NASA Conference Publication 3036

Interstellar Dust: Contributed Papers

NASA Conference Publication 3036

Interstellar Dust: Contributed Papers

Edited by
A. G. G. M. Tielens
and L. J. Allamandola
NASA Ames Research Center
Moffett Field, California

Proceedings of a symposium sponsored by
the National Aeronautics and Space
Administration (Ames Research Center),
the National Science Foundation, and the
International Astronomical Union and held at
Santa Clara University
Santa Clara, California
July 26–30, 1988

National Aeronautics and
Space Administration
Office of Management
Scientific and Technical
Information Division

1989

Frontispiece: Interstellar SiC grains from the Murray meteorite representing extremes of size and shape distribution (scale bar = 1 μm). The interstellar origin of these grains--presumably as stellar condensates--is proven by the highly anomalous isotopic ratios of their Si, C, N, Ne, and Xe, differing from terrestrial ratios by up to 20-fold. These isotopic anomalies are indicative of nucleosynthetic processes in red giants and novae. The grain in the upper right shows well-developed, fresh crystal faces, whereas the remaining grains are fractionated and eroded to varying degrees. (Figure reproduced from Anders, E., Lewis, R.S., Tang, M. and Zinner, E., in IAU Symposium no. 135 on *Interstellar Dust*, Eds. L.J. Allamandola and A.G.G.M. Tielens, (Kluwer, Dordrecht), 1989.)

PREFACE

IAU Symposium 135 on Interstellar Dust was hosted and co-sponsored by NASA Ames Research Center July 26-30, 1988. The symposium was held at Santa Clara University in Santa Clara, California and was made possible by generous grants from the Astronomy and Relativity Branch of the National Aeronautics and Space Administration and the Galactic Astronomy Program of the National Science Foundation. The International Astronomical Union provided travel grants to a number of participants from countries with limited travel funds. We are particularly grateful to the support and services rendered by the dedicated staff at NASA Ames Research Center.

Interstellar dust is of major importance in astrophysics because of its central role in processes such as star formation, the energy balance of gas clouds - including their spectral appearance - interstellar chemistry, the preservation and transport of organic molecules, and so on. The effect of dust on these and other processes is determined by its physical and chemical nature. Until recently, both were the center of controversy and speculation. This situation has improved substantially during the last decade since the previous IAU Symposium on Interstellar Dust in 1972. There has been significant progress observationally, experimentally, and theoretically in areas related to dust research. In particular, the opening up of the IR window by ground-based and air- and spaceborne observatories has provided a touchstone on which theories and experiments can be tested. A good example is the recent realization that polycyclic aromatic hydrocarbon molecules and related species may be a heretofore unrecognized ubiquitous component of the interstellar medium. Likewise the isolation of largely unmodified interstellar grain components in meteorites and in interplanetary dust particles promises to be as revolutionary in the next decade. Thus, it was appropriate to bring researchers together from these various sub-fields in order to integrate the most recent developments. The aim of the symposium was to draw a coherent picture of the dust's composition and its physical characteristics in the various phases of the interstellar medium. The central theme throughout the symposium was the confrontation of theory and laboratory data with observations.

This symposium brought together 199 scientists from 19 different countries. The wide range of interest and expertise of the participants - all in some way related to interstellar dust - is reflected in the great variety of topics that were discussed during the symposium ranging from UV, visible and IR observations of interstellar extinction to quantum-statistical calculations of the IR emission from highly vibrationally excited polycyclic aromatic hydrocarbon molecules. During the course of the symposium, 41 invited review papers and 140 contributed papers were presented. This book is a collection of the contributed papers. The invited reviews will be published in a companion volume by Kluwer Academic Publishers as part of the IAU Symposium Series.

By all accounts, the symposium was a great success. This was due in large measure to the high level of dedication and commitment of the local organizing committee. On behalf of all the participants we thank them for their outstanding effort.

August 1988

Xander Tielens

Lou Allamandola

LOCAL ORGANIZING COMMITTEE MEMBERS

Craig Allen
Betty Baldwin
Barbara Cohen
Luke Dones
Sarah Gibson
Margaret Meixner
Yvonne Pendleton
Bob Rubin
Farid Salama
Scott Sandford
Willem Schutte
Debbie Schwartz
Janice Varney
Bob Walker
Helen Walker
Dora Willoughby

LIST OF SECTIONS

LIST OF INVITED REVIEWS

PRESENTED AT IAU SYMPOSIUM NO. 135 ON INTERSTELLAR DUST

D. Black — Opening Statements

SECTION I: DUST IN THE DIFFUSE INTERSTELLAR MEDIUM

D. Massa: Visible/UV Dust Extinction in the Milky Way
E. Jenkins: Elemental Depletions
E. Fitzpatrick: Visible/UV Observations of Extragalactic Dust
D. Aitken: Dust towards the Galactic Center
P. Martin: Linear and Circular Polarization in the Diffuse ISM
J. Krelowski: Diffuse Interstellar Bands
A. Witt: Visible/UV Scattering by Interstellar Dust

SECTION II: THE OVERIDENTIFIED INFRARED EMISSION FEATURES

K. Sellgren: IR Emission from Reflection Nebulae
J. Bregman: Observations of the IR Emission Features from Planetary Nebulae and HII Regions
J. Puget: The Infrared Cirrus
L. Allamandola: The IR Emission Features and PAH Molecules
W. Duley: The IR Emission Features and Hydrogenated Amorphous Carbon Particles (HAC)
L. Colangeli: Optical Properties of Carbonaceous Materials
S. Leach: Physical and Chemical Properties of PAHs
A. Leger: Visible/UV Properties of PAHs
B. Donn: Problems with PAHs
A. Sakata: Optical Properties of Quenched Carbonaceous Condensates (QCCs)
J. Barker: The Molecular/Quantum-Statistical Approach
L. d'Hendecourt: The Particle/Thermal Approach

SECTION III: DUST IN DENSE CLOUDS

D. Hollenbach: Cloud Heating by Dust
A. Tielens: Grains in Dense Clouds
M. Walmsley: Dust and the Gas Phase Composition of Dense Clouds
R. Hildebrand: Polarized IR Emission from Dust

SECTION IV: DUST IN GALAXIES

G. Helou: Far IR emission from Galactic and Extragalactic Dust
P. Roche: IR Emission from Galaxies

*These will be published separately by Kluwer Academic Publishers/Dordrecht: Holland in their regular IAU Symposium Series.

CONTENTS
(CONTRIBUTED PAPERS)

SECTION I: DUST IN THE DIFFUSE INTERSTELLAR MEDIUM

I-A) INTERSTELLAR EXTINCTION

N91-14898

REDDENING AND EXTINCTION TOWARDS HII REGIONS: A PROGRESS REPORT *

J. Caplan and L. Deharveng
Observatoire de Marseille
2 Place Le Verrier
13248 Marseille Cedex 4, France

The light emitted by the gas in HII regions is attenuated by dust. This extinction can be measured by comparing Hα, Hß, and radio continuum fluxes, since the intrinsic ratios of the Balmer line and thermal radio continuum emissivities are nearly constant for reasonable conditions in HII regions. In the case of giant extragalactic HII regions (c.f. Israel and Kennicutt, 1980), the extinction (from the Hß/radio ratio) has generally been found to be considerably greater than that expected, on the basis of a "standard" law, for the reddening (from the Hα/Hß ratio). More recent work (Caplan and Deharveng, 1986, and van der Hulst, Kennicutt, Crane, and Rots, 1988), although confirming this phenomenon, shows that the discrepancy is less than previously believed.

The extinction excess can be explained in several ways. The dust between us and the emitting gas may have an optical thickness which varies from one point to another over the solid angle subtended by the HII region. The dust may be close enough to the source that scattered light contributes to the flux, or the dust may actually be mixed with the emitting gas. It is difficult to decide which configuration - or combination of configurations - is correct.

The poster presents a rediscussion of the question in the light of our recent observations, with our Fabry-Perot spectrophotometer, of large Galactic HII regions (smaller however than giant extragalactic regions). As these objects are all near the plane of the Galaxy, a large part of the extinction is certainly caused by "interstellar" (i.e. foreground) dust. These regions exhibit definite extinction excesses, which however are rather small with the exception of that of IC 1795, for which a molecular cloud almost totally blocks the light of part of the nebula.

It is instructive to compare the color excesses for stars embedded in these HII regions with those derived (assuming the standard law) from the nebular extinction and reddening. The average value found for stars should indicate the optical depth to the center of the HII region. We find that E_{B-V}(average for stars) > E_{B-V}(from Hß/radio) > E_{B-V}(from Hα/Hß). This result is consistent with various dust distributions, and in particular with internal dust. However, if really large amounts of

dust were located inside the regions, we would expect even greater stellar reddening. In the LMC, we had found E_{B-V}(average for stars) to be about equal to E_{B-V}(from Hα/Hß), but this is clearly due to selection effects: those stars truly inside the HII regions are not observed. Some selection may be present for our Galactic regions too, certain stars being hidden behind opaque clouds.

References

Caplan, J. and Deharveng, L.: 1986, Astron. Astrophys. 155, 297.

Israel, F.P. and Kennicutt, R.C.: 1980, Astrophys. Letters 21, 1.

van der Hulst, J.M., Kennicutt, R.C., Crane, P.C., and Rots, A.H.: 1988, Astron. Astrophys. 195, 38.

* The observations were made at the Observatoire de Haute Provence.

THE RELATIONSHIP BETWEEN IR, OPTICAL, AND UV EXTINCTION

Jason A. Cardelli, Geoffrey C. Clayton, and John S. Mathis
Department of Astronomy, University of Wisconsin
Madison, Wisconsin 53706 USA

ABSTRACT: We present an analysis of the variability of absolute IR, optical, and UV extinction, A_λ, derived through the ratio of total-to-selective extinction, R [$\equiv A_V/E(B-V)$], for 31 lines of sight for which reliable UV extinction parameters have been derived. These data sample a wide range of environments and are characterized by $2.5 \leq R \leq 6.0$. We find that there is a strong linear dependence between extinction expressed as A_λ/A_V and R^{-1} for $1.25\ \mu m \leq \lambda \leq 0.12\ \mu m$. Differences in the general shape of extinction curves are largely due to variations in shape of optical/near-UV extinction ($\lambda \leq 0.7\ \mu m$) corresponding to changes in R, with A_λ/A_V decreasing for increasing R. From a least-squares fit of the observed R-dependence as a function of wavelength for $0.8\ \mu m^{-1} \leq \lambda^{-1} \leq 8.3\ \mu m^{-1}$, we have generated an analytic expression from which IR, optical, and UV extinction curves of the form A_λ/A_V can be reproduced with reasonable accuracy from a knowledge of R. We also find that the absolute bump strength normalized to A_V shows a general decrease with increasing R, suggesting that some fraction of bump grains may be selectively incorporated into coagulated grains. Finally, we find that *absolute extinction* normalized by suitably chosen color indices [e.g. $E(\lambda_1-\lambda_2)$] results in a minimization of the R-dependence of portions of the UV curve, allowing A_λ to be estimated for these wavelengths independent of R.

1. INTRODUCTION

Interpretation of the variability of observed extinction, particularly in the UV, has been confused because most extinction data must be compared in a *relative* way [e.g. $E(\lambda-V)/E(B-V)$], and thus the true nature of the variability may be obscured by the normalization. Conversion of normalized extinction curves to absolute data requires knowledge of the ratio of total-to-selective extinction, R [$\equiv A_V/E(B-V)$]. Clayton and Mathis (1988) have shown that, longward of 0.7 μm, the shape of extinction curves are generally the same and are independent of R. Changes in R arise in the optical/near-UV portion of the curve as a flattening of the observed extinction.

In this paper we examine the variations between R and various UV extinction parameters derived by Fitzpatrick and Massa (1986, 1988; FM88). This represents a continuation of work presented by Cardelli, Clayton, and Mathis (1988a,b). We utilize the data of 31 stars from FM88 for which optical and IR data also exist. For the UV data, FM88 fitted observed extinction curves of the form $E(\lambda-V)/E(B-V)$ with three components; a linear ($1/\lambda$) background, a Lorentzian-like 2175 Å bump in the form of an assumed "Drude function", and a far-UV cubic polynomial. While some aspects of such a parameterization may be more mathematical than physical, the process does provide two

benefits. First, a parameterized curve is easy to reproduce. Second, parameterization of individual curves allows quantitative comparison of specific aspects of UV extinction such as, for example, the position and width of the bump.

The R values used here were derived by fitting the observed near-infrared/optical extinction for $\lambda > 0.7$ μm with the average curve (R = 3.08) of Rieke and Lebofsky (1985). The nature of this fit can be seen in Figure 1 of Cardelli, Clayton, and Mathis (1988a; CCM). Below we descibe the nature of the dependencies between observed extinction and R.

2. VARIABILITY OF GENERAL/TOTAL-TO-SELECTIVE EXTINCTION

2.1 A_λ/A_V versus R^{-1}: The Analytic Dependence

CCM found that there exists a strong relationship between A_λ/A_V and R^{-1} for all UV wavelengths, although the scatter is largest for $\lambda < 0.15$ μm. We have now extended that work to include the optical/near-infrared down to 1.25 μm. An example of this relationship at three wavelengths is shown in Figure 1. We must note that deviations in the shape of optical curves can extend down to and slightly longward of the V bandpass. This is readily apparent by the non-zero slope for the bottom plot in Figure 1. As a result, A_V is perhaps not the best choice, since A_λ/A_V will exhibit some R-dependence at all wavelengths. However, we use this normalization because $A_V/E(B-V)$ has historical significance and a number of the stars lack data at the *R* bandpass ($\lambda = 0.7$ μm). Besides, the deviations below V are generally small, even for lines of sight with R > 4.5.

CCM presented an analytic expression, derived from a least-squares fit between A_λ/A_V and R^{-1} as a function of x ($\equiv 1/\lambda$ μm^{-1}), which can be used to generate UV extinction curves via R which are in relatively good agreement with the observed data. We have combined this with similar fits to optical data so that a complete curve can be generated for 1.25 μm $\leq \lambda \leq$ 0.12 μm. The equation has the form;

$$< A_\lambda/A_V > = a(x) + b(x)/R \qquad (1)$$

where for 0.8 μm^{-1} $\leq x <$ 3.2 μm^{-1} and y=(x-1.82);

$$a(x) = 1 + 0.15020y - 0.34376y^2 + 0.05201y^3 + 0.030339y^4 - 0.01009y^5$$

$$b(x) = 1.75496y + 0.80985y^2 - 0.26666y^3 + 0.01273y^4 - 0.00610y^5$$

and for $x \geq$ 3.2 μm^{-1};

$$a(x) = 1.802 - 0.316x - 0.104/[(x-4.67)^2+0.341] + F_a(x)$$

$$b(x) = -3.090 + 1.825x + 1.206/[(x-4.62)^2 + 0.263] + F_b(x)$$

$$F_a(x) = -0.04473(x-5.9)^2 - 0.009779(x-5.9)^3 \qquad (x \geq 5.9)$$

$$F_b(x) = 0.2130(x-5.9)^2 + 0.1207(x-5.9)^3 \qquad (x \geq 5.9)$$

$$F_a(x) = F_b(x) = 0 \text{ for } x < 5.9 \qquad (x < 5.9)$$

Figure 2 shows a comparison between the formula and real data for three different values of R. The strong dependency of the general level of the UV extinction with R is quite apparent. HD 154445 has been shown because it represents one of the poorest fits in the sample. For the majority of cases, however, the fit is much better. For $R \approx 3.2$, we find excellent agreement between our analytic formula and the standard *average* curves in both the optical and the UV (e.g. Schild 1977; Savage and Mathis 1979; Seaton 1979; Rieke and Lebofsky 1985). However, because these curves correspond to a unique value of R, the dependency shown in Figure 2 clearly indicates that use of these curves to deredden spectra appropriate to R values different from $3.1 \leq R \leq 3.5$ would be inappropriate. Despite the apparent poor fit for HD 154445, our analytic expression for R = 3.61 actually reproduces the observed curve better than using an *average curve* with the same R value. Although R may not be an easy parameter to derive for a particular line of sight, these results indicate that use of the *average curve* with $R > 3.5$ can lead to large systematic errors. Similarly, it is inaccurate to use a *θ Ori-like curve* ($R \approx 5.3$) with $R < 5$.

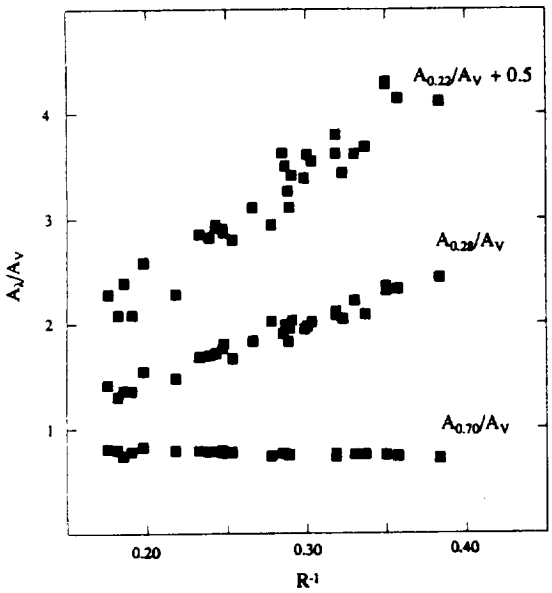

Figure 1: Absolute extinction, A_λ, normalized to A_V versus R^{-1} at three different wavelengths derived from our sample of 31 stars. The top plot has been shifted up by 0.5 units in order to separate it from the middle plot.

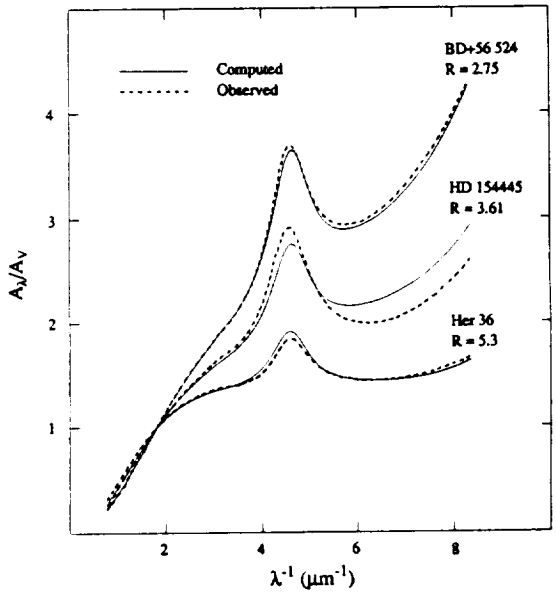

Figure 2: Comparison of the R-dependent relation (eqn. 1) derived from extinction data for the stars in our sample with observed extinction for three stars with different R values. HD 154445 represents one of the most discrepant cases.

2.2 The Variation of A_{bump}/A_V with R^{-1}: Interpretation

Figure 3 shows a comparison between R^{-1} and several UV bump parameters as derived by FM88. In Figure 3a, we find that A_{BUMP}/A_V, the *absolute bump strength* (above the linear background) *normalized by the total visual extinction*, shows a strong dependency on R^{-1} varying between 0.5 ± 0.2 at $R = 5$ and 1.25 ± 0.3 at $R = 3$ (the uncertainties represent the maximum range of the data). This general dependency on R^{-1}

does not necessarily mean that the bump arises from the same species of grains that give rise to the optical extinction. Figures 3b and 3c show plots of bump width ($\gamma \equiv$ FWHM) and central position ($1/\lambda_0$) versus R^{-1} which do not show any clear R-dependence. This would seem to indicate that the bump grains are indeed a separate component which show independent variability. However, the direct relationship between A_{BUMP}/A_V and R^{-1} could be understood qualitatively in a rather simple way. A small value of R^{-1} is most easily explained by an increase in the mean size of the grains which provide the optical extinction. This growth probably involves coagulation, in which small grains are incorporated into larger ones. In most grain models, the carrier of the bump is seen as small grains (usually graphitic carbon). It is easy to imagine that some of these grains would be incorporated into the larger ones under coagulation conditions. In such a scenario, incorporation of some fraction of the bump grains into larger grains, where they do not produce a bump, would result in a decrease in the relative bump strength through a decrease in the column density. The remaining uncoagulated grains are presumably 'free' to respond independently to environmental conditions. Mathis and Whiffen (1989) have made the above arguments quantitative, and other grain models probably could as well.

A similar relationship also exists for the far-UV component (see Cardelli, Clayton, and Mathis 1988b). FM88 found that the shape of the far-UV curvature was essentially the same for all of the stars in their sample and so derived the far-UV component by fitting a single polynomial expression with a variable scale factor. We find that this scale factor, normalized by A_V, also appears to vary with R^{-1}, although the dependence is not as well defined and there are a few lines of sight (e.g. HD 147889, HD 204827) which exhibit strong deviations from the mean.

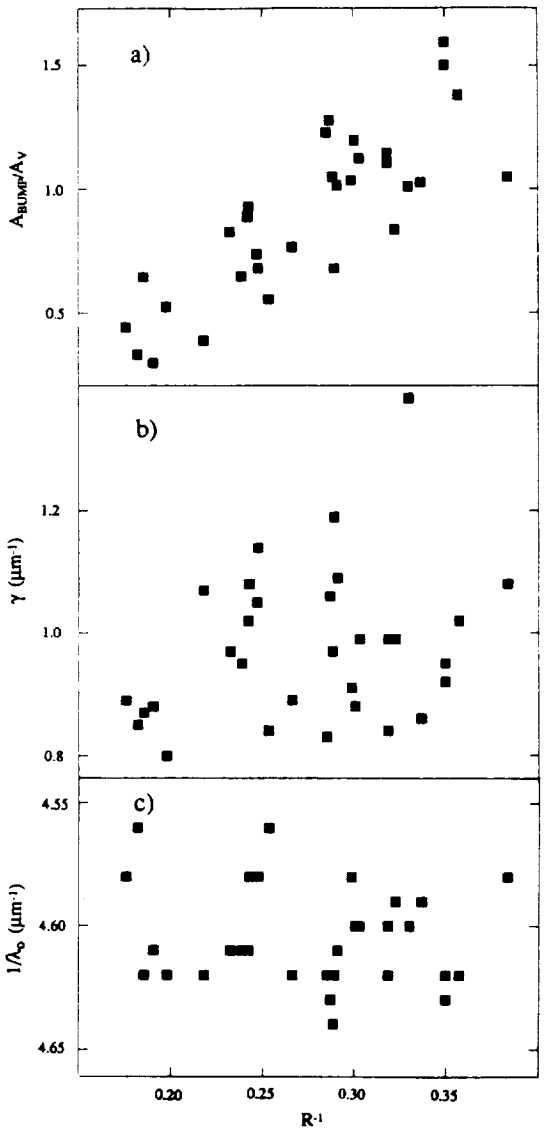

Figure 3: Three different bump parameters for the data in our sample derived by FM88. a) Absolute bump strength, A_{BUMP}, normalized to A_V, b) bump width (γ), and c) central position ($1/\lambda_0$) versus R^{-1}. The behavior shown in b) and c) implies that the bump does vary independently from the grain population responsible for variations in R.

3. COLOR EXCESS NORMALIZATION: $A_\lambda/E(\lambda_1-\lambda_2)$

The strong R-dependence in the shape of extinction curves for $\lambda < 0.7$ μm exhibited in Figure 2 implies that there exists some color excess, $E(\lambda_1 - \lambda_2)$ for $0.7\ \mu m \geq \lambda \geq 0.35$ μm, such that normalized extinction at a particular UV wavelength, $A(\lambda_{uv})/E(\lambda_1-\lambda_2)$, has a minimal dependence on R. Unfortunately, our data base requires that λ_1 and λ_2 be chosen from available broad-band or narrow-band photometry. For our sample of stars, this corresponds to the standard Johnson filters (e.g. U, B, V, or R) which may not correpond to the optimal wavelengths.

Figure 4 shows selected examples of $A(\lambda_{uv})/E(\lambda_1 - \lambda_2)$, where λ_1 and λ_2 correspond to the nominal wavelengths of the B ($\lambda \approx 0.44$ μm), V ($\lambda \approx 0.55$ μm), or R ($\lambda \approx 0.70$ μm) bandpasses, plotted against R. Figure 4a shows that A(0.18 μm)/E(B-V) exhibits a minimal R-dependence, with all but 2 points being within $\leq\pm 10\%$ of the mean value. In Figure 4b we see that A(0.22 μm)/E(B-V) also exhibits a minimal R-dependence, with all but 4 points within $\leq\pm 10\%$. For E(B-V), similar results can be found for $0.24\ \mu m \geq \lambda_{uv} \geq 0.17\ \mu m$. For λ_{uv} outside of this range, normalization by E(B-V) begins to exhibit a moderate R-dependence, as can be seen in Figure 4c for $\lambda_{uv} = 0.26$ μm. However, for this wavelength, normalization by E(B-R) produces a minimal R-dependence with all but 1 point being within $\leq\pm 10\%$. For E(B-R), similar results can be found for $0.30\ \mu m \geq \lambda_{uv} \geq 0.25\ \mu m$. For $\lambda_{uv} > 0.30$ μm, normalization by E(B-R) begins to exhibit a moderate R-dependence as can be seen in Figure 4d.

One can see that normalization by some combination of color excesses utilizing B, V, and R can result in an R-independent value of $A(\lambda_{uv})/E(\lambda_1-\lambda_2)$ for $0.30\ \mu m \geq \lambda_{uv} \geq 0.17$ μm with 1-σ being $<\pm 10\%$. Like the analytic R-dependent results presented above, these results allow UV extinction to be estimated when direct determination is not possible or practical. However, unlike the above results, this procedure *only requires derivation of a color excess from ground-based photometry*, without the near-IR photometry which is needed to derive R.

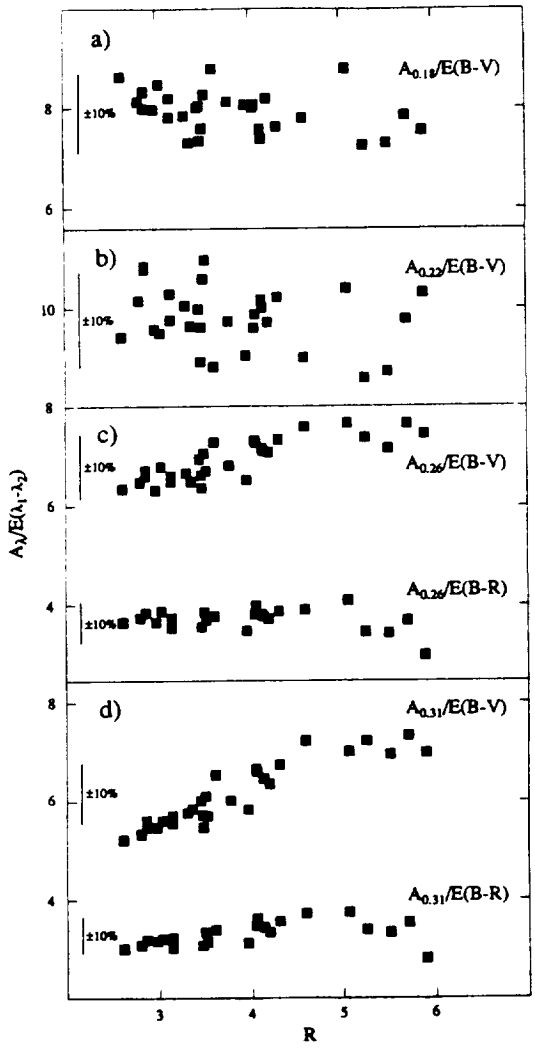

Figure 4: Values of A_λ for selected wavelengths, normalized by various color excesses. For specific wavelengths, a particular choice of color excess results in a minimal R-dependence with 1-σ $<\pm 10\%$. For these cases, A_λ can be estimated independent of R.

REFERENCES

Cardelli, J. A., Clayton, G. C., and Mathis, J. S.: 1988a, *Ap. J. (Lett.)*, **329**, L33 (CCM).

Cardelli, J. A., Clayton, G. C., and Mathis, J. S.: 1988b, *A Decade of UV Astronomy with the IUE Satellite*, in press.

Clayton, G. C, and Mathis, J. S.: 1988, *Ap. J.*, **327**, 911.

Fitzpatrick, E. L., and Massa, D.: 1986, *Ap. J.*, **307**, 286.

Fitzpatrick, E. L., and Massa, D.: 1988, *Ap. J.*, **328**, 734 (FM88).

Mathis, J. S., and Whiffen, G.: 1989, submitted to *Ap. J.*

Rieke, G. H., and Lebofsky, M. J.: 1985, *Ap. J.*, **288**, 618.

Schild, R. E.: 1977, *Astr. J.*, **82**, 337.

Savage, B. D., and Mathis, J. S.: 1979, *Ann. Rev. Astr. Ap.*, **17**, 73.

Seaton, M. J.: 1979, *Mon. Not. Roy. Astr. Soc.*, **187**, 73P.

N91-14900

The Detection of a Broad Interstellar Extinction Feature near 1700Å

David J. Carnochan
Department of Physics & Astronomy
University College London, Gower Street, London WC1E 6BT

Abstract

A statistical examination of 126 extinction curves has revealed the presence of a second broad absorption feature similar in nature to the 2200Å feature. The feature is centred on wavelength 1706Å, has a full-half-width of 350Å and a mean central height of 0.21 magnitudes. The strength of the feature increases with E(B-V) supporting an interstellar origin, and on average it is 18 times weaker than the 2200Å feature.

Extinction curves between 1350 and 2550Å have been produced for 126 normal stars based on data from the S2/68 Ultraviolet Sky Survey in a manner similar to that described by Carnochan (1986a). Following Fitzpatrick & Massa (1988) each curve is initially fitted with the analytic approximation,

$$A(\lambda)/E(B-V) \simeq a_0 + a_1 x + a_2(x-6.0)^2 + b_1 L_1(\lambda) \qquad (1)$$

where $L_1(\lambda)$ is the Lorentz profile,

$$L_1(\lambda) = d_1^2/\{(x-x_1)^2 + d_1^2\} \qquad (2)$$

$x = 1/\lambda$ in microns; a_0, a_1 represent the intercept and slope of the linear extinction continuum; a_2 (which is zero for $x < 6.0$) is a curvature term representing the far uv rise; $b_1 L_1(\lambda)$ is the 2200Å feature with central wavelength x_1 ($\sim 4.6\mu^{-1}$), half-half-width d_1 ($\sim 0.50\mu^{-1}$) and central height b_1 (~ 3.7 mag). The best fit is found using least squares analysis and all six parameters are allowed to vary including the position, x_1, and half-half-width, d_1, of the 2200Å feature. A quantitative measure for the goodness of the fit is obtained by calculating χ_1^2.

The procedure is illustrated in Figure 1(a) where the extinction curve for ζ Oph (HD 129757, O9V, E(B-V)=0.33) is shown together with the the best fit, the three extinction components, and the residuals. It is clear from the residuals that there

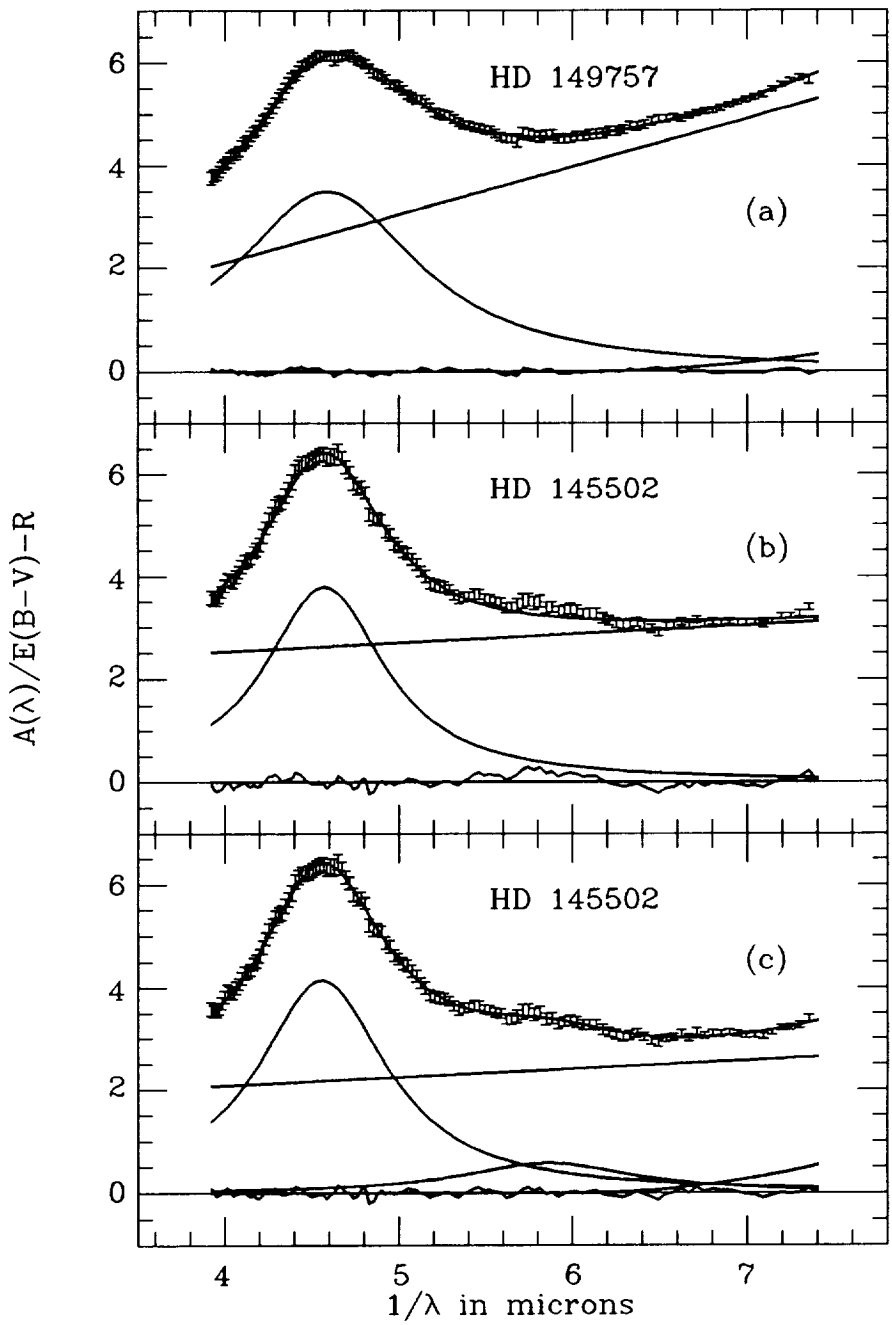

Figure 1: (a) The extinction curve for ζ Oph, HD 149757. Also plotted are the best fit, the three extinction components and the residual extinction. (b) The extinction curve for HD 145502. Note the poorness of the fit between 5.4 and 6.8 μ^{-1}. (c) The revised extinction curve for HD 145502. The best fit uses four components including a contribution from the 1700Å feature. Compare with (b).

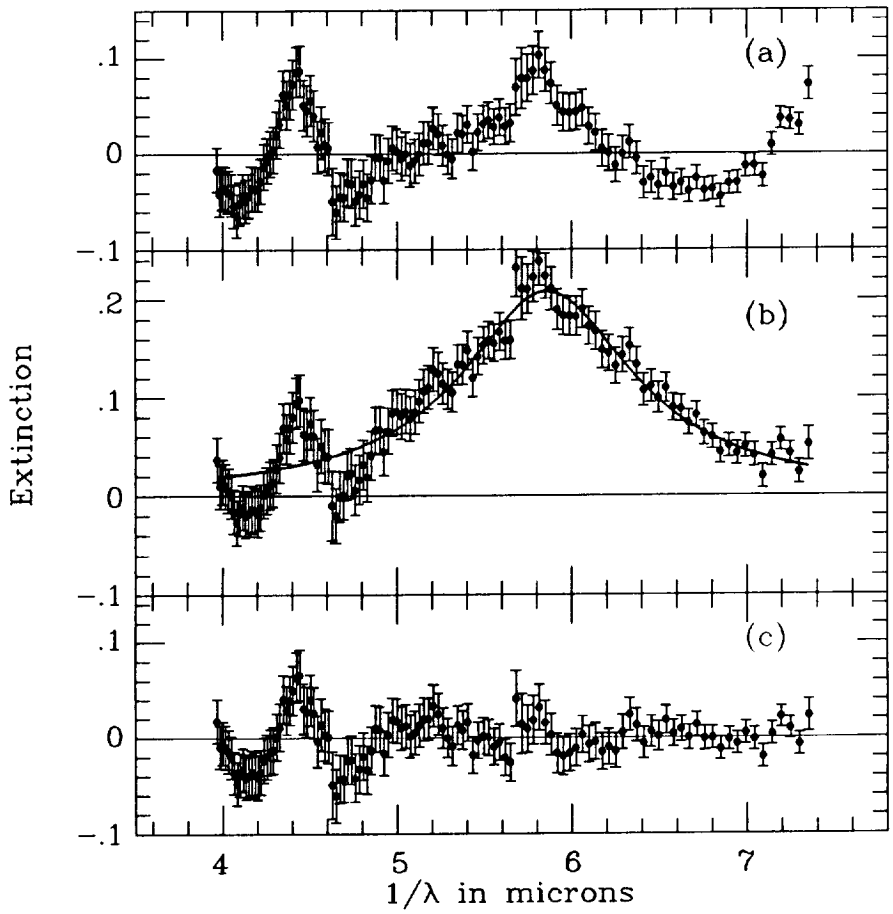

Figure 2: (a) The weighted mean residual extinction averaged over all 126 extinction curves. (b) The profile of the 1700Å feature (including the residuals) averaged over all 126 extinction curves. The best fit Lorentz profile is also shown. (c) The revised mean residual extinction averaged over all 126 extinction curves. This is the same as (b) with the Lorentz 1700Å feature removed.

is no evidence in this star for any additional extinction features. However many stars cannot be fitted quite so well and Figure 1(b) shows the extinction curve for HD 145502 (B2IV, E(B-V)=0.27). It is apparent from the residuals that there are regions where the extinction is either systematically high (around 5.8 μ^{-1}) or systematically low (around 6.5 μ^{-1}), and in this star the long wavelength side of the 2200Å feature does not fit particularly well either.

The weighted mean residuals for all 126 extinction curves are shown in Figure 2(a) and it is now very clear that there is additional structure in the extinction curve that is not accounted for by the three components of equation 1. The ripple between 4 and 5 μ^{-1} is probably associated with the 2200Å feature and indicates that 2200Å is not quite symmetrical, departing slightly from the Lorentz profile

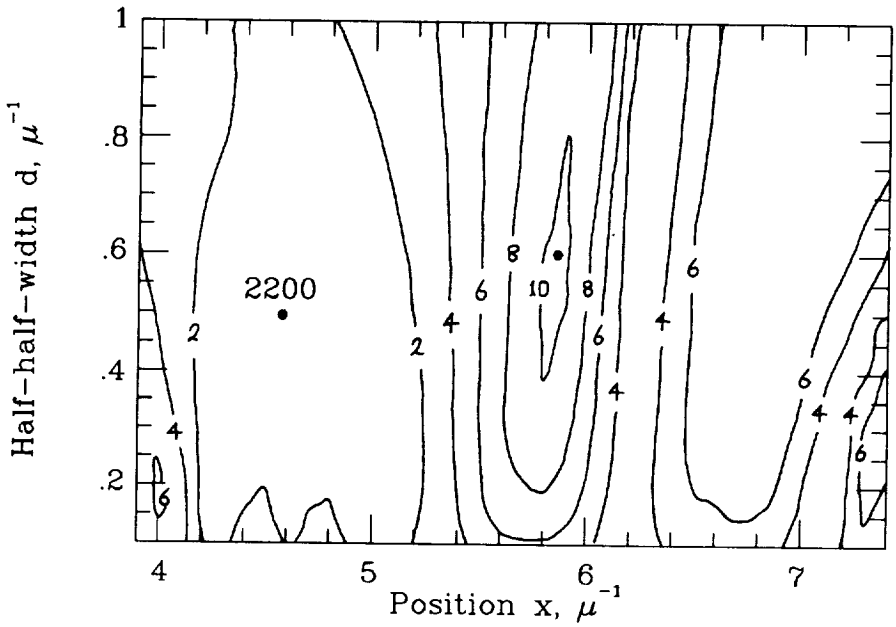

Figure 3: The contour plot of the % improvement in the fit obtained by introducing a feature at wavelength x μ^{-1} and half-half-width d μ^{-1}. The contours are drawn at 2% intervals and the peak of just over 10% occurs at x=5.86, d=0.6 μ^{-1}.

assumed here. If the background is set at about -0.05 then the remainder of the residuals (ignoring the far-uv rise beyond 7 μ^{-1}) can be interpreted as an additional broad absorption feature centred near 5.8 μ^{-1}.

To investigate the possible existence of other features a second Lorentz term was added to equation 1,

$$A(\lambda)/E(B-V) \simeq a_0 + a_1 x + a_2(x-6.0)^2 + b_1 L_1(\lambda) + b_2 L_2(\lambda) \qquad (3)$$

where

$$L_2(\lambda) = d_2^2/\{(x-x_2)^2 + d_2^2\} \qquad (4)$$

The additional feature was assumed to occur at chosen values of position, x_2, and half-half-width, d_2, and a second value for the goodness of fit, χ_2^2, calculated. The percentage improvement in the fit obtained by adding the second feature is simply,

$$(\chi_1^2 - \chi_2^2)/\chi_1^2 \times 100 \qquad (5)$$

A grid search was undertaken for a second feature between $3.9 < x_2 < 7.4$ and $0.1 < d_2 < 1.0$. Figure 3 is the resulting contour map of the improvement in χ^2, meaned over all 126 extinction curves, with contours drawn every 2%. It is clear from this contour map that a 10% improvement can be achieved by postulating the existence of a second absorption feature at 1706Å ($5.86\mu^{-1}$) with a half-half-width of 175Å ($0.60\mu^{-1}$). Statistically the addition of the extra term in equation 3

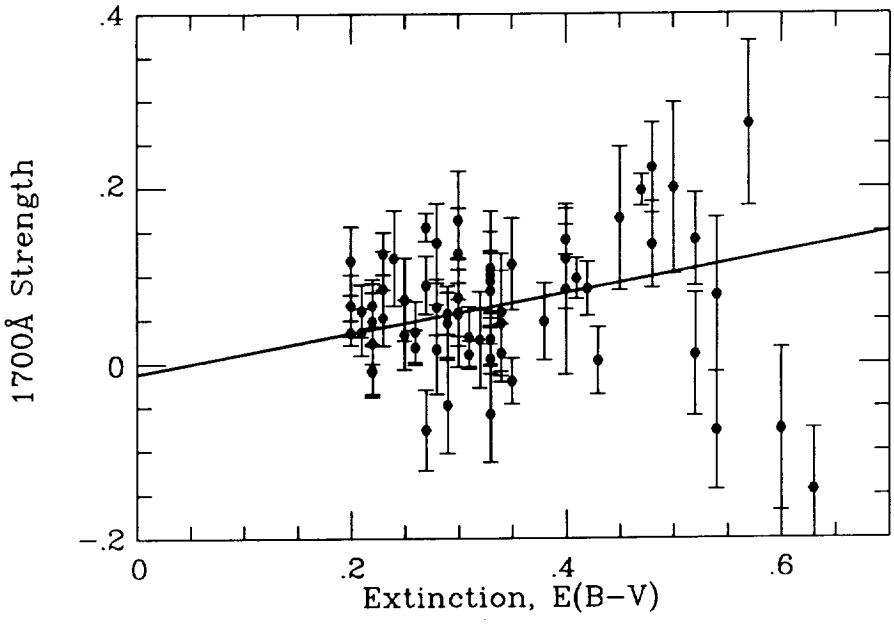

Figure 4: The observed strength of the 1700Å feature plotted against the extinction, E(B-V). The least squares line is also shown which supports an interstellar origin for the 1700Å feature.

should randomly improve χ^2 by about 1%. The actual 10% improvement gives a better than 95% confidence that the 1700Å feature is real. The profile of the feature, $b_2 L_2(\lambda)$, can be checked by inverting equation 3 and Figure 2(b) shows the mean profile averaged over all 126 extinction curves. The mean central height of the 1700Å feature is 0.21 magnitudes which makes it 18 times weaker than the 2200Å feature. The new mean residuals are simply obtained by removing the 1700Å feature from Figure 2(b) and they are shown in Figure 2(c). A comparison of Figures 2(a) and 2(c) demonstrates that the addition of the 1700Å feature makes a considerable improvement to the residuals although the 'ripple' near 2200Å is still present. Figure 1(c) shows the new fit for HD 145502 which again shows considerable improvement over Figure 1(b).

At this point all we have shown is that a significant improvement in fitting the extinction curve can be made by the addition of a 1700Å feature. The most critical task is to demonstrate that such a feature has an interstellar origin. This is quite difficult to accomplish as the feature is weak with relatively large error bars and because it is not observed in all reddened stars (e.g. absent in ζ Oph). The best evidence is to show that its strength, b_2 E(B-V), increases with extinction, E(B-V), and Figure 4 shows the data for 66 stars having mean extinction curve errors smaller than 0.4 magnitudes. Although the scatter is considerable, the best straight line passes very close to the origin and has a positive slope both of which give strong

support to an interstellar origin for the 1700Å feature,

$$b_2 \times E(B-V) = -0.009(\pm 0.010) + 0.221(\pm 0.018)E(B-V) \qquad (6)$$

The mean values of the nine parameters now used to describe the extinction curve are,

$$\begin{array}{lll} a_0 = 2.825 \pm 0.303, & x_1 = 4.575 \pm 0.011, & x_2 = 5.86 \\ a_1 = 0.650 \pm 0.055, & d_1 = 0.495 \pm 0.032, & d_2 = 0.60 \\ a_2 = 0.143 \pm 0.102, & b_1 = 3.765 \pm 0.139, & b_2 = 0.210 \pm 0.133 \end{array}$$

The normalised strength of the 1700Å feature, b_2, varies from star to star and no significant correlations are found with any of the other extinction parameters, supporting the idea of a distinct feature.

As for an explanation of the 1700Å feature, none is immediately forthcoming. However features near 1600Å have been mentioned in three cases. (1) Gilra (1972) has suggested that if silicate grains produce part of the uv extinction then there ought to be a silicate feature near 1600Å. (2) MacLean et. al. (1982) in associating the 2200Å feature with MgO expected a weaker feature near 1600Å. (3) In explaining the 2200Å feature by charge transfer absorption Carnochan (1986b, 1988) has predicted a second charge transfer feature, similar in width to 2200Å and about 30 times weaker in the neighbourhood of 1600Å.

Considerable information is available on the variations and correlations of the nine extinction parameters listed above. These essentially confirm the findings of Carnochan (1986a) and Fitzpatrick & Massa (1986, 1988). A much fuller account of this work will be submitted shortly for publication in Monthly Notices of the Royal Astronomical Society. Finally one interesting coincidence between the 1700Å and 2200Å features is that, within the errors, they have the same value of $\Delta\lambda/\lambda$.

References

Carnochan, D.J. 1986a, M.N.R.A.S. **219**, 903.

Carnochan, D.J. 1986b, *New Insights in Astrophysics*, ESA **SP-263**, 593.

Carnochan, D.J. 1988, M.N.R.A.S. **231**, 455.

Fitzpatrick, E.L. & Massa, D. 1986, Ap.J., **307**, 286.

Fitzpatrick, E.L. & Massa, D. 1988, Ap.J., **328**, 734.

Gilra, D.P. 1972, *Scientific Results from OAO-2*, NASA **SP-310**, 295.

MacLean, S., Duley, W.W. and Millar, T.J. 1982, Ap.J., **256**, L61.

The autocorrelation function of the north pole dust

Jens Knude
Copenhagen University Observatory
Copenhagen, Denmark

N91-14901

1. Abstract

The angular scales on which local interstellar dust is distributed are so far rather unknown as are the geometrical shapes of the dust features.

From the about 5000 color excesses resulting from a north polar survey with 4-5 stars per square degree the two-point autocorrelation function is derived for separations ranging from 10 ' to 3 °.

For intercloud lines of sight, -0.020 < E(b-y) < -0.010 mag, the average cross products $\langle E_1 \times E_2 \rangle_\Theta$ show no variation with separation $\Theta(1,2)$ whereas products of cloud column densities, 0.030 < E(b-y) < 0.040 mag, seem to prefer discrete separations either less than 20', around 75' or finally at about 150'.

Surprisingly the two point autocorrelation function $\omega_E = \langle E_1 \times E_2 \rangle / \langle E \rangle^2 - 1$ equals 0 except for any separation except $\Theta=0$. $\omega_E(\Theta)$'s absence of variation is unexpected because $\omega_H(\Theta)$ is known to vary exponentially above b = 40° for separations less than 3 °. Atomic hydrogen and dust may thus not be entirely mixed or the moments $\langle E_1 \times E_2 \rangle_\Theta$ may not characterize the dust distribution.

2. Angular distribution of almost identical reddening pairs.

Apparently the north polar cap is not completely free from interstellar dust. Figure 1 gives an empression of the dust column densities which may be expected for b > 40° and within ≈ 500 pc from the plane. $A_V = \frac{1}{10}$ corresponds to E(b-y) ≈ 0.024 mag so a substantial fraction of the observed lines of sight, almost one third in fact , is fairly reddened.

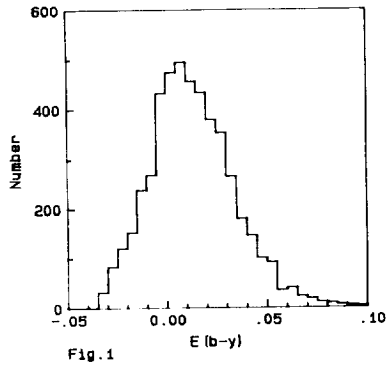

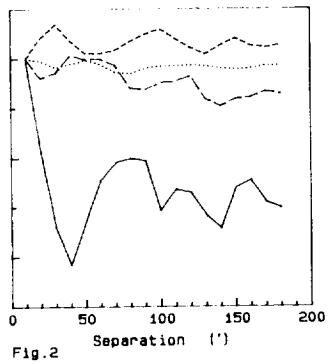

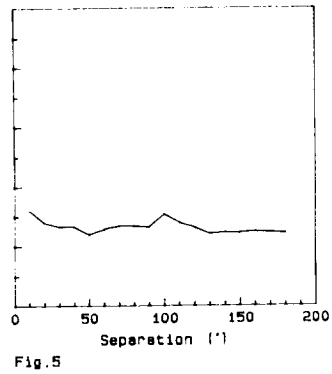

Figure 1. E(b-y) histogram resulting from a survey of the polar area above b=70°. The survey is magnitude compelete for the A5 to G0

stars. The surface density is 4.5 stars per square degree.

Figure 2. Relative frequency of pairs with almost identical color excess: E_2-E_1 = 0.010 mag , as a function of separation. The ordinate is on an arbitrary scale , and the curves are shifted to a common frequency at the 10' separation. The dotted curve corresponds to pairs: -0.020,-0.010. The short dashes corresponds to pairs: 0.010, 0.020. The long dashes corresponds to pairs: 0.020,0.030. The solid curve are for pairs with : 0.030,0.040.

*Figure 5.*Average cross product $\langle E_1 \times E_2 \rangle_\Theta$ versus separation.

First we consider how the average values of products of almost identical color excesses vary with separation. If the diffuse dust clouds have spherical projections the function $\langle E_1 \times E_2 \rangle_\Theta$ will be a representation of typical sizes at a given distance. Figure 2 shows the results for a selection of reddening pairs. A changing shape of the curve is noted when the reddenings are changed from those typical for the intercloud directions, (E_1,E_2) = (-0.020, -0.010) , to those with (E_1,E_2) = (0.030, 0.040) probably crossing regions with enhanced dust density. It is clear that $\langle -0.020 \times -0.010 \rangle_\Theta$ does not change with separations smaller than 3°. So if we consider an intercloud line of sight it will always be located in a region with an extent of at least 3° - its shape untold. For the slightly obscured lines of sight the average product does vary with separation. With E_1 in the range 0.030± 0.005 and E_2 in the interval 0.040± 0.005 the most probable separation is less than 20' but secondary maxima at 75' and 150' are also suggested.

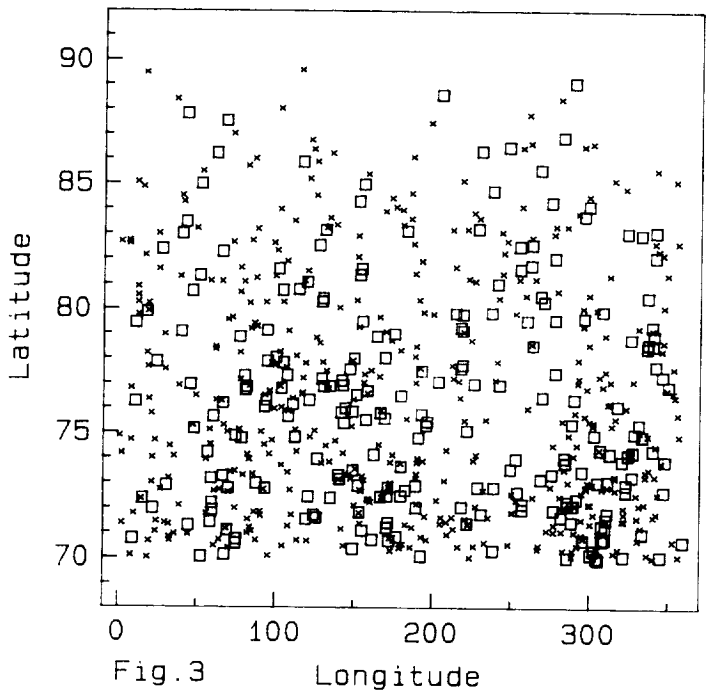

Fig.3

Figure 3. Location of the E_1=0.030± 0.005 (*the* ×'*s*) and the E_2=0.040± 0.005 (□'*s*) lines of sight.

The existence of these preferred separations does, however, not necessarily bear on the angular sizes of discrete clouds. The sequence of preferred separations does not indicate that there are unique upper limits to cloud diameters but more likely it suggests that the dust may not entirely be localized in spherical structures but that it just as well could be confined to elongated features. This qualitative interpretation of Figure 2 may partly find support in Figure 3 where E_1 = 0.030 (*the* ×'*s*) and E_2 = 0.040 (□'*s*) lines of sight are indicated in a (l,b) diagram. What Figure 3 show are several examples where E_1 and E_2 are confined to string-like features. Figure 3 is furthermore instructive by displaying the very inhomogenous distribution of the cloud lines of sight E_1,E_2 and particularly by showing the existence of large solid angles void of these clouds, e.g. the regions centered on (l,b) = (250,75) and (50,79).

3. An overall view of obscured lines of sight.

On Figure 4 is shown the (l,b) distribution of all lines of sight with E(b-y)$\gtrsim$ 0.024 mag on two different scales and in a polar representation. The different scales are chosen to aid the eye to see various structures. The justification of the lower redddening limit 0.024 mag is threefold.

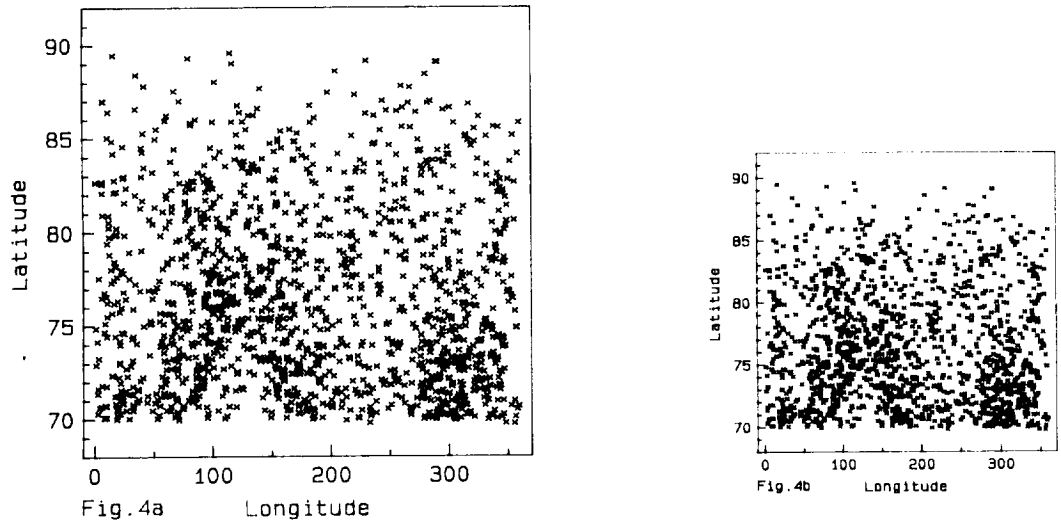

Figure 4a and b. Lines of sight with E(b-y) > 0.024 mag shown in (l,b)-diagrams with different resolution. There is apparently some structure in the distribution of the larger color excesses.

First the lower limit corresponds to $3\times\sigma(E(b\text{-}y))$ so there is a high probability that the plotted lines of sight are significantly reddened. Second , E(b-y) = 0.024 is the reddening expected in the most typical cloud from a decomposition of the color excess distribution in the galactic plane by the method of moments , assuming only one type of clouds. Finally E(b-y) = 0.024 corresponds to $\tau(E{=}250eV)$ = 1 , assuming a canonical gas/dust ratio with no clumping. The E(b-y) > 0.024 mag map may thus indicate where a 250 eV

emission , originating in the more remote halo , could be absorbed. The lower resolution of Figure 4b and 4d suggests the possibility of large more or less coherent systems of extinction at the north galactic pole. Several odd features are also noted in Figure 4a such as the doughnut shaped structure centered at (l,b) = (100,76.5): an isolated ring with $A_V \geq$ 0.1 mag with no absorption at its center. Note also the long string of large excesses at (l,b) = (340-350, 76-84) in an otherwise almost extinction free region.

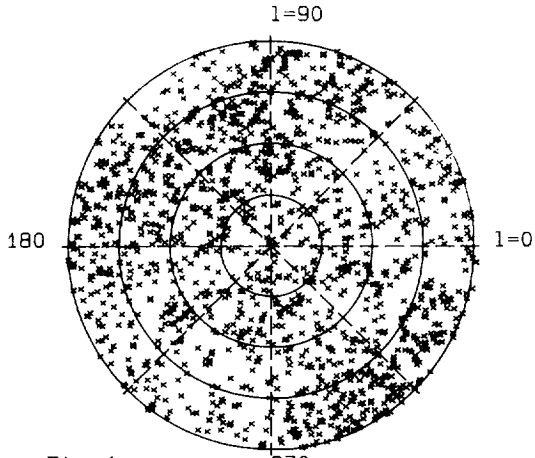

Fig.4c

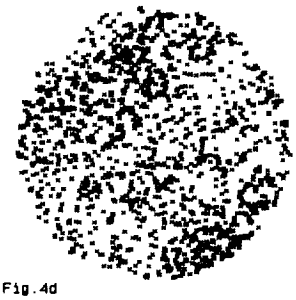
Fig.4d

Figure 4c and d. As Figure 4a and b but in a polar layout. The separation between the latitude circles in Figure 4c is 5°.

Finally Figure 4c,d give the polar presentation of the dust distribution. Particularly the compressed version in which the individual dust features have merged gives an impression of how the dust is located at the NGP.

4. The two-point autocorrelation function.

After the presentation of the complex projected dust distribution in the previous sections it would be interesting to known the behaviour of a statistics as the two point autocorrelation function: $\omega_E(\Theta)=\langle E_1 \times E_2 \rangle / \langle E \rangle^2-1$. As the distribution in Figure 4d is not quite unlike the projected distributions of galaxy counts one might perhaps expect a correlation function similar to those of the galaxy distributions. However , the two-point autocorrelation function of the polar dust distribution is surprisingly found to be constantly equal to zero, except for Θ = 0. The projected dust distribution is apparently uncorrelated conversely to the atomic hydrogen whose autocorrelation follows an exponential law for separations smaller than 3° at latitudes above 40 °.

The different correlation functions could be due to a different spatial distribution of gas and dust or be an artefact of the different observing techniques.

5. Conclusion

The data presented may possibly best be understood if the dust mostly is located in inhomogeneous strings or sheets of substantial angular size.

N91-14902

THE DEPENDENCE OF UV EXTINCTION PROPERTIES ON DUST ENVIRONMENT

Derck Massa, Applied Research Corporation, Landover,
MD 20785

UV extinction data, derived from the Savage et al. (1985) ANS extinction catalog, are analyzed. The data include the normalized extinction at 1550Å, the strength of the 2175Å bump, and a crude estimate of the bump width. The results confirm the systematic increase of far-UV extinction with galactic altitude first uncovered by Kiszkurno-Koziej and Lequeux (1987) and verify that this effect is in fact a result of the dust being away from the plane, and not a generalized density dependence. It is also shown that the width of the 2175Å bump is systematically broader in denser regions (defined by large values of E(B-V) per Kpc), implying that a similar galactic altitude effect seen in this parameter may only be a reflection of the lower densities encountered away from the plane.

The dependence of bump width upon bump strength is also examined. It is shown that a relationship between these two parameters is expected for certain models of the bump, but none is found. However, two factors which could be complicating a straightforward interpretation of the observations are identified and discussed.

REFERENCES

Kiszkurno-Koziej, E., and Lequeux, J. 1987, Astr.Ap., 185, 291.
Savage, B.D., Massa, D., Meade, M., and Wesselius, P.R. 1985, Ap.J.Suppl., 59, 397.

PROPERTIES OF INTERSTELLAR DUST IN THE REGION OF THE CEP OB4 ASSOCIATION

J. Sūdžius
Astronomical Observatory of the Vilnius State University
Vilnius, Lithuania, USSR

1. Introduction

A number of papers have been devoted to the study of regional variations in the interstellar extinction law (see reviews of Savage and Mathis, 1979; Krelowski, 1986). Among the areas with abnormal interstellar extinction law (IEL) the region of Cyg has been noted by a number of authors (see, e. g., Nandy, 1964; Johnson, 1965; Whiteoak, 1966; Goy, 1972; Wampler, 1962; Sūdžius, 1974). Goy (1972) and Wampler (1962) has pointed out that the IEL for the Cyg OB2 association is characteristic of another association, Cep OB4. However, the investigations of interstellar extinction in this association are very scarce and we lack detailed extinction curve for this region of the sky.

Therefore an attempt was made to study interstellar extinction in the region of the Cep OB4 association. The Vilnius seven colour photometric system has been used for this purpose (Straižys, 1977). The effective wavelengths and their reciprocals for the Vilnius photometric system are presented in Table 1.

Table 1

	U	P	X	Y	Z	V	S
λ_e, Å	3425	3730	4037	4650	5149	5429	6500
$1/\lambda_e$, μm^{-1}	2.92	2.68	2.48	2.15	1.94	1.84	1.54

This system has already been applied for the study of variations in the IEL in four regions ofthe sky: Cyg, Cep, Per and Mon (Sūdžius, 1974). It was shown that the Cyg IEL deviates from that for Cep, Per and Mon regions where the IEL was found to be rather uniform. Therefore an average IEL was derived for Cep, Per and Mon regions. It was also found that the interstellar extinction curve has the so-called very broadband structure (VBS) in the visual part of the spectrum. This structure is surprisingly uniform for all the regions investigated. The results of multicolour photometry were combined with the data of Whiteoak (1966) and detailed interstellar extinction curves were derived for Cyg and for Cep-Per-Mon (average) regions in the wavelengths interval of 3000-8000 Å (Sūdžius, 1974).

2. Observations

For the present study OB stars with known Sp/L types were selected from published data. 10 suitable stars were found in the region of the Cep OB4 association. For comparison 18 stars of the Cyg OB2 association were also observed. The observations were obtained with the 48 cm and 1 m telescopes at the observational site near the Maidanak Mountain in Uzbekistan in 1977 and 1985.

The observational procedure and reduction technique were the same as generally accepted for the Vilnius photometric system (Straižys, 1977).

3. Method

The usual way to study possible variations in the IEL is an analysis of differences of colour excess ratios (E/E), E_{ij}/E_{jk}, for different regions of the sky, where magnitudes j and k indicate the normalization points and i is any other magnitude of the photometric system.

In the Vilnius photometric system magnitudes Y and V are chosen for normalization. Therefore colour excess ratios E_{UY}/E_{YV}, E_{PY}/E_{YV}, E_{XY}/E_{YV}, E_{YZ}/E_{YV} and E_{VS}/E_{YV} are calculated. The colour excesses of the observed stars were determined using intrinsic colour indices ofStraižys et al. (1982) and were plotted on two index diagrams. The E/E were calculated by the method of Williamson (1968) and were normalized to Whitford's (1958) IEL: $A_i=(E_{iY}/E_{YV})E_{YV}^{(n)}+A_Y^{(n)}$. This procedure requires the following values of $E_{YV}^{(n)}=0.23^m$ ($E_{BV}=0.32^m$) and $A_Y^{(n)}=1.26^m$. In order to examine the VBS in the interstellar extinction curve deviations of obtained extinction values from Whitford's (1958) IEL, $\Delta A=A_i-A_i^{(w)}$, were determined. It should be noted that in the interval of wavenumbers from 1 to 3 μm^{-1} Whitford's IEL is represented by two straight lines intersecting at 2.24 μm^{-1}.

4. Analysis

The results of calculation of the E/E and their r.m.s. errors are presented in Table 2. This Table also includes the results for the so-called average IEL (Sūdžius, 1974). The plots of colour

Table 2

Area	$\frac{E_{UY}}{E_{YV}}$	$\frac{E_{PY}}{E_{YV}}$	$\frac{E_{XY}}{E_{YV}}$	$\frac{E_{YZ}}{E_{ZV}}$	$\frac{E_{VS}}{E_{YV}}$
Cep OB4	1.791	1.279	0.849	2.173	0.867
	.006	.005	.004	.019	.003
Cyg OB2	1.746	1.237	0.824	1.779	0.885
	.003	.002	.002	.007	.003
Average	1.608	1.138	0.754	1.797	0.843
(Sūdžius,1974)	.009	.006	.005	.021	.007

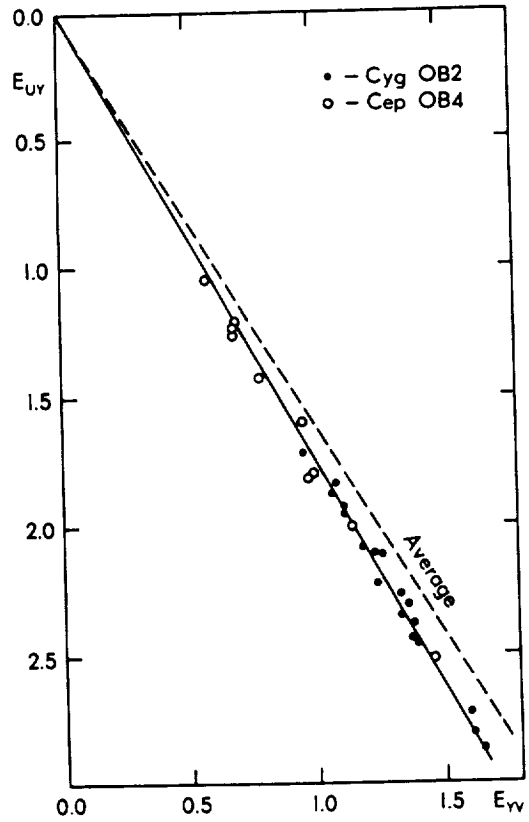

Fig. 1. The diagram E_{UY}, E_{YV} for the observed stars. The continuos line corresponds to the E/E for Cyg OB2 and the dotted one to the average E/E from Sūdžius (1974).

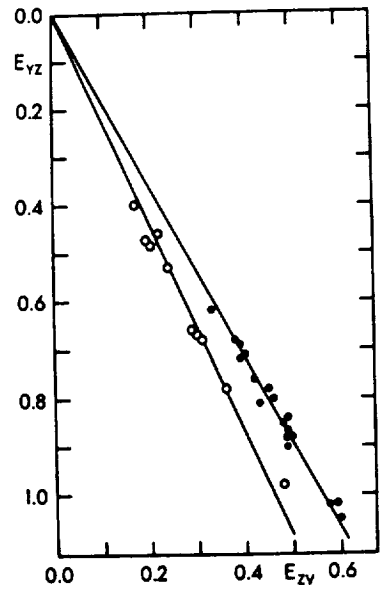

Fig. 2. The diagram E_{YZ}, E_{ZV} for the observed stars. The designations are the same as in Fig. 1.

excesses E_{UY}, E_{YV} and E_{YZ}, E_{ZV} are shown in Figs. 1 and 2 respectively. Pecularities of the IEL are well demonstrated by deviations of the obtained extinction values from those of Whitford's (1958), ΔA. These deviations as well as deviations of the average extinction curve from Whitford's one are plotted in Fig. 3.

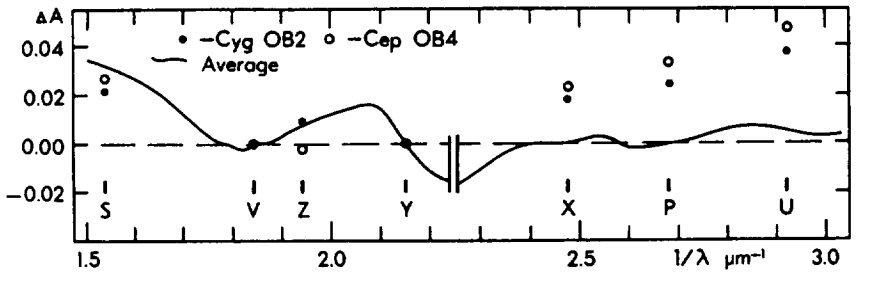

Fig.3. Deviations of Cyg OB2, Cep OB4 and the average extinction laws from Whitford's (1958) one versus wavenumber. The positions of magnitudes of the Vilnius photometric system are indicated.

The obtained results show that in the ultraviolet the IEL for Cep OB4 differs from the average one and is very close to that for Cyg OB2. This conclusion supports the results of Wampler (1962) and Goy (1972) but is in disagreement with the results of Lucke (1980). A little higher values of extinction in the ultraviolet for Cep OB4 in comparison with those for Cyg OB2 confirm the conclusion of Goy (1972). The VBS in the interstellar extinction curve for Cyg OB2 does not differ significantly from the average one and is in agreement with the results of Whiteoak (1966), York (1971), Rex and Hayes (1977) and Krelowski et al. (1986). However, our results indicate that the Cep OB4 extinc-

tion curve probably has no VBS in the interval of wavenumbers 1.84 - 2.15 μm^{-1}. This fact is very important because our results (Sūdžius, 1974) indicate uniformity of the VBS for all the stars investigated.

5. Conclusions

The obtained IEL for the Cep OB4 association does not match any of the laws determined for other regions of the sky. However, it is very close to the Cyg OB2 law in the ultraviolet.

Our results suggest the Cep OB4 IEL to have no VBS in the interval of Wavenumbers 1.84 - 2.15 μm^{-1}.

References

Goy, G.: 1972, Astron. Astrophys., 21, 11.

Johnson, H.L.: 1965, Astrophys. J., 141, 923.

Krelowski, J.: 1986, Studia Soc. Sci. Torun., 6F, No. 4, 53.

Krelowski, J., Maszkowski, R., Strobel, A.: 1986, Astron. Astrophys., 166, 271.

Lucke, D.B.: 1980, Astron. Astrophys., 90, 350.

Nandy, K.: 1964, Publ. Roy. Obs. Edinburgh, 3, 142.

Rex, K.H., Hayes, D.S.: 1977, Preprint.

Savage, B.D., Mathis, J.S.: 1979, Ann. Rev. Astron. Astrophys., 17, 73.

Straižys, V.: 1977, Multicolour Stellar Photometry, Mokslas Publishers, Vilnius.

Straižys, V., Jodinskienė, E., Kurilienė, G.: 1982, Bull. Vilnius Obs., No. 60, 16.

Sūdžius, J.: 1974, Bull. Vilnius Obs., No. 39, 18.

Wampler, E.J.: 1962, Astrophys. J., 136, 100.

Whiteoak, J.B.: 1966, Astrophys. J., 144, 305.

Whitford, A.E.: 1958, Astron. J., 63, 201.

Williamson, J.H.: 1968, Canadian J. Phys., 46, 1895.

York, D.: 1971, Astrophys. J., 166, 65.

THREE-MICRON SPECTROSCOPY OF HIGHLY REDDENED FIELD STARS

M. Tapia[1,4], P. Persi[2], M. Roth[1,3], M. Ferrari-Toniolo[2]

[1]Instituto de Astronomía, UNAM, Ensenada, Mexico.
[2]Istituto di Astrofisica Spaziale, CNR, Frascati, Italy.
[3]Departamento de Astronomía, U. de Chile, Santiago, Chile.
[4]Alexander von Humboldt-Foundation Fellow at E.S.O., Garching, F.R.G.

Broad absorption features centred at 3.45 μm and at 3.0-3.1 μm towards a number of late-type supergiants in the vicinity of the Galactic Centre have been repetedly reported. Here, we present 2.0-2.5 μm and 3.0-4.0 μm spectra of field late-type highly reddened ($A_V \sim 17 - 27$) stars located in different regions of the galactic plane more than 20° away from the Galactic Centre direction. The observations, made with the 3.6m, 2.2m and 1.0m ESO telescopes at La Silla, Chile, consist of CVF spectra with resolution $\lambda/\Delta\lambda \simeq 100$ and IRSPEC spectra with resolution $\lambda/\Delta\lambda \simeq 700$. In the direction of the most highly reddened stars, definitive detections of the 3.45 μm and the 3.0-3.1 μm absorption features are reported. The 3.45 μm feature has been attributed to absorption arising in a vibrational transition resulting from the C-H stretching in organic compounds, while the 3.0-3.1 μm broader feature are tentatively attributed to O-H bonds. The observations strongly support that the agent producing the 3.45 μm feature, presumably organic molecules, is an important component of the diffuse interstellar medium and is not characteristic only of the Galactic Centre environment.

I-B) INTERSTELLAR POLARIZATION

Interstellar Circular Polarization and the Dielectric Nature of Dust Grains

G. Chlewicki
Laboratory for Space Research and Kapteyn Astronomical Institute, Groningen, The Netherlands

J. Mayo Greenberg
Laboratory Astrophysics, University of Leiden, The Netherlands

We have reexamined the implications of the observed relationship between the wavelength dependence of interstellar circular and linear polarization. Mie theory calculations for grains with various optical constants demonstrate that any population of grains which matches the observed wavelength dependence of linear polarization also yields the correct cross-over wavelength of circular polarization. The coincidence of the peak wavelength of linear polarization and the cross-over of circular polarization is therefore independent of the optical constants of the grains and cannot be used as a critical constraint on grain properties. The observed relationship instead reflects a more fundamental connection between linear and circular polarization which has been derived from the Kramers-Kronig relations by Shapiro (1975). Our numerical results fully support Shapiro's conclusions and demonstrate that the apparent upper limit on the visual absorptivity of polarizing grains deduced from earlier Mie theory calculations (Martin, 1972) was spurious and resulted from a violation of the Kramers-Kronig relations in the assumed optical constants of the particles.

The Kramers-Kronig interpretation of circular polarization can be used to place constraints on linear polarization outside the wavelength range in which it has been observed. We use this approach to show that the peak observed in the visual is likely to be the only significant feature in the linear polarization curve, which therefore appears to be well approximated at all wavelengths by the Serkowski formula.

A synthesis of available laboratory data has been used to analyze the properties of dielectric core-mantle grains as the source of visual extinction and polarization. The mantle material is likely to have a low effective energy gap (below 1 eV) and a relatively high visual absorptivity (observations of the albedo of grains suggest an imaginary part of the index of refraction at least as high as 0.15). A multipopulation model, which incorporates the silicate core - organic refractory mantle grains (Hong and Greenberg, 1980), is shown to satisfy all the available constraints on grain properties in the visual.

NEW RESULTS IN THE THEORY OF DUST GRAIN ALIGNMENT

P. Cugnon
Observatoire Royal de Belgique
av. Circulaire, 3 B-1180 Brussel, BELGIUM

Two complementary approaches are used in an attempt to propose an unique appropriate formulation of the solution to the problem of magnetic alignment of grains in the diffuse and/or the more denser clouds, whatever the mechanism of rotational excitation (thermal of suprathermal) can be. The interest of such an unified formulation is mainly that the same theoretical expression for polarization can be used everywhere, allowing for easier comparisons between regions where the physical conditions (temperature, densities, magnetic field, grain size) are highly different.

The first consists in applying a Monte-Carlo method (Purcell and Spitzer, 1971; Cugnon, 1985) to a limited number of representative cases, for which all the torques acting on the grain are taken into account : impulsive random torques due to direct collisions with gas atoms, to evaporations of atoms from the surface, and to exo-energetic recombinations forming hydrogen molecules, followed by violent ejections from peculiar sites; magnetic torques. Three characteristic times are associated with these torques :
- the collisional damping time, related to atomic collisions,
- the time necessary to change completely the actual sites configuration (re-surfacing time) narrowly bound to the correlation time of the suprathermal torque, as defined by Purcell (1979),
- the magnetic damping time.
Also, three temperatures can be defined, which are :
- the rotational temperature of the grain, equal to a weighted mean between the gas temperature, the grain temperature, and the temperature associated with molecular ejection, when this process is random,
- the internal temperature of the grain,
- the "pseudo-temperature" associated to the suprathermal excitation due to molecular ejections from a limited number of peculiar sites.

The Monte-Carlo method implies the random generation of the collisional parameters, among which the time interval between two collisions (or evaporations), the incoming velo-

city of the gas atom, the evaporation and ejection velocities, with the constraint of a maxwellian distribution, and, as a working hypothesis, the rotational and precessional angles, because of the symmetry of the problem and of their fast variations with respect to the other position angles. In order to reduce appreciably the computer running time, it was necessary to increase the mass of the colliding atoms by a factor 10000, and to modify correspondingly the magnetic damping time. For simplicity, also, the surface of the spheroid was divided into 10000 elements, among which the peculiar ejection sites were chosen.

During the time interval separating two impulsive events, the position angles and the angular momentum are incremented by the necessary amount (including a fluctuating part governed by the grain temperature) due to magnetic torques.

The second approach starts from an heuristic (and somewhat speculative) point of view. It consists in a generalization of the author's results (Cugnon, 1983; see also Purcell and Spitzer, 1971; Greenberg, 1978) obtained for thermal alignment to the suprathermal case. It appears indeed that in the two extreme cases, i. e. when the correlation time of the suprathermal torque is very long (short) compared with the collisional and magnetic damping times, the thermal formulation may be used after redefinition of the involved times and temperatures. For example, in the first situation, using the pseudo-temperature quoted above, which is very high, as rotational temperature, and a time characteristic of the changes in the suprathermal torque instead of the collisional damping time leads to perfect Davis and Greenstein alignment, in agreement with Purcell's theory.

The Monte-Carlo method described above appeared to be the most powerful to investigate the intermediate cases. However, at the present time, only a few cases have been run, of which the results are promising, but which do not yet constitute a sufficient sample to make sure that the thermal formulation may be extended to the suprathermal behaviour.

References :

Cugnon, P.: 1983, Astron. Astrophys. 120, 156

Cugnon, P.: 1986, Astron. Astrophys. 152, 1

Greenberg, J.M.: 1978, in "Cosmic Dust", ed. J.A.M. McDonnel, (New-York, Wiley) 187

Purcell, E.M.: 1979, Astrophys. J. 231, 404

Purcell, E.M. and Spitzer, L.: Astrophys. J. 167, 31

POLARIZATION AND EXTINCTION BY ALIGNED GRAINS

M. Matsumura* and M. Seki**
*Astronomical Institute, Tohoku University, Sendai, 980, Japan
**College of General Education, Tohoku University, Sendai, 980, Japan

Abstract. Correlations between ultraviolet extinction and visual polarization are studied. No correlations are found for sampled 272 stars. UV extinction and visual polarization are quite independent phenomena.

1. Introduction

It is well established that wavelength dependence of UV extinction varies from star to star. This variation is usually interpreted as the difference in abundance of grains which characterize the UV extinction (UV grains, hereafter). Other factors, however, may also have effects on this variation. Greenberg and Chlewicki (1987) suggested that the alignment of grains responsible for visual polarization has an effect on UV extinction. In addition, if the UV grains are well aligned, an effect by this alignment may appear in UV extinction, as well as in UV polarization which data is unavailable now (except Gehrels, 1974). The alignment of the UV grains is possible, since the magnetic alignment is more effective for smaller grains (Greenberg, 1978, Seki and Hasegawa, 1986).

Wealth of data provides an opportunity to look for possible correlations between visual polarization and UV extinction. In the present paper, we select the stars for which both visual polarization and UV extinction data are available, and investigate their correlations.

2. Data

Data of visual polarization are cited from Axon and Ellis (1976), and those of UV extinction are from Savage et al (1985) who used results of the Astronomical Netherlands Satellite (ANS). The stars are selected which are well reddened ($E(B-V) > 0.4$ mag), but those are rejected showing UV variability, lying in a cluster, or being identified as double. Thereby we get the sample of 272 stars.

Polarization efficiency $p_v/E(B-V)$ of these stars ranges from 0 to around 10 percent/mag. As is shown in Figure 1,

$p_V/E(B-V)$ increases with l in the range of $l \simeq 50^\circ - 140^\circ$ (l:galactic longitude). This is not inconsistent with the direction of magnetic field being in $l \simeq 50^\circ$ (e.g. Spitzer 1978). Thus the large spread of $p_V/E(B-V)$ in the present sample is mainly due to the difference in angle between the direction of the magnetic field and that of the line of sight.

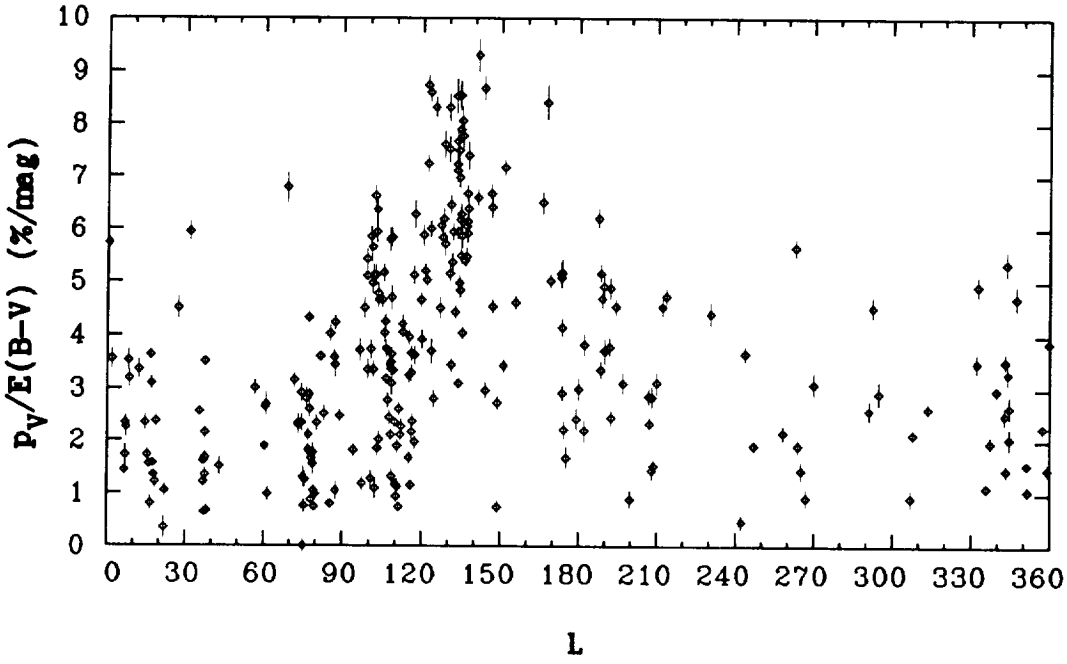

Figure 1. Dependence of $p_V/E(B-V)$ on galactic longitude.

3. Results and Suggestions

Figure 2 shows dependence of the normalized UV color excess $E(\lambda-V)/E(B-V)$ on the optical polarization efficiency $p_V/E(B-V)$, for λ=3300, 2200, and 1550 A. It is apparent that $E(\lambda-V)/E(B-V)$ does not correlate with $p_V/E(B-V)$. Similar results are obtained for λ=2500 and 1800 A. Correlation coefficients are very small: -0.03, 0.09, 0.26, 0.10, and 0.12 for λ= 3300, 2500, 2200, 1800, and 1550 A, respectively. We can safely say that no significant correlations are found.

To get more quantitative information, we divide the sample into four groups according to the value of $p_V/E(B-V)$, and calculate mean and standard deviation of $E(\lambda-V)/E(B-V)$ in each group (Table 1). The means of $E(\lambda-V)/E(B-V)$ are fairly constant against $p_V/E(B-V)$, especially for λ=3300 and 2500 A. Though the model

calculation predicts that the value of $E(\lambda-V)/E(B-V)$ decreases by around 0.5 as $p_V/E(B-V)$ increases from 0 to 9 percent/mag (Greenberg and Chlewicki, 1987), we cannot find such variation in our sample. This may imply that the grains responsible for visual polarization do not have significant contribution to UV extinction. Otherwise, they may be poorly aligned, with their polarization efficiencies being quite high (e.g. magnetite proposed by Shapiro, 1975).

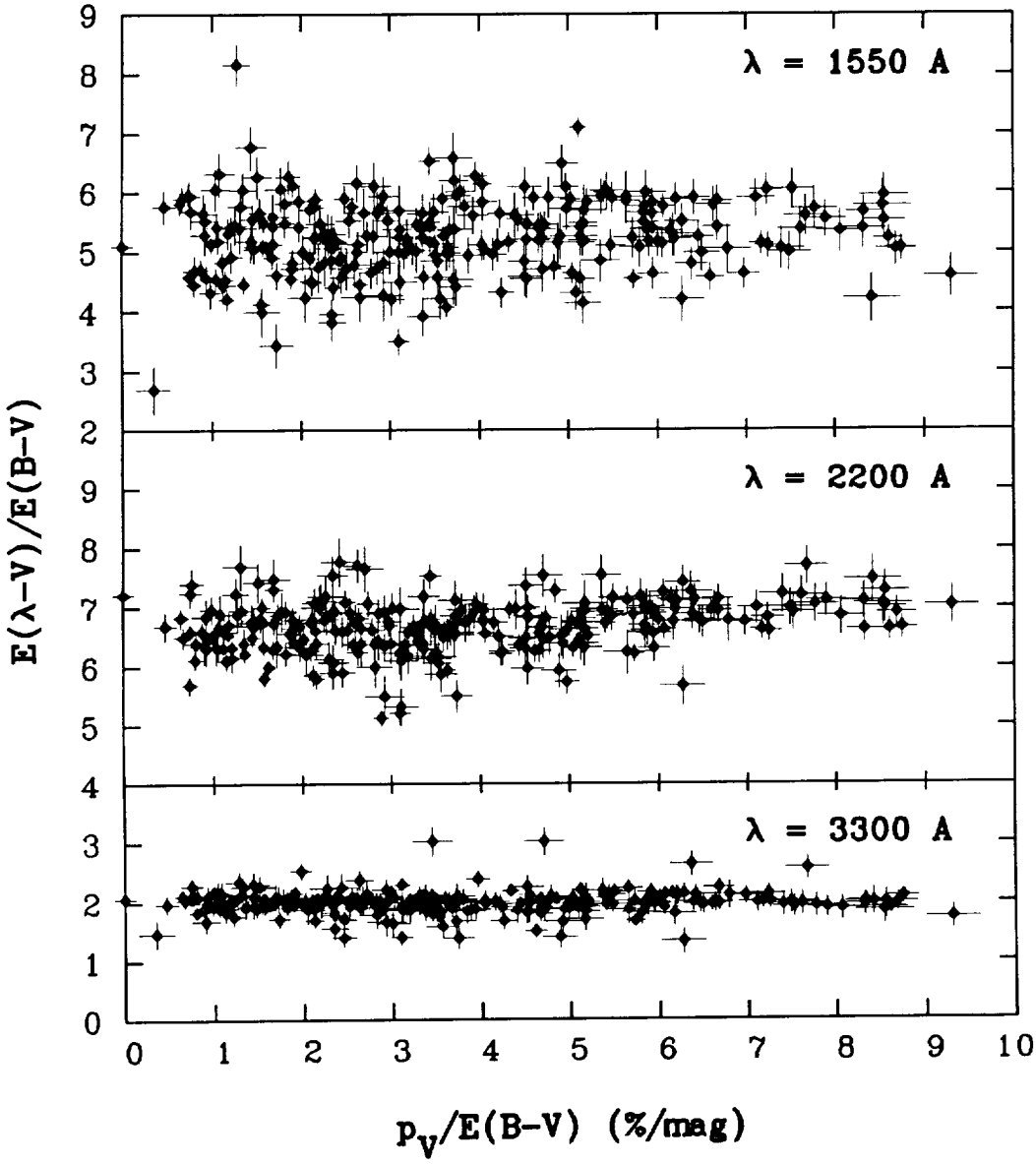

Figure 2. Dependence of $E(\lambda-V)/E(B-V)$ on $p_V/E(B-V)$. The bars show a mismatch of 1 spectral subclass of stars.

Table 1. Means and Standard Deviations of $E(\lambda-V)/E(B-V)$

p / E(B-V)		E(33-V)/E(B-V)	E(25-V)/E(B-V)	E(22-V)/E(B-V)	E(18-V)/E(B-V)	E(15-V)/E(B-V)
0-2 (m=1.28)	m	2.03	4.17	6.58	4.91	5.25
64 stars	σ_{n-1}	0.16	0.38	0.67	0.60	0.81
2-4 (m=2.95)	m	1.97	4.09	6.57	4.77	5.14
99 stars	σ_{n-1}	0.21	0.31	0.50	0.46	0.60
4-6 (m=5.02)	m	1.98	4.13	6.70	4.94	5.39
67 stars	σ_{n-1}	0.20	0.26	0.36	0.39	0.55
>6 (m=7.24)	m	2.02	4.24	6.96	4.96	5.33
42 stars	σ_{n-1}	0.19	0.25	0.32	0.34	0.47
All (m=3.73)	m	2.00	4.14	6.66	4.87	5.26
272 stars	σ_{n-1}	0.19	0.31	0.51	0.47	0.64

References

Axon, D.J., and Ellis, R.S.: 1976, M.N.R.A.S. 177, 499.

Gehrels, T.: 1974, A.J. 79, 590.

Greenberg, J.M.: 1978, in Cosmic Dust, ed. McDonnell, J.A.M., John Wiley & Sons.

Greenberg, J.M. and Chlewicki, G.: 1987, Q.J.R.A.S. 28, 312.

Savage, B.D., Massa, D., Meade, M., and Wesselius, P.R.: 1985, Ap.J. Suppl. 59, 397.

Seki, M. and Hasegawa, T.I.: 1986, Science Rep. Tohoku Univ. Eighth Series, 7, 135 (Sendai Astronomiaj Raportoj N-ro 307).

Shapiro, P.R.: 1975, Ap.J. 201, 151.

Spitzer, L.Jr.: 1978, Physical Processes in the Interstellar Medium, John Wiley & Sons.

ALIGNMENT MECHANISMS OF PARAMAGNETIC GRAINS REVISITED

M. Seki
College of General Education, Tohoku University
Sendai 980, Japan

ABSTRACT

Taking into account the tight coupling of grain axis with angular momentum due to effective dissipation of rotational energy, we have reinvestigated the alignment of spheroidal grains by paramagnetic relaxation. Alignment degree will be significantly improved in diffuse clouds. The inclusions of superparamagnetic (SPM) substances may play a key role in grain alignment in dark clouds as well as in diffuse clouds.

INTRODUCTION

The linear polarization observed in many reddened stars is generally assumed to be produced by alignment of anisotropic grains in the magnetic field. According to Davis and Greenstein (1951, referred to hereafter as "DG"), the angular momentum of a grain J will align with respect to magnetic field B and the principal axis of greatest inertia A tends to line up with J by paramagnetic absorption of the rotational kinetic energy. The magnetic field calculated on the DG theory is much larger than that has been measured. Seki and Hasegawa(1986) reinvestigated the DG mechanism for spheroidal dielectric grains by taking into account the tight coupling of grain axis A with J due to effective dissipation of rotational energy by the internal friction or by the Barnett effect (Purcell 1979). They find that the alignment degree of A with respect to B is distinctly improved.

In some dark clouds, where optical or IR polarizations possibly caused by aligned grains are observed (Vrba et al,1981;Seki and Hasegawa 1987;Hildebrand 1988),the temperatures of the gas and of the dust are so low that alignment by paramagnetic relaxation seems to be difficalt. The "pinwheel" mechanism may be ineffective either,because hydrogen is mai nly in molecular form and there exist few UV photons.

Jones and Spitzer(1967) and Mathis(1986) suggest that a part of interstellar grains are superparamagnetic(SPM). In the present paper, we will examine the effect of the imaginary part of magnetic susceptibility χ'' on polarization efficiency of spheroidal grains on the basis of the "improved" DG mechanism.

DEPENDENCE OF POLARIZATION EFFICIENCY ON χ''

We consider a cloud of identical dielectric spheroids spinning in a uniform magnetic field B. The ratio of polarization P(%) to A_V(mag) is a measure of polarization efficiency of the cloud. If P/A_V is not large and the grain size is smaller than the wavelength at V, we may write the polarization efficiency as follows;

$$P/A_V = (P/A_V)_{pf} \cdot Qa \cdot \sin^2 \nu \ ,$$

where $(P/A_V)_{pf}$ is the polarizing effectiveness for picket-fence alignment, Q_a is the alignment degree of grain axis with respect to magnetic field, and ν is the angle between the line of sight and the direction of magnetic field. Values for $(P/A_V)_{pf}$ are obtained from Rogers and Martin (1978). The alignment parameter is expressed as

$$Q_a = < P_2(\cos (A,B)) > \ ,$$

where angular brackets denote an ensemble average. If the angles (J,B) and (A,J) are uncorrelated, $Q_a = Q_j \cdot Q_x$. Q_j and Q_x are calculated following Seki and Hasegawa(1986) and Purcell and Spitzer(1971).

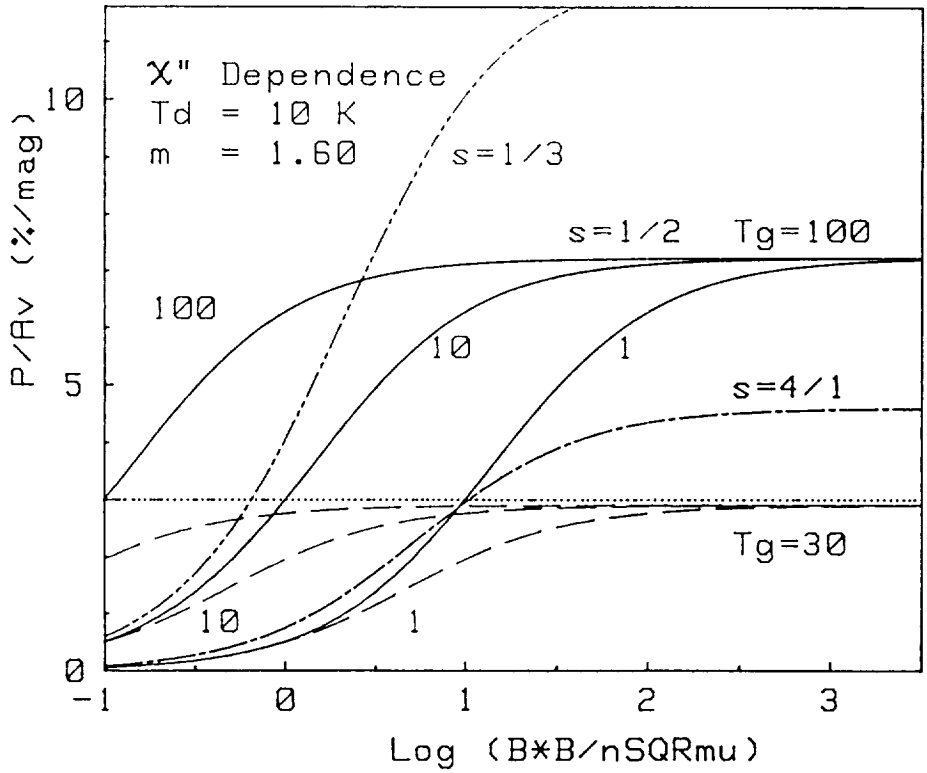

Figure 1. Dependence of P/A_V on the magnetic susceptibility of the grain. The equivalent radius is 0.1μm.

Taking $\nu = 90°$, we show in Figure 1 the polarization efficiency as a function of magnetic field strength for various grain models. The horizontal dotted-line represents the observed efficiency of 3 %/mag. In every case, P/A_V increases monotonously with $B^2/\sqrt{\mu} n_g$ and approaches asymptotically to an upper limit.(μ : the mean molecular weight of the gas; n_g : the number density.) The limiting value depends on the grain's shape (s), the temperatures of the gas (T_g) and of the dust (T_d), and the refractive index (m) via $(P/A_V)_{pf}$.

For $\omega << 10^9$ sec^{-1}, $\chi''(\omega)$ is approximately given as

$$\chi'' = 2.5 \cdot 10^{-12} \, k \omega / T_d,$$

where k = 1 gives χ'' found in most paramagnetic substances. In order to see the effects of SPM inclusions, we have made calculations of P/A_V by simply changing the value of k. The numeral (1,10,or 100) by each curve in Figure 1 represents the value for k. Evidently, the curve of P/A_V vs B^2/n_g shifts in the horizontal direction by changing the paramagnetic susceptibility coefficient k; that is, k is a factor by which the effect of B^2/n_g on the degree of grain alignment is amplified. The effect of SPM inclusions appears significant for low values of B^2/n_g, say, for $B^2/n_g < 10$ $(\mu G)^2/cm^{-3}$. This comes from the fact that Q_j is proportional to the ratio of the magnetic to gas-friction torques δ for a small value of δ, which in turn varies as $(k/(r_{eq} + k) \cdot (B^2/ng)$, where r_{eq} is the equivalent radius of the grain.

Assuming that B scales as $n_g^{0.5}$ and taking $B \approx 10$ μG at $n_g = 10^2$ cm^{-3} (Heiles,1987; Myers and Goodman, 1988), we get $B^2/n_g \approx 10^0$. Then, it seems from Figure 1 that inclusions of SPM substances with $k \approx 10$ are required for oblate grains with $T_d = 10$ K and axial ratio 1/2 in diffuse clouds. The temperature of the gas in a dense and quiet cloud may be much lower than that in the environment. As is demonstrated in Figure 1, polarization efficiency by the same grains may be reduced by a factor of about 2 in the gas of $T_g = 30$ K. However, the reduction factor is not so large at $B^2/n_g \leq 10^{0.5}$ and the derived efficiency at $B^2/n_g = 10^0$ is 2 %/mag. Evidence for the decrease of polarization efficiency with increasing optical depth has been found in several dark clouds (Vrba et al.,1981; Seki and Hasegawa, 1987). Therefore, the calculated efficiency is not necessarily inconsistent with the observed one.

Table 1 is a summary of our results. Alignment degree of dielectric spheroidal grains will be significantly improved if the tight coupling of grain axis with angular momentum is taken into account. Inclusions of SPM substances may play an important role in grain alignment in dark clouds as well as in diffuse clouds.

REFERENCES

Davis,L.Jr. and Greenstein, J.L.: 1951, Astrophys. J. 114, 206
Heiles, C.: 1987, in "Interstellar Processes" (eds. D.J.Hollenbach and Thronson,Jr.), p. 171.

Hildebrand, R.H.: 1988, Astron. Lett. and Communications, 26, 263.
Jones, R.V. and Spitzer, L.Jr. ; 1967, Astrophys. J. 147, 943.
Mathis, J.S.: 1986, Astrophys. J. 308, 281.
Myers, P.C. and Goodman, A.A.: 1988, Astrophys. J. 326, L27.
Purcell,E.M.: 1979, Astrophys. J. 231, 404.
Purcell, E.M. and Spitzer, L.Jr.: 1971, Astrophys. J. 167, 31.
Rogers, C. and Martin, P.G.: 1978, Astrophys. J. 228, 450.
Seki, M. and Hasegawa, T.I.: 1986, Sci. Rep. Tohoku Univ. 7,135 (=Sendai Astronomiaj Raportoj Nr.307).
Seki, M. and Hasegawa, T.I.: 1987, in "Star Forming Regions" (IAU Symp. 115,eds. M.Peimbert, and J. Jugaku), p. 82.
Vrba, F.J., Coyne, G.V. and Tapia, S.: 1981, Astrophys. J. 243, 489.

Table 1. Magnetic Field Strengths Needed for P/Av = 3 %/mag *)

Alignment	Axial Ratio	χ'' **)	$B^2/\bar{\mu}n_g$	B (μG)	
				n_g=10 cm^{-3}	1 cm^{-3}
Classical DG	1 : 2	1	-----	-----	-----
	4 : 1	1	1000	100	30
	4 : 1	10	400	63	20
Improved DG	1 : 2	1	10	10	3
	1 : 2	10	1	3	1
	1 : 2	100	0.1	1	0.3
	4 : 1	1	100	30	10
	4 : 1	10	10	10	3
Tg = 30 K	1 : 2	10	100	30	10 *)
Pin Wheel (PW)	1 : 2	1	1.4	3.7	1.4
	4 : 1	1	6	7.8	2.5

*) For grains with m = 1.6, r_{eq} = 0.1 μm, and Td = 10 K in the gas of μ=1 at Tg = 100 K. Minimum magnetic fields for grains with χ'' = 1 are from Seki and Hasegawa (1986).

**) In units of 2.5×10^{-12} ω / Td .

I-C) DIFFUSE GALACTIC LIGHT

N91-14909

NEW MEASUREMENTS OF THE FAR ULTRAVIOLET SCATTERING PROPERTIES OF INTERSTELLAR DUST

Mark Hurwitz, Stuart Bowyer, and Christopher Martin
Space Sciences Laboratory, University of California Berkeley, CA 94720 USA

We present an analysis of spectra of the diffuse ultraviolet background taken during shuttle flight STS-61C (January 1986). Eight regions of the sky were observed for ~ 20 minutes each, using a spectrograph designed at our lab specifically to perform measurements of the UV background. The field of view was 3.8° ×8′, with imaging along the slit to confine stellar contamination. The instrument featured a shutter mechanism to measure internal background during flight, a low-scatter holographically ruled diffraction grating, photon counting microchannel plate detectors, thorough baffling, and a crystal window to further attenuate stray light. The spectra cover the range 1400 to 1850 Å and have been binned in 50Å bands for this work. We discuss our procedure for subtracting the contribution of stars too faint to be detected as discrete sources during the observations (in general this represents a small fraction of the total intensity detected except at the longest wavelengths). We describe a radiative transfer model used to interpret the data and set confidence intervals on the relevant parameters. We find that the continuum component of the diffuse ultraviolet background arises primarily from two sources. One source is scattering of starlight by interstellar dust with an albedo of about 12% and a relatively isotropic phase function. A second source consists of about 150 photons cm^{-2} sec^{-1} $ster^{-1}$ $Å^{-1}$ of extragalactic light which is attenuated by the dust in our galaxy. Although emission features possibly associated with molecular H_2 are detected in one look direction, fluorescence of H_2 is not a major contributor to the diffuse UV background, at least at galactic latitudes greater than ~10°. This research has been funded by NASA Grants NASA/NGR-05-003-805 and NGT-50185.

INTERSTELLAR DUST AS GENERATOR OF X-RAY RADIATION

S. Ibadov
Institute of Astrophysics, Dushanbe 734670 USSR

Summary. The X-ray generation due to arising of hot dense plasma balls at high-velocity (≥ 70 km s^{-1}) collisions of dust grains in the interstellar medium is considered. Analitical expressions for efficiency of conversion of colliding dust particles kinetic energy into X-ray radiation are presented. The observed intensity distribution of the diffuse component of soft cosmic X-rays (0.1-1 keV) may be partly caused by collisions between the dusty components of high-velocity clouds and of the disk of our Galaxy.

Key words: interstellar dust grains - high-velocity collisions - X-ray generation

1. Introduction

Observations of the diffuse component of cosmic soft X-rays (0.1-1 keV) have indicated that most of these X-rays are emitted from the interstellar medium of the Galaxy by a hot plasma located within 100-200 pc around the Solar system (see e.g. Tanaka and Bleeker, 1977; Apparao, Hayakawa and Hearn, 1979; Kaplan and Pikelner, 1979; Syunyaev, 1986).

There are two approaches to the problem of hot interstellar plasma origin which are connected with the galactic supernova explosions at sufficiently high rate (Cox and Smith, 1974) and the strong stellar wind around early type stars (Castor, McCray and Weaver, 1975). The search for mechanisms responsible for the observed distribution of diffuse soft cosmic X-rays is continuating (Ibadov, 1981; Hirth, Mebold and Müller, 1985).

Interstellar dust is one of the abundant, universal components of the interstellar medium, especially in the directions of the galactic plane and in the cloudy regions, the ratio of spatial densities of dusty ρ_d and gaseous ρ_g matter being $\rho_d/\rho_g \sim 0.01$ in the average (see e.g. Greenberg and Hong, 1975; Spitzer, 1981). At the same time there are observational data indicating the presence of high-velocity (70-300 km s^{-1}) objects and corresponding high-velocity dust grains in the Galaxy. For example, the relative velocities of high-velocity clouds (HVC's) and the disk of our Galaxy have such values at their possible collisions (see e.g. Giovanelli, 1980; Mirabel and Morras, 1984; Dickey and Hailes, 1985; Tenorio-Tagle et al., 1987 and references therein).

High-velocity collisions also occur in the interplanetary and circumsolar medium between cometary and zodiacal dust particles. During high relative velocity ($V \geq V_1 = 70$ km s^{-1}) impacts of dust grains high-density high-temperature plasma balls (initial density and temperature of balls are $n_{io} \approx 10^{22}$ ion cm^{-3} and $T_o \geq T_{o1} = 3\ 10^5$ K) and X-ray radiation may be generated both in the cometary atmospheres and in the interstellar medium (Ibadov, 1980; 1981).

The present report is devoted to theoretical consideration of the efficiency of conversion of colliding high-velocity dust grains kinetic energy into X-ray radiation related to the origin of the diffuse soft cosmic X-ray background.

2. X-ray generation by high-velocity collisions of grains

High-velocity collisions between dust grains of interstellar type, having radii $a \geq 10^{-6}$ cm, are passing the stage of fully thermalization of the kinetic energy of their relative motion as the calculation of the atomic particle transport length shows. During such impacts specific powers of the order of 10^{12}-10^{15} W cm^{-2} are developed and a hot expanding plasma ball with the initial radius $r_o \approx a$ is generated. The comparison of the time for balance of electron and ion temperatures τ_b (Artsimovich, 1961; Spitzer, 1965) and the characteristic time for the plasma ball radiative cooling τ_r with the characteristic ball's expansion time τ_e shows that $\tau_b < \tau_e < \tau_r$, so that the arising plasma is quasi-isothermal and its expansion is quasi-adiabatical.

Since plasma balls produced consist of heavy ions of C, N, O, Si, Mg, Fe etc. with the average atomic number $Z \approx 10$ and the mean multiplicity of charge $z \geq 3$ at $V \geq V_1$ (Ibadov, 1986), the main contribution to the luminosity of plasma balls is supplied (at $T_o \leq 3\ 10^5 Z^2$, K) by recombinational radiation (free-bound transitions) and by emission of excited ions (Artsimovich, 1961; Ginzburg, 1962; Lang, 1978).

The energy, emitted in the X-ray range by a radially expanding plasma ball, is determined as

$$E_x(fb) = 10^{-21} g_{fb} z^4 \int_o^{\tau_x} n_e n_i T^{-1/2} V_p \, dt \quad \text{for } r_o < l_\nu(fb); \quad (1)$$

$$E_x(bb) = \int_o^{\tau_x} \sigma T^4 S \, dt \quad \text{for } r_o \geq 1 \text{ (fb)}. \quad (2)$$

Here τ_x is the hot plasma ball life-time; $l_\nu(fb)$ is the mean free path of plasma photons for free-bound transitions; g_{fb} is the Gaunt factor for electron free-bound transitions; $n_e \equiv n_e(r)$ and $n_i \equiv n_i(r)$ are the number densities of plasma electrons and ions; $T = T(r)$ is the plasma ball temperature; $r \equiv r(t)$ is the radius of plasma ball: the time $t=0$ corresponds to $r=r_o$; $V_p \equiv V_p(r)$ and $S \equiv S(r) = 4\pi r^2$ are the volume and the

surface of the plasma ball; σ is the Stefan-Boltzman constant; the Eq.(1) corresponds to radiation of an optically thin plasma ball and the Eq.(2) - to optically thick plasma (black-body radiation); values are in CGS system.

The spatial-temporal variation of parameters in Eqs. (1) and (2) is determined by the following equations

$$-\frac{3}{2}(N_e+N_i)\frac{k\,dT}{dt} = \frac{(N_e m_e+N_i m_i)}{2}\frac{d}{dt}\left(\frac{dr}{dt}\right)^2, \tag{3}$$

$$(n_e+n_i)kT\frac{dV_p}{dt} = \frac{(N_e m_e+N_i m_i)}{2}\frac{d}{dt}\left(\frac{dr}{dt}\right)^2, \tag{4}$$

where N_e and N_i are the total numbers of electrons and ions in the plasma ball, k is the Boltzman constant, m_e and m_i are the mass of electron and the mean ion mass.

The equation of energy conservation (3) and the equation of motion of the plasma volume as a whole (4) are complemented by following relations

$$V_p = (4\pi/3)r^3, \quad n_e = zn_i, \quad n_i = 3N_i/(4\pi r^3); \tag{5}$$

$$T_o = \frac{Am_h V^2}{12k(1+z+2x_1/3)}; \tag{6}$$

$$z = \begin{cases} z_1(V/V_1)^{2/s_1} & \text{for } V \le V_z; \\ Z & \text{for } V \ge V_z, \end{cases} \tag{7}$$

where A is the mean mass number of atoms in colliding particles, m_h is the mass of hydrogen atom, x_1 is the mean relative energy of ionization; $z_1=3$, $1 \le s_1 \le 2$, $V_z=2\ 10^6 Z$ is the minimal relative velocity of colliding dust grains at which the charge of produced ion equals to charge Z of atomic nucleus (Ibadov, 1986).

From Eqs. (3) and (4), taking into account Eq. (5), we obtain the law of variation of the temperature and radius of the ball in the form

$$T = T_o(r_o/r)^2, \tag{8}$$

$$r^2 = r_o^2+2r_o V_{ro} t+V_a^2 t^2. \tag{9}$$

Here $V_{ro} \equiv (dr/dt)_{r=r_o} = (kT_o/2\pi m_i)^{1/2}$ is the initial radial velocity of ions in plasma ball, $V_a \equiv [V_{ro}^2+3(1+z)kT_o/m_i]^{1/2}$ is the asymptotic velocity of expansion of the ball.

Since $V_{ro} \ll V_a$, during the time $t=r_o/V_a$ the ball temperature decreases, according to Eqs. (8) and (9), up to $T=T_o/2$, so that the X-ray emission pulse from the ball has

the duration $\tau_x = r_o/V_s$.

Inserting into Eqs. (1) and (2) relations (5), (8) and (9) after integrating we have

$$E_x(fb)=2.8\ 10^{-25} g_{fb} Z^{1/2} z^5 n_{io}^2 r_o^4/(1+z)^{1/2} T_o \quad \text{for } r_o<l_\nu(fb); \quad (10)$$

$$E_x(bb)=3.5\ 10^{-8} Z^{1/2} T_o^{7/2} r_o^3/(1+z)^{1/2} \quad \text{for } r_o \geq l_\nu(fb). \quad (11)$$

The kinetic energy of relative motion of two colliding dust grains, expenditured for creating the hot plasma ball, may be presented as

$$E_{in}=(\pi/3) m_p Z n_{io} r_o^3 V^2, \quad (12)$$

where m_p is the proton mass, n_{io} is the initial plasma ions density.

Using Eqs. (10)-(12) we get the efficiency of conversion of kinetic energy of colliding dust grains into X-ray radiation $k_x=E_x/E_{in}$, namely

$$k_x = \begin{cases} 0.17 g_{fb} z^5 n_{io} r_o / [(1+z)Z]^{1/2} T_o V^2 & \text{for } r_o<l_\nu(fb); \\ 1.8\ 10^{16} T_o^{7/2} / [(1+z)Z]^{1/2} n_{io} V^2 & \text{for } r_o \geq l_\nu(fb). \end{cases} \quad (13)$$

It should be noted that the expression for $l_\nu(fb)$ may be be obtained by equating the volume and the surface luminosities - the expressions (10) and (11), at the case of equality of the plasma ball dimension r_o and the mean transport length of photons $l_\nu(fb)$.

Accepting $V=1.5\ 10^7$ cm s^{-1}, $s_1=2$, $x_1=3$, $g_{fb}=1$ and $n_{io}=3\ 10^{22}$ ion cm^{-3} (corresponds to the values of $A=2Z=20$ and of the density of dust grain $\delta=1$ g cm^{-3}) we have $z=6$, $T_o=6\ 10^5$ K, $l_\nu(fb)=3\ 10^{-6}$ cm and by the lower line of Eq. (13) we get $k_x=k_x(bb)=0.1$. This value corresponds to the blackbody emission of the optically thick plasma, produced by the interstellar dust grains ($a \simeq 10^{-6}$-10^{-5} cm), and the most probable energy of photons emitted is $h\nu_m \simeq 3kT_o \simeq 200$ eV; the value of $k_x=0.01$ was used in calculations earlier fulfilled (Ibadov, 1981), which corresponds to the Bremsstrahlung radiation mechanism (free-free transitions) of electrons in the hot optically thin deyterium plasma, produced by picosecond laser pulses (see Basov et al., 1971).

The intensity of the diffuse soft X-ray radiation due to high-velocity collisions of HVC's dust particles with dust grains of the disk of our Galaxy near the zone of interaction may be presented as

$$J_x = (1/8) k_x \rho_{dp} V^3, \quad (14)$$

where ρ_{dp} is the spatial density of dusty component transforming into hot plasma balls.

The observed value of soft X-rays intensity $J_x \simeq 10^{-8}$ erg cm^{-2} s^{-1} is reached according to Eqs.(13) and (14) at $\rho_{dp} = 3\ 10^{-28}$ g cm^{-3}. Hence, if the density of gas in the HVC is $\rho_{gc} = 10^{-25}$ g cm^{-3} and the ratio of densities of dust ρ_{dc} and gas ρ_{gc} in the cloud $\rho_{dc}/\rho_{gc} > 0.01$, the HVC with dimensions $r_c \geq 30$ pc may give appreciable contribution to the diffuse soft cosmic X-rays within distances r = 100 pc considered (see also Ibadov, 1981; Hirth, Mebold and Müller, 1985).

3. Conclusion

Interstellar dust grains high-velocity collisions (70-300 km s^{-1}) result in generation of dense hot plasma balls ($3\ 10^5$-$5\ 10^6$ K) of heavy elements (C, N, O, Si, Mg, Fe etc.), which cause relatively high efficiency of conversion of grains kinetic energy into X-ray radiation at the cost of recombination and line emission mechanisms.

High-velocity collisions between the dusty components of high-velocity clouds and of the disk of our Galaxy may be one of the alternative processes responsible for creating the observed distribution of diffuse component of soft cosmic X-rays in the energy range 0.1-1 keV.

The author is greateful to Prof. O.V. Dobrovolsky for stimulating discussions.

References

Apparao, K.M.V., Hayakawa, S. and Hearn, D.R.: 1979, Astrophys. Space Sci. 65, 419.

Artsimovich, L.A.: 1961, Controlled Fusion, Fizmathgiz, Moscow.

Basov, N.G., Zakharov, S.D., Krokhin, O.N., Kryukov, P.G., Senatsky, Yu.V., Tyurin, E.L., Fedosimov, A.I., Chekalin, S.V. and Shchelev, M.Ya.: 1971, Quantum Electronics USSR, No. 1, 4.

Castor, J., McCray, R. and Weaver, R.: 1975, Astrophys. J. Letters 200, L107.

Cox, D.P. and Smith, B.W.: 1974, Astrophys. J. Letters 189, L105.

Ginzburg, V.L.: 1962, Proc. P.N. Lebedev Phys. Inst. USSR Acad. Sci. 18, 55.

Giovanelli, R.: 1980, Astron. J. 85, 1155.

Greenberg, J.M. and Hong, S.S.: 1975, The Dusty Universe, N. Watson Academic Publ., New York.

Hirth, W., Mebold, U. and Müller, P.: 1985, Astron. Astrophys. 153, 249.

Ibadov, S.: 1980, Comet Circular USSR No. 266, 3.

Ibadov, S.: 1981, Proc. 15th Internat. Conf. on Phenomena in Ionized Gases, Minsk, USSR, v. 1, p. 265.

Ibadov, S.: 1986, Proc. 20th ESLAB Symposium on Exploration of Halley's Comet, Heidelberg, FRG: ESA SP-250, v. 1, p. 377.

Kaplan, S.A. and Pikelner, S.B.: 1979, Physics of the Interstellar Medium, Nauka, Moscow.

Kulkarni, S.R., Dickey, J.M. and Heiles, C.: 1985, Astrophys. J. 291, 716.

Lang, K.R.: 1978, Astrophysical Formulae, v. 1, Mir, Moscow.

Mirabel, F.I. and Morras, R.: 1984, Astrophys. J. 279, 86.

Spitzer, L., Jr.: 1965, Physics of Fully Ionized Gases, Mir, Moscow.

Spitzer, L., Jr.: 1981, Physical Processes in the Interstellar Medium, Mir, Moscow.

Syunyaev, R.A.(ed.): 1986, Physics of the Space, Soviet encyklopaedia, Moscow.

Tanaka, Y. and Bleeker, J.A.M.: 1977, Space Sci. Rev. 20, 815.

Tenorio-Tagle, G., Franco, J., Bodenheimer, P. and Rozyczka, M.: 1987, Astron. Astrophys. 179, 219.

THE SPECTRAL ENERGY DISTRIBUTION OF THE SCATTERED LIGHT FROM DARK CLOUDS

K. Mattila* and G.F.O. Schnur**
* Helsinki University Observatory,
Tähtitorninmäki, SF-00130 Helsinki, Finland
** Astronomisches Institut der Ruhr-Universität
Bochum, Postfach 102148, D-4630 Bochum, F.R.G.

1. Introduction. A dark cloud is exposed to the ambient radiation field of integrated starlight in the Galaxy. Scattering of starlight by the dust particles gives rise to a diffuse surface brightness of the dark nebula. The intensity and the spectrum of this diffuse radiation can be used to investigate e.g. the scattering parameters of the dust, the optical thickness of the cloud and as a probe of the ambient radiation field at the location of the cloud. An understanding of the scattering process is also a prerequisite for the isolation of broad spectral features due to fluorescence or to any other non-scattering origin of the diffuse light.

2. Observations. We have made photoelectric surface brightness observations of the high galactic latitude dark clouds L1642 ($l = 210\overset{\circ}{.}8$, $b = -36\overset{\circ}{.}7$) and L134 ($l = 4\overset{\circ}{.}0$, $b = 36\overset{\circ}{.}0$) at five intermediate bands at 3450, 3850, 4150, 4700 and 5500 Å. The ESO 1-m telescope was used for these observations with exactly simultaneous monitoring observations with the ESO 50-cm telescope to eliminate the influence of airglow variations. Because of the high galactic latitude of these clouds it is possible to find dust-free comparison areas in the neighbourhood. Especially in the case of L1642 an analysis of the IRAS surface brightness data by Laureijs, Mattila and Schnur (1987) was used for this purpose.

The spectral energy distributions (λ = 3450-5500 Å) at $\sim$10 positions in L1642 were determined. They cover a range of extinctions from $A_B \sim 0\overset{m}{.}5$ to $\sim 3^m$. The shape of the spectrum changes systematically as a function of A_B: for increasing A_B it becomes increasingly redder. For intermediate extinctions, $A_B \sim 1\text{-}1\overset{m}{.}5$, the spectrum is very similar to the spectrum of the incident integrated starlight of the Galaxy.

3. Discussion. We present model calculations for multiple scattering in a spherical cloud. These calculations show that the different spectral shapes of the observed diffuse light can be reproduced

with standard dust parameters. We discuss the possibility to use the observed spectrum also as a diagnostic tool for analysing the optical thickness of the cloud and the dust properties.

Reference

Laureijs,R.J., Mattila,K., Schnur,G.F.O.: 1987, Astron. Astrophys. 184, 269

OBSERVATIONS OF THE DIFFUSE UV RADIATION FIELD

J. Murthy,* R.C. Henry,** P.D. Feldman,** and P.D. Tennyson***
*Code 681 NASA/GSFC, Greenbelt, Maryland 20771 USA
**Dept. of Physics and Astronomy, Johns Hopkins University, Baltimore, Maryland 21218 USA
***MIT Lincoln Laboratory, 244 Wood St. Lexington, Massachusetts 02173 USA

We present spectra of the diffuse UV radiation field between 1250 - 3100 Å from eight different regions of the sky (Table 1), which were obtained with the Johns Hopkins UVX experiment. UVX flew aboard the Space Shuttle Columbia (STS-61C) in January 1986 as part of the Get-Away Special project. The experiment consisted of two 1/4 m Ebert-Fastie spectrometers, covering the spectral ranges 1250 - 1700 Å at 17 Å resolution and 1600 - 3100 Å at 27 Å resolution, respectively, with a field of view of 4° x .25°, sufficiently small to pick out regions of the sky with no stars in the line of sight.

TABLE 1
TARGET LIST

Target	Name	Scan	l	b	Notes
1	CLEAR	-	155	58	clear region at high latitude
2	DUST	-	132	40	dusty region at high latitude
3 (start)	COMA	14°	71	82	scan across Coma cluster of
3 (end)			240	84	galaxies
4	HALLEY	-			vicinity of Comet Halley
5	QUIET	-	168	-16	region of low soft X-ray emission
6 (start)	GRADIENT	17°	135	26	scan from region of low HI to
6 (end)			135	9	high HI column density
7 (start)	EXTERNAL	12°	142	47	scan across M81 and Sandage (1976)
7 (end)			142	35	dusty region
8	ERIDANUS	-	216	-39	very active region in Eridanus (Paresce *et al.* 1983)
9 (start)	SPECTRUM	12°	335	86	region observed by Feldman, Brune,
9 (end)			335	74	and Henry (1981)

We find values for the diffuse cosmic background ranging in intensity from 300 to 900 photons cm^{-2} s^{-1} sr^{-1} $Å^{-1}$ (see Table 2) with no correlation with the HI column density in the line of sight, and with a factor of two variation in targets only 11° apart in the sky, implying that either the diffuse cosmic background is not due to starlight reflected from interstellar dust, and therefore is presumably extragalactic in origin, or that, if it is due to reflected starlight, the dust-to-gas ratio varies considerably in different directions.

We also find that the cosmic background is spectrally flat from 1250 - 3100 Å, within the uncertainities of each spectrometer.

The zodiacal light begins to play a significant role in the diffuse radiation field above 2000 Å, and we have determined its brightness relative to the solar emission. Our observed brightnesses of the zodiacal light in the UV remain almost constant with ecliptic latitude, unlike the declining visible brightnesses, possibly indicating that those (smaller) grains responsible for the UV scattering have a much more uniform distribution with distance from the ecliptic plane than do those grains responsible for the visible scattering.

Finally, there is no evidence in our data for the line emission claimed by Feldman, Brune, and Henry (1981) in one of our target regions (Target 9). It should, however, be noted that the errors in our spectra are too large to formally rule out any of those lines.

TABLE 2
BEST FIT PARAMETERS

	Long Wavelength Spectrometer			Short Wavelength Spectrometer	
Target	d[1]	α[2]	b[3]	d[1]	b[3]
1.	.158	81.4 ± 1.9	700. ± 70.	0.67	500
2.	.148	78.0 ± 1.6	950. ± 70.	1.95	500
3.	.194	72.8 ± 2.0	330. ± 80.	2.17	200
5.	.362	86.3 ± 1.9	260. ± 80.	1.46	300
6.	.384	74.6 ± 3.3	420. ± 90.	1.40	700
7.	.255	65.8 ± 3.6	340. ± 100.	1.20	500
8.	.181	58.3 ± 1.6	650. ± 80.	1.07	200
9.	.274	81.3 ± 2.4	520. ± 120.	0.11	100

[1]counts per 20.48 ms bins.
[2]S10 units (6.35×10^{-12} of the solar irradiance per steradian).
[3]photons cm^{-2} s^{-1} sr^{-1} $Å^{-1}$

References

Feldman, P. D., Brune, W. H., and Henry, R. C. 1981, *Ap. J. (Letters)*, **249**, L51.
Paresce, F., Jakobsen, P., and Bowyer, S. 1983, *Astr. Ap.*, **124**, 300.
Sandage, A. 1976, *A. J.*, **81**, 954.

This work was supported by NASA grant NAG 5-619 to the Johns Hopkins University.

N91-14913

THE CAPABILITY OF THE ULTRAVIOLET IMAGING TELESCOPE FOR OBSERVING INTERSTELLAR DUST

Theodore P. Stecher
Laboratory for Astronomy and Solar Physics
NASA, Goddard Space Flight Center

The Ultraviolet Imaging Telescope was designed to be able to obtain deep images of nearby galaxies with a single frame. This ability makes it ideal for many imaging problems of the interstellar dust. The instrument has a forty arc-minute field of view with two arc-second resolution. It has 11 ultraviolet filters and a grating which is used as a grism for full field spectroscopy. In a thirty minute exposure (one orbital night) the limiting magnitude for hot objects is V = 25, or a UV mag of 22 for point sources and a UV mag of 26 for extended sources. Programs are planned for the observation of dust in reflection nebulae, HII regions, planetaries, dark nebulae, the diffuse galactic light,and dust in other galaxies are planned. The UIT has been integrated into the Astro Spacelab Payload and is scheduled to be launched on the Columbia in Nov. 1989.

DIFFUSE GALACTIC LIGHT OBSERVATIONS AT 206 SELECTED AREAS

G. N. Toller
Applied Research Corporation
8201 Corporate Drive
Landover, Maryland 20785

ABSTRACT

Space-based, observational diffuse galactic light (DGL) levels at 4400Å are presented as a function of galactic latitude (b). A peak in the ratio of DGL to direct starlight is apparent at $|b| = 5^{\circ}$ to 15°, where one third of the celestial brightness is due to scattered light. Another salient feature is the general decrease in the relative contribution of the DGL at intermediate and high galactic latitudes. The relationship DGL $(S_{10}(V)_{G2V,4400Å}) = 2.4 \cdot 10^{-20}$ N_{HI} atoms cm^{-2} may be used to estimate the brightness of DGL from neutral hydrogen column densities when $N_{HI} < 2 \cdot 10^{21}$ atoms cm^{-2}.

The results presented here have been used to characterize the interstellar dust in the general interstellar medium. A galaxy model that reproduces observed brightness levels was used to compare theoretical and observed DGL values. This determines two grain parameters - the albedo and the asymmetry of the scattering phase function (g). The results are albedo = .61 ± .07, g = .6 ± .2.

OBSERVATIONS

Photometry from the Pioneer 10 deep space probe permits direct observation of light from beyond the solar system. Accurate DGL information at blue wavelengths can be obtained from comparison of Pioneer photometry with the detailed star counts of Roach and Megill (1961), Sharov and Lipaeva (1973), or Tanabe (1973). The Roach and Megill tabulation is derived from a grid of l^I, b^I entries, obtained by interpolating data from the 206 Kapteyn Selected Areas (hereafter SAs). Subtracting discrete stars and integrated starlight from observations taken beyond the influence of zodiacal light provides the DGL brightness in Table 1. The first two columns give the SA designation followed by its galactic latitude. The third column contains the sum of DGL plus extragalactic background light (EBL), along with the standard deviation. The last column presents the ratio of DGL+EBL to total line of sight starlight (hereafter I_{LOS*}). Corrections for the EBL are generally ignored due to the faintness of the EBL and the observational uncertainties associated with its detection.

Grouping the data into 25 latitude bins, the ratio of DGL+EBL to I_{LOS*} as a function of latitude is plotted in Figure 1. A peak at $5^{o} < |b| < 15^{o}$ and a drop in the relative contribution of DGL at high latitudes are the salient features. Variations from the often used assumption of a constant, latitude-independent ratio are evident.

The observed DGL levels at $|b| > 10^{o}$ and the neutral hydrogen column density (Heiles, 1975) were compared. The well known correlation between the gas and dust spatial distributions suggests that the DGL should vary according to the extinction along the line of sight. The relationship between DGL and N_{HI} at 4407Å is

$$DGL(S_{10}(V)_{G2V}) = 2.4 \cdot 10^{-20} N_{HI} \text{ atoms cm}^{-2},$$

where $1 S_{10}(V)_{G2V} = 1.16 \cdot 10^{-9}$ erg cm^{-2} s^{-1}ster^{-1}Å^{-1}.

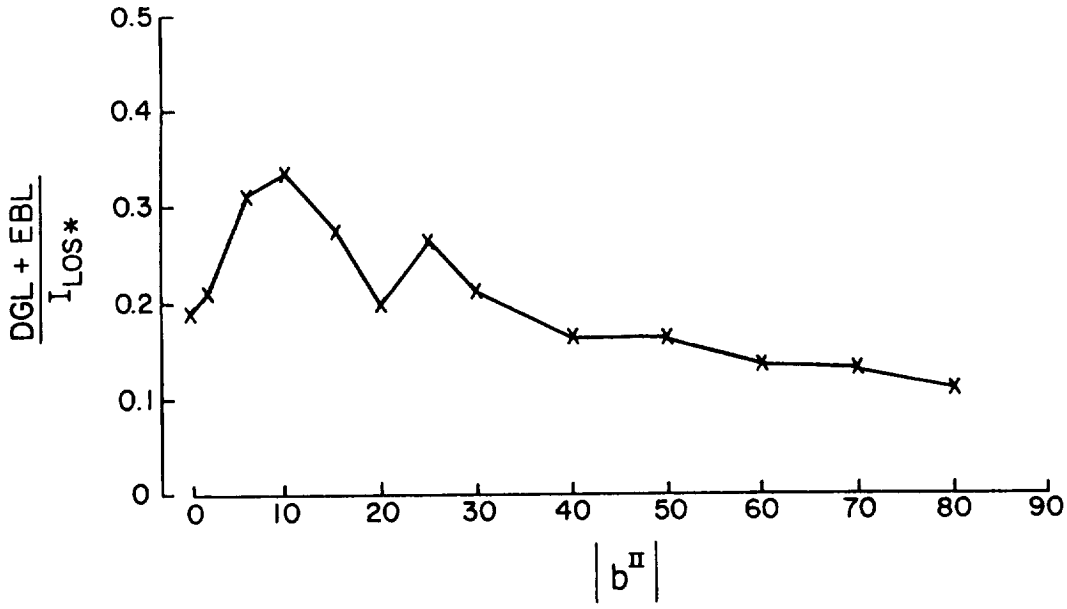

Figure 1. Latitude dependence of (DGL+EBL) divided by direct starlight.

Table 1. Diffuse Galactic Light Plus Cosmic Light at the Selected Areas

SA	b^{II}	DGL+EBL±σ	DGL+EBL I_{LOS}*
1	28.0	20 ± 7	.35
2	13.2	29 ± 7	.27
3	17.6	27 ± 9	.30
4	31.7	7 ± 7	.11
5	42.6	6 ± 7	.12
6	36.3	7.5± 7	.13
7	20.8	22 ± 8	.28
8	- 2.1	47 ± 15	.27
9	2.4	57 ± 16	.43
10	12.7	24 ± 8	.26
11	26.2	13 ± 7	.17
12	40.7	8 ± 7	.16
13	53.3	13 ± 7	.29
14	57.6	3.5± 7	.08
15	48.9	6.5± 7	.13
16	33.3	2 ± 7	.03
17	19.5	15 ± 9	.14
18	7.1	22 ± 13	.13
19	- 0.7	17 ± 20	.09
20	-17.0	12 ± 11	.10
21	-16.5	19 ± 11	.15
22	-12.9	43 ± 12	.33
23	- 7.4	47 ± 12	.38
24	- 0.2	66 ± 26	.55
25	8.0	65 ± 13	.54
26	17.4	30 ± 9	.33
27	27.9	14 ± 7	.21
28	38.7	9.5± 7	.16
30	58.9	12 ± 7	.27
31	68.1	8.5± 7	.20
32	72.8	0.5± 7	.01
33	68.4	8. ± 7	.19
34	60.3	6.5± 7	.14
35	50.1	4 ± 7	.08
36	40.0	1 ± 7	.02
37	28.9	7 ± 8	.08
38	19.3	16 ± 13	.13
39	9.4	0 ± 35	0
40	0.8	75 ± 54	.35
41	- 7.0	31 ± 18	.14
42	-12.4	41 ± 23	.29
43	-16.4	38 ± 20	.33
44	-31.9	2.5± 7	.03
45	-31.4	11 ± 7	.15
46	-27.2	27 ± 8	.41
47	-21.3	46 ± 9	.84
48	-12.4	19 ± 11	.23
49	- 2.4	5 ± 44	.03
50	8.9	42 ± 15	.27
51	20.9	26 ± 9	.29
55	73.1	12.5± 7	.32
56	79.2	6.5± 7	.20
57	85.5	3 ± 7	.10
58	73.8	4 ± 7	.10
59	60.3	6 ± 7	.13
60	48.7	3 ± 7	.06
61	35.4	1 ± 8	.01
62	23.8	7 ± 16	.06
63	10.8	37 ± 22	.19
64	- 0.2	0 ± 58	0
65	-10.7	48 ± 18	.27
66	-19.5	24 ± 11	.23
67	-26.9	24 ± 13	.34
68	-46.1	5.5± 7	.11
69	-46.6	6.5± 7	.13
70	-42.1	13.5± 8	.31
71	-34.8	19 ± 7	.36
72	-24.7	40 ± 9	.79
73	-12.5	39 ± 10	.38
74	0.2	76 ± 53	.32
75	12.9	28 ± 12	.20
79	65.6	25.5± 7	.61
80	75.0	8 ± 7	.21
81	75.7	6 ± 7	.18
82	66.3	8.5± 7	.20
83	54.6	4.5± 7	.10
84	40.9	6.5± 7	.11
85	28.0	17 ± 10	.21
86	14.6	24 ± 12	.17
87	1.7	69 ± 43	.47
88	-10.5	49 ± 18	.26
89	-21.9	21 ± 9	.21
90	-33.1	18.5± 7	.28
91	-41.7	13 ± 7	.25

SA	b^{II}	DGL+EBL±σ	DGL+EBL I_{LOS}*
92	-62.1	4.5± 7	.10
93	-58.1	6 ± 7	.13
94	-49.2	17.5± 7	.38
95	-38.1	30.5± 13	.76
96	-26.0	27 ± 8	.36
97	-12.1	64 ± 20	.67
98	0.0	37 ± 27	.14
99	13.8	27 ± 12	.18
102	50.4	24 ± 7	.54
103	59.2	9.5± 7	.21
104	62.3	0 ± 7	0
105	59.2	8.5± 7	.18
106	50.5	24 ± 7	.45
107	41.3	13.5± 7	.26
108	29.3	18 ± 7	.25
109	14.6	34 ± 12	.33
110	2.1	55 ± 51	.63
111	-10.2	70 ± 25	.55
112	-24.1	10 ± 8	.10
113	-36.8	15 ± 7	.26
114	-48.3	13.5± 7	.28
115	-57.5	7.5± 7	.17
116	-75.0	4.5± 7	.10
117	-75.7	3 ± 7	.07
118	-65.8	2.5± 7	.06
119	-54.4	3 ± 7	.06
120	-40.9	4.5± 7	.08
121	-26.9	35 ± 17	.53
122	-14.5	59 ± 26	.47
123	- 0.8	22 ± 23	.07
124	11.3	28 ± 13	.19
125	22.7	13 ± 8	.14
126	33.9	21.5± 7	.36
127	41.4	6 ± 7	.11
128	46.4	10 ± 9	.20
129	46.8	13.5± 7	.24
130	42.8	10 ± 10	.19
131	34.7	26 ± 8	.38
132	24.5	37 ± 9	.45
133	12.6	66 ± 13	.54
134	0.9	16 ± 35	.05
135	-12.6	21 ± 18	.10
136	-25.2	0 ± 9	0
137	-38.3	8.5± 11	.11
138	-51.8	1.5± 7	.03
139	-65.0	3 ± 7	.06
140	-79.8	6 ± 7	.18
141	-85.8	0 ± 7	0
142	-73.1	2.5± 7	.06
143	-60.8	4 ± 7	.09
144	-47.5	1 ± 7	.02
145	-35.2	0 ± 8	0
146	-23.0	6 ± 14	.06
147	-10.3	49 ± 42	.25
148	0.1	43 ± 39	.14
149	11.5	33 ± 14	.24
150	19.9	25 ± 9	.28
151	26.7	5 ± 7	.06
152	32.1	4.5± 7	.06
153	31.4	7.5± 12	.09
154	28.0	9 ± 8	.10
155	21.0	16 ± 10	.14
156	12.5	66 ± 18	.45
157	1.9	0 ± 50	0
158	- 8.8	171 ± 35	.61
159	-20.7	0 ± 18	0
160	-33.5	10.5± 8	.13
161	-46.8	8 ± 7	.14
162	-58.8	4.5± 7	.09
163	-71.4	3 ± 7	.07
164	-72.9	2.5± 7	.06
165	-70.1	0 ± 7	0
166	-62.3	2 ± 7	.04
167	-52.0	7 ± 8	.15
168	-41.2	0 ± 7	0
169	-30.7	0 ± 12	0
170	-20.6	3 ± 10	.02
171	-11.1	49 ± 52	.27
172	- 1.9	0 ± 54	0
173	5.3	37 ± 52	.19
174	11.4	69 ± 38	.58
175	15.5	23 ± 14	.20
176	17.3	22 ± 17	.13
177	16.2	0 ± 28	0
178	11.8	58 ± 44	.38
179	6.3	91 ± 53	.56
180	- 0.8	47 ± 55	.18
181	- 9.7	136 ± 51	.65
182	-19.7	0 ± 39	0
183	-30.5	1.5± 8	.02
184	-40.3	2.5± 7	.04
185	-51.3	5.5± 7	.10
186	-60.1	0 ± 7	0
187	-69.0	0 ± 7	0

SA	b^{II}	DGL+EBL$\pm\sigma$	DGL+EBL / I_{LOS}*
188	-57.3	15.5± 7	.32
189	-48.3	10.5± 7	.21
191	-19.5	47 ± 15	.48
192	- 6.8	70 ± 27	.24
194	2.1	0 ± 55	0
195	- 1.7	68 ± 54	.29
196	-12.0	28 ± 20	.12
197	-25.4	6 ± 17	.05
198	-40.1	9 ± 7	.10
199	-52.8	0 ± 7	0
202	-20.5	13 ± 11	.11
203	-13.1	47 ± 26	.43
204	-17.2	0 ± 52	0
205	-31.7	17 ± 8	.24
206	-27.9	33 ± 10	.54

THEORY

Comparison between the observed DGL and theoretical levels computed from a reasonable galactic radiative transfer model determines two grain parameters - the albedo and the asymmetry of the scattering phase function (g). Details of this procedure can be found in Toller (1981). The results are albedo = .61 ± .07, g = .6 ± .2. The values derived for the albedo and g apply to particles in the general (intercloud) interstellar medium. Parameters for grains in dense clouds, the interplanetary medium, or circumstellar shells could differ if the chemical composition, size distribution, or shape of the grains depend on their environment. This work will be extended to 6400Å to provide further indications of dust composition.

References

Heiles, C.: 1975, Astron. Astrophys. Suppl. 20, 37.

Roach, F.E. and Megill, L.R.: 1961, Astrophys. J. 133, 228.

Sharov, A.S. and Lipaeva, N.A.: 1973, Soviet Astron. 17, 69.

Tanabe, H: 1973, World Data Center C2 (Airglow), Tokyo, Astron. Obs., Mitaka, Japan, 48.

Toller, G.N.: 1981, Ph.D. Dissertation, SUNY at Stony Brook.

I-D) DIFFUSE INTERSTELLAR BANDS

MATRIX-ISOLATED IONS OF CARBON MOLECULES.

W. Krätschmer
Max Planck Institut für Kernphysik
P.O. Box 103980, 6900 Heidelberg, W.-Germany.

Mixtures of different large carbon molecules were produced in a matrix-isolated state by thermal annealing of matrices initially containing the smaller molecules of carbon vapour. We applied argon ice as matrix material and heated graphite rods resistively to obtain the carbon vapour. Upon annealing, the larger carbon molecules form from the smaller by diffusion and mutual chemical reactions. Amongst the large molecules there are some species which show absorption features similar to those of the diffuse interstellar bands (DIBs). In order to identify these potential DIB carries, we excited the matrix-isolated molecules by the discrete line-spectrum of a Kr laser. Since the amount of molecules was too small to detect a regular Raman effect, we looked for resonance Raman signals. The only strong resonance we found was excited by the 520.8 nm Kr line. In this case a simple progression of Raman lines was detected, of which the first member was located at about 1785 cm-1 displacement. The only molecule with such a ground state vibrational transition energy and an absorption at around 520 nm is the C_2^- ion. Spectral evidence shows that in the matrix-isolated carbon-molecule-mixture the 520 nm line (which is intensity correlated with other molecular features, e.g. at 470 and 247 nm) increases in intensity during the initial phases of thermal annealing. This implies that the C_2^- ions are produced within the matrix, probably by chemical reactions between the initially abundant smaller species. This is surprising, since until now C_2^- ions have been reported to form under input of external energy alone (e.g. by UV-photolysis of acetylene). To preserve overall charge balance in the matrix, a fraction of the larger carbon molecules produced in the chemical reactions may thus become positively charged. Ionized species may be the key to understand the IR and UV-VIS spectra of the large carbon molecules in our matrices.

N91-14915

SIMULTANEOUS INFRARED AND UV-VISIBLE ABSORPTION SPECTRA OF MATRIX-ISOLATED CARBON VAPOR

Joe Kurtz and Donald R. Huffman
Department of Physics, University of Arizona
Tucson, Arizona 85721 USA

Carbon molecules have been suggested as possible carriers of the diffuse interstellar bands. In particular, it has been proposed that the 443 nm diffuse interstellar band is due to the same molecule which gives rise to the 447 nm absorption feature in argon matrix-isolated carbon vapor. If so, then an associated C-C stretching mode should be seen in the IR. By doing spectroscopy in both the IR and UV-visible regions on the same sample, the present work provides evidence for correlating UV-visible absorption features with those found in the IR. Early data indicates no correlation between the strongest IR feature (1997 cm^{-1}) and the 447 nm band. Correlation with weaker IR features is being investigated.

INTRODUCTION

The absorption spectrum of carbon vapor trapped in a solid inert gas matrix was first reported more than 25 years ago (Weltner and Walsh, 1962, Barger and Broida, 1962). Since that time, much has become known about the molecules C_2 and C_3, but, due to the many molecular species present in matrix-isolated carbon vapor, uncertainty remains concerning the assignment of the spectral features that seem to dominate both the UV-visible spectrum of the vapor (Krätschmer, Sorg, and Huffman, 1985) and the infrared spectrum (Thompson, DeKock and Weltner, 1971).

Carbon molecules have been suggested as possible carriers of the diffuse interstellar bands (Douglas, 1977). In particular, Krätschmer (1986) has proposed that the 443 nm diffuse interstellar band is due to the same molecule which gives rise to the 447 nm absorption feature seen in argon-isolated carbon vapor. He has further suggested that the molecule responsible is linear C_7. Theoretical studies of small carbon molecule ground state structures (e.g. Raghavachari and Binkley, 1987) predict IR (vibrational) transitions and can be used as a basis for tentative assignments in this region of the spectrum. Unfortunately, assignment of spectral features in the UV-visible region to a particular carbon molecule based on calculations is even more tenuous. If the 447 nm feature is in fact due to a linear carbon chain such as C_7, then an associated C-C stretching mode absorption feature should be seen in the infrared. Krätschmer's group has studied both spectral regions intensely but in separate experiments. They cannot, therefore, definitely suggest which IR features are due to this same molecule (and which are not). The purpose of this research is to correlate IR absorption features of matrix-isolated carbon vapor to those in the UV-visible by doing spectroscopy in both regions on the same sample. This research should establish correlations between the IR and UV-visible spectra, thus, for the first time, providing direct evidence for the assignment of certain UV-visible features of the long-studied carbon vapor spectrum.

EXPERIMENT

The apparatus consists of a cryostat with a cold finger extending into a vacuum chamber at the intersection of the two monochromator beams. The cryostat is mounted on the sample chamber so as to allow rotation of the cold finger to face either beam. Directly attached to the chamber are the carbon source and the vacuum UV-visible monochromator (see figure 1).

The UV-visible light source is a 75-watt high-pressure Xenon arc lamp which is mounted in a water-cooled chamber under nitrogen purge. The light is focused onto the entrance slits of the Seya-Namioka monochromator with a CaF_2 lens and passes into the monochromator vacuum chamber through a CaF_2 window. The light is dispersed with a 600 line/mm grating then passes through the exit slits directly into the sample chamber and through the sample. It is detected by a phototube whose signal is measured by a picoammeter.

The carbon source consists of an evaporation chamber in which two carbon rods are incandescently heated by passage of a large alternating current (typically 80-120 amps). The flat end of one rod is held against the tapered tip of a smaller rod by a spring under compression in its (water-cooled) mount. The evaporation chamber also has a NaCl window mounted behind the rods (away from the sample) which can be protected somewhat by a shield rotated into position during carbon deposition.

The carbon rods double as an IR light source. For this purpose the window shield is rotated out of the IR beam line and a focusing mirror is placed outside the evaporation chamber. This mirror focuses the IR beam through the sample and sample chamber window, onto the entrance slits of the IR monochromator. This monochromator was taken from a Beckman IR7 Spectrophotometer and has been fitted with a high frequency (~1KHz) light chopper and a liquid N_2 cooled HgCdTe detector. The detector output is amplified and input to a lock-in amplifier. Both the IR and UV-visible systems are operated in single beam mode.

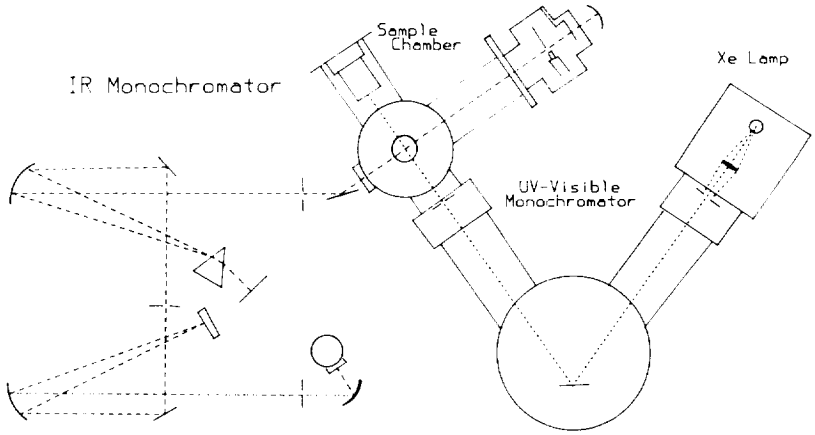

Figure 1 – Optical diagram of both monochromators.

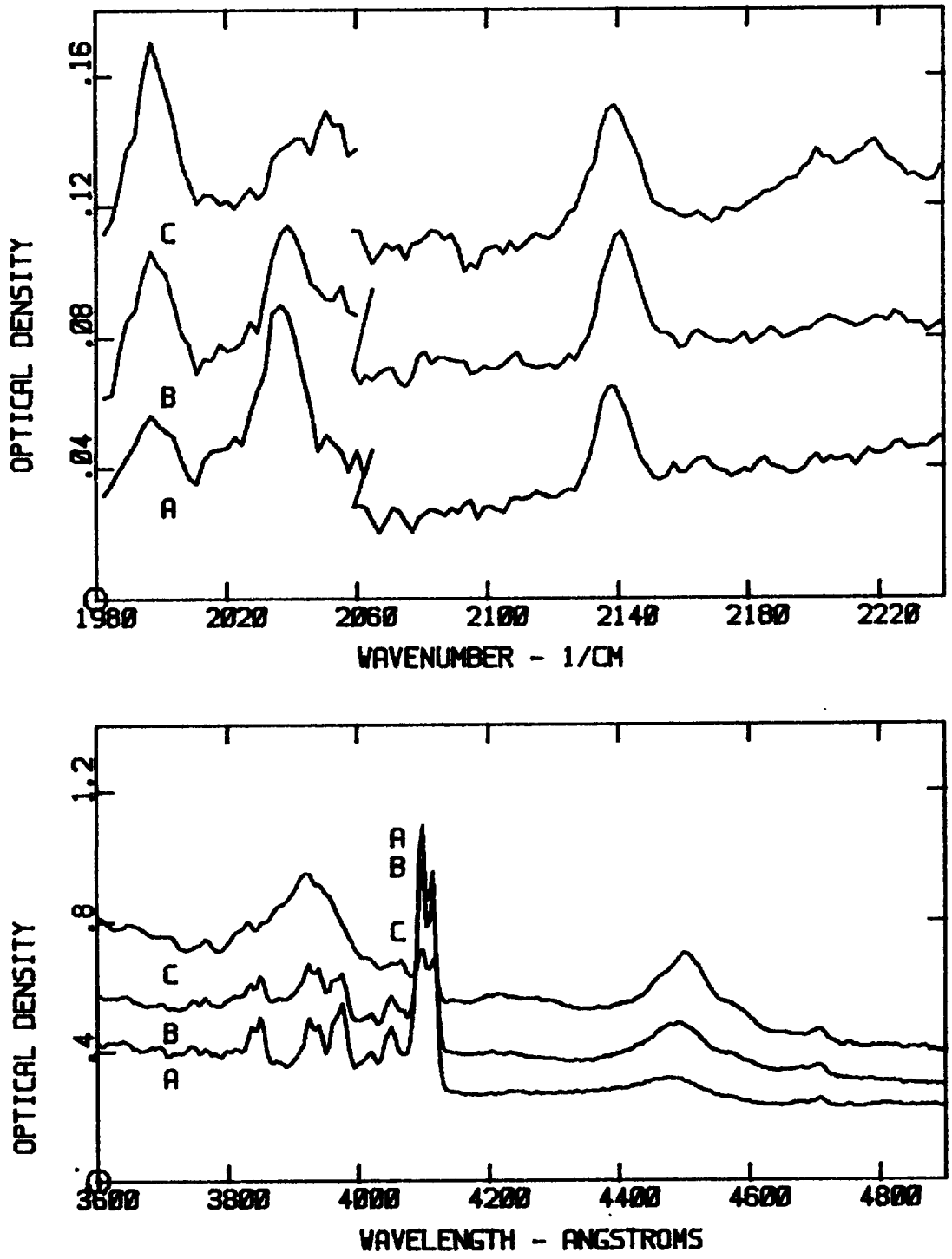

FIGURE 2 - UV-Visible (bottom) and IR (top) spectra.

The cryostat is of the continuous flow type (Oxford Instruments CF-100) wherein temperature control is accomplished by controlling the flow of helium through the cryostat as well as using a resistance heater mounted on the cryostat just above the cold finger. The temperature is measured with a carbon resistor in thermal contact with the cryostat also just above the cold finger.

Samples were prepared by successive depostions of carbon vapor, co-condensing with argon onto a low temperature (~10 K) sapphire substrate on the cryostat cold finger. Subsequent to each deposition, the sample was scanned from 1900 to 6000 Å in the UV-visible and from ~1600 to 2400 cm^{-1} in the IR. After sufficient carbon was deposited, the sample was subjected to a series of increasingly warmer thermal annealings to promote the formation of larger molecular clusters of carbon. After each annealing, the absorption features were again scanned with the sample at 9-10 K.

Data acquisition was accomplished with a 12-bit A-to-D board and an IBM PC. The computer also controls the scanning motors of both monochromators as well as the phototube voltage and a programmable gain op-amp IC which is in-line to the A-to-D input. Software generated by one of the authors (JK) was used to run the monochromators, acquire data and generate the spectral output.

EARLY DATA AND RESULTS

Figure 2 shows portions of spectra from the same experimental run. Curves labeled A, B and C are spectra of the sample after deposition, after two annealing periods and after four annealing periods, respectively. Each annealing period was for about ten minutes. The first was at 20 K with the temperature incremented by about 5 K for each subsequent annealing. Spectra were taken after each annealing, but only two are shown for clarity.

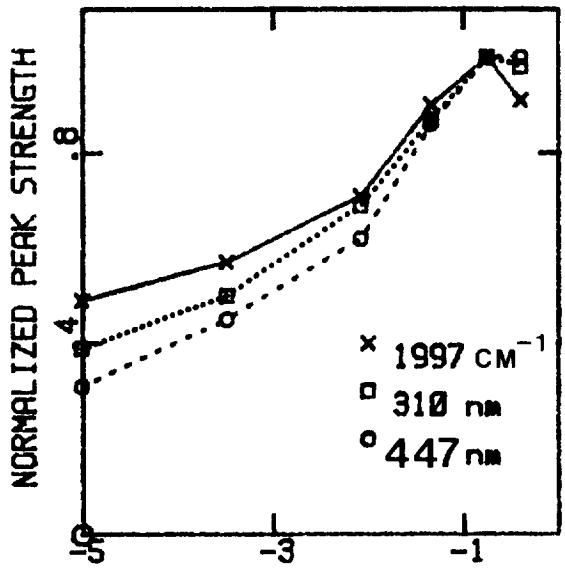

FIGURE 3

Excellent agreement has been observed among the many features found in the UV-visible with the same spectral features found by Krätschmer's group. As annealing proceeds, the known C_3 band at about 410 nm (Figure 2, bottom graph) decreases as the 447 nm band and other bands increase, suggesting that these bands are due to larger clusters of carbon atoms. The infrared spectrum shown in figure 2 (top) also shows a known C_3 feature at about 2039 cm^{-1} which can be seen decreasing as the strong 1997 cm^{-1} feature increases. At 2139 cm^{-1} a large CO feature is present with an unresolved feature at 2128 cm^{-1}. Features growing at 2054, 2200 and 2220 are also shown. Many more IR features are present, but not shown here.

By following the evolution of absorption features in the two regions, correlations can be found. Uncertainties limit the conclusiveness of the possible correlations, particularly because of the low absorption above baseline of the infrared features and the limited IR resolution. With perhaps more certainty, some correlations can be ruled out. Figure 3 shows normalized peak strength above baseline versus an annealing parameter (time and temperature dependent) for two UV-visible features (at 310 nm and 447 nm) and the strongest infrared feature (1997 cm^{-1}).

The 1997 cm^{-1} feature is adequately above the noise even at deposition to conclude that it does not correlate well to the 447 nm feature which is poorly developed at deposition. The 310 nm band seems to be better correlated to this IR feature, although it too is relatively weak in the early stages of annealing. Weaker IR features are being explored, but with the data so far collected, they cannot yet be established as companions of the 447 nm feature.

REFERENCES

Barger, R.L. and Broida, H.P.: 1962, *J. Chem. Phys.* **37**, 1152.

Douglas, A.E.: 1977, *Nature* **269**, 130.

Krätschmer, W.: 1986, *Astrophysics and Space Sciences* **128**, 93.

Krätschmer, W., Sorg, N., and Huffman, D.H.: 1985, *Surface Sci.* **156**, 814.

Raghavachari, K. and Binkley, J.S.: 1987, *J. Chem. Phys.* **87**, 2191

Thompson, K.R., DeKock, R.L., and Weltner, W.: 1971, *J. Am. Chem. Soc.* **93**, 4688.

Weltner, W. and Walsh, P.N.: 1962, *J. Chem. Phys.* **37**, 1153.

N91-14916

CORRELATION PROPERTIES OF INTERSTELLAR DUST: DIFFUSE INTERSTELLAR BANDS

W B Somerville,
Department of Physics and Astronomy, University College, Gower Street, London WC1E 6BT, England

Results are presented here from a research programme in which we attempt to establish the physical nature of the interstellar grains, and the carriers of the diffuse interstellar bands, by comparing relations between different observed properties; the properties used include the extinction in the optical and ultraviolet (including λ2200 and the far-UV rise), cloud density, atomic depletions, and strengths of the diffuse bands. We use our own observations and also data from the literature, selecting particularly sight-lines where some observed property has been found to have anomalous behaviour.

In the case of the diffuse bands, it has been found that the standard catalogue prepared by Snow, York and Welty (1977) contains fundamental compilation errors (Somerville, 1988a). These have been corrected and a revised and updated catalogue compiled. The new dataset for λ4430 is in Figure 1. Values from different observers have been scaled onto a common basis, using a consistent procedure; for stars with several observations a mean value has been used in the diagram. The absolute observational error is obtained by comparing different observations for the same star. It is seen that, while the correlation with E(B-V) is good, the scatter in the distribution is distinctly wider than the spread that would correspond to observational error; further, there are roughly equal numbers of points anomalously strong and anomalously weak relative to the centre of the distribution.

These results indicate that the strength of λ4430 is much more closely related to E(B-V) than it is to the distribution of any known molecule. The similar numbers of sight-lines with strong and weak absorption means that

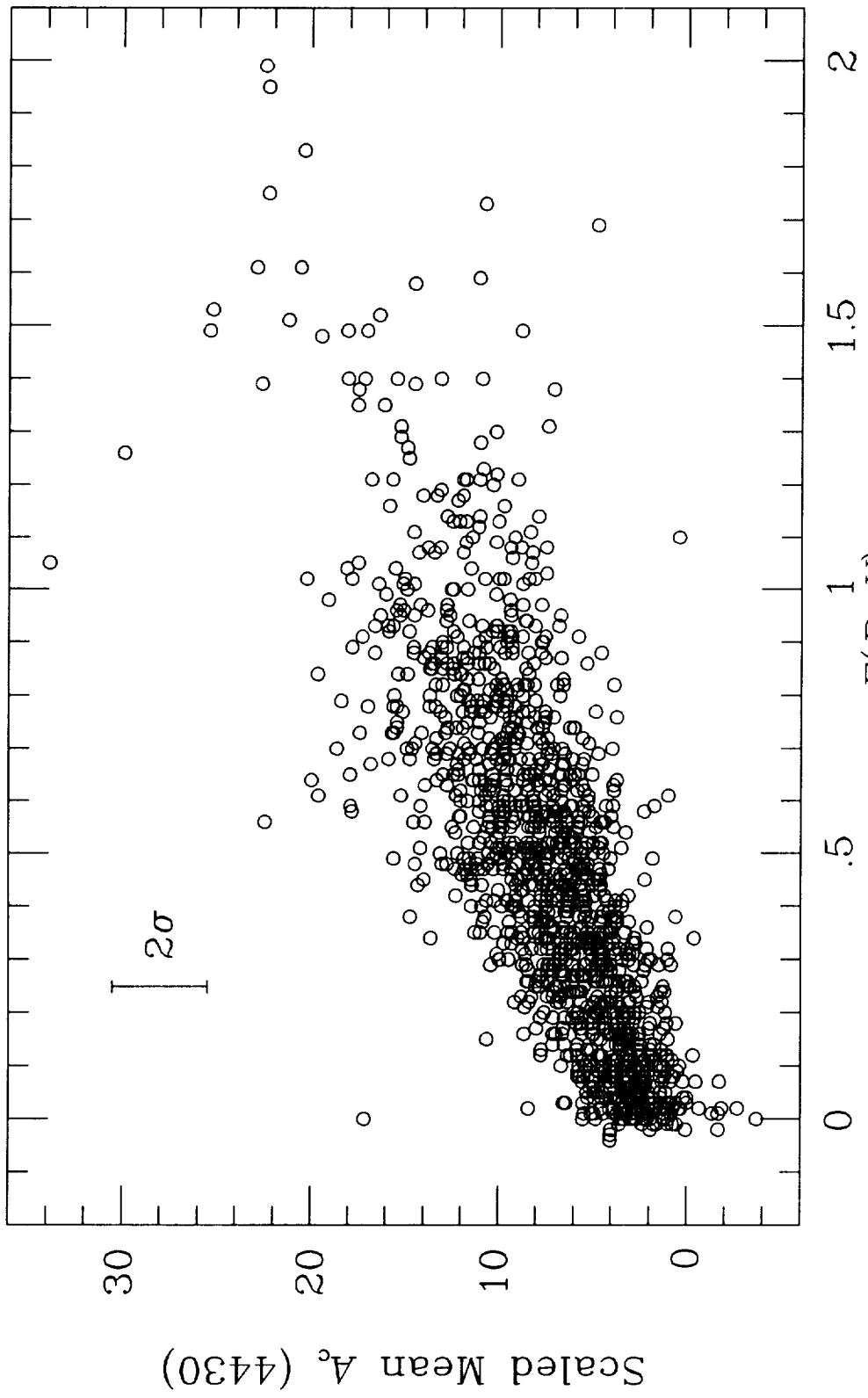

Figure 1. The new λ4430 dataset

the strength is not simply a function of interstellar cloud density - if, for example, the absorption were always weak in regions of low density it cannot be that it is always strong in regions of high density for these are much more widespread. It seems rather that anomalously weak and anomalously strong absorption both occur in particular local regions.

The diffuse bands λ4430 and λ5780 have been examined in relation to atomic depletions and cloud density. It is found that, contrary to previous claims, the strengths of the diffuse bands are independent of these quantities (Somerville, 1988b). Previous analyses (Millar and Duley, 1979; Federman et al., 1984) are in error through the neglect of non-zero intercepts in correlations with E(B-V). It is seen in Figure 2 that the measure P of λ4430 strength per grain used by Millar and Duley is systematically high for low E(B-V), compared with other measures, giving the false appearance of a dependence. This is in consequence of dividing the λ4430 strength - which, as seen in Figure 1, is non-zero at E(B-V)=0 - by a quantity which goes to zero with E(B-V), in this case the total hydrogen column density. The non-zero value at E(B-V)=0 is non-physical; it comes through including weak stellar lines in the profile when it is observed at low spectral resolution (Blades and Somerville, 1977, 1981). Similar considerations show that the systematic trend found by Federman et al. (1984) for λ5780 is unlikely to be real.

This result that the strength of a diffuse band absorption per grain is unrelated to the interstellar cloud density is consistent with what is found from the λ4430 catalogue (Figure 1); it provides strong evidence that these absorptions are not produced either by gas-phase molecules or by surface processes on grains.

In an extended observational programme, we have surveyed nine diffuse bands in the yellow-red region, in 123 stars, from the Lick Observatory (McNally et al., 1987 and in preparation). Detailed error analysis by Rees (1988) leads to the conclusion that for two features, λ5780 and λ6283, there is a real physical scatter relative to E(B-V). For the seven other features, there is no unambiguous evidence for any scatter beyond what can be attributed to observational error.

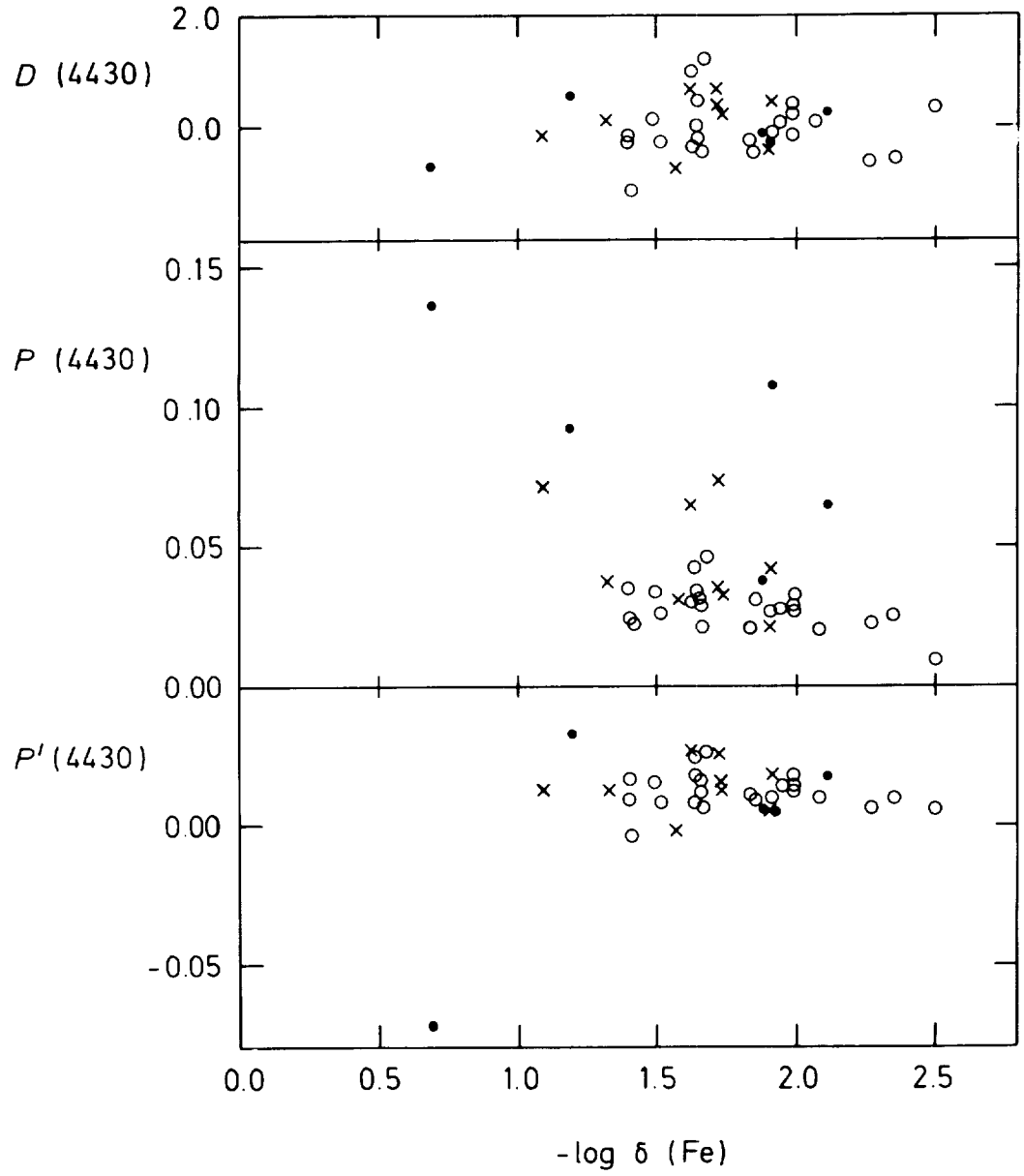

Figure 2. The relation of three measures of '4430 strength per dust grain' to iron depletion. Solid points: E(B-V)<0.1, crosses: 0.1<E(B-V)<0.2, open circles: 0.2<E(B-V). The quantity P(4430), used by Millar and Duley (1979), shows a false dependence not seen for the two other quantities (Somerville, 1988b).

Taking all these results together, they indicate that the carriers of the bands must be very closely related to the grains that produce optical extinction, and absorb by some mechanism independent of the cloud density. This favours a mechanism involving internal processes in grains, or some bulk property of the grains, that operates independently of the gaseous environment.

References

Blades, J.C. and Somerville, W.B.: 1977, Mon. Not. R. Astr. Soc. 181, 769.

Blades, J.C. and Somerville, W.B.: 1981, Mon. Not. R. Astr. Soc. 197, 543.

Federman, S.R., Kumar, C.K. and Vanden Bout, P.A.: 1984, Astrophys. J. 282, 485.

McNally, D., Ashfield, M., Baines, D.W.T., Fossey, S., Rees, P.C.T., Somerville, W.B. and Whittet, D.C.B.: 1987, IAU Symposium 120: Astrochemistry, ed. M.S. Vardya and S.P. Tarafdar (Dordrecht: Reidel), 321.

Millar, T.J. and Duley, W.W.: 1979, Mon. Not. R. Astr. Soc. 187, 379.

Rees, P.C.T.: 1988, Ph.D. thesis, University of London.

Snow, T.P., York, D.G. and Welty, D.E.: 1977, Astr. J. 82, 113.

Somerville, W.B.: 1988a, Astr. J., submitted.

Somerville, W.B.: 1988b, Mon. Not. R. Astr. Soc., in press.

SECTION II: THE OVERIDENTIFIED INFRARED EMISSION FEATURES

II-A) OBSERVATIONS OF THE IR EMISSION FEATURES

HIGH RESOLUTION SPECTROSCOPY OF THE 11.3um EMISSION BAND

J.M. Achtermann, J.H. Lacy, and D.E. Bruce
Dept. of Astronomy, Univ. of Texas, Austin

High resolution spectra of the 11.3um emission band in M82 and NGC 7027 have been obtained using the Univ. of Texas IR echelle spectrometer on the IRTF in April 1988. The spectral resolution was 0.004 um, with coverage from 11.0um to 11.6um. Spectra were measured at ten positions along a 10" long slit.

Analysis of the data is still in progress, but initial results show no clear evidence of narrow structure within the feature. The analysis will involve comparison of the observed spectra to laboratory and predicted spectra of PAH's and QCC's to determine which may be responsible for the emission. The spectra will be examined with a goal of determining whether the emission is caused by molecular or solid state material.

The data will also be examined for evidence of variations in the shape and strength of the 11.3um feature with position on the sky. In NGC 7027 the 10" long slit went across the edge of the ionized nebulae, allowing comparison of emission from both ionized and neutral regions.

INFRARED IMAGES OF REFLECTION NEBULAE AND ORION'S BAR : FLUORESCENT MOLECULAR HYDROGEN AND THE 3.3 μm FEATURE

M.G. Burton*, A. Moorhouse**, P.W.J.L. Brand**,
P.F. Roche*** and T.R. Geballe****

* NASA Ames Research Center, Moffett Field, California 94035, USA.
** Department of Astronomy, University of Edinburgh, Blackford Hill, Edinburgh, EH9 3HJ, Scotland.
*** Royal Observatory Edinburgh, Blackford Hill, Edinburgh, EH9 3HJ, Scotland.
**** Joint Astronomy Center, 665 Komohana Street, Hilo 96720, USA.

Abstract

Images have been obtained of the (fluorescent) molecular hydrogen 1–0 S(1) line, and of the 3.3 μm emission feature, in Orion's Bar and three reflection nebulae. The emission from these species appears to comes from the same spatial locations in all sources observed. This suggests that the 3.3 μm feature is excited by the same energetic UV–photons which cause the molecular hydrogen to fluoresce.

Observations

We have obtained infrared images of emission from molecular hydrogen and the 3.3 μm feature in the ionisation front Orion's Bar, and in portions of three reflection nebulae, NGC 1333 SVS 3, NGC 2023 and Pars 18. In all these sources ultra–violet radiation is beleived to be responsible for the excitation of the molecular hydrogen. The data was obtained at the UKIRT in January of 1988 using the infrared camera IRCAM with 0.6" pixel scale. Narrow band (1%) filters were used to image the 3.3 μm emission feature, the molecular hydrogen v=1–0 S(1) line (2.12 μm), and the atomic hydrogen Brackett γ line (2.16 μm). The images shown here were constructed by mosaicing together several overlapping frames (note that East is to the right in the figures). Typical integration times were 5 minutes a frame. Images were also obtained through narow band filters at 2.1 μm and 3.1 μm to assess the

contribution of continuum radiation to the emission. Apart from emission from stars, there was essentially no continuum detected at any of the positions observed.

Contour maps of the H_2 line emission from the two reflection nebulae NGC 1333 SVS 3 and NGC 2023, overlapped on those of the 3.3 μm emission feature, are shown in Figures 1 & 3 (the image for Pars 18 is not shown). In all three nebulae there is a tight correlation between the location of the 3.3 μm feature emission and the fluoresced molecular hydrogen emission. Although the relative proportions of S(1) and 3.3 μm emission vary between the sources, this correlation suggests they arise from the same spatial locations in each source. Brackett γ recombination line emission from ionised gas was not detected in these sources.

In Orion's Bar the 3.3 μm emission feature is clearly defined by a sharp, linear, ridge (Fig. 2). The ridge is parallel to the ionisation front seen in optical recombination lines (Munch & Taylor 1974), but lies behind it. The emission reaches a maximum within 5" of the ionisation front, and then falls off approximately exponentially. The feature is still detected 30" away. There are two components to the H_2 line emission beyond the ionisation front, with the strongest emission located in a layer about 15" away from it. There is 3.3 μm emission in front of and behind this layer.

The Reflection Nebulae

In the reflection nebulae observed, the H_2 and 3.3 μm emission arises in photo-dissociation fronts. Beyond the front there are insufficient UV photons with enough energy to photo-dissociate the molecules. The structure of such fronts has been modelled by several authors (*e.g.* Tielens & Hollenbach 1985, Black & Van Dishoeck 1987). The UV flux can heat, through the photo-electric mechanism, a column of gas near the cloud surface to high temperatures ($\sim$ 100 to 1000 K). UV-pumping can excite the molecular hydrogen, leading to an appreciable amount of vibrationally excited H_2 in the gas. Cooling occurs primarily by the OI 63 μm and CII 158 μm lines. The near-infrared spectrum of NGC 2023 is dominated by emission from high-vibrational states of molecular hydrogen (Gatley *et al.* 1987), demonstrating that the emission is fluorescently excited.

In all of the reflection nebulae observed the 3.3 μm emission arises in almost exactly the same regions as the (fluorescent) H_2 emission. The correlation is particularly tight in NGC 2023. These emission regions form shell-like structures around the exciting stars of the nebulae, with the fluoresced H_2 located at an optical depth

$A_v \sim 1$ from the stars. The relative intensity of the H_2 and 3.3 μm emission does vary between sources, and in the northern portion of NGC 1333 SVS 3, H_2 line emission was not detected. This may just be a sensitivity effect, the S(1) line flux falling below the detection limit. In addition, the extinction to the S(1) line, at 2.1 μm is greater than to the 3.3 μm feature; the variation may result from variable extinction.

The 3.3 μm emitting gas must therefore also lie in the photo-dissociation region with the excited H_2. This strongly suggests that the same UV–photons which excite the molecular hydrogen (with $\lambda = 912 - 1100$Å) can also excite the 3.3 μm emission feature. This is in fact slightly surprising for it is likely that UV photons with wavelengths greater than 1100Å can also excite the 3.3 μm feature, whereas they cannot induce H_2 to fluoresce. This may account for the more extended 3.3 μm emission region in NGC 1333 SVS 3 than the H_2, with lower energy photons penetrating further into the surrounding molecular cloud. However in NGC 2023 and Pars 18 the emission regions appear coincident. If the optical depth is rising rapidly behind the emission shell, then all energetic photons will be effectively stopped and neither H_2 nor 3.3 μm feature will be excited beyond it.

Alternatively the 3.3 μm emitting material may be preferentially formed in the hot, dense photo-dissociation regions. If this were the case, though, we might expect to observe the feature away from the photo-dissociation front if UV photons were not responsible for its excitation. This has not been observed in the reflection nebulae. The absence of Br γ line emission in any of the sources indicates that the excitation of the 3.3 μm emission feature is not related to presence of ionised gas.

Orion's Bar

Orion's Bar appears is a classical example of an edge-on ionisation front. The edge is well defined by the 3.3 μm image of the Bar (Fig. 2), lying just behind the ionisation front. It shows clearly that the 3.3 μm emission feature arises from the neutral region behind the front, as other evidence indicates (*e.g.* Sellgren 1981, Aitken *et al.* 1979). The approximately exponential fall-off of the emission strength with distance from the front is consistent with what would be expected if UV radiation were responsible for the feature's excitation, with the optical depth of the emitting region increasing linearly with distance into the cloud from the source of UV photons.

The H_2 v=1–0 S(1) line emission is more complicated, possibly containing two components. There is in fact diffuse H_2 line emission from all over the mapped

region. The emission may arise from both shocked and fluorescent line emitting regions in the gas (Hayashi *et al.* 1985). The H_2 line emission nearer the front, around the 3.3 μm emission ridge, is probably excited by UV-fluorescence, as in the reflection nebulae. The emission is weaker, relative to the 3.3 μm emission, than the H_2 line emission from the reflection nebulae. This could result from an underabundance of H_2 molecules, which may occur if the grains become so hot that reformation of dissociated hydrogen molecules is inefficient. The carriers of the 3.3 μm feature are then presumably not dissociated to a comparable extent as the hydrogen molecules.

The strongest H_2 line emission observed originates 15" behind the front, in a layer assigned as shocked emission by Hayashi *et al.* There is 3.3 μm emission behind and in front of this layer. If this is indeed a shocked layer, it would indicate that that the shock does not significantly affect the material responsible for the feature emission.

We feel it more likely, however, that the H_2 line emission from this layer arises in a dense photo-dissociation region rather than behind a shock. It is hard to drive a shock wave by an expanding HII region into molecular gas sufficiently fast to excite the molecular hydrogen. The shock front would also be expected to lie adjacent to the ionisation front, rather than be offset 15" from it. If the molecular gas is sufficiently dense ($\geq 10^5 - 10^6$ cm^{-3}), collisions can thermalise the fluoresced molecules before they can radiate. The emission spectrum from such a region can therefore appear similar to that from hot, shocked gas, although UV-fluorescence is responsible for its excitation.

References

Aitken, D.K., Roche, P.F., Spenser, P.M. & Jones B., 1979. *Astron. Astrophys.*, **76**, 60.

Black, J. & Van Dishoeck, E., 1987. *Astrophys. J.*, **322**, 412.

Gatley, I., Hasegawa, T., Suzuki, H., Garden, R., Brand, P., Lightfoot, J., Glencross, W., Okuda, H. & Nagata, T., 1987. *Astrophys. J. (Lett)*, **318**, L73.

Hayashi, M., Hasegawa, T. Gatley, I., Garden, R. & Kaifu N., 1985 *Mon. Not. R. astr. Soc.*, **215**, 31p.

Munch, G. & Taylor, K., 1974. *Astrophys. J. (Lett)*, **192**, L93.

Sellgren, K., 1981. *Astrophys. J.*, **245**, 138.

Tielens, A.G.G.M. & Hollenbach, D.J., 1985. *Astrophys. J.*, **291**, 722.

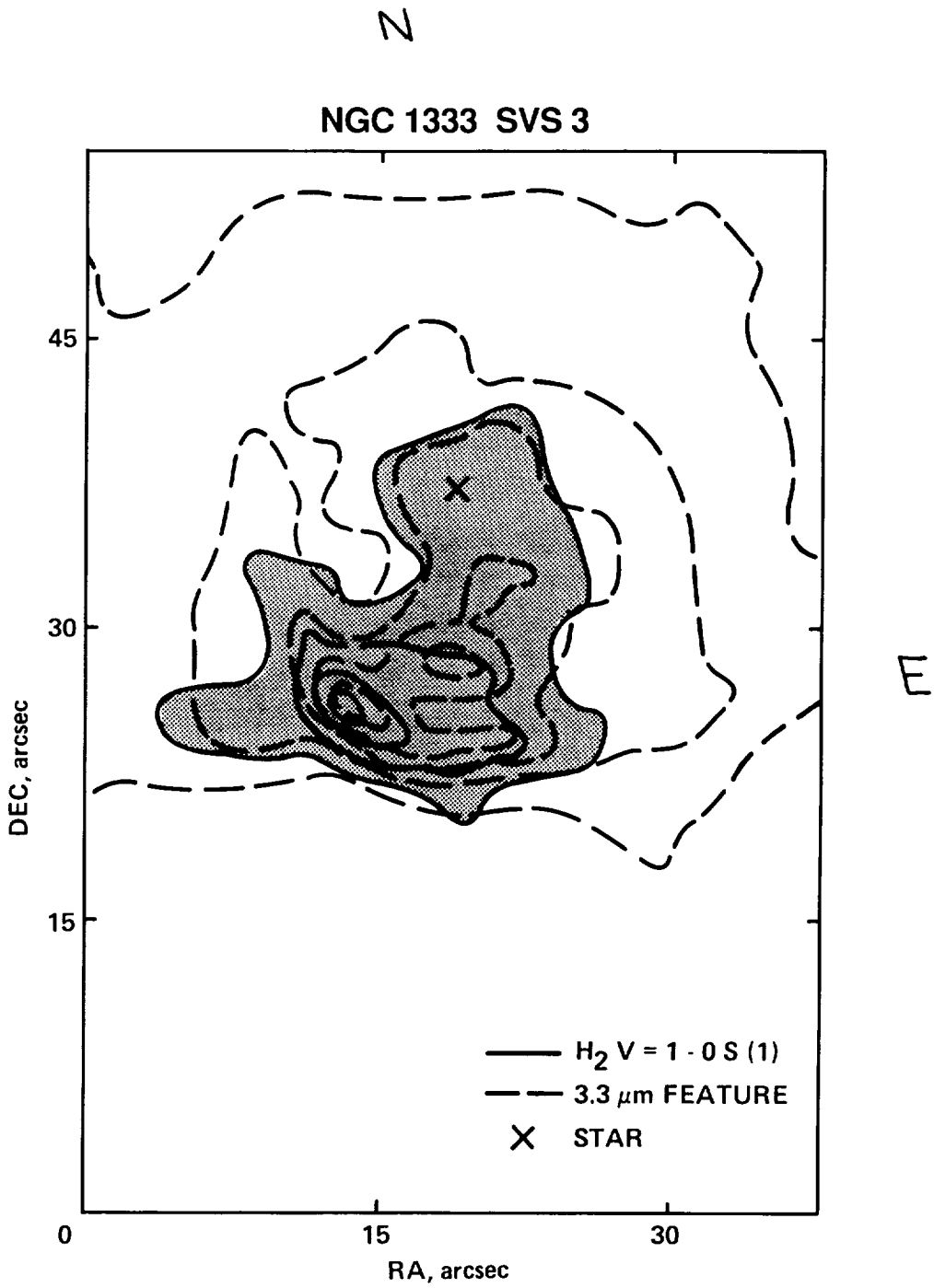

Figure 1. Contour maps of the molecular hydrogen v=1-0 S(1) line (2.12μm) (continuous line, shaded region) and the 3.3μm emission feature (dashed line) in the refelction nebula NGC 1333 SVS 3. The location of the exciting star is marked by the X. The image scale is 0.6" and the map consists of two overlapping frames.

Figure 2.

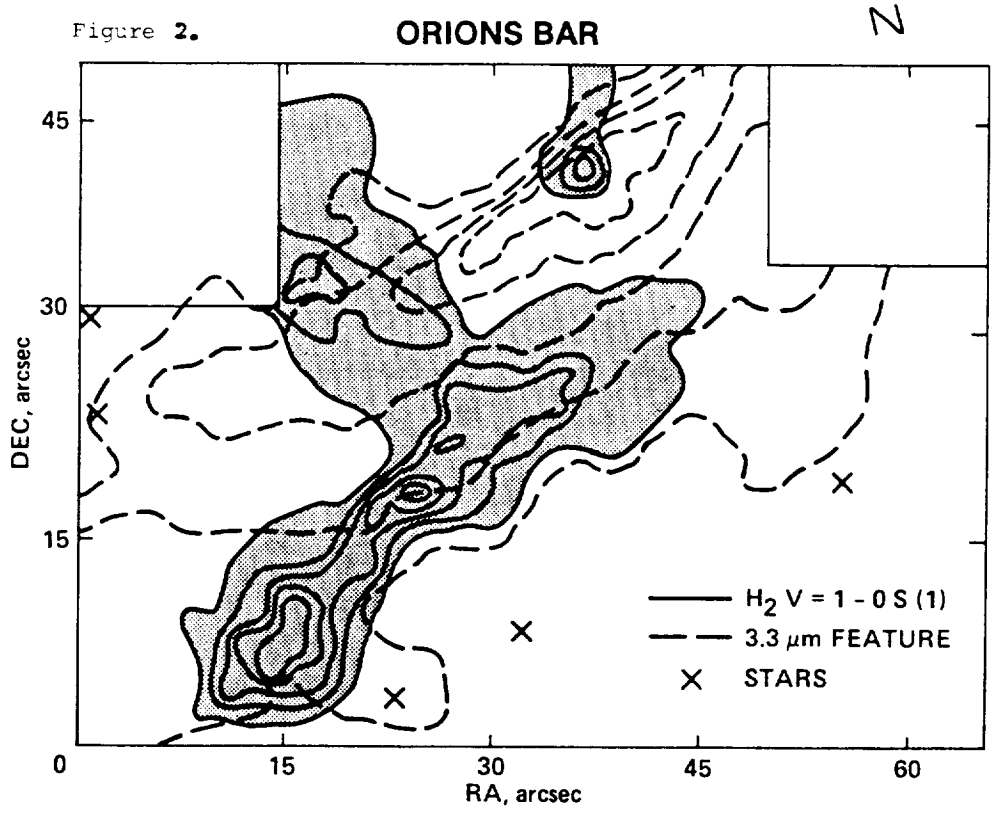

Figure 3.

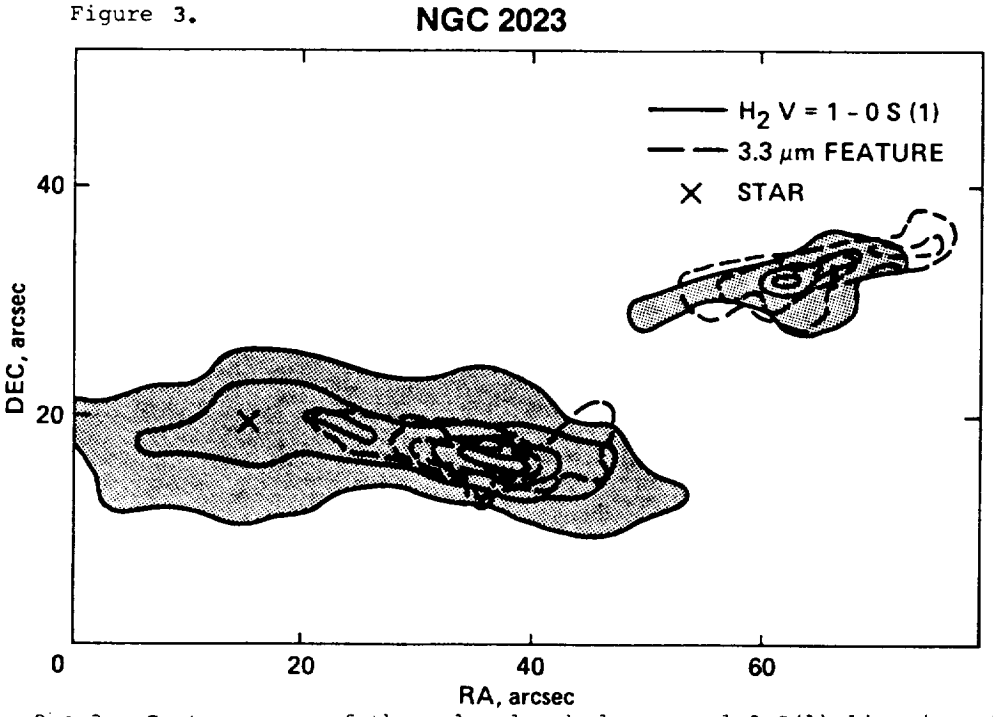

Figures 2 & 3. Contour maps of the molecular hydrogen v=1-0 S(1) line (continuous line, shaded region) and the 3.3μm feature (dashed line) in Orion's Bar and the reflection nebula NGC 2023. The ionisation front of the HII region of the Bar is to the NW of the ridge of 3.3μm emission. The exciting star for NGC 2023 is located 80" N of the peak of the molecular hydrogen emission.

N91-14919

AIRBORNE OBSERVATIONS OF THE INFRARED EMISSION BANDS

M. Cohen, D. Wooden, A.G.G.M. Tielens, J. Bregman, F. Witteborn
D. Rank and L.J. Allamandola

Earlier airborne studies of the infrared bands between 5 and 8 microns have now been extended to a sample of southern sources selected from the IRAS LRS atlas. The correlation between the strongest bands at 6.2 and 7.7 microns is now based on a total sample of 40 sources and is very strong. A new emission band at 5.2 microns, previously predicted for PAHs, is recognized in 27 sources; it too correlates with the dominant 7.7 micron band, showing that the 5.2 micron feature also belongs to the "generic" spectrum of PAH features at 3.3, 5.6, 6.2, 6.9, 7.7, 8.7, 11.3, and 12.7 microns.

We have sufficient sources now to define the relative strengths of most of these bands in three separate nebular environments: planetaries, HII regions, and reflection nebulae. We detect significant variations in the generic spectra of PAHs in these different environments which are echoed by variations in the exact wavelength of the strong "7.7" micron peak.

Our earlier suggestion that, in planetaries, the fraction of total emission observed by IRAS that is carried by the PAH emissions is correlated with nebular gas-phase C/O ratiom is supported by the addition of newly-observed southern planetaries, including the unusually carbon-rich [WC10] nebular neculei. These [WC10] nuclei also exhibit a strong "plateau" of emission linking the 6.2 and 7.7 micron features.

A SURVEY FOR "PAH" EMISSION IN H II REGIONS, PLANETARY AND PROTO-PLANETARY NEBULAE

M. de Muizon,* P. Cox,** and J. Lequeux***
*Sterrewacht Leiden, Postbus 9513, 2300 RA Leiden NL and Observatoire de Paris
**MPI für Radioastronomie, Auf dem Hügel 69, D 5300 Bonn, FRG
***Radioastronomie, Ecole Normale Supérieure, 75231 Paris CEDEX 05 F and Observatoire de Paris

SUMMARY

We report on preliminary results of a systematic investigation of PAH emission in H II regions, planetary nebulae (PN) and proto-planetary nebulae (PPN). This emission occurs in a vast majority of H II regions showing the ubiquity of the carriers. With the remarkable exception of NGC 6302, PAH emission is only seen in carbon-rich PNs and PPNs and is quite common in this case. This shows that PAHs are formed at least in part in carbon-rich evolved objects.

INTRODUCTION

We are engaged in a systematic search for infrared emission features in the IRAS/LRS (Low Resolution Spectra) data base. This data base contains a total of about 170 000 individual spectra of various qualities concerning about 50 000 IRAS sources. These spectra cover the spectral ranges 7.8 to 13.5 μm and 10.5 to 22.5 μm. A selection has been published in the LRS Atlas (IRAS Science Team, 1986) but many good quality spectra are still in the data base. We have systematically examined the individual spectra of known H II regions, planetary nebulae (PN) and proto-planetary nebulae (PPN) as well as all spectra with emission lines or with a flat or rising continuum in the LRS Atlas. The resulting selection constitutes a new data base which, although being neither complete nor homogeneous, contains a very large amount of information. An extensive literature search has added to this base a number of objects with published emission lines in the near IR (up to about 30 μm)

In the course of this work we experienced a number of difficulties with the Low Resolution Spectra:
1) Many individual spectra are affected by spurious "spikes" which sometimes superimpose over a real emission line. This problem is discussed by de Muizon et al. (1988) and necessitates examination of individual spectra. A revised version of the LRS Atlas where correction has

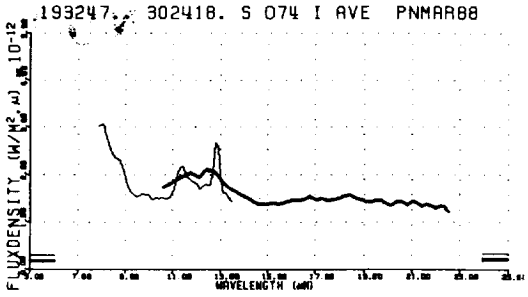

1a) BD+30°3639 PN

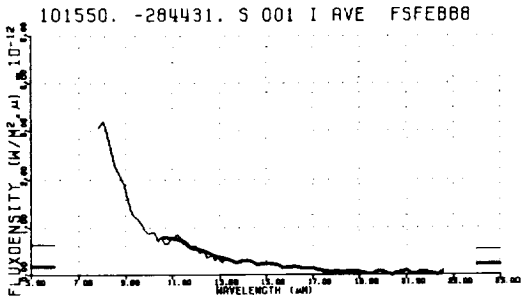

1b) HR 4049 PPN

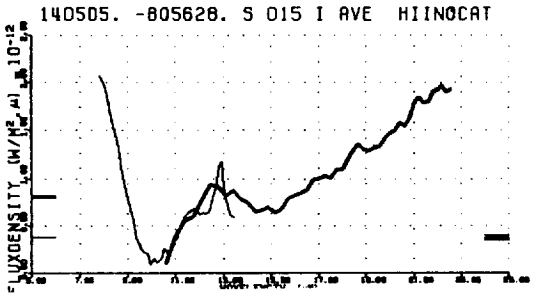

1c) G 312.112 H II

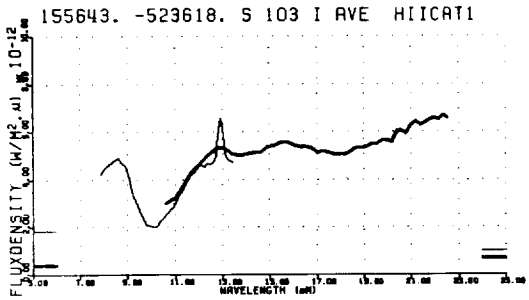

1d) G 329.353 H II

Figure 1: IRAS Low-Resolution Spectra of representative objects

been made for spikes is in preparation.

2) The automatic classification given in the LRS Atlas can be misleading: a confusion is possible for example between silicate absorption centered at 9.7 μm and PAH emission at 7.7, 8.6 (generally unresolved) and 11.3 μm.

3) The LRS instrument being a slitless prism spectrograph, wavelength resolution varies with wavelength and with the angular extent of the source and the wavelength scale may be somewhat displaced depending on the brightness distribution over the source.

RESULTS

IR emission bands form a spectrum of features at 3.3 + 3.4, 6.2, 7.7, 8.6 and 11.3 μm which appear together in a variety of objects (see e.g. Cohen et al. 1986 and references herein). These features are generally attributed to a mixture of Polycyclic Aromatic Hydrocarbons (PAH): Léger and Puget (1984). Usually the observations with a single instrument do not cover the whole spectrum and one must combine observations made in various ways, resulting in a variable signal-to-noise ratio for a single source. The LRS include the 7.7 μm feature (on the edge of the spectra), the 8.6 μm one (often unresolved from the previous one) and the 11.3 μm band. Examples are shown on Fig. 1 for one PN (BD+30°3639, Fig. 1a), one PPN (HR 4049, Fig.1b, see Waelkens et al. 1987) and two H II regions: G312.112 (Fig. 1c), not in the LRS Atlas, is a typical spectrum with PAH emission while G329.353 (Fig. 1d) shows strong silicate absorption and apparently no PAH emission. The interpretation of this sort of objects at the shortest

wavelengths may be ambiguous but there is no feature at 11.3 μm. Either there are no PAHs or their emission is very absorbed. There are only 2 certain H II regions without PAH emission and without silicate absorption. Both are of high excitation and deserve further attention.

We have added to our sample objects with PAH emission detected by other observers (the list of references is too lengthy to be given here). It should be remarked that higher-resolution spectra such as those of Roche ad Aitken (1986 and references herein) are more sensitive than LRS, but much less objects have been observed.

Provisional results are given in the following Table 1. Information on C/O ratios and exciting stars of PNs is mainly from Zuckerman and Aller (1986).

TABLE 1

STATISTICS FOR H II REGIONS

Certain H II regions	with certain PAH emission.....	83
	with possible PAH emission.....	31
	without PAH but strong silicate absorption.	14
	without PAH, without silicate absorption...	2
	Total...	130
Objects of unknown nature (many being probably H II regions)		
	with certain PAH emission.....	34
	with possible PAH emission.....	13
	without PAH but strong silicate absorption.	15
	without PAH, without silicate absorption...	3
	Total...	65

Note: strong silicate absorption may mimic or hide PAHs on LRS

STATISTICS FOR PNs AND PPNs

Carbon-rich, or ionized by a WC star		
	with certain PAH emission.....	15
	with possible PAH emission.....	5
	C/O>1, no detected PAHs (NGC 6543 and 6884)	2
	Total...	22
Oxygen-rich	certain PAH emission (NGC 6302).....	1
	possible PAH emission.....	3
	Total...	4

Notes to Table 1

CRL 618 = AFGL 618, in a transition stage from PPN to PN, is a carbon-rich object (from chemistry) showing rather surprisingly silicate emission. We class it as an object with possible PAH emission as a marginal emission at 3.3 and 6.2 μm can be seen on Fig. 1 of Russell et al. (1978). The good LRS shows no PAH feature. Radio continuum and recombination-line emission have been detected and there are fast increases in the continuum flux (Martin-Pntado et al. 1988). It may be

that PAHs, if really absent, have not had time to form or to be excited by UV photons. Further observations of this fascinating object are clearly needed.

NGC 6302 is a type-I PN which has been consistently classed as carbon-rich (C/O>1): see Zuckerman and Aller (1986). However as discussed by Roche and Aitken (1986) the value of C/O may be suspect in view of the very high range of ionizations which goes from Ne II to Ne VI. On the other hand it shows OH maser emission (Payne et al. 1988) which tends to confirm a low C/O ratio. This object clearly deserves further studies.

The 3 oxygen-rich objects with possible PAH emission are NGC 2440, 3242 and Hb 12. The only evidence for PAHs is the 3.3μm emission reported by Martin (1987). There is no visible accompanying 3.4μm emission and we suspect that one may be dealing with Pfδ rather than PAH emission.

CONCLUSIONS

From Table 1 and the previous discussion we can reach conclusions which although not really new (see e.g. Barlow, 1983, Cohen et al. 1986, Roche and Aitken, 1986, Zuckerman and Aller, 1986) are based upon a substantially increased data base, especially for the 7.7μm feature which cannot be observed from the ground.

1) "PAH" emission is ubiquitous. It obviously requires the presence of UV photons and is seen near essentially all H II regions (presumably at the interface with neutral gas). This confirms the ubiquity of PAHs in the general interstellar medium.

2) In PNs and PPNs, "PAH" emission is seen only where an ionizing flux is present (for PPNs) and in carbon-rich objects, with the remarkable possible exception of NGC 6302. Most objects with C/O>1 show PAH emission: there are only 2 clear exceptions. Clearly carbon-rich evolved stars are sites for the formation of PAHs.

3) We confirm the existence of important variations in the 7.7/11.3μm band intensity ratio first discussed by Cohen et al. (1986).

REFERENCES

Barlow, M.J.:1983, IAU Symposium 103 "Planetary Nebulae", ed. D. Flower Reidel, Dordrecht, p. 105

Cohen, M., Allamandola, L., Tielens, A.G.G.M., Bregman, J., Simpson, J. P., Wittebord, F.C., Wooden, D., Rank, D.:1986, Astrophys. J. 302, 737

IRAS Science Team:1986, Astron. Astrophys. Suppl. 65, 607

Léger, A., Puget, J.L.:1984, Astron. Astrophys. 137, L5

Martin, W.:1987, Astron. Astrophys. 182, 290

Martin-Pintado, J., Bujarrabal, V., Bachiller, R., Gomez-Gonzalez, J., Planesas, P.:1988, Astron. Astrophys. 197, L15

de Muizon, M., Cox, P., Lequeux, J.:1988, Astron. Astrophys. in press
Payne, H.E., Phillips, J.A., Terzian, Y.:1988, Astrophys. J. 326, 368
Roche, P.F., Aitken, D.K.:1986, Month. Not. Roy. Astron. Soc. 221, 63
Russell, R.W., Soifer, B.T., Willner, S.P.:1978, Astrophys. J. 220, 568
Waelkens, C., Lamers, H., Waters, R.:1987, The Messenger (ESO) 49, 29
Zuckerman, B., Aller, L.H.:1986, Astrophys. J. 301, 772

PAH EMISSION FROM NOVA CEN 1986

N91-14921

A.R. Hyland and P.J. McGregor
Mount Stromlo and Siding Spring Observatories,
Institute of Advanced Studies,
The Australian National University,
GPO Box 4, ACT 2601, Australia.

ABSTRACT. We report the discovery of broad emission features between 3.2μm and 3.6μm in the spectrum of Nova Cen 1986 (V842 Cen) some 300 days following outburst and remaining prominent for several months. The general characteristics of these features are similar to those attributed to PAH molecules in other dusty sources, although the relative strengths are different, and these observations provide the first clear evidence for molecular constituents other than graphite particles in the ejecta of novae.

1. INTRODUCTION

Since the original discovery of a dust emission phase in FH Ser (Hyland and Neugebauer 1970), and subsequent investigations which show that a dust phase is common to many novae (Ney and Hatfield 1978, Gehrz et al. 1980 a, b 1988), it has been realised that novae provide unparalleled opportunities for the investigation of the formation and dispersal of dust particles into the interstellar medium. Studies of the nature of the dust found in novae outbursts should provide clues on the abundance characteristics of the ejecta, and of the physical conditions existing during dust formation and destruction.

Photometric infrared studies of several novae have been reported in the literature (Ney and Hatfield 1978, Gehrz et al. 1980 a,b, 1988, Geisel, Kleinmann and Low 1970, Mitchell et al, 1985). Although these show remarkable similarities in the infrared secular development of novae, with a number of intermediate speed novae exhibiting strong dust emission, there exist wide differences in the optical depth of dust formed.

Little definitive information regarding the nature of the dust particles has so far been obtained, and the determination of the relative contributions of various dust constituents in novae ejecta remains one of the key issues to be addressed. The smooth black-body nature of the continua and apparent lack of silicate or other emission features in the 8-13μm region as determined from broad and intermediate-band photometry (other than in Nova Aql 1982, Bode et al. 1984) has led to a consensus view of dust in most novae as carbon particles, probably in graphitic form (see Bode and Evans 1983 for a discussion of this point). It might be expected that the UV radiation field experienced by carbon rich dust in novae ejecta would be conducive to the excitation of PAH type molecules if they are present in the outflow. However, data of sufficient resolution to determine whether weak dust emission features are present in novae ejecta have not been available. Infrared spectroscopic observations have been at a premium and have not had the time coverage of the photometric data. One of the key motivations for the present program of observations has been to obtain secular spectroscopic data in the 1-5μm region with sufficient resolution to determine if and when dust emission

signatures reveal themselves.

2. THE SPECTRAL DEVELOPMENT OF NOVA CEN 1986

Nova Cen 1986 (V842 Cen) was discovered in 1986 November several days before maximum light (McNaught 1986). Because of its brightness, position, and the availability of previously scheduled time, Nova Cen has provided us with one of the best opportunities yet for significant secular studies of the infrared spectrum development of a nova. The first spectrum was obtained on 1986 December 19, and since then data has been obtained at roughly regular intervals for about 18 months.

Spectroscopic and photometric infrared data have been obtained with the cooled grating spectrometer (CIGS) and photometric systems on the ANU 2.3m telescope at Siding Spring Observatory, and also with the infrared spectrometer (FIGS) on the Anglo-Australian telescope. Wherever possible, spectroscopic data were obtained with a resolving power of $\lambda/\delta\lambda$~500, covering the 1-5μm windows. A selection of spectra in the 2.9-4.1μm wavelength range obtained on five different occasions between 1986 December and 1988 January is shown in Figure 1.

Early spectra of the nova, taken some 30 days after outburst, when no dust emission was evident,showed the presence of strong emission lines of H, He, OI as well as CO first overtone emission similar to that seen in NQ Vul (Ferland et al. 1979). In the three micron region, strong atomic emission lines mask the appearance of any dust or molecular features. As expected for this relatively slow nova, by analogy with FH Ser, dust formation occurred around 55 days following outburst, and produced an optically thick dust shell which lasted for some 75 days. The dust emission dominated all wavelengths longer than the J(1.25μm) band until early 1988. Spectra taken soon after the formation of the dust shell (1987 January) show the presence of an extremely smooth dust continuum with a blackbody temperature of about 650K (Hyland and McGregor, 1987). Examination of the spectrum in the three micron region, where dust and molecular signatures are expected, showed no significant features against the smooth continuum.

However, spectra taken in 1987 September, when the shell temperature was closer to 800K, and subsequent measurements up to 1988 May, all show the presence of broad spectral features between 3.25 and 3.5μm with characteristics similar to those of the proposed PAH bands. We believe that this is the first time that such features have been seen in the spectrum of a nova.

The absolute integrated strength of the feature in 1987 September (~1.2×10^{-17} W/cm^2), was such that it would not have been visible against the continuum when the dust shell first formed, and so it is not possible to say whether the PAH molecules formed simultaneously with the graphitic like dust, or was formed subsequently by processing of the dust. By 1987 July it should have been possible to measure a feature with the strength of that found in September, although this is greatly hampered by imperfect division of telluric features close to 3.3μm. Nevertheless, it appears (Fig. 1) that the 3.4μm emission was not present in July, and we favor the formation of molecules by the processing of existing graphitic grains.

The integrated strength of the features decreased by a factor of ~2.5 between 1987 September, and 1988 January, while the continuum dropped by a factor of ~6 during the same period as the dust became progressively more optically thin. This can be attributed to an increase in the relative number of excited PAH type molecules.

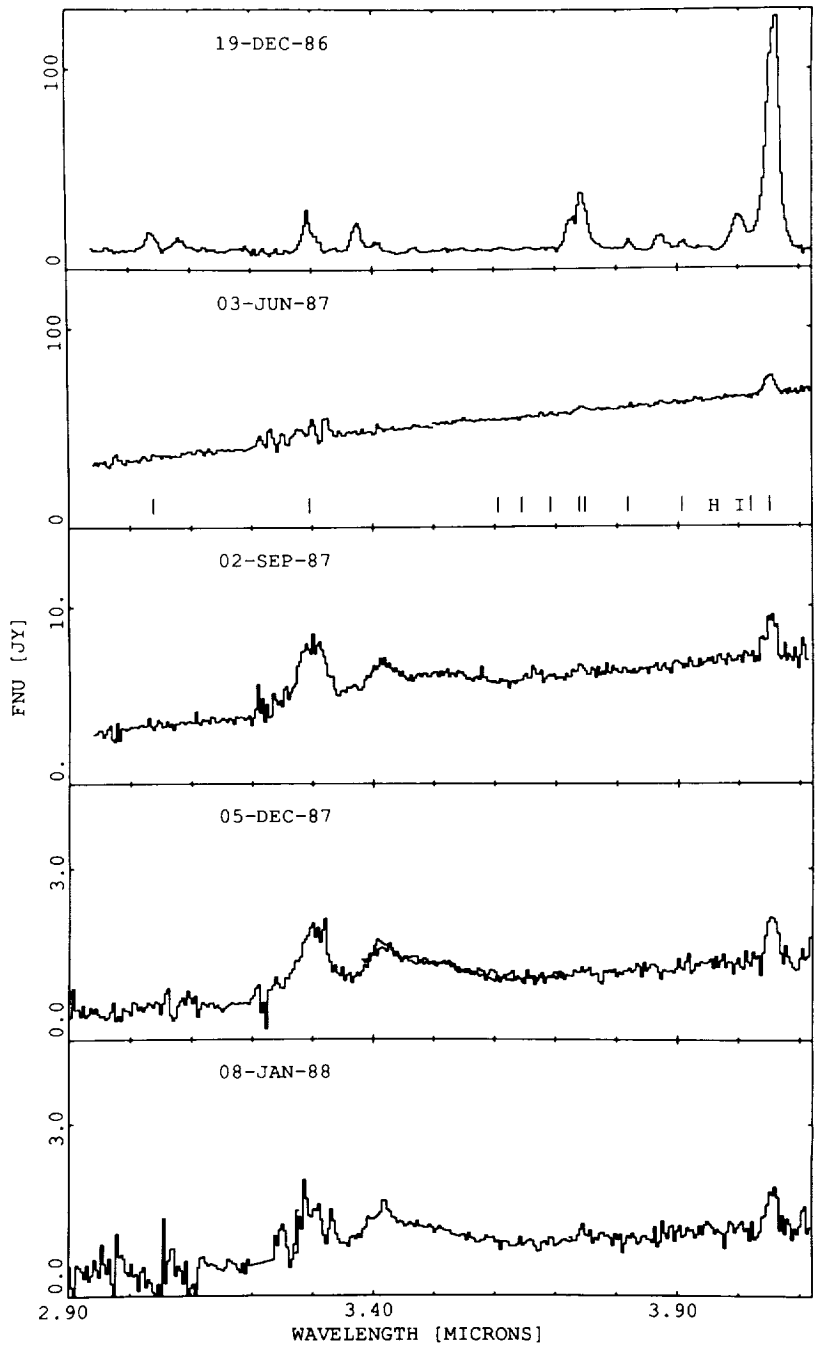

Fig. 1 Spectra of V842 Cen from 2.9-4.1μm obtained on five different occasions showing the development of the 3.3 and 3.4μm features. The top three spectra were obtained with CIGS on the MSSSO 2.3m telescope, while the remainder were obtained with FIGS on the AAT.

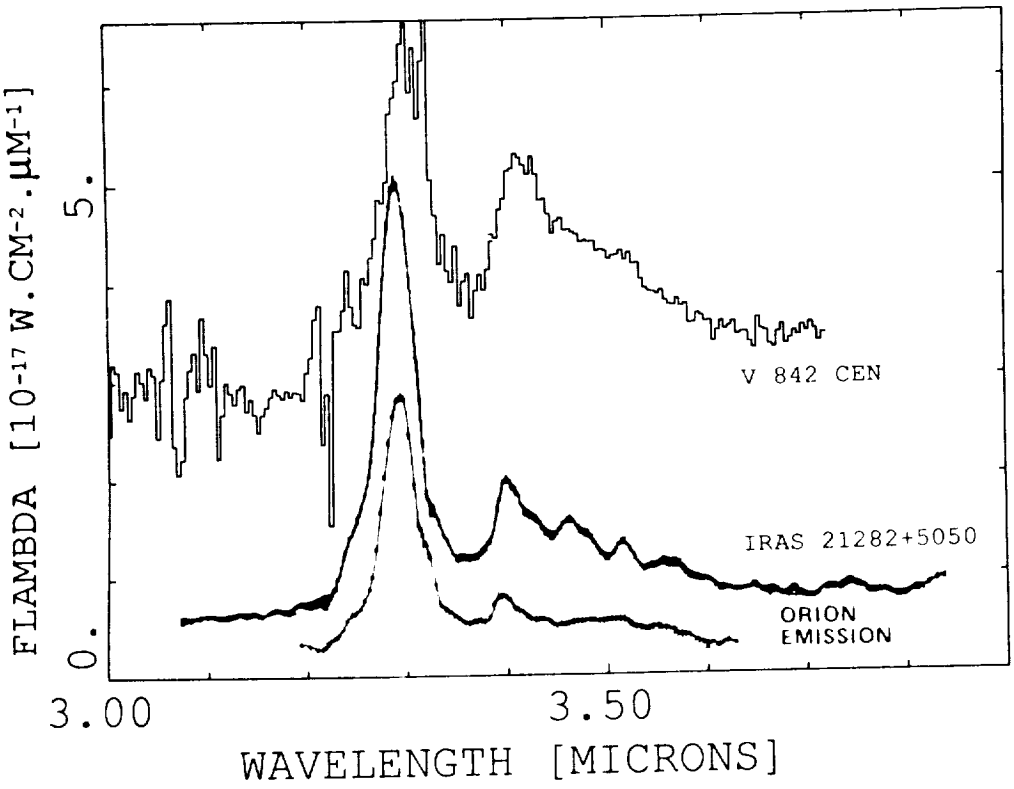

Fig. 2 A comparison of the observed 3μm spectrum of V842 Cen with spectra of IRAS 21282+5050 and the Orion Bar (see text). The spectrum of the nova has been arbitrarily shifted by the addition of a constant (10^{-17}).

3. PAH CHARACTERISTICS

The emission features observed in V842 Cen are compared with observations of PAH features in IRAS 21282+5050 (de Muizon et al. 1987) and the Orion Bar (Allamandola et al. 1987) in Fig. 2. Despite considerable similarities of the emission features in these three sources, V842 Cen also differs significantly from the other two sources in two respects. These are, 1) the relative strength of the 3.28μm feature to the blended group between 3.4 and 3.6μm is much lower in V842 Cen and 2) the feature seen strongly in 21282+5050 at 3.45μm is either absent or weak in the nova, rendering the shape of the feature between 3.4μm and 3.6μm intermediate between that of the two comparison objects. These characteristics should be diagnostic of the conditions and relative number densities of various molecular species in the nova ejecta. For example, it is possible that the relative strength of the 3.28μm and 3.4-3.6μm features is directly related to the temperature of the molecular species. Allamandola et al. (1987) have pointed out that a change from 400 to 480K is sufficient to alter the relative strengths of these features in observed char spectra remarkably in the sense that the longer wavelength features are

enhanced at lower temperature. On the other hand, the exact wavelength of the C-H stretching vibration depends on the precise nature of the molecules involved (see de Muizon et al. 1987), and the relative strength of the features at different wavelengths may provide important constraints on the exact mix of molecular species. The 3.28μm feature is dominant in aromatics, while in saturated hydrocarbons such as alkanes the C-H mode lies in the 3.4-3.6μm range, and depends upon whether the C-H bond is in CH_3, CH_2, or CH. The 3.46μm feature is thought to be due to a C-H bond in CH. It is possible therefore, that the weakness of the 3.28μm feature relative to those between 3.4-3.6μm may be due to a low ratio of unsaturated to saturated hydrocarbons. At the present time we have no explanation for the apparent differences in the feature at 3.45μm. Clearly the use of features in the 3μm region as molecular diagnostics in dust spectra has great potential, but at present is still in its infancy and will require both high quality astronomical and laboratory data for further advances to be made.

REFERENCES:

Allamandola, L.J., Tielens, A.G.G.M. and Barker, J.R.: 1987,in *Polycyclic Aromatic Hydrocarbons and Astrophysics*, eds. Léger, A., Hendecourt, L.B. d', and Boccara, N., (D. Reidel Publishing Co., Dordrecht), p. 255.

Bode, M.F. and Evans, A.: 1983, *Q.J.R.A.S.*, **24**, 83.

Bode, M.F., Evans, A., Whittet, D.C.B., Aitken, D.K., Roche, P.F. and Whitmore, B.: 1984, *M.N.R.A.S.*, **207**, 897.

Ferland,G.J., Lambert, D.L., Netzer, H., Hall, D.N. and Ridgway, S.T.: 1979, *Ap. J.*, **227**, 489.

Gehrz, R.D., Grasdalen, G.L., Hackwell, J.A. and Ney, E.P.: 1980a, *Ap. J.*, **237**, 855.

Gehrz, R.D., Hackwell, J.A., Grasdalen, G.L., Ney, E.P., Neugebauer, G. and Sellgren, K.: 1980b, *Ap. J.*, **239**, 570.

Gehrz, R.D., Harrison, T.E., Ney, E.P., Matthews, K., Neugebauer, G., Elias, J., Grasdalen, G.L. and Hackwell, J.A.: 1988, *Ap. J.*, **329**, 894.

Geisel, S.L., Kleinmann, D.E. and Low, F.J.: 1970, *Ap. J.*, **161**, L101.

Hyland, A.R. and Neugebauer, G.: 1970, *Ap. J.(Letters)*, **160**, L177.

Hyland, A.R. and McGregor, P.J.: 1987, in *Infrared Astronomy with Arrays*, eds. Wynn-Williams, C. G. and Becklin, E.E., (University of Hawaii, Honolulu), p.388.

McNaught, R.H.: 1986, *IAU Circular* 4274.

Mitchell, R.M., Robinson, G., Hyland, A.R. and Neugebauer, G.: 1985, *M.N.R.A.S.*, **216**, 1057.

Muizon, M. de, Hendecourt, L.B.d' and Geballe, T.R.: 1987, in *Polycyclic Aromatic Hydrocarbons,* eds. Léger, A., Hendecourt, L. d' and Boccara, N., (D. Reidel Publishing Co., Dordrecht, Holland), p. 287.

Ney, E.P. and Hatfield, B.F.: 1978, *Ap. J. (Letters)*, **219**, L111.

SPATIAL VARIATIONS OF THE 3 μm EMISSION FEATURES WITHIN NEBULAE

A. Moorhouse,* T.R. Geballe,** L.J. Allamandola,***
A.G.G.M. Tielens,*** and P.W.J.L. Brand,*

* Department of Astronomy, University of Edinburgh, Blackford Hill, Edinburgh, EH9 3HJ, Scotland.
** Joint Astronomy Center, 665 Komohana Street, Hilo 96720, USA.
*** NASA Ames Research Center, Moffett Field, California 94035, USA.

We present 3 μm spectra of the Orion bar region and the Red Rectangle. In both objects spectra were obtained at more than one location, corresponding to different distances from the excitation source. The well known 3.3 μm and 3.4 μm emission bands are seen in both objects as well as the recently discovered features at 3.46, 3.51 and 3.57 μm in the Orion's bar spectra. The spectra show that the relative strengths of the 3 μm emission features vary within Orions bar. As distance from the exciting star increases, the 3.4 μm and 3.51 μm features increase, and the 3.46 μm feature decreases in strength, relative to the strong 3.3 μm feature. There are two possible interpretations which we postulate, each of which involves the breaking of bonds by UV radiation, which removes the modes responsible for the 3.4 μm emission near the star. The two possible bond ruptures are (a) the CH bond in small PAHs, or (b) the bond to an aliphatic subgroup. It has to be pointed out that neither interpretation appears entirely satisfactory. The vibrational overtone interpretation cannot explain the presence or behaviour of the 3.46 μm feature, whereas the laboratory spectra of aliphatic sidegroups contain many more features in the 3 μm region than are observed in the astronomical sources.

THE WAVELENGTH DEPENDENCE OF POLARIZATION IN NGC2023

C.D.Rolph & S.M.Scarrott
Department of Physics, University of Durham, U.K.

NGC2023 is a bright reflection nebula illuminated by the central star HD37903. At 2 microns the nebula is seen solely by reflected light from the central star but in the NIR there is excess radiation that is supposed to arise from thermal emission from a population of small grains (Sellgren, 1984). The unexpectedly high surface brightness at R and I wavelengths has led to the suggestion that even at these wavelengths there is a significant contribution from this thermal emission process (Witt, Schild and Kraiman, 1984).

If the nebula is seen by reflected starlight then this radiation will be linearly polarized. The level of polarization depends on the scattering geometry, grain size distribution etc and is typically 20-40% for nebulae such as NGC1999 which is morphologically similar to NGC2023. If, in any waveband, there is a contribution of radiation from emission processes this radiation will be unpolarized and will serve to dilute the scattered radiation to give a lower level of observed polarization. A study of the wavelength dependence of polarization in nebulae in which there may be thermal emission from grains will indicate the contribution from this process to the total luminosity.

We have produced polarization maps in BVRI wavebands for the NGC2023 nebulosity which confirm that at all wavelengths it is a reflection nebula illuminated by a central star. In fig.1 we show the wavelength dependence of polarization at representative points in the nebula and in fig.2 a scatter plot of polarization in V and I wavebands at all points at which we have measurements is given.

Our results indicate that throughout the nebula there is a general trend for the level of polarization to increase with wavelength and that maximum levels of polarization occur at the longest wavelengths. We see no evidence in our data for any significant contribution from the thermal emission from grains in the BVRI luminosity of NGC2023.

Sellgren, K.: 1984, Astrophys.J. 277, 623
Witt, A.N., Schild, R.E. and Kraiman, J.B.: 1984, Astrophys.J. 281, 708

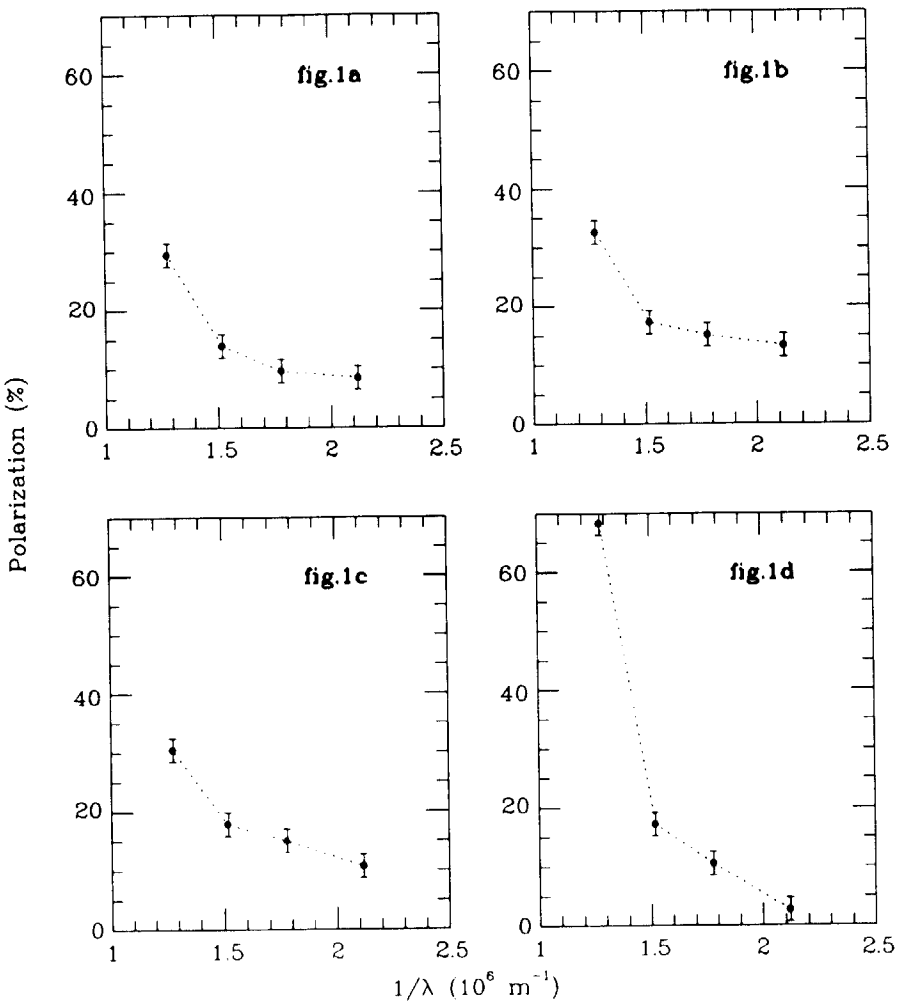

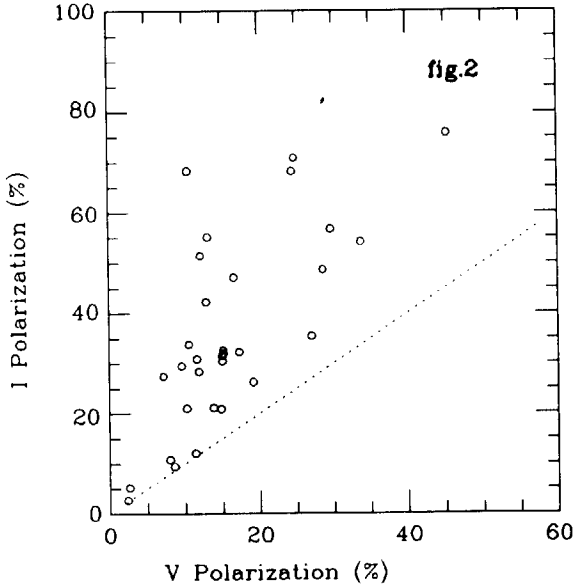

Fig.1 : Wavelength dependence of polarization
- **a** 75 arcsecs SE of HD37903
- **b** 100 arcsecs NE of HD37903
- **c** 150 arcsecs SE of HD37903
- **d** 200 arcsecs NW of HD37903

Fig.2 : Scatter plot of polarization in V and I wavebands.

RED FLUORESCENCE AND 3-12 MICRON EMISSION IN NGC 2023, HD 44179, M 82, AND LYNDS 1780.

C. Ryter* and L. d'Hendecourt**
*Service d'Astrophysique, DPHG/SAP, C.E.N.
Saclay, 91191 GIF SUR YVETTE CEDEX, France.
**Groupe de Physique des Solides de l'E.N.S.,
Université de Paris VII, 2, place Jussieu,
75251 PARIS CEDEX 05, France.

A red excess observed by Cohen et al. (1975) in the Red-Rectangle (HD 44179), studied by Greenstein and Oke (1977) and attributed by them to a possible molecular fluorescence mechanism, has also been discovered in NGC 2023 by Witt et al. (1984) and analysed in subsequent work (Witt and Schild, 1986, 1988) in this and other nebulae. An unexpected red light excess has also been noticed in a high latitude dark cloud L 1780 (Lynds, 1962) by Mattila (1979).

The fluorescence has been attributed to hydrogenated amorphous carbon by Duley (1985), on the basis of laboratory work. Alternatively, transitions between electronic states of free polycyclic aromatic hydrocarbon molecules, by-passing the cascade along the vibrational states, has been considered by d'Hendecourt et al. (1986) and Léger et al. (1988). In L 1780, the red excess has been related to the 12 μm emission detected by IRAS by Chlewicki and Laureijs (1987).

A quantative comparison of the intensity of the red fluorescence and that of the 3 - 12 μm features is thus warranted in helping assess the physical properties of large interstellar molecules.

The red fluorescence radiation, F(R), appears as a bump on the spectra between 0.6 and 0.9 μm. Values were deduced from the spectra published by Witt and Schild (1988) for NGC 2023, Cohen et al. (1975) for HD44179, and by Mattila (1979) for the high latitude cloud L 1780. Corrections for the extinction, both interstellar and internal to the nebulae, were included.

The 3 - 12 μm brightness, F(IR), was obtained through integration of the spectra published by Sellgren et al.(1985) for NGC 2023, and by Russel et al. (1979) for HD 44179 after removal of a smooth continuum due to hot large grains (Dainty et al., 1985). For the cloud L 1780, F(IR) was deduced from the 12 μm IRAS in-band flux, which can be

shown to be about 0.77 of the 3 - 12 μm flux. The galaxy M 82 could be included by evaluating the red fluorescence flux superimposed on the smooth stellar spectrum measured by Peimbert and Spinrad (1970), and adopting the infrared spectrum published by Willner et al. (1977).

The values of the ratio of the fluorescence flux to the infrared flux, F(R)/F(IR), are summarized in table 1, where estimates of the radiation density have also been included.

Table 1. Summary of results.

Object	Fluorescence F(R) [w m^{-2}]	3 - 12 μm F(IR) [w m^{-2}]	F(R)/F(IR)	density [eV cm^{-3}]
NGC 2023	$4.9\ 10^{-6}$ *	$7.5\ 10^{-5}$ *	0.065	10 - 100
HD 44179	$3.1\ 10^{-13}$	$1.9\ 10^{-11}$	0.016	>100
M 82	$1.8\ 10^{-21}$	$4.1\ 10^{-20}$	0.044	100-1000
L 1780	$2.4\ 10^{-8}$ *	$1.2\ 10^{-7}$ *	0.23	0.4

*per steradian

As shown by Léger et al. (1988), large molecules or ions should exhibit fluorescence emission upon UV excitation, with a yield very sensitive to the number of atoms they contain, and to the energy of the UV photons. Léger's et al. original calculation has been extended to larger molecules, and the ratio F(R)/F(IR) computed. In any case, the exciting radiation field contains numerous hard photons, and the highest photon energy, E = 13.6 eV, is appropriate. The result is displayed on fig. 1 as a function of the number of atoms per molecules.

The sizes deduced from table 1 and fig.1 are of about 70 atoms for the nebulae, and 50 atoms for the interstellar cloud L 1780. They fall well within the range of sizes deduced by de Muizon et al. (1987) through an anlysis of the ratio of the intensities of the 3.3 μm and 11.3 μm lines obtained on 14 IRAS sources.

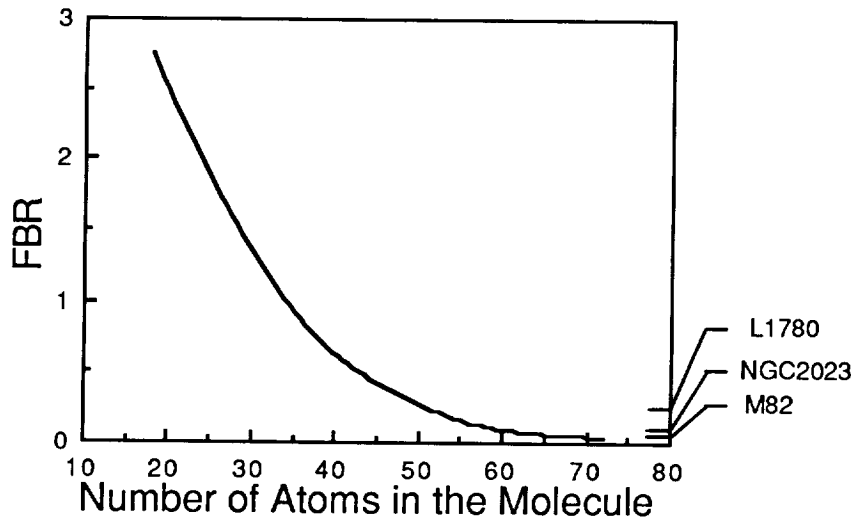

Figure 1. Ratio of the fluorescence flux to the infrared flux, FBR = F(R)/F(IR), as a function of the number of atoms in the aromatic molecules. Adapted from Léger et al. (1988). The exciting photon energy is 13.6 eV.

Red fluorescence and infrared radiation are two separate ways to access to the size of the molecules through observation, and it is rewarding that both approches give similar results. These findings bring a striking coherence into the physical description of the paricles, and add further support to the initial attribution of the infrared features to polycylic aromatic hydrocarbons (PAH).

A detailed account of this work will be presented elsewhere (submitted to Astronomy and Astrophysics).

Chlewicki, G. and Laureijs, R.: 1987, in "Polycyclic Aromatic Hydrocarbons and Astrophysics", ed. Léger, d'Hendecourt and Boccara (Reidel: Dordrecht), p.335.

Cohen et al., 1975: Ap. J. 196, 179.

Dainty,J.C., Pipher, J.L., Lacasse, M.G.: 1985, Ap. J. 293, 530.

Duley, W.W.: 1985, Mon. Not. R. Astr. Soc. 215, 259.

Greenstein, J.L. and Oke, J.B.: 1977, Pub. Astr. Soc. Pac. 89, 131.

d'Hendecourt, L.B., léger, a., Olofsson, G.,Schmidt, W.: 1986, Astron. Astrophys. 170, 91.

Léger, A. Boissel, P., d'Hendecourt, L.: 1988, Phys. Rev. Letters, 60, 921.

Lynds, B.T.: 1962, Ap. J. suppl. 7, 1.

Mattila. K.: 1979, Astr. Astrophys.78, 253.

de Muizon, M., d'Hendecourt, L.B., Geballe, T.R.: 1987, in "Polycyclic Aromatic Hydrocarbons and Astrophysics", ed. Léger, d'Hendecourt and Boccara (Reidel: Dordrecht), p. 287.

Russel, R.W., Soifer, B.T., Willner, S.P.: 1978, Ap. J. 220, 568.

Peimbert, H, Spinrad, H.: 1970, Ap. J. 160, 429.

Sellgren, K., Allamandola, L.L., Bregman, J.D., Werner, M.W., Wooden, D.H.: 1985, Ap. J. 299, 416.

Willner, S.P., Soifer, B.T., Russel, R.W., Joyce, R.T., Gillet, F.C.: 1977, Ap. J. Letters, 217, L 121.

Witt, A.N., Schild, R.E., Kraiman, J.B.: 1984, Ap. J. 281, 709.

Witt, A.N., Schild, R.E.: 1986, Ap. J. Suppl. 62, 839.

Witt, A.N., Schild, R.E.: 1988, Ap. J. 325, 837

N91-14925

HIGH-SPECTRAL RESOLUTION OBSERVATIONS OF THE 3.29 μm EMISSION FEATURE: COMPARISON TO QCC AND PAHS.

A.T. Tokunaga,* K. Sellgren,* A. Sakata,** S. Wada,**, T. Onaka,***
Y. Nakada,***, and T. Nagata****
*Inst. for Astronomy, Univ. of Hawaii, 2680 Woodlawn Dr., Honolulu, HI 96822
**Univ. of Electro-communications, Chofu-shi, Tokyo 182, Japan
***Dept. of Astronomy, Univ. of Tokyo, Bunkyo-ku, Tokyo 113, Japan
****Univ. of Kyoto, Sakyo-ku, Kyoto 606, Japan

Two of the most promising explanations for the origin of the interstellar emission features observed at 3.29, 3.4, 6.2, 7.7, 8.6, and 11.3 μm are: quenched carbonaceous composite (QCC) and polycyclic aromatic hydrocarbons (PAHs). Details can be found in Sakata et al. (1987) for QCC and in Leger and d'Hendecourt (1987) for PAH.

In Fig. 1 we show high-resolution spectra of the 3.29 μm emission feature which were taken with the Cooled-Grating Array Spectrometer at the NASA IRTF at Mauna Kea and previously published by Nagata et al. (1988) and Tokunaga et al. (1988). These spectra show that the peak wavelength of the 3.29 μm feature is located at 3.295 ± 0.005 μm and that it is coincident with the peak absorbance of QCC. The peak wavelength of the 3.29 μm feature appears to be the same in all of the sources we have observed thus far. However, the width of the feature in HD 44179 and Elias 1 is only 0.023 μm, which is smaller than the 0.043 μm width in NGC 7027, IRAS 21282+5050, the Orion nebula, and BD+30°3639.

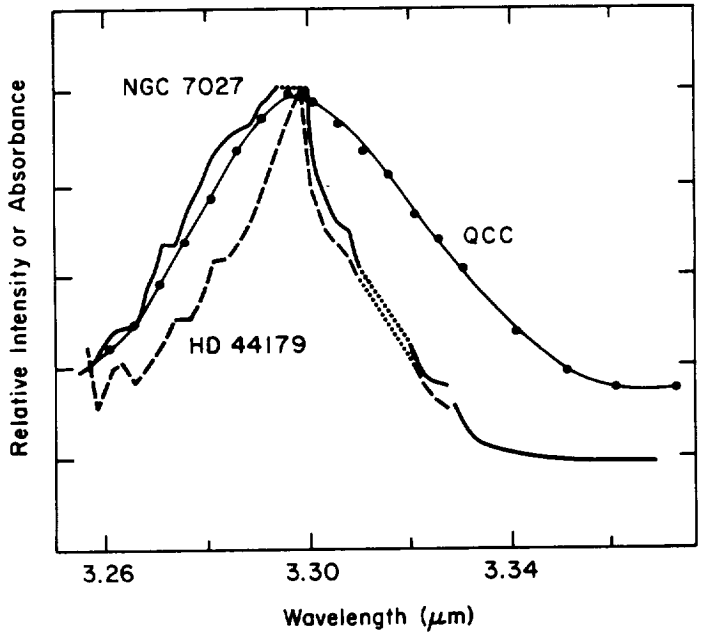

Fig. 1. Spectra of NGC 7027 and HD 44179 at a resolving power of 1400 compared to the absorbance of QCC.

Spectra of NGC 7027, QCC, and PAHs is shown in Fig. 2. The spectrum of QCC shown was taken after the QCC was heated to 500 °C in a vacuum, and at this temperature, the QCC bands at 3.4-3.6 μm are much weaker compared to the room temperature sample. The spectra of PAHs shown were taken at room temperature.

In Fig. 2 we show only the PAHs which have a peak near 3.295 μm; many others were measured but did not provide such a good match to the interstellar emission feature. Indeed, we measured over 30 PAHs and only benzene and benz(a)pyrene showed a peak exactly at 3.295 μm. Note that the width of the interstellar emission feature is less than or equal to 0.043 μm (40 cm^{-1}), so that combining the spectra of many PAH molecules would give rise to a feature at 3.29 μm which is much broader than what is observed. Also, the aromatic C-H bond of PAHs produces multiple features near 3.28-3.29 μm which is not observed in the interstellar medium.

In summary, QCC matches the 3.29 μm interstellar emission feature very closely in the wavelength of the peak, and it produces a single feature. On the other hand, PAHs rarely match the peak of the interstellar emission feature, and characteristically produce multiple features. We therefore suggest that QCC produces a much better match to the 3.29 μm interstellar emission feature.

We show in Fig. 3 and 4 additional spectra obtained in the same manner as the spectra published by Nagata et al. (1988) and Tokunaga et al. (1988). NGC 7027, Orion (position 4), and BD+30°3639 all have a profile for the 3.29 μm that is the same within observational errors. Also, Nagata et al. (1988) show that this emission feature is the same for NGC 7027 and IRAS 21282+5050 as well. On the other hand, spectra of HD 44179 and Elias 1 (see Fig. 4) show that these objects have a profile which is similar in shape but quite different that of the other objects shown in Fig. 3. A detailed comparison of the NGC 7027 and HD 44179 profiles is given by Tokunaga et al. (1988). In summary, high-spectral resolution observations of the 3.29 μm feature shows at least two types of emission profiles for this feature. The reason for this difference is not known at this time.

Leger, A., and D'Hendedourt, L.B.: 1987, in Polycyclic Aromatic Hydrocarbons and Astrophysics, ed. A. Leger, L. d'Hendecourt, and N. Boccara (Dordrecht: Reidel), p.223.

Nagata, T., Tokunaga, A.T., Sellgren, K., Smith, R.G., Onaka, T., Nakada, Y., and Sakata, A.: 1988, Ap. J. **326**, 157.

Sakata, A., Wada, S., Onaka, T., and Tokunaga, A.T.: 1987, Ap. J. Lett. **320**, L63.

Tokunaga, A.T., Nagata, T., Sellgren, K., Smith, R.G., Onaka, T., Nakada, Y., Sakata, A., and Wada, S.: 1988, Ap. J., **328**, 709.

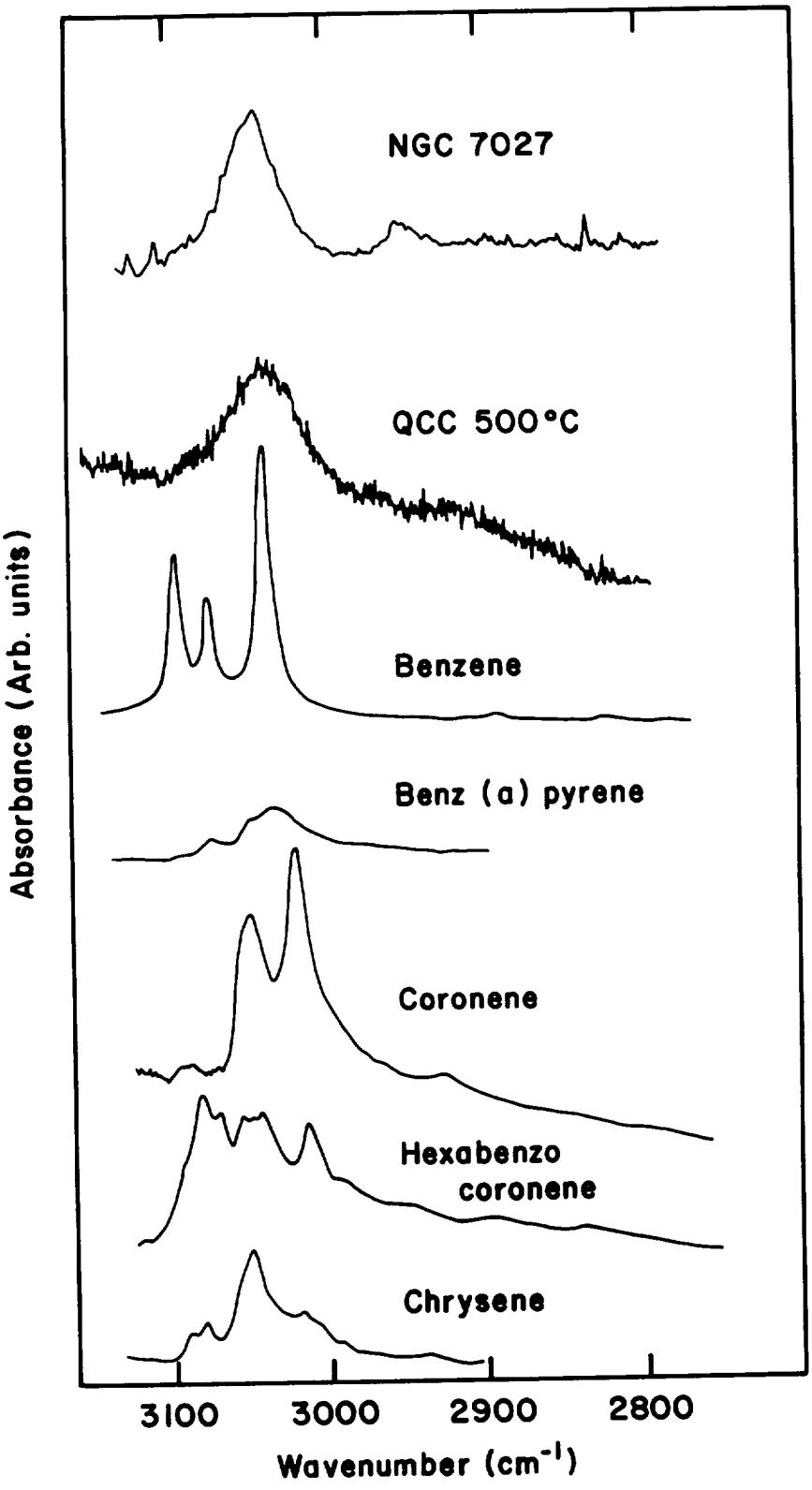

Fig. 2. The absorbance of QCC and PAHs taken at a resolution of 1 cm^{-1} compared to the emission spectrum of NGC 7027. The very strong Pf-δ line at 3.297 μm has been removed from the spectrum of NGC 7027.

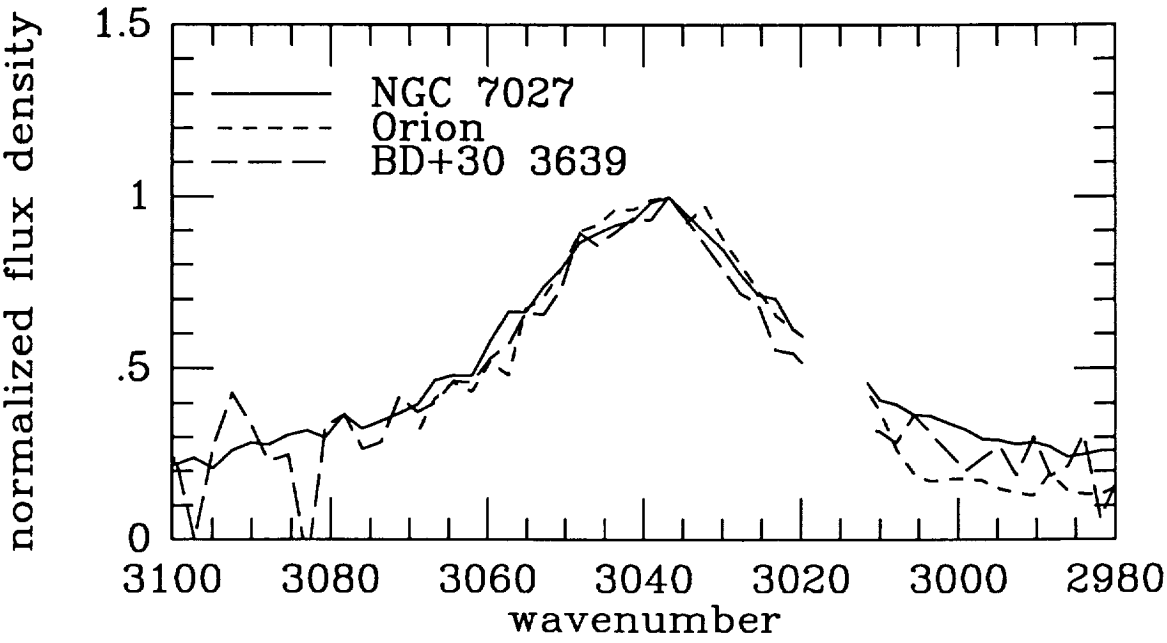

Fig. 3. Spectra of NGC 7027, Orion (at position 4), and BD+30°3639 taken at a resolving power of 1400. The strong Pf-δ line has been removed from the spectrum of NGC 7027 and BD+30°3639. The strong telluric methane band precludes data from being taken between 3010 and 3020 cm^{-1}. The point-to-point scatter is indicative of the noise level.

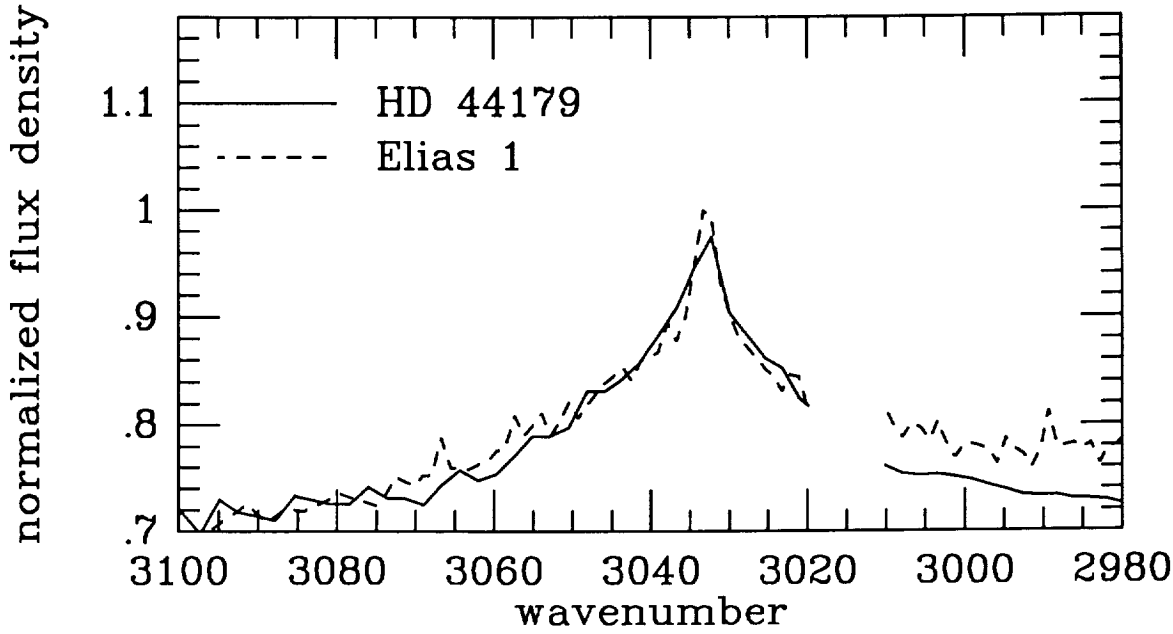

Fig. 4. Spectra of HD 44179 and Elias 1 at a resolving power of 1400.

"Spectral Structure Near the 11.3 Micron Emission Feature"

F.C. Witteborn, S.A. Sandford, J.D. Bregman, L.J. Allamandola,
M. Cohen, and D. Wooden

If the 11.3μm emission feature seen in the spectra of many planetary nebulae, HII regions, and reflection nebulae is attributable to polycyclic aromatic hydrocarbons (PAHs), then additional features should be present between 11.3 and 13.0μm. Moderate resolution ($\lambda/\Delta\lambda$ = 140) spectra of NGC 7027, HD 44179, BD+30°3639, and IRAS 21282+5050 are presented which show evidence for new emission features centered near 12.0 and 12.7 μm. These are consistent with an origin from PAHs and can be used to constrain the molecular structure of the family of PAHs responsible for the infrared features. There is an indication that coronene-like PAHs contribute far more to the emission from NGC 7027 than to the emission from HD 44179. The observed asymmetric profile of the 11.3μm band in all the spectra is consistent with the slight anharmonicity expected in the C-H out-of-plane bending mode in PAHs. A series of repeating features between 10 and 11μm in the spectrum of HD 44179 suggests a simple hydride larger than 2 atoms is present in the gas phase in this object.

II-B) THE NEAR INFRARED CIRRUS

SMALL SCALE VARIATIONS OF ABUNDANCES OF TRANSIENTLY HEATED GRAINS IN MOLECULAR CLOUDS

F. Boulanger[1,2], E. Falgarone[1,3], G. Helou[2], J.L. Puget[1]

[1] Laboratoire de Physique, Ecole Normale Supérieure, Paris
[2] IPAC, California Institute of Technology, Pasadena
[3] Downs Laboratory of Physics, California Institute of Technology, Pasadena

IRAS images of a variety of fragments in nearby molecular clouds show that the energy distribution of their IR emission varies widely from cloud to cloud and from place to place within a given cloud (see Figure 1 and other examples in Puget, 1988). These variations at small scale are all the more unexpected that the colors of the IR emission of cold material differ very little at large scale: the colors of the cirrus emission above the 3kpc molecular ring are the same as those of the cirrus emission in the solar neighborhood (Pérault et al., 1988).

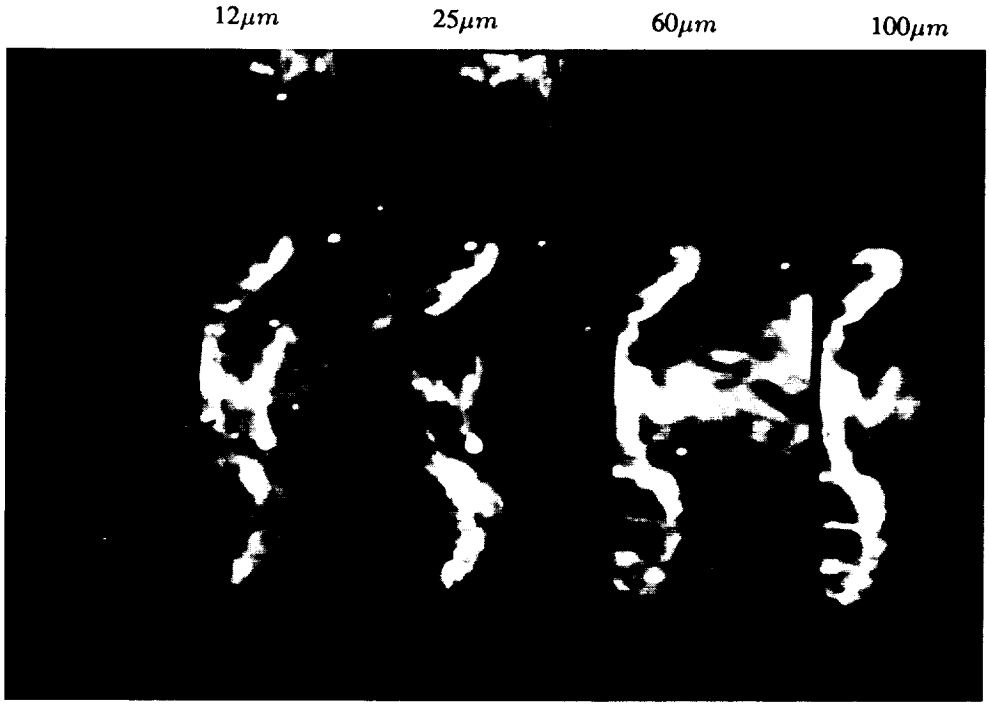

Figure 1.: *Molecular filament near ζ Oph. Different morphologies in the four IRAS bands illustrate color differences*

To quantitatively study these variations, we obtained $12\mu m$, $60\mu m$ and $100\mu m$ brightnesses of small areas centered at different positions within the set of clouds and complexes listed in the Table. The range

of observed $I_\nu(12\mu m)/I_\nu(100\mu m)$ colors is given for each cloud. Variations by an order of magnitude are found in most clouds. Variations by a factor 2 to 3 are observed within a cloud on scales as small as 0.5pc, the resolution of our study. Maximum observed $I_\nu(12\mu m)/I_\nu(100\mu m)$ values are roughly 3 to 4 times larger than the average value obtained by Boulanger and Pérault (1988) for the nearby interstellar medium; the lowest upper limits are more than a factor of 10 lower than this value. For a subset of our measurements, we derived an estimate of the visual extinction from ^{13}CO observations or star counts. This estimate enables us to measure the $100\mu m$ emissivity per proton. The $I_\nu(12\mu m)/I_\nu(100\mu m)$ color is plotted against the $100\mu m$ brightness, the $100\mu m/A_v$ ratio and the $I_\nu(60\mu m)/I_\nu(100\mu m)$ color in figures 2, 3 and 4. In figure 4, we separated the data in two families on the basis of their $100\mu m$ brightness: on the one hand, clouds or fragments of clouds with $I_\nu(100\mu m) < 10 MJy/sr$ which show little extinction ($A_v < 1 mag$) on optical plates (translucent clouds), on the other hand dark clouds brighter at $100\mu m$ and more opaque in the visible ($A_v > 2 mag$).

Table

Cloud or complex	Size (pc)	$I_\nu(12\mu m)/I_\nu(100\mu m)$	$A_v(mag)^{(*)}$	Type of cloud
Taurus Auriga Perseus	50	<0.015-0.12	1.5-6	dark
Ophiuchus filaments	10	0.02-0.13	1-3	dark
Ophiuchus core	2	<0.01-0.1	5-50	dark
Chamaeleon	10	<0.003-0.16	0.5-3	translucent/dark
Ursa Major	10	0.035-0.15	0.1-1	translucent
High Latitude Clouds	5	<0.02-0.16	0.1-1	translucent

(*). *Range of visual extinction at an angular scale of a few arcmin.*

I. Observational facts.

The elements directly derived from observational data are the following:

1) large variations of the $I_\nu(12\mu m)/I_\nu(100\mu m)$ color are found from one cloud to another and within molecular clouds on scales as small as the resolution of our study, $\sim 0.5pc$ (Table),

2) the amplitude of the variations is not related to the nature of the clouds. Dark and translucent clouds exhibit a similar range of $I_\nu(12\mu m)/I_\nu(100\mu m)$ colors (Figure 2). These clouds are all molecular or closely associated with a molecular cloud. There is presently no evidence for a similar scatter among isolated HI clouds: for comparison, colors obtained for a small sample of atomic clouds are also plotted in figure 2,

3) color variations do not depend on the intensity of the heating radiation field (Figure 3). In this figure, we use the $100\mu m/A_v$ ratio as an indicator of the average intensity of the radiation field along the line of sight. This implicitely assumes that the absorptivity of large grains (emitters of the $100\mu m$) and the fraction of the total energy they radiate in the $100\mu m$ band do not vary much within our sample of clouds. The latter condition is met for an equilibrium temperature of large grains between 18K and 32K assuming an emissivity law in λ^{-2}.

4) dark clouds show a correlation between $I_\nu(12\mu m)/I_\nu(100\mu m)$ and $I_\nu(60\mu m)/I_\nu(100\mu m)$ colors while translucent clouds do not (Figure 4). The difference between the two families suggests that the size

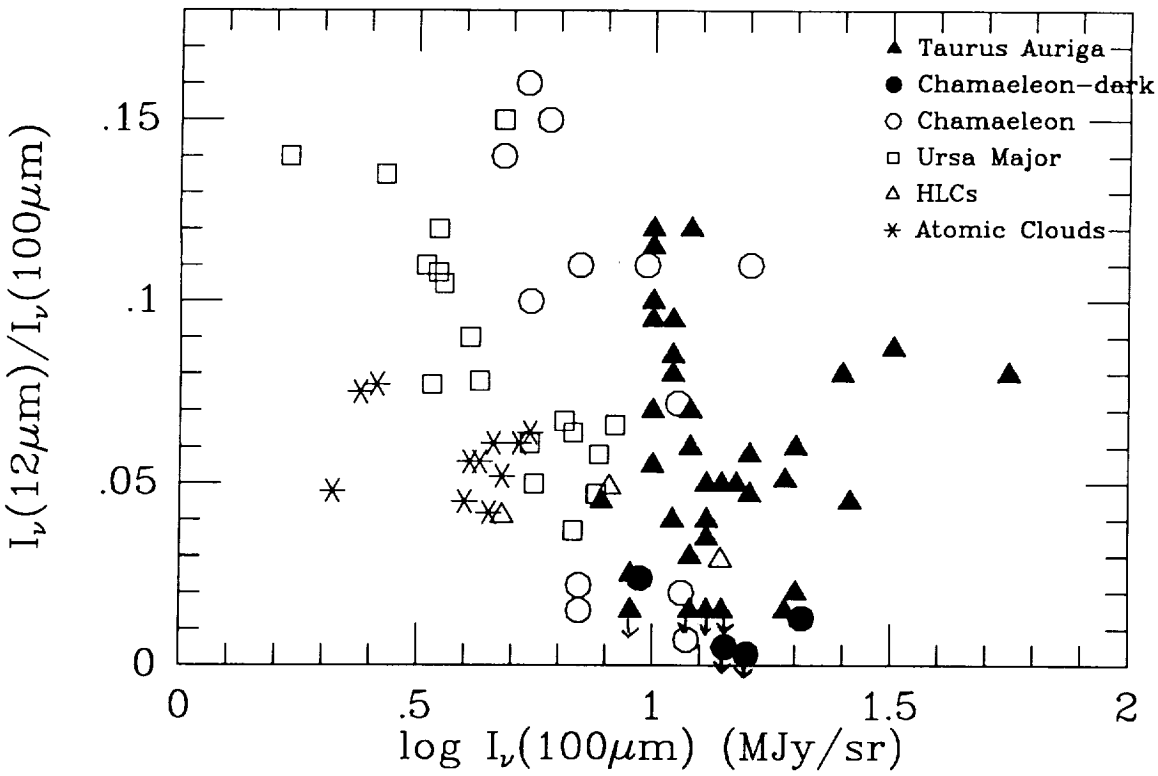

Figure 2.: *$I_\nu(12\mu m)/I_\nu(100\mu m)$ color versus $100\mu m$ brightness. The symbols are solid for dark clouds and open for translucent clouds.*

distribution of the small particles (the radiation of which is caused by temperature fluctuations) is not the same for the two sets of clouds. In the dark clouds, the observed correlation indicates that (i) part of the $60\mu m$ emission is due to small grains and (ii) what makes the $12\mu m$ emission vary, simultaneously affects the $60\mu m$ emission. In the other family, either there is no contribution of small grains to the $60\mu m$ emission or there is a contribution but no link between the particles responsible for the $12\mu m$ and $60\mu m$ emission.

II. Elements of interpretation.

The color variations seen here cannot be accounted for by the $12\mu m$ limb brightening of the kind discussed by Beichman et al. (1988) for the B5 cloud or by Puget (1988) at the edges of filaments and fragments in the Ophiuchus cloud. In these cases, part of the effect is due to the reddening of the spectrum of the heating radiation as the depth within the cloud increases: in the outer layers most of the heating comes from UV photons, in the inner layers dust is heated by visible and near-IR light. The amplitude of the variations reported on here cannot be reproduced by any reasonable density structure of the cloud (see models in Beichman et al., 1988).

We thus conclude that large variations of the abundances of small particles with respect to those of the large grains responsible for the $100\mu m$ emission are required to explain the observed color variations and that these abundances have to vary by large factors: an order of magnitude from cloud to cloud and 2 to 3 from place to place within one cloud.

Several physical mechanisms may be invoked to account for these variations at small scale. Agglomeration between the smallest particles and/or condensation on large grains, desorption of small particles and large molecules from the surface of large grains triggered either by UV photons or via collisions with the gas, inhomogeneities possibly driven by the disordered velocity field within clouds or shock chemistry.

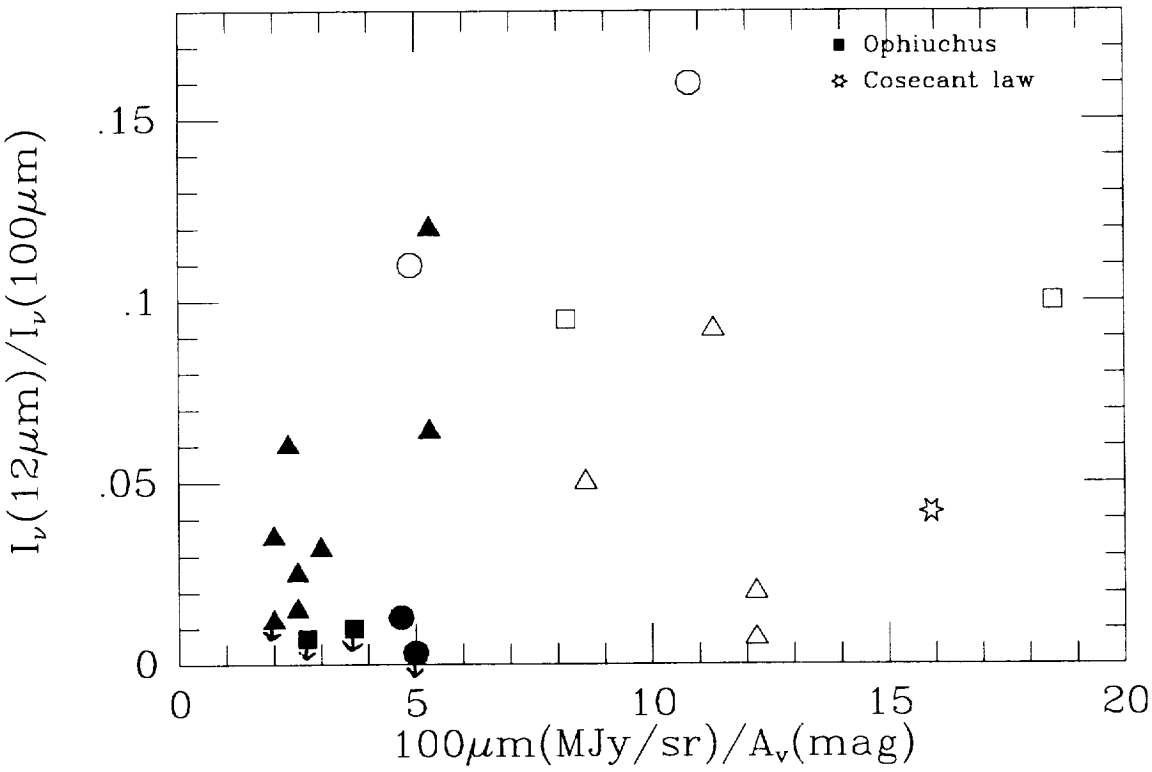

Figure 3.: *$I_\nu(12\mu m)/I_\nu(100\mu m)$ versus $100\mu m/A_v$ for the subset of measurements for which visual extinction has been estimated. Unspecified symbols are the same as in figure 2.*

Any interpretation faces the problem of the short mixing timescale, $\tau \sim 5\,10^5 yr$ over $\sim 0.5pc$ for internal cloud velocities of the order of $1km/s$.

References

Beichman C.A., Wilson R.W., Langer W.D., Goldsmith P.S 1988: *Astrophys. J.* in press

Boulanger F. and Pérault M. 1988: *Astrophys. J.* **330**, 964

Puget J.L. 1988: IAU Symposium 135 on Interstellar Dust

Pérault M., Boulanger F., Puget J.L., Falgarone E. 1988: *Astrophys. J.* submitted

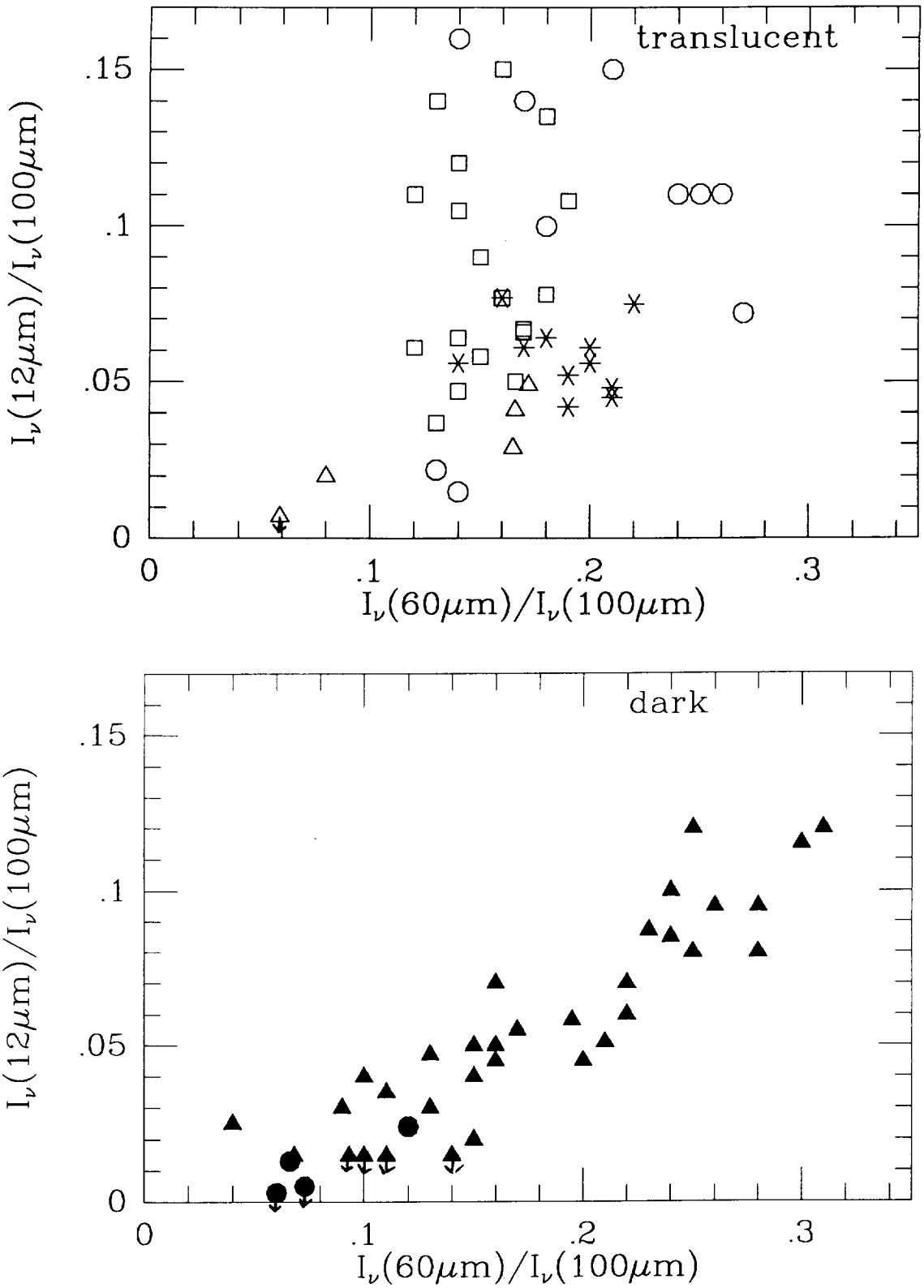

Figure 4.: *$I_\nu(12\mu m)/I_\nu(100\mu m)$ versus $I_\nu(60\mu m)/I_\nu(100\mu m)$ for the two families of clouds. Symbols are the same as in figure 2.*

THE 3.3μm EMISSION FEATURE : MAP OF THE GALACTIC DISK, 10° < l < 35°, - 6° < b < 6° .

M. Giard*, F. Pajot**, E. Caux*, J.M. Lamarre**
and G. Serra*
*Centre d'Etude Spatiale des Rayonnements,
9, avenue du Colonel Roche, BP 4346,
31029 Toulouse Cedex, France.
**Laboratoire de Physique Stellaire et Planétaire,
BP 10, 91370 Verrières-le-buisson Cedex, France.

The 3.3μm aromatic feature has been detected in the diffuse galactic emission with the AROME*** balloon borne instrument. (Giard et al., 1988, submitted to Astronomy and Astrophysics-Letters). We present here the results in the form of an (lxb) map of the 3.3μm feature's intensity.

The AROME instrument consists in a Cassegrain telescope (D = 140 mm) with wobbling secondary mirrors (fm ≈ 18 Hz, amplitude on the sky = 1.7°) and a liquid/solid nitrogen cooled photometer. The field of view is 0.52° and the feature is detected by difference of the fluxes measured in a wide (2.8μm < λ < 3.7μm) and a narrow (3.22μm < λ < 3.38μm) photometric band. The observationnal procedure is a slow azimuthal scanning (speed = 0.8°/s) at a constant elevation angle (≈ 30°). The pointing accuracy is ± 5' relative and 0.5° absolute. The instrumental noise is dominated by the photon noise of the background emission of warm optics. The rms value of the fluctuations is equivalent to a surface brightness $\lambda.I\lambda \approx 1.3\ 10^{-6}$ Wm^{-2} sr^{-1} in both bands .

The instrumental output is modified by the impulse response of the system. So the galactic surface brightness was restored in Fourier space by an inverse optimal filtering (Helstrom 1967). The map of the feature's intensity is presented in Figure 1 for the region of galactic coordinates 10° < l < 35°, -6° < b < 6°. All the known HII-giant molecular cloud complexes are visible in the 3.3μm "feature" emission showing a good correlation with the infrared dust emission. In addition to this "source"

*** The AROME instrument is funded by the Centre National d'Etudes Spatiales , France.

emission there is a diffuse galactic emission wich extends to the highest latitudes observed (b = ± 6°).

The observation of the 3.3μm feature in the galactic emission had been predicted by Puget, Léger and Boulanger (1985). It allows to identify the very small grains wich are responsible for the near and mid infrared emission of the Galaxy, to polycyclic aromatic hydrocarbons (PAHs). These molecules were first introduced by J. Platt (1956) to explain some properties of the interstellar extinction. They were recently proposed as being at the origin of the unidentified infrared bands at 3.3, 6.2, 7.7, 8.6 and 11.3 μm observed in emission in a wide variety of sources (Léger and Puget 1984, Allamandola, Tielens and Barker 1985).

≈≈≈≈≈≈≈≈≈≈≈≈≈≈≈

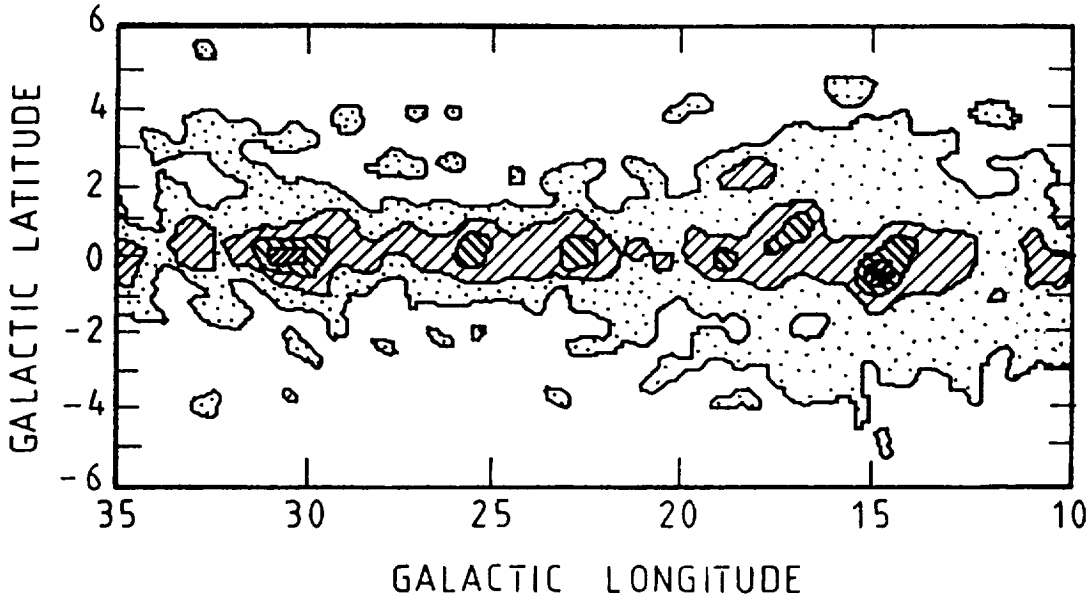

Figure 1: Isophote map of the 3.3μm feature's intensity in galactic coodinates. The resolution is (Δl×Δb)=(0.74°×0.90°). The first level and the step are equal to $6\ 10^{-8}$ W/m2/sr and the r.m.s. noise fluctuation is $1.2\ 10^{-8}$ W/m2/sr.

≈≈≈≈≈≈≈≈≈≈≈≈≈≈≈

References:

Allamandola, L.J., Tielens, A.G.G.M. and Barker, J.R.: 1985, Ap.J., 290, L25

Helstrom, C.W. : 1967, J. Opt. Soc. Am. 57, 297.

Léger, A., Puget, J.L.: 1984, Astron. and Astrophys. 137,L5

Platt J. : 1956, Ap.J., 123, 486.

Puget J.L., Léger A. and Boulanger F. : 1985, Astron. and Astrophys., 142, L19.

IR EMISSION AND UV EXTINCTION IN TWO OPEN CLUSTERS

J. A. HACKWELL AND J. H. HECHT
Space Sciences Laboratory, The Aerospace Corporation, Los Angeles, California 90009 USA

Recent models of interstellar extinction have shown the importance of understanding *both* the UV and IR properties of interstellar dust grains. (~~Draine and~~ Anderson, 1985; Hecht, 1986). IRAS data have shown variations in 60 and 100 μm emissions presumably due to the presence of IR cirrus, while recent observations in the UV by Fitzpatrick and Massa (1986,1988) have identified components in the UV extinction curve which vary in different star regions. The Draine and Anderson (1985) model connects these results by proposing that different size variations in interstellar grains would cause distinct changes in both the IR emission and the UV extinction.

In order to test this model it is necessary to make observations in well defined locations away from peculiar extinction regions. In the infrared this means looking away from the galactic plane so as to limit non-local sources of IR radiation. In the UV variations in extinction are best understood by studying clusters of B stars since the underlying spectra of these stars are well understood and all of the stars in a given cluster are at the same distance from us (Massa et al., 1985). Thus, any differences observed in the measured extinction will presumably be due to changes in the intervening cirrus dust. If the star clusters are distant than the IR emission should be primarily from dust in front of the clusters.

We have chosen to study two open clusters that are out of the galactic plane and which contain a number of late B and early A stars suitable for UV extinction studies, and whose IRAS data show variations in the 60/100 μm ratio (IC 4665 and NGC 1647) . Based on the Draine and Anderson (1985) model, we would expect to see variations in their UV extinction curves that correlate with the IR cirrus emission. We have obtained low resolution spectra of the cluster members with IUE and we will present results showing the correlation between the IR emission and the UV extinction curve shape, using the parameterization described by Fitzpatrick and Massa (1986, 1988).

Draine, B. and N. Anderson: 1985, Ap.J. **292** 494
Fitzpatrick, E. L. and D. Massa: 1986 Ap. J. **307**, 286
Fitzpatrick, E. L. and D. Massa: 1988 Ap. J. **328**, 734
Hecht, J. H.: 1986 Ap. J. **305**, 817
Massa, D. and E. L. Fitzpatrick: 1985 Ap. J. Suppl. **60**, 305

Dust Emission from High Latitude Cirrus Clouds

Rene J. Laureijs, G. Chlewicki, F.O. Clark, P.R. Wesselius

Laboratory for Space Research and Kapteyn Astronomical Institute
P.O. Box 800, 9700 AV Groningen
The Netherlands

Abstract

In order to study dust emission from grains in the interstellar medium, we analyzed the infrared properties in a number of isolated high latitude dust clouds ($b \geq 10^{\circ}$) which contain no dominant internal heating sources. The clouds are spatially resolved, have a simple geometry and are mapped in the IRAS bands at 12, 25, 60 and 100 μm. For a number of these clouds we obtained extinction data (A_B) from starcounts.

A significant part (30 to 50 %) of the infrared radiation of the clouds in the IRAS wavelength range of 8-130 μm is emitted in the short wavelength bands at 12 and 25 μm. The 60/100 μm ratios for the integrated fluxes of the clouds have a typical value of 0.19 ± 0.05. The 12/100 μm ratios in the sample show a considerable variation and range from 0.03 to 0.14 with an average value of 0.07. We find a ratio $I_\nu(100\ \mu m)/A_B$ between 5 and 8 MJy/mag, which is significantly lower than the ratio found in other studies. From the 12 and 25 μm morphology, which is dramatically different from the morphology at 60 and 100 μm, we infer that the short wavelength emission emerges from the outer parts of the clouds.

Examination of the individual brightness profiles of the clouds shows a nearly constant 60/100 μm brightness ratio as a function of opacity in the cloud. The brightness distribution in several of the most regular clouds shows an initial rise in the ratio towards higher opacities. This observation directly proves that the emission in the two bands cannot be due to a single population of equilibrium grains. The 12/100 μm ratio drops steadily as a function of opacity. Such a relationship must be caused by particles which absorb strongly in the UV. The 100 μm surface brightness remains proportional to blue extinction up to almost 2 magnitudes. The very slow decline of the grain temperature that the relation implies can only be reproduced in models if the particles are allowed to absorb at wavelengths as long as 1 μm.

To model the observations we require particles absorbing mainly at UV wavelengths and emitting at 12 and 25 μm, an emission component around 60 μm due to particles at a high (50 K) temperature, and strongly absorbing grains in the visual and near infrared to account for the linear relationship between $I_\nu(100\ \mu m)$ and A_B.

THE SPATIAL DISTRIBUTION OF INFRARED RADIATION FROM VISIBLE REFLECTION NEBULAE

L. Luan[1], M.W. Werner[2], E. Dwek[3], and K. Sellgren[4]

[1]Astronomy Department, University of California at Berkeley
[2]NASA-Ames Research Center
[3]NASA-Goddard Space Flight Center
[4]Institute for Astronomy, University of Hawaii

I. Introduction

The emission at IRAS 12μm and 25μm bands of reflection nebulae is far in excess of that expected from the longer wavelength equilibrium thermal emission (Sellgren *et al.* 1987). The excess emission in the IRAS 12μm band is a general phenomenon, seen in various components of interstellar medium such as infrared cirrus clouds (Boulanger *et al.* 1985; Weiland *et al.* 1986), reflection nebulae (Castelaz *et al.* 1987; Sellgren *et al.* 1987), HII regions, atomic and molecular clouds (Boulanger and Pérault 1988), and also normal spiral galaxies (Helou 1986). This excess emission has been attributed to ultraviolet-excited fluorescence in polycyclic aromatic hydrocarbon (PAH) molecules (Léger and Puget 1984; Allamandola *et al.* 1985) or to the effect of temperature fluctuations in very small grains (Draine and Anderson 1985; Weiland *et al.* 1986).

We present here results to date of studies of IRAS data on reflection nebulae selected from the van den Bergh (1966) reflection nebula sample and the van den Bergh and Herbst (1975) reflection nebula sample. Detailed scans of flux ratio and color temperature across the nebulae were obtained in order to study the spatial distribution of infrared emission. We have used a model to predict the spatial distribution of infrared emission from dust grains illuminated by a B-type star. We have also used the model to explore the excitation of the IRAS 12μm band emission as a function of stellar temperature. Our model predictions are in good agreement with the analysis of reflection nebulae, illuminated by stars with stellar temperature ranging from 21,000K down to 3,000K, presented at this meeting by Sellgren.

II. Data Processing and Results

We have used co-added intensity images at 12μm, 25μm, 60μm and 100μm obtained from the IRAS data-base. All data have been smoothed to the IRAS 100μm band resolution ($3' \times 5'$) using an algorithm developed by W. Rice at IPAC; this facilitates comparison between different IRAS channels.

For each nebula, we obtained a $2.5° \times 2.5°$ field with the nebula located at the center. The sizes of the nebulae in our study vary from 15 to 45 arcminutes. The large field makes it easier to subtract the global background emission. Zodiacal light and galactic emission were removed by fitting a plane to all bands, based on the fact that the zodiacal light and galactic emission are large scale features. Local background was measured using four $3' \times 3'$ boxes around the nebula. The standard deviation in the background measurements defined a 3-σ threshold to exclude the outermost regions of the nebula, where the excitation contribution from

other sources, e.g. interstellar radiation field and sometimes nearby stars, may be comparable to that of the illuminating starlight. The flux ratios thus obtained reveal the spatial distribution of nebular colors as a function of the intensity of the radiation field of the illuminating star.

Flux ratios obtained for three reflection nebulae are shown in Figure 1a, 1b and 1c, for NGC7023 (illuminating star spectral type B5, apparent visual magnitude m_V=7.39); Merope Nebula (B6, m_V=4.18) and vdB10 (A0, m_V=5.81), respectively. They all show that $F_\nu(60)/F_\nu(100)$ decreases as distance from the star increases. This is expected from emission from large grains which are heated in thermal equilibrium by starlight. On the other hand, the high values of $F_\nu(12)/F_\nu(25)$ even in the outer regions of the nebulae are far in excess of what is expected from equilibrium thermal emission.

The scan line across the Merope Nebula we used was close to that adopted by Castelaz *et al.* (1987), and almost the same answers were obtained. In vdB10, the stellar type of the illuminating star is A0, but $F_\nu(60)/F_\nu(100)$ shows higher values, which imply higher temperature of grains, compared with the Merope nebula which is illuminated by a B star. This may be due to the fact that vdB10 is much less spatially extended than NGC7023 and the Merope Nebula, where dust grains at different distances along the line of sight contribute to the flux. In vdB10, this effect is much smaller, so the flux observed represents more closely the nebular emission from the immediate vicinity of the star. In some cases of our reflection nebulae sample, $F_\nu(12)/F_\nu(25)$ ratio goes down significantly at the position of the star, as seen in vdB10 (Figure 1c). Examples of this phenomenon occur more frequently in reflection nebulae illuminated by OB stars and with smaller angular sizes, where the emission from dust grains in high energy density radiation field is less diluted by the layers of dust grains along the line of sight. The decrease in the $F_\nu(12)/F_\nu(25)$ ratio in regions of high starlight energy density may be attributable to the destruction of 12μm band emitters (Ryter *et al.* 1987; Boulanger *et al.* 1988), and/or to the enhancement of 25μm band equilibrium-emission from large grains as they are hotter in the vicinity of the star.

Simple models in which all geometrical effects are ignored predict that the 60μm/100μm temperature should vary with θ, as $logT_c(60/100) \sim -k\ log\theta$ (k=2/(4+n)). Here θ is the angular offset from the star and n is the exponent of the grain emissivity power law ($Q(\lambda) \sim 1/\lambda^n$). For n between 1 and 2, the commonly adopted range, we expect that the temperature to vary inversely as the .33 to .40 power of the angle. In Figure 3, we show $T_c(60/100)$ *vs* θ for four nebulae. The data are well fit by straight lines with slopes between .25 and .41, consistent with the theoretical expectation. This provides further evidence for equilibrium thermal emission as the explanation of the 60-to-100μm radiation.

III. Model Calculations

The model we used incorporates the conventional MRN (Mathis, Rumpl, and Nordsieck 1977) size distribution which is a graphite and silicate grain mixture with a power law size distribution $n(a)=n_o a^{-3.5}$ as the large grain component, with size range extended to cover 50Å $< a \leq 1\mu$m, together with an enhanced population of

graphite grains with $n(a)=n_o a^{-5.0}$ and $3\text{Å} \leq a \leq 50\text{Å}$, as the small grain component. In the studies of high galactic latitude infrared cirrus clouds (Weiland *et al.* 1986) and reflection nebulae in the Pleiades (Werner *et al.* 1988), this enhanced small grain population was needed to fit the IRAS data. Small silicate grains are not included in the small grain component because the silicate 9.6μm emission feature is not observed in reflection nebulae (Sellgren *et al.* 1985). The mass ratio of small grains ($a \leq 50\text{Å}$), to large grains ($a > 50\text{Å}$), are assume to be 0.5 in all cases. The model predictions of flux ratio $F_\nu(12)/F_\nu(25)$ and $F_\nu(60)/F_\nu(100)$ for dust illuminated by a B1.5 star and visual magnitude $m_V = 7$ are shown in Figure 2. The effect of temperature fluctuations in the very small grain dominates the $F_\nu(12)/F_\nu(25)$ ratio. $F_\nu(60)/F_\nu(100)$ is dominated by the equilibrium emission from the large grains. Also in this model, we predict appreciable values for the ratio $R = \nu F_\nu(12)/\nu F_\nu(100)$ even for stars with effective temperature below 5000K. Figure 4 is the result of calculation of stellar spectral types ranging from B0 to M5, with fixed angular offset $\theta = 3'$ and visual magnitude $m_V = 8$. Thus in this model, the fraction of the stellar energy radiated in the ultraviolet (below 2500Å, for example), falls much more rapidly with spectral type than does the fraction of the absorbed stellar radiation reradiated at 12μm band.

IV. Conclusions

1. The 100μm and 60μm band emission of reflection nebulae show the behavior expected from thermal emission from large dust grains which are in thermal equilibrium, heated by the illuminating stars of the nebulae. On the other hand, for the cooler diffuse interstellar medium, which is heated by the diffuse interstellar radiation field, there is considerable amount of non-equilibrium emission in 60μm band from small grain components (Draine and Anderson 1985).
2. The 12μm and a large part of the 25μm band emission are produced in a non-equilibrium process. The independence of the ratio $F_\nu(12)/F_\nu(25)$ of the intensity of the starlight is expected from temperature fluctuations in very small grains. In some cases, $F_\nu(12)/F_\nu(25)$ decreases significantly in the immediate vicinity of the illuminating star. Careful comparison between analysis of IRAS data and model calculation may help to distinguish if the decrease of $F_\nu(12)/F_\nu(25)$ in the immediate vicinity of the illuminating star is attributable to dust destruction or merely to enhancement of thermal emission at of 25μm.
3. A two-component model of dust grains, including the effect of temperature fluctuations of very small grains, predicts that the excess 12μm emission is readily excited by photons softer than the ultraviolet, in agreement with the data presented at this meeting by Sellgren. This agreement suggest that a broad range of photon energies intending into the visual is capable of exciting the excess 12μm emission.

Acknolegements

We thank Dr. Allamondola for helpful discussions. LL specially thank Professor Heiles for many helpful discussions. This work was supported by IPAC and by NASA-Ames Consortium Agreement NCA2-269.

References

Allamandola, L.J., Tielens, A.G.G.M., and Barker, J.R. 1985, *Ap.J.Lett.*, **315**, L61.

van den Bergh, S. 1966, *Astron.J.*, **71**, 990.

van den Bergh, S., and Herbst, W. 1975, *Astron.J.*, **80**, 208.

Boulanger, F., Baud, B., and van Albada., G.D. 1985, *Astr.Ap.Lett.*, **144**, L93.

Boulanger, F., and Pérault, M. 1988, *Ap.J.*, **330**, 964.

Boulanger,F. *et al.* 1988, *Ap.J.*, to be published.

Castelaz, M.W., Sellgren, K. and Werner, M.W. 1987, *Ap.J.*, **313**, 853.

Draine, B.T., and Anderson, N. 1985, *Ap.J.*, **292**, 494.

Léger, A., and Puget, J.L. 1984, *Astr.Ap.*, **137**, L5.

Ryter, C., Puget, J.L., and Pérault, M. 1987, *Astr.Ap.*, **186**, 312.

Sellgren, K., Allamandola, L.J., Bregman, J.D., Werner, M.W., and Wooden, D.H. 1985, *Ap.J.*, **299**, 416.

Sellgren, K., Castelaz, M.W., Werner, M.W., and Luan, L. 1987, *Proceedings of Third IRAS Conference*, Queen Mary College: to be published.

Weiland, J.L., Blitz, L., Dwek, E., Hauser, M., Magani, L., Rickard, L.J. 1986, *Ap.J.Lett.*, **306**, L101.

FIGURE CAPTIONS

Figure 1a, 1b, 1c. One-dimensional scans of $F_\nu(12)/F_\nu(25)$ and $F_\nu(60)/F_\nu(100)$ through the central stars for three reflection nebulae NGC7023, Merope Nebula and vdB10, respectively.

Figure 2. Two-component model predictions of $F_\nu(12)/F_\nu(25)$ and $F_\nu(60)/F_\nu(100)$ ratios of dust emission, illuminated by a B1.5 star with apparent visual magnitude $m_V = 7$, as a function of angular offset. The relative roles that two grain components play are clearly shown in $F_\nu(12)/F_\nu(25)$ and $F_\nu(60)/F_\nu(100)$ ratios.

Figure 3. One-dimensional color temperature $T_c(60/100)$ scans (derived from the 60μm to 100μm flux ratio) through the central stars for four reflection nebulae. The lines, labelled by the slope k ($T_c(60/100)$ varies as angular offset to the -k power), are least-square fits to the data.

Figure 4. Model prediction of IRAS $\nu F_\nu(12)/\nu F_\nu(100)$ ratio of dust emission at a fixed angular offset from star ($\theta = 3'$), as a function of stellar temperature, assuming mass ratio of very small grains to big grains b=0.5 and visual magnitude $m_V = 8$. Also plotted are fractions of stellar energy in the ultraviolet (below 2500Å) and observational data of reflection nebulae presented at this meeting by Sellgren (the arrows represent the upper limits of the data). This result suggest that a broad range of photon energies extending into the visual are capable of exciting the excess 12μm emission.

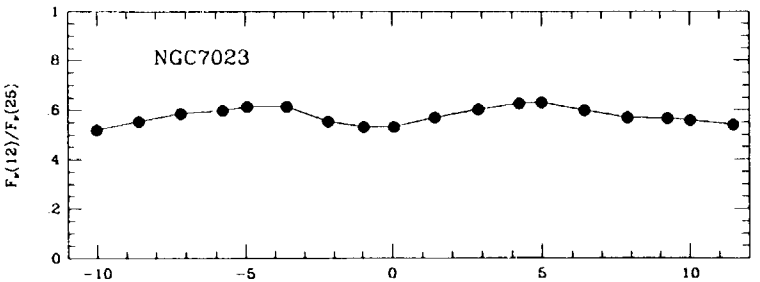

Figure 1a

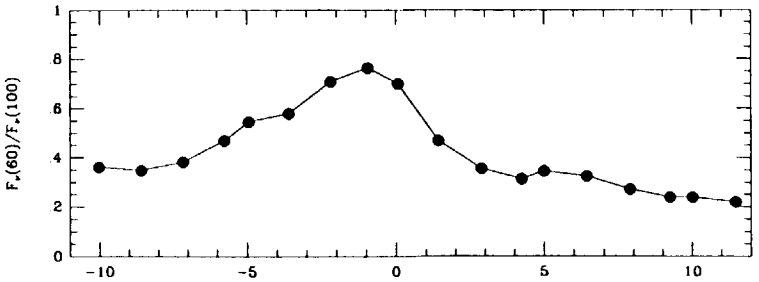

Figure 1a

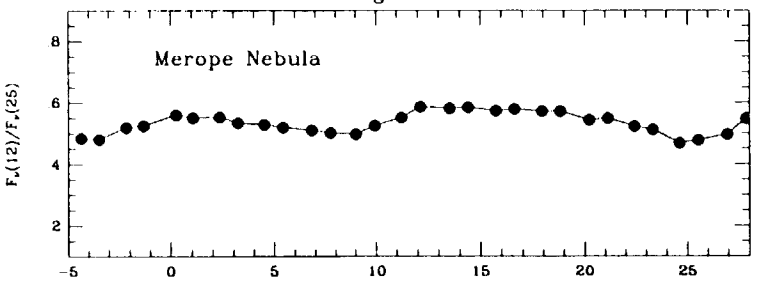

Figure 1b

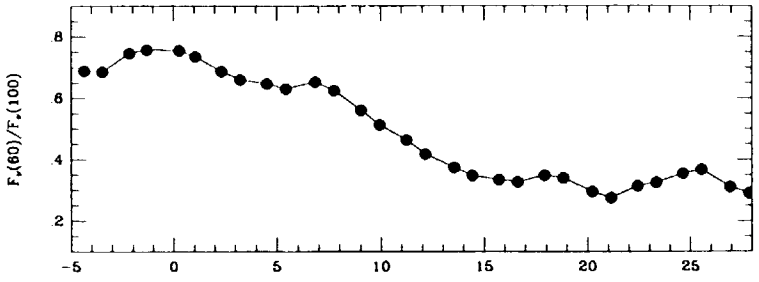

Figure 1b

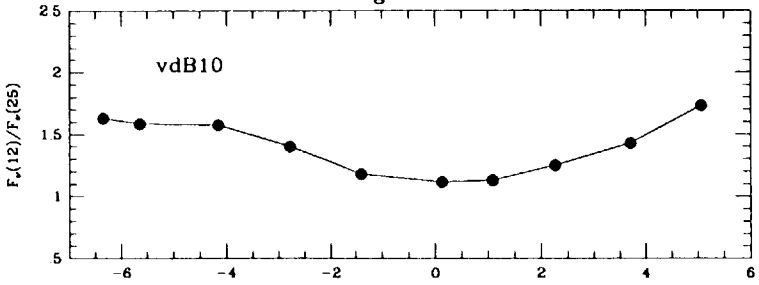

Figure 1c

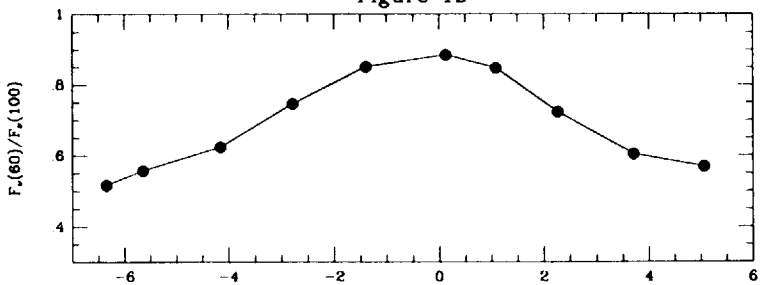

Figure 1c

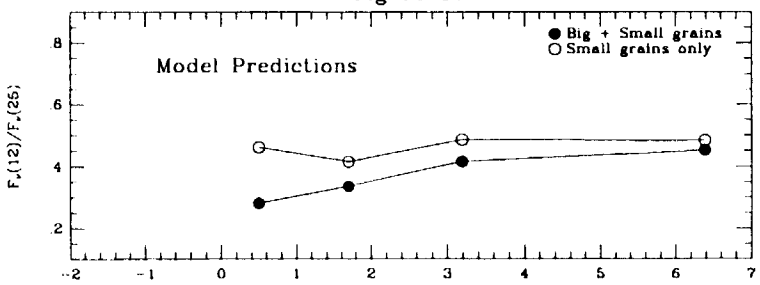

Figure 2

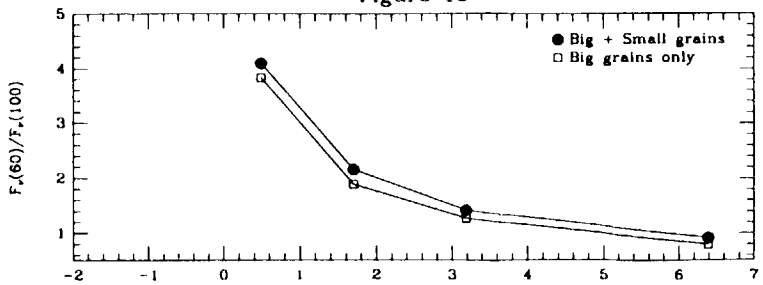

Figure 2

Angular Offset from star (arcmin)

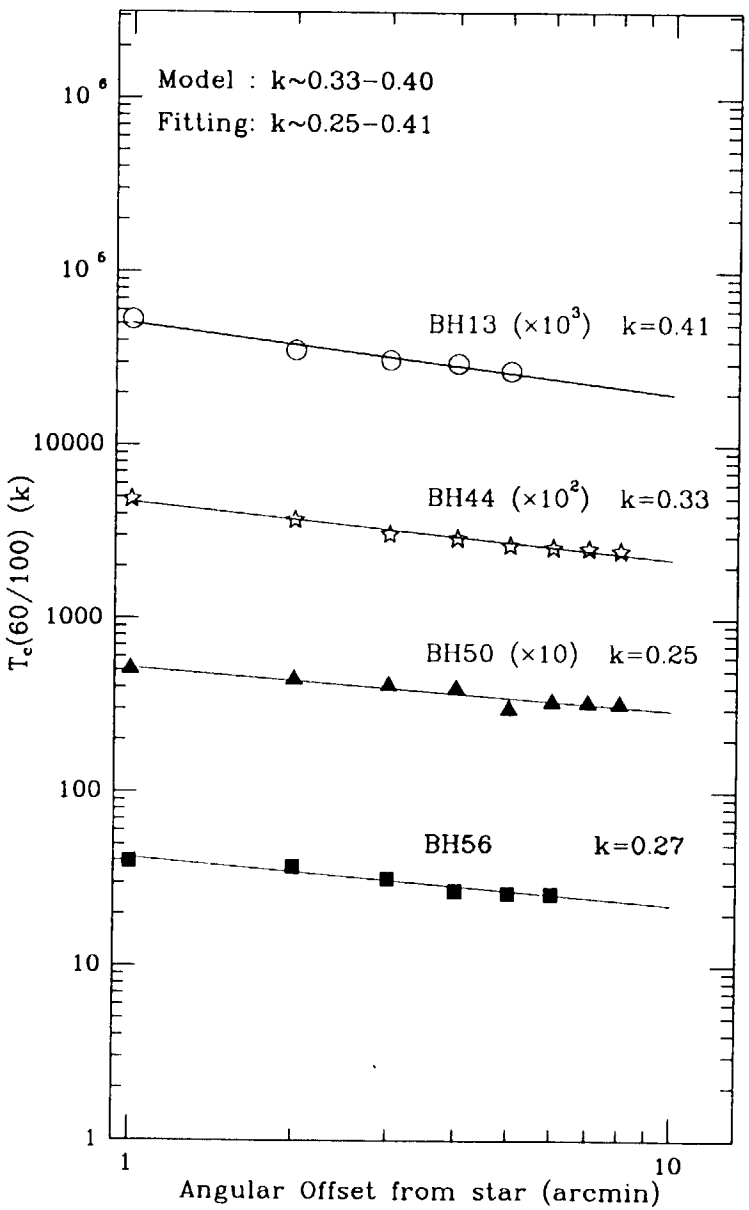

Figure 3

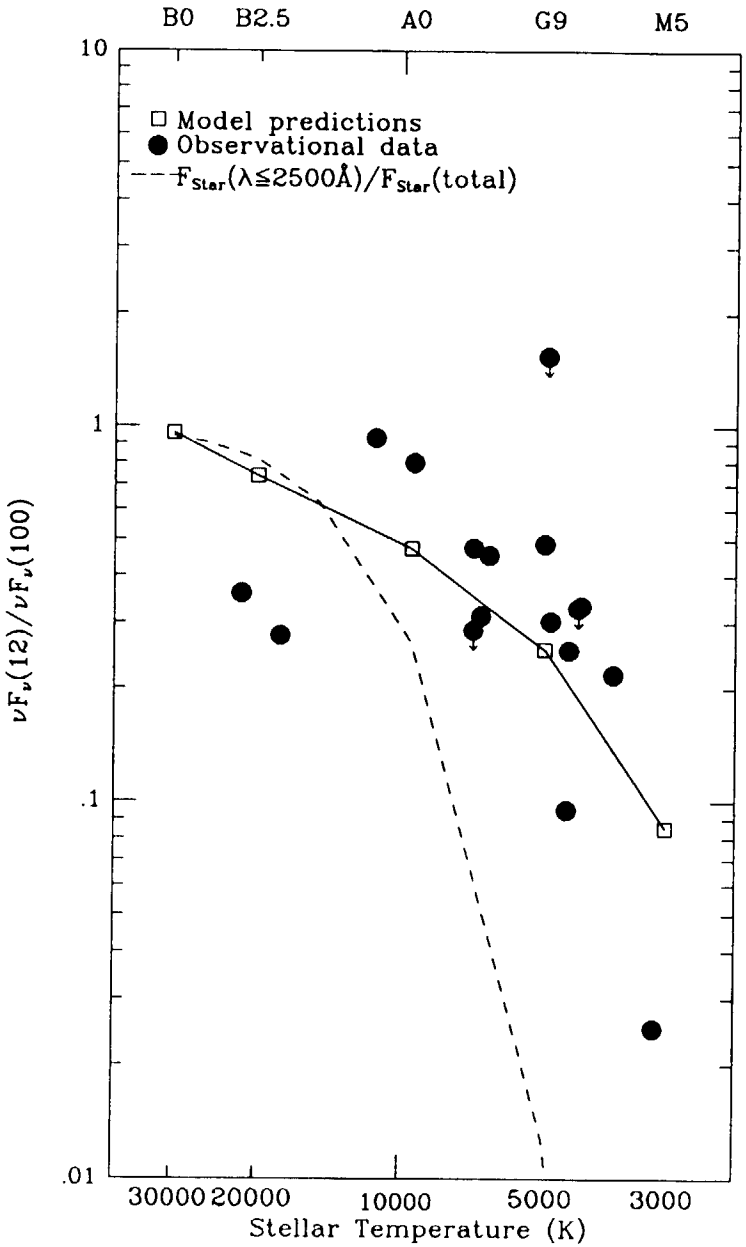

Figure 4

II-C) LABORATORY STUDIES OF CANDIDATE MATERIALS

INFLUENCE OF TEMPERATURE ON THE INFRARED SPECTRUM OF THE CORONENE MOLECULE

J.P. BERNARD*, L. D'HENDECOURT**, A. LEGER**
* Laboratoire de Physique Stellaire et Planetaire, BP n° 10, 91371 Verrières le Buisson cedex, France.
**Groupe de Physique des Solides de l'ENS, Université Paris VII, T23, 4 pl. Jussieu, 75251 Paris cedex 05, France.

ABSTRACT

Laboratory experiments were done to investigate the temperature dependence of the absorption spectrum of the coronene ($C_{24}H_{12}$) molecule in the infra-red. Because of it's compactness, the coronene is believed to be typical of the interstellar medium (ISM) polycyclic aromatic hydrocarbons (PAHs) population (see ref. 1).

The main result is that the spectrum is temperature independent in the explored range, supporting the modelisation of the astronomical infrared bands with emission from PAHs.

In the fine structure of the spectrum, very small temperature correlated fluctuations are observed which are not detected with actual photometric means in the interstellar medium. Qualitative arguments are given to investigate wether this structure is due to coronene or laboratory experiment artefacts.

LABORATORY EXPERIMENT RELEVANCE

In the ISM, the emitted intensity is $I_\lambda(T)=\varepsilon_\lambda(T).B_\lambda(T)$

where
- $\varepsilon_\lambda(T)$ is the emissivity
- $B_\lambda(T)$ is the Planck function.

In the laboratory, it is easier to take absorption spectra.
One measures, for an optically thin sample, the absorptivity :

$$A_\lambda(T) = \frac{J_0 - J_\lambda}{J_0} = 1 - e^{-N\sigma_\lambda(T)} \approx N\sigma_\lambda(T)$$

where
- J_0 and J_λ are the incident and transmitted intensities respectively
- N the column density of the molecule in the sample
- σ_λ the absorption cross section.

From Kirchhoff's law, one can compute the emitted spectrum at the temperature T, knowing $A_\lambda(T)$:

$$I_\lambda(T) = B_\lambda(T)\, A_\lambda(T)$$

which is in agreement with the observed spectra assuming that $A_\lambda(T)$ is mostly independent of the temperature.

With the increase in temperature, the population of the vibrational levels is suspected to change : upper levels (v=2, 3, ...) can be populated and thus, emission from these upper levels is expected (v=1→2, v=2→3, ...)

So, IR bands emitters identification is partly based upon temperature independence of the PAHs spectra which are usually known at room temperature.

EXPERIMENTAL TECHNIQUES

Spectra were recorded in solid phase. This technique had to be used because coronene is a solid up to 470 K so that gaseous phase spectra cannot easily be obtained at intermediate temperatures and require otherwise long path cells for sufficient absorption.

pellets :

Coronene was mechanically mixed in C_sI (to obtain an optical depth $\tau \approx 1$ at 3.3 μm) and pressed to make a pellet.
In the same conditions, we made a blank pellet (without coronene), which spectrum is used as reference to subtract the C_sI component.

cell :

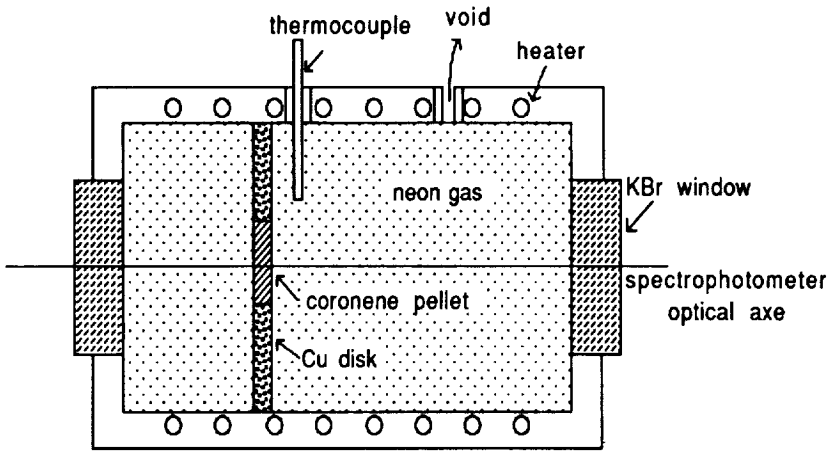

figure n°1 : Schematical view of the warmed cell used to obtain spectra at high temperatures(300-492 K). C_u disk and neon gas ensure a good thermal equilibrium between the heater and the coronene pellet. KB_r is used for the windows because of its transparancy in the IR. Temperature is measured with a thermocouple with an accuracy better than ≈1 K.

We used the warmed cell shown in fig. n°1. The pellet is fixed on a C_u disk and the cell is filled with 10 mbar of an inert gas (neon) to ensure a good thermal equilibrium between the cell and the pellet. Windows are made of KB_r which is transparent in the IR and the temperature is measured by a thermocouple.

Spectrophotometer :

Fourrier transform spectrophotometer of the BOMEM DA3 series.

Experimental parameters :

-Explored range of temperature : 300 K-500 K known with an accuracy better than $\Delta T = 1K$.

-Frequency range : between 400 and 4000 cm^{-1} (25 μm and 2,5 μm) with a $\Delta\nu$=1 cm^{-1} spectral resolution.

RESULTS

Coronene evaporation from the pellet was not detected. For temperatures higher than 500 K, we were limited by coronene evaporation from C_sI matrix. Contamination by residual CO_2 or H_2O is identified in their strong IR activity regions (around 1600 cm^{-1} for H_2O and 670 cm^{-1} for CO_2) and contamination is find to be weak near the features of interest.

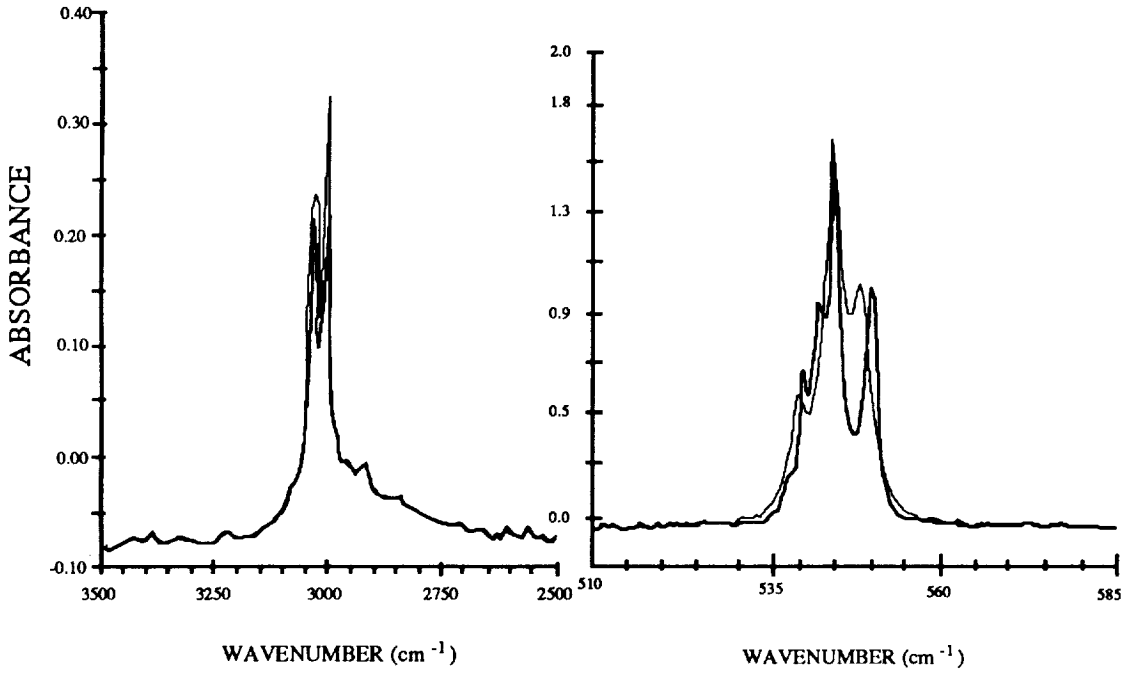

figure n°2: spectra at two extreme temperatures for the 3.3 μm and 18 μm lines.
bold line : spectrum at 298 K
normal line : spectrum at 497 K

Two typical bands are shown on fig. n°2 for different values of the temperature.

In fig. n°3, we have shown the values of the integrated intensities over the emission line and λ_{gc} the line gravity center.

These quantities appear to be constant if one accepts an error of 6,3% and 2,3% for I and λ_{gc} respectively. The error at 3.3 μm is larger because of the incertitude on the baseline due to the shape of the continuum at this wavelength neighborhood.

So, we can conclude that the shape of the spectrum for the coronene between 400 and 4000 cm^{-1} is not sharply temperature dependent in the range 300 K - 500 K.

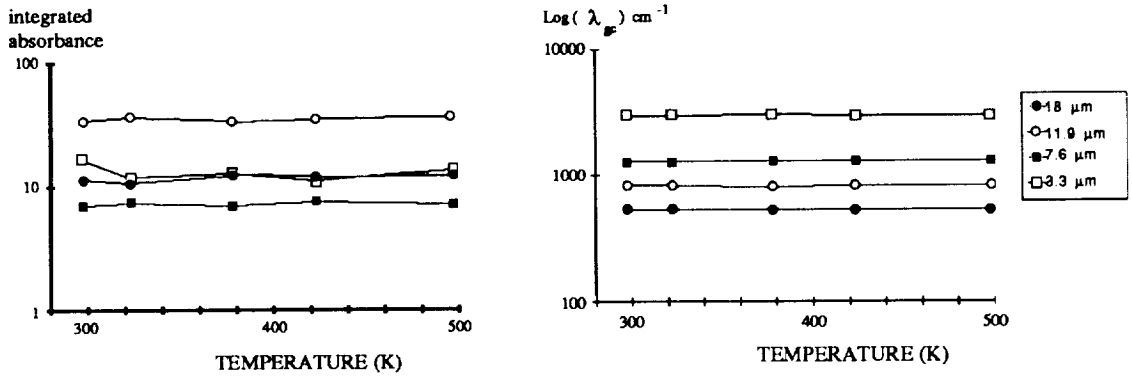

figure n°3 : results of the experiment showing that coronene absorptivity is temperature independent.

- Integrated absorbance for each strong IR absorption line of the coronene spectrum between 400 and 4000 cm^{-1} versus temperature between room temperature and 492 K. Units are arbitrary. These intensities are constant over the explored range of temperature at a 6.3%, 1.4%, 1.8%, 2.5% level for 3.3, 7.6, 11.9 and 18 µm respectively.

- same graphic for λ_{gc} the gravity center of each line in logarithmic scale. Errors are smaller than : 1.7%, 0.1%, 2.3 %, 0.4% for 3.3, 7.6, 11.9 and 18 µm respectively.

IDENTIFICATION OF THE FINE STRUCTURE

Each strong absorption line in the spectrum presents the aspect of fig. n°2. It is composed of several lines (≈ 5 cm^{-1} and ≈ 55 cm^{-1} distant from each other at 11.8 and 3.3 µm respectively). Each individual line of the group is broadened when the temperature is increased. The same behavior is observed for each strong absorption line in the spectrum of the coronene.

We can try to explain the existence of such a fine structure by two different processes :

- An intramolecular one : Fermi coupling with harmonics or mode combinations
- An extra-molecular process : dipole-dipole interaction between coronene molecules.

FERMI COUPLING

The 102 natural modes of the coronene molecule can be grouped under the 12 symmetry types of the D_{6h} symmetry group. The IR active ones are in good agreement with the principal features of the laboratory spectra.

Due to the anharmonicity of the potential, harmonics and combinations (HCs) transitions are allowed with very small probabilities and can interact with strong natural modes lines via Fermi coupling process and become strong enough to be observed in the natural lines vicinity giving rise to such a fine structure.

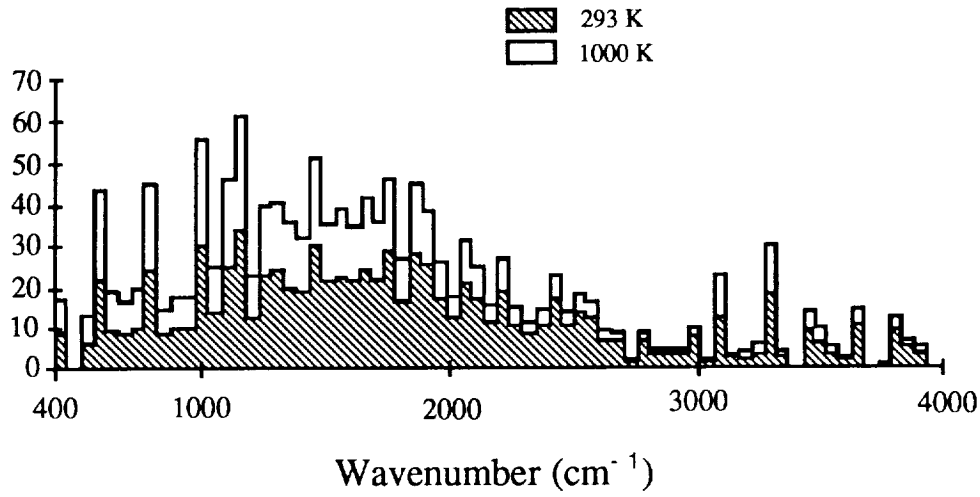

figure n°4 : Histogram in arbitrary units of the density probabilities of the IR active harmonics and mode combinations in the 400 - 4000 cm^{-1} range of wavenumbers for the two extreme temperatures of 300 K and 1000 K.

We have calculated (from the data in ref.2 and 3) the frequencies and symmetry types for all the possible HCs involving two phonons processes issued from the 102 natural modes of the coronene and selected the IR actives ones. A plot of these HCs is presented on fig. n°4. It shows that one cannot explain the continuum observed under the 3.3 μm line in the ISM (a grey body spectrum at ≈ 1000 K), by emission from HC lines. Nevertheless, This probability distribution being a priori symmetry group dependent, it as to be investigated for other PAHs of astrophysical interest.

When plotted near the features of the spectrum, it appears that :

- There is no HC in the vicinity of 850 and 545 cm^{-1} which means that it would be difficult to explain the structure of this features with this process.
- On the other hand, there is 17 HCs in the range 2900-3100 cm^{-1}.

So Fermi coupling can explain the 3.3 μm line doubling but not the 11.8 μm and 18.3 μm features structure because there are no candidates for such a coupling.

DIPOLE-DIPOLE INTERACTION

In our sample, there are still some small pieces of coronene crystal. The structure of this crystal is described in ref. 4. We have verified that the shift in frequency due to dipole-dipole interaction is in agreement with the observed spectra in order of magnitude.

For instance, for the 11.9 μm mode which is attributed to the out of plane bending of the C-H bond, the energy interaction between two bonds due to electrical field created by dipoles is $u = d.E = -d^2/R^3$ leading to a force $F_r = d^2/R^4$ where d is the dipolar moment and R the distance of the bonds. Motion equations assuming small amplitudes, gives the shift $\Delta\omega$ from the unperturbed frequency :

$$\frac{\Delta\omega}{\omega} = (1+\frac{4d^2}{kR^5})^{1/2} - 1 \approx \frac{2d^2}{kR^5}.$$

The shift being very distance dependent, we can only consider the closest bonds couples. Careful examination of the crystal structure shows that these couples are intermolecular ones with R≈1.8 Å involving approximately one half of the C-H bonds in the crystal. With $d \approx 1$ debye, and $k \approx 0.5\ r^2\ 10^5$ dynes/cm where r is the length of an individual C-H bond in Å, one find $\Delta\nu_{11.9\ \mu m} \approx 16\ cm^{-1}$ which is compatible in order of magnitude with the observed shift for this line.

So this effect cannot be ruled out to explain the observed fine structure.

references

(1) LÉGER, A., PUGET, J.L. : 1984, Astron. & Astrophys. 137, L5-L8

(3) CYVIN, B.N., BRUNVOLL, J., CYVIN, S.J., KLAEBOE, P. : 1984, Spec. Lett. 17, 559-567

(2) CYVIN, S.J. : 1982, Journ. Molec. Struct. 79, 423-442

(4) RUSTON, W.R., RÜDORFF, W. : 1947, Bull. Soc. Chim. Belg. 56, 97-105

N91-14933

RAMAN PROPERTIES OF VARIOUS CARBONACEOUS MATERIALS AND THEIR ASTROPHYSICAL IMPLICATIONS

A. Blanco,[*] A. Borghesi,[*] E. Bussoletti,[**] L. Colangeli,[***] S. Fonti,[*] M. Lugara',[****] V. Orofino[*] and G. Scamarcio[****].

[*]Physics Department, University of Lecce, Italy
[**]Istituto Universitario Navale and Osservatorio Astronomico di Capodimonte, Napoli, Italy
[***]ESA, Space Science Department, ESTEC, Noordwijk, The Nederlands
[****]Physics Department, University of Bari, Italy.

It is well known that a large number of celestial objects exhibit, in the range 3-12 μm, a family of emission features called unidentified infrared bands (UIR). They usually appear together and are associated with UV sources (Russel et al., 1977, de Muizon et al., 1986). Recently various authors (Duley and Williams, 1981, Sellgren, 1984, Leger and Puget, 1984, Allamandola et al., 1985) have suggested that these features could be attributed to solid carbonaceous materials. Following this interest, we have performed a systematic analysis of various types of amorphous carbon grains and polycyclic aromatic hydrocarbons (PAH), produced in laboratory. The samples have been studied by transmission techniques (Borghesi et al., 1987, Blanco et al., 1988a) and more recently by Raman spectroscopy (Blanco et al., 1988b).

In fact Raman and IR active vibrational modes are complementary for PAH molecules highly symmetric characterized by an inversion centre of symmetry. Meanwhile Raman and IR spectra can be very similar in presence of a not very symmetric vibrational force field. This last case applies to PAHs clusters and carbon particles which always occur in chain-like structures.

Raman spectra of different types of graphite have been already studied by Tuinstra and Koenig (1973), and Raman techniques have also been applied to the study of atmospheric pollution by carbonaceous materials (Rosen and Novakov, 1978). However a systematic analysis of carbonaceous materials of astrophysical relevance has not yet been carried out.

We present here updating results of Raman measurements performed on several carbonaceous materials, chosen according to their astrophysical interest. The measurements have been made by means of a Jobin-Yvon double monochromator HG2S and standard DC electronic. We used the line at 5145 Å of an Ar^+ laser as excitation source.

Allamandola, L.J., Tielens, A.G.G.M. and Barker, J.R.: 1985, Astrophys. J. (Letters) 290, L25.

Blanco, A., Bussoletti E. and Colangeli L.,: 1988a, Astrophys. J. in press.

Blanco, A., Bussoletti, E., Colangeli L., Fonti S. and Orofino, V.: 1988b, Infrared Phys., in press.

Borghesi, A., Bussoletti, E. and Colangeli L.: 1987, Astrophys. J., 314, 422.

De Muizon, M., Geballe, T.R., D'Hendecourt, L.B. and Baas, F.: 1986, Astrophys. J. (Letters) 306, L105.

Duley, W.W. and Williams, D.A.: 1981, Mon. Not. R. Astr. Soc. 196, 269.

Leger, A. and Puget, J.L.: 1984, Astr. Astrophys. 137, L5.

Rosen, H. and Novakov, T.: 1978, Atmos. Envirom. 12, 923.

Russell, R.W., Soifer, B.T. and Willner, S.P.: 1977, Astrophys. J. (Letters) 217, L149.

Tuinstra, F. and Koenig, J.L.: 1973, J. Chemical Phys. 53, 1126.

Sellgren, K.: 1984, Astrophys. J. 277, 623.

INFRARED FLUORESCENCE FROM PAHs IN THE LABORATORY

Isabelle Cherchneff and John R. Barker
Department of Atmospheric, Oceanic and Space sciences
Space Physics Research Laboratory
The University of Michigan, Ann Arbor, MI 48109-2143

1 - Introduction

Several celestial objects, including UV rich regions of planetary and reflection nebulae, stars, HII regions and extragalactic sources, are characterized by the unidentified infrared emission bands (UIR bands). This family consists of features at 3050 cm^{-1} (3.3μm), 2950 cm^{-1}(3.4μm), 1615 cm^{-1}(6.2μm), 1310 cm^{-1} (7.7μm), 1150 cm^{-1} (8.6μm) and 85 cm^{-1} (11.8μm), with weaker signatures at 1785 cm^{-1} and 1430 cm^{-1}, and was first detected in the planetary nebula NGC 7027 (Gillet et al., 1973; Merrill et al., 1975; Russel et al., 1977). The features have typical widths of 3% to 10% of their wavelength (Allamandola, 1984; Willner, 1984).

A few years ago, it was proposed that polycyclic aromatic hydrocarbon species (PAHs) are responsible for most of the UIR bands. (Duley and Williams, 1981; Lèger and Puget, 1984; Allamandola, Tielens and Barker, 1985). This hypothesis is based on a spectroscopic analysis of the observed features. The 3050 cm^{-1} band for example is known to be characteristic of the aromatic stretching vibration in PAHs (Bellamy, 1968), as is the 6.2 μm signature.

Comparisons of observed infrared spectra with laboratory absorption spectra of PAHs support the PAH hypothesis. (Lèger and d' Hendecourt, 1987; Allamandola, Tielens and Barker, 1987). An example spectrum is represented in Fig 1, where the Orion Bar 3.3 micron spectrum is compared with the absorption frequencies of the PAHs Chrysene ($C_{18}H_{12}$), Pyrene ($C_{16}H_{10}$) and Coronene ($C_{24}H_{12}$).

This paper presents the laser-excited 3.3 μm emission spectrum from a gas phase PAH (azulene, $C_{10}H_8$). The infrared fluorescence theory (IRF) is briefly explained, followed by a description of the experimental apparatus, a report of the results and discussion.

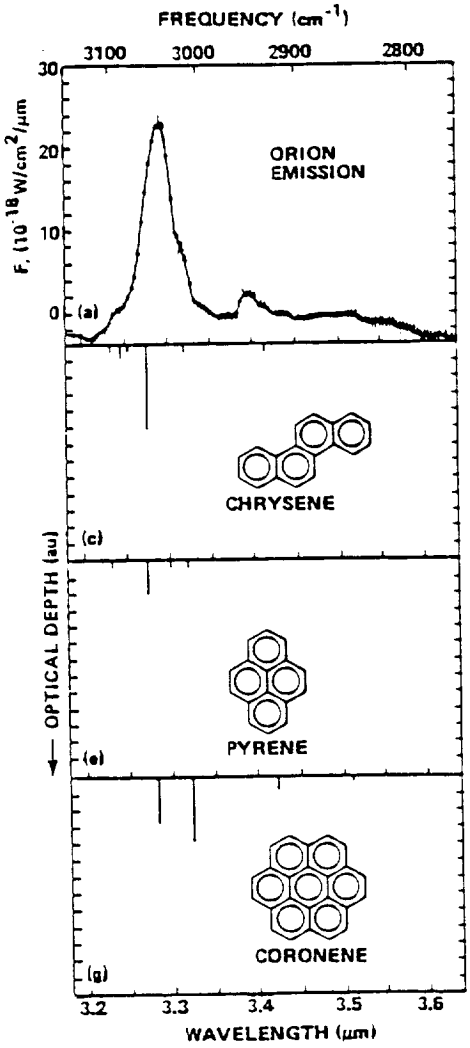

Fig 1 : The 3 micron emission spectrum from the Orion Bar compared with the absorption spectra of chrysene, pyrene and coronene.

2 - Infrared Fluorescence Theory

The IRF emission due to a $\Delta v = 1$ vibrational transition in a polyatomic molecule of total vibrational energy E can be calculated from the basic expression for a single oscillator (Herzberg, 1968; Durana and MacDonald, 1976; Rossi et al., 1983)

$$I(E,i,v) = N_v(E)\ h\nu_i\ A_i^{v,v-1}$$

where ν_i is the frequency of the emitting mode, $A_i^{v,v-1}$ is the Einstein coefficient for the $v \rightarrow v-1$ transition (equal to $v\ A_i^{1,0}$ in the harmonic oscillator approximation), and $N_v(E)$ is the number of molecules with total energy E and v quanta in the i^{th} vibrational mode.

Under the ergodic assumption, the energy is distributed statistically among the accessible vibrational states of the molecule, and

$$N_v(E) = N(E) \frac{\rho_{s-1}(E - v h\nu_i)}{\rho_s(E)}$$

where N(E) is the total number of excited molecules, s is the number of oscillators, $\rho_s(E)$ is the total density of states with vibrational energy E, and $\rho_{s-1}(E-h\nu_i)$ is the density of states, omitting the emitting mode i and its vibrational energy content. Hence the theoretical IRF intensity for a particular $\Delta v=1$ transition and for the emitting mode i

$$(1) \qquad I(E,i,v) = N(E)\ h\nu_i\ v\ A_i^{1,0} \frac{\rho_{s-1}(E - v h\nu_i)}{\rho_s(E)}$$

The reliability of the IRF theory recently has been tested by experimental data that showed excellent agreement with theoretical predictions (Shi, Bernfeld and Barker, 1988).

Emission spectra from PAHs can be predicted using equation 1 and an assumed Lorentzian profile (30 cm^{-1} width) as shown in Fig 2 where the calculated emission spectrum is for a C-H stretch mode (3050 cm^{-1}) of chrysene as a function of the vibrational energy content of the molecule (Barker, Allamandola, and Tielens, 1987). The main peak corresponds to the transition between the vibrational states v=1 and v=0. The second peak represents the transition v=2→ 1; the shift is due to the anharmonicity of the vibrational potential of the molecule. A more realistic simulation would include the other C-H stretch modes, which may have slightly different frequencies. All PAH species would exhibit a similar spectrum, but the peak locations are peculiar to each molecule and will be somewhat shifted.

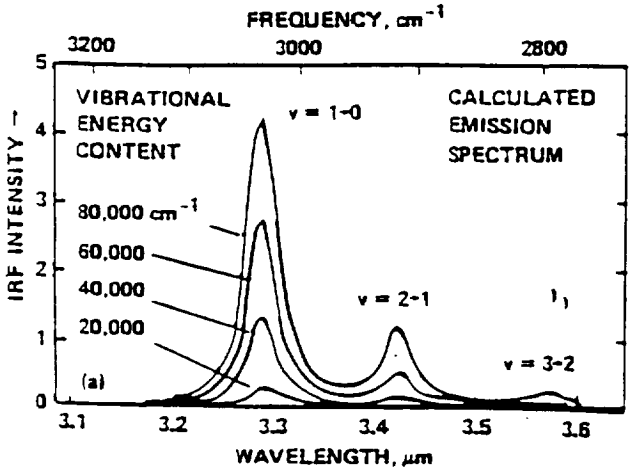

Fig 2 : The calculated emission spectrum for chrysene in the C-H stretching region as a function of vibrational energy content.

3 - Experimental

Azulene ($C_{10}H_8$) is a very convenient laboratory subject because its rapid interconversion (IC) processes can be exploited in order to prepare vibrationally excited molecules in the electronic ground state. In this experiment, a 308 nm (32000 cm^{-1}) UV laser is used to excite azulene to its S_2 excited electronic state and subsequent IC to high vibrational levels of the electronic ground state takes place in ~1.4 ns, a lifetime much shorter than the interval between collisions. This method thus provides an ensemble of vibrationally excited molecules which emit infrared light via fluorescence.

The present experiment employs both IRF and optoacoustic techniques (Shi, Bernfeld and Barker, 1988). The first method measures the IRF emission intensity while the second one determines the number of vibrationally excited molecules. The IRF emission per azulene molecule can be deduced from the ratio of these two measurements.

The experimental apparatus is presented schematically in Fig 3. The fluorescence cell is fitted with Suprasil fused silica windows for the laser beam. The fluorescence is viewed through a sapphire window by a 77 K InSb photovoltaic detector (5 μs time-response) and matched preamplifier. A spherical gold mirror with a 5 cm focal length is placed inside the cell so that the detector matches the mirror center of curvature. The detector image is then located on the detector itself, which views a 77 K background. This method improves the fluorescence signal by collecting more light and by reducing the background noise. The azulene vapor pressure in both cells is regulated by maintaining the azulene reservoirs at fixed temperature with a temperature-regulated bath

The fluorescence emisson is isolated by a 2.5-5 μm bandpass filter (BPF) and wavelength resolved by a CVF filter maintained at 77 K. The resolution of the system is defined by an ajustable slit placed between the BPF and the CVF. A 40 cm^{-1} resolution was chosen in this experiment. The sensitivity of the instrument is essentially constant over the wavelength range of interest. Both the IRF emission and the optoacoustic signal are simultaneously acquired and averaged using a digital oscilloscope. The data are transfered to a computer and analysed using non-linear least squares.

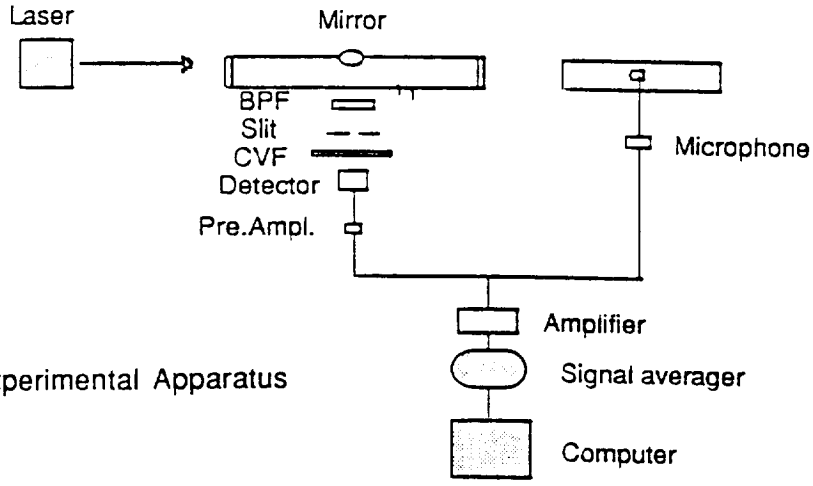

Fig 3 : Experimental Apparatus

4 - Results and discussion

A typical fluorescence decay signal is shown in Fig 4. The decay is due to collisional deactivation and is fitted by an exponential function. The IRF intensity at t=0 is then extrapolated from the intensity at t= 5μs, the time response of the system.

A preliminary IRF emission spectrum is presented in Fig 5. This spectrum resembles the observed IR spectrum, although azulene, used in this experiment for its photophysical properties, is probably not responsible for the IR emission in the interstellar medium, where a typical PAH size would range between 20 and 50 carbon atoms (Allamandola, Tielens and Barker, 1987). The peak position in Fig 5 is 3075 ± 20 cm^{-1}, which corresponds to the $v=1 \longrightarrow 0$ C-H stretching transition frequency. The measured spectrum is for all azulene C-H stretch modes, which have frequencies between 3020 cm^{-1} and 3080 cm^{-1}(Chao and Khanna, 1977). The asymmetry in the spectrum may result from the convolution of the $\Delta v=1-0$ and $\Delta v=2-1$ with the bandpass of the system, which is about 40 cm^{-1}. Thus the $v=2 \longrightarrow 1$ transition can not be resolved under these conditions. Nevertheless, the preliminary results presented in this paper are consitent with the hypothesis that PAHs are responsible for the UIR bands emission.

Experiments now underway are using a higher resolution (28 cm^{-1}) and should provide a better-resolved IR fluorescence spectrum from azulene. Future work will investigate other PAHs, both in cells and in cold molecular beam expansions, which mimic temperatures found in the interstellar medium.

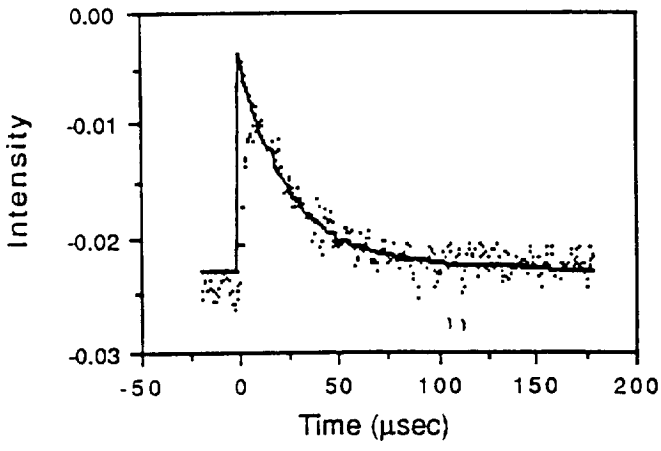

Fig 4 : IRF decay curve for azulene.

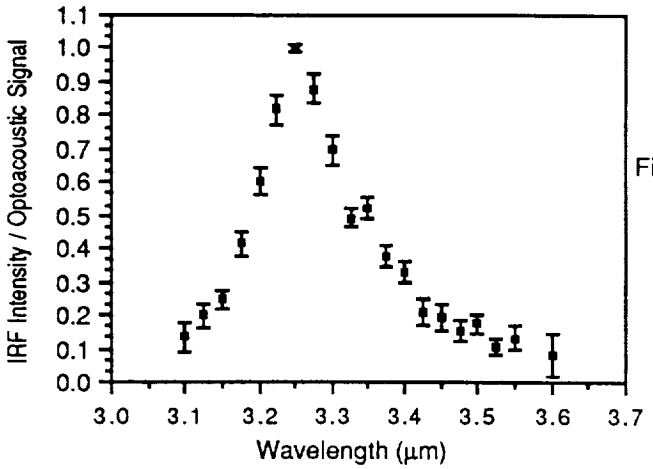

Fig 5 : IRF emission spectrum for azulene

Acknowledgements : This work is funded, in part, by the National Science Fundation, Gallactic Astronomy Program.

References :

Allamandola, L.J.: 1984, in *Galactic and Extragalactic Infrared Spectroscopy*, eds. M.F Kessler, J.P. Phillips, Reidel, Dordrecht

Allamandola, L.J., Tielens, A.G.G.M and Barker, J.R.: 1985, Ap. J. Letters 290, L25

Allamandola, L.J., Tielens, A.G.G.M and Barker, J.R.: 1987, in *Interstellar Process*, eds. D.J. Hollenbach and H.A. Thronson, Jr, Reidel, Dordrecht

Barker, J.R., Allamandola, L.J. and Tielens, A.G.G.M.: 1987, Ap. J. Letters 315, L61

Bellamy, L.J., 1958, The Infrared Spectra of Complex organic Molecules, eds. J. Wiley and Sons, New York

Chao R.S and Khanna, R.K: 1977, Spectroschimica Acta 33A, 53

Durana, J.F. and MacDonald, J.D.: 1977, J. Chem. Phys. 64, 2518

Duley, W.W. and Williams, D.A.: 1981, M.N.R.A.S, 196, 269

Gillett, F.C., Forrest, W.J. and Merrill, K.M.: 1973, Ap. J. 183, 87

d' Hendecourt L.B. and Lèger, A.: 1987, in *Planetary and Proto-Planetary Nebulae : from IRAS to ISO*, 203-220, eds. Preite martinez, A., Reidel

Herzberg, G.H.: 1968, Infrared and raman Spectra of plyatomic molecules, eds. D. van Nostrand Co., Princeton

Lèger, A. and Puget, J.L.: 1984, Astronomy and Astrophysics 137, L5

Merrill, K.M., Soifer, B.T. and Russel, R.W.: 1975, Ap. J. Letters 200, L37

Rossi M.J., Pladziewicz, J.R. and Barker, J.R.: 1983, J. Chem. Phys. 78, 6695

Russel, R.W. Soifer, B.T. and Willner, S.P.: 1977, Ap. J. Letters 217, L149

Shi, J., Bernfeld, D. and Barker, J.R.: 1988, J. Chem. Phys. 88, 6211

Willner S.P.: 1984, in *Galactic and Extragalactic Infrared Spectroscopy*, eds. M.F. Kessler, J.P. Phillips, Reidel, Dordrecht

Si_3N_4 EMISSIVITY AND THE UNIDENTIFIED INFRARED BANDS

R. W. RUSSELL, M. A. CHATELAIN, J. H. HECHT
Space Sciences Laboratory, The Aerospace Corporation,
Los Angeles, California 90009 USA
and
J. R. STEPHENS
Los Alamos National Laboratory
Los Alamos, New Mexico 87545

INTRODUCTION

Infrared spectroscopy of warm (about 150-750 K), dusty astronomical sources has revealed a structured emission spectrum which can be diagnostic of the composition, temperature, and in some cases, even size and shape of the grains giving rise to the observed emission. The successful identifications of silicate emission in oxygen-rich objects and SiC in carbon-rich objects are two examples of this type of analysis. Cometary spectra at moderate resolution (e.g. Merrill, 1974, and Campins and Tokunaga 1987) have similarly revealed silicate emission, tying together interstellar and interplanetary dust.

However, Goebel (1987 and 1988) has pointed out that some astronomical sources appear to contain a different type of dust which results in a qualitatively different spectral shape in the 8-13 micron region. Furthermore, the association of the unidentified infrared (UIR) bands at 3.3/3.4, 6.2, 7.7/7.9, 8.6, and 11.3 microns with regions of thermal dust emission and regions of reflection nebulosity has led several authors to attempt to relate that emission to structure in the wavelength dependent emissivity curve of a grain or molecular cluster material. Gas phase species seem to be unlikely, in view of the constancy of central wavelength of the features in such a variety of source types and environments. It is crucial that the wavelength dependence of the emissivity (not extinction, which usually includes significant scattering effects that can qualitatively change the appearance of the spectrum) of proposed dust components be measured in the laboratory over the entire range of wavelengths available for the celestial sources before a positive identification can be made. This poster presents part of an ongoing effort in our laboratory to obtain such data for proposed or likely celestial dust constituents.

THE SAMPLES

Goebel (1987 and 1988) suggested that silicon nitride might be a viable candidate for at least one component of celestial grains, based on the wavelength and the width of the bands at 9-12 microns in the spectra of the celestial sources Nova Aql 1982 and NGC 6572 and the absorption shape in the laboratory spectra of this material. This poster reports the results of an emissivity study of both crystalline and amorphous samples of silicon nitride prepared at the Los Alamos National Laboratory.

The samples were prepared by G. J. Vogt by injecting SiH_4 and NH_3 into a thermal RF coupled plasma which dissociates them. The Si_3N_4 condenses in the cooler plasma flame and is collected in a cyclone separator for analysis. Electron diffraction patterns obtained in the Material Sciences Lab at Aerospace showed a

mix of alpha and beta silicon nitride with some silicon particles in the crystalline sample. The amorphous sample, as expected, gave no diffraction peaks. Energy dispersive analysis of x-rays (EDAX) showed the crystalline sample to be all Si and N with a ratio of about 2:3 to 1:1. The results for the amorphous sample were consistent with this range, but might possibly be consistent with up to 5 % oxygen. No silicon oxide or silicate electron diffraction peaks were seen, however.

The samples were spread thinly on copper blocks and studied in the same vacuum emissivity chamber (see Figure 1) used in earlier studies of interstellar and cometary dust (Stephens and Russell, 1979, Cohen et al., 1980, and Hecht et al., 1986). The spectra were obtained with a circular variable filter (CVF) wheel spectrometer with a resolving power of about 50. The spectra were sampled at about two points per spectral resolution element to better define the structure in the emissivity curve. The samples were heated to 350 K for these studies, although we do not expect the emissivity to exhibit much temperature dependence in this regime. Spectra of black felt and 3M black velvet were used as blackbody references.

DISCUSSION

Figures 2 and 3 present the emissivity curves for amorphous and crystalline silicon nitride. Three points should be emphasized regarding the application of these data to the task of identifying the celestial grain components responsible for the UIR bands and the emission features seen in the spectra of Nova Aql 1982 and the planetary nebula NGC 6572. First, the spectra of the amorphous and crystalline samples of silicon nitride are remarkably similar, in direct contrast with the behavior of the spectra of amorphous and crystalline silicates. The only significant difference seen here is that the amorphous silicon nitride spectrum exhibits a long wavelength tail not present in the spectrum of the crystalline emission. Note that although the EDAX data suggested that only the amorphous sample might have had some oxygen (less than or about 5 %) and thus possibly some silicon oxide which could contribute to a 9 micron peak, that peak appears quite the same in the spectra of both samples. Also, the 12.5 micron silicon oxide peak is absent from both spectra, strengthening the contention that silicon oxide is not present in any significant amount.

Secondly, the ratio of the 9 micron to 11 micron emissivity is **much** higher here than that seen in published absorption spectra (e.g., Nyquist and Kagel, 1971). This effect could be due to particle size effects or the scattering contribution in the extinction data. This makes the spectra reported here look quite different from the Nova spectrum (Gehrz et al. 1984), which shows much less emissivity at 9 microns than at either 11 or 12 microns. The spectrum of NGC 6572 (Willner et al. 1979) exhibits an even higher ratio of 11 to 9 micron fluxes, but the temperature of the grains is much more difficult to determine making it hard to derive the ratio of emissivities. Thus, no strong quantitative statement can be made, but qualitatively the slopes in the lab sample spectra are very different from the slopes in these two astronomical spectra.

Third, the rise toward 3 microns needs to be investigated over a wider wavelength range and at a higher temperature to permit a valid comparison of the silicon nitride emission with the 3.3 micron UIR emission. Again, the shape of the spectrum at these wavelengths in the extinction data is usually dominated by a

scattering component, and a peak such as this would be hard to detect against the scattering continuum.

SUMMARY

The spectra shown here make it appear unlikely that silicon nitride can be identified as the source of the 8-13 micron emission in either NGC 6572 or Nova Aql 1982. The similarity between the general wavelength and shape of the 10 micron emission from some silicates and that from the two forms of silicon nitride reported here could allow a mix of cosmic grains which includes some silicon nitride if only the 8-13 micron data are considered.

A feature is seen near 3.3 microns in the spectra of silicon nitride which requires further study. It might help explain the UIR emission at this wavelength. However, if the spectral shape at shorter wavelengths is different from that seen in the astronomical data, it would permit strong upper limits on the amount of silicon nitride present in spite of the potential ambiguity due to the similarity between the silicate and silicon nitride 10 micron features.

ACKNOWLEDGEMENTS

We thank G. J. Vogt for preparing the samples at LANL. Joe Uht and Paul Adams made essential, timely sample characterizations at Aerospace for which we are grateful. This work was supported by the Aerospace Sponsored Research program in the Space Sciences Laboratory.

Campins, H. and A. Tokunaga: 1987, "Infrared Observations of the Dust Coma" in *Infrared Observations of Comets Halley and Wilson and Properties of the Grains*, ed. by M.S. Hanner, (NASA Conference Publication), in press, p. 1.

Cohen, N. L., J. F. McCarthy, R. W. Russell, and J. R. Stephens: 1980, B.A.A.S., **11**, 610.

Gehrz, R. D., E. P. Ney, G. L. Grasdalen, J. A. Hackwell, and H. A. Thronson, Jr.: 1984, Ap. J., **281**, 303.

Goebel, J. H.: 1987, B.A.A.S., **18**, 1003.

Goebel, J. H.: 1988, preprint.

Hecht, J.H., R. W. Russell, J. R. Stephens, P. R. Grieve: 1986, Ap. J., **309**, 90.

Merrill, K.M. 1974, Icarus, **23**, 566.

Nyquist, R.A. and R. O. Kagel: 1971, *Infrared Spectra of Inorganic Compounds*, (Academic Press, Inc., Orlando, Florida), p. 114.

Stephens, J.R. and R. W. Russell: 1979, Ap. J., **228**, 780.

Willner, S.P., B. Jones, R. C. Puetter, R. W. Russell, and B. T. Soifer: 1979, Ap.J., **234**, 496.

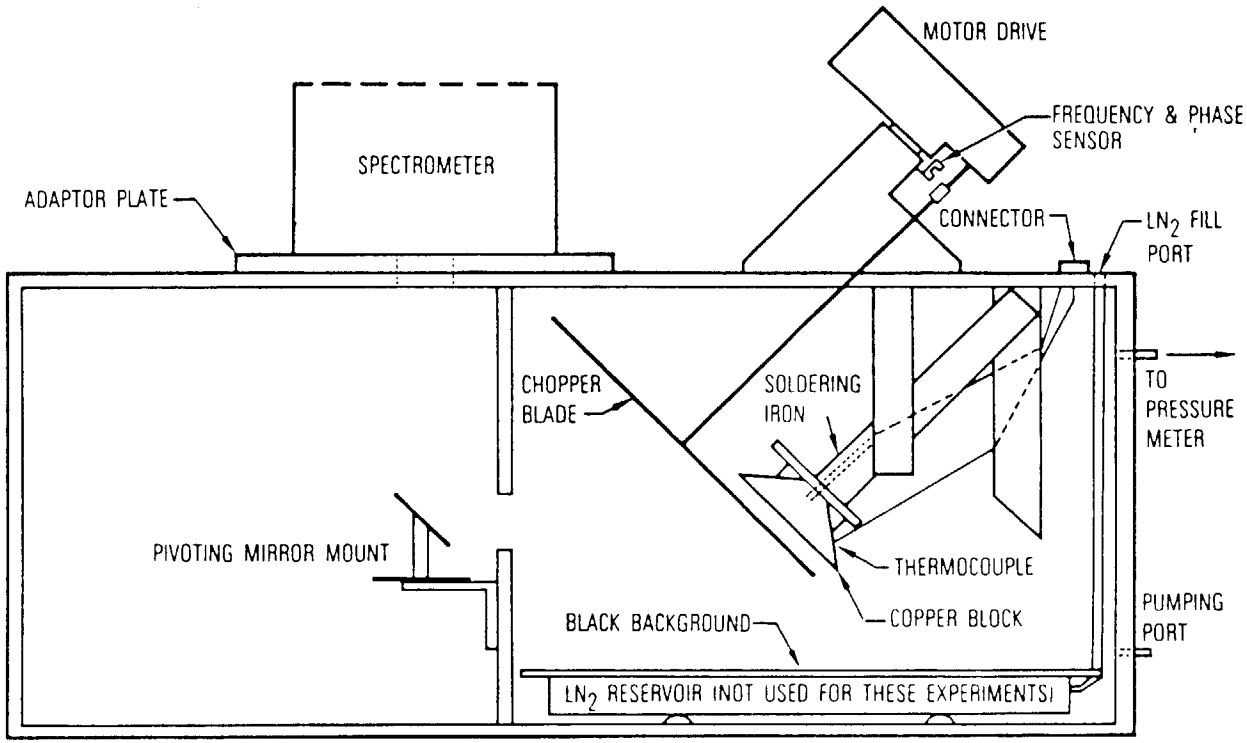

Figure 1. A top schematic view of the emissivity chamber used to make the emission measurements.

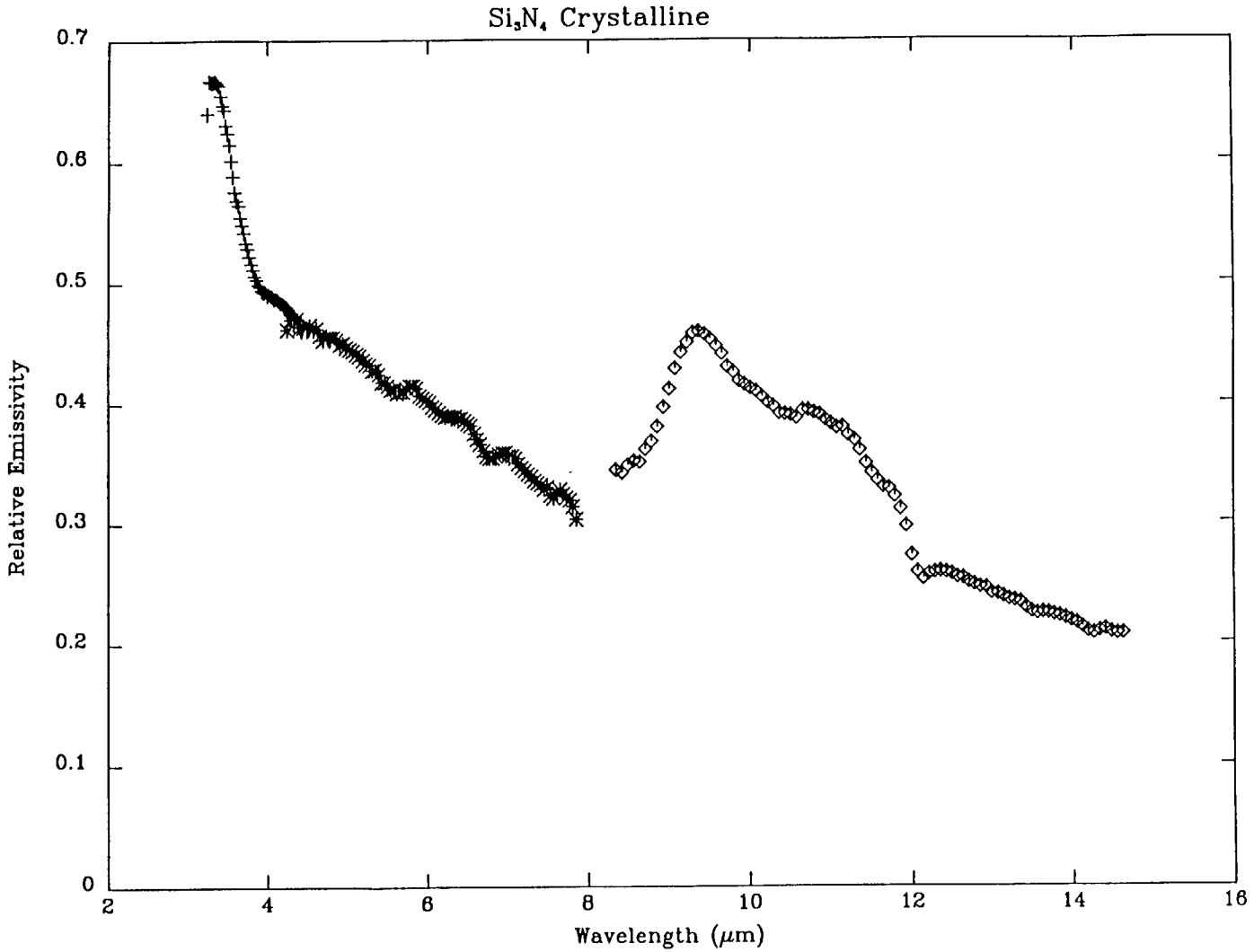

Figure 2. Relative emissivity of crystalline silicon nitride.

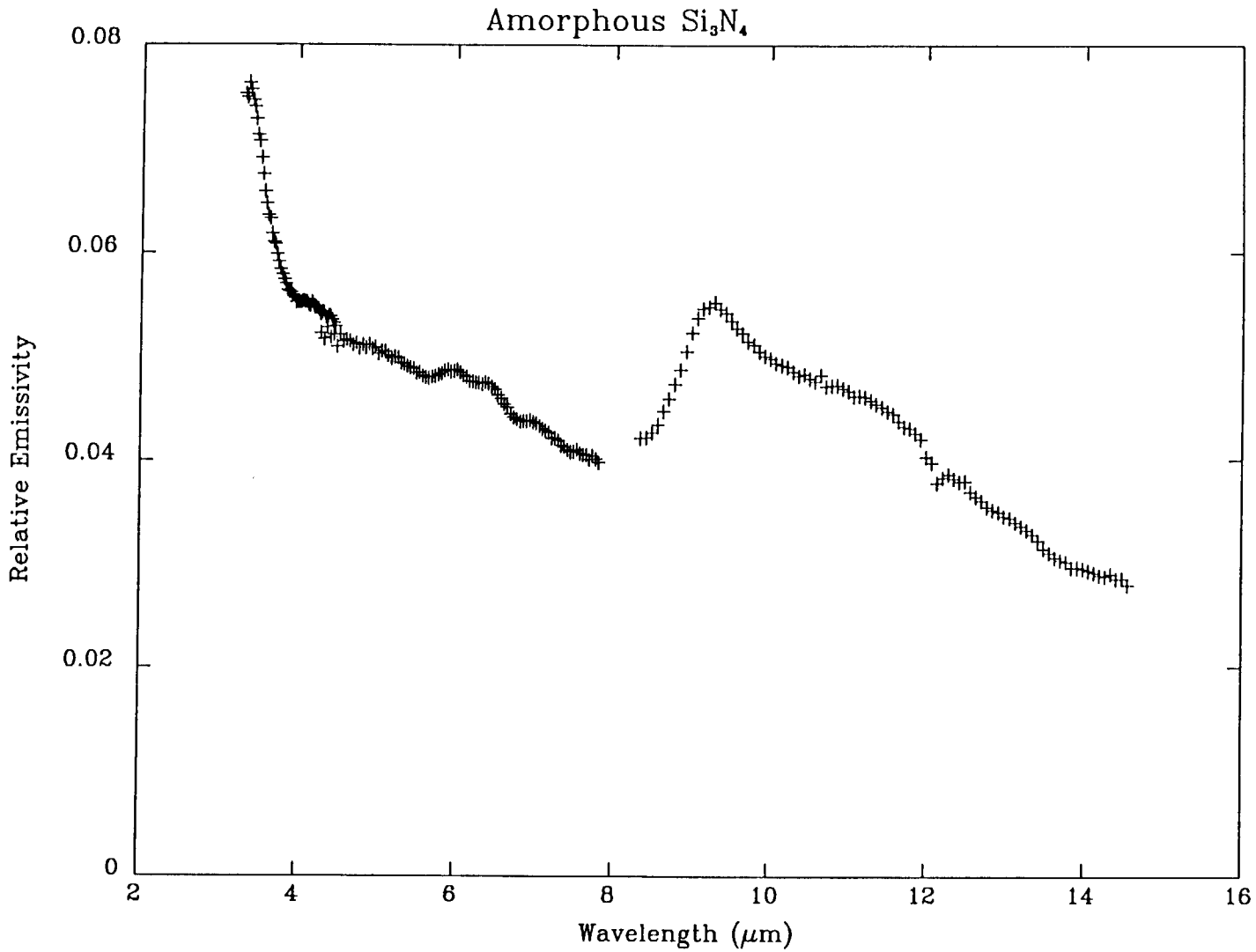

Figure 3. Relative emissivity of amorphous silicon nitride.

PAH IN THE LABORATORY AND INTERSTELLAR SPACE

Thomas J. Wdowiak, Gregory C. Flickinger, and David A. Boyd
Physics Department, University of Alabama at Birmingham,
UAB Station, Birmingham, Alabama 35294 USA

ABSTRACT. The hypothesis that polycyclic aromatic hydrocarbons (PAH) are a constituent of the interstellar medium, and a source of the infrared emission bands at 3.3, 6.2, 7.7, 8.6, and 11.3 microns is being studied using PAH containing acid insoluble residue of the Orgueil CI meteorite and coal tar. FTIR spectra of Orgueil PAH material that has undergone thermal treatment, and a solvent insoluble fraction of coal tar that has been exposed to hydrogen plasma are presented. The ultraviolet excited luminescence spectrum of a solvent soluble coal tar film is also shown. Comparison of the laboratory measurements with observations appears to support the interstellar PAH hypothesis, and demonstrates the process of dehydrogenation expected to take place in the interstellar medium.

The presence of polycyclic aromatic hydrocarbon molecules (PAH) in the interstellar medium is inferred from the observation of infrared emission bands at 3.3, 6.2, 7.7, 8.6, and 11.3 microns. (for a review of the field see "Polycyclic Aromatic Hydrocarbons and Astrophysics:, ed. A. Leger, L. d'Hendecourt, and N. Boccara, D. Reidel, 1987). Demonstration that this assignment is correct is important because it would mean PAH is a major form of interstellar carbon and that PAH molecules could play a role in charge exchange reactions leading to chemical pathways radically different from what has been considered previously. The latter situation leads to new estimates of abundances of interstellar molecules, such as formaldehyde in dark clouds, that are orders of magnitude greater than previous results. (Lepp and Dalgarno 1988) The difficulty in making definite the PAH assignment is that the kinds of PAH samples generally available to the experimenter from supply houses and laboratory sources are probably not of the type considered to exist in the interstellar medium. The 11.3 micron emission band mandates PAH molecules that have single hydrogen atoms per aromatic ring (Bellamy 1975, Cohen, Tielens, and Allamandola 1985), while most laboratory samples have 2, 3, or 4 hydrogen atoms per ring. Also, interstellar PAH molecules must be composed of >20 carbon atoms in order to survive the interstellar ultraviolet radiation field (Leger and Puget 1984). Laboratory experiments with PAH candidates having >20 carbon atoms are difficult because of low solubility and low volatility. While available pure PAH samples are useful for exploring basic mechanisms, we have turned our attention toward PAH in carbonaceous chondrites and the PAH products of the coking process, pyrolysis, plasma chemistry, and combustion with the intent of determining if the PAH assignment for the UIR bands is reasonable.

The acid insoluble residue of the Orgueil (CI) carbonaceous chondrite has been shown to have substantial aromatic content (Cronin, Pizzarello, and Frye 1987). After vacuum treatment it exhibits an infrared absorption spectrum similar to that observed in emission from the Orion Nebula (Wdowiak, Flickinger, and Cronin, 1988). The Orion emission spectrum in the 5 to 14 micron region and the KBr pellet absorption spectrum of Orgueil

acid insoluble residue after vacuum heating to 500C are shown in Figure 1. The Orgueil FTIR spectrum has had a continuum subtracted to remove the effect of scattering in the KBr pellet, revealing the maximum of the broad absorption "hump" is at ~7.8 microns in addition to the peaks at 6.2 and 11.3 microns. The coincidence of the wavelength of the heated treated residue "hump" maximum and the observed 7.7 micron emission band is interesting.

The Orgueil acid insoluble residue has other interesting IR spectral features besides those shown in Figure 1. Figure 2 shows the heat treated Orgueil acid insoluble residue has absorption bands at 16 and 19.6 microns (625 cm^{-1} and 510 cm^{-1}). These features are intrinsic to the residue and are evident in untreated material. They are probably due to bending of the PAH aromatic structure and are of interest as a candidate for the cause of the broad 25 micron band emission observed with IRAS (Hauser et al., 1984; Lynch et al., 1988). Because of the absence of a 10 micron (1000 cm^{-1}) band one can conclude the 16 micron (625 cm^{-1}) and 19.6 micron (510 cm^{-1}) bands are not due to silicate material that has escaped being dissolved by HF. Sandford and Walker (1985) have published an IR spectrum of an interplanetary dust particle (IDP "Conehead") having bands at 16.8 micron (595 cm^{-1}) and 23.1 micron (433 cm^{-1}) attributed to an hydrous Al_2O_3 or Fe_2O_3. The Orgueil 16 micron (625 cm^{-1}) and 19.6 micron (512 cm^{-1}) absorption features could therefore be due to microgram amounts of mineral in the milligram amount of sample residue.

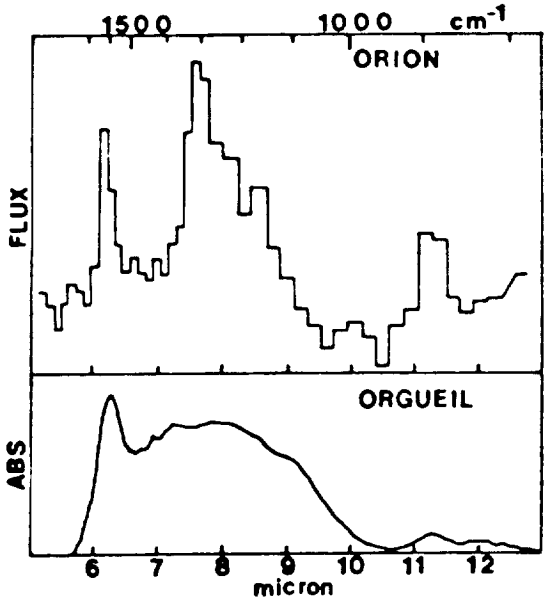

Fig. 1 Orion Bar (Allamandola et al. 1987) and heat treated Orgueil PAH residue.

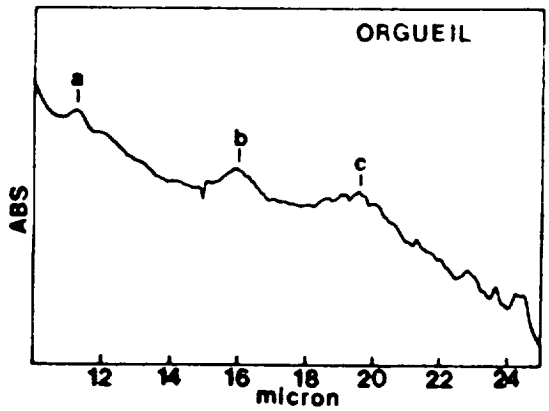

Fig. 2 Orgueil heat treated PAH residue a-11.3, b-16 and c-19.6 micron bands.

Coal tar prepared by coking coal at 1400 K in the absence of air is utilized as a PAH mixture that is an analog to interstellar PAH mixtures. Bulk coal tar mixed with acetone was filtered and the filtrate evaporated afterwards to concentrate a solvent soluble fraction used to prepare air dried films. As the solvent is evaporated away a dramatic spectral shift of ~2000A from blue to orange-red occurs in the near ultra-violet excited luminescence. The solvent soluble fraction coated on a substrate as a film and excited with ultraviolet radiation exhibits luminescence having a spectral signature in the 5500A to 7500A range similar to that of the Red Rectangle and other dusty regions (Figure 3). This result suggests the Red Rectangle emission is due to excited-dimer (excimer) emission of PAH molecules clumped together (Wdowiak 1986). In the excimer process which requires adjacent PAH molecules (as in the film), an excited dimer is formed from an excited singlet molecule and an unexcited one. This is followed by a radiative transition emitting light at longer wavelengths than single molecules would, followed by rapid dissociation into monomers. Duley and Williams (1988) have demonstrated PAH clumps would have an infrared emission spectrum similar to that of free molecules, making the excimer process plausible for the source of the optical emission of objects such as the Red Rectangle which also exhibits IR band emission (Russell, Sofier, and Willner 1978).

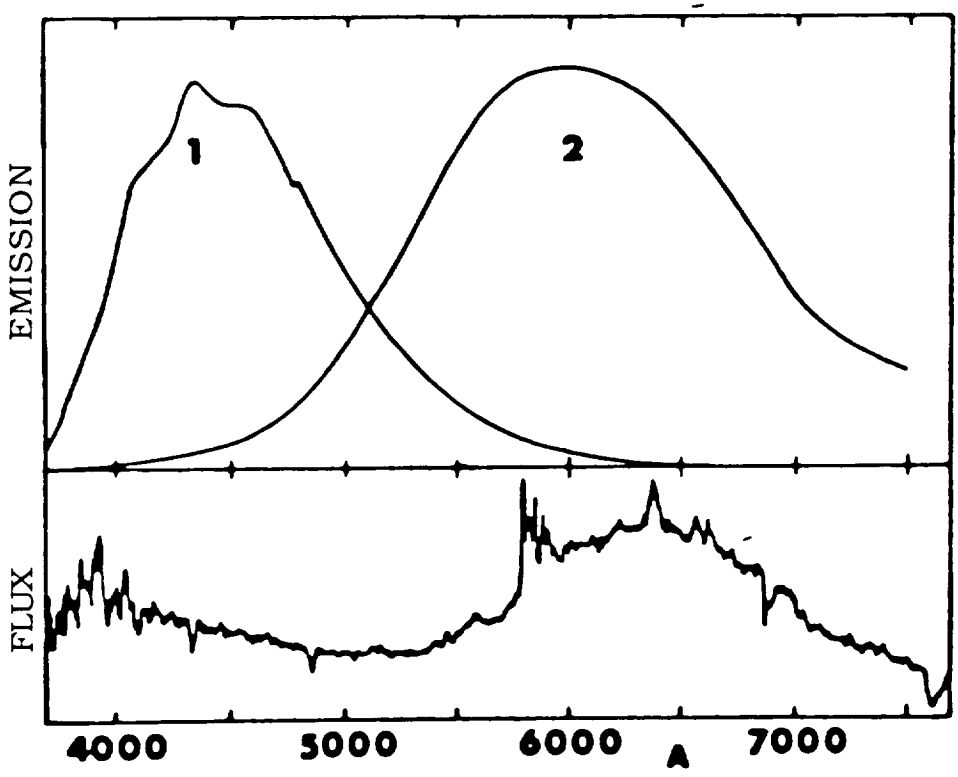

Fig. 3 Luminescence of 3070A excited coal tar in ethyl alcohol (1) and as a film on quartz (2) corrected for R928 PMT sensitivity shown with the spectrum of the Red Rectangle (Schmidt, Cohen, and Morgan 1980).

The coal tar residue obtained in the filtering process was washed repeatedly with benzene to remove soluble material and then air dried prior to pressing it into KBr pellets or subjecting it to further processing. The solvent insoluble fraction of coal tar has infrared spectral characteristics similar, but not identical to that of the heat treated acid insoluble residue of the Orgueil meteorite. In particular the presence of 3.3 micron (3030 cm^{-1}) absorption and other features longward of 11.3 micron (885 cm^{-1}) suggests it is more hydrogenated. An experiment was performed to try to simulate in a gross, but rapid manner the effect of H atom, H ion, and ultraviolet exposure on interstellar PAH. The benzene insoluble coal tar residue was placed in a boat, and subjected to a microwave excited hydrogen plasma at a pressure of 1.5 Torr for 35 minutes. The processing reduced the strength of the 13.4 micron (746 cm^{-1}) band, probably associated with aromatic rings having 3 or 4 adjacent hydrogens per ring, relative to the 11.3 micron (885 cm^{-1}) band associated with 1 hydrogen per ring (Figure 4). This experiment may demonstrate why the 11.3 micron interstellar emission band dominates the 10 to 15 micron region, by simulating the dehydrogenation expected to take place in the interstellar environment.

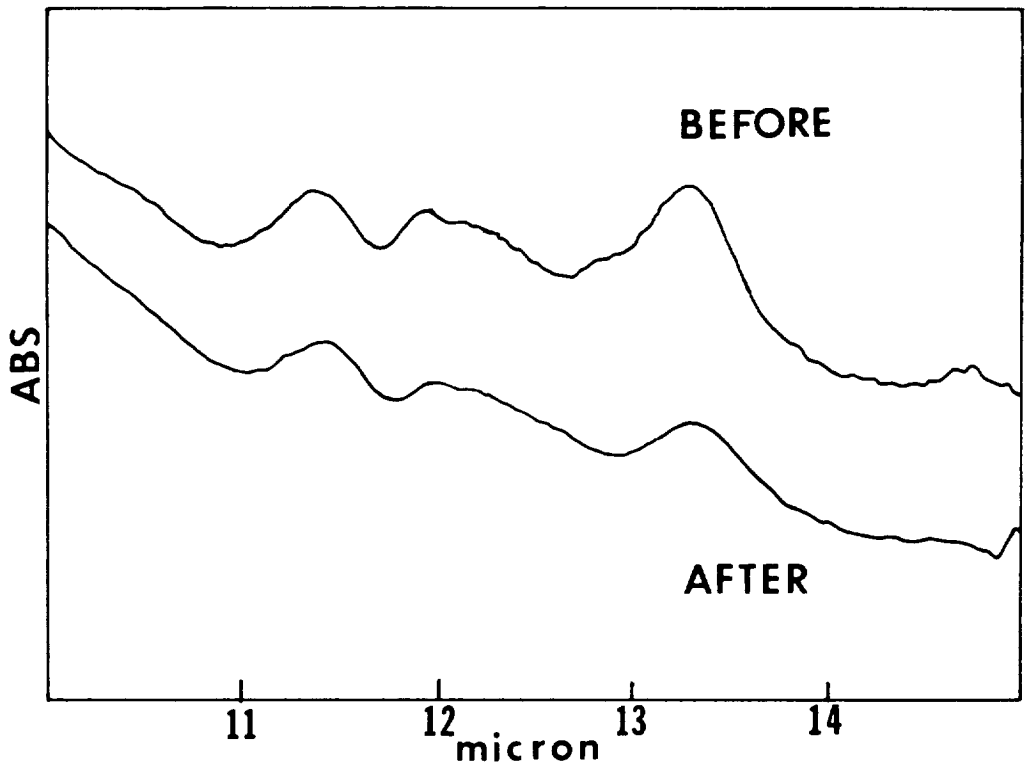

Fig. 4 FTIR spectra in the 10 to 15 micron region of the solvent insoluble fraction of coal tar before and after being subjected to a hydrogen plasma environment.

Comparison of the laboratory measurements discussed here and observations indicates the linking of the IR emission bands to a PAH source is not inconsistent with our laboratory experience. However a laboratory analog that exhibits precisely all of the spectral features of a source such as the Red Rectangle (HD 44179) still eludes the laboratory worker and is troubling. It may be that the PAH species have a special character, or that there is stratification of various populations of PAH species in a unique manner in the source of IR emission and no single analog or analog system will suffice. Still to be exploited are the structured features superimposed upon the Red Rectangle 5500A - 7500A emission "hump" (Schmidt, Cohen, and Margon 1980, Warren-Smith, Scarrott, and Murdin 1981). Those features may be due to simple radicals or ions trapped in relatively inert ices such as CO or N_2 (Wdowiak 1981) or are the signatures of complex molecules. Perhaps even stimulated emission may be involved. What is need are observations of the Red Rectangle quality of other similar sources. This work was supported by NASA grant NAGW-749.

Allamandola, L.J., Tielens, A.G.G.M., and Barker, J.R.: 1987 in Polycyclic Aromatic Hydrocarbons and Astrophysics (ed. Leger, A., d'Hendecourt, L., and Boccaro, N, D. Reidel).
Bellamy, L.J.: 1985, The Infra-red Spectra of Complex Molecules (Chapman and Hall, London).
Cohen, M., Tielens, A.G.G.M., and Allamandola, L.J.: 1985, Ap.J. 299, 193.
Cronin, J.R., Pizzarello, S., and Frye, J.S.: 1987, Geochim. Cosmoschim Acta 51, 299.
Duley, W.W. and Williams, D.A.: 1988, M.N.R.A.S. 231, 969.
Hauser, M.G. et al.: 1984, Ap.J. 278, L 115.
Leger, A. and Puget, L.L.: 1984, Astron.. Astrophys. 137, L5.
Lepp. S. al Dalgarno, A.: 1988, Ap.J. 324, 553.
Lynch, D.K., Hackwell, J.A., Wesselius, P., Olling, R., and Isreal, F.P.: 1988, Bull. Am. Astron. soc. 20, 732.
Sandford, S.A. and Walker, R.M.: 1985, Ap.J. 291, 838.
Schmidt, G.D., Cohen, M., and Margon, B.: 1980, Ap.J. 239, L133.
Russell, R.W., Soifer, B.T., and Williams, S.P.: 1978, Ap.J. 220, 568.
Warren-Smith, R.F., Scarrott, S.M., and Murdin, P.: 1981, Nature 292, 317.
Wdowiak, T.J.: 1981, Nature 293, 724.
Wdowiak, T.J.: 1986, in Interrelationships Among Circumstellar, Interstellar, and Interplanetary Dust (NASA CP 2403), A41.
Wdowiak, T.J., Flickinger, G.G., and Cronin, J.R.: 1988, Ap.J. 328, 175.

II-D) THEORETICAL STUDIES

DIRECT PHOTODISSOCIATION OF CH BONDS IN PAHS: IMPLICATIONS FOR THE INFRARED EMISSION BANDS

V. Buch
Department of Chemistry, University of Illinois at Chicago

Direct photodissociation is proposed as the dominant destruction mechanism for the CH bonds in large interstellar molecules exposed to UV radiation. The implications for the unidentified infrared emission bands (UIR) are examined assuming that polycyclic aromatic hydrocarbons (PAHs) are the carriers of the bands. Direct photodissociation explains extensive dehydrogenation of PAHs which was inferred from the UIR spectra. The relative intensities of the UIR bands are proposed as a probe of molecular structure of PAHs, and as a diagnostic of the ratio of the density and the UV flux within the sources.

THE EFFECT OF IONIZATION ON THE INFRARED ABSORPTION SPECTRA OF PAHs: A PRELIMINARY REPORT

D. J. DeFrees* and M. D. Miller**
*Molecular Research Institute, Palo Alto, CA 94304
**IBM Almaden Research Center, San Jose, CA 95120

The emission lines observed in many interstellar infrared sources at 3050, 1610, 1300, 1150, and 885 cm^{-1} (3.28, 6.2, 7.7, 8.7, and 11.3 microns) are hypothesized to originate from polycyclic aromatic hydrocarbon molecules (PAHs). (Léger & Puget, 1984, Allamandola et al., 1985) These assignments are based on analyses of laboratory infrared spectra of neutral PAHs. However, it is likely that in the interstellar medium the PAHs are ionized, i.e., are positively charged. Furthermore, as pointed out by Allamandola et al. (1987), "although the IR emission band spectrum resembles what one might expect from a mixture of PAHs, it does not match in details such as frequency, band profile, or relative intensities predicted from the absorption spectra of any known PAH molecule." The PAH hypothesis is far from proven.

One source of additional information to test the PAH hypothesis is *ab initio* molecular orbital theory. (Hehre et al., 1986) It can be used to compute, from first principles, the geometries, vibrational frequencies, and vibrational intensities for model PAH compounds which are difficult to study in the laboratory. We have used the Gaussian 86 computer program (Frisch et al., 1984) to determine the effect of ionization on the infrared absorption spectra of several small PAHs: naphthalene and anthracene. This brief article contains a preliminary report of the results of these calculations.

The vibrational spectra were computed at the HF/3-21G level of theory. Previous studies (DeFrees & McLean, 1985, Yamaguchi et al., 1986) show that after simple scaling, *ab intio* frequencies are accurate to ± 50 cm^{-1} and intensities are correct to within a factor of two. Calculations performed on benzene demonstrate that these conclusions, reached on studies of small molecules, apply as well to the study of PAHs. Computed transmittance spectra were generated with lorentzian curves (constant half-height width of 15 cm^{-1}) centered at the HF/3-21G wavelengths with an area equal to the computed intensity. The spectra are scaled to give a maximum transmittance of 5%. Figures 1 and 2 are computed transmittance spectra of naphthalene (C_8H_{10}) and its radical cation ($C_8H_{10}^+$), respectively, while figures 3 and 4 show computed vibrational spectra of anthracene ($C_{10}H_{14}$) and its radical cation ($C_{10}H_{14}^+$), respectively. Frequencies have not been scaled in these plots; for comparison with experiment multiply each frequency by 0.89. (DeFrees & McLean, 1985)

Ionization of naphthalene and anthracene has a striking effect on the predicted infrared absorption spectrum. In each case, strong C-H stretching bands around 3300 cm^{-1} in the neutrals are absent in spectra of the cations. In the region from 400 to 2000 cm^{-1} there are also some large changes. In naphthalene, the neutral has two strong absorptions in this region whereas the ion has 5; anthracene has three strong, narrow peaks while its cation has one strong, wide, peak resulting from the blending of several strong absorptions.

Analysis of these results is on-going. We will determine the cause for the large changes that occur in the absorption spectra on ionization. With this understanding, we hope to be able to make at least qualitative extrapolations to larger systems. We also intend to examine the effects of ionization on the emission spectra.

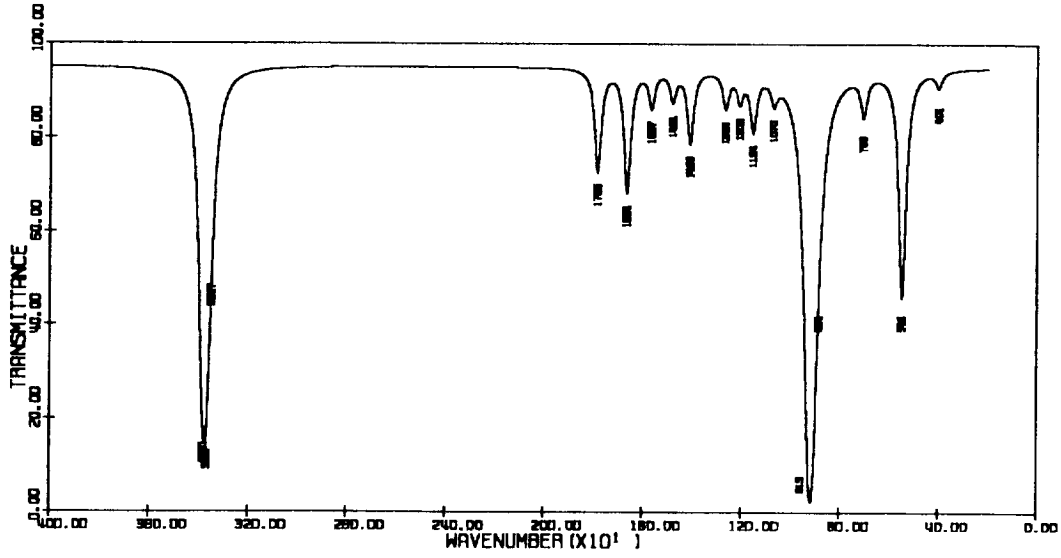

Fig. 1 Computed transmittance spectrum of naphthalene

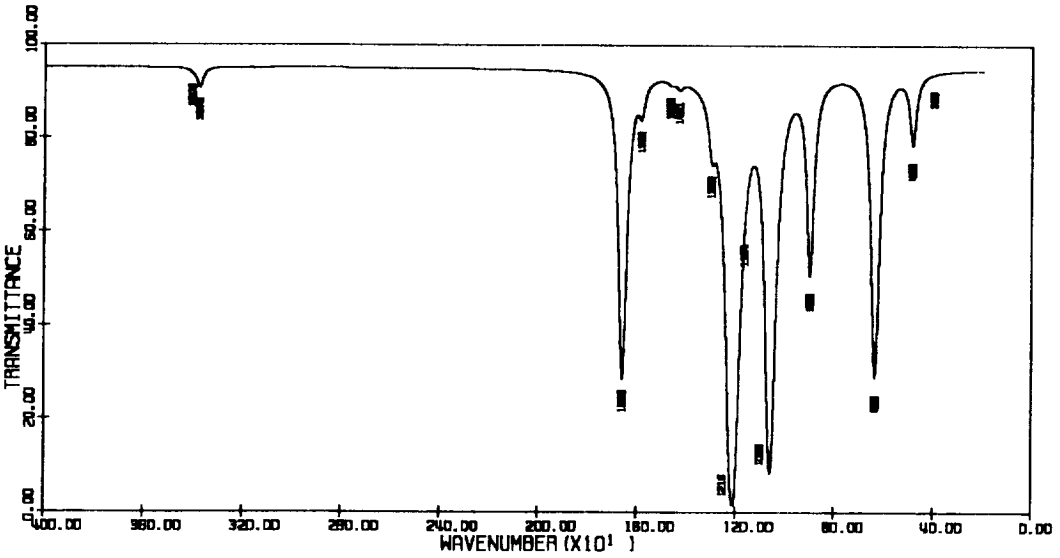

Fig. 2 Computed transmittance spectrum of naphthalene radical cation

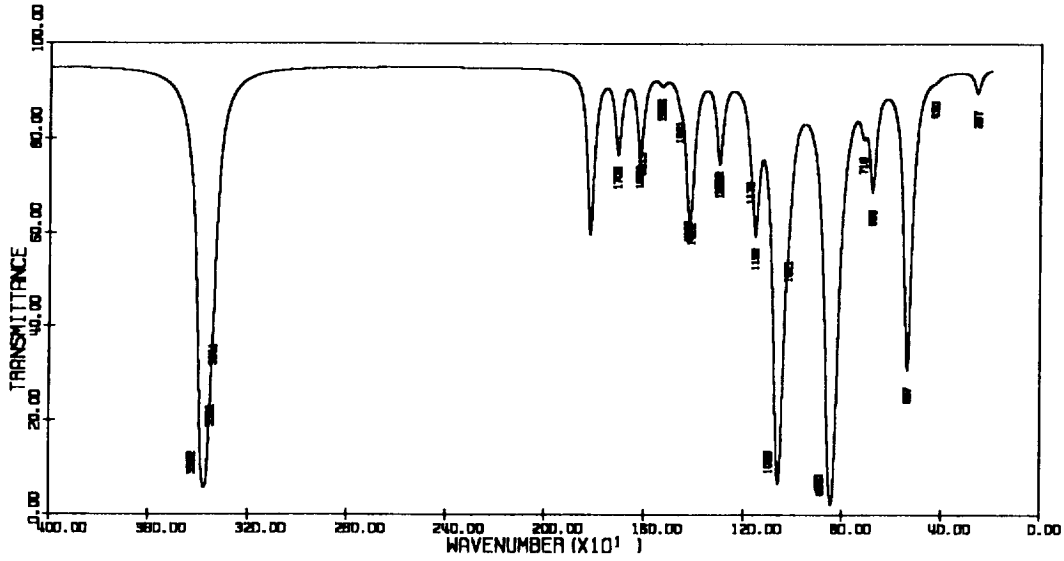

Fig 3 Computed transmittance spectrum of anthracene

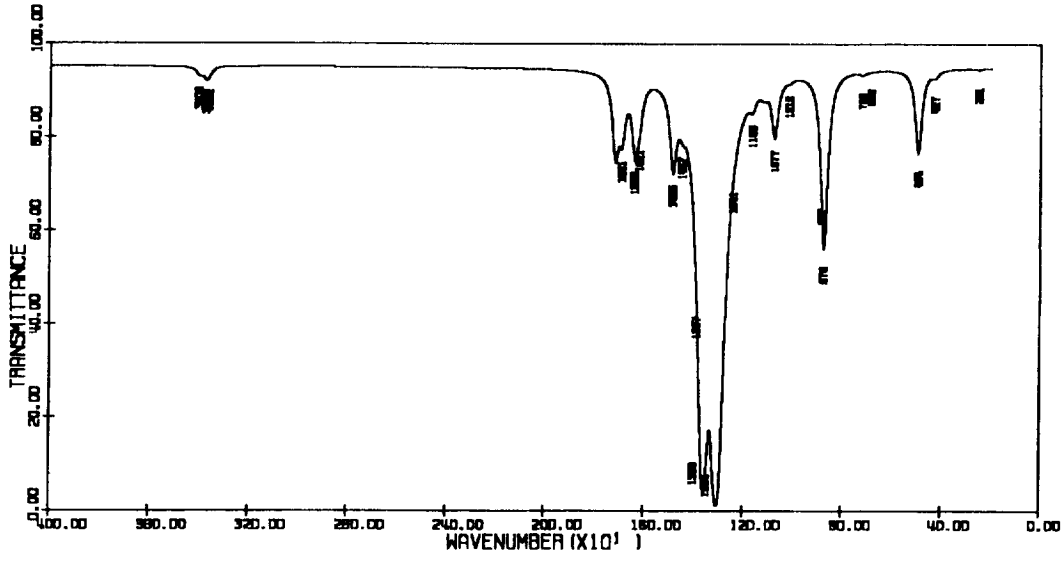

Fig 4 Computed transmittance spectrum of anthracene radical cation

References

L. J. Allamandola, A. G. G. M. Tielens, & J. R. Barker. (1985) *Ap. J. Letters*, **290**, L25.

L. J. Allamandola, A. G. G. M. Tielens, & J. R. Barker. (1987) Infrared emission from interstellar PAHs. in G. E. Morfill & M. Scholer, editor, *Physical Processes in Interstellar Clouds*, pages 305.

D. J. DeFrees & A. D. McLean. (1985) *J. Chem. Phys.*, **82**, 333.

M. J. Frisch, J. S. Binkley, H. B. Schlegel, K. Raghavachari, C. F. Melius, R. L. Martin, J. J. P. Stewart, C. M. Rohlfing, L. R. Kahn, D. J. DeFrees, R. Seeger, R. A. Whiteside, D. J. Fox, E. M. Fluder, & J. A. Pople. (1984) *Gaussian 86*. Pittsburgh, PA: Carnegie-Mellon Quantum Chemistry Publishing Unit.

W. J. Hehre, L. Radom, P. v. R. Schleyer, & J. A. Pople. (1986) *Ab Initio Molecular Orbital Theory*. New York, NY: John Wiley and Sons.

A. Leger & J. L. Puget. (1984) *Astro. Ap.*, **137**, L5.

Y. Yamaguchi, M. Frisch, J. Gaw, H. F. Schaefer III, & J. S. Binkley. (1986) *J. Chem. Phys.*, **84**, 2262.

ANGULAR MOTION OF A PAH MOLECULE IN INTERSTELLAR ENVIRONMENT

D.Rouan(*) , A.Léger(**) , A.Omont(***) , M.Giard(****)

*Laboratoire de Recherches Spatiales,Observatoire de Paris-Meudon
F92195 Meudon Principal Cedex, France
**Groupe de Physique des Solides de l'ENS, Université Paris 7,
2 pl Jussieu, F75251 Paris Cedex 05, France
***Groupe d'Astrophysique, Université de Grenoble, CERMO,
B.P.68, F38402 Saint Martin d'Hères Cédex, France
****Centre d'Etude Spatiale du Rayonnement, 9. av du Col. Roche,
BP4346, F31029 Toulouse Cédex, France

The Polycyclic Aromatic Hydrocarbon (PAH) molecules have recently been proposed as an important and hitherto undetected component of the ISM. The hypothesis was based on an attractive explanation of the "Unidentified IR Emission Bands" (Léger and Puget 1984). It has already led to a verified prediction on extended galactic and extragalactic emissions measured by IRAS (Boulanger et al., 1986), or by a recent balloon-borne experiment (Giard et al., 1988). We study here the physics that rules the motion of such molecules in the ISM, taking into account their coupling with the ambiant gas, the radiation field (absorption and emission) and the static magnetic field. This study is important for many implications of the PAH hypothesis such as the radio emission by these molecules or the expected polarization of their IR emission (Sellgren et al. ,1988).

We consider a reflection nebulae where the situation is rather well known (Omont, 1986). Every day life of a mean PAH molecule in such a region is as follows: every three hours a UV photon is absorbed heating the molecule to a thousand degree; the temperature decay due to cooling by infrared emission follows then within a few seconds. A collision with a molecule of gas occurs typically once every week, while an H atom is ejected or captured at the same rate. The figure 1 gives a typical cooling cycle after a heat impulse.

The PAH molecule we have considered as representative of the family has typically 50 atoms, a radius of 4.5 $\AA$, is circular and has a molecular mass $M = 300$; its permanent dipole moment is 3 Debye.

The four basic questions we try to answer are: *i)* what are the interactions that make the molecule rotating; what is the rotational velocity or more precisely the statistical distribution n(J) of the angular momentum $\vec{J}$; *ii)* does the molecule rotate preferentially around an axis normal to its plane ? or more precisely what is the distribution n(K) of the projection of $\vec{J}$ on the main axis of inertia; *iii)* is alignment possible, either on the magnetic field or on the line of sight of a source of photons through *streaming* process ? iv) finally what are the implications in terms of observations of the rotation of PAHs ?

Rotational velocity: The distribution n(J) results from a random walk where the different events giving rise to a variation of J are a collisions, the accretion or the ejection of a H atom, the emission or the absorbtion of a photon (UV, IR or radio). Rotational drag from the interstellar gas, radio emission of rotational photons or self-regulating disymetry of the probalities of IR photo-emission will limit the growth of the rotational velocity.

PAHs eject H-atoms by thermo-dissociation; this uses a fraction of a vibration quanta (.04 eV) and produces suprathermal H-atoms (900K). Photo-dissociation is another possible mechanism (Buch, 1988), however not yet proven in large molecules, much more efficient (2.5 eV and 30 000K). When absorbing or emitting a photon, the angular momentum exchange is $\Delta J = 0, \pm 1$. The absorption of one UV photon is followed by the emission of a burst of typically 50 IR photons.

We give in table I the different contributions of each process to the random-walk building-up and to its limitation by drag type effects.

Physical process	**Rate**	**ΔJ** (random)	δJ **(drag)**
Collision with a H atom	once a week	$\pm$ 10 $\hbar$	$-J/150$
Ejection of a H atom (thermo-dissociation)	once a week	$\pm$ 6 $\hbar$	$-J/100$
Emission of an IR photon (vibr-rot)	50 each 3 hours	$\pm$ $\hbar$	$-\frac{[J-<J>]}{3000}$
Emission of a radio photon (rot)	one photon per day		$-\hbar$

All these contributions can be handled through a Focker-Planck equation describing the global diffusion-like process.

We have shown that the dominant mechanism in the building-up of J is either photo-dissociation, if real, with $< J >= 220$ and $T_{rot} = 760K$, or IR emission which leads typically to $< J >= 80 \pm 70$ and $T_{rot} = 130K$. ***Radio emission is in both cases very efficient.*** The figure 2 displays the distribution of J for the second case, the most likely. One shows that this distribution is thermal with a temperature $T_{rot} = \frac{h\nu_0}{6}$, where ν_0 is the -properly averaged- frequency of IR vibration-rotation photons.

Alignment of $\vec{J}$ perpendicular to the molecule plane: The distribution n(K) results from internal energy exchange with the vibration modes of the molecule, allowing the conservation of $\vec{J}$ and total energy $E = E_{rot} + E_{vib}$. This Intramolecular Vibration-Rotation Energy Transfert (IVRET) is caused by Coriolis and centrifugal interactions. As $\vec{J}$ is fixed, the change in E_{rot} must be the result of a change in K, thus affecting the precession angle (β) the symmetry axis makes with $\vec{J}$. This angle changes many times during each UV photon event and K is statistically distributed with the vibrational temperature T_{vib} at each moment. When the rotational temperature T_J which characterizes J is much higher than T_K, the molecule axis aligns along $\vec{J}(K \rightarrow J)$; when $T_J \ll T_K$, the axis is isotropically distributed around $\vec{J}$ (uniform distribution of K from: -J to + J) :

this happens just after the absorption of a UV photon.

Cooling of the molecule tends thus to a rapid (a few hundred seconds) alignment of the rotation vector normal to the plane, and memory of the direction of the UV photon is thus immediately lost after its absorption.

Streaming: Alignment of non-spherical grains by streaming supposes that a driving force, the radiative pressure, at least equal to the gas pressure times the surface area of the grain maintains a velocity of the particle with respect to the gas (Roche and Aitken 1985). The resulting unbalance of the collision directions tends to favorise a spinning with an axis preferentially oriented perpendicular to the stream. We have shown that the radiative pressure is in general too weak in a typical reflecting nebula to drive a PAH molecule at a velocity significantly different from the thermal velocity: *streaming is thus unefficient* .

Coupling with $\vec{B}$: The coupling of the molecule with the interstellar magnetic field $\vec{B} = 10\mu Gauss$ causes its precession around the field direction with a period $\nu_{Larmor}^{-1} \simeq 3000s$ *much larger than the cooling time* ($t_{IR} = 3s$). This results from the evaluation of the permanent magnetic moment (μ) of the molecule, considering rotation of a charged system when ionized, diamagnetism, Barnett effect, electronic orbital and spin magnetic moment; the last two ones could be in principle as large as one Bohr magneton (μ_0). However the quenching to zero of the orbital momentum in aromatic molecules reduces $< \vec{L} >$ directly and $< \vec{S} >$ via the spin-orbit coupling.

A second possible effect of $\vec{B}$ we have investigated is the Davis-Greenstein alignment mechanism proposed for interstellar grains. However the very large imaginary part of the susceptibility it supposes (super ferro-magnetism, Mathis 1986) can hardly be found in PAH molecules, and we do not believe such a mechanism of aligment can be efficient.

Radio emission:because of the rapid rotation one expects a significant radio emission due to tansitions between rotational levels. Because the molecule rotates most of the time around its largest axis of inertia, we have used the approximation of linear molecules to evaluate the power radiated by PAHs. The different quantities of interest are given below, and the radio spectrum is displayed on figure 3.

- Spontaneous emission: $A_{J \to J-1} = 910^{-12} (\frac{\mu}{3Debye})^2 J^3 \ \ s^{-1}$
- Emission spectrum: $P_\nu \ \propto \ \nu^5 \exp[-\frac{h^2\nu^2}{4\bar{B}kT_{rot}}]$
- $\nu_{max} \ = \ 87 \ (\frac{N_{at}}{24})^{-\frac{5}{4}} \ GH_z \implies \lambda_{max} \ = \ 3.4 \ (\frac{N_{at}}{24})^{\frac{5}{4}}$ mm
- Integrated emited power per molecule:
  $6.5 \ 10^{-21} \ (\frac{\mu}{3D})^2 \ (\frac{N_{at}}{24})^{\frac{5}{2}} \ erg \ s^{-1}$
- Radiated power per h atom:
  $L_H^{PAH} \ = \ 4.5 \ 10^{-34} \ (\frac{\mu}{3D})^2 \ (\frac{N_{at}}{24})^{\frac{3}{2}} \ W \, H_{at}^{-1}$

- Source brightness (for $A_v = 1$):
  $B^{PAH}_{(3mm)} = 1.0\,(\frac{N_{at}}{24})^{\frac{3}{2}}\ MJ_y sr^{-1} mag^{-1}$
- For comparison:
  - Thermal grain emission:
    $B^{dust}_{(3mm)} = .006\ MJ_y\ sr^{-1} mag^{-1}$
  - Average molecular brightness (Galactic Center direction):
    $B^{molec}_{(3mm)} = .2\ MJ_y sr^{-1} mag^{-1}$

We conclude that *the radio emission of PAH molecules would dominate the millimetric radio continuum from reflecting nebula.*This represents a new observational test of the PAH hypothesis.

References:

- D.K. Aitken, J.A. Bailey, P.F. Roche, J.M. Hough, 1985, MNRAS **215**, 815
- F. Boulanger, B. Band, and G.D. van Albada, 1985, Astr. and Astrophys., **144**,L9
- V. Buch, 1988 preprint
- M. Giard et al., 1988, to appear in Astr. and Astrophys. and this meeting
- A. Léger and J.L. Puget, 1984, Astr. and Astrophys., **146**, 81
- A. Léger and L. d'Hendecourt, 1986, in *Polycyclic Aromatic Hydrocarbons and Astrophysics* , ed. A. Léger, L. d'Hendecourt and N. Boccara, Reidel
- J.S. Mathis, 1986, Astrophys. J. **308**, 281
- G. M. McClelland, G.M. Nathanson, J.H. Frederick, F.W. Farley, 1988, in *Excited States* , Vol. 7, Academic Press
- A. Omont, 1986, Astr. and Astrophys., **164**, 159
- K. Sellgren, D. Rouan, and A. Léger, 1988, Astr. and Astrophys. **196**, 252

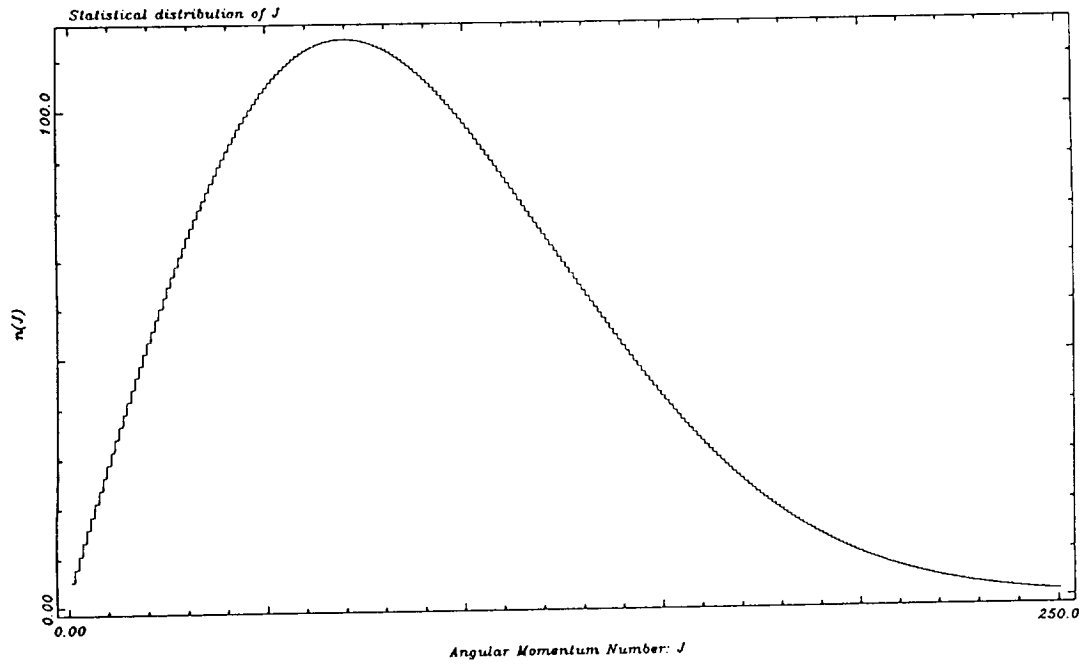

Figure 2

Statistical distribution of the angular momentum number J when governed by the emission of IR vibration-rotation photons.

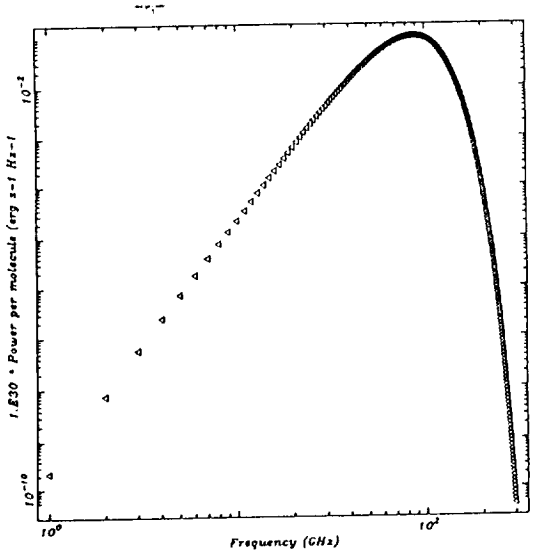

Figure 3

Radio emission spectrum of a population of PAHs

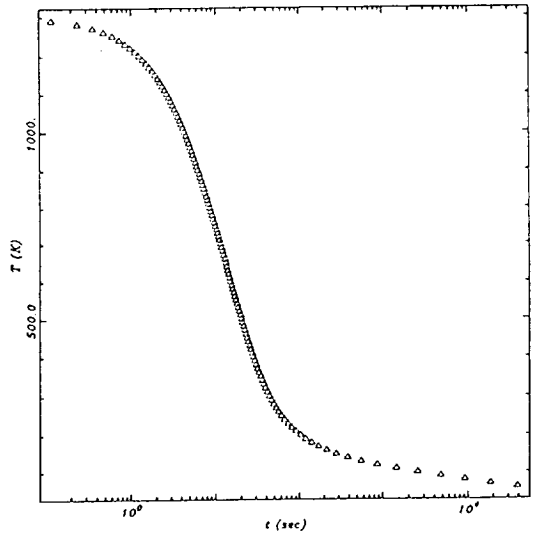

Figure 1

Cooling of a PAH after a heat impulse

PAHs MOLECULES AND HEATING OF THE INTERSTELLAR GAS

L. Verstraete*,A. Léger*,L. d'Hendecourt*,O. Dutuit**,
D. Défourneau*
*Groupes de Physique des Solides de l'ENS,Université
Paris 7,Tour 23 - 2,place Jussieu - 75251 PARIS Cedex 05
France
**Laboratoire de Physico-Chimie des Rayonnements - Bat.351
- 91405 Orsay - France

Until now it has remained difficult to account for the rather high temperatures (T=80-100 K) observed in many diffuse interstellar clouds (Spitzer and Jenkins,1975).

Various heating mechanisms have been considered: photoionization of minor species (C,Fe,Si) and ionization of H by cosmic rays (Dalgarno and McCray,1972), photoelectric effect on small grains (Jura 1976,Draine 1978). Yet all these processes are either too weak (ionization by cosmic rays, photoionization of trace elements) or efficient under too restricting conditions (photoemission from dust grains) to balance the observed cooling rates (Pottasch et al.,1979). A major heat source is thus still missing in the thermal balance of the diffuse gas.

Recently (Léger and Puget,1984) a new molecular component : the Polycyclic Aromatic Hydrocarbons (PAH),was introduced in the description of the interstellar medium to account for infrared emission features observed in a wide variety of astronomical objects. Those molecules were found to contain about 6% of the cosmic abundance of carbon.

Hence d'Hendecourt and Léger (1987) have reconsidered the problem of the heat input in the diffuse gas and proposed that photoionization of PAHs might be a significant (if not major) heat source. Indeed the photoionization of PAH molecules appears to be very efficient with respect to other processes. This for 2 reasons: first the photoelectron once produced do escape the molecule as opposed to grains in which it has to undergo several scattering processes(Jura,1976), second the recombination cross-section of a PAH is much larger than those for atoms or ions because of the presence of many internal vibrational modes likely to be excited by the recombining electron.Thus the ionization balance results in the presence of a large number of neutral molecules allowing further ionization and heating.

Ionization balance and heating rate per molecule

Following d'Hendecourt and Léger(1987) we write the ionization rate as:

$$R_{ion} = \int_{IP}^{13.6eV} 4\pi F(E)\,\sigma_{ion}(E)\,dE \qquad (1)$$

where F(E) is the mean interstellar radiation field(Draine,1978) , $\sigma_{ion}(E)$ and IP the photoionization cross-section and first ionization potential of the PAH considered
The recombination rate is:

$$R_{rec} = n_e \langle v . \sigma_{rec}(v) \rangle \qquad (2)$$

where n_e is the electronic density and v, $\sigma_{rec}(v)$ are the speed and recombination cross-section for an electron.The average is to be taken over a Maxwell distribution.
Assuming that the PAH bears a single positive charge and that it is spherical one finds:

$$\sigma_{rec}(v) = Y\ \sigma_0\ (1+ 2eU(a)/mv^2) \qquad \text{(Spitzer,1978)} \qquad (3)$$

with $a=0.9\sqrt{Nc}$ Å (Omont,1986) radius of the molecule where Nc is the number of carbon atoms and $\sigma_0 = \pi a^2$ the geometrical cross-section of the PAH , the mean electrostatic potential at r=a is thus defined as U(a) = e/a. Y is the sticking probability for recombination assumed equal to 1 (d'Hendecourt and Léger,1987) and m the electron mass.

After averaging , R_{rec} can be rewritten as:

$$R_{rec}=n_e\ \sigma_0\ (1+ eU(a)/kT)\ \sqrt{(8kT/\pi m)} \qquad (4)$$

The fractional ionization is then: $\beta = R_{ion}/(R_{ion}+R_{rec})$
The mean heat input to the gas phase is:

$$Q=(1-\beta)\int_{IP}^{13.6eV} 4\pi dE . F(E) . \sigma_{ion}(E)\ (E-IP) . \gamma(E) \quad - \quad n_e\beta \langle 1/2mv^2 . v\sigma_{rec}(v) \rangle \qquad (5)$$

where $\gamma(E)$ is the fraction of the energy E-IP that goes in kinetic energy of the photoejected electron.We shall further assume: $\langle\gamma(E)\rangle = 0.5$, a value inferred from measurements of photoionization of benzene (Terenin and Villessov,1964).
The Maxwell averaged recombined energy is:

$$E_{rec}=n_e . \beta \langle 1/2mv^2 . v\sigma_{rec}(v) \rangle = 2kT . \beta . R_{rec}(1 - eU/2kT\ /(1+eU/kT)) \qquad (6)$$

for the temperatures considered: $eU/kT>>1$, hence:

$$E_{rec} \approx \beta . kT . R_{rec}$$

defining: $$\langle E_e \rangle = 1/R_{ion} \int_{IP}^{13.6eV} 4\pi dE . F(E) (E-IP)\ \gamma(E)\ \sigma_{ion}(E)$$

as the mean energy of the photoelectron, we can express the heat input per molecule as:

$$Q = \beta . R_{rec} (\langle E_e \rangle - kT) = \langle E_e \rangle . \beta . R_{rec} (1 - 2T/3\theta) \qquad (7)$$

with : $\langle Ee \rangle = 3/2 k\theta$, defining a mean temperature θ for the ejected electron.

Thus for heating it is necessary that : $T < 3/2\ k\theta$.

Photoionization cross-sections of 2 PAH's:coronene and pyrene

Measurements of the photoionization cross-sections of coronene($C_{24}H_{12}$) and pyrene($C_{16}H_{10}$) have been carried out using the ACO synchrotron radiation facility of Paris-Sud University.

The experimental process was the following:the species were vaporized in a cylindrical oven where 2 holes were made at both ends to let the light beam through.The photoions where collected on an electrode at -50 V.
The calibration has been performed using absolute cross-sections of ethylene and benzene(Berkowitz,1979) and we dispose now of cross-sections from the IP(~1700Å) up to 600Å for both species.
The cross-sections per carbon atom are presented here below (fig.2) for coronene, pyrene and benzene (as extrapolated by d'Hendecourt and Léger,1987).Note that the cross-sections scaled to the number of C atoms in the PAH are very similar except that of the extrapolated benzene.

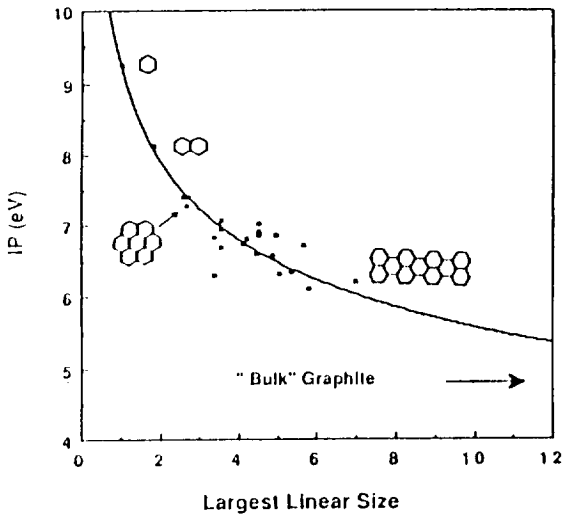

Figure 1 - *Ionization potential (IP) of various PAH molecules versus the largest linear size of the molecule in unit of the benzene ring diameter. The reported values are from Eifeld and Schmidt, (1981).*

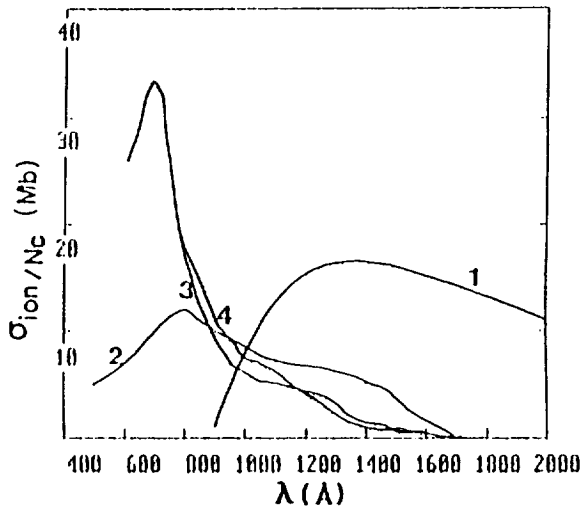

Figure 2: *Photoionization cross-sections per C atom in Mb (1 Mb= 10^{-18} cm^{-2}) for benzene (2) as extrapolated by Léger and d'Hendecourt (1987) , pyrene (3) and coronene (4) . The mean UV field taken from Draine (1978) is also shown (1) .*

Heating per molecule and abundance required to balance the cooling of a cold diffuse cloud.

For a cold diffuse cloud with : $T \approx 80K$ $n_e = 3.10^{-2} cm^{-3}$ $n_H = 10 cm^{-3}$ the numerical values found for the ionization fraction, β, the mean temperature of the photoelectron: θ, and the heat input Q/N_C per carbon atom are:

$\beta = 1.5\%$ $\theta = 1.39.10^4 K$ $Q/Nc = 1.10^{-21}$ erg.s^{-1}.C^{-1}

for both coronene(Nc=24) and pyrene(Nc=16).
Taking a mean cooling rate per H atom from Pottasch et al.:

$$\Lambda/n_H = 1.10^{-25} \text{ erg.s}^{-1}.\text{H}^{-1}$$

and assuming thermal equilibrium (cooling rate = heating rate) it is possible to derive what fraction f of the cosmic carbon would have to be carried by PAH's,namely:

$$f = (\Lambda/n_H) / (Q/Nc) . (C/H)^{-1}$$

With the above values one finds: $f \approx 25\%$.

This value has to be compared to the abundance deduced from the infrared emission bands.
Léger and d'Hendecourt (Les Houches,1986) found that PAH's would represent 6% of the cosmic carbon in the diffuse interstellar medium and calculated that the mean total number of atoms for a PAH in a reflection nebula should be : $N \sim 50$.
Furthermore Ryter and d'Hendecourt (this meeting) find a minimum size of $N \sim 50$ atoms from an analysis of visible fluorescence in a diffuse HI cloud.
Assuming a hydrogen coverage of 10% for the diffuse medium(Léger and d'Hendecourt,1986) we come to a mean number of $Nc \sim 45$ carbon atoms.
Our laboratory studies were carried out on smaller species but it is possible to estimate the heat input per carbon for a PAH with Nc =45 from the present data.This can be done assuming that the ionization cross-sections are proportional to Nc (see fig.2 here and Léger and d'Hendecourt,1987) and adopting the empirical evolution of the first IP of a PAH versus its size (fig.1).
Hence the heat input per C atom,and the abundance:

$Q/Nc = 1.7.10^{-21}$ erg.s^{-1}.C^{-1} and $f \approx 15\%$

This latter value is compatible with that inferred from the IR emission features since the IR emission bands should be dominated by the small-size molecules so that the value of 6% should be

considered as a lower limit.
The thermal equilibrium of the warm HI intercloud medium ($T \approx 8.10^3 K$) is not well accounted for (Draine,1978) and it is instructive to estimate the contribution of PAH's to the heat input in such regions.
Assuming $f \approx 15\%$, the same mean energy per photoelectron: 1.8 eV (i.e. $\theta = 1.39.10^4 K$) and taking:

$T \approx 810^3 K$ $\quad n_H \approx 0.3 cm^{-3}$ $\quad n_e/n_H = 0.1$

the heating rate per H atom turns out to be:

$$\Gamma/n_H = 2.5.10^{-26} \text{ erg.s}^{-1}.H^{-1}$$

This result is comparable to the value of the interstellar cooling function (Dalgarno and McCray,1972) at this temperature:

$$\Lambda/n_H = 3.10^{-26} \text{ erg.s}^{-1} \text{ per H atom.}$$

Conclusion:

Using photoionization cross-sections measured in the laboratory we have shown that in order to balance the observed cooling rates in cold diffuse clouds ($T \approx 80K$) the PAH's would have to contain 15% of the cosmic abundance of carbon.This value does not contradict the former estimation of 6% deduced from the IR emission bands since this latter is to be taken as a lower limit.

Further on we have estimated that the contribution to the heating rate due to PAH's in a warm HI cloud ($T \approx 8.10^3 K$) , assuming the same PAH abundance as for a cold HI cloud , would represent a significant fraction of the value required to keep the medium in thermal balance.

Hence photoionization of PAH's might well be a major heat source for the cold and warm HI media.

It should be noted that the PAH abundance found depends on:

- the fraction of the incident photon that is converted in kinetic energy of the photoelectron: $\gamma(E)$
- the recombination cross-section,the mean UV interstellar field
- the observed cooling rate.

It would be useful to obtain measurements of the cooling function Λ for a variety of regions corresponding to different values of the mean UV energy density and of the near IR fluxes thus allowing a study of the evolution of the heating rate with respect to the size distribution of PAH's.

Finally supplementary laboratory studies are needed for an extension to other PAH species and for the measurement of $\gamma(E)$.

References :

Berkowitz, J.: 1979, Photoabsorption , photoionization and photoelectron spectroscopy , John Wiley and sons

Dalgarno, A., McCray, R.A.: 1972, An.Rev.Astr.& Ap.,**10**,375

Draine, B.T.: 1978, Ap.J. Suppl.,**36**,595

Eifeld, P., Schmidt, W.: 1981, Jal of Electron. Spec. and Related Phenomena,**24**,101

d'Hendecourt, L., Léger, A.: 1987, Astr.Ap.Letters, **180**,L9

Jura, M.: 1976, Ap.J,**204**,12

Léger, A., d'Hendecourt, L.: 1987, in " Polycyclic Aromatic Hydrocarbons and Astrophysics", ed. Léger, d'Hendecourt and Boccara (Reidel: Dordrecht), p.223

Omont, A.: 1986, Astr.Ap.,**164**,159

Pottasch, S.R., Wesselius, P.R., Van Duinen, R.J.: 1979, Astr.Ap. Letters,**74**,L15

Spitzer, L.: 1978, Physical processes in the interstellar medium, John Wiley and sons.

Spitzer, L., Jenkins, F.B.: 1975, An.Rev.Astr.Ap.,**13**,133

Terenin, A., Vilessov, F.: 1964, Adv. in Photochemistry,**2**,385

SECTION III: DUST IN DENSE CLOUDS

III-A) STUDIES OF DARK CLOUDS AND STAR FORMING REGIONS

THE COMPACT FAR INFRARED EMISSION FROM THE YOUNG STELLAR OBJECT IRAS 16293-2422

H. M. Butner,* N. J. Evans II,* D. F. Lester,* L. G. Mundy,** P. M. Harvey,* and M. F. Campbell***
*Dept. of Astronomy, University of Texas at Austin, Austin, Tx 78712 USA
**Owens Valley Radio Observatory, California Institute of Technology,Pasadena, CA 91125 USA
***Dept. of Physics and Astronomy, Colby College, Waterville, ME 04901 USA

High resolution far infrared observations at 50 and 100 microns have been made of the young stellar object, IRAS 16293-2422. The observations were made using the Kuiper Airborne Observatory in 1988 April. They are part of a systematic high resolution study of nearby YSO's. The purpose of the project is to obtain resolution in the far infrared comparable to that at other wavelengths. Until recently, the highest resolution that has been available in the far infrared has been from either IRAS(angular resolution of ~4') or the KAO using standard FIR photometry(~35"). With scanning techniques (Lester et al. 1986), it is possible to obtain 10" resolution on bright sources. Such a resolution is necessary to better determine the physical conditions of the YSO, and to compare with models of star formation.

IRAS 16293-2422 first drew attention as a strong infrared source associated with strong CS emission (Walker et al. 1986) and a very compact CO outflow (Wootten and Loren, 1986). Located in the filamentary dark cloud L1689, part of the Rho Oph complex, the YSO has a luminosity similiar to that of L1551, about 30 solar luminosities. Mundy, Wilking and Myers (1986) found IRAS 16293-2422 has an elongated region (11" by less than 5") of thermal dust emission at 2.7 mm, as well as a compact ^{13}CO core of similiar dimensions. The major axis of the disk-like structure lies roughly perpendicular to the CO outflow. Mundy, Wilking and Myers found that the spectral

energy distribution of the source from 25 microns to 2.7 mm could be fit by a single dust temperature(41 K) assuming a $\lambda^{-1.5}$ dust emissivity law. In addition, they argued that their models were consistent with a sharp edged dust distribution for the YSO.

In order to better constrain the models for the source, we observed the YSO at both 50 and 100 microns on several flights in 1988 April from the KAO. Along the major axis we resolve the source at 100 microns, and find a FWHM size of 15" using Maximum Entropy deconvolution. This size is consistent with the disk size found by Mundy et al. We present estimates of the size both along the major and minor axis of the disk, as well as estimates of the dust temperature and 100 micron opacity for the YSO.

Lester, D. F., Harvey, P.M., Joy, M. and Ellis, H. B. Jr.: 1986, Ap. J., 309, 80.

Mundy, L.G., Wilking, B.A., and Myers, S. T.: 1986, Ap. J.(Letters), 311, L75.

Walker, C. K., Lada, C. J., Young, E. T., Maloney, P. R., and Wilking, B.A.: 1986, Ap. J.(Letters), 309, L47.

Wootten, A., and Loren, R. B.: 1986, Ap. J. 317, 220.

DUST CLOUDS IN ORION AND THE INTERSTELLAR NEUTRAL HYDROGEN DISTRIBUTION

N.V.Bystrova
Special Astrophysical Observatory,
USSR Academy of Sciences,Leningrad
Branch of the SAO,Pulkovo,
Leningrad,196140 USSR

According to published examples of the far infrared observations in the Orion and its surroundings several well-defined dust clouds of different sizes and structure are present there.

For comparison of these clouds with the neutral hydrogen distribution on the area of approximately thousand square degrees the data from Pulkovo Sky Survey in the interstellar neutral Hydrogen Radio Line as well as special observations with the RATAN-600 telescope in 21 cm line were used.From the materials of Pulkovo HI Survey we took the data about the line emission at ten velocities between - 21.8 and + 25.6 km/s LSR for the structural component of the interstellar hydrogen emission.

The results given in the poster concern mainly the Orion's Great Dust Cloud and the Lambda Orionis region where the information about the situation with the dust and interstellar hydrogen is very essential for interpretation.

INFRARED EMISSION FROM ULTRACOMPACT H II REGIONS

Ed Churchwell*, Mark Wolfire**, and Douglas O. S. Wood*
*Dept. of Astronomy, University of Wisconsin, 475 N. Charter St., Madison, WI 53706
**Dept. of Astron. & Astrophys., University of Chicago, 5640 S. Ellis, Chicago, IL 60637

Models of circumstellar dust shells around ultracompact (UC) HII regions have been constructed that accurately fit the observed infrared flux distributions. The models assume spherically symmetric dust shells illuminated by stars whose bolometric luminosity is inferred from the integrated FIR flux densities. Assuming ionization by a single zero-age main sequence (ZAMS) star, we use the relations of Panagia (1973) to infer the stellar radius and effective temperature for a given luminosity. The grain mixture in the dust shell consists of bare graphite and silicate grains with the optical properties of Draine and Lee (1984, 1987) and the size distribution of Mathis, Rumpl, and Nordsieck (1977). The computer code of Wolfire and Cassinelli (1986) was used to solve the radiative transfer equations through a spherical dust shell. The model provides monochromatic luminosities, dust temperatures, and opacities through the shell. Aside from the stellar properties (L_*, R_*, and T_{eff}) and dust properties, the only other input parameters to the model are the distance to the shell (used to convert fluxes to luminosities), the form of its density distribution $\rho(r)$, and its outer radius. All the latter input parameters have independent constraints which permit only a small range in their values for a given object. For example, the outer radius of the dust shell is determined by the point at which the dust temperature can no longer be distinguished from the ambient temperature of the molecular cloud. The inner radius of the dust shell is determined by the dust sublimation temperature (~1500 K for silicates and ~2000 K for graphite) and is not an input parameter. Because of the size distribution and different compositions of grains, the inner radius is different for different kinds of dust (i.e. the inner shell boundary is not very sharp).

Predictions of the model are compared with observations of a typical UC HII region and the run of dust temperature with radius and the optical depth with frequency are discussed. An important result of these models is the prediction that UC HII regions as a class are among the coolest and most luminous single objects in the Galaxy. They occupy an extreme position in FIR color-color plots and are therefore easily recognized.

N91-14943

DUST IN A FEW SOUTHERN HII REGIONS

S.K. Ghosh, K.V.K. Iyengar, T.N. Rengarajan, S.N. Tandon,
R.P. Verma and R.R. Daniel
Tata Institute of Fundamental Research, Homi Bhabha Road,
Bombay, 400005, INDIA

We discuss the property of dust in four southern HII region/molecular cloud complexes - RCW 108, RCW 57, RCW 122 and G351.6-1.3. These regions were observed at an effective wavelength of 150 μm using TIFR balloon borne 1 m telescope and deconvolved maps with a resolution of 1' were obtained. We have combined our data with other available data to derive the properties of the infrared emitting dust in these regions.

1. RCW 108 (IRAS 16362-4845)

This region has only one compact source which has a flux density of 12,000 Jy at 150 μm. Our flux density along with those of IRAS is consistent with a dust temperature of 40 K (for deriving temperatures we assume that emissivity $\propto 1/\lambda$). Optical depth at 150 μm is 0.07. IRAS LRS spectrum of this source shows silicate feature at 10 μm and NeII emission line at 12.8 μm. We fitted the spectrum around the absorption feature (7.5-12 μm) using two types of emissivity functions - lunar silicate (lunar rock 14321, Knacke and Thomson, 1973) and the Trapezium type (Gillett et al. 1975). The parameters for the fit were, the temperature of the emitting source (assumed to be black body), and the optical depth of the surrounding shell. The best fits for these two types of grains along with the parameters are shown in Fig. 1. It can be seen that the lunar silicate gives a much better fit to the observed data than the Trapezium type of dust.

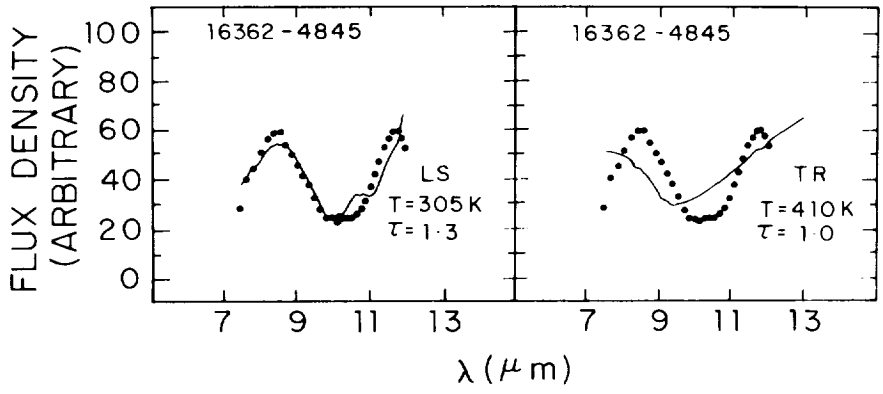

Fig. 1. The observed LRS spectrum (filled circles) of IRAS 16362-4845 along with the two fitted spectra - a) lunar silicate grains (LS) ; b) Trapezium type grains (TR).

2. RCW 57

This region has one strong source and two weaker sources. The main source has a flux density of 24,000 Jy at 150 μm. Our flux density and the IRAS flux densities are consistent with a dust temperature of 40 K. The optical depth at 150 μm is 0.09. If we combine our flux density with that at 1 mm by Cheung et al. (1980), we get a very flat wavelength dependence for emissivity (slope = -0.2) between 150 μm and 1 mm.

3. RCW 122

The map for this region has two bright sources, three isolated weak sources and diffuse emission around the brightest source. The brightest source has a flux density of 21,300 Jy. By combining our data with the flux density at 69 μm observed by McBreen et al. (1985) we get a dust temperature of 60 K. The optical depth at 150 μm is 0.04. Comparing our flux density with that at 1 mm by Cheung et al. (1980) we get a flat emissivity dependence with a slope of -0.6.

4. G351.6-1.3

This region has two HII regions G351.6-1.3 and G351.7-1.2. The source associated with G351.6-1.3 has a flux density of 12,000 Jy at 150 μm. Our flux density and those from IRAS are consistent with a dust temperature of 55 K. The optical depth at 150 μm is 0.03. Our flux density combined with that at 1 mm from Arnold et al. (1978) give the slope for emissivity dependence as -1.2. We did radiation transfer calculations based on the model given by Scoville and Kwan (1976) to fit the spectrum of the source from 2 μm to 1 mm. It is found that the dust distribution with density decreasing inversely with distance fits the observed spectrum better than that with uniform density. The source corresponding to G351.7-1.2 has a total flux density of 8,000 Jy at 150 μm. This source is more extended than G351.6-1.3. The derived dust temperature is 35 K and the optical depth at 150 μm is 0.01.

REFERENCES

Arnold, E.M., Kreysa, E., Schultz, G.V. and Sherwood, W.A.: 1978, Astr. Ap., 70, L1.

Cheung, L.H., Frogel, J.A., Gezari, D.Y. and Hauser, M.G.: 1980, Ap. J., 240, 74.

Gillett, F.C., Forrest, W.J., Merrill, K.M., Capps, R.W. and Soifer, B.T.: 1975, Ap. J., 200, 609.

Knacke, R.F. and Thomson, R.K.: 1973, Pub. A. S. P., 85, 341.

McBreen, B., Fazio, G.G., Loughran, L. and Rengarajan, T.N.: 1985, Astr. J., 90, 88.

Scoville, N.Z. and Kwan, J.: 1976, Ap. J., 206, 718.

DISTRIBUTION OF DUST IN W31 COMPLEX

S.K. Ghosh, K.V.K. Iyengar, T.N. Rengarajan, S.N. Tandon,
R.P. Verma and R.R. Daniel

Tata Institute of Fundamental Research
Homi Bhabha Road, Colaba
Bombay - 400005 INDIA

W31 is a HII region - molecular cloud complex in the galactic plane at a distance of 6 Kpc. This complex consists of two prominent radio continuum sources G10.2-0.3 and G10.3-0.1 representing HII regions. An extended region ($\sim$ 25' x 30') covering both these HII regions has been mapped in the far infrared (FIR) (120 - 300 μm) using the TIFR 1 m balloon-borne telescope with an angular resolution of $\sim$ 1' and a dynamic range of 100 (see Ghosh et al. 1988, for details). The resulting flux density distribution at an effective wavelength of 160 μm (for $\epsilon_\lambda \propto 1/\lambda$ & T = 30K) is presented in Fig. 1(c). The coadded IRAS survey scan data at 60 μm (1'.5 x 5' HPBW) and 100 μm (3' x 5' HPBW) have been deconvolved using a maximum entropy method to generate the flux density maps of the same region. These 60 μm and 100 μm maps are shown in Fig. 1(a) & (b) respectively.

Despite the dissimilar resolutions, the 60, 100 & 160 μm maps have striking structural similarities demonstrating the effectiveness of FIR radiation as dust tracer.

All three maps clearly show two regions (North & South) of extended FIR emission around the two prominent HII regions. These two HII regions are most likely physically associated as evident from their radio recombination line velocities (Downes et al. 1980). Because of the superior angular resolution at 160 μm, ten additional sources have been resolved in addition to the two HII regions (S1-S12, see Fig. 3(c)). Our sources S4, S6, S7 & S10 correspond to the IRAS Point Source Catalog sources 18060-2005, 18064-2008, 18064-2020 and 18065-2026 respectively and they are denoted by a + mark in Fig. 3(c). The corresponding 5 GHz radio continuum source positions (from Altenhoff et al. 1979) are depicted by a $\square$ symbol. The dust temperatures of the 160 μm sources which have IRAS counterparts have been estimated to be in the range 30 - 38 K for a $\epsilon_\lambda \propto 1/\lambda$ emissivity law. The dust optical depth at 160 μm is 0.048 for the brightest source (S7); the same for S4, S9, S6 and S3 are 0.029, 0.027, 0.005 and 0.004 respectively. The logs of FIR luminosities (in units of $L_\odot$) of S1, S3, S4, S6, S7, S8, S10, S11 and S12 are 4.43, 4.49, 5.76, 4.65, 6.30, 5.32, 4.52, 4.23 and 4.71 respectively.

Large scale extended emission from cooler dust at as large a distance as ~ 9 pc (d = 6 Kpc) has been clearly detected. The diffuse 160 μm dust emission has been estimated by modelling the emission by a linear superposition of ten pointlike sources with their flux densities as parameters to be fitted; their positions chosen near the local maxima in the map. A comparison of the observed emission with that of the superposed pointlike sources of the best fit model leads to the conclusion that about 35 % of the emission in W31 complex (both the North and the South regions) is of diffuse origin.

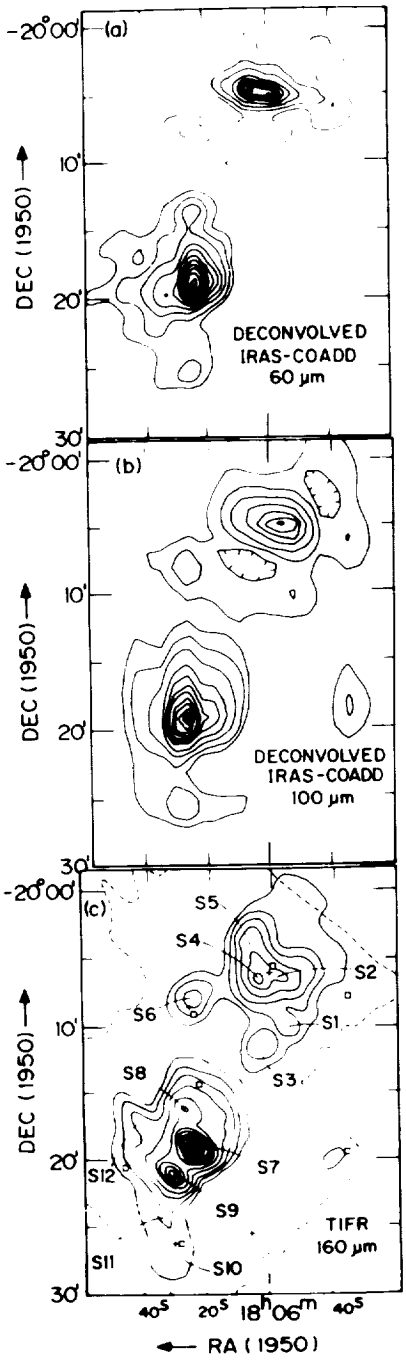

Figure 1.(a) Deconvolved IRAS survey coadd map of the W31 complex at 60 μm. The contour levels are 0.95, 0.9, 0.8, 0.7, 0.6, 0.5, 0.4, 0.3, 0.2, 0.1, 0.05 and 0.025 of the peak (3490 Jy / Sq. arc min.). (b) Same as (a) at 100 μm with peak = 5940 Jy / Sq. arc min. (c) TIFR map at 160 μm with peak = 3680 Jy / Sq. arc min. In addition to the contour levels of (a), 0.01 is also included here.

REFERENCES :

Altenhoff, W.J., Downes, D., Pauls, T. and Schraml, J.: 1979, Astr. Ap., 35, 23.

Downes, D., Wilson, T.L., Bieging, J. and Wink, J.: 1980, Astr. Ap. Sup., 40, 379.

Ghosh, S.K., Iyengar, K.V.K., Rengarajan, T.N., Tandon, S.N., Verma, R.P. and Daniel, R.R.: 1988, Ap. J. (in press).

N91-14945

LONGWAVE SPECTRAL DEPENDENCE OF EMISSION FROM WARM DUST CLOUDS

M. A. GORDON
NATIONAL RADIO ASTRONOMY OBSERVATORY
CAMPUS BUILDING 65, 949 NORTH CHERRY AVENUE
TUCSON, ARIZONA 85721-0655, USA

Observations (Gordon and Jewell, 1987) of the continuum emission from warm dust clouds at 230 GHz, or 1300 μm, enable us to determine the frequency dependence of the optically thin, longwave emission. Integrating the emission over the solid angle of the clouds gives a flux independent of the beam size and of the internal temperature structure of the clouds. The frequency resolving power of 64 allows us to correct these fluxes for the contribution of free-free emission from nearby HII regions—at the price of reduced sensitivity, of course. We (Gordon, 1988) combine these observations with similar observations made by others in the submillimeter and far infrared regimes to determine the continuum spectra of the dust-clouds.

To determine mean characteristics for these clouds, we fit these spectra with the simple transfer equation,

$$F_\nu = \Omega B_\nu(T)\,(1 - e^\tau)\,, \tag{1}$$

where the optical depth is modeled by

$$\tau = (\nu/\nu_o)^\beta\,. \tag{2}$$

Here F_ν is the integrated flux at frequency ν; Ω, the solid angle of the source; $B_\nu(T)$, the frequency form of the Planck function at a temperature T; ν_o, the frequency at which the average opacity of the cloud τ is 1, and β, the frequency dependence of the opacity and emissivity. At millimeter and submillimeter wavelengths where usually $\tau \ll 1$, the flux $F_\nu \propto \nu^{\beta+2}$.

The first result is that the color temperature T may represent an average dust temperature for a cloud. Our fits to Eq. (1) show the derived solid angles of the sources, Ω, are only $\leq 10\%$ of the actual solid angles subtended by the clouds. Most are $\leq 3\%$. Interpreting these values as filling factors, we suggest that the clouds are highly fragmented on angular scales much less than the 0.5–1.0 arc min beamwidths normally used to map the clouds. The implication of this fragmentation is that the FIR photons may be able to escape from the clouds so that the continuum spectra may represent the distribution of photons within the cloud in spite of substantial opacities of the cloud fragments, and therefore that the color temperatures T may also represent the temperatures of the dust grains averaged over the clouds.

Under the assumption that the continuum spectra *do* represent the real distribution of flux within the clouds and the color temperatures T of Eq.(1) may be indicative of the dust temperatures, Fig. 1 shows the distribution of these dust temperatures for the 11 clouds observed. The lower limit probably results from the sensitivity limit to our observational technique, but the upper limit may be an intrinsic property of dust clouds in general. For example, the upper limit may mean that photons with $\lambda \leq 46\mu$m — the wavelength of the maximum of $B_\nu(110\ \mathrm{K})$ — may have difficulty

escaping from the cloud fragments, or that the cloud has a regulatory mechanism to maintain its average color temperature below 110 K.

The longwave spectral dependence of the flux may tell us something about the average property of the dust grains. Fig. 2 shows the variation of β as a function of T. It appears that $\beta \approx 2$ for all but the warmest clouds, those of OMC-1 indicated by the filled circles.

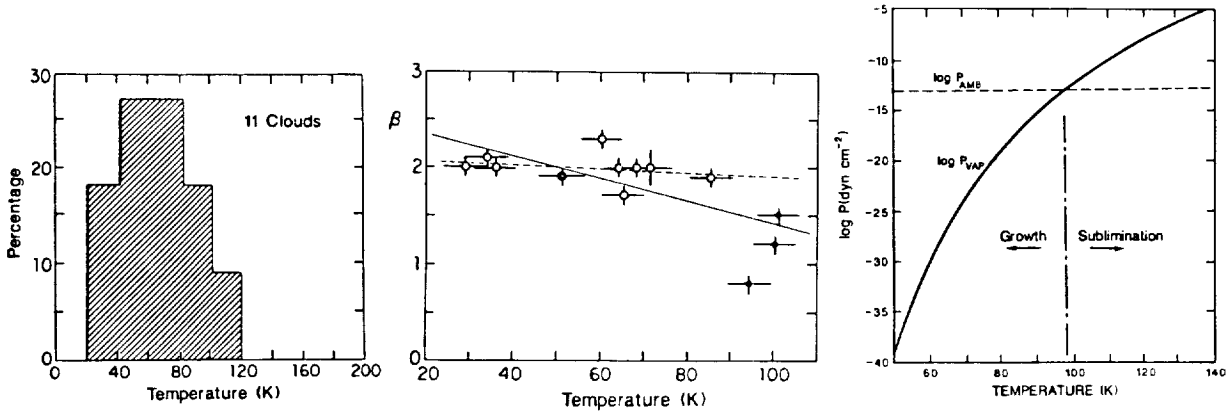

(*left*) **Fig. 1**—The histogram of color temperatures. (*center*) **Fig. 2**—Opacity exponent β plotted against color temperature. The broken line is a least squares fit to all but the OMC-1 data. (*right*) **Fig. 3**—The ambient pressure of H_2O for OMC-1 and the vapor pressure of ice plotted against temperature. The regions of the growth and sublimation of the ice mantles are marked.

Because β is lower for each of the components of OMC-1, we believe the explanation lies in something unusual about the cloud's dust grains and not just the presence of a cold cloud along the line of sight. Fig. 3 is a plot of the vapor pressure of ice (van de Hulst, 1949) against the ambient pressure of H_2O, where we assume a density of 8 molecules per cm^3 (Phillips *et al.*, 1978; Waters *et al.*, 1980) which may be an appropriate density for OMC-1. At temperatures greater than the intersection temperature (98 K) of the 2 curves, ice mantles will sublime. At lower temperatures, they will grow. The average T for OMC-1 is $\approx$ 100 K. Could the lower βs for OMC-1 result from evaporation of ice mantles, thereby altering the grain emissivities (Aannestad, 1975) from the normal characteristics of most grains in the ISM? Under these condition, the time required for the evaporation of the ice mantles would be $\approx$ 5000 yr, a short time compared to the lifetime of the contiquous HII region, the Great Nebula in Orion.

Aannestad, P. A.: 1975, *Ap. J.*, **200**, 30.

Gordon, M. A.: 1988, *Ap. J.*, **331**, in press.

Gordon, M. A., and Jewell, P. R.: 1987, *Ap. J.*, **323**, 766.

Phillips, T. G., *et al.*: 1978, *Ap. J. (Letters)*, **222**, 159.

van de Hulst, H. C.: 1949, *Rech. Astr. de l'Obs d'Utrecht*, **11**, P.2, Chap.II.

Waters, J. W., *et al.* 1980, *Ap. J.*, **235**, 57.

HI AND DUST IN THE HIGH LATITUDE DARK CLOUD L1642

T. Liljeström and K. Mattila
Observatory and Astrophysics Laboratory, Helsinki University
Tähtitorninmäki, SF-00130 Helsinki, Finland

Abstract. We have mapped the high latitude dark cloud L1642 ($l=210^{\circ}.8$, $b=-36^{\circ}.7$) in the 21-cm HI line using the 100-m radio telescope at Effelsberg. A remarkable HI line broadening from 2.5 to 2.9 km/s is observed over a small area on the "bright side" of L1642, i.e. the side facing the galactic plane. Results are presented concerning the effects of the asymmetrical UV radiation field of OB stars on the HI gas and the very small dust grains associated with L1642.

RESULTS AND DISCUSSION

The line width map of HI (Fig. 1) shows an increase from 2.5 to 2.9 km/s near the centre of the L1642 cloud peaking on the "bright side" of L1642. The spectra are narrow and do not reveal any sign of a second velocity component which could explain the line broadening as a blend effect. Although an explanation in terms of increased turbulence cannot be excluded, the fact that the IRAS 12μm surface brightness map of Laureijs et al. (1987) shows a maximum at the same position as the HI line broadening maximum (see Fig. 1) supports the thermal line broadening model where the heating of the HI gas is due to the photoelectric emission from very small grains and/or PAHs.

Assuming that the turbulent and large scale motions are the same in the broadened HI line region and immediately outside this area a temperature enhancement of 47 K is obtained for the HI gas. Adopting for the L1642 HI cloud the temperature $T_k = 81$ K, an average value for diffuse clouds (Spitzer and Cochran, 1981), the increase of the HI line width corresponds to an increase of T_k from $\sim$80 to 130 K.

A simplified thermal balance model where the photoelectric heating function of very small grains (Spitzer, 1978) is balanced by the cooling functions of C^+, CO and C (Langer, 1976) can explain a $\sim$50 K temperature enhancement if the mean projected surface area of grains/cm^3 per H atom is $2.0\ 10^{-21}$ cm^2. This value is consistent with the value of dust area as given by Spitzer (1978) if the extinction efficiency for these small grains is $Q_e \sim 1$. The requirement for additional grain area can be fullfilled by introducing the very small grains.

A ridge of excess HI emission has been detected at the outer edge of the dark cloud on its "bright side". From Fig. 2 it is seen that the ratio $N_{HI}/N_H(tot)$ vs. A_V tends to be higher for the "bright side" than for the "shadow side" of L1642. Fig. 2 shows a general agreement between the $H+H \rightleftarrows H_2$ equilibrium model of Hollenbach et al. (1971) and observations for $A_V > 1.4$ mag which corresponds to the projected distance $\rho < 0.85\ R$ (R=cloud radius) from the cloud centre. Based on the observations of Opal and Weller (1984) we estimate that the background UV radiation field in the vicinity of L1642 is about two times stronger on the "bright side" as compared to the "shadow side" of the cloud. Adopting for the model calculations a radiation

field value half of that used by Hollenbach et al. (1971) we obtain the result shown by the dashed curve in Fig. 2.

REFERENCES

Hollenbach, D., Werner, M., Salpeter, E.: 1971, Astrophys.J. 163,165

Langer, W.: 1976, Astrophys.J. 206, 699

Laureijs,R., Mattila,K., Schnur,G.: 1987, Astron.Astrophys. 184, 269

Opal, C.B., Weller, C.S.: 1984, Astrophys.J. 282, 445

Spitzer, L.,Jr.: 1978, Physical Processes in the Interstellar Medium, Wiley, New York

Spitzer, L.,Jr., Cochran, W.D.: 1973, Astrophys.J.Letters 186, L23

FIG. 1

The line width (FWHM) of HI in L1642. Unit is km/s. The right-hand cross is the centre of the molecular cloud. The dashed oval shows the maximum in the 12μm map of Laureijs et al. (1987), and the thin dashed line the direction of the galactic equator

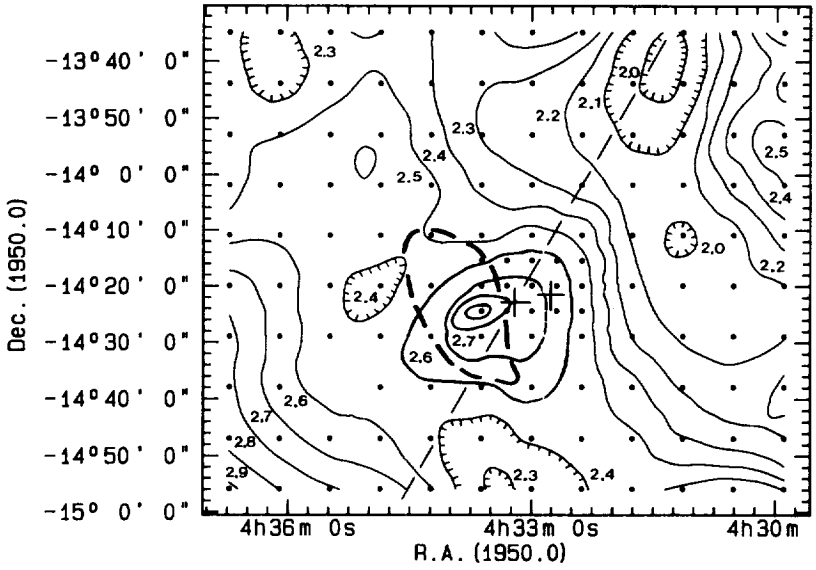

FIG. 2

The ratio $N_{HI}/N_H(tot)$ vs. A_V. The results of the "bright side" of L1642 are marked with open circles and the results of the "shadow side" with crosses. The three continuous curves correspond to the Hollenbach et al. (1971) $H+H \rightleftarrows H_2$ equilibrium model. The dashed line corresponds to a gas density of 9 10^3 cm^{-3} and to an ambient UV radiation field value half of that used by Hollenbach et al. (1971)

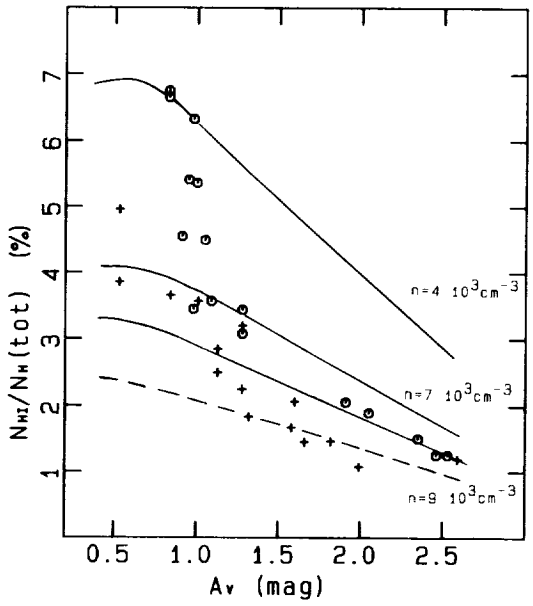

DUST EMISSION IN THE SAGITTARIUS B2 MOLECULAR CLOUD CORE

DARIUSZ C. LIS AND PAUL F. GOLDSMITH

FIVE COLLEGE RADIO ASTRONOMY OBSERVATORY, DEPARTMENT OF PHYSICS AND ASTRONOMY, UNIVERSITY OF MASSACHUSETTS, AMHERST, MA 01003

ABSTRACT

We present a model for the dust emission from the Sagittarius B2 molecular cloud core which reproduces the observed spectrum between 30 μ and 1300 μ, as well as the distribution of the emission at 1300 μ. The model is based on the assumption that Sgr B2(N) continuum source is located behind the dust cloud associated with Sgr B2(M) continuum source. The fact that Sgr B2(N) is stronger at 1300 μ can be attributed to a local column density maximum at the position of this source. Absence of a 53 μ emission peak at the position of Sgr B2(N) suggests that the luminosity of the north source is lower than that of the middle source.

I. OBSERVATIONS

We have observed the 1300 μ continuum emission in the Sgr B2 molecular cloud core, using the 14 m FCRAO radome enclosed telescope at New Salem, Massachusetts. The receiver system comprised two cooled Schottky diode receivers sensitive to orthogonal linear polarizations with an IF bandwidth of approximately 500 MHz. The LO frequency of 230.2 GHz was selected to be free of any strong line emission. The data were taken on three days in February and March 1988 and consist of 45 positions with 15″ spacing and 16 positions with 20″ spacing centered at the position of Sgr B2(M) continuum source ($\alpha_{1950} = 17^h44^m10.5^s$, $\delta_{1950} = -28°22'05''$). The size of the mapped region is $1' \times 2'$. The receivers were tuned for double sideband operation. A typical double sideband system temperature referred to above the Earth's atmosphere at the low elevation characteristic of Sgr B2 was 1900 K. A 4 minute integration time gave an

observed r.m.s. fluctuation level of about 40 mK (1σ). Saturn was used for pointing and calibration. The FWHM beam size was measured to be 23″, and the beam efficiency was about 0.1 . The resulting conversion from the observed antenna temperature to the unpolarized flux density in 23″ beam is 185 Jy K^{-1}. A contour map of the emission, presented in Fig. 1, shows a qualitative agreement with the first data set obtained in 1986 (Goldsmith, Snell and Lis 1987), except of a small difference in declination of the peak of the emission. Each of the three data sets which are averaged in Fig. 1 shows the same distribution of the emission. The peak antenna temperature of 0.31 K (equivalent to the flux density of 58 Jy) is observed at the (0,40″) position corresponding approximately to the Sgr B2(N) continuum source. The antenna temperature observed at the position of the Sgr B2 (M) source is 0.24 K (equivalent to 45 Jy).

II. MODEL OF THE SOURCE

An acceptable model of the source should be able to reproduce the observed spectrum of the continuum emission, as well as to explain the absence of the 53 μ emission peak coincident with the maximum of the 1300 μ emission at the position of Sgr B2(N) (Harvey, Campbell, and Hoffmann 1977). We have modeled the source structure using the radiation transfer code of Egan, Leung, and Spagna (1988). We first find an equilibrium temperature distribution for Sgr B2(N) and Sgr B2(M) assuming spherical symmetry and no interaction between both sources. Then we compute the observed flux convolved with a Gaussian beam assuming that Sgr B2(N) is located behind the dust cloud associated with Sgr B2(M), and the emission from this source is therefore attenuated by cold foreground dust. The observations of the J=1→0 transition of $C^{18}O$ (Lis and Goldsmith 1988) suggest that the molecular cloud associated with Sgr B2(M) has a radius of about 22.5 pc and consists of a constant density envelope with an H_2 density of about 2200 cm^{-3} surrounding a central region with a power law density distribution with an exponent of -2 extending inward to about 1.25 pc. The average density within inner 1.25 pc is about 5.7×10^4 cm^{-3}. We have used this as a starting point for our calculations. From the small source size at 1300 μ it is clear that the emission originates from a small high density core of the cloud. Due to small beam filling factor and high temperature this core does not show up in the $C^{18}O$ emission. We have assumed the core to be a Gaussian and have taken the FWHM size (D_N) and central density (n_N) as parameters of the model. For Sgr B2(N) we have assumed a simple Gaussian core and a constant density envelope of the same density as for Sgr B2(M). For simplicity we have assumed the same radii of the envelopes. Density distributions for

Fig. 1.

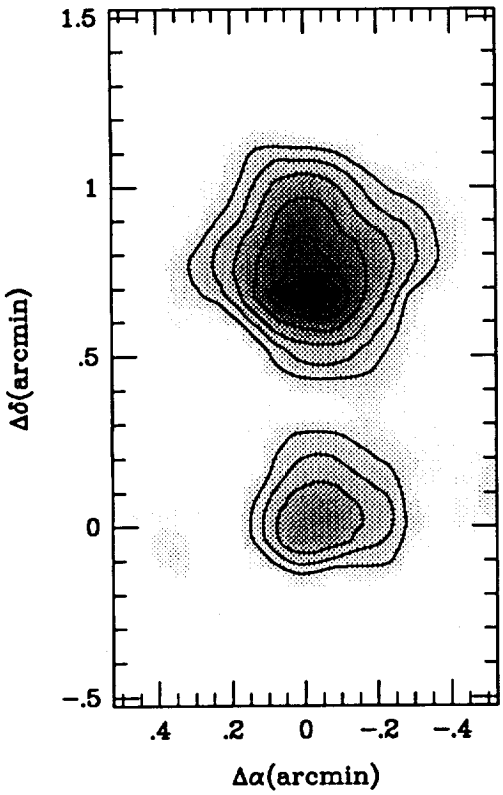

Fig. 2.

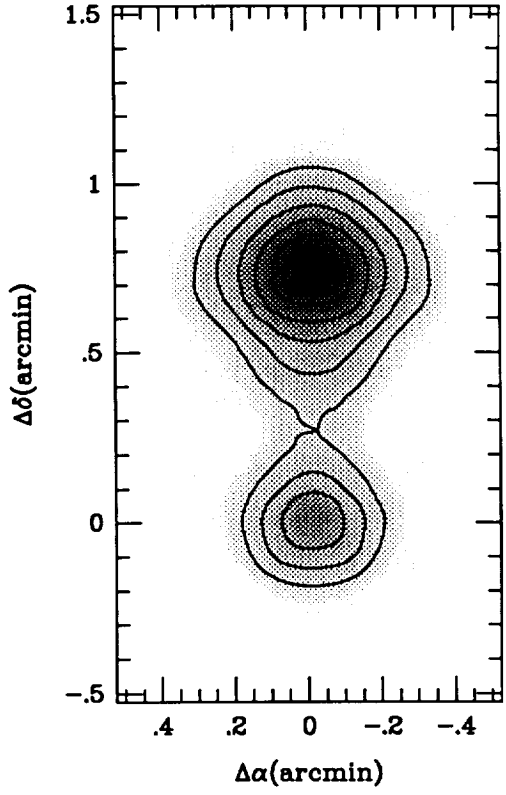

Fig. 3.

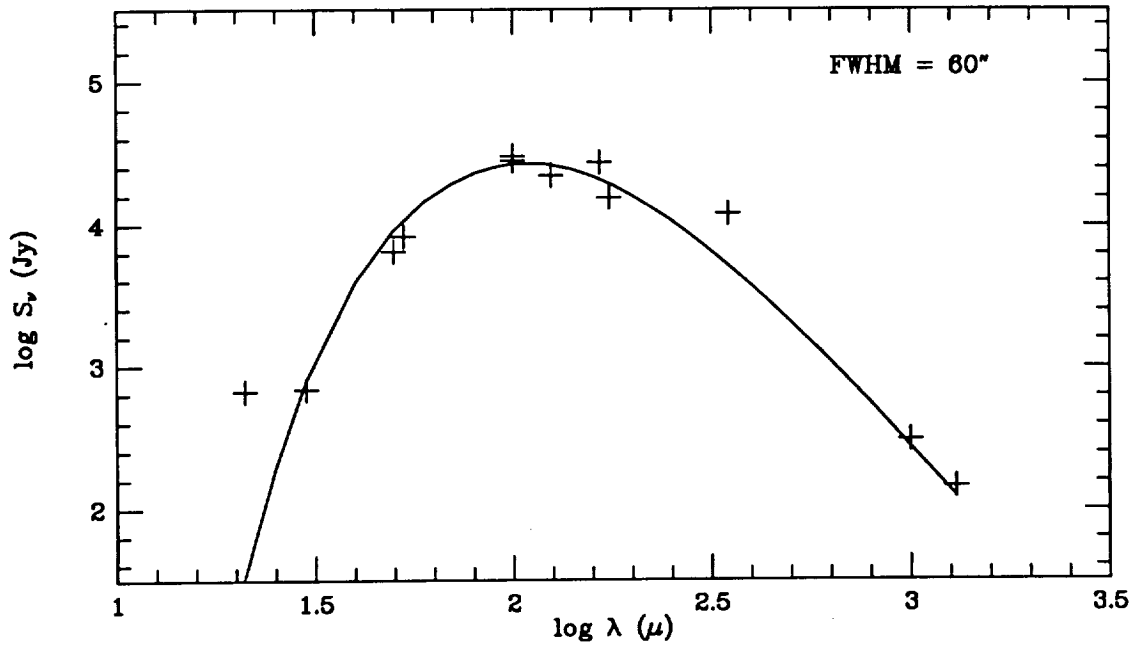

both sources as described above have been then scaled to give a required optical depth at 100 μ. Other important input parameters of the model are luminosities and temperatures of the central objects (L_N, L_M, T_N, T_M). We have used standard grain model with 0.1 μ radius and density of 3 g cm^{-3}. The grain emissivity varies as λ^{-1} between 0.1 and 100 μ and as λ^{α} for wavelengths longer than 100 μ, α being again a parameter varied in the computations. Based on a series of test runs we conclude that the wavelength of the peak of the convolved spectrum is sensitive mainly to the optical depth of the middle source (τ_M). The fact that the peak occurs at the wavelength of about 100 μ suggests that the optical depth at this frequency is relatively high. The flux at the peak is a function of the luminosity of the middle source. The 1300 μ flux is not very sensitive neither to the luminosity nor the temperature of the central star. It is mainly a function of the column density (or τ) and α. The 100 μ optical depth of the north source (τ_N) is, therefore, given by the optical depth of the middle source and the north-to-middle peak flux ratio at 1300 μ. The absence of the peak of the 53 μ emission at the position of Sgr B2(N) imposes an upper limit for the luminosity of the north source.

In this paper we present a model that successfully predicts distribution of the emission at 1300 μ, observed spectrum between 20 and 1300 μ and is consistent with the $C^{18}O$ data. The range of relevant parameters for which a good fit to the data is obtained has yet to be determined. The parameters of our model are presented in Table 1. Figure 2 presents distribution of the emission from our model cloud at 1300 μ, and Figure 3 the observed flux in 60″ beam as a function of wavelength.

III. CONCLUSION

We have presented a model for the dust emission from the Sgr B2 molecular cloud core. The model successfully predicts the observed spectrum of the continuum emission between 30 μ and 1300 μ and the observed distribution of the emission at 1300 μ. Sgr B2(N) is less luminous than Sgr B2(M) and the peak of the 1300 μ emission at the position of the north source is a result of a local column density maximum. This together with the fact that Sgr B2(N) is located behind the dust cloud associated with Sgr B2(M) continuum source explains why no peak of the 53 μ emission is detected at the position of Sgr B2(N). Observations of the 350 μ emission would be especially useful to test our model, because it predicts the peak fluxes from both sources to be approximately equal at this frequency.

Table 1. - Model parameters.

Parameter	M	N
$L(L_\odot)^a$	1.0×10^7	5.1×10^6
$T(K)^b$	$4. \times 10^4$	$4. \times 10^4$
$\tau_{100}(0'')^c$	2.2	2.1
$\tau_{100}(23'')$.....	1.7	-
$\tau_{100}(60'')$.....	0.9	-
$D_{core}(pc)^d$.....	0.5	1.1
$n_{grain}(cm^{-3})^e$ ..	7.0×10^{-6}	3.5×10^{-6}
$n_{H_2}(cm^{-3})^f$	2.5×10^6	1.3×10^6
α^g	1.4	1.4
$N_{H_2}(0'')^h$	5.4×10^{24}	-
$N_{H_2}(23'')$	2.0×10^{24}	-
$N_{H_2}(60'')$	1.1×10^{24}	-
$N_{H_2}(core)^i$	4.1×10^{24}	4.4×10^{24}

[a]Total luminosity of the central star.

[b]Temperature of the central star.

[c]100 μ optical depth for different beam sizes.

[d]FWHM size of the core.

[e]Grain density at the center.

[f]H_2 density at the center assuming standard gas to dust ratio of 100 by mass.

[g]Grain emissivity law slope for $\lambda > 100$ μ.

[h]H_2 column density for different beam sizes.

[i]H_2 column density through the core.

REFERENCES

Goldsmith, P.F., Snell, R.L., and Lis, D.C. 1987, *Ap. J.*, **313**, L5.

Egan, M.P, Leung, C.M., and Spagna, G.F 1988, *Comput. Phys. Commun.*, **48**, 271.

Harvey, P.M., Campbell, M.F., and Hoffmann, W.F. 1977, *Ap. J.*, **211**, 786. 271.

Lis, D.C., and Goldsmith, P.F. 1988, *Ap. J.*, in press.

ADDITIONAL RED AND REDDENED STARS IN Cyg 0B2 ASSOCIATION

M. Parthasarathy and S. K. Jain
Indian Institute of Astrophysics
Bangalore 560 034, India

ABSTRACT

Several new red and reddened stars are detected in the most heavily reddened association Cyg OB2. About 47 IRAS sources are detected in Cyg OB2. Their flux distributions, and colours, suggest that they are young stellar objects embedded in dust envelopes or disks (some of them may be proto stars) and are most likely members of the Cyg OB2 association. The large values of the flux ratio L_{IR}/L_{VIS} suggests that the central objects are obscured because of very large extinction.

1. INTRODUCTION

The Cyg OB2 (VI Cygni) association consists of a group of luminous O-B stars some of which are extremely reddened ($A_V \sim 4$-10 mag). Cyg OB2 is the most heavily reddened association in the northern sky. The association is centered around $\alpha = 20^h\ 31^m\ 0.5$, $\delta = 41°\ 16'$ (1950) with an angular diameter of about 1°. Spectroscopic and photometric investigations of the Cyg OB2 association have been carried out by Johnson and Morgan (1953); Morgan et al. (1954); Schulte (1956a,b, and 1958); Reddish et al. (1967); Leitherer et al. (1982); and Voelcker (1975). The initial very low dispersion spectroscopic survey of Schulte (1956a,b, and 1958) revealed several heavily reddened bright O-B stars. We have carried out a very low dispersion spectroscopic survey similar to that made by Schulte (1956a,b) to detect fainter red and reddened stars in the region of Cyg OB2. Cyg OB2 is a heavily reddened young association. There can be several very young objects embedded in the dust. We have searched the IRAS point-source catalogue (Beichman et al., 1985) for infrared sources in the Cyg OB2 region. In this paper we present results of our very low dispersion spectroscopic survey and also an analysis of the IRAS data of the Cyg OB2 association.

2. OBSERVATIONS

The very low dispersion spectra of stars in the Cyg OB2 region were obtained with the f/2 Cassegrain slitless spectrograph with a 3° quartz prism at the Cassegrain focus of the 102-cm Ritchey Chretien reflector at Kavalur Observatory. The spectra are unwidened. Each exposure covers a field of 40 min of arc diameter. The exposure times ranged from 5 to 45 min with Eastman Kodak 103a-E emulsion. The 103a-E emulsion and quartz prism (3°) combination gives spectra from 350 to 6600 Å. The dip in the sensitivity of the 103a-E emulsion at 5200 Å enables us to distinguish the blue and red portions of the spectrum.

3. REDDENED STARS

The principal criterion for classification is the shape of the stellar spectrum and also the density in different portions of the image. Because of the very low dispersion, we reach fainter magnitudes in short exposure times, and also overlapping of the spectra is almost avoided. The spectral classification criteria and the method of detection of red and reddened stars have been described by Schulte (1956a,b), Bappu and Parthasarathy (1977) and Parthasarathy (1978). Employing the very low dispersion (10,000 Å/mm) technique, Schulte (1956a,b) found several reddened early-type stars in Cyg OB2 association. We have used the spectral types and colours of Schulte's (1958) (see also Leitherer et al., 1982) reddened O-B stars, and also other bright stars in the field to compare and calibrate our classification. We have detected a number of new red and reddened stars in Cyg OB2 association. A few are given in table 1 and are also shown in figure 1. Some of the red stars detected by us have UBV photometric observations made by Reddish et al. (1967) (see table 1). The UBV data of Reddish et al. and our micro spectra clearly suggest that these are reddened stars.

4. IRAS OBSERVATIONS

We found 47 IRAS sources in the region of the Cyg OB2 association. Some of the bright IRAS sources in the Cyg OB2 association region are given in table 2. The 12-μm, 25-μm, 60-μm, and 100-μm fluxes, total integrated fluxes, F_{IR}, and the dust temperatures T_d of 19 sources are given in table 2. All the IRAS sources in Cyg OB2 association show flux increasing with increasing wavelength, similar to that observed in young stellar objects (Lada, 1987). We identified the optical counterparts of some of these IRAS sources. Some of the IRAS sources in Cyg OB2 association appear to be associated with OB stars. Some of the IRAS sources in Cyg OB2 association show very high luminosities $L_{IR}/L_O \sim 2\times10^4$ (table 2) and also show very large values of the ratio L_{IR}/L_{VIS}. The flux distribution's location clearly suggests that these are young stellar objects embedded in thick circumstellar dust envelopes or disks and are most likely members of Cyg OB2 association. The large values of the flux ratio L_{IR}/L_{VIS} suggest that the central optical objects are obscured because of very large extinction.

5. CONCLUSIONS

We have detected several new red and reddened stars in Cyg OB2 association. We have found about 47 IRAS sources in the Cyg OB2 association. Their flux distributions and colours suggest that these are young stellar objects embedded in dust envelopes or disks.

REFERENCES

Bappu, M.K.V. and Parthasarathy, M. 1977, Kodaikanal Obs. Bull. Ser., A 2, 1.

Beichman et al., 1985, IRAS point source catalogue, JPL.

Johnson, H.L. and Morgan, W.W. 1953, Astrophys. J., 117, 313.

Lada, C.J. 1987, IAP Symposium, 115, 1.

Leitherer, C. et al., 1982, Astron. Astrophys., 108, 102.

Morgan, W.W. et al., 1954, Astrophys. J., 120, 506.

Parthasarathy, M. 1978, IAU Symposium, 80, 25.

Reddish, V.C. et al., 1967, Pub. Roy. Obs. Edinburgh, 5, 111.

Schulte, D.H., 1956a, Astrophys. J., 123, 250; 1956b, Astrophys. J., 124, 530; 1958, Astrophys. J., 128, 41.

Voelcker, K. 1975, Astron. Astrophys. Suppl., 22, 1.

TABLE 1.– SOME OF THE REDDENED STARS WHOSE LOW DISPERSION SPECTRA ARE SHOWN IN FIGURE 1

Star no.	m_V	B-V	U-B	Comments
12	15.56	1.04	---	R1073
15	15.17	1.32	0.58	R 816
23	14.8	---	---	New
24	13.71	1.76	0.51	R 815
40	15.5	---	---	New
44	13.92	1.63	0.65	R 826
51	13.02	2.68	0.83	R 887
57	15.7	---	---	New
64	15.37	1.05	0.56	R 763
65	16.0	---	---	New
73	13.21	1.58	1.66	R 637
98	15.39	1.21	---	R 960
99	14.15	1.90	0.99	R 961
104	15.8	---	---	New
112	15.4	---	---	New
115	15.4	---	---	New
124	13.0	---	---	New
125	13.97	2.02	1.21	R 600
130	12.77	2.39	---	R 702
135	14.02	1.93	0.76	R 603
155	13.97	1.50	0.52	R 719
434	14.0	---	---	New
463	14.0	---	---	New
491	12.5	---	---	New
495	14.7	---	---	New
498	14.5	---	---	New
500	14.4	---	---	New
539	13.5	---	---	New
550	12.5	---	---	New

Note: The prefix "R" means the number refers to the catalogue number of Reddish et al.

TABLE 2.– SOME BRIGHT IRAS SOURCES IN Cyg OB ASSOCIATION

S. No.	Coordinates (1950)		IRAS FLUXES (Jy)				F_{IR}	T_d K	$L_{IR/L_\odot}$
	R.A.	Dec.	12-μm	25-μm	60-μm	100-μm	$\times 10^{-13} Wm^{-2}$		
1	$20^h28^m40.6^s$	+41°05'39"	12.91	91.9	789.89	1387.02	916.40	47	1.15×10^4
2	20 29 03	+40 52 15	0.58	5.62	65.67	136.29	76.93	43	9.62×10^2
3	20 29 32.9	+41 26 30	0.46	2.08	7.42	133.0	50.08	22	6.26×10^2
4	20 29 42	+40 52 42	1.3	2.8	34.1	150.6	69.10	32	8.64×10^2
5	20 30 2.2	+40 58 47	2.01	6.08	47.59	159.09	81.80	35	1.02×10^3
6	20 30 28.4	+40 59 00	4.21	10.29	179.8	800.2	360.10	32	4.50×10^3
7	20 31 28.1	+41 06 51	1.78	4.08	61.26	---	39.40	63	4.93×10^2
8	20 31 30.3	+40 48 39	1.48	4.26	49.71	142.2	74.90	38	9.37×10^2
9	20 32 8.0	+41 12 22	5.22	28.27	427.89	920.61	529.60	42	6.62×10^3
10	20 32 10.6	+41 46 10	1.58	2.52	44.38	88.72	52.98	36	6.63×10^2
11	20 32 26.3	+40 57 58	14.53	37.01	76.68	147.43	155.81	44	1.95×10^3
12	20 32 43.5	+41 20 22	11.56	17.54	286.67	631.4	363.90	38	4.55×10^3
13	20 32 46.0	+41 48 20	1.21	1.40	42.19	163.23	75.44	34	9.43×10^2
14	20 32 52.8	+40 42 32	3.63	8.73	76.3	---	53.80	71	6.73×10^2
15	20 33 12.3	+40 34 39	1.2	2.5	45.6	125.72	65.60	38	8.20×10^2
16	20 33 12.9	+41 24 24	11.44	77.46	909.21	1376.07	950.00	51	1.19×10^4
17	20 33 21.3	+41 02 53	22.85	74.88	1246.12	2477.62	1472.00	44	1.84×10^4
18	20 33 46.5	+41 04 56	4.42	7.8	192.37	542.43	277.00	38	3.46×10^3
19	20 34 19.5	+41 29 33	22.12	151.76	690.2	1035.34	822.00	17	1.03×10^4

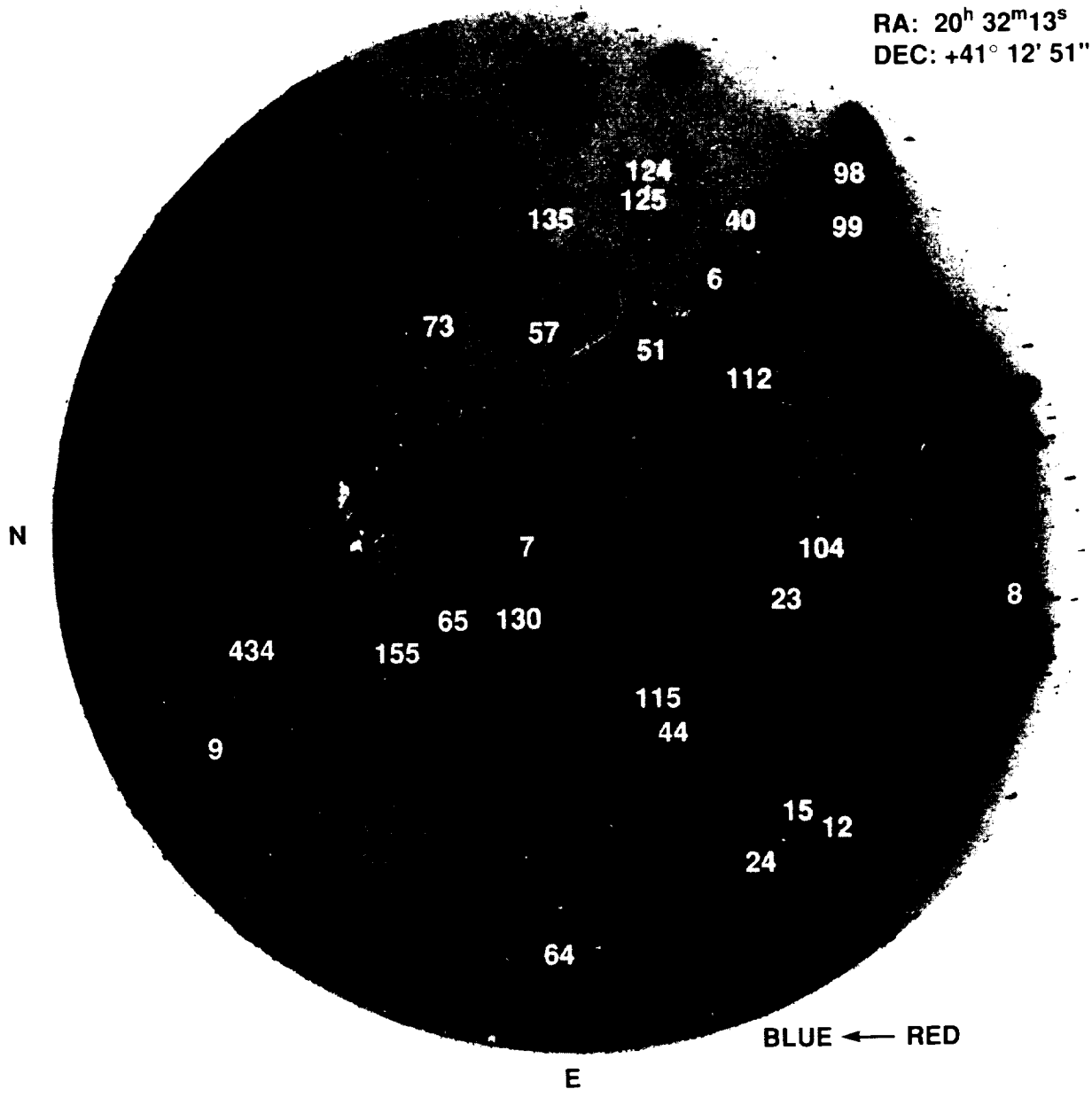

Plate 1: Low dispersion spectrograms of the Cyg OB2 association. Some of the red and reddened stars listed in table 1 are shown here. The encircled stars represent some of the IRAS sources listed in table 2.

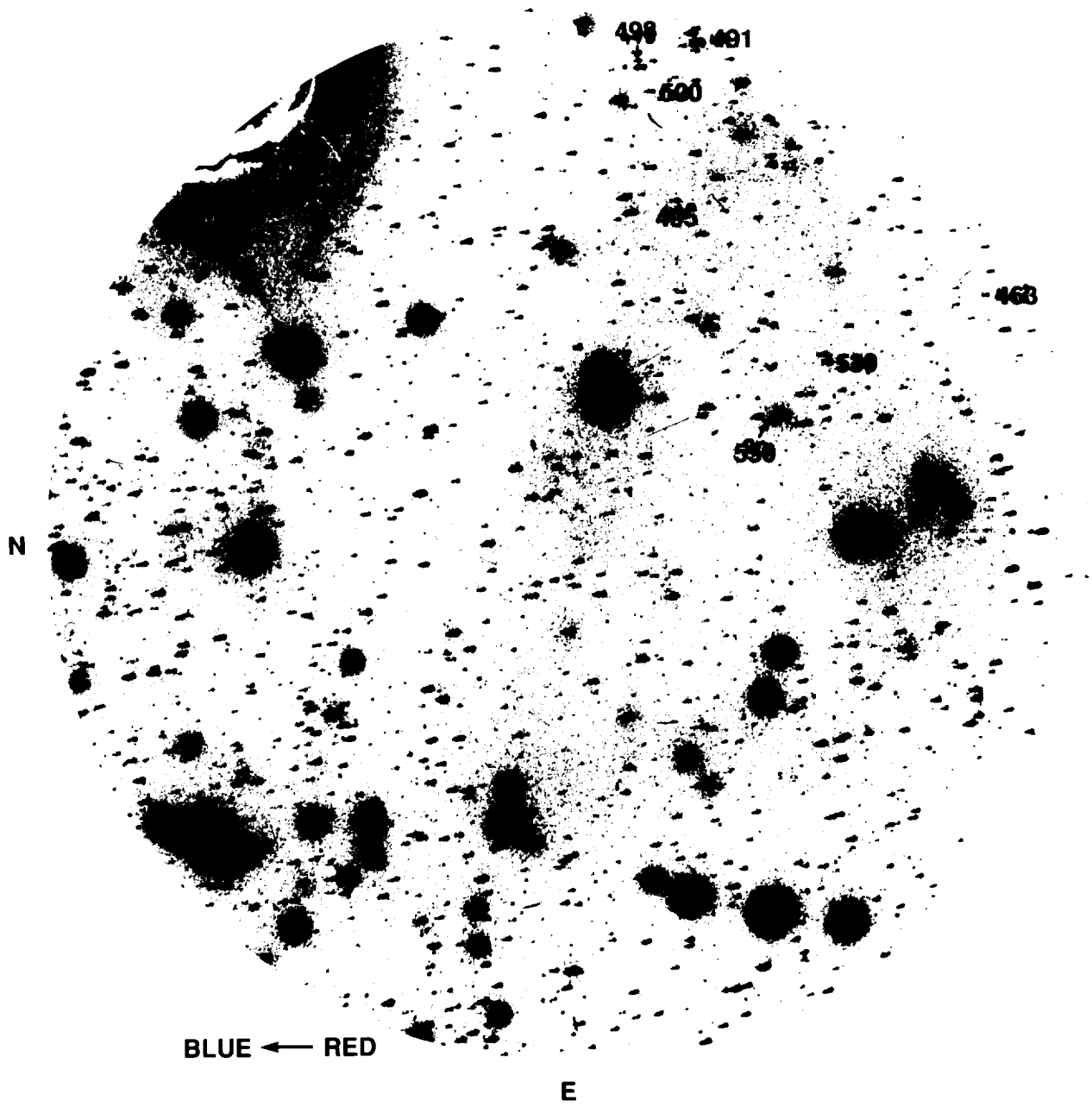

Plate 1: Concluded.

The Embedded Objects in ε Cha I Cloud

T. Prusti R. Assendorp P. Wesselius

Laboratory for Space Research, Groningen

Abstract

We have carried out a study of the embedded objects in the ε Cha I cloud. General shapes of the spectra have been constructed for the members in the cloud. The near infrared data have been compiled from the literature and combined with the IRAS Point Source Catalog information. Pointed observations by the IRAS have been used in the regions of high source density where the Point Source Catalog is confused. Member objects near the late B star HD 97300 have been measured recently in the $3 - 10$ μm bands using the ESO 2.2 meter telescope in order to investigate the effects of disks seen in other young stellar objects.

We present a picture of the complete initial luminosity function in the ε Cha I cloud. Individual objects of interest are discussed separately. Finally we compare the observations with the theoretical views on low mass star formation.

INTERFEROMETRIC MOLECULAR LINE OBSERVATIONS OF W51

Alexander Rudolph[1,2], William J. Welch[1], Patrick Palmer [3], and Bérengère Dubrulle[1,4]

[1] *Radio Astronomy Laboratory, University of California, Berkeley Ca 94720, USA*

[2] *Department of Physics, University of Chicago, Chicago, Illinois 60637, USA*

[3] *Department of Astronomy and Astrophysics, University of Chicago, Chicago, Illinois 60637, USA*

[4] *École Normale Supérieure, 45 rue d'Ulm, 75230 Paris Cedex 05, France*

This abstract presents observations of the HII region complex in W51 made with the Hat Creek millimeter interferometer. W51 is a region of massive star-formation approximately 7 kpc distant from the sun (cf. Bieging, *et.al.* 1975). This region has been extensively studied in both the infrared and submillimeter (Genzel, *et.al.* 1982, Jaffe, *et.al.* 1984, Jaffe, *et.al.* 1987) and the radio (Scott 1978, Genzel, *et.al.* 1982, Ho, *et.al.* 1983) as well as in maser transitions (Genzel and Downes 1977). These previous observations have revealed three regions of interest: (1) W51MAIN, a knot of bright maser emission near two compact HII regions W51e1 and W51e2 (Genzel and Downes 1977, Scott 1978). W51MAIN is also the peak of the 400 μm emission indicating that the bulk of the mass ($\approx 50{,}000\ M_\odot$) is centered here (Jaffe, *et.al.* 1984). However, there is no 20 μm emission towards W51MAIN (Genzel, *et.al.* 1982) implying a large extinction in that direction. This is consistent with a dense molecular cloud shrouding the forming O and B stars. (2) W51IRS1 is a long curving structure seen at 20 μm and at 2 and 6 cm but not at 400 μm. (3) W51IRS2 (also known as W51NORTH) is another compact HII region slightly offset from an 8 μm and a 20 μm peak and a collection of H_2O masers (Genzel, *et.al.* 1982, Genzel and Downes 1977). In both W51MAIN and W51IRS2 there is hot (100 K) ammonia seen (Ho, *et.al.* 1983) and evidence for outflow activity (red- and blue-shifted masers, shock-excited H_2, and high-velocity wings of SiO (Genzel, *et.al.* 1981, Schneps, *et.al.* 1981, Beckwith and Zuckerman 1982, Downes, *et.al.* 1982).

These observations were made with 8 configurations of the three 6.1m antennas at the Hat Creek millimeter interferometer. The observations were made with a 512-channel digital correlator allowing simultaneous observations of the HCO^+ $J = 1 \rightarrow 0$ transition, the SO $2_2 \rightarrow 1_1$ transition, and the $H^{13}CN$ $J = 1 \rightarrow 0$ transition, all with $\approx 5'' \times 6''$ resolution. In addition, a 3.4mm continuum emission map was made from the channels with no molecular emission.

SO and $H^{13}CN$ Emission

Figure 1 shows maps of SO and $H^{13}CN$ emission towards W51. In each case the distribution of the emission consists of three point sources (emission peaks 1, 2, and 3), surrounded by weak, diffuse emission. These point sources coincide with extensive evidence for outflow activity: H_2O maser proper motions, quadrupole lines of H_2, and high-velocity line wings of SiO, as well as hot ($T > 100$ K) NH_3 emission (Ho, *et.al.* 1983, and references therein). The compactness of the SO emission in conjunction with the large extent of the emission from HCO^+, a molecule requiring equally high densities to excite, implies that there is an SO abundance enhancement near these star-forming regions. Compact SO emission is also seen in association with Orion, W49, SgrB2, and G34.3+0.2 (Hat Creek results in preparation). Thus, this result seems to be universal to high-mass star-forming

regions with outflows, and it may be possible to use such small-scale SO emission as a signpost of outflow activity. In addition, a fourth $H^{13}CN$ emission peak is detected $\approx 13''$ northwest of W51MAIN.

Continuum Map

Figure 2 shows the 3.4mm continuum map. W51 e1, e2, IRS1, and IRS2 are detected. The overall structure of the emission is very similar to that seen at 1.3cm (Ho, *et.al.* 1983). W51 e1 and e2 are unresolved, while IRS2 has a size $6''.7 \times 9''.7$ which deconvolves to $\approx 3'' \times 8''$. W51IRS1 also shows some evidence for the curving structure to the south seen at 6cm and 20μm. A new source, not seen at 1.3cm, and therefore likely due to thermal dust, is detected. This source, labeled W51DUST, is coincident with the source $H^{13}CN$-4, and may constitute a region in very early stages of star formation.

HCO^+ Spectra

Figure 2 also shows spectra of HCO^+ towards the four main continuum sources, e2, e1, IRS1, and IRS2. All four spectra show red-shifted absorption, indicating the presence of infalling gas. These spectra are consistent with overall collapse of the W51 region towards the mass concentration at W51MAIN. This result is similar to that found by Welch, *et.al.* (1987) for W49. Thus these observations confirm that large O-B associations are formed by overall collapse of the molecular cloud.

The spectrum towards W51IRS1 shows both red-shifted *and blue-shifted* absorption. If the infall picture is correct then the detection of both red-shifted and blue-shifted absorption towards W51IRS1 suggests that it may be behind the collapsing sphere of material and thus the emission is absorbed by material in both directions of the infall.

Continuum Spectra : Evidence for Dust Emission at 3.4mm

Figure 3 contains a table of fluxes for the sources in W51, and shows the spectra plotted below. W51e2 is an ultracompact HII region closely associated with the maser emission W51MAIN. The long wavelength emission of this source is consistent with optically thick free-free emission with a turnover frequency of ≈ 23 GHz. If the source has a temperature of 10000 K, then the implied emission measure is 2×10^9 cm^{-6} pc, the size is 3×10^{16} cm, the density is 5×10^5cm^{-3}. These all imply 8×10^{47} ionizing photons/sec, consistent with a single O9 star.

Extrapolating the 1.3cm free-free emission of 0.38 Jy to 3.4mm, one finds an excess of 0.9 Jy. This excess is due to dust. The 3.4mm excess plotted along with the peak fluxes of the lower resolution 1.2mm and 400μm maps, fit a power law of $\lambda^{-3.4\pm0.1}$, consistent with thermal dust with an emissivity $\epsilon \propto \lambda^{-1.4\pm0.1}$.

W51e1 shows an essentially flat spectrum from 6cm to 1.3cm, indicating that it is optically thin at these wavelengths. This is consistent with e1 being a more evolved region that e2. The 3.4mm flux of 0.39 Jy again shows an excess over the 1.3cm flux of 0.18 Jy.

The 400μm, 1.2mm, 3.4mm, and 1.3cm fluxes, integrated over a region $\approx 40''$ in size, including W51 e2, e1, and DUST, are plotted as W51MAIN. Fitting the 3.4mm excess with

the shorter wavelength measurements gives an excellent fit to a power law of $\lambda^{-3.2\pm0.1}$. Thus, the dust around W51MAIN is in two components:

1) A point source concentrated within the ultracompact HII region e2 ($d < 2 \times 10^{16}$ cm).

2) Extended emission within 40″ of W51MAIN, primarily in W51e1 and W51DUST.

W51IRS2 also shows a 3.4mm/1.3cm excess. The 3.4mm flux is 5.41 Jy and the 1.3cm flux is 3.34 Jy. The fit to the 3.4mm dust contribution, and the 1.2mm and 400μm integrated fluxes is $\lambda^{-3.1\pm0.1}$.

Conclusions

The conclusions are as follows:

1) SO and $H^{13}CN$ emission are similar and coincide with outflow activity

2) HCO^+ spectra show evidence for overall collapse of the W51 cloud towards W51MAIN. W51IRS1 is behind this collapsing sphere.

3) A previously undetected continuum peak, W51DUST, coincides with the molecular peak $H^{13}CN$-4. This may be a region in the very early stages of star-formation.

4) Dust emission at 3.4mm reveals that about half the 400μm emission comes from the ultracompact HII region e2, and the rest from W51e1 and W51DUST. W51IRS2 also shows evidence for dust at 3.4mm.

References

Beckwith, S., and Zuckerman, B. 1982, *Ap. J.*, **255**, 536.

Bieging, J. 1975, in HII *Regions and Related Topics*, ed. T. L. Wilson and D. Downes (Berlin: Springer-Verlag), p.443.

Downes, D., Genzel, R., Hjalmarson, A., Nyman, L. A., and Ronnang, B. 1982, *Ap. J. (Letters)*, **252**, L29.

Genzel, R., and Downes, D. 1977, *Astr. Ap. Suppl.*, **30**, 145.

Genzel, R., *et.al.* 1981, *Ap. J.*, **247**, 1039.

Genzel, R., Becklin, E. E., Wynn-Williams, C. G., Moran, J. M., Reid, M. J., Jaffe, D. T., and Downes, D. 1982, *Ap. J.*, **255**, 527.

Ho, P. T. P., Genzel, R., and Das, A. 1983, *Ap. J.*, **266**, 596.

Jaffe, D. T., Becklin, E. E., and Hildebrand, R. H. 1984, *Ap. J. (Letters)*, **279**, L51.

Jaffe, D. T., Harris, A. I., and Genzel, R. 1987, *Ap. J.*, **316**, 231.

Schneps, M. H., Lane, A. P., Downes, D., Moran, J. M., Genzel, R., and Reid, M. J. 1981, *Ap. J.*, **249**, 124.

Scott, P. F. 1978, *M. N. R. A. S.*, **183**, 435.

Welch, W. J., Dreher, J. W., Jackson, J. M., Terebey, S., and Vogel, S. N. 1987, *Science*, **238**, 1550.

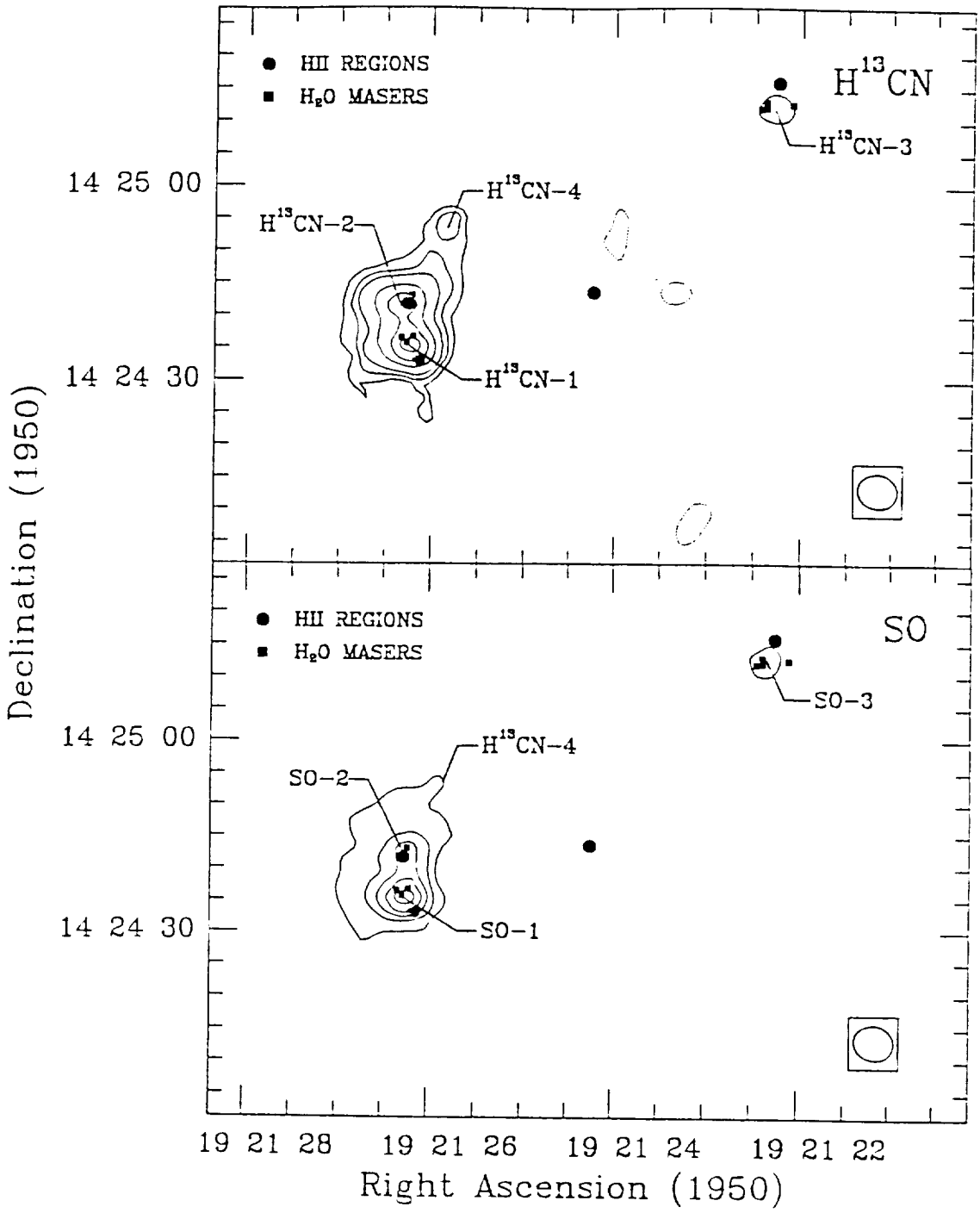

Figure 1

Top - $H^{13}CN(J=1\rightarrow0)$ emission from W51. Contour levels are -.2,-.1,.1,.2,.3,.5,.7,.9 of the peak flux of 7.7 K (1σ = 0.3 K). Bottom - SO ($2_2 \rightarrow 1_1$) emission from W51. Contour levels are -.1,.1,.3,.5,.7,.9 of the peak flux of 6.1 K. (1σ = 0.3 K). Peaks are marked by numbers 1,2,3,4. Squares are HII regions, circles are prominent H_2O maser clusters. The beam is 6".4x5".3.

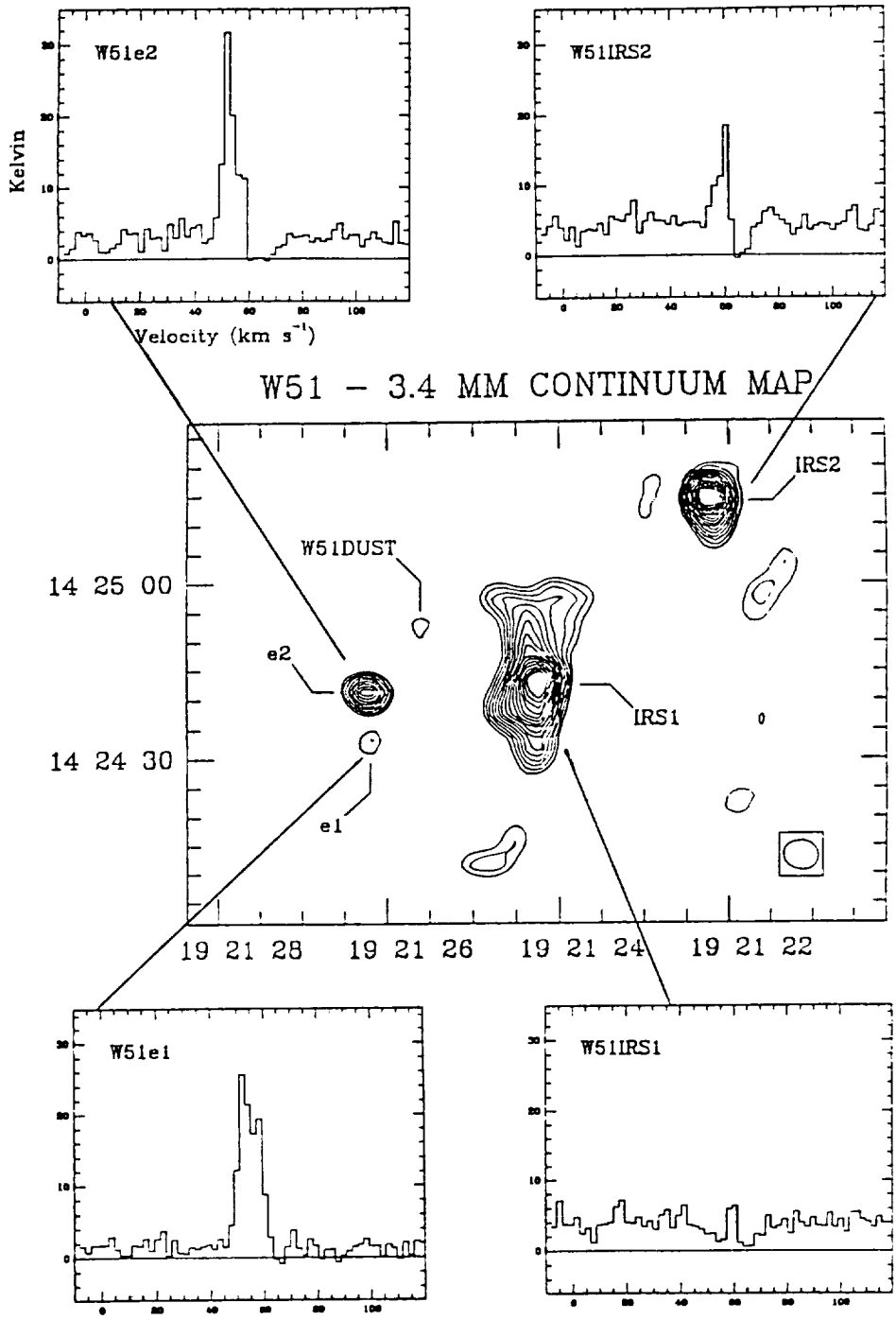

Figure 2

3.4 mm continuum map of W51. Contour levels are -5,-4,4,5,6,7,8,9,10,11, 12, 13,14,15,16,17,18,19 times 0.060 Jy/beam (1σ). The four spectra are HCO^+(J-1→0) emission towards the four main continuum emission features. All four spectra show red-shifted absorption indicating the presence of infalling gas. The spectrum towards W51IRS1 shows both red- and blue-shifted absorption indicating that it is behind the infalling cloud.

Fluxes for W51[a]

Source	6cm	2cm	1.3cm	3.4mm	$3.4^{(dust)}$mm	1.2mm	400μm	α^{dust}
W51e2	<0.02	0.15	0.38	1.23	0.90	26[b]	1200[b]	3.4±0.1
W51e1	0.14	0.19	0.18	0.39				
W51MAIN[c]			0.56	3.25	2.76	74	2500	3.2±0.1
W51IRS2[d]			3.34	5.41	2.95	54	1800	3.1±0.1

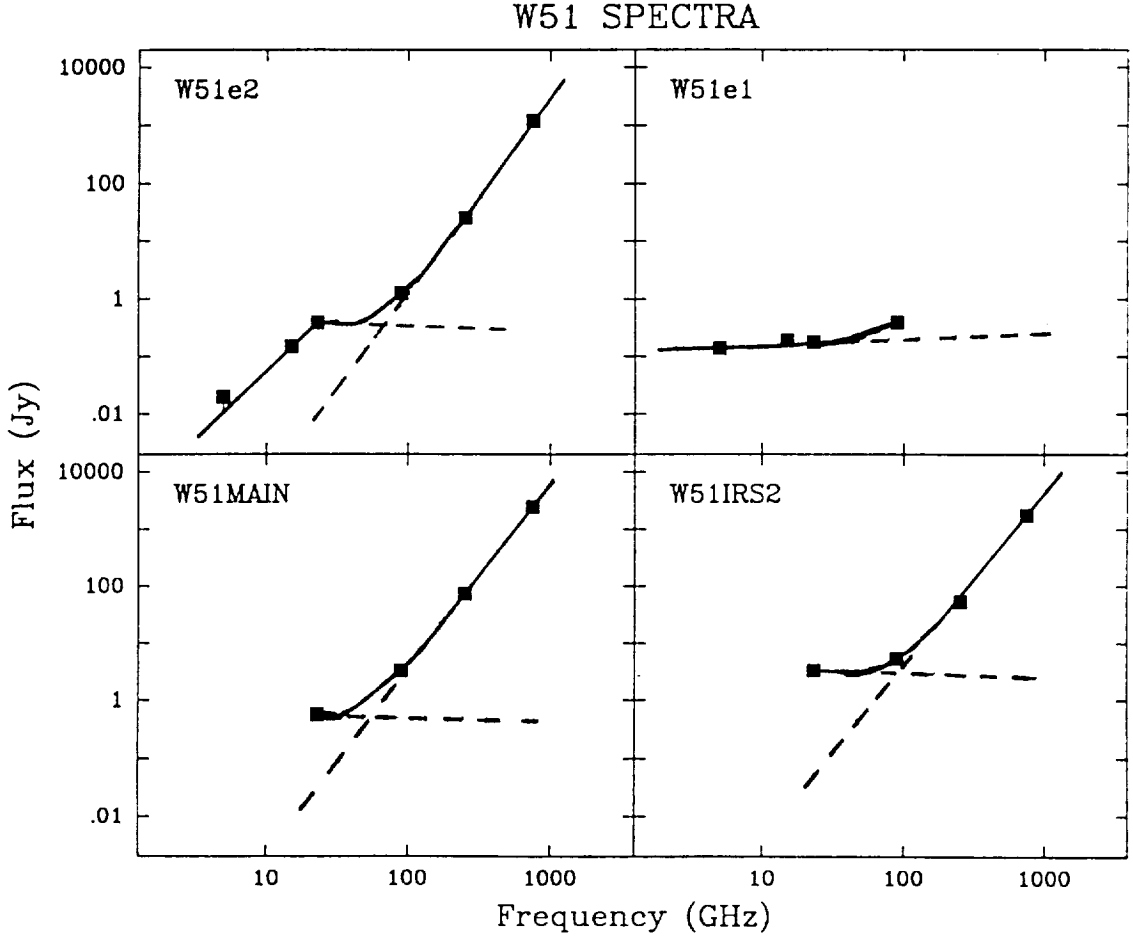

Figure 3

Spectra of W51 e2, e1, MAIN, and IRS2.

2,6 cm Scott (1978)
1.3 cm Ho, et al (1983)
3.4 mm This work
1.2 mm Martin (1987)
400 μm Jaffe, et al (1984)

[a]All fluxes in Jy except as noted
[b]Peak flux in Jy/beam
[c]Total flux from 40" area
[d]1.3cm and 3.4mm are primary beam corrected

DUST EMISSION FROM BARNARD 35: GAS HEATING ANOMALY RESOLVED

Howard A. Smith
Naval Research Laboratory
Washington, D.C. 20375

ABSTRACT

The molecular cloud B35 has puzzled observers because it contains gas which is at $T_g \approx 23K$, hotter than the surrounding dust whose $T_d \approx 10K$. An investigation of the IRAS data, however, shows a previously unreported dust component at $T_d \approx 33K$ whose luminosity is ample to heat the gas. IRAS also finds that about 12% of the total luminosity around the core, and about 20% along the rim, arises from the small grain component with T≤300K. The temperatures of these two components vary across the source, and this behavior is discussed. The results illustrate the presence of multiple components of dust in these clouds, and emphasize the need for data at multiple wavelengths.

1. INTRODUCTION

Barnard 35 is a bright-rimmed dark cloud, one of a ring of such clouds located at the edge of the large HII region excited by the λ Ori OB association. It is about 18'x4' in overall size, and has a far infrared point source at the densest part of the cloud, at the western edge close to the bright rim. It has gas and dust temperatures that resemble in general those in other dark clouds and globules. Along the bright ridge, however, the CO is heated to $T_g=23.4\pm3.5$ K, while measurements of the dust temperature in this ridge give $T_d=10\pm5$ K (Lada et al., 1981). Because the usual model for gas heating uses gas-dust collisions, alternative mechanisms for heating the dust in this cloud have been investigated, but found inadequate or inconclusive. These including shock heating, magnetic viscous heating, and heating from the nearby star FU Ori (Lada and Wilking, 1980; Smith et al., 1982).

2. IRAS DATA

We have used the IRAS coadded data on B35 to analyze the emission from dust in three zones: the outer rim of the cloud, the small inner core along the line-of-sight to the embedded star, and the intervening region ("limb") between the two. Figure 1 shows the 60 μm IRAS image

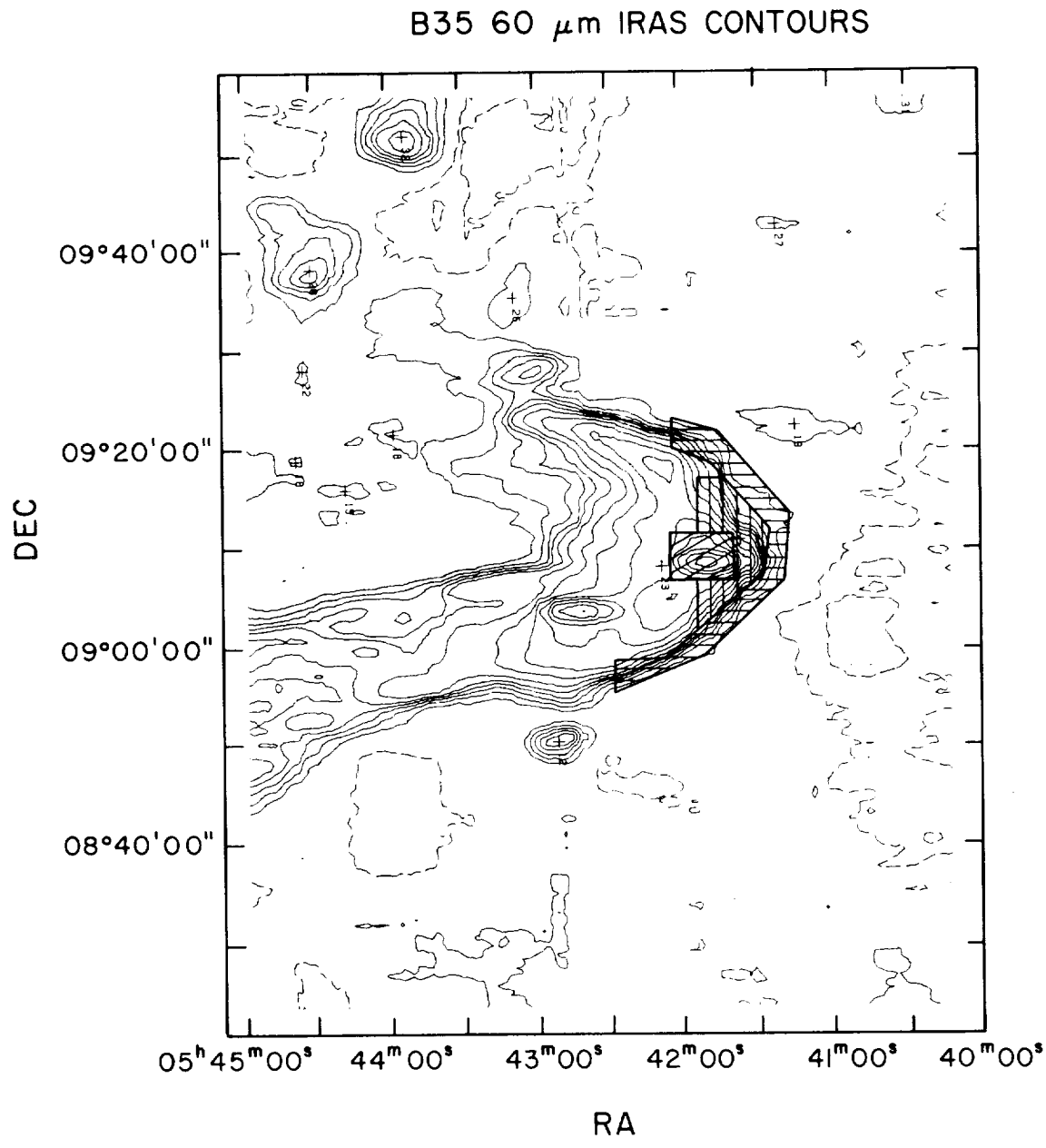

Figure 1: The IRAS 60 μm contours of the B35 cloud, with coordinates for epoch 1950.0. The three areas used for dust analysis (see text) are shown.

of B35, with the three zones indicated. The data reduction procedure first approximately corrected for overlying zodiacal emission by measuring the background at several locations away from the source, fitting that emission to a plane, and subtracting the plane from the entire image, at all four IRAS bands. Next the 12, 25 and 60 μm images were degraded to the same resolution as the 100 μm image, so that approximately equivalent areas were being compared; in each wavelength band the area examined was the same to within 5%. The AIPS software package was then used to measure the integrated intensity in each of the areas, in each of the bands, and the corresponding statistics. Next the data were color-corrected according to standard procedures as described in the IRAS Explanatory Supplement (Beichman et al., 1985). Finally the flux values were fit to a two temperature greybody model, whose emissivity was also varied according to υ^{β} with β=0, 1 or 2. Table 1 lists the results of this data reduction.

3. DISCUSSION

The data of Lada et al. were obtained from the Kuiper Airborne Observatory with a set of four far infrared filters, 80 μm being the shortest wavelength passed by the filters and diffraction limiting the long wavelength response. As a result the KAO system was very sensitive to the cold dust ($T_g \approx 10K$), which emits at wavelengths longer than about 140 μm, but was not sensitive to a warm component which IRAS easily detects. On the other hand the IRAS 100 μm filter passes very little radiation longward of about 110 μm

The IRAS data on B35 in fact reveal a warm 33K dust component not seen by the Lada et al. KAO observations. Figure 2 is a plot of the continuum emission from the 2′ region around the core, showing both the IRAS data and those from the KAO. The two data sets are mutually consistent because at IRAS wavelengths the flux from a λ^{-1} cold greybody is on the modified Wien tail and in this case down by a factor of 16 from the KAO data point. IRAS and KAO data each sample a different component of the dust. IRAS finds the luminosity in the ≈30K dust component around the core to be about 3.4 $L_{\odot}$, and over the entire region of warm CO gas about 700$L_{\odot}$, more than enough to provide the necessary gas heating and an order-of-magnitude larger than the previous estimates of cloud luminosity (Lada et al., 1981). We expect that multiple dust temperature components are the norm in dark clouds, and CO temperatures can provide a clue that warmer dust is present than is indicated by the data longward of 100 μm. The results emphasize the importance of observations at multiple wavelengths.

The IRAS data also show a strong component of high temperature emission, the small grain contribution, at a characteristic temperature of ≤ 300K, and cooling noticeably as the line-of-sight moves from the edge to the core of the cloud. The total luminosity in this high

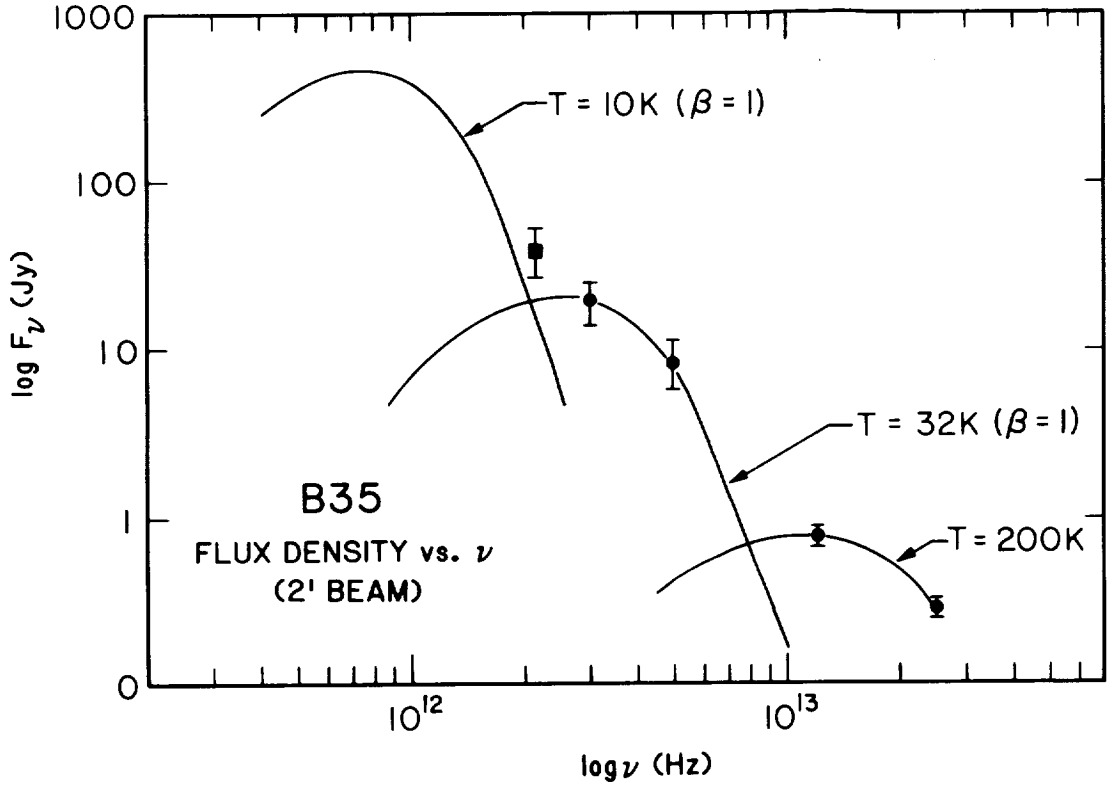

Figure 2: The continuum spectrum of B35 in a 2′ region around the core. The dots are from IRAS data, and the square from the KAO data of Lada et al. (1981). Curves are best fits to the data points, with assumed dust emissivity laws as indicated. The KAO data were obtained with a set of four long-wavelength pass filters, and the shape of the T=10K curve is determined by more data than this single point.

temperature component is between 10-20% of the total source luminosity, an amount comparable to that seen in other clouds. The low temperature component is at about 30K, and warms noticeable as the line-of-sight moves inward, behavior expected because of the presence of the embedded hot young star. Figure 3 plots the temperatures of these two components versus sampled area as the line-of-sight moves inward from the rim toward the cloud core. The optical depth of the dust at 100 μm in each of the three zones is $\approx 10^{-4}$.

The small grain component might itself contribute to the heating of the gas since its temperature and luminosity are more than ample. However the usual gas heating mechanism is collisional, and proportional to n_{gr}(hot)σ (Burke and Hollenbach, 1983). The total abundance of small grains n_{gr} is estimated at $<10^{-2}$ by mass of the total dust (Sellgren, 1983), with the amount being hot at any time given approximately by the ratio of the cooling time to the time

between collisions, $\approx 10^{-2}$ (Dwek, 1984; private communication). In addition their geometrical cross-section is 4-5 orders-of-magnitude smaller than that of the normal dust component. If these grains are to heat the gas significantly, therefore, it must be through some more efficient mechanism, perhaps involving photoelectric heating (Draine and Sutin, 1987).

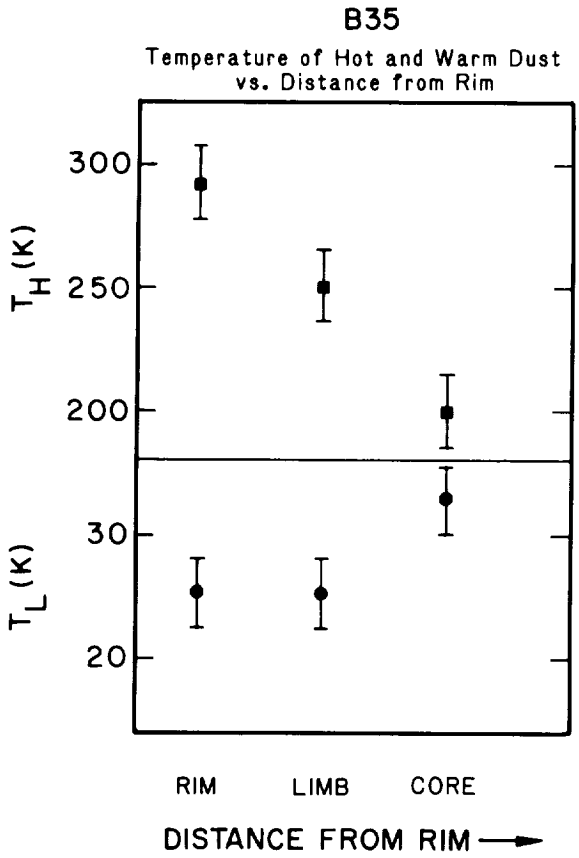

Figure 3: Plot of the temperature of the hot and warm dust components versus distance from the cloud rim. The uncertainties reflect both statistical flux errors and uncertainties in the appropriate spectral shape to use for color corrections and temperature fitting. All data are from the IRAS coadded scans.

REFERENCES

Beichman, C.A., Neugebauer, G., Habing, H.J., Clegg, P.E., and Chester, T.J.: 1985, *IRAS Catalogs and Atlases Explanatory Supplement* (Pasadena, JPL)

Burke, J.R. and Hollenbach, D.J.: 1983, Ap.J., 265, 223

Draine, B.T. and Sutin, B.: 1987, Ap.J., 320, 803

Dwek, E: 1986, Ap.J., 302, 363

Lada, C.J. and Wilking, B.A.: 1980, Ap.J., 242, 1056

Lada, C.J., Thronson, H.A., Smith, H.A., Harper, D.A., Keene, J., Loewenstein, R.F., and Smith, J.: 1981, Ap.J., 251, L91

Sellgren, C.: 1983, Ph.D. Thesis

Smith, H.A., Thronson, H.A., Lada, C.J., Harper, D.A., Loewenstein, R.F. and Smith, J.: 1982, Ap.J., 258, 170

TABLE 1
IRAS FLUXES AND DUST TEMPERATURES[a,b]

	12 μm	25 μm	60 μm	100 μm	T_H	T_L	L_H	L_H
	(Jy)				(K)		($L_\odot$)	
Outer Rim (area$\approx 1.8\times10^{-4}$ sr)	47.5	50.7	318	1702	292	25.5	81	312
Inner Limb (area $\approx 5.1\times10^{-5}$ sr)	33.3	48.7	292	1607	251	25.3	61	296
Central Core (area $\approx 7.8\times10^{-6}$ sr)	7.1	18.9	203	475	200	33.0	18	87

[a] IRAS color corrected fluxes, assumming for the correction a T≈200K blackbody (β=0) for the 12 and 25 μm fluxes, and a β=1 emissivity dependence to the 60 and 100 μm emission. The corrected raw data points were then fit to β=0 and 1 blackbodies, respectively, and the corrected fluxes and derived temperatures and luminosities listed here.

[b] We have estimated the 3σ error bars as ±10% in the 12 and 25 μm data, and ±30% in the 60 and 100 μm data. These error bars reflect both uncertainties in the raw data, the color correction values, the two temperature fits, and possible variations in β.

A TWO MICRON POLARIZATION SURVEY TOWARD DARK CLOUDS

M. Tamura[1], S. Sato[2], I. Gatley[3], J. H. Hough[4]
[1]Kyoto University, Kyoto 606, Japan
[2]Tokyo Astronomical Observatory, Tokyo, Japan
[3]ADP, NOAO, Tucson, AZ85726, USA
[4]Hatfield Polytechnic, Hertfordshire AL109AB, UK

A near-infrared (2.2 μm) polarization survey of about 190 sources has been conducted toward nearby dark clouds. The sample includes both background field stars and embedded young stellar objects. The aim of the project is (i) to determine the magnetic field structure in the densest regions of the dark clouds and study the role of magnetic fields in various phases of star formation processes, and (ii) to study the grain alignment efficiency in the dark cloud cores.

From the polarization of background field stars and intrinsically unpolarized embedded sources, we have determined the magnetic field structure in these clouds. In Heiles Cloud 2, the Rho Oph core, and the NGC 1333 region, the observed intracloud polarization vectors are coincident in direction with the optical polarization in the outer regions of the clouds and are well aligned in a direction perpendicular to the long axis of the cloud elongation. These suggest that the magnetic field lines are smoothly connected from the outer regions to the inner regions of the clouds and run perpendicular to the major axis of these denser regions of the clouds. Thus, these clouds might have formed by contraction along the magnetic field, resulting in the flattened shape. On the other hand, in some regions in the clouds, like the L1641 as a part of the Orion A cloud complex and the Rho Oph streamers, the clouds are elongated roughly parallel to the magnetic field. These regions are relatively tenuous compared to the Ori BN/KL region and the Rho Oph core, respectively. This might be due to an expansion/flowing of matter along the magnetic field lines. Polarization efficiency ($P(K)/A_V$) ranges from 0.06 to 0.33 $\%mag^{-1}$.

From the intrinsic polarization of young stellar objects, we have determined the spatial distribution of circumstellar dust around young stars. A remarkable perpendicularity has been found between the ambient magnetic field and the infrared polarization of young stellar objects which exhibit mass outflow phenomena. This indicated the presence of circumstellar disk/torus whose plane is perpendicular to the ambient magnetic field; the mass outflows expand in the polar regions of the disk and the polarization arises in the direction parallel to the disk plane due to scattering by dust grains in the reflection nebulosity. The relationship is clearly seen in the NGC 1333 cloud, the Taurus cloud, and even L1641.

Combining the perpendicularity between the disks and magnetic fields with perpendicularity between the cloud elongation and magnetic fields, we conclude that the magnetic fields might have dominated nearly all aspects of cloud dynamics, from the initial collapse of the clouds right through to the formation of disks/tori around young stars in these low-to-intermediate mass star forming clouds of the Taurus, Ophiuchus, and Perseus. Although such geometrical relationship is less clear in the Orion cloud where high-mass stars are forming, the geometry of circumstellar structure might be also preferentially determined by the magnetic field in the clouds.

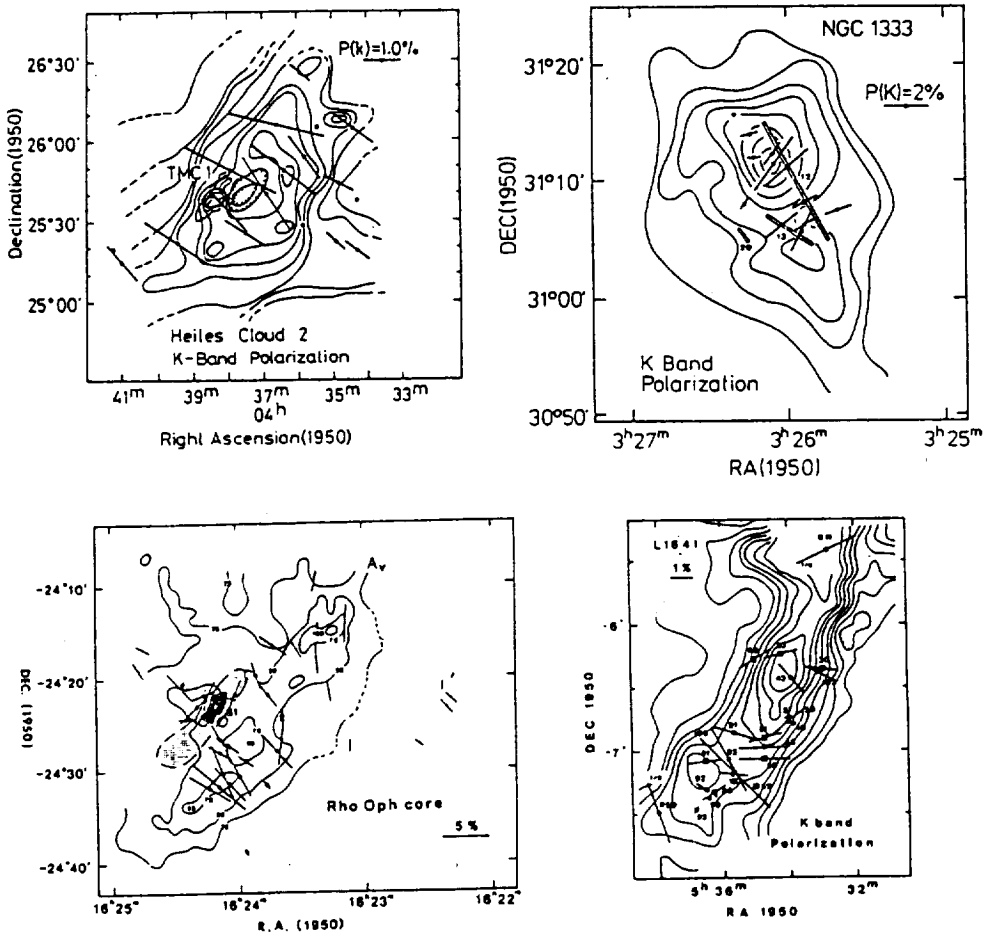

Fig. 1. 2.2 micron polarization maps of Heiles Cloud 2, the Rho Oph core, the NGC 1333 cloud, and L1641 superposed on the A_v or CO line contour maps.

REFERENCES

Loren, R. B. 1976, Ap. J., **209**, 466.
Maddalena, R. B. et al. 1986, Ap. J., **303**, 375.
Sato, S. et al. 1988, Mon. Not. R. astr. Soc., **230**, 321.
Sherwood, W. A., and Wilson, T. L. 1981, A. Ap., **101**, 72.
Snell, R. L. et al. 1982, Ap. J., **255**, 149.
Tamura, M. 1988, Ph. D. thesis.
Tamura, M. et al. 1987, Mon. Not. R. astr. Soc., **224**, 413.
Tamura, M. et al. 1988, Mon. Not. R. astr. Soc., **231**, 445.
Wilking, B. A., and Lada, C. J. 1983, Ap. J., **274**, 698.
Wilking, B. A. et al. 1979, A. J., **84**, 199.

IRAS RESULTS ON OUTER GALAXY STAR FORMATION

Susan Terebey*, Michel Fich**
* California Institute of Technology 105-24, Pasadena CA 91125
** Physics Dept.,University of Waterloo, Waterloo
Ontario N2L3G1, Canada

We have systematically studied an infrared defined (60 μm) sample of IRAS sources in order to investigate star formation in the outer Galaxy. Five percent of the sample are point sources with IRAS spectra that suggest the emission is from a dust shell surrounding a mature star. Ninety-five percent have spectra where flux density strictly rises with wavelength. The sources are extended, and we show that Point Source Catalog fluxes seriously underestimate total fluxes. We have reliably assigned CO kinematic distances to two thirds of the sources. Most of the infrared luminosities correspond to B spectral types. We detect 6 cm continuum emission from all sources inferred to have spectral type B1 or earlier. The combined IRAS/CO/6 cm data show these sources are young, moderately massive stars that are embedded in interstellar clouds. The young embedded sources define a distinct band in an IRAS color-color diagram. Normal IRAS galaxies fall in the same band, consistent with the interpretation that their infrared emission is due to star formation.

HIGH RESOLUTION OBSERVATIONS OF COMPACT HII REGIONS AT 230 GHZ

J. E. Wink,*** P. G. Mezger,* R. Zylka*

* Max-Planck-Instut für Radioastronomie, 5300 Bonn, W.- Germany

** Instute de Radioastronomie Millimétrique, 38406 St. Martin d'Héres, France

Based on the idea that star formation goes on progressively in molecular clouds, we conducted a search for protostars by mapping compact HII regions at a frequency of 250 GHz. We used the IRAM 30-m radio telescope in Spain with the ^{3}He-cooled bolometer of the MPIfR (Kreysa, 1985). The beam has a full width to half power of 11″at this frequency.

We observed twenty compact HII regions usually obtaining twice the expected free-free flux density, positionally coincident with the HII region. Even fine structure within the HII regions can be traced in our maps as in the case of G75.84+0.40 near ON-2 (Fig 1). The high degree of coincidence between our 250 GHz and the 5 GHz map of Harris (1976) shows that the excess flux density we observe must come from dust mixed with the ionized gas. Part of the dust must however be accumulated in the outer parts of the HII region, since in some cases our contours are shifted outwards relative to the radio maps. This is consistant with the fact that in those cases where we have enough information to make a model fit we derive temperatures of 80± 30 K. We use for our fits longward of 80μm a modified Planck curve with a dust emissivity proportional to λ^2.

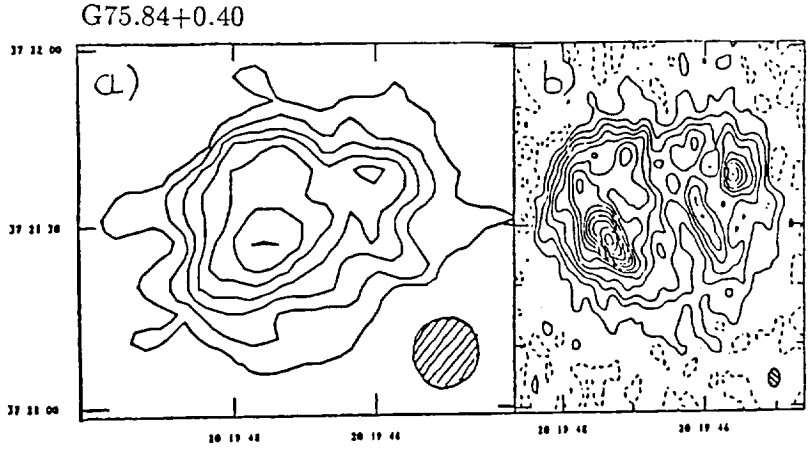

Fig. 1. a) our 250 GHz-map. Contours start at 0.28 Jy/beam and increase by 0.14 Jy/beam. b) the 5 GHz map of Harris (1976) made with the Cambridge 5-km-telescope. The respective beams are shown by the hatched ellipses.

In a few cases, we detect structures not seen before. The best example is our map of NGC2024 (Mezger *et al.* 1987). Another is in the W3A complex in Fig 2b. Components A and B are compatible with free-free emission, component D is hardly visible, component C has twice the free-free flux density and the arc below has no counterpart in ionized gas. The only other evidence for this arc is in the HCN map of Wright *et al.* (1984). The peak in the NW of component A is shifted outwards relative to the peak at 5 GHz. Perhaps the most interesting case is W3OH (Fig 3). A cross cut indicates 3 separate regions: i) the central source W3OH itself. It is unresolved, has 9.4 Jy, compared to a free-free flux density of 3.4 Jy. The major contribution must come from hot dust mixed with the ionized gas; ii) a second, resolved, much weaker source below W3OH is consistent with emission from dust outside the HII region; iii) very extended emission. This could be the dust in the diffuse molecular cloud from which W3OH formed.

REFERENCES:

Arnal, E.M., Goss, W.M., Dickel, H.R., Forster, J.R.: 1982, Mon. Not. R. Astr. Soc. **201**, 317

Harris, S.: 1976, Mon. Not. R. Astr. Soc. **174**, 1

Kreysa, E.: 1985, Proc. URSI Intern.Symp. "mm- and submm-wave Astronomy", Granada 1984, Spain, p. 153

Mezger, P.G., Chini, R., Kreysa, E., Wink, J.E., Salter, C.J.: 1988, Astron. Astrophys. **191**, 44

Wright, M.C.H., Dickel, H.R., Ho, P.T.P.: 1984, Astrophys.J. **281**, L71

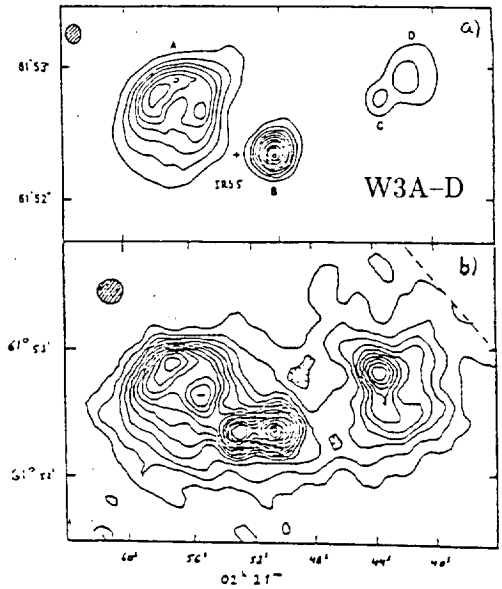

Fig. 2. b) our 250 GHz map of W3 A–D. The dashed line shows the limit of the map. Contours are in Jy/beam. They start at .233 and increment by the same amount. a) the 5 GHz map of Arnal *et al.*(1972).

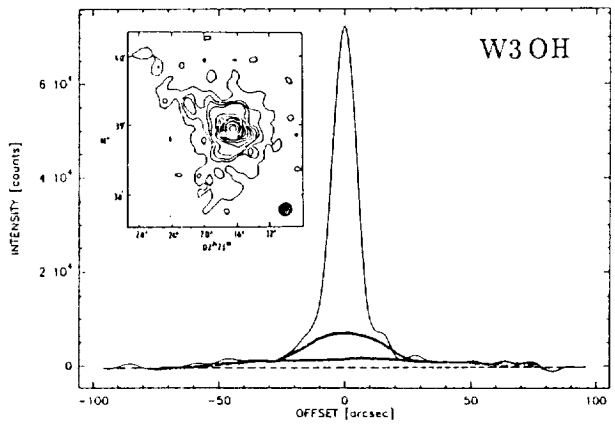

Fig. 3. the insert is our 250 GHz map of W3 OH. Contours are at .21 .42 .63 .84 1.26 1.68 2.24 2.94 3.78 4.76 5.88 7.14 8.65 10.08 Jy/beam. The curve is the average of delination- and right ascension cut through the peak. Our decomposition into three features of different widths is indicated.

N91-14955

SURVEY OBSERVATIONS OF EMISSION-LINE STARS IN THE ORION REGION

S. D. Wiramihardja,* T. Kogure,** S. Yoshida,**
K. Ogura,*** and M. Nakano****

* Department of Astronomy and Bosscha Observatory
Institute of Technology Bandung, Indonesia
** Department of Astronomy, Faculty of Science
University of Kyoto, Kyoto, Japan
*** Department of Natural Science
Kokugakuin University, Tokyo, Japan
**** Department of Earth Science, Faculty of Education
Oita University, Oita, Japan

We have conducted survey observations for Hα-emission stars in the Orion region using the Kiso Schmidt telescope and partly the CTIO Curtis Schmidt telescope. In the area of about 25 square degrees, centered at R.A. = 5^h40^m and Dec. = $0^o.0$, a total of 236 Hα-emission objects, mostly supposed to be T Tau type stars, have been detected among which 155 are new ones including 6 non-stellar objects.

Celestial coordinates and V-magnitude are measured for the detected objects. Eye estimation of the Hα-emission intensity is also made at three epochs in a time span of about two years, where we found notable variation of Hα intensity in 68 out of 236 objects.

Besides a remarkable concentration along the northern dark cloud complex, a loose concentration is noticed near the Orion Belt region, fairly well coinciding with the distribution of the Orion OBIb association members. A comparison with the Av-map is also made to see the relationship between the distribution of emission-line objects and that of interstellar dust.

III-B) INTERSTELLAR GRAIN MANTLES

MATRIX ISOLATION AS A TOOL FOR STUDYING INTERSTELLAR CHEMICAL REACTIONS

David W. Ball, Bryan J. Ortman, Robert H. Hauge, John L. Margrave,
Department of Chemistry, Rice University, Houston, Texas, 77251

Since the identification of the OH radical as an interstellar species (Barrett and Lilly, 1957), over 50 molecular species have been identified as interstellar denizens. While identification of new species appears straightforward, an explanation for their mechanisms of formation is not. While most astronomers concede that "large" bodies like interstellar dust grains are necessary for adsorption of molecules and their energies of reactions (Watson and Salpeter, 1972; Allen and Robinson, 1975), many of the mechanistic steps are unknown and speculative.

We propose that data from matrix isolation experiments involving the reactions of refractory materials (especially C, Si, and Fe atoms and clusters) with small molecules (mainly H_2, H_2O, CO, CO_2, and O_2) are particularly applicable to explaining mechanistic details of likely interstellar chemical reactions. In many cases, matrix isolation techniques are the sole method of studying such reactions; also in many cases, complexations and bond rearrangements yield molecules never before observed. The study of these reactions thus provides a logical basis for the mechanisms of interstellar reactions.

Table 1 shows a list of reactions studied in our laboratory that would simulate interstellar chemical reactions. These reactions were studied using FTIR-matrix isolation techniques. This Table does not represent an exhaustive list of reactions studied; we only include reactions of species having astronomical interest. We do point out, however, that the preponderance of reactive pathways shown here hints that true interstellar space is certainly a "soup" of chemical species, about which much is still unknown.

REFERENCES

Allen, M., and Robinson, G.W.: 1975, Astrophys. J., 195, 81.
Barrett, A.H., and Lilly, A.E.: 1957, Astron. J., 62, 5.
Fredin, L., Hauge, R.H., Kafafi, Z.H., Margrave, J.L.: 1985, J. Chem. Phys., 82, 3542.
Harding, L.B.: 1983, J. Phys. Chem., 87, 441.
Kafafi, Z.H., Hauge, R.H., Fredin, L., Kauffman, J.W., Margrave, J.L.: 1982, J. Chem. Phys., 77, 1617.
Kafafi, Z.H., Fredin, L., Hauge, R.H., Margrave, J.L.: 1982, J. Chem. Phys., 77, 1626.
Kauffman, J.W.: 1981, PhD Thesis, Rice University.
Ortman, B.J.: 1987, PhD Thesis, Rice University.
Watson, W.D., and Salpeter, E.E.: 1972, Astrophys. J., 174, 321.

TABLE 1

REACTION	REFERENCE
$C + CO \longrightarrow C_2O$	Ortman, 1987
$C_2 + CO \longrightarrow C_3O$	
$C_3 + CO \longrightarrow C_4O$	
$C_3 + H_2O \longrightarrow C_3 \cdots H_2O$	
$C_3 \cdots H_2O \xrightarrow{400\ nm} HO\text{-}C{\equiv}C\text{-}C\text{-}H \xrightarrow{UV}$ propynal	
$C + O_2 \longrightarrow CO_2$	
$C + 2\,O_2 \longrightarrow CO + O_3$	
$C_3 + O_2 \longrightarrow C_3 \cdots O_2$	
$C_3 \cdots O_2 \xrightarrow{400\ nm} C_3O + O \longrightarrow CO_2 + C_2$	
$C + H_2 \not\longrightarrow CH_2$ (evidence of barrier: Harding, 1983)	
$C_2 + H_2 \longrightarrow C_2H_2$	
$Si + H_2 \longrightarrow SiH_2$	Fredin, 1985
$Si + H_2O \longrightarrow HSiOH$	Kafafi, 1982
$Si + HF \longrightarrow HSiF$	Kafafi, 1982
$Fe + HX \longrightarrow HFeX$ (X = CH_3, NH_2, OH, F)	Kauffman, 1981

NEW INSIGHTS IN THE PHOTOCHEMISTRY OF GRAIN MANTLES: THE IDENTIFICATION OF THE 4.62 AND 6.87 μm BANDS

by

Ruud Grim, Willem Schutte, Bernard Schmitt and Mayo Greenberg

Laboratory Astrophysics, University of Leiden
P.O. Box 9504, 2300 RA, Leiden, The Netherlands

The mid-IR spectral region of molecular clouds is known to show the fingerprints of molecules frozen in the icy mantles of the interstellar grains. So far, only a few molecules have been positively identified: H_2O, CO, OCS, H_2S and CH_3OH. With the recent identification of the 4.62 μm absorption band in W33A with the OCN^- ion (Grim and Greenberg 1987) a new field of potential candidates became available. To study in more detail the complex chemical and physical interactions going on in the ice mantles accreted on grains in molecular clouds we performed numerous experiments involving UV irradiation and diffusion experiments. We present here some new ideas about the photochemistry of molecular ices, whereas the diffusion will be addressed in the paper by Schmitt *et al.*.

Although our ultimate aim was to study irradiated astrophysically relevant molecular ices for comparison with interstellar spectra, we have started our research with the irradiation of binary ices. Using isotopic labelling on NH_3/CO and NH_3/O_2 ices we have identified numerous compounds, of which the OCN^-, NO_2^-, NO_3^-, and NH_4^+ ions are the most interesting ones since they reveal a new type of chemical reactions. It appeared that these compounds were formed by proton transfer reactions induced by the interaction between an acid (HNCO, HNO_2, HNO_3) and a base (NH_3) through a hydrogen bond. This mechanism has been confirmed by a study of photolyzed diluted argon mixtures ($Ar/NH_3/CO$ and $Ar/NH_3/O_2$) that were allowed to anneal slowly, permitting the transfer reactions to occur. Using the collected data of these two particularly studies, we reached a better understanding of the effects of UV irradiation of such complex mixtures as $H_2O/NH_3/CO/O_2 = 10/1/1/1$.

The main astrophysically relevant results from the overall study are presented. Firstly, the 4.62 μm band in W33A can be reproduced with NH_3/CO containing irradiated ices and has been identified with OCN^- (Grim and Greenberg 1987). The 6.87 μm band in W33A and other protostellar objects is reproduced with NH_3/O_2 containing ices (Figure 1a) and is identified with NH_4^+.

For W33A the following column densities relative to H_2O have been calculated: $[OCN^-]/[H_2O] \sim 1\%$ and $[NH_4^+]/[H_2O] \sim 2\%$. The 5-8 μm spectrum of W33A shows significant line of sight effects. The 6.0 μm H_2O band is carried by grains that have a relatively low temperature, but the position of the 6.87 μm indicated grains that are heated to higher temperatures. The more complex 5-8 μm spectrum of Mon R2/IRS 2 shows three interesting regions (Figure 1b): (i) an absorption excess from 5.2 to 5.8 μm which is not understood yet, (ii) a very steep rise at 6.1 μm that constrains the maximum contribution of H_2O and requires the presence of other compounds to account for the observed 6.0 μm band, and (iii) the broad 6.87 μm band can not be explained solely by NH_4^+, but ammonium salts might explain the observed broadening.

References:

Grim, R.J.A. and Greenberg, J.M., 1987, *Ap. J. Letters*, **321**, L91

Tielens, A.G.G.M., and Allamandola, L.J., 1987, in *Physical processes in interstellar clouds*, eds. Morfill, G., and Scoles, M.

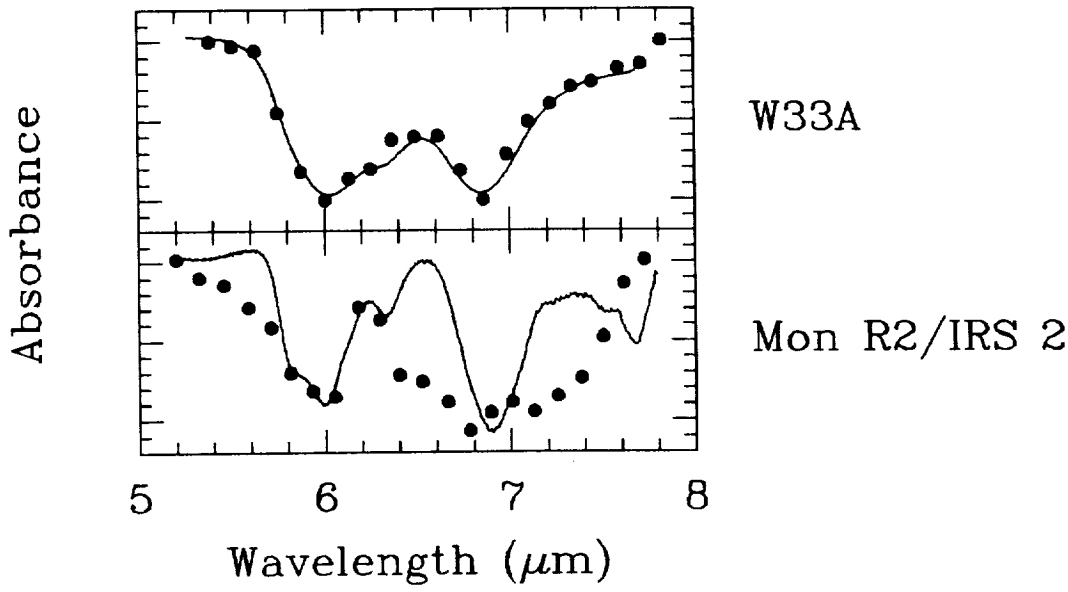

Figure 1: The 5-8 μm spectrum of W33A compared with $H_2O/NH_3/CO/O_2 = 10/1/1/1$ after UV irradiation and annealing to 176 K (a), and the 5-8 μm spectrum of Mon R2/IRS 2 compared with the same mixture but after sufficient time at 176 K to sublimate all H_2O (b). The observational data are taken from Tielens and Allamandola (1987).

DISTRIBUTION OF THE 3.1 μm FEATURE IN CEPHEUS A

K. -W. Hodapp* and C. Eiroa**

*Institute for Astronomy, University of Hawaii, Honolulu, USA

**Observatorio Astronómico Nacional, Madrid, Spain

Near-infrared absorption features produced by core-mantle dust grains are observed in the line of sigth of many protostellar objects. Most of the observations have been made with relatively large beams, around 10". Very often, however, extended structures are associated with the young objects. Since the absorptions are formed under different physical and chemical conditions, the large beam observations might be providing a somehow inexact information on aspects like spatial distribution of the features, where and how they are built up, optical depths, etc. It seems, therefore, that high spatial resolution observations, $\theta \leq 3$", could be helpful to monitor the expected changes of the features.

Cep A/IRS 6 is a suitable candidate to carry out such a kind of study. This source is located in an active star formation region and consists of a young object associated with an extended reflection nebula. Rapid changes in the extinction across the object and a deep 3.1 μm ice feature (12" beam) are observed (Lenzen et al., 1984).

We have observed the ice feature in four positions of Cep A/IRS 6 with a 2".7 aperture. The observations have been carried out at the IRTF using the cooled grating array spectrometer, CGAS (Tokunaga et al., 1987). As an example of our results Figure 1 shows the 2.4 - 3.8 μm spectra of two positions. Position (0",0") is the maximum of the reflection nebula, and Position (-6",-8") is located at a position close to the suspected energy source where a molecular disk causes a rapid increase in the extinction (Lenzen et al., 1984). We see noticeable changes in the infrared continuum and in the 3.1 μm ice optical depth. The spectra also show some small but qualitative differences in the band shape. At Position (-6",-8") a shoulder at about 3.4 μm in the long wavelength wing of the ice feature is fairly present. In contrast, the shoulder is either not present or very weak at Position (0",0"). More details are given in a paper submitted to Astrophysical Journal.

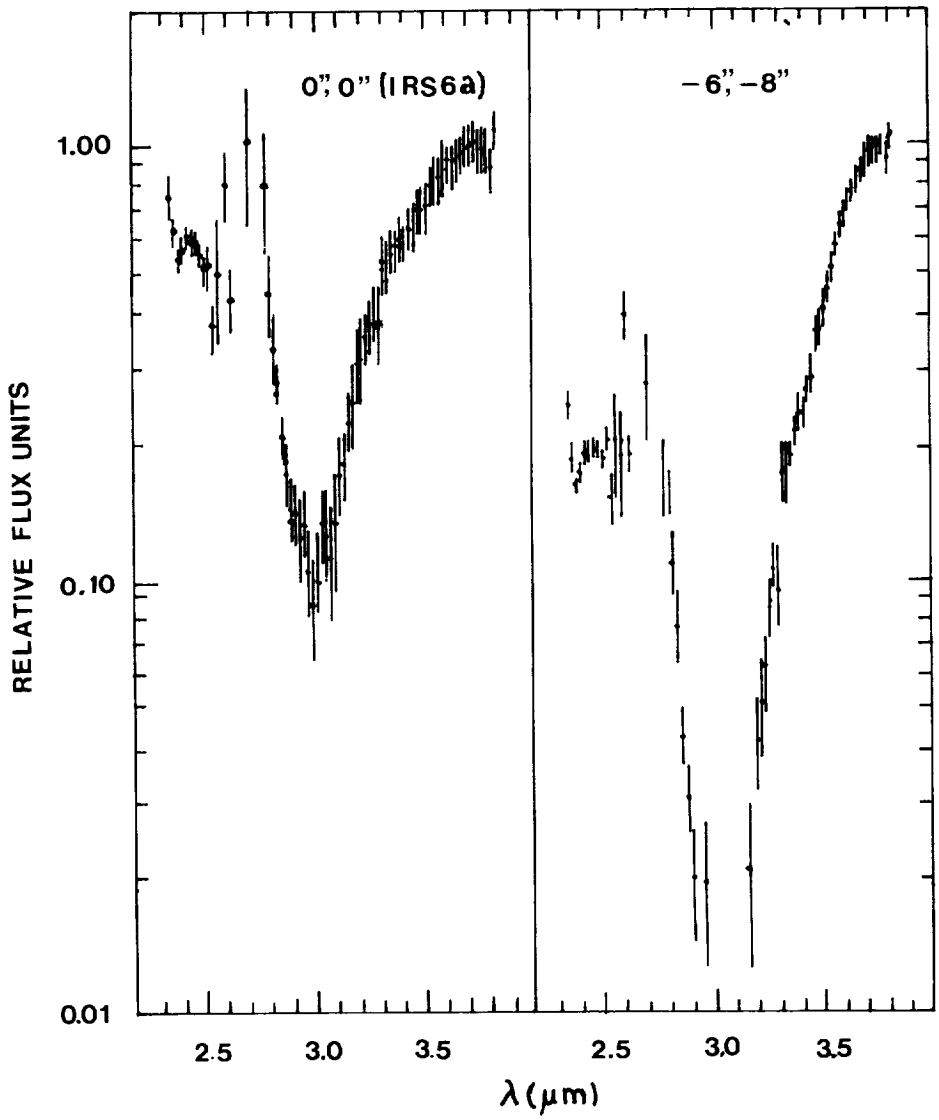

Figure 1: 2.4 - 3.8 μm spectra of two positions in Cep A/IRS 6 in relative flux units. Error bars include all kinds of uncertainties in the object and standard star observations.

REFERENCES

Lenzen, R., Hodapp, K. -W. Hodapp and Solf, J.: 1984, Astron. Astrophys. 137, 202

Tokunaga, A. T., Smith, R. G. and Irwin, E.: 1987, in "Infrared Astronomy with Arrays", eds. C. G. Wynn-Williams and E. E. Becklin (University of Hawaii, Honolulu), page 367

C.4

GRAIN GROWTH, OPTICAL POLARISATION AND EXTINCTION IN INTERSTELLAR CLOUDS

A P Jones
Department of Mathematics, UMIST, PO Box 88,
Manchester M60 1QD, England, UK

Increases in the wavelength of maximum polarisation and the ratio of total to selective extinction are generally assumed to be the result of grain growth in interstellar clouds (McMillan, 1978; Whittet and Blades, 1980; Clayton and Mathis, 1988). Using a grain model in which the interstellar extinction is explained by amorphous carbon (a-C) and hydrogenated amorphous carbon (a-C:H) mantles on silicate cores (Duley, 1987; Jones, Duley and Williams, 1987; Duley, Jones and Williams, 1988) we have theoretically studied the effects of these absorbing carbonaceous mantles on the polarising properties of large (500 Å - 2500 Å radius) silicate grains. We adopt the polarisation model of Mathis (1986) and show that carbon-coated silicate grains can explain the relationship between the wavelength of maximum polarisation (λ_{max}) and R observed toward dark clouds.

References

Clayton, G.C. and Mathis, J S.:1988, Ap. J. 327, 911.

Duley, W.W.:1987, Mon. Not. R. astr. Soc. 229, 203.

Duley, W.W.,Jones, A.P. and Williams, D.A.:1987, Mon. Not. R. astr. Soc. 229, 213.

Jones, A.P., Duley, W.W. and Williams, D.A. : 1988, Mon. Not. R. astr. Soc. in press.

McMillan, R.S.:1978, Ap. J. 225, 880.

Whittet, D.C.B. and Blades, J.C.:1980, Mon. Not. R. astr. Soc. 191, 309.

GRAIN MANTLES: THE IMPACT ON GRAIN EVOLUTION AND SELECTIVE EXTINCTION

Charles L. Joseph

Princeton University Observatory
Princeton, New Jersey 08544 USA

Depletion studies are used to infer the presence of mantles and to constrain grain evolutionary models in the diffuse interstellar medium. The presence of these mantles appears to be important in the evolution of the grains inside diffuse as well as dense clouds. In dense clouds where the element-to-element abundances sometimes differ from those found in diffuse clouds (Joseph *et al.* 1986), empirical relationships are starting to emerge between gas abundances and various types of peculiar selective extinction. These peculiar extinction curves may be the result of nonvolatile mantle formation on grain cores or may reflect chemical differences due to variations in the intrinsic metalicity from one cloud to another.

In a recent diffuse cloud study, using high-quality data found in the literature, Joseph (1988) inferred that the relative gas abundances of Fe, P, Mn, and Mg are probably set early in the lifetime of the grains and are not altered substantially thereafter, even though significant grain processing is likely to occur. A simple theoretical model (Figure 1) as well as the observational results (Figure 2) are reproduced from Joseph (1988). For a given level of overall depletion, the sightline-to-sightline rms variance in the depletion for each of these 4 elements was found to be significantly smaller than the element-to-element variance. Joseph discovered that the Fe, P, Mn, and Mg depletions in his sample, spanning approximately 1.0 (dex) in mean line-of-sight depletion, are linearly correlated with each other and have regression slopes near unity. Thus, his data suggest that the element-to-element abundances are remarkably similar, even though substantial differences in the overall level of depletion are observed from one line of sight to another. This result is at variance with many depletion models, which predict the element-to-element depletions as well as the overall level of depletion to be altered via dust-gas interactions inside diffuse clouds. Further, the results of Joseph (1988) are inconsistent with the grain destruction models of Seab and Shull (1983), probably indicating most grain-grain collisions in the aftermath of shocks result in grains that are shattered rather than vaporized.

Duley (1980) and Joseph (1988) both conclude that most of the iron in the diffuse interstellar medium exists preferentially in grain cores under substantial nonvolatile mantles that are chemically-distinct. These mantles appear to be consistent with a picture where the mantles are destroyed by shocks, but are replenished repeatedly between shocks in such a manner as to preserve the logarithmic element-to-element abundance differences. Occasionally, however, some clouds are severely shocked or are shocked a second time before the protective grain mantles can be established. In these few cases, the element-to-element abundances are changed. The formation of these mantles also helps to preserve the exceptionally large levels of depletion of certain elements such as calcium, despite the constant injection of small amounts of undepleted gas (Jura 1986).

While the selective extinction curve from one line of sight to another is remarkably

similar in the diffuse interstellar medium, the number of sightlines with peculiar extinction rises dramatically for dense clouds. Over the past few years, peculiar extinction has been studied intensively in an effort to relate differences in the selective extinction of starlight to various other physical parameters (e.g. Massa, Savage, and Fitzpatrick 1983, Witt, Bohlin, and Stecher 1984). Both of these studies, which relied on broad-band optical photography to infer dense clouds, concluded that the far-UV extinction in dense clouds is generally lower than that found for diffuse clouds. In contrast, Joseph *et al.* (1986) used the presence of molecules as an indicator of density and they found enhanced far-UV extinction in lines of sight through dense clouds [as did Cardelli and Savage (1988)].

Following up earlier work, Joseph, Snow, and Seab (1988) discovered that dense clouds, which have a large CN/Fe I abundance ratio, have a shallow ($\sim$1.0 dex less than the Seaton (1979) average) 2200 Å extinction bump relative to the underlying extinction (see figure 3). The sightlines with a large CN/Fe I abundance ratio also exhibit enhanced far-UV extinction. While the CN/Fe I abundance ratio is sensitive to the wavelength dependence of extinction, preferential depletion of some elements or differences in the intrinsic element-to-element abundances must also be invoked to account for all of the observed abundance differences. Additional studies are already under way in an attempt to find other abundance ratios that could be used to predict various types of selective extinction as well as to predict the relative change in the abundances due to depletion.

Cardelli, J.A. and Savage, B.D.: 1988, Ap.J., 325, 864.

Duley, W.W.: 1980, Ap.J. (Letters), 240, L47.

Joseph, C.L.: 1988, Ap.J., in press.

Joseph, C.L., Snow, T.P., and Seab, C.G.: 1988, Ap.J. (Letters), submitted.

Joseph, C.L., Snow, T.P., Seab, C.G., and Crutcher, R.M.: 1986, Ap.J., 309, 771.

Jura, M.: 1986, in *Interstellar Processes,* D.J. Hollenbach and H.A. Thronson, eds.

Seab, C.G. and Shull, M.J.: 1983, Ap.J., 275, 652.

Seaton, M.J.: 1979, M.N.R.A.S., 187, 73P.

Witt, A.N., Bohlin, R. C. and Stecher, T.P.: 1984, Ap.J., 279, 698.

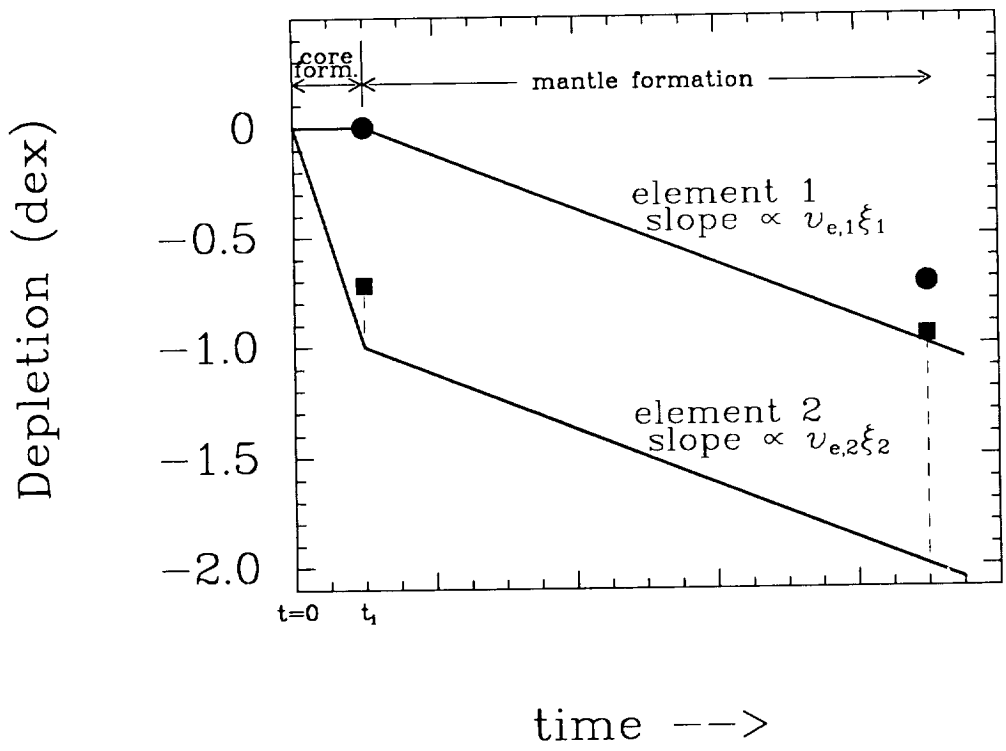

Figure 1 depicting a simple model of the time evolution of a parcel of gas and dust as observed by the depletions of two elements. At time, t=0, grains start to form in the outer atmospheres of late-type giants and grow until they are deposited into the diffuse interstellar medium at time, t_i. Much of the differences in the element-to-element depletions occur in this initial stage. Dust-gas interactions inside the interstellar medium take over for $t > t_i$ with the gas going into mantles and depleting onto the grain cores according to the rate equation:

$$dn_i/dt = -n_i n_d <\sigma v> \xi_i$$

where n_i, n_d, $<\sigma v>$, and ξ_i are the density of element i, the particle density of the dust, the effective collisional coefficient, and the sticking probability, respectively.

A commonly held belief (contradicted by the observational results in Figure 2) is that depletion or sputtering processes in diffuse clouds usually result in line segments for $t > t_i$ that diverge (i.e. the element-to-element difference in depletion changes as the total overall level of depletion increases).

If elements 1 and 2 have comparable cosmic abundances, then the depletions represented above will form grains with a core-mantle structure. The solid circles and squares show approximately the resulting depletions of elements 1 and 2 if 10% of the grains are suddenly destroyed. This type of destruction (suggested by some shock models) is unlike sputtering, which normally only removes mantle material.

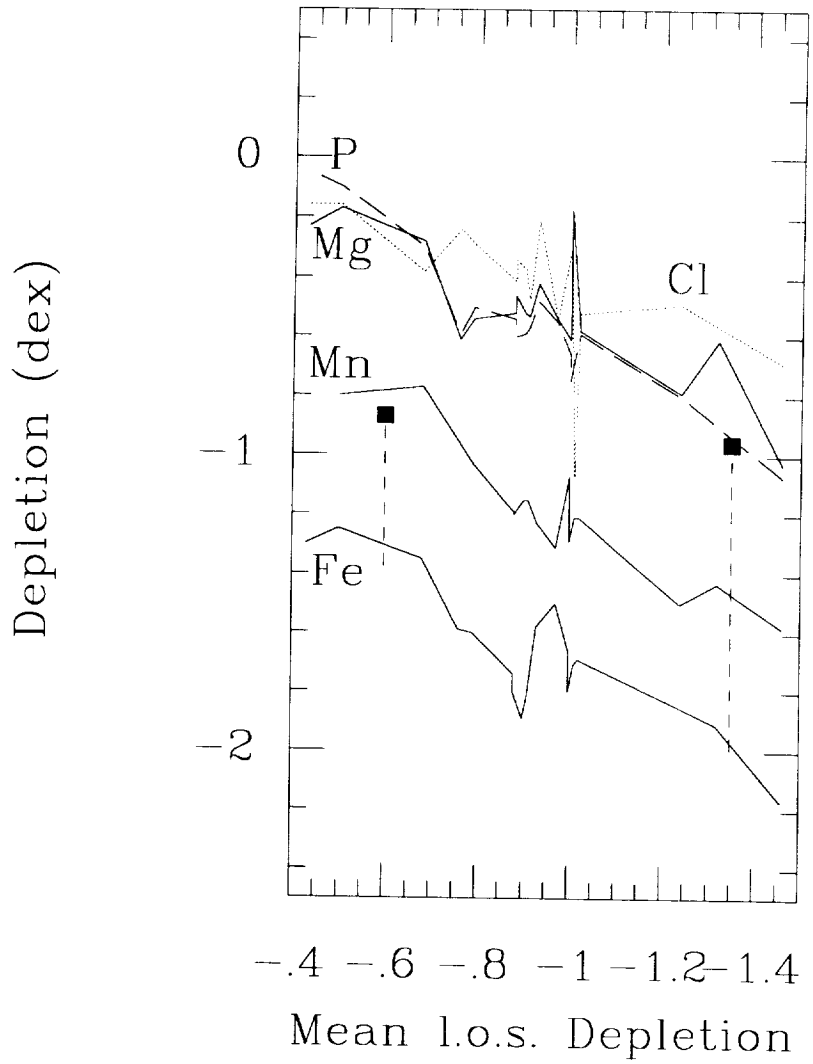

Figure 2 showing the observational results of Joseph (1988) that are based on measurements by Jenkins, Savage, and Spitzer (1986). The mean line-of-sight depletion, defined as the sum of the logarithmic depletions of the elements divided by the number of elements measured for the line of sight, is a general measure of the net amount of the available material deposited onto the grains. As is readily evident, none of these elements appears to deplete preferentially faster than any of the others. The two solid boxes show the approximate gaseous abundances of iron that would result if 10% of the grains in a line of sight with comparable depletion are suddenly destroyed.

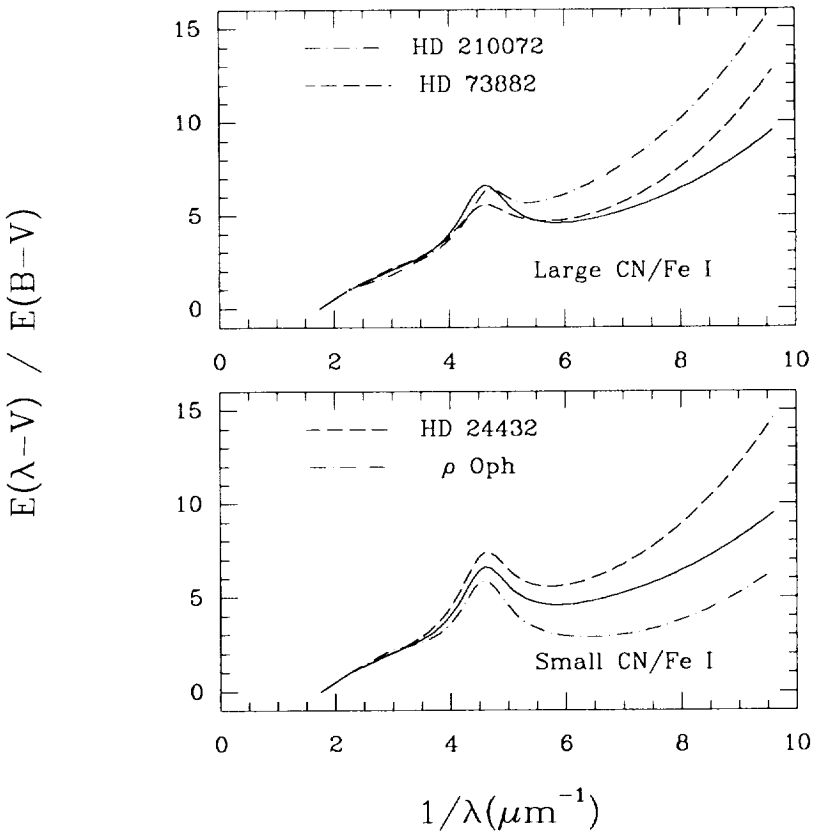

Figure 3 showing typical examples of the selective extinction curves for each of the 2 types of dense clouds in a study by Joseph *et al.* [1988, Ap.J. (Letters), submitted]. Joseph t, examined the molecular and neutral atomic abundances for 19 lines of sight through dense clouds known to have peculiar extinction curves. Lines of sight, which have a gaseous CN/Fe I abundance ratio greater than about 2 (0.3 dex), have a shallow ~1.0 dex less than normal) 2200 Å bumps relative to the underlying extinction. The solid lines are the Seaton (1979) average for comparison.

MOLECULAR AND MASS SPECTROSCOPIC ANALYSIS OF ISOTOPICALLY LABELED ORGANIC RESIDUES[a].

C.X. Mendoza-Gómez*, J.M. Greenberg*, P. McCain**, J.P. Ferris**, R. Briggs***, M.S. de Groot* and W.A. Schutte*,

* Laboratory Astrophysics, Huygens Laboratory, University of Leiden, The Netherlands
** Department of Chemistry, Rensselaer Polytechnic Institute, Troy, N.Y., U.S.A.
*** Center for Laboratories and Research, N.Y. State Department of Health, Albany N.Y., U.S.A.

INTRODUCTION

Experimental studies aimed at understanding the evolution of complex organic molecules on interstellar grains have been performed.

The photolysis of frozen gas mixtures of various composition containing H_2O; CO; NH_3 and CH_4 was studied. These species were chosen because of their astrophysical importance as deduced from observational as well as theoretical studies of ice mantles on interstellar grains.

These ultraviolet photolysed ices were warmed up in order to produce refractory organic molecules like the ones formed in molecular clouds when the icy mantles are being irradiated and warmed up either by a nearby stellar source or impulsive heating.

The laboratory studies give us among other results, estimates of the efficiency of production of such organic material under interstellar conditions. There is sufficient production of organic material in molecular clouds (Schutte, 1988) to maintain organic refractory mantles against the destructive processes in diffuse clouds (Greenberg, 1982 and 1986).

RESULTS

ANALYSIS OF ORGANIC RESIDUES (O.R.)

Non-isotopically labeled samples.

The O.R. was analysed by GC-MS and HPLC. Previous studies (Agarwal et al, 1985 and Schutte, 1988) showed that the O.R. consists of a number of small molecules containing hydroxy, carbonyl and amine-groups. In table 1 a summary of the photoproducts from different ratios of the mixture H_2O:CO:NH_3:CH_4 is shown.

[a] Work supported in part by NASA grant nr. NGR33-018-148 and one of us (C.X. Mendoza-Gómez) acknowledges a fellowship from the University of Mexico.

TABLE 1. Molecular composition of O.R. made from the gas mixture H_2O: CO: NH_3: CH_4 in the following ratios:
Sample one: 5:5:1:0, sample two: 3: 1: 0.3: 1 and sample three: 8: 0: 1: 2.5.
(from Agarwal el al 1985, Ferris 1987 and Schutte 1988).

PHOTOPRODUCTS		SAMPLE NR.		
		1	2	3
Name	Formulae	Abundances		
Glycolic Acid	$HOCH_2COOH$	0.50	0.38	0.21
3-Hydroxypropanoic acid	$HOCH_2CH_2COOH$	(*)	(*)	0.06
Formamidine	$HN{=}CHNH_2$	-	-	0.20
Hydroxy-acetamide	$HOCH_2CONH_2$	0.18	0.13	0.11
Hexamethylene-Tetramine	$C_6H_{12}N_4$	(*)	(*)	0.13
Urea/Biuret (**)	H_2NCONH_2/ $H_2NCONHCONH_2$	0.01	-	-
Oxamic acid	$H_2NCOCOOH$	0.02	0.05	-
Ethanol-amine	$H_2NCH_2CH_2OH$	0.006	-	0.10
Glycerol	$HOCH_2CHOHCH_2OH$	0.04	0.06	0.06
Glycine	H_2NCH_2COOH	-	-	0.02
Oxamide	$H_2NCOCONH_2$	0.07	0.15	0.06
Glyceric acid	$HOCH_2CHOHCOOH$	0.06	0.07	0.05
Glyceramide	$HOCH_2CHOHCONH_2$	0.12	0.16	0.002

Notes:
(*) Detected, but amount not measured
(**) Urea and biuret analyzed together

Isotopically labeled samples.

Because of being able to prepare only very small samples in the laboratory, there are always problems of contamination to be worried about. Therefore one has to be cautious of all sources of contamination, not only leaks in the system, but also residual deposits left over from earlier experiments in the apparatus.

In order to detect contamination and to better identify the molecules, we started on a new program using isotopically labeled mixtures. One first result

was that glycerol, one of the less abundant products - and thus with more possibilities of having come from contamination - has been clearly identified in the residues with isotopic labelling.

A proposed scheme for the process leading to glycerol is shown in the following diagram:

$$CH_4 \xrightarrow[h\nu]{} CH_2 + H_2$$

Direct photolysis of methane at $h\nu < 1440\,\text{Å}$ (Calvert and Pitts, 1966)

$$CH_2 + H_2O \longrightarrow CH_2 - O \begin{cases} H \longrightarrow CH_3OH \\ H \longrightarrow CH_2O + H_2 \end{cases}$$

obtaining thus formaldehyde (CH_2O). Then,

$$CH_2O + CH_2O \longrightarrow \begin{matrix} CH_2O \\ | \\ C = O \\ | \\ H \end{matrix}$$

$$\begin{matrix} CH_2O \\ | \\ C = O \\ | \\ H \end{matrix} + CH_2O \longrightarrow \begin{matrix} CH_2OH \\ | \\ CHOH \\ | \\ C = O \\ | \\ H \end{matrix} \xrightarrow{2H} \begin{matrix} C_2OH \\ | \\ CHOOH \\ | \\ CH_2OH \end{matrix}$$

(Glycerol)

CONCLUSIONS

Our ultimate aim is to understand the evolution of mantles of interstellar grains and to account for both their chemical and physical properties - including their optical properties from the submillimeter to the ultraviolet.

The gradual carbonization of organic mantles in the diffuse cloud phase leads to higher and higher visual absorptivity - yellow residues become brown in the laboratory.

Our results are being applied to explaining the organic components of comets and their relevance to the origin of life.

REFERENCES

Agarwal, V.K., Schutte, W., Greenberg, J.M., Ferris, J.P., Briggs, R., Connor, S., van de Bult, C.P.E.M. and Baas, F.: 1985, Origins of Life, 16-21.

Calvert, J.C. and Pitts, J.N.: 1966, Photochemistry, p. 87. J. Wiley & Sons, Inc.

Ferris, J.P.: 1987, private communication.

Greenberg, J.M.: 1982, Submillimetre Wave Astronomy, 261-305, Ed. J.E. Beckman and J.P. Phillips, Cambridge University Press.

Greenberg, J,M.: 1986, Light on Dark Matter, 177-188, Ed. J.P. Israel, D. Reidel Publishing Company.

Schutte, W.A.: 1988, Ph. D. Thesis "The Evolution of Interstellar Organic Grain Mantles" Leiden, The Netherlands.

SYNTHESIS OF H_2 IN DIRTY ICE MANTLES BY FAST ION ENERGY LOSS: NEW EXPERIMENTAL RESULTS INCREASE THE RELEVANCE OF THIS MECHANISM

V. Pirranello,[1] *W. L. Brown,*[2] *L. J. Lanzerotti,*[2], *D. A. Averna*[3]

Abstract

We point out that recent experimental results obtained at Bell Laboratories support the importance of H_2 production in molecular clouds by cosmic ray bombardment of the mantles of grains.

1. INTRODUCTION

H_2 is one of the most important interstellar molecules, both because of its abundance and because of the central role played in the development of the chemistry, which occurs in both diffuse and in dense clouds. H_2 is, in fact, the molecule which, when ionized either by UV photons or by cosmic rays, triggers the gas phase ion-molecule reaction chains; for this reason it is sometimes emphatically called the "seminal" molecule. This fact makes molecular hydrogen also relevant for the collapse and the fragmentation of interstellar clouds, and hence for the formation of stars and the structure and dynamics of galaxies.

It has long been recognized that radiative association of two hydrogen atoms in the gas phase cannot be responsible for the presence of interstellar H_2: the molecule is formed in a highly excited state and it is not able to emit a photon carrying the formation energy before dissociating. A third body is therefore required to absorb the formation energy. In interstellar conditions, the third body can only be a grain, acting as a catalyst.

2. RECOMBINATION OF H ATOMS ON GRAINS

The mechanism accepted for many years is the recombination of hydrogen atoms adsorbed on grain surfaces. Two atoms stick on a grain and, if they are mobile enough, can encounter each other, before evaporating, and form an H_2 molecule. This has been treated by many authors and, in particular, by

1 Dipartimento di Fisica, Universita'della Calabria, Rende, Italy

2 AT&T Bell Laboratories, Murray Hill, New Jersey, USA

3 Isitituto di Arstronomia, Universita'di Catania, Catania, Italy

Hollenbach and Salpeter (1971).

Hollenbach and Salpeter treated crystalline grains, solids with periodic structures in which the wave packet describing an adsorbed atom spreads quickly, assuring the required mobility. The process gives almost equal probability of finding the atom in any suitable adsorption site. In these conditions, the temperature independent rate R of H_2 formation is

$$R \sim 10^{-13} cm^{-3} s^{-1}$$

Smoluchowski (1983) questioned the choice of a crystalline structure for interstellar grains and considered the formation of H_2 on amorphous surfaces. This is, in fact, likely to be the most suitable structure of grain mantles in dense molecular clouds.

Amorphous ice differs from crystalline ice in its lack of periodicity in the distribution of molecules and of adsorption sites. In such conditions Smoluchowski showed that, because of the non-periodic spacing of potential wells, the wave packet describing the adsorbed atom quickly becomes localized into the deepest traps and, therefore, becomes almost immobile. Smoluchowski evaluated the production rate of H_2 as a function of the grain temperature and the density of atomic and molecular hydrogen in the gas phase.

A general feature of Smoluchowski's results is that the rate of formation of H_2 is orders of magnitude lower than that obtained considering crystalline ice, especially at $T < 18K$. These new results may render other processes competitive in producing interstellar H_2.

3. H_2 PRODUCTION BY COSMIC RAYS

In a recent paper (Pirranello and Averna, 1988) considered as an alternative process the production of H_2 in molecular clouds by cosmic ray bombardment of icy mantles on grains (as already suggested by Pirranello, 1987). The laboratory results of Brown et al. (1982) were used. Brown et al. found that, for H_2O irradiated by MeV helium ions, H_2 molecules are formed and released into the gas phase. More generally, H_2 is ejected by incident ions from any hydrogen rich frozen gas. For details on the experimental equipment the reader is referred to the paper by Brown et al. (1982).

The formation of molecules different from those originally present in the irradiated layer can be explained by the production of molecular fragments induced by the release of energy of the impinging fast particle. One way of considering the process is in terms of a transiently hot cylinder, initially about 50Å in diameter, that exists around the track of an individual fast ion. Since ice has a relatively low thermal conductivity, energy lost by the ion in the ice layer remains confined around the track for a time long enough to be thermalized. The hot cylinder increases in diameter and decreases in temperature on a time scale of $10^{-11}-10^{-10}$ sec. Molecular fragments that are

formed in this high temperature region acquire enough mobility to recombine with different partners, forming new molecules.

The production rate of molecular hydrogen at depth "d", in a dense cloud, per unit volume per second is

$$R(H_2) = 4\pi^2 \int_{a_{min}}^{a_{max}} \int_0^{E_{max}} Y_{H_2}(E')\, n_g \frac{dJ'}{dE'}\, a^2 dE' da \qquad (1)$$

where a = radius of the grain
n_g = size distribution of grains
E' = residual kinetic energy
Y = production yield of H_2 by an ion of energy E'
dJ'/dE' = distorted differential energy spectrum

A Monte Carlo simulation of the interaction between cosmic rays and grain mantles, at various depths in the core of a spherical molecular cloud, has been performed. The simulation has been continued until 40000 ions had hit each grain of the type and size chosen.

Pirranello and Averna used as a model of small molecular clouds one of those built by Boland and de Jong (1984). Their predictions seem in good agreement with observed column densities of several molecular species in L134, L183 and TMC-1. These are hydrostatic, self-gravitating spherical models of small molecular clouds supported against gravity by turbulent and thermal pressure, without internal heat sources. Spherical grains at depths $A > 1$ magnitudes, following the size distribution given by Mathis eta al. (1977), were used. The grains considered by Pirranello and Verna were assumed to be constituted by a refractory core, made of graphite or silicates, with a superimposed dirty ice layer consisting of H_2O, CH_4, NH_3, and CO in the relative abundances 5:3:2:1. For production of H_2 from CH_4 and NH_3 they assumed (there are not yet quantitative measurements of yields for these species) the (very conservative) yields of 3.96 and 4.62 per incident 1.5 MeV He ion. The ratio between the core radius and the mantle thickness has been taken to be about 1.

The cosmic rays were taken to be only low energy proton and helium particles with $E < 1$ GeV (taken from Morfill et al., 1976). These ions are the most abundant and their stopping power "dE/dx" (i.e. the energy lost per unit path length) is larger at these energies.

The energy lost by each ion interacting with the gas inside the cloud, before impinging on the grain, was subtracted from the initial energy. In this way it was possible to obtain, from the differential ion energy spectrum "dJ/dE" of the cosmic rays impinging on the clouds from the outside, the distorted differential energy spectrum "dJ'/dE'" at depth "d" inside the cloud.

The Pirranello and Averna (1988) paper gives the production rate of molecular hydrogen per cubic centimetre per second "R (T_g,d)" as a function of the grain temperature "T_g" and the depth in the core of the cloud. The results show that, especially in the low temperature region ($T < 18K$, the region of interest in the core of dense clouds), cosmic ray bombardment of grain mantles is more efficient in producing H_2 than is the recombination of adsorbed H atoms on the amorphous surface of grains. Only in restricted ranges of temperature is this second mechanism more relevant.

4. NEW EXPERIMENTAL RESULTS AND CONSEQUENCES

Using the same experimental techniques and roughly the same equipment as described in Brown et al. (1982), we have irradiated, with 1.5 MeV helium beams, thin icy films made of H_2O and CD_4 mixed in the gas phase and deposited on a "cold finger" at 9K. Among synthesized molecules are found H_2, HD and D_2.

A preliminary calibration of the mass spectrometer output obtained by means of the Rutherford backscattering technique shows that the yields per impinging particle should be raised by almost two orders of magnitude over those Pirranello and Averna assumed for the mixture of water and methane ice (details of the new experimental results will be presented elsewhere). Scaling the results of the previous Monte Carlo simulation with this difference in the assumed yields would then increase the rates at the various depths in the cloud by roughly two orders of magnitude. This fact gives greater relevance to the process of production of molecular hydrogen by cosmic rays impinging on icy organic grain mantles, especially when compared with the recombination of adsorbed H atoms on grains, even if the mobility of H atoms is not as low as that deduced by Smoluchowski.

REFERENCES

Boland, W., de Jong, T.: 1984, Astron. Astrophys. 134, 87.

Brown, W. L., Augustiniak, W. M., Simmons, E., Marcantonio, D. J., Lanzerotti, L. J., Johnson, R. E., Boring, J. W,, Reimann, C. T., Foti, G., Pirranello, V.: 1982, Nucl. Inst. Meth. 198, 1.

Hollenbach, D. J., Salpeter, E. E.: 1971, Astrophys. J. 163, 155.

Mathis, J. S., Rumpl, W., Nordisieck, K. H.: 1977, Astrophys. J. 217, 425.

Morfill, G. E., Volk, H. J., Lee, M. A.: 1976, J.G.R. 81, 5841.

Pirranello, V.: 1987, Proc. Summer School on "Genesis and Propagation of Cosmic Rays", M. M. Shapiro ed., Reidel Publ. Co., Dortrech, in press.

Pirranello, V., Averna, D.: 1988, Astron. Astrophys. 196, 201.

Smoluchowski, R.: 1983, J. Phys. Chem. 87, 4229.

DIFFUSION AND INFRARED PROPERTIES OF MOLECULES IN ICE MANTLES

Bernard Schmitt, Ruud Grim and Mayo Greenberg

Laboratory Astrophysics, University of Leiden,
P.O. Box 9504, 2300 RA, Leiden, The Netherlands

Within dense molecular clouds the formation of frozen icy mantles on interstellar dust grains is thought to be the result of various growth processes. The molecules, which make up the ice mantles are probably completely mixed. To study the physical properties of such ice mixtures we performed experiments on the evaporation processes and on the spectroscopic properties of CO, CO_2 and CH_4 in water rich ices.

The decrease in concentration of volatile molecules in ice samples deposited at 10 K and subsequently heated is found to occurs essentialy in two steps. The first one, corresponding to an evaporation of part of the volatile molecules, starts at about 25 K for CO, 32 K for CH_4 and 70 K for CO_2. During the crystallization of H_2O ice at $T > 120$ K a second evaporation occurs leading to the complete disappearance of the volatile molecules in the solid phase. The rates of disappearance are closely connected with the crystallization rates of H_2O ice. These crystallization rates have been measured between 125 and 150 K and the activation energy of the amorphous to cubic transition has been determined.

We show that when CO is trapped in water rich ice mixtures at 10 K the 2137 cm^{-1} (4.68 μm) absorption undergoes an initial irreversible change in shape upon warmup. Subsequent changes in intensity with temperature are reversible. These phenomena can be understood by considering two different interactions between CO and H_2O. The formation of a quite strong hydrogen bond between the carbon atom and a hydrogen atom explains the existence of the 2152 cm^{-1} (4.64 μm) CO satellite. Rearrangement of the water hydrogen bonding network during warmup explains its disappearance. The thermal reversibility of the CO 2137 cm^{-1} line intensity suggests either the involvement of a localized mode or dipolar interactions between CO and H_2O molecules.

The main astrophysical implications of the diffusion and spectroscopic behaviors are presented. We focus on the possible effects of a heating source on the fraction of volatile molecules, such as CO, trapped in grain mantles observed towards protostars. Furthermore, we explain how the spectroscopic effects observed have important implications on the use of laboratory spectra in the interpretation of column densities, temperature and thermal history of interstellar grain mantles.

THE EVOLUTION OF ORGANIC MANTLES ON INTERSTELLAR GRAINS

by

Willem Schutte and Mayo Greenberg

Laboratory Astrophysics, University of Leiden
P.O. Box 9504, 2300 RA, Leiden, The Netherlands

Observations of the galactic center source IRS 7 (Butchart *et al.* 1986) revealed the presence of interstellar absorption features at 3, 3.26 and 3.4 μm. In fig. 1 these observations are compared to the spectrum of an amorphous carbon material, being a mixture of saturated and unsaturated hydrocarbons. The interstellar 3.4 μm band is matched by the C−H stretching mode of tetrahedrally bonded carbon ($R_3 - C - H$, here 'R' denotes either an H atom or an organic carbon chain). The 3.26 μmfeature seems to correspond with the C−H stretching mode of trigonally bonded carbon ($R = CH - R$) at 3.28 μm. Thus the features seen towards IRS 7 point to the presence of solid organics in the interstellar medium. The deduced amount of organic carbon is about 30 % of the cosmic abundance, while the amount of organic oxygen is much smaller. Thus a hydrocarbon-type, unsaturated material is indicated.

The observed broad 3 μm band can be matched very well with the H_2O band in a laboratory ice mixture (fig. 1). Also the presence of a CO line in the spectrum of Sgr AW (Willner *et al.* 1979) points to molecular cloud extinction towards the galactic center. The H_2O/CO line intensity ratio is consistent with the ratio's observed in local clouds.

Direct data on the composition of interstellar grains was obtained by the PUMA mass spectrometer on board the Vega 1 Halley mission (Kissel and Krueger 1987). It was found that an important fraction of the grains in the coma consisted of unsaturated hydrocarbon type of materials, consistent with the IRS 7 observations.

By laboratory simulation of the chemical processes on dust grains we have investigated how solid organic materials can be produced in the interstellar medium. Our model as well as the observational constraints were discussed by Schutte (1988). The ice mantles that accrete on grains in molecular clouds, consisting primarily of H_2O, CO, H_2CO, NH_3 and O_2, are irradiated by the internal UV field, resulting in the storage of radicals upon photodissociation of the original molecules. Transient heating events lead to the production of oxygen-rich organic species by recombination reactions. The experiments indicated that in this way the observed amount of organic material can be produced

if a grain passes a few times through a molecular cloud during its life.

After the destruction of the cloud the grains enter a more diffuse medium. Here they are subjected to the interstellar UV field as well as to colissions with atomic hydrogen. Experiments show that the intense photoprocessing results in the removal of small species like H_2O and NH_3 as well as in carbonization of the organic molecules. Contrary to this, the atomic H flux will maintain a certain hydrogen level in the mantle. These processes likely convert the original, oxygen-rich organics into an unsaturated hydrocarbon type material such as that observed towards IRS 7 and in Comet Halley grains.

References :

Butchart, I, McFadzean, A.D., Whittet, D.C.B., Geballe, T.R., and Greenberg, J.M., 1986, *Astron. Ap. Lett.*, **154**, L5.

Kissel, J., and Krueger, F.R., 1987, *Nature*, **326**, 755.

Schutte, W.A., 1988, *The Evolution of Interstellar Organic Grain Mantles*, Ph. D. thesis, University of Leiden, the Netherlands.

Willner, S.P., Russell, R.W., Puetter, R.C., Soifer, B.T., and Harvey, P.M., 1979, *Ap. J. Lett.*, **229**, L65.

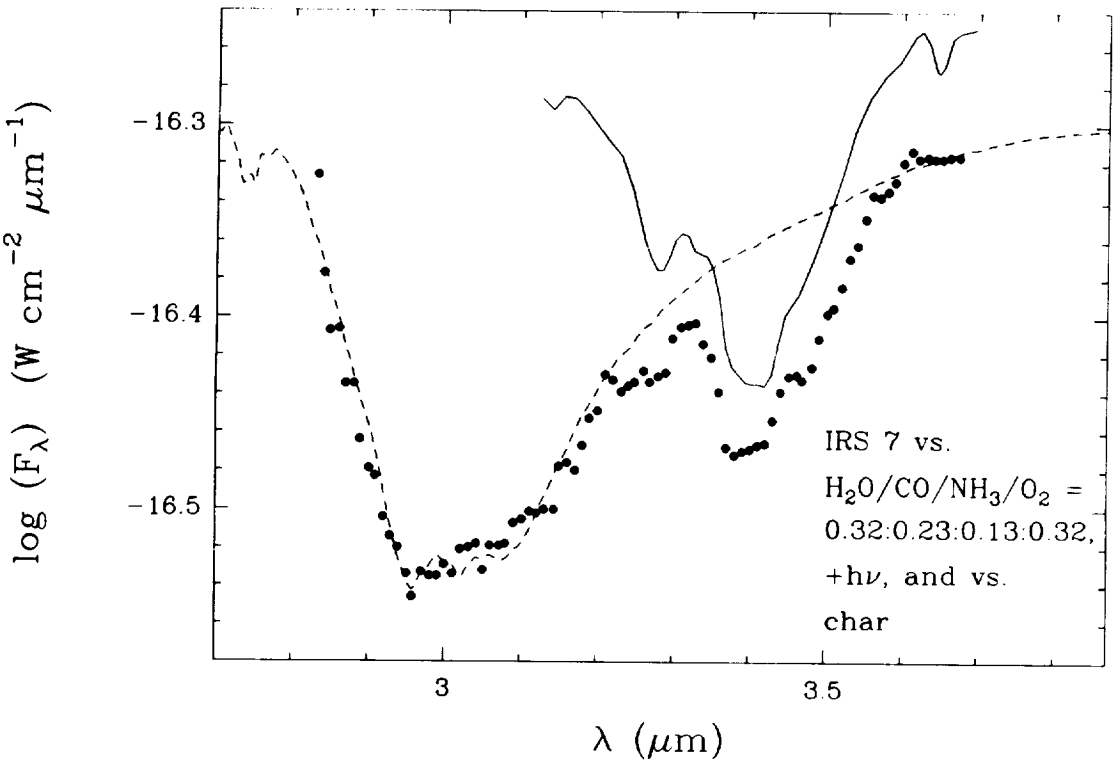

Figure 1. A comparison of the IR spectrum of IRS 7 with the spectra of an amorphous carbon material (solid line) and the H_2O feature of the ice mixture $H_2O/CO/NH_3/O_2$ = 0.32:0.23:0.13:0.32 (dashed line).

ABSORPTION FEATURES IN THE 3 μm SPECTRA OF HIGHLY OBSCURED OBJECTS

R.G. Smith*, K. Sellgren**, and A.T. Tokunaga**
*Max-Planck-Institut für extraterrestrische Physik, 8046 Garching bei München, West Germany
**Institute for Astronomy, University of Hawaii, Honolulu, HI 96822, U.S.A.

Using the IRTF cooled-grating spectrometer (CGAS; Tokunaga et al. 1987) we have obtained moderate resolution 2.4-3.8 μm spectra ($\lambda/\Delta\lambda$ ~ 160) of a selection of infrared protostars and one object located behind the Taurus dark cloud (Elias 16; Elias 1978). Two examples of the spectra are presented in Figure 1. These observations were obtained with aim of comparing the shapes of the 3.07 μm H_2O ice absorption and the long wavelength wing at $\lambda > 3.07$ um. It is clear that the absorption near 3.07 μm is dominated by H_2O ice and a comparison between the spectra and a simple H_2O ice model allows a temperature estimate for the hottest ice-coated grains in these sources. Of particular interest is the fact that BN, Mon R2/IRS-3 and AFGL 2591 have absorption features near 3.07 μm that indicate grain temperatures of $\geq$ 70K. In addition, absorption which cannot be explained by H_2O ice exists on both sides of the H_2O ice absorption feature. The short wavelength absorption peaks near 2.8 μm and is associated with additional absorption at $\lambda > 3.07$ μm. The additional absorption longwards of 3.07 μm appears as a strong absorption peaking near 3.3 μm combined with a slightly weaker but broader absorption peaking near 3.45 μm. Higher resolution observations ($\lambda/\Delta\lambda$ ~ 640) showed no indication of the absorption due to the N-H stretching vibration of NH_3 near 2.963 μm in the spectra of BN and AFGL 989. This rules out NH_3 ice as an explanation for the 2.97 μm absorption feature observed by Knacke et al. (1982) and a $NH_3.H_2O$ ice mixture as an explanation for the absorption at $\lambda > 3.07$ μm. The most plausible explanation for the 3.3 and 3.45 μm features appears to be absorption by a mixture of hydrocarbons, although we cannot identify them with features already attributed to hydrocarbons in the ISM, reflection nebulae and Comets. However, at this resolution, these features appear the same for all sources in the sample, including Elias 16, thus implying a very similar mixture of molecules in each source.

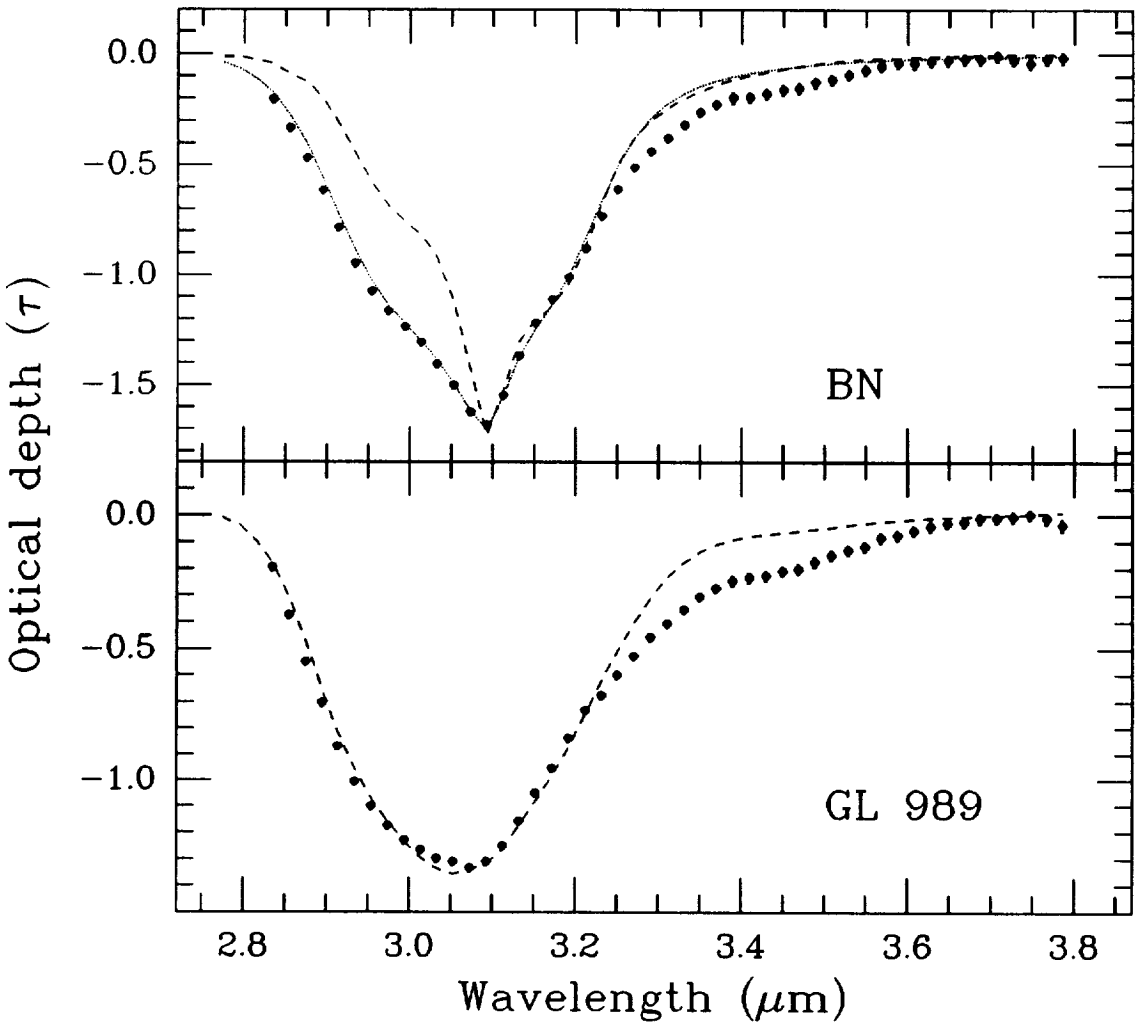

Figure 1. Spectra of two protostars, BN and AFGL 989, plotted in terms of optical depths. A simple model based on Mie Theory has been used to model the H_2O ice absorption in each source. For BN, the dashed line is a 150K ice model and the dotted line is a mixture of 23K, 77K, and 150K ices. For AFGL 989, the dashed line is a 23K ice model.

Elias, J.H.: 1978, Ap. J., 224, 857.

Knacke, R.F., McCorkle, S., Puetter, R.C., Erickson, E.F., and Kratschmer, W.: 1982, Ap. J., 260, 141.

Tokunaga, A.T., Smith, R.G., and Irwin, E. 1987, in Infrared Astronomy with Arrays, eds. C.G. Wynn-Williams and E.E. Becklin, (Institute for Astronomy, Univ. of Hawaii), p. 367.

III-C) PHYSICS OF DUST IN DENSE CLOUDS

PRODUCTION AND TRANSFER OF UV PHOTONS IN NON-HOMOGENEOUS SPHERICAL CLOUDS

S. Aiello*, C. Cecchi-Pestellini*
F. Mencaraglia**
B. Barsella***, F. Ferrini***

*Dipartimento di Fisica, Universita' di Firenze
**CNR - IROE, Firenze
***Istituto di Astronomia, Universita' di Pisa

1. Introduction

Due to screening by dust particles, the UV radiation field of intersteellar origin is practically inexistent within very dense interstellar clouds. However, as argued first by Prasad and Tarafdar (1983), it appears possible that the cosmic-ray excitation of the Lyman and Werner systems of the hydrogen molecule could originate a chemically-significant flux of UV photons even within such dense clouds.

This suggestion by Prasad and Tarafdar was investigated later by Lepp et al (1986), Sternberg et al (1987), Gredel et al (1987), who found that cosmic-ray induced photon production may significantly affect the chemistry of dense clouds.

In view of the important implications that the existence of such photons may have for the gas and dust evolution, and taking into account that the transfer of radiation inside a cloud is strongly affected by extinction and scattering properties of dust particles, as well as by their distribution, it seemed worthwhile to re-analyze the c.r.- induced production of UV photons, giving particular emphasis to the treatment of the transfer of the emitted photons.

Elsewhere (Aiello et al, 1987) we computed the c.r. - induced UV flux in a homogeneous spherical cloud as a function of the extinction and scattering properties of dust. In the present work we extended the analysis to the case of clouds with radial gas and dust density gradients.

2. UV Photons production and transfer

The equation of statistical equilibrium for the vibrational levels of the upper electronic states ($B^1\Sigma u^+$, $C^1\Pi u$) is:

$$n_u[\sum_1^{14}{}_j(A_{uj} + B_{uj} \langle I_{uj}\rangle] = n_o(C_{ou} + B_{ou} \langle I_{ou}\rangle) + \sum_1^{14}{}_j n_j B_{ju} \langle I_{uj}\rangle \quad [1]$$

where n_u, n_o, n_j are, respectively, the populations of the upper electronic vibrational level, of the ground electronic level with $v''= 0$ and of the jth vibrational level of the electronic ground.

Because of the low level of expected UV fluxes we can disregard the stimulated emission with respect to the spontaneous emission. We can also overlook the absorption from electronic ground states with $v''>0$.

Finally, since the photons emitted in the ($u \rightarrow v''=0$) transitions are absorbed very close to the point at which they are generated ("on the spot"), we can put the corresponding fields as equal to the source functions.

So, the equation [1] becomes:

$$n_u = n_o C_{ou} (\sum_1^{14}{}_j A_{uj})^{-1} \quad [2]$$

The transfer of emitted photons has been computed by using a method the outlines of which have been given by Van de Hulst and Davis (1961), adapted to a spherical symmetry with a radial gradient of dust density.

The approach is the following: let I_0 be the intensity of the zero order and let I_n, the intensity of the light which has been scattered n times in succession. We will proceed step by step from the I_n to the I_{n+1}, and will then compute the total scattered light: $\langle I \rangle = \langle I_0 \rangle + \Sigma_n \langle I_n \rangle$. The intensities are averaged over the line profiles as well as over the solid angle.

The source function for the scattering of order n in each point of the cloud is related to the intensity of the order n-1. In other words the calculation scheme is:

S_0 (molecular emission) $\Rightarrow I_0 \Rightarrow S_1 \Rightarrow I_1 \Rightarrow S_2 \Rightarrow I_2 \Rightarrow$ .....

Mathematical and computational details can be found in Aiello et al (1984).

For the photon fluxes we obtain the following expression:

$$N_{uj} = C_{ou}\, R\, F(r/R, \nu_{uj};\, \tau, \gamma, g)\, A_{uj}\, n_o (1-\psi)\, (\sum_{1}^{14} A_{uj})^{-1} \quad [3]$$

Let us to discuss the quantities involved in [3]:

ψ is a correction factor that allows for the fraction of absorption events that lead to the dissociation of the molecules. Following Jura (1974) we put $\psi = 0.1$.

The excitation coefficients, C_{ou} were computed by making use of the results from analysis of the effects of the energy deposition by c.r. within a molecular hydrogen cloud performed by Aiello & Cecchi-Pestellini (1987). In this computation the interstellar proton spectrum by Webber & Yushak (1983), extrapolated down to 1 MeV, was adopted. A check on the validity of our choice is represented by the value of the resulting ionization rate $\zeta = 3 \times 10^{-17}$ s^{-1} per H_2 molecule, wich is in good agreement with the values derived from the analysis of thermal balance within dark clouds (Duley & Williams, 1984).

The efficiency factor F is a function of the cloud structure as well as of the extinction and scattering properties of the dust.

a) Extinction properties

The wavelength dependence of the optical depth depends on the extinction law adopted. The latter has been studied in the direction of many thousands of stars located in different galactic regions and astrophysical environments. The mean extinction curve (MIEC) so derived (Savage & Mathis, 1979) can be considered as representative of the general properties of dust in the diffuse medium and in old associations (Aiello et al., 1988). However, extinction and polarization data show that in dense clouds and in regions of recent star formation, dust grains are likely to have different properties: in particular, their size distribution appears to be biased towards larger radii that results in a more or less marked flattening of the extinction curve in the far UV

spectral region. Therefore, the use of MIEC in radiation transfer computations could be completely inappropriate in the case of dense clouds. Because of this, we shall adopt here the extinction law derived for σ-Sco (Snow & York, 1975), assumed as representative of the extinction curve in a class of dense clouds. It is worthwhile noting that the σ-Sco extinction curve is a conservative choice. Indeed, the mean extinction curve towards inner region of ρ-Oph is even lower.

b) Scattering properties

γ and g can be derived, in principle, from observations of reflection nebulae and of the diffuse galactic light. However this task is more difficult to accomplish than the observation and interpretation of the interstellar extinction law. in fact only under exceptional conditions is it possible to derive the albedo and the asymmetry factor independently of one another. Furthermore, the determination of γ and g can be affected by the uncertainty of the geometrical relationship of the sources of illumination and the scatters, as well as and by the uncertainty of the illuminating spectrum. The observational results are particularly ambiguous in the far UV region.

Nor does the situation look much better when we turn to the existing models of the interstellar dust. Indeed, since the interstellar extinction curve is quite insensitive to the exact composition of the dust, it can be matched by models which exclude each other. So existing models of dust based on the fitting of the interstellar extinction curve give different values of the scattering parameters for the same spectral interval. Moreover, as stated above, the properties of dust inside the dense clouds may differ from the properties of the dust in the general interstellar medium, so the uncertainty is even greater.

It is possible, however, to derive from the observational results some indications about the scattering properties of interstellar dust. Indeed it appears that the dust is basically forward scattering and that the its albedo is smaller towards shorter wavelengths than in the visual (De Boer, 1986). Moreover, it appear possible, independent of particular grain models, to put constraints on the values allowed for the mean albedo and asymmetry factor of the dust responsible for the MIEC (Chlewicki and Greenberg, 1984). So it is possible to exclude from consideration the cases of very low values of the asymmetry factors coupled with large values of the albedo or of very large albedo coupled with completely forward scattering. Both the Mathis,Rumpl and Nordsieck (1977) and Greenberg and Chlewicki (1983) models give allowed values.

The validity of this analysis is limited to the grains as defined by the mean extinction curve. No scattering models, in our knowledge, have been worked out for the dust within the dense clouds. Some indications, however, can be obtained if the deficiency of small grains in size distribution is taken into account.

In the present computations, we used the scattering parame-

ters measured in Orion by Mathis et al (1981). The adopted data are those of their model 5. The reason of this choice is that Orion, being a region particularly suitable for investigating the scattering properties of the dust, exhibits in the same time a flat extinction.

Finally, A_{uj}, the probability for the 629 transitions considered in the present work are from Allison and Dalgarno (1970).

3. Results

We carried out computations of photon fluxes for two different model of radial density distribution inside the cloud (gas and dust densities are assumed to have the same density distribution):

I. The cloud has a small uniform density core (r_c = 0.1 pc, $n(H_2) = 10^4$ cm^{-3}) plus a r^{-1} density gradient. The resulting total visual optical depth (edge to center) is 10.

II. The cloud has a small uniform density core (same parameters as in the case I) plus a r^{-2} density gradient. The total visual optical depth is 6.

In both cases the cloud radius is assumed to be equal to 1 pc.

The assumption that the interstellar UV radiation cannot penetrate inside the cloud obviously implies the existence, around our object, of an extended envelope, or that the object is located in a less dense but larger region (an example of such objects is the dark cloud B5 (Stenholm, 1985)).

The photon fluxes obtained at the center (C), in the middle (M) and at the edge (E) of the cloud are given in table 1. The resulting line spectrum is shown in fig. 1.

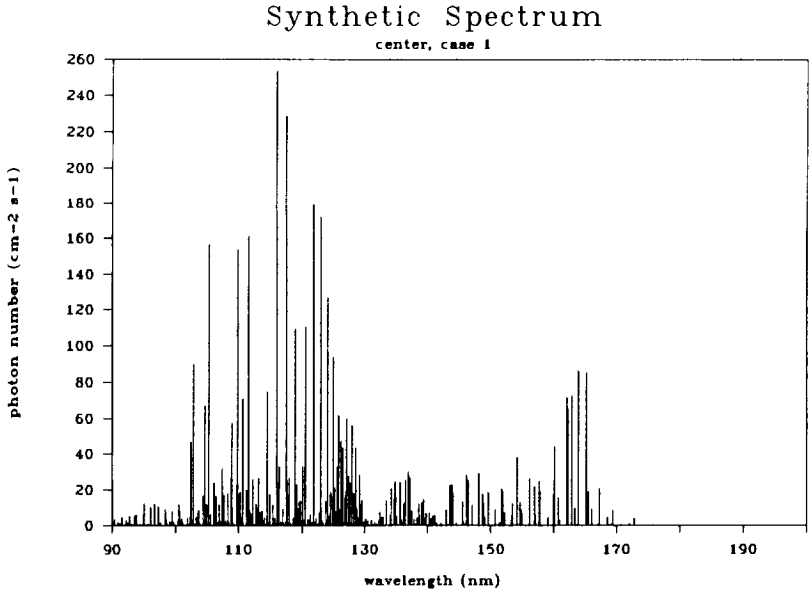

Fig.1 Synthetic emission spectrum in the Lyman and Werner bands

Our results strongly support the suggestion that the low energy cosmic rays may generate, inside dense interstellar clouds, UV radiation fields that may significantly contribute to the gas and dust evolution.

Table 1. PHOTON FLUXES (cm^{-2} s^{-1}) x 10^{-1}

	CASE I			CASE II		
	C	M	E	C	M	E
Lyman	275	220	115	470	225	80
Werner	300	240	125	515	260	90

4. References

Aiello S., Rosolia A., Barsella B., Ferrini F., Iorio D., 1984, *Nuovo Cim.*, **7**, 840.

Aiello S., Barsella B., Cecchi-Pestellini C., Mencaraglia F., 1987, *Proceeding of the Conference "Molecular Clouds in the Milky Way and External Galaxies"*, Amherst, November 1987.

Aiello S., Cecchi-Pestellini, 1987, ibidem.

Aiello S., Barsella B., Chlewicki G., Greenberg J. M., Patriarchi P., Perinotto M., 1988, *Astron. Astrophys.*, **73**, 195.

Allison A. C., Dalgarno A., 1970, *Atomic Data*, **1**, 289.

Chlewicki G., Greenberg J. M., 1984, *Mon. Not. R. astr. Soc.*, **211**, 719

de Boer K. S., 1986, *ESA SP-263*, 551.

Duley W. W., Williams D. A., 1984, *Interstellar Chemistry*, Academic Press.

Gredel R., Lepp S., Dalgarno A., 1987, *Ap. J.(letters)*, **323**, 4137.

Greenberg J. M., Chlewicki G., 1983, *Ap. J.*, **272**, 563.

Jura M., 1974, *Ap. J.*, **191**, 397.

Lepp S., Dalgarno A., Sternberg A., 1986, *Preprint n. 2379 of the Center for Astrophysics*.

Mathis J. S., Rumpl V., Nordsieck K. M., 1977, *Ap. J.*, **217**, 425.

Mathis J. S., Perinotto M., Patriarchi P., Shiffer F. M., 1981, *Ap. J.*, **249**, 109.

Prasad S. S., Tarafdar S. P., 1983, *Ap. J.*, **267**, 608.

Savage B., Mathis J. S., 1979, *Ann. Rev. Astron. Astrophys.*, **17**, 73.

Snow T. P., York D. G., 1975, *Astrophys. Space Sci.*, **34**, 19

Stenholm L. G., 1985, *Astron. Astrophys.*, **144**, 179

Sternberg A., Dalgarno A., Lepp S., 1987, *Preprint n. 2434 of the Center for Astrophysics*.

Van de Hulst H. C., Davis M. M., 1961, *Proc. K. Ned. Akad. Wet., Ser. B*, **64**, 220.

Webber W. R., Yushak S. M., 1983, *Ap. J.*, **275**, 391.

GRAINS CHARGES IN INTERSTELLAR CLOUDS

N91-14967

N. Bel, J.P. Lafon, Y.P. Viala
Observatoire de Paris-Meudon
92195 Meudon Principal Cedex, France

The charge of cosmic grains is a parameter which could play an important role in many astrophysical phenomena. It probably has an influence on the coagulation of grains and more generally on grain-grain collisions, and on the interaction between charged particles and grains which could lead to the formation of large grains or large molecules. It is of deciding importance when the interaction with cosmic magnetic field is taken into consideration, both in quiet or perturbed media. For example, the dynamics of the grains, through the action of the magnetic field on the particle trajectories, could be completely perturbed in interstellar shocks. Moreover, the coupling between neutral and ionised matter controls the drift of the magnetic field across "normal" interstellar clouds: this process could be influenced by grains, if the charge were sufficiently large, with well known effects on protostar formation processes.

The electrostatic charge of grains depends mainly on the nature of the constitutive material of the grain and on the physical properties of its environment: it results from a delicate balance between the plasma particle collection and the photoelectron emission, both of them depending on each other; the properties of the medium in which the grain is embedded have to be determined by modelling the cloud. Now, the charge of a grain is obtained in two steps: we compute the characteristics of the environment of the grain, i.e. the chemical structure of the cloud and the intensity of the radiation field at each stage of its propagation through the cloud; for this we use the numerical model developped by Clavel et al. (1978) and improved by Viala (1986). Then, we determine the charge of a grain which is

embedded in this environment by using the recent and general study of Lafon et al. (1981). This treatment is fully justified because the electrical equilibrium state of the cloud is not affected by the charge of the grains, since in interstellar clouds the ratio of the number density of grains to that of the gas is very low, of the order of 10^{-12}.

We have obtained (Bel et al. 1988) the profile of the equilibrium charge of some "typical" grains through different types of interstellar clouds (hot diffuse, moderately diffuse and dense cloud, with hydrogen number density spanning from 10 to 10^4 cm^{-3}) as a function of the depth of the cloud.

The grain charge can reach high values (up to 130 proton charges) in hot diffuse clouds. In such clouds, the charge is practically constant throughout the cloud; on the other hand, in clouds with higher densities ($\sim$ 100 cm^{-3}), it can also reach rather high values ($\sim$ 40) but it strongly depends on the position of the grain inside the cloud. The results are very sensitive to the mean UV interstellar radiation field (whose determinations could fairly differ from one author to another). Three parameters appear to be essential but with different levels of sensitivity of the charge: the gas density, the temperature and the total thickness of the cloud. In addition, the charge of grain is investigated in a model mimicking the physical conditions in the cloud in front of the particular star ζ Oph.

Bel, N., Lafon, J.-P. J., Viala, Y.P., Loireleux, E.: 1988, to be published in Astron. Astrophys.

Clavel, J., Viala, Y.P., Bel, N.: 1978, Astron. Astrophys. 65, 435

Lafon, J.-P. J., Lamy, Ph., Millet, J.M.: 1981, Astron. Astrophys. 95, 295

Viala, Y.P.: 1986, Astron. Astrophys. Suppl. 64, 391.

Dust Coagulation in ISM

A. Chokshi, A.G.G.M. Tielens, and D. Hollenbach

Coagulation is an important mechanism in the growth of interstellar and interplanetary dust particles. In astrophysics, the coagulation process is usually treated very crudely. Sticking coefficients are assumed to be either zero or unity depending on whether the particle collision occur at energies greater or less than the attractive van der Waal's potential between the particles.

We have theoretically analysed the microphysics of the coagulation process as a function of the physical properties of the coagulating grains, i.e., their size, relative velocities, temperature, elastic properties, and the van der Waal interaction. Upon collision, the two spheres elastically deform at the contact point forming a contact circle (c.f. Fig. 1). Part of the kinetic (E_K) and the binding energy (E_b) is used for this elastic deformation (elastic energy E_e). This energy is available again for springing the spheres apart (c.f. Fig. 2). The remainder of the collision energy ($E_K + E_b$)is transformed into compressional waves that travel back and forth in the colliding particles. Part of this wave energy (fraction f) may be dissipated by phonon interaction or internal scattering during the collision and thus sticking will occur if the dissipated fraction of the wave energy is greater than the initial kinetic energy of the colliding particles.

Numerical calculations of collisions between linear chains provide the wave energy in individual particles and the spectrum of the mechanical vibrations set up in colliding particles. Sticking probabilities are then calculated using simple estimates for elastic deformation energies and for the attenuation of the wave energy due to absorption and scattering processes.

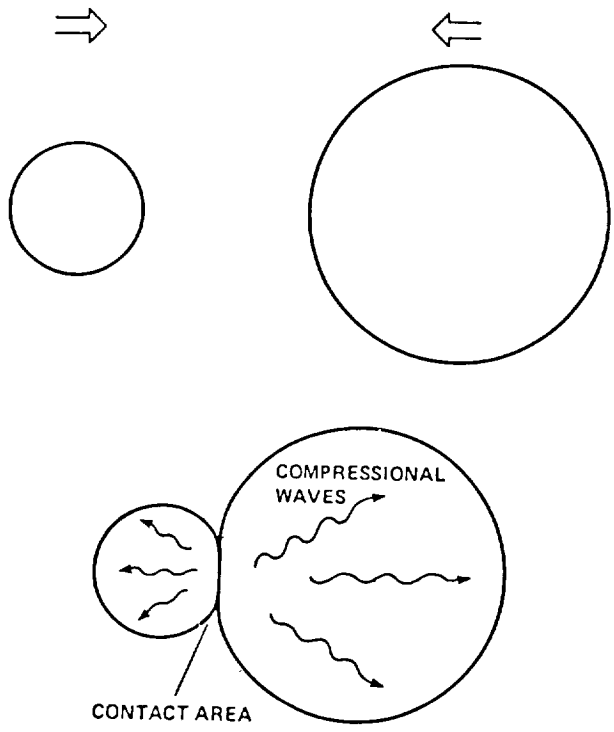

Fig. 1

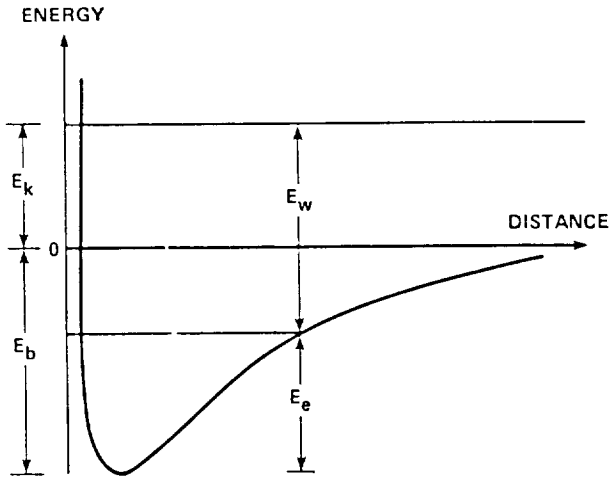

Fig. 2

ON THE POLARIZATION MECHANISM IN THE R MON / NGC 2261 COMPLEX

François Ménard and Pierre Bastien

Département de Physique, and Observatoire du mont Mégantic
Université de Montréal
C.P. 6128, Succ.A , Montréal
H3C 3J7
CANADA

ABSTRACT. We report the detection of circular polarization in R Mon and NGC 2261. This detection implies that the mechanism responsible for the linear and circular polarization is most likely multiple scattering in a flattened distribution. It replaces the previously suggested scenario where dichroic extinction by elongated dust grains aligned by a toroidal magnetic field was producing the polarization. The multiple scattering interpretation of linear polarization maps also means that these maps now provide *direct* evidence for a circumstellar disk around R Mon and possibly around many other YSO's.

I. INTRODUCTION

It is generally admitted that NGC 2261 is a reflection nebula, the illuminating source being R Mon. Evidence for this comes from the centrosymmetric pattern of the measured linear polarization vectors (Gething et al. 1982; Aspin, McLean, and Coyne 1985; Warren-Smith, Draper, and Scarrott 1987). All the vectors lying perpendicular to the radial direction to R Mon. Such a centrosymmetric pattern is typical of reflection nebulae where single scattering is responsible for the polarization since the polarization vectors are usually perpendicular to the scattering plane.

However, departure from this simple scattering pattern is clearly seen in a band close to and including R Mon itself. In this band the polarization vectors are roughly perpendicular to the symmetry axis of the bipolar nebula. The presence of such a region of aligned polarization vectors is common in YSO's associated with reflection nebulosity (Bastien 1988).

Until recently, these patterns of aligned polarization vectors were usually interpreted in terms of dichroic extinction by elongated grains aligned by a toroidal magnetic field. However, whether or not such a field actually exists is not yet clear. Competing scenarios where the magnetic field is poloidal rather than toroidal have been proposed by Pudritz and Norman (1983) and Pudritz and Silk (1987).

We do not feel however that aligned grains are the answer to the problem. In fact, multiple scattering polarization models of YSO's (Bastien and Ménard 1988) show that the linear polarization maps of all YSO's can be interpreted as due to single scattering in two optically thin bipolar lobes combined with multiple scattering around an optically thick equatorial disk. Single scattering in the optically thin lobes naturally gives a centrosymmetric pattern while the large optical depth in the equatorial disk ensures multiple scattering. The model makes no assumption about the grain size and shape and requires no magnetic field. It also predicts a typical circular polarization pattern.

In an attempt to confirm the validity of our model, we made circular polarization measurements of R Mon and its nebulosity NGC 2261. R Mon is a good candidate for such an experiment since it is a bright reflection nebula already suspected to have a disk.

II. OBSERVATIONS AND DISCUSSION

The observations were made on 1988 January 22, 23 and 27 with the 1.6m Ritchey-Chrétien telescope of the mont Mégantic Observatory in Québec, Canada. The circu-

lar polarization data are given in Table 1. Instrumental and/or interstellar origins for the detected circular polarization can be rejected for various reasons. These reasons include a null detection at position 1 and different signs for the circular polarization of R Mon when measured with two different diaphragms. (see Ménard, Bastien and Robert 1988 for details).

We are then left with a circumstellar origin for the polarization. To explain the data, the linear polarization maps and the circular polarization, one can readily show that elongated grains are not suitable. They cannot be responsible for both the aligned linear polarization vectors and the circular polarization at the same time. If *extinction by aligned elongated grains* is invoked to produce the circular polarization then the direction of alignment of the grains has to rotate across the nebula (Kemp and Wolstencroft 1972; Bandermann and Kemp 1973; Martin 1974) and the linear polarization vectors are not aligned anymore. The large amount of extinction needed to produce the high linear polarization observed also suggests that multiple scattering is present.

On the other hand, if *scattering on elongated grains* is considered we have the same problem. Scattering on such grains could produce the circular polarization but then the polarization vectors would be centrosymmetric.

Consequently, we are left with multiple scattering in a flattened distribution, a disk, to explain the data. This mechanism can easily explain the aligned vectors in the linear polarization maps but also offers an easy explanation to the circular polarization. Further support for multiple scattering is also coming from the discovery of a halo, bluer than the star, surrounding R Mon (Beckwith *et al.* 1984).

We therefore suggest that R Mon has positive (right handed) circular polarization as detected with our 3.9" diaphragm. The equatorial disk begins to dominate the polarization at an angular size between 4" and 8"(as inferred from our measurements of R Mon with these two apertures). This thick equatorial structure governs

the production of linear and circular polarization close to the star via multiple scattering (evidence is coming from the aligned linear polarization vectors and circular polarization at position 3 and 4, and marginally at position 2, see Figure 1). Farther away from the star, where the density is lower, single scattering is responsible for the polarization. We can see a centrosymmetric linear polarization pattern and detect no circular polarization at position 1.

At this point we must note that, even though we do not detect exactly the typical circular polarization pattern predicted by our model, we clearly detect an effect caused by multiple scattering in the region around R Mon where the density is enhanced when compared to the bipolar lobes.

This region corresponds to a probable optically thick equatorial disk but is somewhat larger than the inferred 6" upper limit of Sargent and Beckwith (1987) based on Owens Valley Radio Interferometer maximum resolution. It is however much smaller than the ^{12}CO counterpart of this equatorial disk (Cantó *et al.* 1981).

In summary, the fact that the detected circular polarization can be explained *only* by multiple scattering in an equatorial disk and that all linear polarization maps can be interpreted easily by the same model provide direct evidence for the presence of a flattened structure around R Mon.

A more detailed account of the observations will appear in the 1988 December 1st issue of Ap.J.

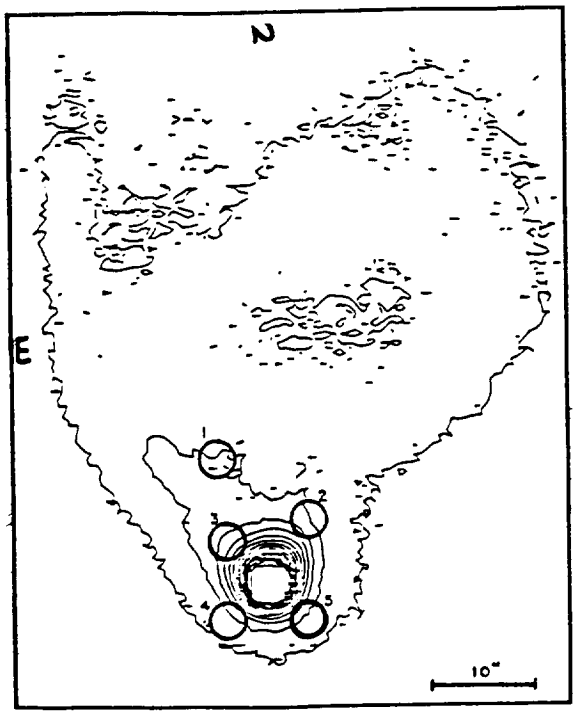

Fig.1 Isophotal contour map of R Mon. Position of circular polarization measurements are shown to scale.

Table 1

Circular polarization data for R Mon and NGC 2261

Position	ϕ_d	V/I	$\sigma(V/I)$
	°	10^{-4}	10^{-4}
R Mon	3.9	10.9	2.2
R Mon	8.3	-13.5	1.3
1	3.9	-1.2	4.5
2	3.9	-16.8	6.3
3	3.9	-20.4	6.7
4	3.9	-37.2	5.6
5	3.9	-11.1	6.2

REFERENCES

Aspin, C., McLean, I. S. and Coyne, G. V.: 1985, Astr. Ap. 149, 158.

Bandermann, L. W. and Kemp, J. C.: 1973, M. N. R. A. S. 162, 367.

Bastien, P.: 1988, in *Proc. Vatican Observatory Conf. on Polarized Radiation of Circumstellar Origin*, eds. G. V. Coyne *et al.*, (Vatican: Vatican Press), in press.

Bastien, P. and Ménard, F.: 1988, Ap.J. 326, 343.

Beckwith, S., Zuckerman, B., Skrutskie, M. F. and Dyck, H. M.: 1984, Ap. J. 287, 793.

Cantó, J., Rodriguez, L. F., Barral, J. F. and Carral, P.: 1981, Ap. J. 244, 102.

Gething, M. R., Warren-Smith, R. F., Scarrott, S. M. and Bingham, R. G.: 1982, M. N. R. A. S. 198, 881.

Kemp, J. C. and Wolstencroft, R. D.: 1972, Ap. J. Lett. 176, L115.

Martin, P. G.: 1974, Ap. J. Lett. 187, 461.

Ménard, F., Bastien, P. and Robert, C.: 1988, to appear in 1988 December 1^{st} issue of Ap.J.

Pudritz, R. E. and Norman, C. A.: 1983, Ap. J. 274 ,677.

Pudritz, R. E. and Silk, J.: 1987, Ap. J. 316, 213.

Sargent, A. I. and Beckwith, S.: 1987, Ap. J. 323, 294.

Warren-Smith, R. F., Draper, P. W. and Scarrott, S. M.: 1987, Ap. J. 315, 500.

INFRARED STUDIES OF DUST GRAINS IN INFRARED REFLECTION NEBULAE

Y.J. Pendleton, A.G.G.M. Tielens, and M.W. Werner
NASA Ames Research Center

Infrared reflection nebulae, regions of dust which are illuminated by nearby embedded sources, have been observed in several regions of ongoing star formation. Near infrared observations and theoretical modelling of the scattered light from infrared reflection nebulae can provide information about the dust grain properties in star forming regions. We have modelled infrared reflection nebulae as plane parallel slabs assuming isotropically scattering grains. The intensity of the reflected light is given by

$$I = I_0 \omega f(\omega) e^{-\tau_{ext}}$$

where I_0 is the incident intensity, ω is the albedo, τ_{ext} is the foreground extinction optical depth, and the function $f(\omega)$ includes the geometric factors. In the optically thick case and when ω is small, $f(\omega)$ is independent of ω and is 0.25 for angles of incident and reflected light of 30°. Thus, $I \sim \omega$. In the optically thin limit this equation reduces to the familiar

$$I = I_0 \tau_{sca} e^{-\tau_{ext}}$$

where τ_{sca} is the scattering optical depth. For the grain scattering properties (angle averaged), we use graphite and silicate grains (Draine and Lee, 1984) with a power law grain size distribution (MRN model: $0.005 \leq a \leq 0.25$ and Large grain model:$0.225 \leq a \leq 0.8\mu m$). The former is the well known Mathis, Rumpl, and Nordsieck (1977;MRN) model which provides a good fit to the visible and UV interstellar extinction curve. Among the free parameters of the model are the stellar luminosity and effective temperature, the optical depth of the nebula, and the extinction by foreground material.

Figure 1 shows a typical result from our model. The intensity of the reflected light increases with decreasing wavelength due to the increase in the scattering cross section. At the shortest wavelengths, it decreases again due to the rapid decrease in the intensity of the incident light for the assumed cool blackbody (T=800K). As shown in figure 1, the MRN grain model can explain the overall near infrared brightness of a typical infrared reflection nebula. However, larger grains can also explain the observed intensity distribution.

Besides polarization, a possible discriminant of grain size is the shape of the 3.08 μm ice band which has been observed in reflection nebulae in OMC-1 (Knacke and McCorkle, 1987), OMC-2 and Cep-A (Pendleton, 1987). Our models show that for an MRN distribution, the addition of ice mantles has little effect on the scattering cross sections. In contrast, for the large grain case, the ice produces a pronounced minimum at about 2.9 μm (fig. 2a&b). Thus, if large ice grains are present in the reflection nebula, the ice band may show structure at this wavelength unless large amounts of foreground ice extinction obfuscate this.

References:

Knacke, R. and McCorkle, S. 1987, *A. J.*,**94**, 972.
Mathis,J., Rumpl, W., and Nordsieck, K. 1977, **217**, 425.
Pendleton, Y. 1987, Ph.D. thesis, U. C. Santa Cruz.

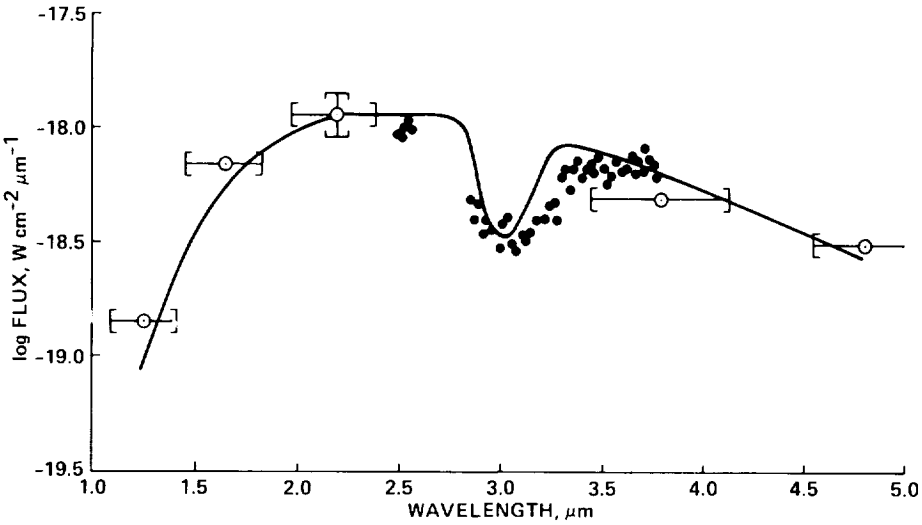

Figure 1. A comparison of model results with observations of the OMC 2 IRS1 nebula. The solid line represents isotropic scattering in an optically thick nebula over an MRN distribution of grains ($0.005 \leqslant a \leqslant 0.25$ μm) with 10% Oxygen in the form of ice mantles (Δa_{ice} = 30 Å). The broadband data for a position 5"E, 5"N of IRS1 are shown by open circles with brackets denoting the wavelength coverage. A typical error bar for the broadband points is shown for the 2.2 μm point. Beamsizes were 6" and 2.7" for the broadband and spectroscopic measurements, respectively. The broadband data have been multiplied by the ratio of the areas of the two beams to allow comparison to the spectroscopic data.

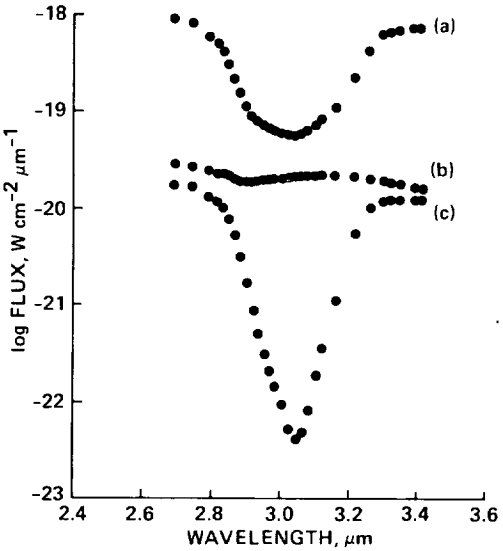

Figure 2a. A plot of flux (W cm^{-2} μm^{-1}) vs. wavelength (μm) for isotropic scattering by an MRN distribution of grains ($0.005 \leqslant a \leqslant 0.25$ μm) with 100% Oxygen in the form of ice mantles (Δa_{ice} = 145 Å). Nebular optical depth effects are shown by comparison of the optically thick curve (a) ($\sim \omega$) to the optically thin curve (b) ($\sim \tau_{sca}$). Curve (c) demonstrates the effect of adding foreground extinction by ice particles to (b). The foreground extinction was normalized by $\tau(3.1\ \mu m) = 7.0$.

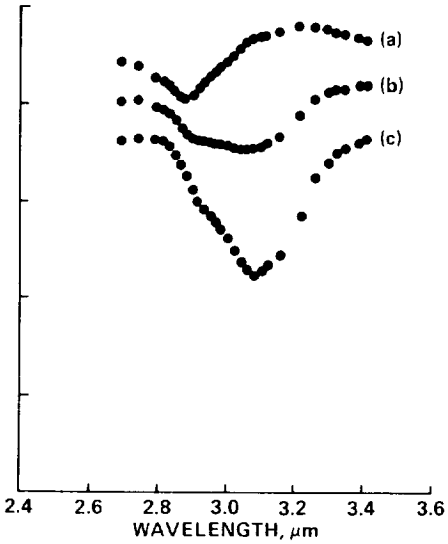

Figure 2b. A plot of flux (W cm^{-2} μm^{-1}) vs. wavelength (μm) for isotropic scattering by a distribution of large grains ($0.225 \leqslant a \leqslant 0.8\ \mu m$) with 100% Oxygen in the form of ice mantles (Δa_{ice} = 2600 Å). In (a) we show results from an optically thin nebula while (b) and (c) represent an optically thin nebula with foreground extinction normalized such that $\tau(3.1\ \mu m) = 1.5$ and 3.0, respectively.

LABORATORY INVESTIGATION OF ELECTRIC CHARGING OF DUST PARTICLES BY ELECTRONS, IONS AND UV RADIATION

J. Svestka*, S. Pinter**, and E. Grün**
*Prague Observatory, Petrin 205, 11846 Prague 1, Czechoslovakia
**Max-Planck-Institut für Kernphysik, Postfach 103980,
6900 Heidelberg 1, Federal Republic of Germany

There exists many cosmic environments where electric charging of dust particles occurs by electrons, ions and UV radiation (e.g. review of Whipple 1981). In case of interstellar dust particles the value of their electric charge can have, for instance, very important consequences for their destruction rate in SNR's shock-waves and can globally influence the overall life cycle of dust particles in galaxies (see e.g. Seab, 1987). There are many phenomena in case of dust particles within the solar system which can be explained by their electric charging with consequent interactions with electromagnetic fields and/or electrostatic fragmentations (see e.g. Morfill and Grün, 1979; Sekanina and Farrell, 1980; Fechtig et al., 1979; Grün et al., 1984; Mendis et al., 1984). Theoretical calculations of charging are often based on unreliable data extrapolated from the results of measurements with plane surfaces (parameters of secondary electron emission, photoemission, capture probalilities of electrons and ions etc.). The experimental laboratory work on the simulation of charging processes and the study of physical phenomena related to them (e.g. electrostatic fragmentation) promise the possibility to improve our knowledge in this field of research. For charging of particles at MPIK we used a vacuum chamber in which particles fall through an electron or ion beam of energies up to 10 kev. Some of the particles attaining the proper charge-to-mass ratio were then suspended in an electrodynamic quadrupole. After isolation of a single particle the charge-to-mass ratio of the particle could be determined from the oscillation frequency of the particle and amplitude and frequency of alternating voltage applied to the quadrupole electrode. The charge itself was possible to determine by means of the charge induced on the metallic cylinder placed below quadrupole, through which the particle is forced to pass after completion of a charging process. In a similar suspension system Vedder (1963,1978) charged particles for subsequent acceleration. The aim of these experiments was, however, to attain maximum charge of dust particles and the charging processes were not explicitly studied. To simulate the cosmic charging processes requires finding out the influence of strong electric field inside quadrupole which can result in induced charge of the particles and in strongly modified energy distributions of electron and ion beams. Furthermore to be determined is the influence of the rest gas because electrons and ions produced by collisional ionization of rest gas can result in significant effects. For measurements at MPIK we used particles of size 1 to 100μm from glass, carbon, aluminium, iron, MgO and very loosely bound conglomerates of aluminium oxide particles. The main aim of initial measurements was to reach high values of charge-

to-mass ratio and to study the dependence of maximum attainable charge-to-mass ratio on ion energy and applied voltage (see Svestka et al., 1987). In the course of time the experimental set-up has been improved by e.g. installation of a two dimensional opto-electronic damping system for damping of particle motions at low vacuum pressures, better control of electron and ion beams as well as optical and vacuum system, better characterization of dust particles etc. Measurements of the dependences of maximum attainable charge-to-mass ratio and charge itself on the energy of ion and electron beams at different vacuum pressures and applied voltages have been performed. Further secondary electron emission from particles has been studied by determination of the equilibrium surface potentials of particles at different vacuum pressures and then by solving the set of equations describing respective equilibrium states. At present the similar apparatus for charging of dust particles is under construction at Prague Observatory with the aim to study at the beginning the parameters of the photoemission to UV radiation. Study of photoemission from aluminium, glass and aluminium oxide particles of size 1 to $10\mu m$ under illumination by UV radiation of wavelengths 200 to 300 nm has already begun and preliminary results have been obtained. Results of measurements from both set-ups are presented and possible consequences discussed.

Fechtig, H.; Grün, E. and Morfill, G.E.: Planet. Space Sci. 27, 511.

Grün, E.; Morfill, G.E. and Mendis D.A.: 1984, in: Planetary Rings (Eds. R. Greenberg and A. Brahic; Univ. of Arizona Press), p. 275.

Mendis, D.A.; Hill, I.R.; Ip, W-H; Goertz, C.K. and Grün, E.: 1984, in: Saturn (Eds. T. Gehrels and M.S. Matthews; Univ. of Arizona press), p. 545.

Morfill, G.E. and Grün, E.: 1979, Planet. Space Sci. 27, 1269.

Seab, C.G.: 1987, in: Interstellar Processes (Eds. D.J. Hollenbach and H.A. Thronson; Reidel, Dordrecht).

Sekanina, Z. and Farrell, J.A.: 1980 Astron. J. 85, 1538.

Svestka, J.; Grün, E.; Pinter, S. and Schumacher, S.: 1987, Publications of Astronomical Institute of the Czechoslovak Academy of Sciences, 67, 277.

Vedder, J.F.: 1963, Rev. Sci. Instr. 34, 1175.

Vedder, J.F.: 1978, Rev. Sci. Instr. 49, 1.

Whipple, E.C.: 1981, Rev.Prog.Phys. 44, 1197.

N91-14972

DUST IN REGIONS OF MASSIVE STAR FORMATION

M. G. Wolfire,* and J. P. Cassinelli **
*Astronomy and Astrophysics Center, University of Chicago,
Chicago, Illinois 60637 USA
**Astronomy Department, University of Wisconsin
Madison, Wisconsin 53706 USA

Obsevational evidence suggests that stars greater than 100 $M_\odot$ exist in the Galaxy and LMC (Humphreys and Mc Elroy 1984), however classical star formation theory (Larson and Starrfield 1971, Kahn 1974) predict stellar mass limits of only ≈ 60 $M_\odot$. A protostar increases mass by accreting the surrounding gas and dust. Grains are destroyed as they near the central protostar creating a dust shell or cocoon. Radiation pressure acting on the grains can halt the inflow of material thereby limiting the amount of mass accumulated by the protostar. We first consider rather general constraints on the initial dust-to-gas ratio and mass accretion rates that permit inflow. We further constrain these results by constructing a numerical model, including radiative deceleration on grains and grain destruction processes.

At the outer boundary of the flow, grains see the infrared field emitted by warmer grains in the shell's interior . The outward radiative acceleration must be less than the inward gravitational acceleration

$$\Gamma = \left|\frac{\text{radiation}}{\text{gravity}}\right| = \frac{k_F L/4\pi r^2 c}{GM/r^2} < 1\,, \qquad (1)$$

where k_F is the flux mean of the dust opacity. We approximate k_F by $k_B(T_{rad})$ the Planck mean of the radiation pressure coefficient, where T_{rad} is some characteristic temperature of the radiation field. The maximum of T_{rad} has been chosen to be 2000 K since grains at the cocoon's inner edge will be destroyed before they can be heated to such a temperature. The opacity is calculated using an assumed grain model. As a standard we use the Mathis, Rumpl, and Nordsieck (1977) (MRN) grain model consisiting of graphite and silicate grains ranging in radius between $a_- = 0.005\mu$m and $a_+ = 0.25\mu$m, and distributed in radius as $a^{-3.5}$. Adopting the optical constants of Draine and Lee (1984), we find the outward radiative acceleration exceeds the inward pull of gravity for core masses as low as ~ 10 $M_\odot$. Furthermore, infall onto a 100 $M_\odot$ core is allowed, for a wide range in T_{rad}, only if the total grain number abundance is reduced by a factor of 4 relative to the standard MRN grain model and graphite grains larger than 0.2 times the MRN maximum size are depleted.

At the shell's inner edge, the outward radiation pressure must be less than the dynamic pressure of infalling material. If all of the stellar radiation field is absorbed in a thin region

at the inner edge of the dust shell, r_1, then it is necessary that

$$\left|\frac{\text{radiation pressure}}{\text{dynamic pressure}}\right| = \frac{L/c}{\dot{M} v_{ff}(r_1)} < 1 \qquad (2)$$

where $\dot{M}$ is the mass accretion rate and $v_{ff}(r_1)$ is the free-fall velocity at the dust destruction radius, r_1. We estimate the dust destruction radius by equating radiative heating by the central star to radiative cooling at the grain sublimation temperature. Since the free-fall speed is the largest possible inflow speed, we get an estimate of the minimum rate of mass inflow necessary for accretion to continue. Using the largest graphite grain size that satisfies the outer boundary condition, $a_+ = 0.05\mu$m, and assuming here $T_{\rm sub} = 1800$ K, we find that inflow into a 100 $M_\odot$ core requires a mass accretion rate of $> 10^{-3}$ $M_\odot$ yr^{-1}.

Proper estimates of the limits on $\dot{M}$ and the intial grain conditions require us to account for the deceleration of the flow between shell boundaries due to radiation pressure and to calculate grain destruction processes acting in the inflow. Processes of sublimation and vaporization by grain-grain collisions are considered for both graphite and silicates, plus surface reactions for graphites. We use the radiation transfer program of Wolfire and Cassinelli (1986) to calculate the grain temperatures and radiation field throughout the accrection flow. The rate of grain destruction depends mainly on the grain temperature, therefore grains of different sizes and compositions are destroyed at different radial distances.

Accretion onto a 100 $M_\odot$ core was maintained for $\dot{M} = 5 \times 10^{-3}$ $M_\odot$ yr^{-1} and a dust-to-gas ratio of 1/8 times the standard Galactic value. This is a higher mass inflow and lower grain abundance than that estimated by the simple boundary conditions which neglected the deceleration of the flow by infrared radiation.

In conclusion, we have investigated the constraints on dust properties which allows the formation of massive stars. We find the dust-to-gas ratio of the MRN standard model must be reduced by a factor of 4, and graphite grains larger than $\approx 0.05\mu$m in radius must be depleted. Furthermore, the accretion rate onto massive protostars (> 60 $M_\odot$) must be maintained at a fairly large value ($> 10^{-3}$ $M_\odot$ yr^{-1}) during the formation process. These findings seem to suggest that massive star formation requires rather extreme preconditioning of the grain and gas environment.

Draine, B.T. and Lee , H.M. 1984, Ap. J., 385, 89.

Humphreys, R. M., and Mc Elroy, D. B. 1984, Ap. J., 284, 565.

Kahn, F.D. 1974, Astr. Ap., 37, 149.

Larson, R.B., and Starrfield, S. 1971, Astr. Ap., 13, 190.

Mathis, J.S., Rumpl, W., and Nordsieck, K.H. 1977, Ap. J., 217, 425 (MRN).

Wolfire, M.G. and Cassinelli, J.P. 1986, Ap. J., 310, 207.

SECTION IV: DUST IN GALAXIES

IV-A) GALACTIC FAR INFRARED EMISSION

DOES CO TRACE H_2 AT HIGH GALACTIC LATITUDE?

D. Bazell[1], L. Blitz[2], and F.X. Désert[3]

[1]Applied Research Corporation

[2]Astronomy Program, University of Maryland;
and Institute for Advanced Study

[3]Laboratory for Astronomy and Solar Physics,
NASA/Goddard Space Flight Center

We have recently completed a CO survey of 342 Infrared Excess Clouds (IRECs) distributed uniformly across the sky. Following comparison of the integrated CO brightness Wco (K km s^{-1}) with the 100 μm infrared brightness B_4 obtained from the *IRAS* data, we have found evidence for a threshold in B_4 of 4 - 5 MJy sr^{-1} below which CO does not form.

In an attempt to find an unbiased method to determine the location of High Latitude Molecular Clouds, Désert, Bazell, and Boulanger (1988) (DBB) studied the correlation between the 100 μm infrared brightness from the *IRAS* survey and the integrated HI column density from several HI surveys. They cataloged regions characterized by an excess of infrared radiation above what was expected from the local B_4-N_{HI} correlation, producing a list of several hundred statistically significant infrared excess clouds or IRECs. The physical nature of the IRECs was not totally clear. Hence, in order to determine whether they corresponded to molecular clouds we performed a CO survey of the DBB clouds.

The original correlation study by DBB had spatial resolution of 1/3 degree. To accurately determine the observational positions we made a 2x2 degree map at 2 arc min resolution from the 100 μm *IRAS* Sky Flux plates centered on the peak of infrared excess for each cloud. The search position corresponded to the peak of 100 μm brightness within a 0.5 degree box coincident with the center of the map, after subtracting a background equal to the lowest value in the 2x2 degree map.

In the figure we show the detection success rate R = No. det./No. obs. as a function of B_4. A clear cutoff or threshold is evident between 4 and 5 MJy sr^{-1} in B_4. Above 4 MJy sr^{-1} the average detection rate is 71%. Below 4 MJy sr^{-1} the average detection rate is 3% (consisting of over 100 observations). Using the conversion B_4/A_V = 16 MJy sr^{-1}/mag the threshold value corresponds to about 0.25 mag of visual extinction. Above 5 MJy sr^{-1} a plot of W_{CO} vs. B_4 shows no direct correlation. We will also present evidence that this threshold effect can be seen within an individual cloud, providing evidence for a phase transition between atomic and molecular gas.

While the main thrust of our observing program was to examine the CO content of the IRECs, we also attempted to detect CO toward a number of UV stars so we could correlate CO brightness with direct measurements of H_2 column density and E(B-V). We observed 26 stars selected from the list of Bohlin, Savage, and Drake (1978) which had been observed in the UV by the Copernicus satellite. Of the 26 observed stars in the sample we detected CO toward 6. Excluding ϵ Per, which appears to have a large amount of CO behind it, CO is detected only for those stars with E(B-V) above 0.3 mag. corresponding to A_V = 0.9 mag. This is consistent with our results obtained using infrared data which would be expected to show a lower value for A_V because the smooth background and foreground component of the image has been removed.

There are a number of ways to explain the excess infrared brightness observed in the clouds in which CO was not detected. The most interesting is that they are clouds containing H2 but not CO, indicating that CO is not necessarily a good tracer of the total gas content of the diffuse interstellar medium. It is possible that the clouds have an abnormally high dust to gas mass ratio, producing excess IR due to larger column density of dust. Finally, it may be that these clouds

are heated by some distant heating source that 'beams' its radiation in a certain direction due to inhomogeneities in the interstellar medium.

References

Bohlin, R.C., Savage, B.D., and Drake, J.F. 1978, Ap. J., **224**, 132

Désert, F.X., Bazell, D., and Boulanger, F. 1988, to appear in Nov. 15 issue of Ap. J.

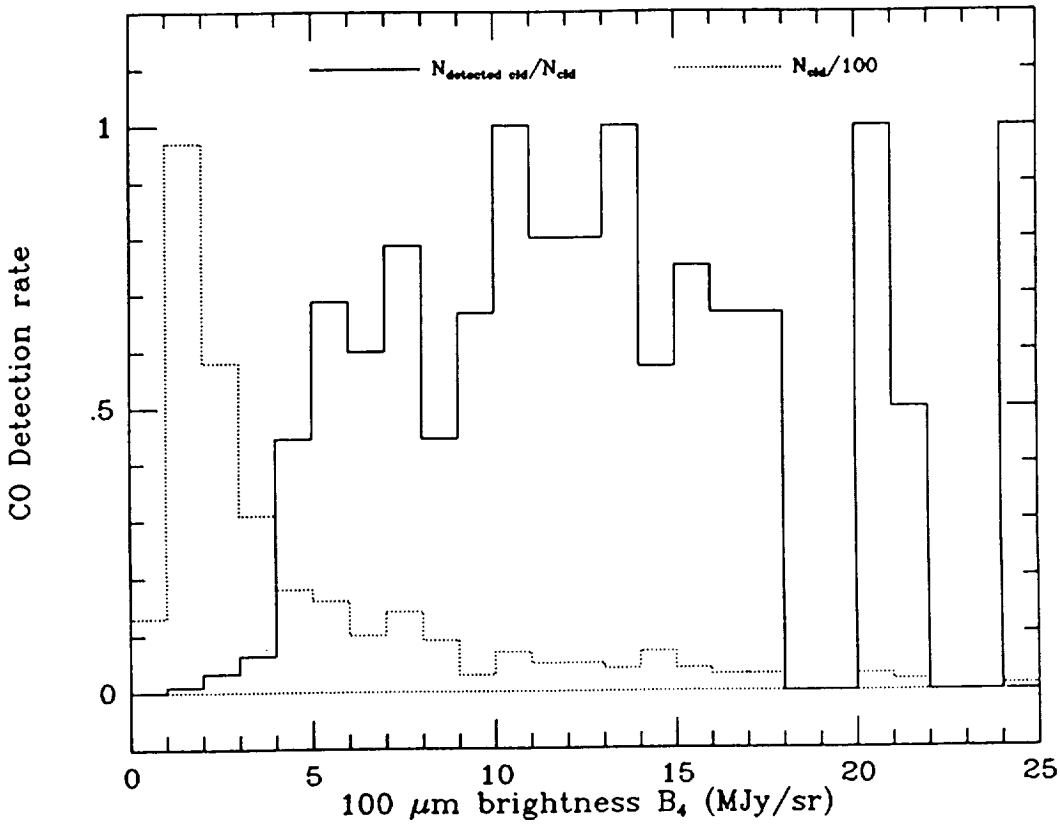

Figure Caption

The solid line shows the detection success rate as a function of 100 μm infrared brightness, B_4. Below the threshold value of 4 MJy sr^{-1} the average detection success rate is about 3%. Above the threshold it is about 71%. The dotted line shows the number of clouds in each brightness bin divided by 100.

N91-14974

THE ORIGIN OF THE GALACTIC EMISSION IN IRAS DATA

E. Caux*, P.M. Solomon** and T.J. Mooney**

*CESR CNRS/UPS, BP 4346, 31029 Toulouse Cedex, France.
**Astronomy Program, State University of New York at Stony Brook, New-York USA

Using the high resolution IRAS data in one hand, and the radial distribution of gaseous material and those of the interstellar radiation field (ISRF) in the other hand, we have built a model of the Galactic infrared emission.

The first step consisted of a separation of the diffuse emission in IRAS data from that of the well-defined strong Galactic sources. This was done using a morphologic separation of the two components based on their spatial distributions which are not the same in Galactic longitude as well as in Galactic latitude (Caux, Solomon and Mooney, in preparation).

A well accepted idea is that IR emission comes from dust heated either by the ISRF and/or by internal cloud heating sources. We have thus modelled the IR galactic emission from radial distributions of gas and ISRF and the following three main hypothesis : i/ The dust to gas ratio is the same in the whole Galaxy, ii/ IR emission is proportionnal to local dust density, iii/ IR emission is also proportionnal to the local ISRF.

For H1, we took Burton and Gordon (1978) radial distribution. The molecular material consists of two components, cold H2 (H2c) connected to molecular clouds having not or not yet formed high mass stars, and warm H2 (H2w) connected to active star forming regions associated with HII regions. We took the axissymetric distribution computed using FCRAO data (Solomon et al., private communication). The ISRF is derived from Innanen (1973) for the disc population and from the Lyman continuum photons distribution computed by Gusten and Mezger (1983) for star forming regions.

The IR emission as modelled in this way has been integrated over each line of sight and compared with observed IRAS data. The results show that the IR diffuse component emission comes from dust associated with H1 and heated by the general ISRF. For the dust embedded in cold H2 component, the heating source is also the general ISRF while the warm component is explained by dust embedded

in molecular clouds and heated by high-mass stars born in the close vicinity of the clouds in one hand (≈ 2/3) and by the disc population ISRF in the other hand (≈ 1/3).

The table summarizes the different radial properties of each component. Total IR luminosities were computed using a bolometric correction determined by integration of IR spectra on a large sample of sources (λ > 120μm data are from Caux et al., 1985). IRE (ratio of IR luminosity over ionizing star luminosity) was computed using total IR luminosities (H1+H2c+H2w) and the number of Lyman continuum photons given by Gusten and Mezger, 1983. The main result is that we don't observe variations of IRE and $(L/M)_{H1}/(L/M)_{H2C}$ and $(L/M)_{H1}/(L/M)_{H2w}$ with galactic radius, showing that the physical properties of starlight to IR conversion are about the same in the whole Galaxy. The detailed results of this model will be given in a forthcoming paper (Caux, Solomon and Mooney, in preparation).

R (kpc)	L_{H1} (Lo/pc^2)	M_{H1} (Mo/pc^2)	$(L/M)_{H1}$	L_{H2c} (Lo/pc^2)	M_{H2c} (Mo/pc^2)	$(L/M)_{H2c}$
4.0-6.5	27.4	3.1	8.8	10.4	4.2	2.5
6.5-9.0	18.2	3.9	4.7	5.3	4.8	1.1
9.0-11.0	9.2	4.1	2.2	1.3	2.4	0.5
11.0-13.0	4.9	4.2	1.15	0.2	0.65	0.3
13.0-15.0	1.9	2.5	0.75	0.05	0.25	0.2

R (kpc)	L_{H2w} (Lo/pc^2)	M_{H2w} (Mo/pc^2)	$(L/M)_{H2w}$	$\frac{(L/M)_{H1}}{(L/M)_{H2c}}$	$\frac{(L/M)_{H1}}{(L/M)_{H2w}}$	IRE
4.0-6.5	45.6	6.1	7.5	3.5	1.2	15.2
6.5-9.0	8.0	2.1	3.8	4.3	1.2	15.0
9.0-11.0	0.2	0.15	1.3	4.4	1.7	15.6
11.0-13.0	-	-	-	3.8	-	-
13.0-15.0	-	-	-	3.8	-	-

References:

Burton, W.B. and Gordon, M.A. : 1978, Astron. and Astrophys. 63, 7.

Caux, E., Puget, J.L., Serra, G., Gispert, R. and Ryter, C. : 1985, Astron. and Astrophys. 144, 37.

Gusten, R. and Mezger, P.G. : 1983, Vistas in Astronomy, 26, 159.

Innanen, K.A.: 1973, Astrophysics & Space Science, 63, 7.

MOLECULES, GRAINS, AND SHOCKS: A COMPARISON OF CO, H I AND IRAS DATA

Carl Heiles, William T. Reach, and Bon-Chul Koo
Astronomy Department, University of California, Berkeley

We have compared the IR and H I properties, and CO content, of a set of 26 isolated, degree-sized interstellar clouds. The comparisons offer some conclusions concerning the effects of kinematics on molecular content and grain size distribution, although these conclusions are provisional because of the small sample. The departure of S_{100}/N_{HI}, where S_{100} is the 100μm surface brightness, from the theoretically-predicted value is a measure of the H_2 content of clouds. This is confirmed by the detection of CO in clouds with large S_{100}/N_{HI}. Even clouds with low column density, $\lesssim 2.4 \times 10^{20}$ H-nuclei cm^{-2}, may contain more H_2 than H I, in contrast to results obtained from UV absorption line studies. The [H_2/H I] ratio is large only for quiescent clouds.

The dependence of S_{60}/S_{100} on cloud velocity implies that fast shocks preferentially destroy large grains and/or produce small grains. The marginally defined dependence of S_{12}/S_{100} on velocity, if real, probably implies that very small grains (VSG's) are formed in shocks in the 10 to 20 km s^{-1} velocity range, and destroyed at slightly higher velocities. Two neighboring clouds have been affected by the same shock, but with different degrees of completion; comparison of these two allows us to estimate a time scale for VSG formation. Nearly *all* clouds, independently of kinematics, appear to contain VSG's.

Some members of our cloud sample emit more power in the IRAS 12μm band than in the 100μm band. Such clouds must have very large fractions of their total Carbon in the form of polycyclic aromatic hydrocarbons (PAH's), if VSG's are exclusively PAH's. Finally, the absence of correlation of S_{12}/S_{100} with S_{60}/S_{100} implies that VSG's are not formed preferentially from the breakup of large grains.

A ROCKET-BORNE MEASUREMENT OF INTERSTELLAR DUST EMISSION AT HIGH GALACTIC LATITUDE

A.E. Lange,* D. Alsop,* S. Hayakawa,** T. Matsumoto,**
H. Matsuo,** H. Murakami,** P.L. Richards,* and S. Sato,**

* Dept. of Physics, Univ. of California, Berkeley, California 94720 USA
**Dept. of Astrophysics, Nagoya Univ., Nagoya 464, Japan

We have measured the diffuse brightness of the sky in six submillimeter passbands, using a rocket-borne, liquid helium-cooled, absolute radiometer (Lange et al., 1987). During the flight, the 7.6° field-of-view of the radiometer repeatedly scanned a 31° diameter circle centered at b=35°, l=203°. In Matsumoto et al (1988) we reported the average brightness observed in each of the passbands, and tentatively identified the dominant source of emission in the three shortest wavelength bands (centered at 102, 137 and 262 μm) as interstellar dust (ISD).

Spatial structure was observed in these bands, as would be expected for emission from the ISD. We have calculated the average column density of HI in each field-of-view along the scan path, using the Bell Laboratories 21 cm survey (Stark et al., 1988). The correlation of submillimeter emission with HI column density is shown in Fig. 1.

All three bands show a significant correlation with HI. The striking degree of correlation of the 137 μm data with HI column density implies that the dust to gas ratio and the dust temperature are extremely constant over this large region of the sky. The ratio of ISD emission to HI column density is 19±4, 30±5, and 6±3 $10^{-33}\{(W/cm^2sr)/n(HI)\}$ at 102, 137, and 262 μm, respectively. These values are in excellent agreement with those computed by Draine and Anderson (1985) for a mixture of graphite and silicate grains. The 102 μm value is in good agreement with the range of values reported for the IRAS 100 μm data (Tereby and Fich, 1986).

A significant residual emission, not correlated with the HI column density, is evident in all three channels. The origins of this emission will be discussed elsewhere (Lange et al., 1988).

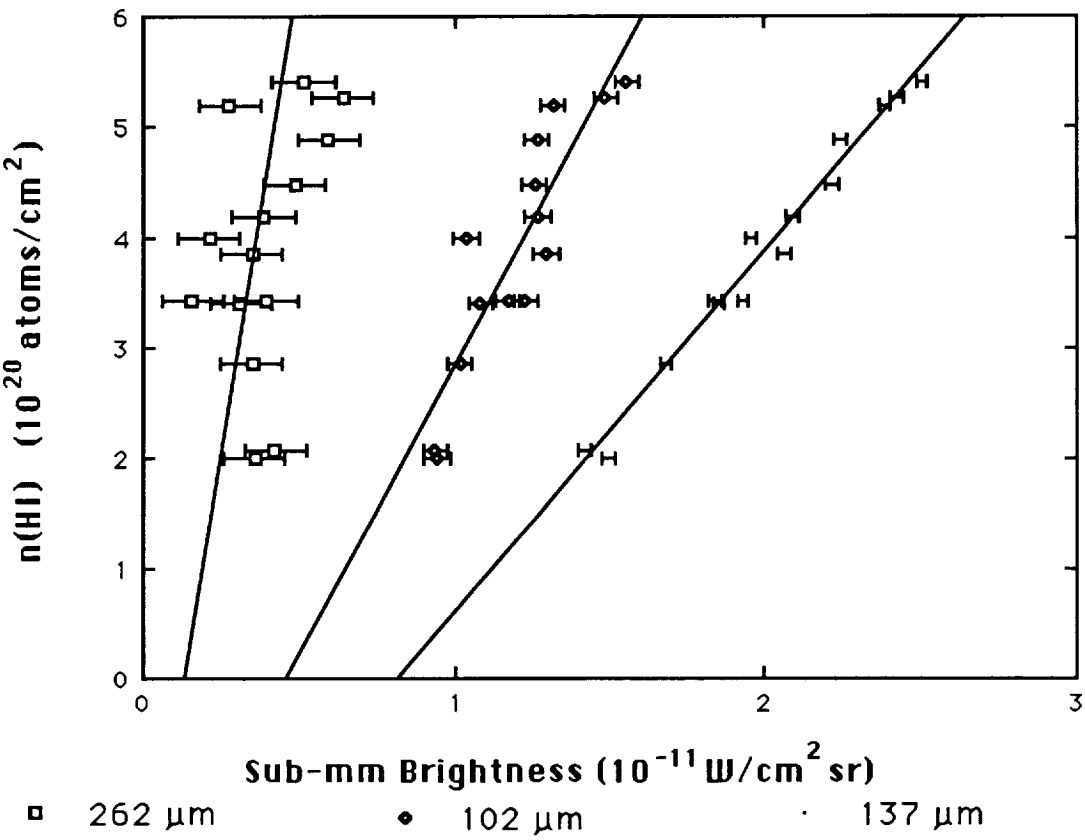

Figure 1. The correlation of HI column density with submillimeter brightness. The horizontal error bars indicate 1σ statistical errors only. The uncertainty in the calibration of the submillimeter data is ±20%, ±15%, and ±3% for the 102, 137 and 262 μm channels, respectively.

Acknowledgments

It is a pleasure to thank Prof. Y. Ogawara and other staff of the Institute of Space and Astronautical Science for launch support. This project was supported by the Japan-U.S. Cooperative Science Program administrated by the Japan Society for the Promotion of Science and the U.S. National Science Foundation, by the Scientific Research Fund of the Japanese Ministry of Education, Science and Culture (Nos. 58420003 and 58460037), by the National Aeronautics and Space Administration No. NGL05-003-497, and by the California Space Institute No. CS73-83.

References

Draine, B.T. and Anderson, N.: 1985, Ap. J. 292, 494.

Lange, A.E., Hayakawa, S., Matsumoto, T., Matsuo, H., Murakami, H., Richards, P.L., and Sato, S.: 1987, Appl. Optics 26, 401.

Lange, A.E., Richards, P.L., Hayakawa, S., Matsumoto, T., Matsuo, H., Murakami, H., and Sato, S.: in preparation.

Matsumoto, T., Hayakawa, S., Matsuo, H., Murakami, H., Sato, S., Lange, A.E., and Richards, P.L.: 1988, Ap. J. 329, 567.

Stark, A.A., Bally, J., Linke, R.A., and Heiles, C.: in preparation.

Tereby, S. and Fich, M.: 1986, Ap. J. 309, L73.

N91-14977

MOLECULES IN AN INFRARED CIRRUS CLOUD

Horst Meyerdierks* and Nathalie Brouillet**
* Radioastronomisches Institut der Universität Bonn,
Auf dem Hügel 71, D-5300 Bonn, Fed. Rep. of Germany
** Observatoire de l'Université de Bordeaux I,
B.P. 21, F-33270 Floirac, France

High latitude dark and bright nebulae were already catalogued by Lynds (1962, 1965) and re-detected in the 100 μm band of IRAS (Low et al. 1984). CO was detected in a number of high-latitude clouds (e.g. Goerigk et al. 1983, Magnani et al. 1985). A prominent feature at 100 μm is the Polar Loop (e.g. Wesselius and Fejes 1973, "Polar Ridge"). It is expanding at a velocity of 5 or 10 km/s (Heithausen and Meyerdierks 1987). One of the clouds that form the Polar Loop was observed in the $1_{10}-1_{11}$ 4.8 GHz transition of formaldehyde and in the J=1-0 transitions of ^{12}CO and ^{13}CO at 115 GHz and 110 GHz resp.

The cloud, which has an extent of 2.5° by 4°, consists of several filaments 1° or 2° long and 0.5° wide. From the correlation of IRAS 60 μm and 100 μm intensities we derive a colour temperature of the dust of 21 K and a maximum optical depth of $3 \cdot 10^{-4}$ (assuming $\tau \propto \nu^2$). At one local maximum of the 100 μm intensity, the hyperfine structure of formaldehyde could be resolved. While the H_2CO column density is (4.4 ± 2.0) 10^{13} cm^{-2}, the excitation temperature of 2.43 K implies a gas density of $(2 \pm 1) \cdot 10^5$ cm^{-3} for kinetic temperatures of 10 to 20 K according to Garrison et al. (1975). Maps of this region in H_2CO and CO show the size of the molecular clump to be 7'. LTE calculations for the observed CO isotopes (cf. Dickman 1978) result in a peak ^{13}CO column density of $(2.3 \pm 0.8) \cdot 10^{15}$ cm^{-2}. Converting this to H_2 column density (Dickman) and assuming a distance of 100 pc, the H_2 density should be 2000 cm^{-3}. Obviously the molecule distribution is very clumpy on a scale of less than 1 pc and the observations suffer from beam dilution (3' and 4.4' beams).

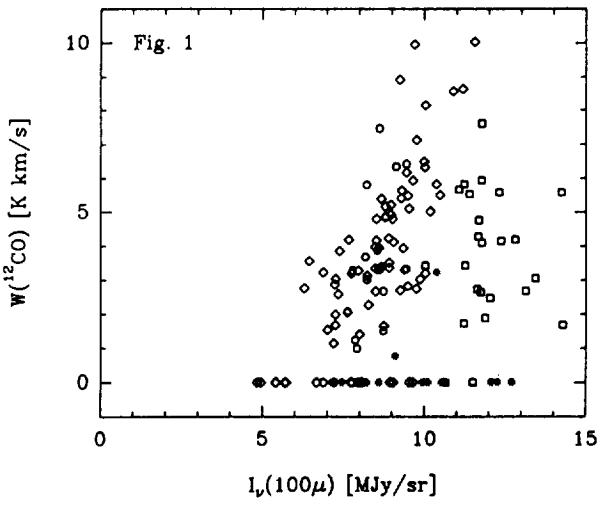

Since the infrared optical depth is small, the 100 μm intensity can be used as a measure of dust column density. Figure 1 compares this with the observed ^{12}CO line integral. Different

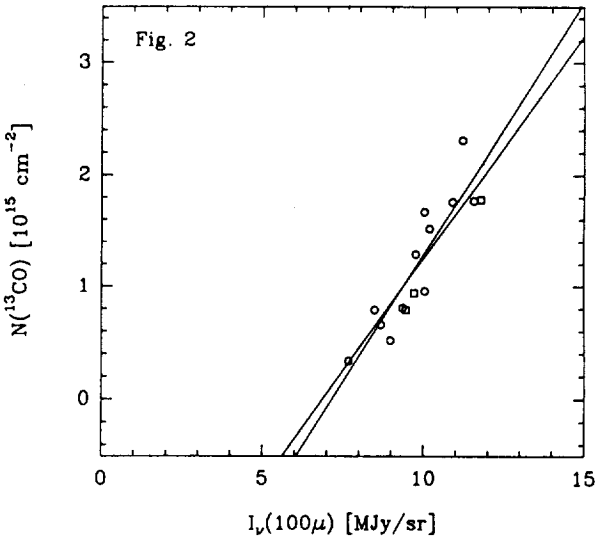

symbols denote different parts of the cloud. The 100 μm intensity jumps when moving from one part to the other but is roughly constant within each of these parts. On the other hand, the CO line integral varies within each part between 0 and 10 K·km/s. This behaviour seems to contradict the assumption that ^{12}CO is optically thick. Figure 1 can be understood as follows: The dust emission per nucleon is equal for dust related to HI or to H_2 (de Vries et al. 1987). Figure 1 then indicates that most of the proton column density is in HI. Only where dense clumps are on the line of sight (i.e. where ^{13}CO is detected), is the molecular column density comparable to the atomic one of the surrounding, less dense envelope. This is demonstrated by figure 2, which shows the correlation of ^{13}CO column density and 100 μm intensity. Roughly half of the dust column density seems to be related to non-molecular gas even at the peak molecular column density.

Finally, the stability of the molecular clump described above can be considered. At an assumed distance of 100 pc the H_2 mass would be 0.6 $M_\odot$, while the virial mass for a radius of 0.1 pc and a line width of 1.3 km/s would be 35 $M_\odot$. Thus the clump is anything but gravitationally bound and will probably disperse on a time scale of $6 \cdot 10^4$ years. Similarly, the filaments which would be 1 pc across would disperse in $3 \cdot 10^5$ years.

It remains to be seen, if this transient nature is a general property of cirrus clouds. The cloud investigated here may well be special because it belongs to an expanding loop. On the other hand, shocks moving through the interstellar medium may hold a key to the understanding of the filamentary morphology of the infrared cirrus.

References:

de Vries, H.W., Heithausen, A., Thaddeus, P.: 1987, *Astrophys. J.* **319**, 723
Dickman, R.L.: 1978, *Astrophys. J. Suppl.* **37**, 407
Goerigk, W., et al.: 1983, *Astron. Astrophys.* **120**, 63
Garrison, B., et al.: 1975, *Astrophys. J.* **200**, L175
Heithausen, A., Meyerdierks, H.: 1987, *Mitt. Astron. Ges.* **70**, 417
Low, F.J., et al.: 1984, *Astrophys. J.* **278**, L19
Lynds, B.T.: 1962, *Astrophys. J. Suppl.* **7** 1
Lynds, B.T.: 1965, *Astrophys. J. Suppl.* **12** 163
Magnani, L., Blitz, L., Mundy, L.: 1985, *Astrophys. J.* **295** 402
Wesselius, P.R., Fejes, I.: 1973, *Astron. Astrophys.* **24** 15

INFRARED CIRRUS POINT SOURCES

William T. Reach, Carl Heiles, and Bon-Chul Koo
Astronomy Department, University of California, Berkeley

The Infrared Astronomical Satellite (IRAS) discovered a large number of unresolved sources which were much more intense at 100μm than at shorter infrared wavelengths. We have isolated a sample of these point sources (Heiles *et al. 1987*) which are located in regions of very low Galactic H I column density, as determined from the Hat Creek 21-cm line survey. Whereas we initially believed these sources to be prime candidates for a class of previously unknown astronomical object, our observations have now proven that most of the sources are associated with the interstellar medium (ISM) of our Galaxy.

Using the NAIC Arecibo telescope to search for Galactic and redshifted 21-cm emission, we have found that:
(1) The excess H I column density at the position of the the IRAS source is less than 10^{19} cm^{-2} over the 3′ beam of the telescope.
(2) Some (roughly 1/3) of the point sources are associated with features in nearby, catalogued spiral galaxies with large angular size.
(3) Many of the point sources are associated with clouds at anomalous LSR velocities. One extraordinary source is associated with a small high velocity cloud, at $v_{LSR} = +133$ km/s.

Using the NRAO Kitt Peak 12-m telescope to search for Galactic ^{12}CO J=1-0 line emission, we have found that:
(1) A large fraction (65% detection rate at the 0.2 K antenna temperature level) of the IRAS source positions reveal CO in position-switched observations.
(2) The CO lines are frequently at anomalous velocities, identical to the H I line velocities.
(3) There is a correlation between the IRAS 100μm flux and the CO antenna temperature. This correlation suggests that the CO emission may be optically *thin*. We are performing ^{13}CO observations (1988 June 11-15) in order to determine the CO optical depth at the location of the IRAS sources; the results will be presented in our poster.

Heiles, C., McCarthy, P. J., Reach, W. T., and Strauss, M. A. 1987, in *Star Formation in Galaxies*, NASA CP-2466, ed. C. J. Lonsdale, p. 553.

Dust in Stellar Wind Bow Shocks

Dave Van Buren - STScI & JHU

A number of high velocity O stars have associated parsec-sized structures visible in the *IRAS* infrared. They can most readily be explained as the dense shells of stellar wind bow shocks. The infrared emission arises from starlight-heated post-shock dust, and possibly also from ionic lines. Emission from pre-shock dust is often seen as well, and allows in principle the empirical determination of the effects of shocks on dust. Since the observed bow shocks span a range of velocities a comparison with theories for shock destruction of dust is possible.

STUDYING THE SPATIAL DISTRIBUTION OF INTERSTELLAR DUST

H.Walker,*,** M.Werner,* C.Allen,* R.Henry,*** R.Kimble,*** J.Wofford,*** J.Murthy****

* NASA Ames Research Center, Moffett Field, CA 94035
** SETI Institute, Moffett Field, CA 94035
*** Center for Astrophysical Sciences, The Johns Hopkins University, Baltimore, MD 21218
**** NASA Goddard Space Flight Center, Greenbelt, MD 20771

I. Introduction

The spatial distribution of interstellar dust reflects both interstellar dynamics and the processes which form and destroy dust in the interstellar medium. The IRAS survey, because of its high sensitivity to thermal emission from dust in the infrared, provides new approaches to determining the spatial distribution of the dust. We report here the initial results of an attempt to use the IRAS data to probe the spatial distribution of dust - by searching for thermal emission from dust in the vicinity of bright stars.

It can easily be shown that a bright, luminous star embedded in a region of "average" interstellar density, i.e. n(H) = 1, and "typical" dust-to-gas ratio, will heat the nearby dust and produce infrared emission readily detectable from IRAS. Consider for example a B3 star at a distance of 50pc from the earth. At a radial distance of 0.25 pc from the star (angular distance 0.25° as seen from earth), the heat input into the interstellar dust from this star is 1.1×10^{-21} erg cm^{-3} s^{-1} H-atom^{-1}, more than 200 times that due to the "mean" interstellar radiation field. Assuming n(H) = 1 and a path length of 0.25 pc through the material within 0.25 pc of the star, the reradiated infrared luminosity due to this heat input will be 6.6×10^{-5} erg cm^{-2} sr^{-1} s^{-1}. If 50% of this reradiated power lies in either of the two long wavelength IRAS bands, the resulting surface brightness will be 1-3MJy/sr, detectable by IRAS in regions where the background is smooth, due to the large number of pixels involved.

II. Results to Date

The above analysis has motivated us to search for diffuse infrared emission in the vicinity of bright, luminous stars, in order to assess the probability with which they are associated with interstellar dust clouds in certain density ranges. We began with a list of 25 stars selected on the basis of high visible brightness or high ultraviolet brightness, with $|b| > 15°$. The 60μm and 100μm IRAS Sky Flux plates from HCONS 1 & 2 (resolution 6 arcmin) were examined in a search for infrared emission associated with these stars. In five of the twenty-five cases, extended infrared emission was found close to or at the position of the star. In each case, this emission shows 60μm/100μm flux ratio appreciably higher than that which characterizes the diffuse emission elsewhere on the same plate. The higher color temperature indicates that the infrared emission is due to dust heated by the star rather than background or foreground "cirrus" clouds.

III. Analysis

We list below the properties of the diffuse infrared emission associated with these five stars. α Lyr (Vega) is included in the table as a comparison object, known to have a very cool circumstellar dust shell, and one of the IRAS standard point sources, α Boo (Arcturus), is also listed. The table gives the peak surface brightness (I_{peak}) of the emission at the location of the star, with the background subtracted (in MJy/sr). The background is found by taking a ring around the area used for the summation and finding the mean of the lowest 25% of the values. This avoids the problems of nearby sources of emission and of stripes, and since the areas involved are small, the assumption of a single value for the background is acceptable. The flux density, with the background subtracted, is summed over a region usually 22 arcmin by 22 arcmin ($\sum I_{net}$ in Jy). The values are shown in brackets when the emission peak is not precisely centred on the source position. For α Vir two boxes were used to sum the emission, one centred on the 12μm source and one on the 100μm source. One box was used for δ Sco, but its size was increased to 48 arcmin by 38 arcmin to accomodate the extended emission at 100μm. The 60μm/100μm flux density ratio is shown in two forms. The subscript "net" means that the preceeding two rows of summed background subtracted flux are divided to give the ratio. The subscript "sub" means that the two maps with the backgound subtracted from each were divided and the value of an appropriate pixel given. The same ratio for cirrus is 0.2 (Weiland et al., 1986). The numbers in brackets are the temperatures derived from the ratio, assuming a blackbody. The ratio of the infrared luminosity to the stellar luminosity at earth is given, showing how small an optical depth is detected.

Also given is the heating rate 1 parsec from the star (Γ). The stellar input spectra are derived from Kurucz (1979) models (a blackbody is used for α Boo). These spectra are then folded through the absorption properties of dust in the model by Mathis, Mezger and Panagia (1983) to determine the heat input, assuming the

dust is optically thin. The canonical relationship between extinction and hydrogen column density is assumed, $E_{B-V} = N_H/6\times10^{21}$.

IV. Conclusions

These preliminary results show that this technique - which relies on finding infrared emission associated with randomly selected stars - can ultimately be used to study the distribution of dust in the ISM.

The density of the cloud producing the infrared emission may be derived by assuming that the dust is at its projected distance from the star and that the heating is due to the star's (known) radiation field. The heating radiation will be folded into a Draine (1985) grain model, and the number of emitting grains adjusted to reproduce the observed energy distribution. We note that this technique is capable in principle of detecting dust densities much lower than those typical of the cirrus clouds, because we are looking preferentially at regions near stars where the heating flux is far higher than the diffuse radiation field which produces the cirrus emission.

References

Draine, B.T., 1985. Astrophys. J. Suppl. **57**, 587.

Kurucz, R.L., 1979. Astrophys. J. Suppl. **40**, 1.

Mathis, J.S., Mezger, P.G., Panagia, N., 1983. Astron. Astrophys. **128**, 212.

Van Buren, D., McCray, R., 1988. Astrophys. J. (in press)

Weiland, J.L., Blitz, L., Dwek, E., Hauser, M.G., Magnani, L., Rickard, L.J., 1986. Astrophys. J. **306**, L104.

Notes for the Table

α Vir is also classified as B1III-IV. The fluxes for α Vir in brackets show that the flux given is not centred on the star, but about 14 arcmin away. The 12μm/25μm map shows a single peak at the stellar position, showing the star dominates the emission here. The 60μm/100μm shows two features, one at the stellar position and one at the peak of the 100μm flux. The flux ratios include both the star and the dust.

For δ Sco the peak 12μm flux from the star is not coincident with the peak of the 100μm flux map. Van Buren and McCray (1988) suggest the longer wavelength emission is a bow shock associated with the star. In the 12μm/25μm map the star is at a peak in the ratio map, and the cool dust is near a minimum. The structure is poorly defined in the contour plot for the 60μm/100μm map, but the "bow shock" structure is present.

ν Sco has a companion about 40 arcsec away, which is itself double. The 12μm/25μm map shows a minimum in the ratio at the star's position, and there is a maximum in the 60μm/100μm map, as the cool dust dominates the surroundings.

π Sco is visible at all 4 wavelengths, and appears much larger than a point source.

Star	α Vir	δ Sco	ν Sco	π Sco	η Hya	α Lyr	α Boo
Sp Type	B1III+B2V	B0.3IV	B3V+B8V	B1V+B2V	B3V	A0Va	K1IIIbp
V	0.98	2.32	4.01	2.89	4.30	0.03	–0.04
r (pc)	43	~200	33	100	~160	8	10
FWHM 60μm	0.80°	0.40°	0.52°	0.26°	0.52°		
I_{peak} 12μm (MJy/sr)	3.9	2.0	1.8	4.0	0.3	17.2	422.5
I_{peak} 25μm	1.0	9.0	8.6	40.0	0.9	4.1	94.6
I_{peak} 60μm	(3.2)	17.0	9.6	31.7	0.3	3.8	11.8
I_{peak} 100μm	(1.9)	10.4	5.1	16.1	0.3	2.9	3.0
$\sum I_{net}$ 12μm (Jy)	(35.3)	79.9	23.8	26.7	14.2	40.5	861.4
$\sum I_{net}$ 25μm	(120.5)	344.9	104.8	390.6	32.6	15.1	179.0
$\sum I_{net}$ 60μm	(275.8)	1184	213.6	930.1	17.2	15.3	31.1
$\sum I_{net}$ 100μm	(226.2)	1173	329.9	710.8	30.6	25.4	24.9
$(60/100)_{net}$	1.2 (85)	1.0 (70)	0.7 (55)	1.3 (90)	0.6 (50)	0.6 (50)	1.3 (85)
$(60/100)_{sub}$	2.0 (150)	1.2 (85)	0.9 (65)	2.1 (180)	0.8 (60)	0.3 (40)	3.6
L_* (ergs.s^{-1})	4.10^{37}	4.10^{37}	1.10^{37}	3.10^{37}	1.10^{37}	3.10^{35}	3.10^{35}
L_{IR}/L_*	$1.8.10^{-3}$	0.18	$5.3.10^{-3}$	$4.3.10^{-2}$	$1.3.10^{-2}$	$8.3.10^{-4}$	$4.1.10^{-3}$
Γ (ergs.cm^{-3}s^{-1}n$_H^{-1}$)	4.10^{-22}	1.10^{-21}	4.10^{-22}	5.10^{-23}	4.10^{-22}	5.10^{-25}	3.10^{-25}

The 12μm/25μm shows a minimum in the ratio at the source position, and the 60μm/100μm map shows a peak.
The luminosities of the stars, shown in the table, are from Allen's Astrophysical Quantities.
Γ is the heating rate 1 parsec from the star.

THERMAL EMISSION FROM INTERSTELLAR DUST IN AND NEAR THE PLEIADES

Richard E. White*
*Five College Astronomy Department, Smith College, Northampton, Massachusetts 01063 USA and
Department of Physics and Astronomy, University of Wyoming, Laramie, Wyoming 82071 USA

ABSTRACT

IRAS survey coadds for a $8.7^\circ \times 4.3^\circ$ field near the Pleiades provide evidence for dynamical interaction between the cluster and the surrounding interstellar medium. The far-infrared images show large region of faint emission with bright rims east of the cluster, suggestive of a wake. Images of the far-infrared color temperature and 100 μm optical depth reveal temperature maxima and optical depth minima near the bright cluster stars, as well as a strong optical depth peak at the core of the adjacent CO cloud. Models for thermal dust emission near the stars indicate that most of the apparent optical depth minima near stars are illusory, but also and provide indirect evidence for small scale interaction between the stars and the encroaching dust cloud.

INTRODUCTION

The encounter of the Pleiades star cluster with a small interstellar cloud (Gordon and Arny 1984; Federman and Willson 1984; White 1984a,b; Breger 1986, 1987) has created a laboratory for the investigation of interstellar processes. The Infrared Astronomical Satellite (IRAS) opened new windows to that laboratory, revealing for the first time the distribution of long wavelength radiation emitted by the dust in the familiar optical reflection nebulae. Castelaz, Sellgren, and Werner (1987, CSW) reported on an initial examination of IRAS data for a $2.25^\circ \times 2.25^\circ$ region centered on the cluster. They concluded that the 60 μm and 100 μm data could be understood as thermal emission from typical interstellar grains, whereas the 12 μm and 25 μm data required the action of single-photon excitation of small grains or large molecules.

This paper presents preliminary results from an investigation of new IRAS survey coadds. The data set is a mosaic of eight $2.25^\circ \times 2.25^\circ$ fields, covering $8.7^\circ \times 4.3^\circ$, a much larger region than studied by CSW.

The data have received processing to remove some of the artifacts present in the earlier data and the slope of the zodiacal background, but detectable signatures of the satellite and the data processing remain.

The analysis follows the interpretation of CSW that the 60 μm and 100 μm images primarily represent optically thin thermal emission, and yields images of color temperature, T_c, and 100 μm optical depth, τ, for an assumed dust emissivity varying as λ^{-1}. [Although the derived values of T_c and τ depend on the emissivity law, qualitative characteristics of the images do not.]

LARGE SCALE STRUCTURE

Figure 1 is a contour diagram of the 60 μm surface brightness mosaic. The 100 μm mosaic exhibits the same features. The dominant features of both images are: (1) bright emission to the right of center, at the position of the Pleiades; and (2) the elongated region to the left (east) of the cluster, which exhibits faint emission and a brighter rim. The orientation of this feature is consistent with the east-west alignment of streamers in the Pleiades reflection nebulae (Arny 1977), and appears to be the wake left by the passage of the cluster through the interstellar medium.

The individual subimages in the mosaic received entirely separate treatment in the data processing. Consequently, although the surface brightness mosaics appear nearly seamless, images of far- infrared color temperature and optical depth clearly reveal the subimage boundaries. This circumstance renders difficult further interpretation of the large scale structure at the present time. The bright emission near the cluster, however, is insensitive to small differences in background between subimages.

THE CLUSTER ENVIRONMENT

The maximum surface brightness at both 60 μm and 100 μm occurs at a position south of 23 Tau (Merope), although there are secondary peaks near positions of luminous cluster stars. The images of color temperature and 100 μm optical depth clarify the physical situation.

Figure 2 shows prominent peaks in T_c, up to 46 K, at or near the positions of bright stars, above a broad plateau emission with $T_c \sim 30$ K. This pattern fulfills the expectation that a star cluster embedded in an interstellar dust cloud would yield local temperature maxima within a larger region heated by the collective ultraviolet emission of the cluster stars.

Figure 3 exhibits a strong τ peak that coincides with the core of the small CO cloud southwest of 23 Tau (Federman and Willson 1984; Bally and White 1989), fainter structure to the southwest of the peak that matches the morphology of the CO cloud, and a ridge that details the dust distribution that is roughly outlined by optical polarization data (Breger 1986, 1987).

The figure also exhibits local minima near the positions of the brightest stars,

and a minimum that extends eastward from the cluster core. The latter feature corresponds to the 21-cm "hole" discussed by Gordon and Arny (1984) and confirmed by Breger (1986). Its larger structure is confused by mosaic boundaries, but it suggests that the large scale "hole" present in Figure 1 results primarily from a dearth of dust, not from unusually low dust temperatures.

SMALL SCALE STRUCTURE

Preliminary analysis of these images has included construction of simple models for the thermal emission near several stars, under the assumption that the dust is optically thin both in the infrared and in the ultraviolet, with parameters adjusted to give reasonable representations of the T_c- and τ-profiles within 15' of the star. Results to date include the following.

1. Apparent minima in τ occur at the positions of luminous stars even for uniform layers, as a consequence of the single temperature analysis of the surface brightness ratios.
2. The most luminous Pleiades star, η Tau, lies in a real cavity in the dust distribution that is evident both in T_c and τ.
3. Unless the 100 μm dust emissivity is unexpectedly large, >0.005, all the stars examined require unresolved cavities to account for the relatively modest color temperatures observed.

Thus, although apparent τ-minima near the stars must be regarded with caution, the analysis indicates that small scale interactions between the stars and the surrounding interstellar medium do occur. Possible mechanisms for interaction between the stars and the surrounding interstellar medium include ram pressure from stellar winds, the direct influence of radiation pressure, and thermal pressure resulting as the interstellar gas is heated indirectly by starlight.

CONCLUSIONS

1. Far-infrared images of an $8.7° \times 4.3°$ region near the Pleiades provide evidence for a "wake" produced by passage of the cluster through the ambient interstellar medium.
2. Images of the far-infrared color temperature and 100 μm optical depth in a $2.6° \times 2.6°$ region near the cluster show:
   a. temperature peaks and optical depth minima near the positions of luminous stars;
   b. an optical depth peak and fainter structure corresponding to that seen in CO emission, plus more extended features previously inferred from polarization data.

3. Models for the thermal emission near the stars provide indirect evidence for unresolved cavities resulting from dynamical interaction between the stars and the surrounding interstellar medium.

4. The optical depth distribution therefore suggests the presence of both large scale and small scale dynamical interactions between the Pleiades and an interstellar cloud that appears to be encroaching from the western side of the cluster (Arny 1977; Gordon and Arny 1984).

REFERENCES

Arny, T. 1977, Ap. J., **217**, 83.

Bally, J. and White, R. E. 1989, in preparation.

Breger, M. 1986, Ap. J., **309**, 311.

Breger, M. 1987, Ap. J., **319**, 754.

Castelaz, M., Sellgren, K., and Werner, M. W. 1987, Ap. J., **313**, 509.

Federman, S. R., and Willson, R. F. 1984, Ap. J., **283**, 626.

Gordon, K. J., and Arny, T. T. 1984, A. J., **89**, 672.

White, R. E. 1984a, Ap. J., **284**, 685.

White, R. E. 1984b, Ap. J., **684**, 695.

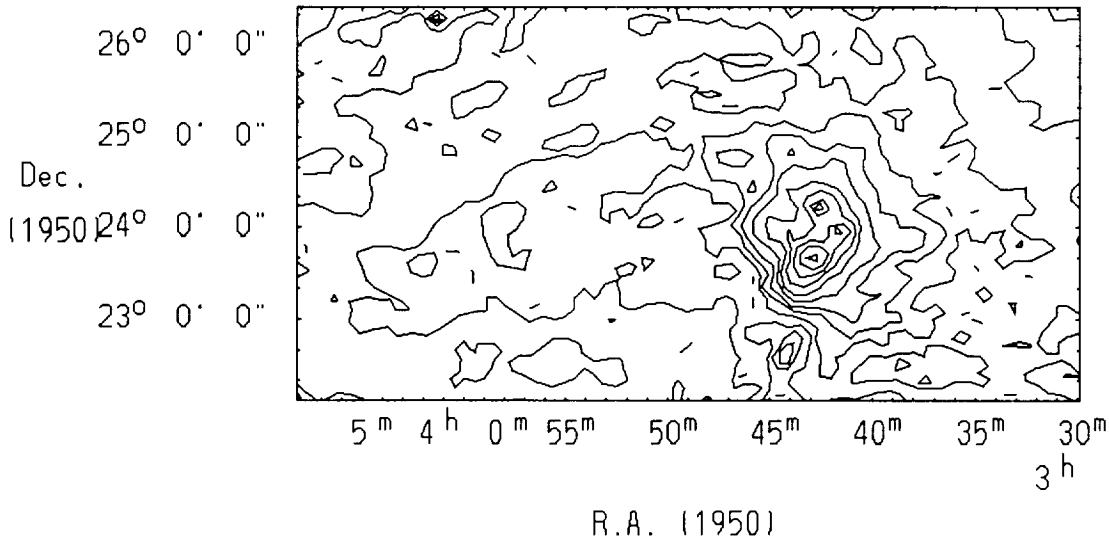

Figure 1. Contour diagram of 60 μm surface brightness mosaic, which covers $8.7° \times 4.3°$ near the Pleiades. The contour interval is 0.25 dex. The brightest contour represents log S_{60} (Jy sr^{-1}) = 8.0. The peak value is 8.15.

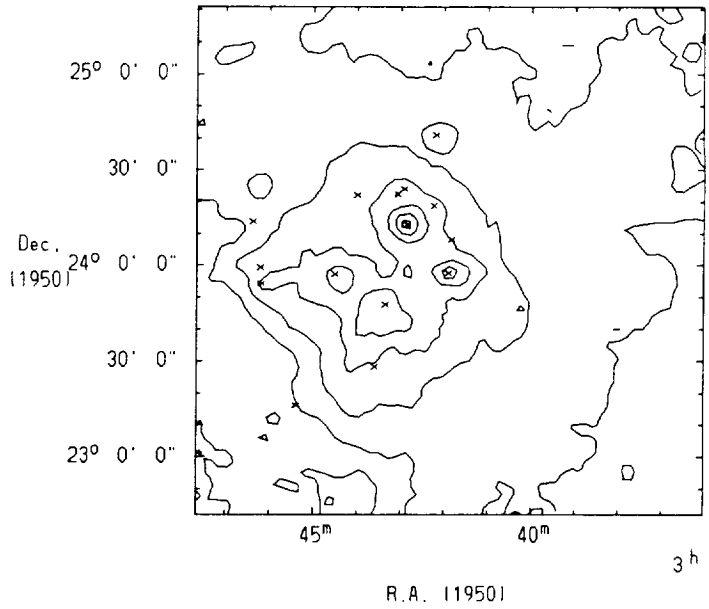

Figure 2. Color temperatures in the immediate vicinity of the Pleiades, derived from the ratio of 60 μm and 100 μm surface brightnesses assuming that the opacity varies as λ^{-1}.

The contour interval is 4 K. The brightest contour represents 44 K, and the peak value is 45.3 K. The crosses represent positions of the most luminous cluster stars.

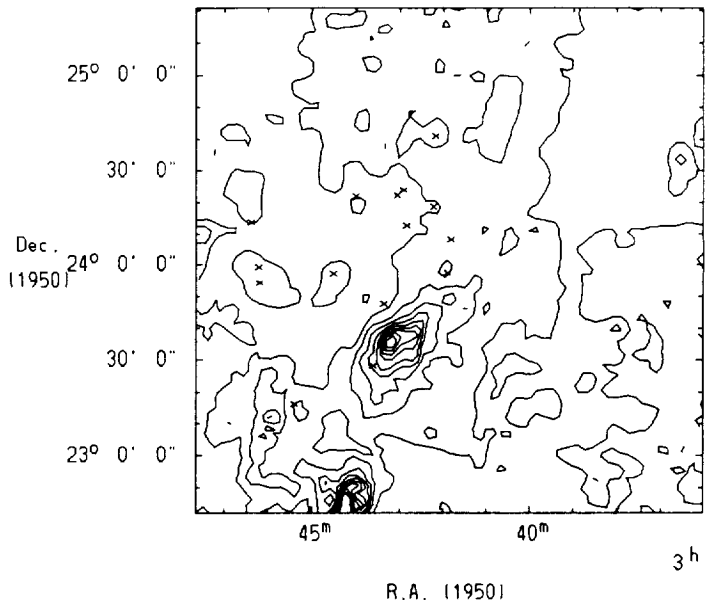

Figure 3. Optical depths derived from the 100 μm surface brightnesses and the color temperatures in Figure 3. The contour interval is 5×10^{-5}. The highest contour represents 6×10^{-4}. The peak value near the cluster is 5.6×10^{-4}. The crosses represent positions of the most luminous cluster stars.

IV-B) DUST IN EXTERNAL GALAXIES

TEMPERATURE DISTRIBUTION OF DUST IN LUMINOUS IRAS GALAXIES

David P. Carico
Downs Laboratory of Physics, 320-47
California Institute of Technology, Pasadena, CA 91125

INTRODUCTION

Work is currently in progress to obtain temperature distributions of dust in the most infrared-luminous galaxies. The results presented herein are of a preliminary nature, representing a zeroth-order approximation (see **WORK YET TO BE DONE**, below). The objects which have been analyzed so far are all galaxies from the *IRAS* Bright Galaxy Sample with infrared luminosities $L_{IR} \geq 10^{11}\ L_{\odot}$ (see Carico *et al.*, 1988). They are: **Arp 220, Mrk 231, Mrk 273, NGC 1614, NGC 3690, NGC 6285/6,** and **Zw 049.057.** The analysis utilized 3.7 μm data from the Palomar 5 m Hale telescope, *IRAS* data at 12, 25, 60, and 100 μm, and 1 mm continuum data from the CalTech Submillimeter Observatory on Mauna Kea.

METHOD

A cloud of N spherical dust grains at a distance d from the observer produces an observed flux density at a wavelength λ given by

$$f_\nu(\lambda) = \int_0^\infty \pi B_\nu(\lambda, T) \left(\frac{a}{d}\right)^2 Q_{abs}(\lambda) \frac{dN}{dT}\, dT\ , \tag{1}$$

where a is the radius of the dust grains, $Q_{abs}(\lambda)$ is the absorption efficiency of the dust grain material, and $B_\nu(\lambda, T)$ is the Planck function. If a mean mass density is adopted for the grain material (a value of 3 g cm^{-3} was used to obtain the accompanying results), N can be rewritten in terms of the total mass of dust, M, and eqn. (1) can be put in the form

$$f_\nu(\lambda) = C\, \frac{Q_{abs}(\lambda)}{a}\, \frac{1}{\lambda^3} \int_0^\infty \frac{1}{e^{\frac{hc}{\lambda kT}} - 1} \frac{dM}{dT}\, dT\ , \tag{2}$$

where C is a constant for a given emission source, depending only on the mean mass density of the grain material and the distance to the source. For $\lambda \gg a$, the quantity $Q_{abs}(\lambda)/a$ is independent of a (see, e.g., Hildebrand, 1983); thus, for infrared emission from spherical interstellar dust grains, the observed flux density does not depend on the size of the grains.

In numerical form, eqn. (2) becomes

$$f_\nu(\lambda_i) = C\, \frac{Q_{abs}(\lambda_i)}{a}\, \frac{1}{\lambda_i^3} \sum_j \frac{1}{e^{\frac{hc}{\lambda_i kT_j}} - 1} \left(\frac{dM}{dT}\right)_j dT_j\ .$$

Using logarithmic intervals for λ and T, so that $\lambda_i = \lambda_o\, x^i$, $T_j = T_o\, y^j$, and $dT_j = T_j - T_{j-1} = T_j(1 - \frac{1}{y})$, where x, y, λ_o, and T_o are constants, and defining

$$f_i = \frac{\lambda_o^3 a}{C Q_{abs}(\lambda_i)} (1 - \frac{1}{y})\, f_\nu(\lambda_i)$$

$$K_{ij} = \left[x^i (e^{\frac{hc}{\lambda_i kT_j}} - 1)\right]^{-1}$$

$$g_j = \left(\frac{dM}{d(\ln T)}\right)_j$$

one obtains

$$f_i = \sum_j K_{ij}\, g_j \tag{3}$$

which must be solved for the g_j.

For the analysis presented here, eqn. (3) was solved using a modified version of the least-squares computer program described by Pajot *et al.* (1986) (which was generously provided by J. L. Puget when this author's own program failed to cooperate for as yet unknown reasons – my sincerest thanks!). A wavelength range from 3.7 μm to 1000 μm was used for all objects. The results are shown in the accompanying figures.

RESULTS

The results for three representative galaxies are shown in Figures 1 and 2. In each plot, three curves have been drawn, representing results for three different emissivity laws:

$Q_{abs} \propto \lambda^{-1}$: solid line

$Q_{abs} \propto \lambda^{-1.5}$: dotted line

$Q_{abs} \propto \lambda^{-2}$: dot – dashed line

where Q_{abs} is the absorption efficiency, normalized to $Q_{abs}(100\ \mu m)/a = 133.3\ \mathrm{cm}^{-1}$, and a is the effective grain size.

Figure 1 shows the mass of dust (in units of $M_\odot = 2 \times 10^{33}$ gm) per logarithmic temperature interval. The total mass is thus the area under the curve shown.

In Figure 2 is shown the fraction of the total luminosity emitted by dust at a temperature T (in the top half of each plot), and the fraction of the luminosity which is being emitted by dust which is at temperatures $\geq T$. These plots tend to bring out the differences between the galaxies much more clearly than the mass distribution plots of Figure 1, due to the extreme temperature dependence of the luminosity ($L \propto T^{4+\beta}$, for $Q_{abs} \propto \lambda^{-\beta}$). In particular, one can compare the very sharply peaked distribution for Arp 220, centered at 50 K, and falling to 5% of the luminosity at temperatures $\lesssim 25$ K and $\gtrsim 100$ K, with the broad distribution for Mrk 231, which peaks at roughly 150 K and falls to 5% of the luminosity for temperatures $\lesssim 40$ K and $\gtrsim 350$ K. This difference can also be seen in the bottom plots where, for Arp 220, $\lesssim 10\%$ of the luminosity is being emitted by dust with temperatures > 100 K, whereas for Mrk 231, the contribution to the luminosity from $T > 100$ K dust is $\sim 60\%$.

Figure 2 also indicates how uncertain estimates of the mass of cold dust can be. For the case of Mrk 231, Figure 2 suggests that more than 90% of the luminosity is being emitted by dust at temperatures $\gtrsim 50$ K. However, from Figure 1 it is seen that most of the estimated dust mass for Mrk 231 is at temperatures $\lesssim 50$ K. Hence, significant changes in the total mass of dust would not necessarily be reflected in the energy distribution.

WORK YET TO BE DONE

As mentioned previously, the work presented here is preliminary, intended to obtain a qualitative feel for the analysis and the results that can be obtained. The main simplifications which have gone into this analysis, and which will be addressed in subsequent work, are as follows:

1. The dust was assumed to be everywhere optically thin to infrared radiation. This is almost certainly not the case, particularly for the compact central regions of such galaxies as Arp 220 and Mrk 231.
2. The $1 - 3\ \mu m$ data has not yet been utilized, due to the complexities of accurately accounting for contamination from stellar emission. These wavelengths will clearly be important in understanding the hottest dust, particularly for temperatures in excess of 1000 K.
3. The contribution to the emission from very small grains, presumably PAHs (polycyclic aromatic hydrocarbons), has not been addressed, and may be significant in some sources.

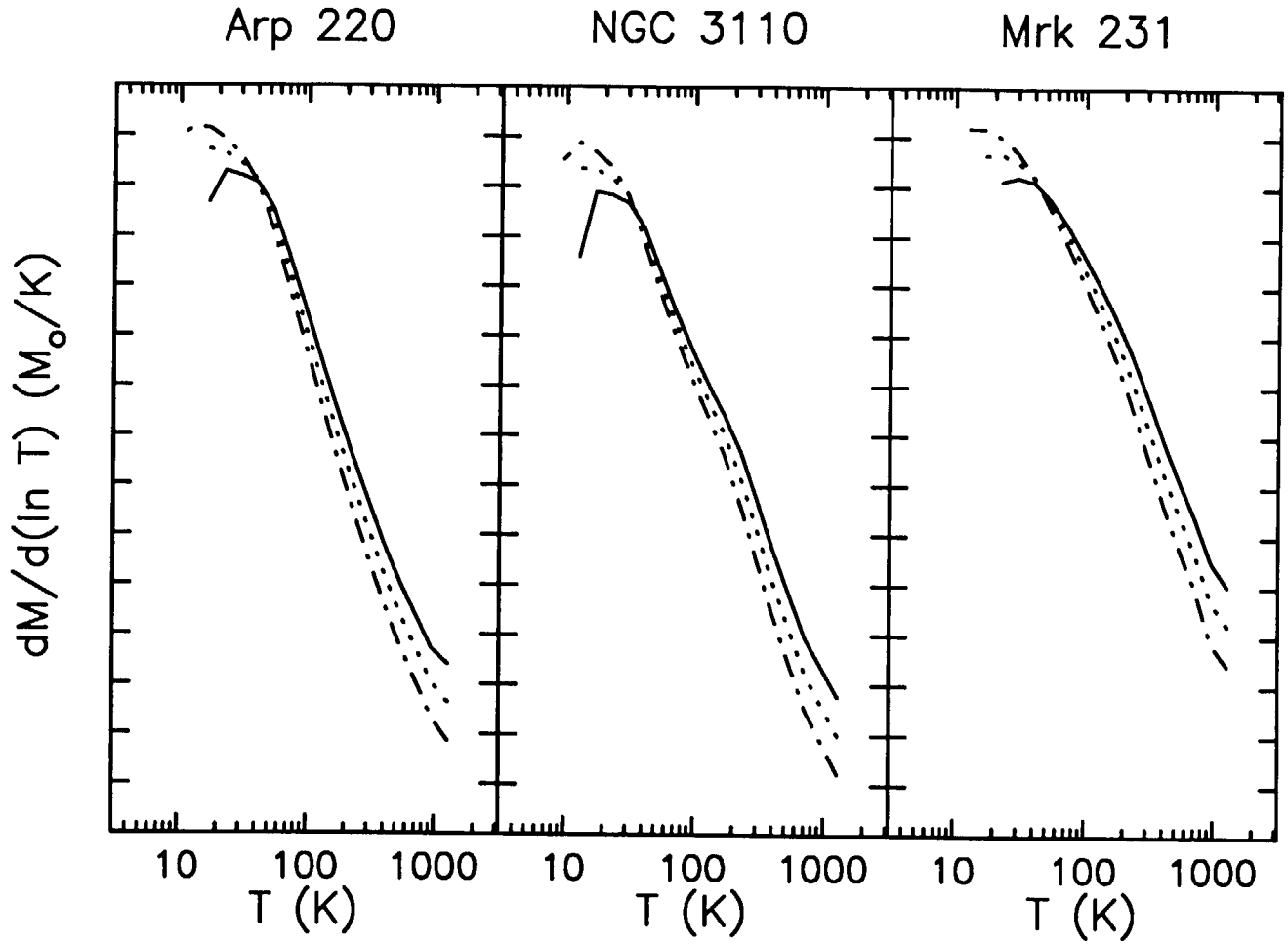

Figure 1: The mass of interstellar dust as a function of temperature for three infrared-luminous galaxies. The different curves on each plot are discussed in the text.

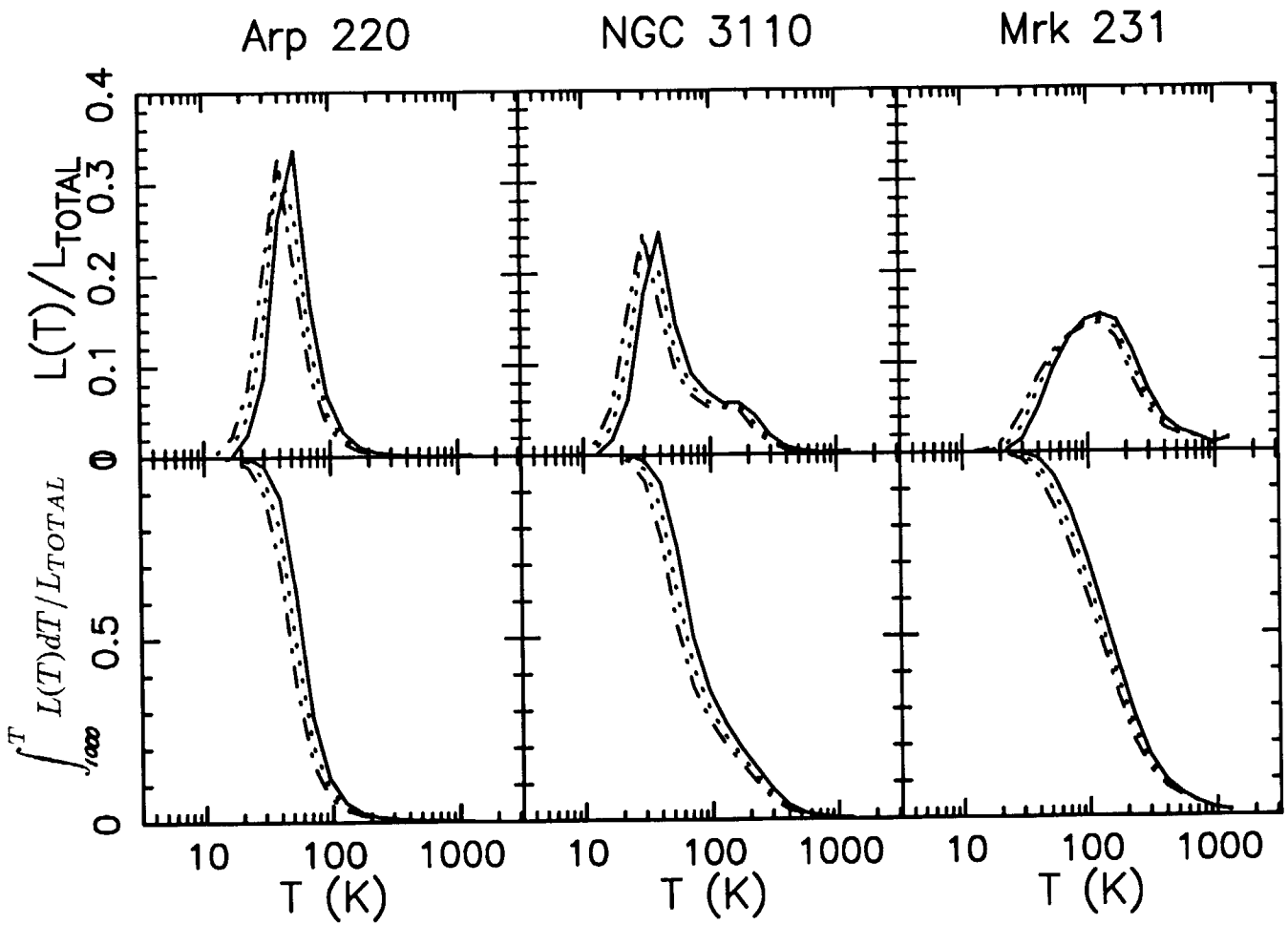

Figure 2: (*top*) The fraction of the luminosity emitted by dust at temperature T (*bottom*) The fraction of the luminosity emitted by dust at all temperatures $\geq T$.

The author is grateful to J. L. Puget and B. T. Soifer for extremely helpful discussions, J. Keene for vital assistance in obtaining the 1 mm measurements at the CalTech Submillimeter Observatory, and B. T. Soifer and G. Neugebauer for financial support while attending the symposium.

REFERENCES

Carico, D.P., Sanders, D.B., Soifer, B.T., Elias, J.H., Matthews, K., and Neugebauer, G.: 1988, *Astron.J*, **95**, 356.

Hildebrand, R.H.: 1983, *Q.J.R.A.S.*, **24**, 267.

Pajot, F., Boissé, P., Gispert, R., Lamarre, J.M., Puget, J.L., and Serra, G.: 1986, *Astron.Astrophys.*, **157**, 393.

100 AND 160 MICRON MAPS OF THE DUST REEMISSION FROM THE NUCLEUS AND INNER-ARM REGIONS OF NGC 6946

G. ENGARGIOLA AND D.A. HARPER
Yerkes Observatory

D.T. JAFFE
Department of Astronomy, University of Texas at Austin

ABSTRACT

Dust reemission from the Scd galaxy NGC 6946 has been measured at 100 and 160 μm with the 32-channel University of Chicago Far-Infrared Camera. We present fully sampled maps of the nucleus and inner spiral arms at 45" resolution. The far-infrared morphology of the galaxy is a bright peak centered on a diffuse disk, where the peak occurs about 24" NE of the Dressel and Condon optical center. The 100/160 μm color temperature is correlated with the Hα surface brightness. Assuming the distance from earth to the galaxy is 10.1 Mpc, we determine that Tc is 32°K at the nucleus and at radius 5.4 kpc, where there is a concentration of HII regions. In the intermediate annulus of relatively low Hα surface brightness, the temperature drops to a local minimum of 25°K at radius 3 kpc. The ratio of reradiated to transmitted stellar luminosity is ~3.0 at the nucleus and ~0.9 for the disk. The optical depth at 100μm increases from .0005 at the edges of our map to .0035 at the FIR peak. Combining our observations with a fully sampled map of similar spatial extent in CO(1->0), we determine that the ratio F_{IR}/I_{CO} at the center of the galaxy is almost twice that for the disk, where the value is more or less constant.

I. INTRODUCTION

NGC 6946 is a nearly, face-on Scd type galaxy having an especially prominent northern spiral arm (Arp 1966) and a bright, compact, starburst nucleus (Telesco and Harper 1980). This galaxy has been studied extensively from X-ray to radio wavelengths. The blue and I-band fluxes have been measured by Ables (1971) and Elmgreen and Elmgreen (1984). DeGioia-Eastwood et al. (1984) have made a determination of the massive star formation rate based on measurements of Hα, but the the most detailed study of the ionized gas morphology to date has been prepared by Bonnarel (1986). All optical measurements of the galaxy reveal that surface brightness tapers off exponentially from the nucleus. The nonthermal radio continuum (van der Kuit, Allen, and Rots 1977; Klein et al 1982) and the CO (Young and Scoville) have smooth emission profiles similar to the optical disk, but the distribution of thermal radio emission is clumpy: concentrations coincide with the nucleus and a circumnuclear ring of prominent HII regions. X-rays occur throughout the optical disk but peak at the starburst nucleus and in the vicinity of the bright northern arm (Fabbiano and Trinchieri, 1987). X-ray intensity declines more steeply with radius than the optical surface brightness, possibly because of a relative excess of X-rays from a gaseous component associated with star-forming regions in the active nucleus. The global far-infrared emission properties at $\lambda \leq 100\mu m$ have been determined from IRAS observations by Rice

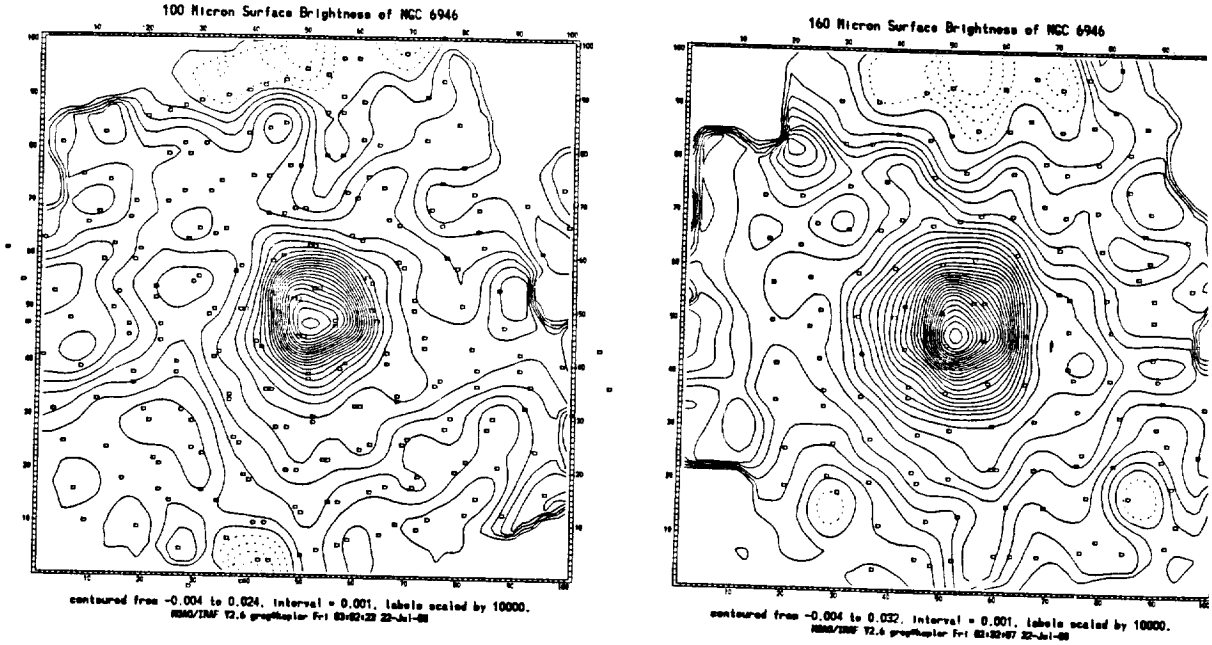

Fig. 1.- Contour maps of NGC 6946 at 100 and 160 microns. The resolution of both maps is ~45". The contours are linear and in signal units (volts).

et al. (1987). The ratio of far-infrared to blue luminosity is ~.9 indicating that half the starlight of the galaxy is reradiated by dust. The infrared and blue diameter are the same (~13'), hence the entire optical disk is obscured by quantities of dust. IRAS scans at 12, 25 and, to some extent, at 60 microns show the far-infrared emission peaks strongly on a disk of diffuse emission. Hence, the morphology of NGC 6946 is similar at all wavelengths, but with some interesting differences. In addition to an exponential disk, there is an excess of far-infrared and x-ray emission at the nucleus. Also, the distribution of HI integrated intensity has a hole 16 kpc in diameter centered at the nucleus (Tacconi and Young), beyond which the intensity rises steeply but then declines exponentially with a scalelength of 14.5 kpc. This falls outside the 4-6 kpc range of scalelengths for other surface brightness profiles.

The starlight continuum of NGC 6946 peaks strongly in the near infrared at ~1 micron and in the far-infrared at ~120 microns. In addition, there is a small peak which occurs at ~10 microns. The near-infrared peak is stellar light; the far-infrared peak is thermal reradiation of stellar photons absorbed by interstellar dust, while the mid-infrared peak is believed to be emission from small grains heated to high temperatures by absorption of UV photons from hot stars. In general, the functional form F_υ=constant x $\nu B_\nu(T_c)$ can be fit to the far-infrared peak. Tc may be regarded as a representative, but not the actual, temperature of the interstellar dust. If measurements of the galaxy are made at two wavelengths on the Rayleigh-Jeans side of spectrum, a color temperature for the dust can be computed which depends linearly on the ratio of the two measurements. However, the dependence of the emissivity on wavelength is required: for this paper, we shall assume the dependence is inverse linear.

Array detector systems developed at the University of Chicago have been used to map extensive, large scale morphology of nearby face-on galaxies such as M 51 (Smith et al.,1984) and NGC 6946 (Smith, Harper, and Loewenstein, 1984). More completely sampled maps of the inner disk and nucleus of NGC 6946 made at 100 and 160 microns are presented in this paper. For the

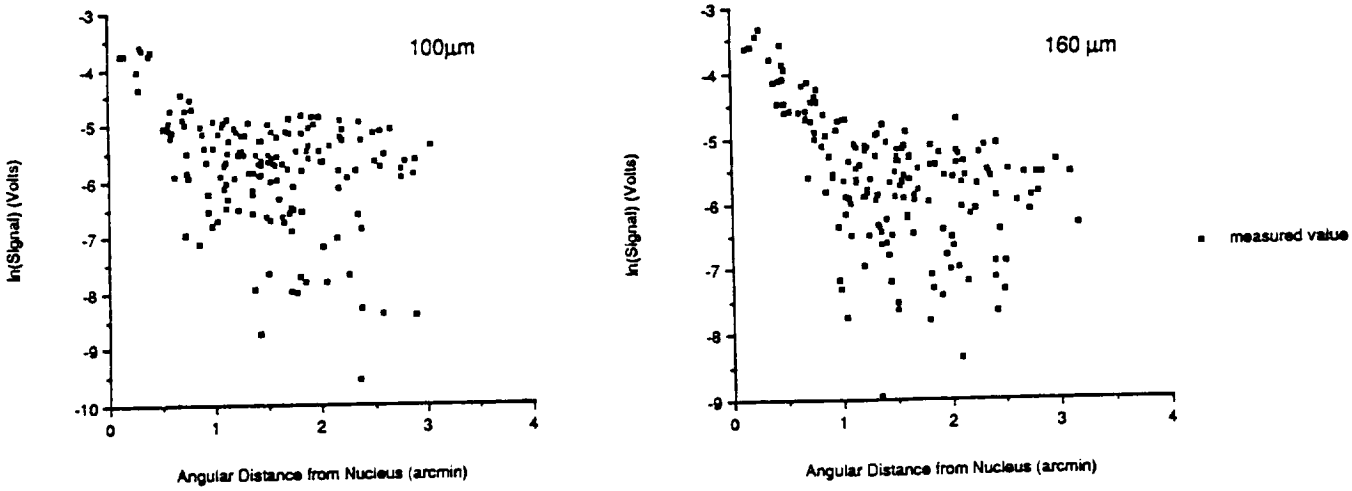

Fig. 2.- Radial distribution of the 100μm and 160μm surface brightness of NGC 6946. The logarithm of the signal measured with the camera is plotted versus the angular distance from the nucleus.

discussion, we adopt 10.1 Mpc (Rogstad, Shostak, and Rots, 1975) for the distance to NGC 6946. At this distance, our beamwidth projects to 2.9 kpc. We shall examine the dust reradiation morphology of NGC 6946 in greater detail than previous studies. Moreover, we shall study the variation of 100 micron optical depth and 100/160 micron color temperature over the galaxy, and consider the relation of these quantities to other characteristics of the interstellar medium.

II. OBSERVATIONS AND DATA ANALYSIS

NGC 6946 was mapped at 100 and 160 microns with the 32-channel University of Chicago Far-Infrared Camera mounted on the .91 m telescope of the NASA-Kuiper Airborne Observatory. The observations were made in June 1986. A brief description of the instrument and calibration procedures can be found in Engargiola et al. (1988). The detector array consists of a closed packed array of bolometer detectors having 45" beams (FWHM) and 48" center to center spacings. The boresite for the camera was found by observing M 82. Thermal background was removed by chopping the secondary mirror 4.5' off the source. W51 was the calibrator and all measured signals were corrected for atmospheric extinction due to water vapor. We estimate that the far-infrared positions are good to 5".

The galaxy was mapped by stepping the detector array through a configuration of eight points described by the corner points of two overlapping 22."5 x 22."5 squares offset diagonally from each other by about a quarter beam diameter. Such eight-point maps are oversampled. The integration time at each point was two minutes, and a single eight point map was made at each broad-band filter setting. The effective wavelengths were 100 and 160 microns. Since the sky rotates relative to the focal plane, the data points when mapped onto the celestial sphere are irregularly spaced. Using a gaussian weighting function with σ = 12."6, these points were interpolated to a regular 100x100 grid. The final maps have a resolution of ~47".

III. RESULTS

Contour maps of the 100 and 160μm surface brightness made with 45" resolution are shown in figure 1. The maps are in signal units (volts). The peak is 76Jy/beam at 100μm and 66Jy/beam at 160μm, where the beam area of each detector element is .8 square arcminutes and the dimensions of the IRAF viewport are 6'x6'. The images are oriented sky right (north-up, east-left) and are centered at (α,δ)=(20: 33: 50.4, +59: 59: 11), the far-infrared peak. When compared to a Hα map with the same resolution (figure 3), it seems clear that emission from four spiral arms has been detected at 100μm. Unfortunately, the 160μm map is not sampled as far to the east of the nucleus, and some of the spiral structure observed at 100μm has been missed. Small open boxes mark points where the surface brightness has been measured. The distribution of signals measured by the far-infrared camera versus the angular distance from the nucleus are shown in figure 2. The linear dispersion out to 1' is evidence of the oblong shape of the bright infrared peak. The distribution past 1' appears to bifurcate, where one branch is an apparent continuation of the steeply decreasing nuclear flux and the other is the true disk of the galaxy, which is fragmented into spiral arms.

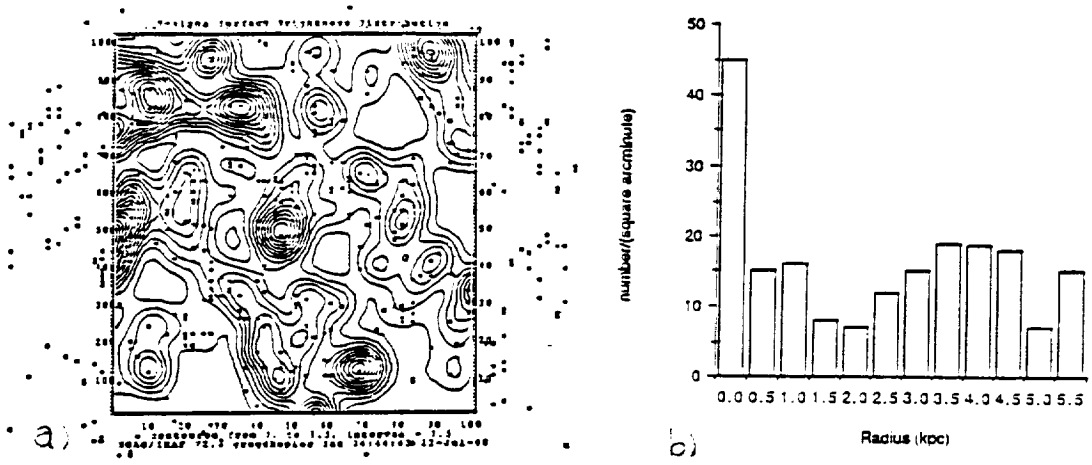

Fig. 3.- a) A linear contour map of the Hα surface brightness distribution. Light from two compact HII regions, one in the nucleus and one to the SW have been excluded. Together, they are less than 10% of the total emission, but would have dominated the extended features of the contour map. b) The radial number distribution of HII regions in the galaxy. Data from Bonnarel et al. (1986).

From the energy distribution for the central 45" of the galaxy (figure 4), it can be inferred that nearly 3/4 of the stellar luminosity from this region is absorbed by dust. The 100 and 160 μm points are from our maps; the optical and near infrared points are from Lebofsky and Rieke (1979); and, the 12, 25 and 60 μm points are obtained from IRAS maps (Rice et al.,1987) by integrating down to the 20% contour and scaling the fluxes to our beamsize of 45". The hot and cold dust components which peak at ~10 and ~100μm can be fit by the sum of a 200 and 32°K modified blackbody, respectively. Integrating under the far-infrared peaks gives $\equiv 3 \times 10^{-12}$ W m^{-2}, which corresponds to a

luminosity of $9.6\times10^{+9}$ $L_{\odot}$. The distribution of starlight transmitted by NGC 6946, which peaks at 1μm, is $\equiv 1.0\times10^{-12}$ Wm^{-2}. Hence, the ratio of transmitted to reradiated energy from the central 45" is ~3. When calculated for the disk, this ratio is ~0.9.

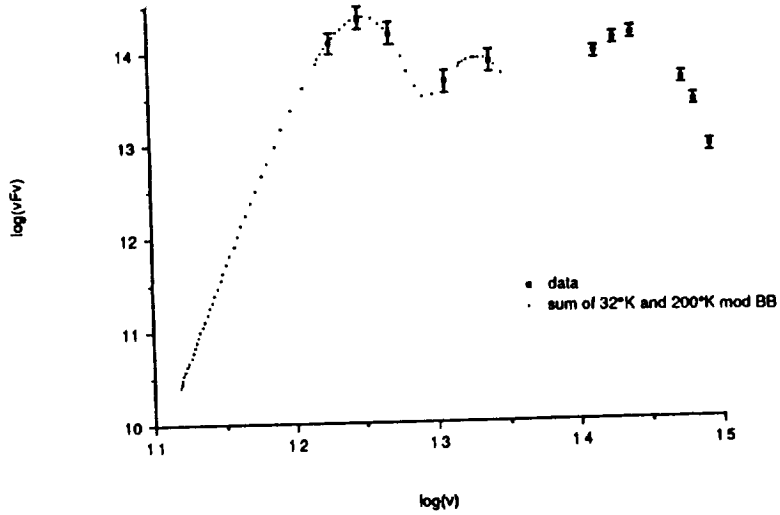

Fig. 4.- Optical/Infrared specrum of the central 45" of NGC 6946. Far-infrared data is from KAO; mid-infrared data is from Rice et al. (1986); and near-infrared and optical is from Rieke and Lebofsky (1979).

The contour map of Hα surface brightness with 45" resolution (figure 3a) has been made from data of Bonnarel et al. (1986). Note the ring of bright HII regions which surrounds the nucleus. The relative Hα radial surface brightness distribution is shown along with the 100/160μm color temperature in figure 5. The 100/160μm color temperature for dust in the nucleus and in the ring is 32°K. The intermediate ring of low Hα surface brightness is 25°K. Figure 3b is a histogram of the number of HII regions versus distance from the nucleus; note fewer are observed at radii where the color temperature is low. We also computed the 100μm optical depth as a function of radial distance from the nucleus by inverting the relation $F_{\upsilon}(r)= \pi B_{\upsilon}[T(r)](1-\exp(-\tau(r)))\Delta\Omega$, where $\Delta\Omega$ is the beam area of our instrument. The radial variation of the 100μm optical depth and the color temperature are plotted in figure 6.

We divided our 100 and 160μm maps by a fully sampled CO(1->0) map with 45" resolution (Tacconi and Young,1987). The ratio of 100 and 160 μm flux to integrated CO(1->0) luminosity is 2/3 higher for the central 2' than for the rest of the galaxy (figure 7). Beyond the central region, the 160μm/CO(1->0) ratio is nearly constant to the edges of the map while the 100μm/CO(1->0) ratio is gradually increasing toward larger radii. The oscillations in these profiles are very likely due to sampling artifacts in the CO map: the sample points were equally spaced on concentric circles.

Finally, we mention that the ratio of 100μm to Hα intensity rises sharply toward the nucleus for the regions we mapped. This could be due either to an intrinsic difference in the 100μm to Hα ratio in the radiating source or to increased attenuation of Hα by dust in the nucleus.

IV. Conclusions

We have mapped the nucleus and inner-arm regions of the Scd type galaxy NGC 6946 at 100 and 160μm with an array of 45" beams. From these observations, combined with other published data, we find the following:

1. The dust reemission of NGC 6946 at 100 and 160 microns shows a peak at the center superposed on an exponential disk with a scale-length of 5.6 kpc.
2. The peak is offset 24" NE of the Dressel and Condon optical position. This displacement is over four times our estimated RMS pointing error.
3. Approximately 20% of the flux at 100 microns comes from the central 3 kpc. The percentage of the total 160 micron flux from this region is somewhat smaller.
4. The 100 and 160 micron light follows closely, but not exactly, the Hα; the inner spiral arms have been resolved at both wavelengths, but the structure is clearer at 100 microns.
5. Our analysis shows that the 100/160 micron color temperature is correlated with regions of prominent Hα emission. If a similar process generates all the dust reemission in the far-infrared and the color temperature is representative of the actual dust temperature, this correlation strongly suggests that the the dust is being heated by photons from young, luminous stars.
6. The nucleus is more optically thick at 100 microns than the edge of the disk. An upward inflection of the optical depth occurs at 3 kpc, where the color temperature is a local minimum.
7. The strength of the 100 micron relative to the Hα light increases toward the nucleus. If the far-infrared flux is reemission of OB stellar radiation, one might expect the two quantities to scale, unless larger concentrations of dust in the nucleus are attenuating the Hα more than in the disk. This is consistent with statement #6. Alternatively, this could be due to an intrinsic difference in the radiating source.
8. The F_{IR}/I_{CO} ratio is fairly constant over the disk but abruptly increases by 2/3 for the central 2' region.

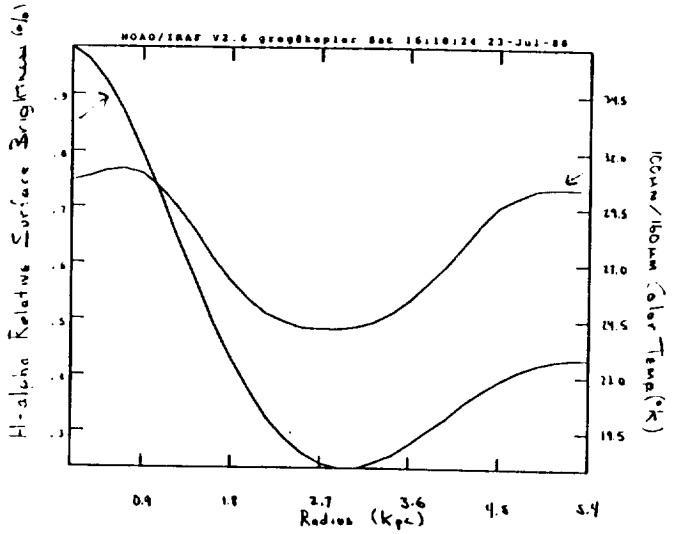

Fig. 5. - The relative Hα radial surface brightness distribution plotted with the 100/160μm color temperature.

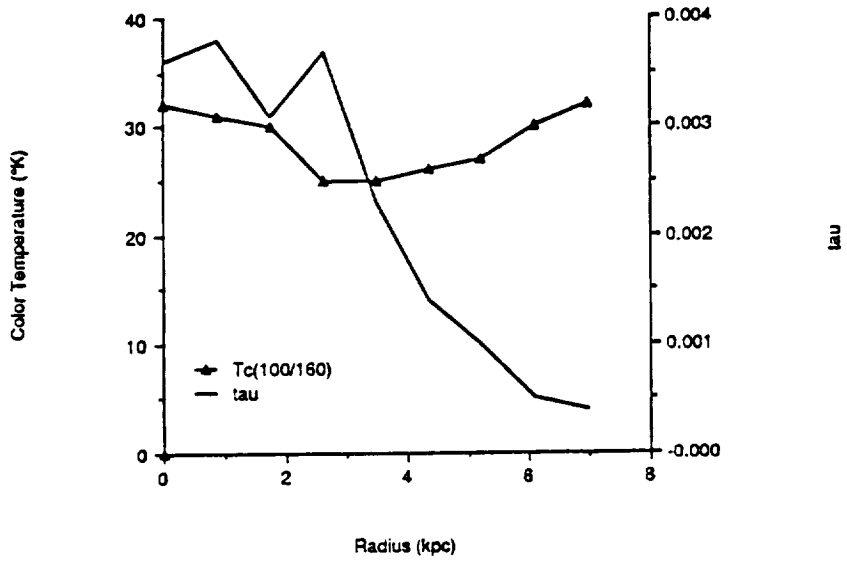

Fig. 6. - The radial variation of the 100μm optical depth and the 100/160μm color temperature.

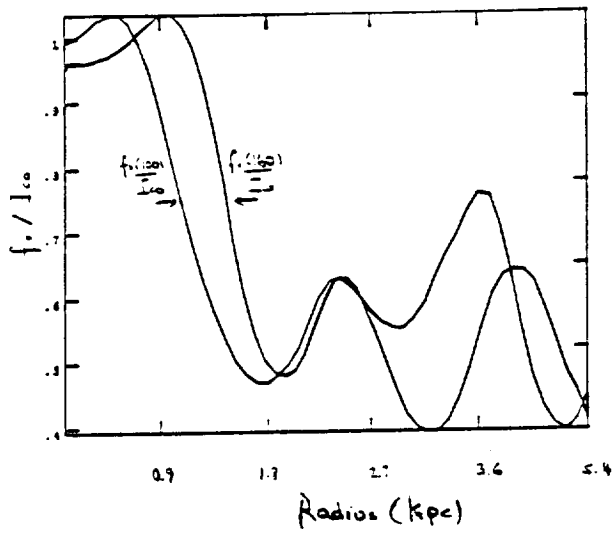

Fig.7. - The ratio of the 100 and 160μm flux to integrated CO(1->0) intensity.

References

Ables, H.D. 1971, Publ. U.S. Naval Obs. Sec. Ser. Vol. XX, Part IV, Washington D.C.

Arp, H.G. 1966. Ap. J. Suppl. Ser.,**14**, 1

Bonnarel,F.,Boulesteix, J., and Marcelin, M. 1986 Astro. Ap., Suppl. Ser.,**66**, 149

Condon, J.J., Condon, M.A., Gisler, G., and Puschell, J.J. 1982, Ap. J., **253**, 102

De Gioia-Eastwood, K., and Grasdalen, G.L. 1984, Ap. J., **278**, 564

Elmegreen, D.M., and Elmegreene, B.G. 1984, Ap. J. Suppl. Ser., 54, 127

Engargiola, G., Harper, D.A., Willner, S.P., and Elvis, M. 1988, Ap. J. ,(submitted)

Fabbiano, G., and Trinchieri, G. 1987, **315**, 46
Rieke, G.H., Lebofsky, M.J., Thompson, R.I., Low, F.J., and Tokunaga, A.T. 1980, Ap. J., **238**, 24
Rogstad, D.A., Shostok, G.S., and Rots, A.H. 1973, Astro. Ap., **22**, 11
Smith, J. 1984, Ap. J., **261**, 463
Smith,J., Harper, D.A., and Loewenstein, R.F. 1984, from proceedings of the Airborne Astronomy Symposium, NASA Conference Publication 2353
Tacconi, L.J., and Young, J.S. 1986 Ap. J., **235**, 392
Tacconi, L.J., and Young, J.S. 1988, Ap. J., (submitted)
Telesco, C.M., and Harper, D.A. 1980, Ap. J., **235**, 392
van der Kruit, P.C., and Allen, R.J. 1977, Ann. Rev. Astr. Ap. ,**16**, 103
van der Kruit, P.C., Allen, R.J. , and Rots, A.H. 1977, Astr. Ap., **55**, 421
Young, J.S., Schloerb, F.P., Kenney, J.D., and Lord, S.D. 1986, **304**, 443
Young, J.S., and Scoville, N.Z., 1982, Ap. J., **258**, 467

GRAINS IN GALACTIC HALOES

N91-14984

A. Ferrara*, B. Barsella*, F. Ferrini*, J.M. Greenberg** and S. Aiello***
* Istituto di Astronomia, Università di Pisa, piazza Torricelli 2, 56100 Pisa, Italy
** Laboratory Astrophysics, University of Leiden, Huygens Laboratorium, Postbus 9504, 2300 RA Leiden, The Netherlands
*** Dipartimento di Fisica, Università di Firenze, via Pancaldo 3/45, 50127 Firenze, Italy

INTRODUCTION

We considered the effect of extensive forces on dust grains subjected to the light and matter distribution of a spiral galaxy (Greenberg et al. (1987), Ferrini et al. (1987), Barsella et al. (1988), hereafter Paper I). We have shown that the combined force on a small particle located above the plane of a galactic disk may be either attractive or repulsive depending on a variety of parameters. We found, for example, that graphite grains from 20 nm to 250 nm radius are expelled from a typical galaxy, while silicates and other forms of dielectrics, after initial expulsion, may settle in potential minimum within the halo. We have discussed only the statical behaviour of the forces for 17 galaxies whose luminosity and matter distribution in the disk, bulge and halo components are reasonably well known.

We present here the preliminary results of the study of the motion of a dust grain for NGC 3198, the same galaxy we have discussed in Paper I.

THE MODEL

The forces present in the equation of motion are:

(a) - **Gravitation**

The force on a dust grain of mass m_g may be written:

$$\vec{F}_G(\vec{r}) = m_g \vec{G}(\vec{r})$$

where $\vec{G}(\vec{r})$ is the gravitational field intensity at the point $\vec{r}$.

(b) - **Radiation pressure**

The force on a grain of radius a and radiation pressure coefficient $Q_{pr}(a,\nu)$ is:

$$\vec{F}_R(\vec{r}) = \pi a^2 \int d\vec{\rho} \int d\nu Q_{pr}(a,\nu)\vec{\Psi}(\vec{r},\vec{\rho},\nu)$$

where $\vec{\Psi}$ is the radiation field due to a small portion of the galaxy at $\vec{\rho}$ on the grain at position $\vec{r}$ at frequency ν . We assume that the luminosity function of the galaxy may be splitted into two parts: a global luminosity function, depending on the galactic position, and a spectral function, which depends only on the Hubble type of the galaxy. Hence the radiation field function may be written: $\vec{\Psi}(\vec{r},\vec{\rho},\nu) = \vec{\Xi}(\vec{r},\vec{\rho})\Omega(\nu)$.

To perform the integration over ν, we adopt the spectral energy distribution for Sc type galaxies as given by Pence (1976) and Yoshii and Takahara (1988).

(c) – **Gas drag**

The drag force exerced by the gas is:

$$F_{gas} = 2\pi a^2 nkT \left\{ \left(s^2 + 1 - \frac{1}{4s^2} \right) \mathrm{erf}(s) + \left(s + \frac{1}{2s} \right) \frac{e^{-s^2}}{\sqrt{\pi}} \right\}$$

$$s = \left(\frac{m_H v^2}{2kT} \right)^{\frac{1}{2}}$$

where v is the grain velocity, T is the temperature of the gas and n is its number density (see Draine and Salpeter (1979)).

We assume that the gas in the region outside of the galactic disk is composed of atomic hydrogen with an exponentially decreasing number density n and a pressure $p/k = nT$ also described by an exponential function with a scale length comparable to the thickness of the halo gas. This stratified structure of the gas in the halo may be changed in the equations of motion by specifying the density and pressure scale lengths, the density and the temperature at the edge of the disk, and the thickness of the gas halo. As a guide, we have adopted the scheme proposed by Savage (1986):

$$n \approx 0.5\,\mathrm{cm}^{-3} \text{ at } 100 \text{ pc}$$

$$T \approx 5000\,\mathrm{K} \text{ at } 100 \text{ pc}$$

and we have assumed a thickness of the gas halo equal to one tenth of the galactic halo radius.

The system of ordinary differential equations that describes the motion of a dust grain has been numerically solved with Livermore Solver for Ordinary Differential Equations (LSODE).

RESULTS

We have solved the equation of motion for single grains in some selected cases. The galaxy we have chosen was the same of Paper I (NGC 3198), a "typical" galaxy. Our preceding static analysis of the forces had lead us to select, for this preliminary study, only astronomical silicate grains of intermediate radii (in particular $a = 100$, 200 and 300 nm).

The initial conditions we have chosen are: starting point 100 pc high on the galactic plane of simmetry; galactocentric radii: $0, 2, 4, \ldots, 10$ kpc, initial velocity equal to the rotational velocity of the galaxy at that position as measured from 21 cm observations of HI. We have integrated the equations of motion with a display step of 2 Myr for a total integration time of 1 Gyr.

The results are presented in Figures 1,2 3 and 4. The most interesting results are the following:

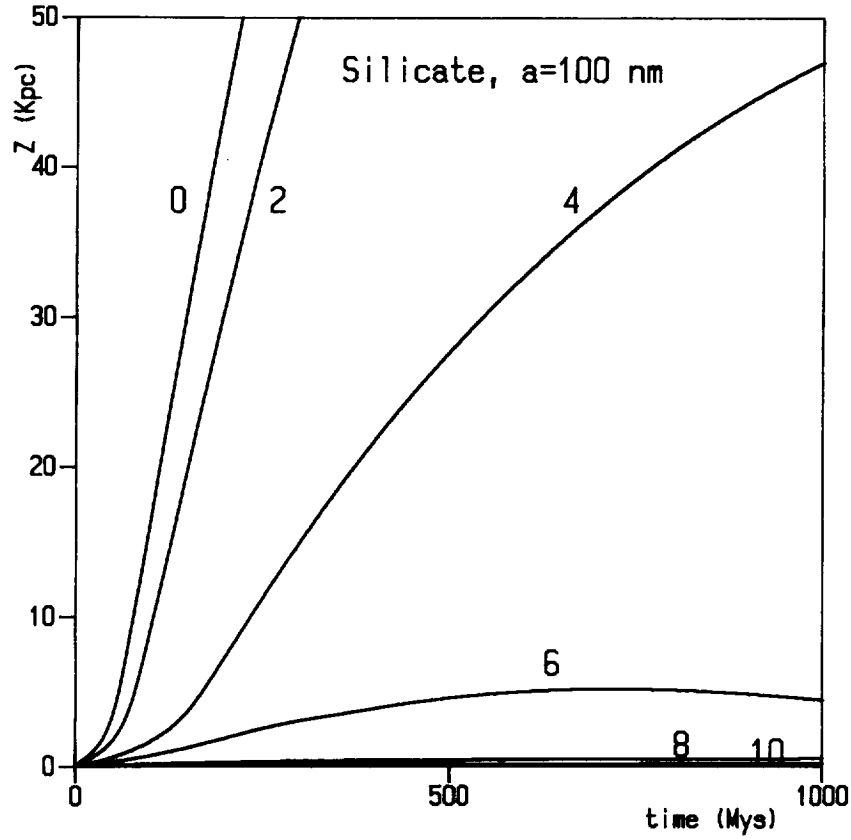

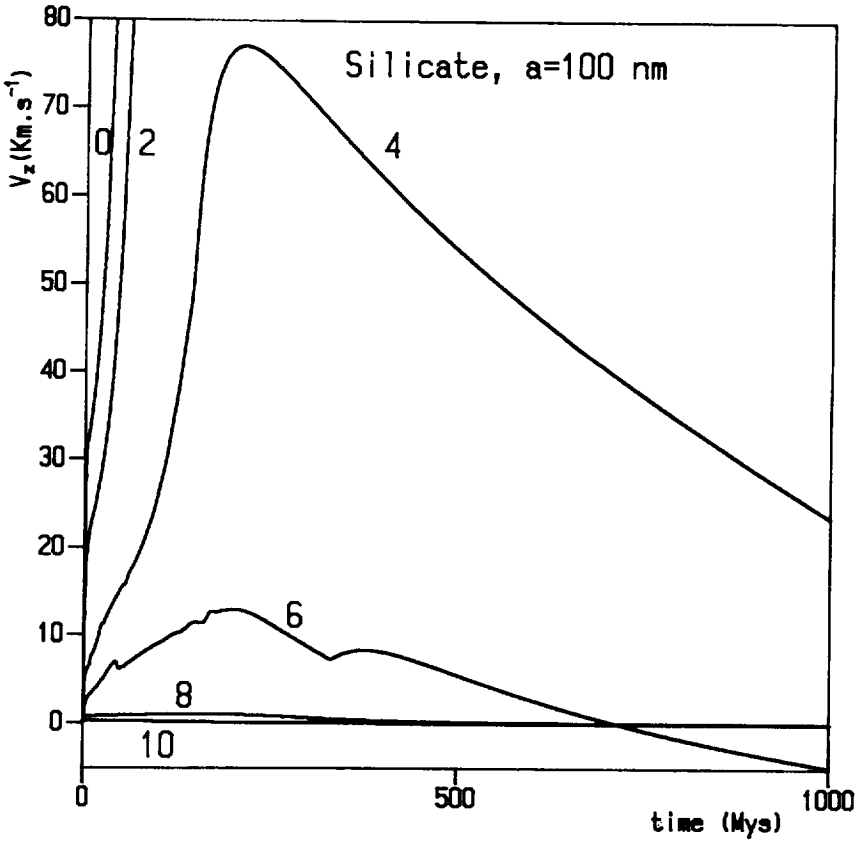

Figs. 1 and 2 – z position and z component ot the velocity, as a function of time, for a grain of astronomical silicate of radius $a = 100\,\mathrm{nm}$ (The numbers on the lines represent the starting distance in kpc).

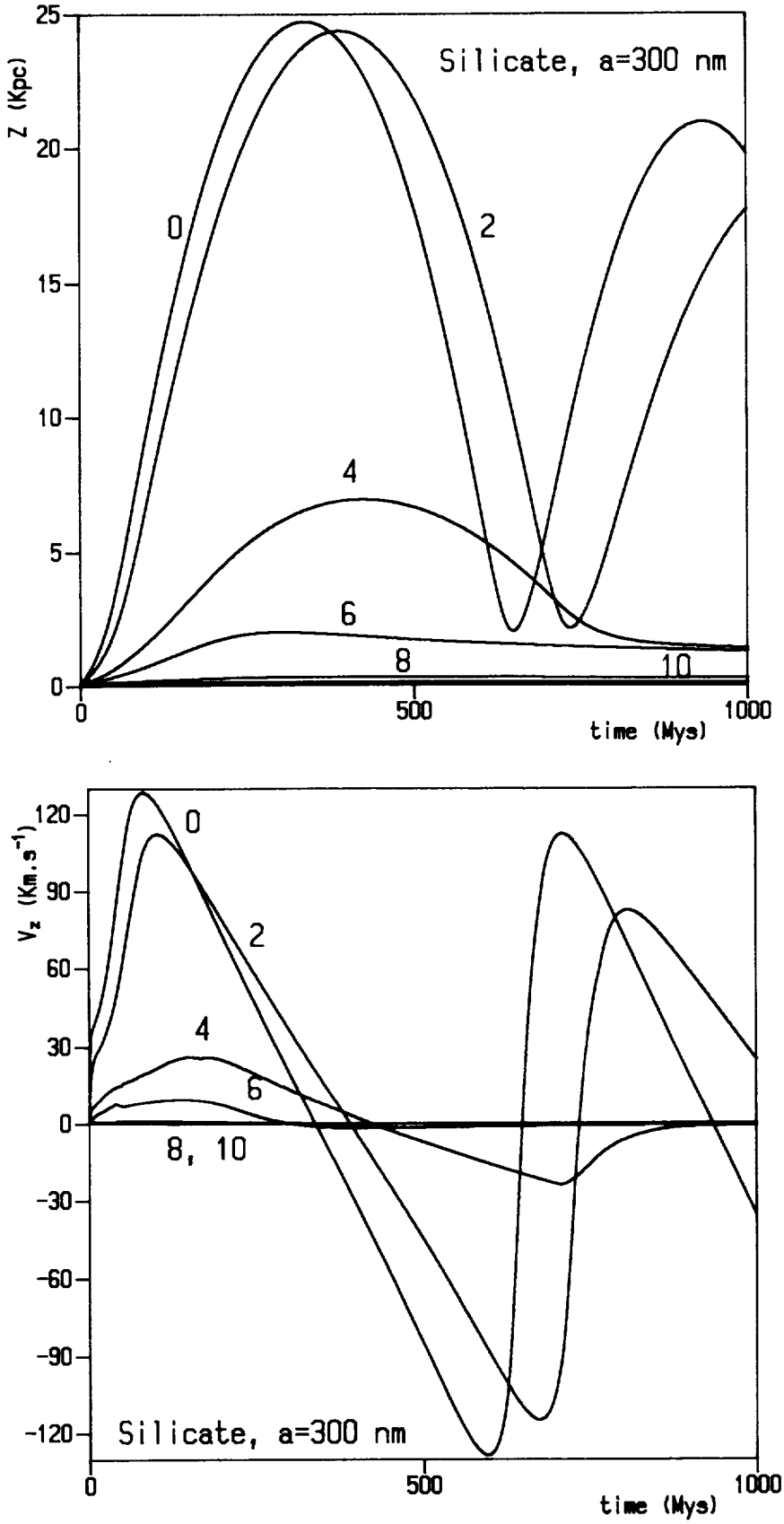

Figs. 3 and 4 – z position and z component ot the velocity, as a function of time, for a grain of astronomical silicate of radius $a = 300\,\mathrm{nm}$ (The numbers on the lines represent the starting distance in kpc).

- the expulsion is effective, in this case, only for grains of radii $a = 100$ and 200 nm. In addition, the region of the galactic plane where the expulsion may take place is limited to about half of the luminosity radius, which for NGC 3198 is about 10 kpc.
- the time scale for crossing the hot gas region is dependent on the galactocentric distance and on the grain radius, and is approximately $8 \div 15$ Myr for $a = 100$ nm and $20 \div 30$ Mr for $a = 200$ nm. This means that the grain may suffer considerable erosion in the hot medium; this effect must therefore be introduced in the model. In any case, these time intervals are not larger than the life–time for destruction of the grain by sputtering (Draine and Salpeter (1979)), and therefore a certain amount of dust may be expelled. A careful analysis of the size evolution of the grain may give an idea of the metallicity increase of the diffuse halo gas due to this mechanism.

ACKNOWLEDGEMENTS

As we have said before, the solution of the system of differential equations of motion has been done using the LSODE package . Thanks are due to A. Hindemarsh who has written it and to J. Dongarra who has put it on the networks.

REFERENCES

Barsella, B., Ferrini, F., Greenberg, J.M., Aiello, S.: 1988, submitted to Astron. Astrophys.

Draine, B.T., Salpeter, E.E: 1979, Astrophys. J. **231**, 77

Ferrini, F., Barsella, B., Greenberg, J. M., communication presented to "Dust in the Universe", Manchester 1987, to be published

Greenberg, J.M., Ferrini, F., Barsella, B., Aiello, S.: 1987, Nature **327**, 214

Pence, W.: 1976, Astrophys. J. **203**, 39

Savage, B.D.: 1986, in New Insights in Astrophysics, Proc Joint NASA/ESA/SERC Conference, London, ESA SP–263, 259

Yoshii, Y., Takahara, F.: 1988, Astrophys. J. **326**, 1

DOES THE FAR-INFRARED/RADIO CORRELATION IN SPIRAL GALAXIES EXTEND TO THE SPATIAL DOMAIN?

N.A. Howarth and A.J. Fitt.
M.R.A.O., Cavendish Laboratory, Cambridge, England.

A comparison is made between the spatial distribution of the thermal far-infrared and non-thermal radio emission of nearby spiral galaxies. This is done in an attempt to improve our understanding of the well known correlation between the integrated IRAS far-infrared and radio emission of spiral galaxies, *e.g.* de Jong *et al.*, 1985, Helou *et al.*, 1986.

A physical explanation for this correlation is not straight forward due to the ambiguous nature of the origin of the far-infrared and radio, and the dependence of the non-thermal radio on each galaxies' magnetic field. It is now widely believed that the infrared emission detected in the longer wavelength IRAS wavebands ($> 50\mu$m) arises from at least two distinct sources, *e.g.* Cox *et al.*, 1986, Persson and Helou, 1987:

i) a warm (T~40K) component associated with dense dust clouds heated by embedded O and B type stars.

ii) a cooler (T~20K) component associated with diffuse dust distributed throughout the ISM heated by the interstellar radiation field.

A link between the warm component and the radio via electrons originating in Type II supernovae (the ultimate fate of many of the O and B type stars responsible for the warm component) has been suggested by numerous authors. The supporting evidence is scarce and inconclusive. The dominant source of the radio is not yet known, discrete supernova remnants contributing only a few per cent of the total. Indeed diffusive shock acceleration theory diverts the question away from the class of objects responsible for the radio radiating cosmic-ray electrons. Instead the origin of a much less energetic reservoir of electrons and the means by which some of these electrons are accelerated to relativistic energies becomes the central issue, *e.g.* Bloemen, 1987. When account is taken of our sketchy knowledge regarding extragalactic magnetic fields, (but see Hummel, 1986) it can be seen why the far-infrared/radio correlation is so puzzling.

We have attempted to provide some insight into the problem by looking at the spatial distribution of the different components in some nearby spiral galaxies, starting with the face-on spiral M51. The source of the far-infrared data is the IRAS CPC instrument. This has a resolution of ~1.5 arcmin at 50 and 100μm, compared to that of the Survey detectors, 4.3 by 6.9 arcmin at 100μm. Warm and cold far-infrared fluxes integrated over all wavelengths and the radio intensity at two frequencies are plotted against radius in Figure 1 below. All plots are to a common resolution of 100 arcsec, the radio data originating from the Cambridge Low Frequency Synthesis Telescope (151 MHz) and the VLA (1490 MHz, from Condon, 1987). The warm and cold regions are assumed to be represented

Figure 1: The Radial Distribution of the Far-Infrared and Radio Emission in the Face-on Spiral Galaxy M51.

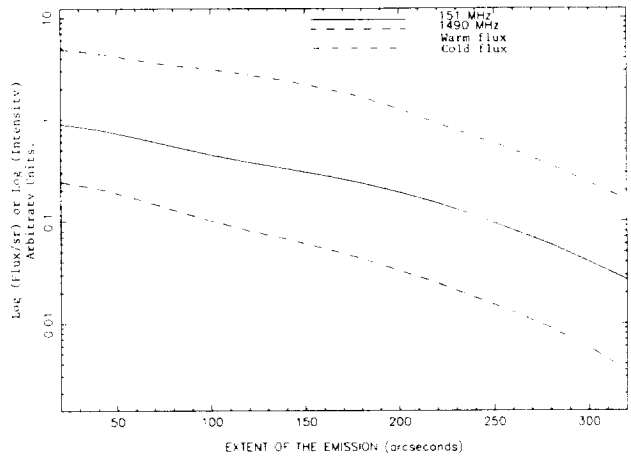

by a single galactic wide temperatures of 50 K and 20 K respectively. A dust emissivity of 1 has been assumed. The form of the plots is little effected by varying these assumptions. As can be seen the radio and cold component curves appear to follow each other most closely, in contradiction to the simple OB star/type II supernovae hypothesis mentioned above. The significance of this result awaits analysis of more galaxies and an interpretation of the dominant influences on the distribution of each of the components.

References

Bloemen, H., 1987, 'Interstellar Processes', 143, D. Reidel Pub. Company.

Condon, J.J., 1987, Astrophys. J. Supp., 65, 485.

Cox, P., Krügel, E. and Mezger, P.G., 1986, Astron. and Astrophys., 155, 380.

Helou, G., Soifer, B.T. and Rowan-Robinson, M., 1985, Astrophys. J., 298, L7.

Hummel, E., 1986, Astron. and Astrophys., 160, L4.

de Jong, T., Klein, U., Wielebinski, R. and Wunderlich, E., 1985, Astron. and Astrophys., 147, L6.

Persson, C.J.L. and Helou, G., 1987, Astrophys. J., 314, 513.

MULTICOLOR OPTICAL POLARIMETRY OF REDDENED STARS IN THE SMALL MAGELLANIC CLOUD

A.M. Magalhães,* G.V. Coyne,** V. Piirola,*** and C.V. Rodrigues*
*Instituto Astronômico e Geofísico, Universidade de São Paulo, Caixa Postal 30.627, São Paulo 01051, Brazil
**Vatican Observatory, V-00120 Cittá del Vaticano
***Observatory and Astrophysics Laboratory, University of Helsinki, Tahtitorninmaki, SF-00130 Helsinki 13, Finland

SUMMARY

First results of an on-going program to determine the wavelength dependence of the interstellar optical polarization of reddened stars in the Small Magellanic Cloud are presented.

I. INTRODUCTION

IUE observations of reddened stars in the Small Magellanic Cloud (SMC) (Bouchet et al. 1985) generally show marked differences in the extinction law as compared to both the Galaxy and the Large Magellanic Cloud. Our aim is to determine the wavelength dependence of the optical linear polarization in the direction of several such stars in the SMC in order to further constrain the dust composition and size distribution in that galaxy.

II. INSTRUMENTATION

The observations reported here were mostly gathered with the VATPOL polarimeter (Magalhães et al. 1984) of the Vatican Observatory at the 2.15m argentinan national telescope in San Juan and with the MINIPOL polarimeter (Frecker and Serkowski 1976) at CTIO. A few observations were also obtained with PISCO polarimeter (Stahl et al. 1986) at ESO/La Silla. Later in this season, observations are scheduled with both VATPOL and the University of São Paulo IAGPOL polarimeter (Magalhães and Velloso 1988) at the 1.60m brazilian national telescope.

III. FOREGROUND GALACTIC POLARIZATION

The observed optical linear polarization in the SMC in our sample is typically fairly small (section IV below), which makes the correction due to foreground galactic dust fairly critical, despite the low ($0^m.02$) foreground reddening (McNamara and Feltz 1980). Schmidt (1976) presents a rather detailed study of the foreground polarization in the SMC

direction, dividing it into five fields and suggesting the necessary foreground corrections in each section.

We also considered separately, from Schmidt's sample, stars in each field at distances larger than 400 pc; most of the foreground reddening occurs within this distance (McNamara and Feltz 1980). We also considered averages of SMC stars from the sample of Magalhães et al. (1987) and from the present sample with visual polarization smaller than 0.4%.

These estimates are compared in Table 1 below. We then corrected the SMC observation in each filter employing Serkowski's (Coyne et al. 1974) relation for the galactic interstellar polarization,

$$P(\lambda) = P_{max} * \exp\{-K \ln^2(\lambda_{max}/\lambda)\},$$

chosing to use for P_{max} the P value from galactic stars with r > 400pc and the relation between K and λ_{max} as given by Wilking et al. (1982). We used 0.55um for λ_{max}, consistent with own multicolor observations of foreground stars.

IV. RESULTS

With one exception, our sample contains stars which have been observed for ultraviolet extinction by Bouchet et al (1985) and we refer to them according to their number in the catalogue of Azzopardi and Vigneau (1982). The exception is AV 211 which (as far as we know) has not had its UV extinction determined. We employ colour excesses from Bouchet et al. For AV 211, we have estimated the colour excess using photometric and spectroscopic data in Azzopardi and Vigneau and the calibration by Brunet (1975).

Fig. 1 presents the correlation we obtain between P_{max} and E_{B-V}. P_{max} was obtained by fitting the data with Serkowski's relation, using the galactic relation between K and λ_{max}. As can be seen, the intrinsic polarization for most of the stars is fairly small, albeit consistent with their colour excesses. The galactic envelope is also indicated for comparison.

For the three more polarized objects, AV 211, AV 398 and AV 456, we present details of the fits in Figs. 2 through 4 and in Table 2. The derived values of P_{max} and λ_{max} stay the same within the errors even if a allowing the fit to include the parameter K as a free parameter as well as rather insensitive to the foreground polarization choice. We include in Table 2 the ratio between R ($=A_V/E_{B-V}$) and λ_{max}, assuming R=2.7 ± 0.2 for the SMC as given by Bouchet et al. (1985). These values should be compared to the galactic one of about 6.7 (Clayton and Mathis 1988) and are meant to be taken as indicative only, since many more stars will have to be studied. More observations should allow us to check more closely the relation between K and λ_{max} for the SMC.

AV 456 has an extinction law (Lequeux et al. 1982) and gas-to-dust ratio (Bouchet et al. 1985) close to galactic values and its λ_{max} (Table 2) seems to reflect that the grains responsible for the optical interstellar polarization in that direction are indeed similar to those in the Galaxy. AV 398, the most heavily reddened object, is also the most polarized one and presents UV extinction law typical of the SMC (Bouchet et al. 1985), with a steep rise into the UV and absence of a

strong 2200 Å peak. Its λ_{max}, although somewhat smaller, is still quite comparable to galactic values. AV 211 presents the smaller λ_{max} of the three objects.

Even values of λ_{max} close to "normal" should have an important bearing on grain modelling for the SMC. For instance, if the details mentioned above in the SMC extinction law are interpreted, in the context of the Mathis et al. (1977) model, as the result of a smaller role of graphite grains in the visible, the size distribution of silicate grains would have to be shifted in the direction of larger grains (Bouchet et al. 1985) in order to account properly for the visual extinction. If, as expected, variations in λ_{max} reflect distinct size distributions of dust particles (as for the Galaxy - Clayton and Mathis 1988), the preliminary results of Table 2 point either against that conclusion or to a size distribution of aligned grains (probably still silicates) in the SMC distinct from the one producing the extinction. Clearly, the forthcoming observations of this program will be of importance regarding the grain population in the SMC.

Finally, Table 2 shows a comparison between the optical (this work) and radio polarization position angles (from Loiseau et al. 1987). Since the latter is of non-thermal origin and would indicate a magnetic field direction orthogonal to that of a similarly oriented optical polarization vector, it is quite probable that the radio and optical polarixations originate from distinct regions in and around the SMC (Loiseau et al. 1987; Magalhães et al 1987).

ACKNOWLEDGEMENTS

A.M.M. and C.V.R. would like to acknowledge support from Fundação de Amparo à pesquisa do Estado de São Paulo (FAPESP) for this project. A.M.M. also acknowledges support for his travel from FAPESP through grant nº 88/1415-4 and the IAU through the Local Organizing Committee.

REFERENCES

Azzopardi, M. and Vigneau, J.: 1982, Astron. Astrophys. Suppl. Ser. 50, 291.

Bouchet, P., Lequeux, J., Maurice, E., Prevot, L.,and Prevot-Burnichon, M.L.: 1985, Astron. Astrophys. 149, 330.

Brunet, J.P.: 1975, Astron. Astrophys. 43, 345.

Clayton, G.C. and Mathis, J.S.: 1988, Ap. J. 327, 911.

Coyne, G.V., Gehrels, T. and Serkowski, K.: 1974, A.J. 79, 581.

Frecker, J. and Serkowski, K.: 1976, Appl. Opt. 15, 605.

Lequeux, J., Maurice, E., Prevot, L. and Prevot-Burnichon, M.L.: 1982, Astron. Astrophys. 113, L15.

Loiseau, N., Klein, U., Greybe, A., Wielebinski, R. and Haynes, R.F.: 1987, Astron. Astrophys. 178, 62.

Magalhães, A. M., Benedetti, E. and Roland, E. H.: 1984, Publ. Astron. Soc. Pac. 96, 383.

Magalhães, A. M., Loiseau, N. and Piirola, V.: 1987, Workshop in "Magnetic Fields and Extragalatic Objets", Corsega, p. 185.

Magalhães, A.M. and Velloso, W.F.: 1988, in "Instrumentation for Ground-Based Optical Astronomy: Present and Future" (ed. L.B. Robinson), Springer-Verlag (N. York), p. 638.

Mathis, J.S., Rumpl, W. and Nordsiek, K.H.: 1977, Ap. J. 217, 425.

McNamara, D.H. and Feltz Jr., K.A.: 1980, Publ. Astron. Soc. Pac. 92, 587.

Schmidt, Th.: 1976, Astron. Astrophys. Suppl. 24, 357.

Stahl, O., Buzzoni, B., Kraus, G., Schwarz, H., Metz, K. and Roth, M.: 1986, Messenger 46, 23.

Wilking, B.A., Lebofsky, M.J. and Rieke, G.H.: 1982, A.J. 87, 695.

TABLE 1. FOREGROUND POLARIZATION IN THE DIRECTION OF THE SMC

Field	Schmidt (1976) P ± σ (%)	Schmidt (1976) θ (°)	r > 400 pc P ± σ (%)	r > 400 pc θ (°)	SMC stars* P ± σ (%)	SMC stars* θ (°)
I	.37 ± .15	111	.36 ± .05	110	.22 ± .01	129
II	.27 ± .15	123	.27 ± .03	125	.32 ± .01	118
III	.06 ± .09	139	.18 ± .03	132	.09 ± .01	139
IV	.14 ± .12	125	.25 ± .02	127	.09 ± .03	159
V	.16 ± .12	93	.35 ± .04	102	.16 ± .04	117

* $w/P_V < 0.4\%$

TABLE 2. FITTED PARAMETERS FOR THE MORE HIGHLY POLARIZED OBJECTS

Star	P_{max} (%)	λ_{max} (A)	R/λ_{max}	θ opt (°)	θrad (°)
AV 211	1.01 ± .05	.41 ± .05	6.6 ± .9	128	135
AV 398	1.70 ± .05	.49 ± .04	5.5 ± .6	135	135
AV 456	1.19 ± .05	.55 ± .05	4.9 ± .6	166	140

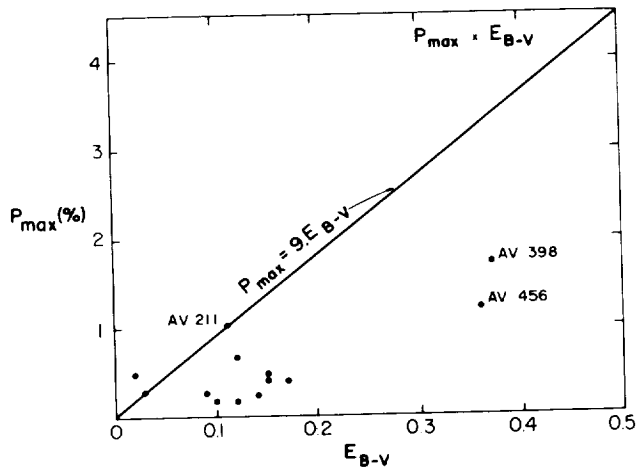

Fig. 1 - Maximum polarization as a function of colour excess for the observed SMC stars.

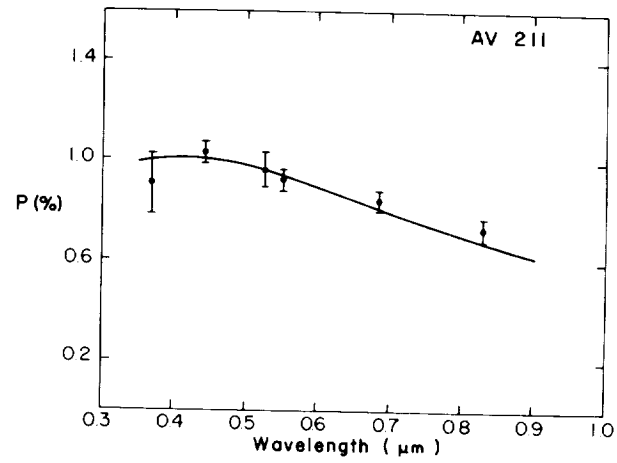

Fig. 2 - Wavelength dependence of the linear polarization for the SMC star AV 211.

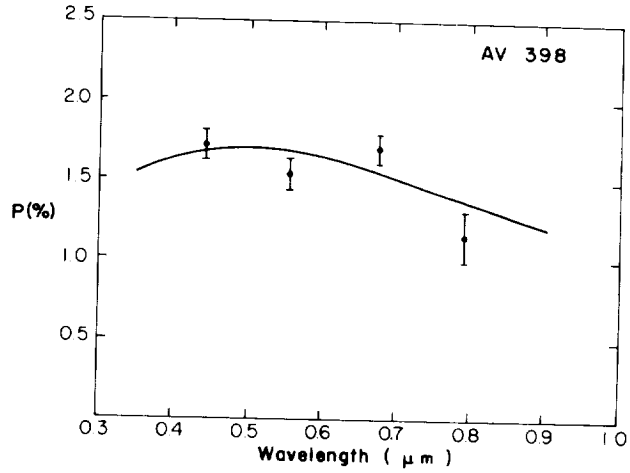

Fig. 3 - Same as Fig.2 for AV 398.

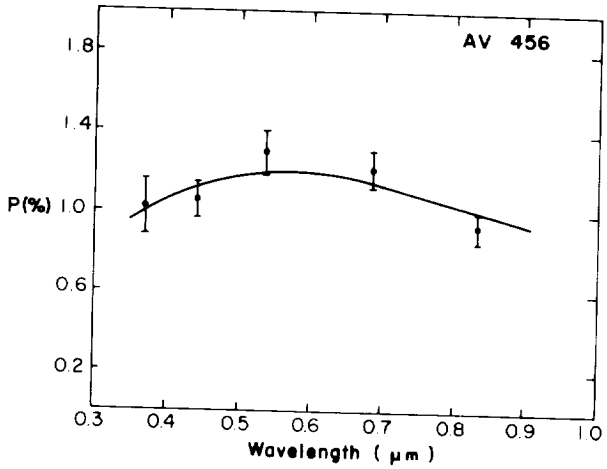

Fig. 4 - Same as Fig.2 for AV 456.

ON THE ORIGIN OF EXTINCTION IN THE COMA CLUSTER OF GALAXIES

Y. Rephaeli*, Eli Dwek**, and John C. Mather**
*Center for Astrophysics and Space Sciences,
University of California, La Jolla, CA 92093, USA,
and School of Physics and Astronomy, Tel Aviv University,
Tel Aviv, 69978, Israel
**Laboratory for Astronomy and Solar Physics, Infrared Astrophysics Branch,
NASA-Goddard Space Flight Center
Greenbelt, MD, 20771, USA

SUMMARY: Visual extinction of distant clusters seen through the Coma cluster seem to suggest that dust may be present in the hot X-ray emitting intracluster gas. However, IRAS failed to detect any infrared emission from the cluster at the level expected from the extinction measurements. We have carried out a detailed analysis of the properties of intracluster dust in the context of a model which includes continuous injection of dust by the cluster galaxies, grain destruction by sputtering, and transient grain heating by the hot plasma. Our computed infrared fluxes are in agreement with the upper limit obtained from the IRAS. The calculations, and the constraint implied by the IRAS observations, suggest that the intracluster dust must be significantly depleted compared to interstellar abundances. We discuss possible explanations for the discrepancy between the observed visual extinction and the IRAS upper limit.

The presence of metal-enriched intracluster (IC) gas in clusters of galaxies has been extensively established by X-ray spectral and line measurements. This IC gas is likely to be of galactic origin, suggesting that dust grains, which may have been ejected from galaxies, may also be present in the IC gas. Since any (hypothetical) primordial intergalactic dust accreted into the cluster would not have survived sputtering by the ambient hot gas, the presence of dust in the IC gas can be considered as further evidence for its galactic origin. The detection of dust in the IC gas may therefore provide important clues for galaxy and cluster evolution theories. If the dust-to-gas mass ratio in the cluster is not much smaller than its interstellar value, clusters may constitute the most extended infrared (IR) sources in the Universe.

The possible existence of dust in the IC space had been deduced from extinction measurements. Zwicky (1962) was first to estimate the extinction of light from distant clusters by nearby ones. For the Coma cluster he found $A_V \sim 0.4$m. Using the same method,

Karachentsev and Lipovetskii (1969) found a value of $A_V \sim 0.3$m for the Coma cluster, and averaging over 15 clusters they estimated a mean cluster extinction of $A_V \sim 0.2\text{m}\pm$ .05m. An upper bound on A_V comparable to these values has been deduced by Hu, Cowie, and Wang (1985; hereafter HCW) from UV-to-optical line ratios. If all the extinction is attributed to IC dust, then the IC dust-to-gas mass ratio in the central $\sim 10'$ of the cluster should be about 0.1xZ, where Z=0.0075 is its galactic value.

The presence of IC dust can also be inferred from its IR emission. An early theoretical estimate of IC dust emission (Yahil and Ostriker 1973) was quantitatively improved by Silk and Burke (1974). Based on the study of the interaction of dust particles with a hot gas (Burke and Silk 1974), they found that a typical dust temperature in the cluster is about 30 K. Voshchinnikov and Khersonskij (1984; hereafter VK) used more recent studies on the interaction of dust particles with hot plasmas (Draine and Salpeter 1979), and dust optical properties (Draine and Lee 1984), to present more detailed calculations of the IR emission from dust grains in clusters of galaxies. In their analysis, VK assumed that the observed extinction can be attributed to the presence of dust in the hot gas. By normalizing the dust abundance to the observed extinction they in effect adopted a dust-to-gas mass ratio equal to $\sim$ 0.1xZ. Assuming a constant gas temperature throughout the cluster they calculated a dust temperature of $\sim$ 40 K in the center of the Coma cluster. The dust spectrum peaks at about 100 μm has a flux density of $\sim 3\text{x}10^3$ MJy sr^{-1} at that wavelength in the center of the cluster. HCW also considered IR emission from IC dust, and found typical dust temperatures of $\sim$ 20 K. Based on the measured extinction and X-ray determined gas mass in the cluster core, HCW derived a 100 μm flux density of $\sim 3\text{x}10^4$ Jy sr^{-1}. We obtain similar values, in spite of HCW's incorrect expressions for the dust heating rate and luminosity.

We have carried out a more detailed model for the infrared emission from the Coma cluster (Dwek, Rephaeli and Mather 1987). Here we briefly summarize the results of our work, concentrating only on the most basic considerations (see our paper for a more extensive and quantitative discussion). In our model, the abundance of IC dust is determined by the combined effects of continuous mass loss from galaxies and destruction by the hot gas. Our approach improves upon previous studies in two respects. First, in all earlier calculations the dust temperature was assumed to attain an equilibrium value, obtained by equating the collisional heating rate of the dust to its cooling rate by IR emission. This assumption breaks down below a certain grain size that depends on the temperature and density of the ambient plasma (Dwek 1986). Below this size a dust particle is stochastically heated by the ambient plasma and its temperature will fluctuate. In the central region of the Coma cluster this effect is important for all grains with sizes below ~ 0.15 μm. Second, an additional simplifying assumption made in the earlier calculations is that the IC grain size distribution is equal to that in the interstellar medium. In our model we obtain a more realistic characterization off IC dust by assuming that its injection rate into the IC medium is proportional to the spatial density distribution of galaxies in the cluster. The grain size distribution has been obtained assuming a steady state between destruction and injection. In all our calculations, the gas temperature and density profile are based on the most recent best-fit analysis of X-ray observations of the Coma cluster (Henriksen and Mushotzky 1986).

The results of our calculations show that the average dust-to-gas mass ratio in the

central 3 Mpc region of the Coma cluster is significantly smaller, by about two orders of magnitude, than that in the average interstellar medium. As a result, only about 10% of the observed extinction through the cluster can be attributed to dust in the IC gas. We have compared the 100 μm brightness predicted by our model with IRAS observations, which set a limit of 7 MJy sr^{-1} on the emission from the cluster at this wavelength. This value is a strict upper limit on the diffuse emission from the cluster, since we have made no attempt to correct the observations for any contribution from foreground emission, or emission from the cluster galaxies. Even so, this limit is about 400 times lower than the brightness predicted by VK, but consistent with values derived also by HCW. The discrepancy between the VK model and the IRAS observations therefore suggests that IC dust is significantly underabundant compared with its abundance in the interstellar medium. Thus, the observed visual extinction through the cluster cannot be attributed to dust within the central 3 Mpc region.

There are several possible ways to explain the discrepancy between the observed extinction measurements and lack of corresponding IR emission from the cluster. First, consider the possibility that the extinction is due to dust in the cluster galaxies. (Note that only a small fraction of the dust and gas can be present in pressure-confined clouds outside galaxies - Rephaeli and Wandel 1985.) If so, the average mass of gas, containing a normal dust-to-gas mass ratio, required to be present within the central 3 Mpc region is about $9x10^{13}$ $M_\odot$. The number of galaxies within this region is about 1200 (Rood et al. 1972), requiring the average mass of gas and dust in a galaxy to be $\sim 7x10^{10}$ and $\sim 5x10^{8}$ $M_\odot$, respectively. This gas mass is significantly larger than the typical value of $\sim 5x10^{9}$ $M_\odot$, deduced by Canizares, Fabbiano, and Trinchieri (1987) for a sample of early-type galaxies. Spiral galaxies may contain more gas and dust, but they comprise only 20% of all galaxies in Coma, and are found mostly outside the central region of the cluster. If the observed emission is attributed to dust in spirals, the required mass of dust in each galaxy would be $\sim 3x10^{9}$ $M_\odot$, implying a gas mass of about $4x10^{11}$ $M_\odot$. This is much higher than the average value of $\sim 10^{10}$ $M_\odot$ of gas in spiral (Bothun 1984, Verter 1987). A second possibility is that the observed extinction could be due to dust at large distances, R>3 Mpc from the cluster center. Assuming that dust is undepleted at such distances, and that the extrapolated gas density profile remains unchanged, this dust can at most account for about one third of the observed extinction. We emphasize, however, that this value should be regarded as a strict upper limit since the assumptions made in its derivation are quite unrealistic. We expect the dust to be depleted somewhat during its transit to the IC space. Moreover, our assumed gas density profile (which has been deduced from the X-ray measurements) in the central cluster region is too shallow, and must steepen in the outer cluster region in order to avoid mass divergence. Hu (1987) suggests that dust responsible for the extinction may have been only recently injected into the IC space. But this dust must have been injected at large distances from the cluster center, otherwise it would give rise to observable IRAS emission. Gas poor spirals should therefore preferentially lie on orbits that take them into the outer regions of the cluster, contrary to the conclusions reached by Dressler (1986). In addition, excessive amount of gas has to be injected by the cluster spirals.

We conclude that the observed visual extinction cannot be explained by any distribution of dust in the central region of the Coma cluster and cannot be attributed to dust in galaxies. We also have to bear in mind the possibility that the visual extincion may have

been significantly overestimated. The visual extinction is deduced from a decrease in the number of clusters seen through Coma. The number of observed clusters is 11, whereas 20 are expected on the basis of statistical arguments. Because of the small number of clusters in the sample, the resulting value for the extinction is only a 2 sigma effect. On the other hand, if confirmed, the visual exctinction will imply the presence of dust and by gas at large distances from the cluster center. We hope that future observations will resolve the current discrepancy, or ambiguity, between the observed extinction and the IRAS observations.

REFERENCES

Bothun, G. D.: 1984, Ap. J., 277, 532.
Burke, T.R., and Silk, J.: 1974, Ap. J., 190, 1.
Canizares, C.R., Fabbiano, G., and Trinchieri, G.: 1987, Ap. J., 312, 503.
Draine, B.T., and Salpeter, E.E.: 1979, Ap. J., 231, 77.
Draine, B.T., and Lee, H. M.: 1984, Ap. J., 285, 89.
Dressler, A.: 1986, Ap. J., 301, 35.
Dwek, E.: 1986, Ap. J., 302, 363.
Dwek, E., Rephaeli, Y., and Mather, J.C.: 1987, Ap. J., submitted.
Henriksen, M.J., and Mushotzky, R.F.: 1986, Ap. J., 302, 287.
Hu, E.M., Cowie, L.L., and Wang, Z.: 1985, Ap. J. Suppl., 59, 447.
Hu, E.M. 1987, in Cooling Flows in Clusters and Galaxies. Procedings of the NATO Advanced Research Workshop, ed. A. C. Fabian (Cambridge: England).
Karachentsev, I.D., and Lipovetskii, V.A.: 1969, Soviet Phys., 12, 909.
Rephaeli, Y., and Wandel, A.: 1985, M. N. R. A. S., 215, 453.
Rood, H.J., Page, T.L., Kintner, E.C., and King, I.R.: 1972, Ap. J., 175, 627.
Silk, J., and Burke, J.R.: 1974, Ap. J., 190, 11.
Verter, F.: 1987, Ap. J. Suppl., 65, 555.
Voshchinnikov, N.V., and Khersonskij, V.K.: 1984, Ap. Sp. Sc., 103, 301.
Yahil, A., and Ostriker, J.P.: 1973, Ap. J., 185, 787.
Zwicky, F.: 1962, in Problems of Extragalactic Research, ed. G. C. McVit (New York: Macmillan), p. 149.

Far Infrared Structure of Spiral Galaxies From the IRAS CPC Images

Richard J. Wainscoat, Arati Chokshi*, and Laurance R. Doyle
S.E.T.I. Institute, N.A.S.A. Ames Research Center
M.S. 245-7, Moffett Field, CA. 94035
(* NAS-NRC Research Associate)

Significant extended far infrared ($50\mu m$ and $100\mu m$) structure has been found for five face-on spiral galaxies (NGC2403, M51, M83, NGC6946, and IC342) from fourteen galaxies searched in the IRAS CPC catalogue. Images were initially processed to remove instrumental and background artifacts, the isophotal centroids of each image determined, and multiple images of each galaxy (for each wavelength) superimposed and averaged to improve signal-to-noise. Calibration of these images was performed using IRAS survey array data. Infrared isophotes were then superimposed on optical (blue) images so that direct structural comparisons could be made.

GALAXY FORMATION BY DUST?

Boqi Wang and Goerge B. Field

Harvard-Smithsonian Center for Astrophysics

It has been known since the early 1940's[1] that radiation can cause an instability in the interstellar medium. Absorbing dust particles in an isotropic radiation field shadow each other by a solid angle which is inversely proportional to the square of the distance between the two particles, leading to an inverse-square attractive force – "mock gravity". The effect is largest in an optically thin medium. Recently Hogan and White[2] (HW, hereafter) proposed that if the pre-galactic universe contained suitable sources of radiation and dust, instability in the dust distribution caused by mock gravity may have led to the formation of galaxies and galaxy clusters. In their picture of a well-coupled dust-gas medium, HW show that mock gravity begins to dominate gravitational instability when the perturbation becomes optically thin, provided that the radiation field at the time is strong enough. The recent rocket observation of the microwave background at submillimeter wavelengths by Matsumoto *et al.*[3] might be from pre-galactic stars, the consequence of the absorption of ultraviolet radiation by dust, and infrared reemission which is subsequently redshifted. HW's analysis omits radiative drag, incomplete collisional coupling of gas and dust, finite dust albedo, and finite matter pressure. These effects could be important. In a preliminary calculation including them, we have confirmed that mock gravitational instability is effective if there is a strong ultraviolet radiation at the time, but any galaxies that form would be substantially enriched in heavy elements because the contraction of the dust is more rapid than that of the gas. Moreover, since the dust moves with supersonic velocity through the gas soon after the perturbation becomes optically thin, the sputtering of dust particles by gas is significant[4], so the dust could disappear before the instability develops significantly. We conclude that the mock gravity by dust is not important in galaxy formations. The detailed results of our calculations will be presented elsewhere.

REFERENCES

[1] Spitzer, L. 1941, *Ap. J.*, **94**, 232.
[2] Hogan, C.J. and White, S.D. 1986, *Nature*, **371**, 575.
[3] Matsumoto, S. *et al.* 1988, *Ap. J.*, in press.
[4] Draine, B.T. and Salpeter, E.E. 1979, *Ap. J.*, **231**, 77.

SECTION V: OPTICAL PROPERTIES OF GRAINS

VUV-VISIBLE MEASUREMENTS ON DIFFERENT SAMPLES OF AMORPHOUS CARBON

A. Blanco*, A. Borghesi*, E. Bussoletti**, L. Colangeli***, S. Fonti*,
H.E. Gumlich****, Ch. Jung****, V. Orofino*, G. Schwehm***
* Physics Department, University of Lecce, Lecce, Italy
** Istituto Universitario Navale and Osservatorio Astronomico di Capodimonte, Napoli, Italy
*** Space Science Department of ESA/ESTEC, Noordwijk, The Netherlands
**** Technische Universitat Berlin, West Germany

1. INTRODUCTION

Among various candidate materials for interstellar dust, amorphous carbon (AC) is playing an increasingly important role (Greenstein, 1981; Hecht et al., 1984; Jura, 1983, 1986). Furthermore, recent "in situ" measurements have clearly shown the presence of carbonaceous grains in the coma of comet Halley (Kissel et al., 1986). Laboratory investigations on AC grains may be very useful to better interpret observations and to support theoretical elaborations.

Previous extinction measurements on AC grains (Borghesi et al., 1985; Colangeli et al., 1986; Bussoletti et al., 1987) have evidenced an UV hump, quite similar to the 220 nm "interstellar extinction bump". In addition, the near IR absorption spectrum of AC particles shows bands which match some of the so-called interstellar "unidentified infrared bands", detected in many celestial sources (Borghesi et al., 1987; Blanco et al., 1988), and the 3.4 μm emission band observed in Halley's spectrum (Colangeli et al., 1988).

Recently, we have started an international research program which also includes UV extinction analyses on AC samples, by using synchrotron light. We present here preliminary results obtained in a first shift of measurements, last june.

2. EXPERIMENTAL

The AC dust particles have been produced by arc discharge between two amorphous carbon electrodes, in a controlled Ar atmosphere (p = 1 Torr) and collected on Litium Fluoride (LiF) windows (cutoff = 105 nm). The UV extinction measurements have been performed using the BESSY-synchrotron light facility in West Berlin. Two sets of samples have been analyzed, so far, allowing also for low temperature tests:

Set	Samples	d (cm)
I	1,2,3,4	3,5,7,10
II	5,6	5, 10

where "d" is the collecting distance of the samples from the arc discharge. The LiF windows used in the two series of measurements show slightly different

transmission properties (Figure 1). Furthermore, the samples of each set are characterized by almost the same surface density of dust, σ, but samples of set II have σ values higher than those of set I.

3. RESULTS

Some examples of the obtained spectra are summarized in Figures 2-4. At the present stage of the data analysis we can only draw some preliminary considerations:

a) a wide band falling at around 240 nm is detected in all the analyzed samples. Its intensity seems to decrease with increasing the dust collecting distance (Figure 2).

b) a peak at 150 nm decreases in intensity with increasing the collecting distance. The band seems absent in the samples characterized by a larger amount of dust (Figure 3).

c) a feature at about 200 nm is detected in some samples. At the moment we tend to attribute it to the transmission properties of the LiF substrates at that wavelength (Figure 1) and/or to some problems in the experimental setup.

d) it is unclear if a hump at 120 nm is real or due to instrumental effects.

e) the profile of the spectra does not show substantial changes when the samples are cooled down to about 100 K (Figure 4).

The present results appear to be in general agreement with previous findings, but their analysis is in progress and the interpretation is still on the way.

Blanco, A., Bussoletti, E. and Colangeli, L.: 1988, Astrophys. J., in press.

Borghesi, A., Bussoletti, E. and Colangeli, L.: 1985, Astron. Astrophys. 142, 225.

Borghesi, A., Bussoletti, E. and Colangeli, L.: 1987, Astrophys. J. 314, 422.

Bussoletti, E., Colangeli, L., Borghesi, A., Orofino, V.: 1987, Astron. Astrophys. Suppl. Ser. 70, 257.

Colangeli, L., Capozzi, V., Bussoletti, E. and Minafra, A.: 1986, Astron. Astrophys. 168, 349.

Colangeli, L., Schwehm, G., Bussoletti, E., Blanco, A., Fonti, S., Orofino, V.: 1988, Astrophys. J., submitted

Greenstein, J. L.: 1981, Astrophys. J. 245, 124.

Hecht, J. H., Holm, A. V., Donn, B. and Wu, C. C.: 1984, Astrophys. J. 280, 228.

Jura, M.: 1983, Astrophys. J. 267, 647.

Jura, M.: 1986, Astrophys. J. 303, 327.

Kissel, J., et al.: 1986, Nature 321, 280.

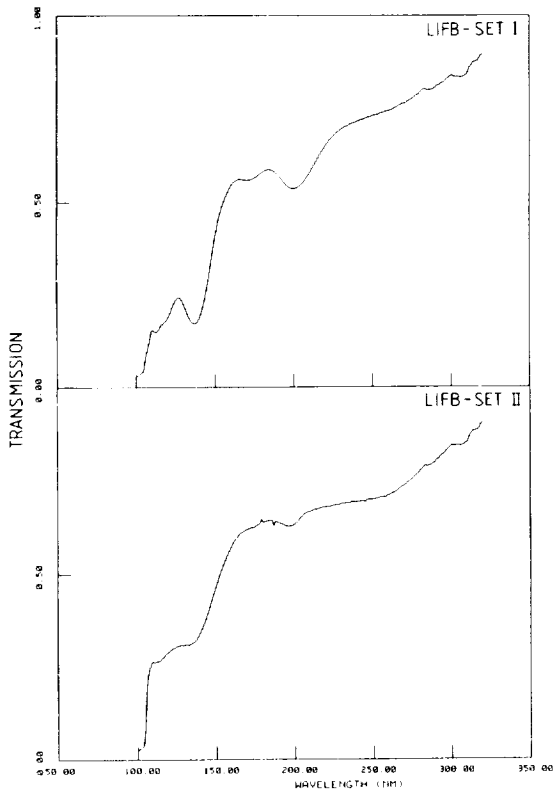

Figure 1. Transmission spectra of Litium Fluoride windows (LiFB) used in the two sets of measurements.

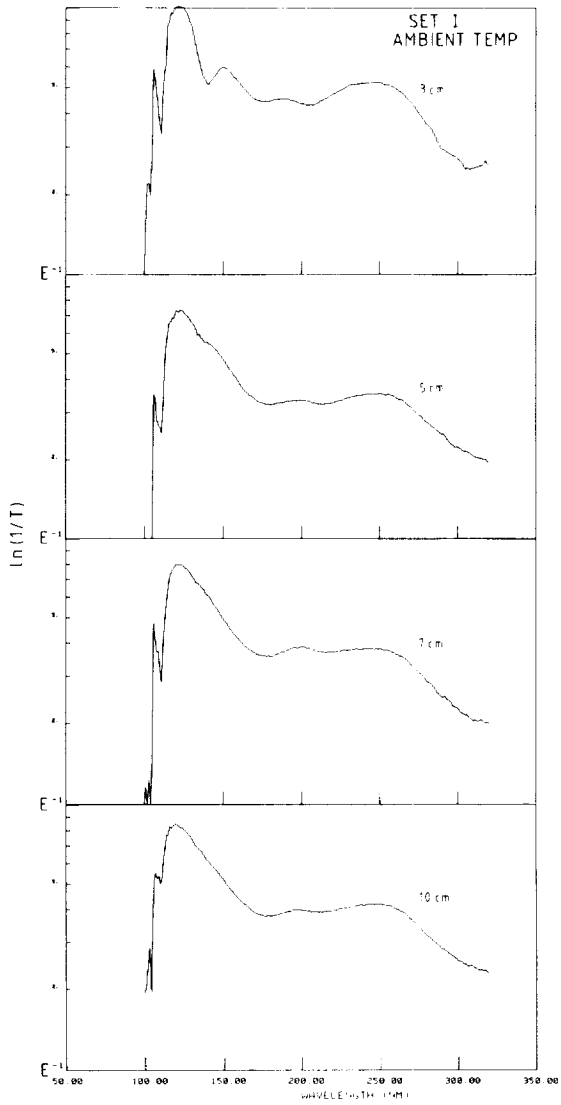

Figure 2. Normalized extinction coefficient at ambient temperature for AC samples of set I.

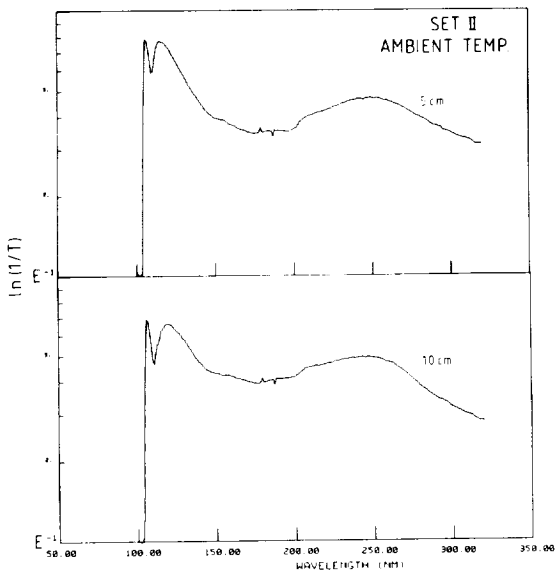

Figure 3. Normalized extinction coefficient at ambient temperature for AC samples of set II.

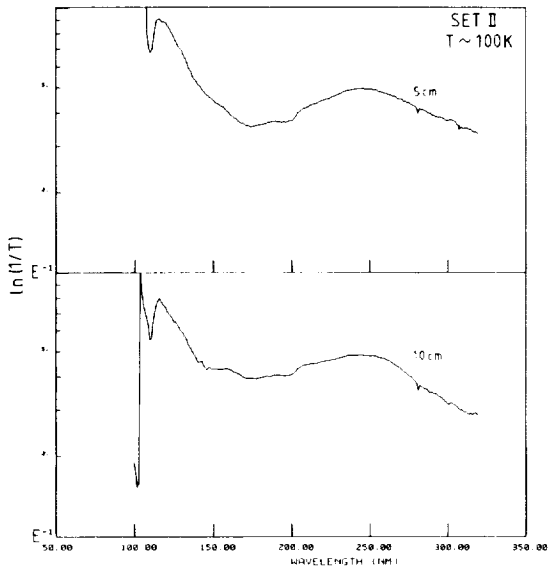

Figure 4. Normalized extinction coefficient at 100 K for AC samples of set II.

STEPS TOWARD INTERSTELLAR SILICATE DUST MINERALOGY

J. Dorschner, J. Gürtler, and Th. Henning
Universitäts-Sternwarte, Jena, DDR-6900, G.D.R.

One of the most certain facts on interstellar dust is that it contains grains with silicon oxygen tetrahedra (SOT), the internal vibrations of which cause the well known silicate bands at 10 and 18 μm. The broad and almost structureless appearance of them demonstrates lacking translation symmetry in these solids that must be considered amorphous or glassy silicates. There is no direct information on the cations in these interstellar silicates and on the number of bridging oxygens per tetrahedron (NBO). Comparing experimental results gained on amorphous silicates, e.g. silicate glasses, of cosmically most abundant metals (Mg, Fe, Ca, Al) with the observations is the only way to investigate interstellar silicate dust mineralogy (cf. Dorschner and Henning, 1986).

At Jena University Observatory IR spectra of submicrometer-sized grains of pyroxene glasses (SSG) have been studied. Pyroxenes are common minerals in asteroids, meteorites, interplanetary, and supposedly also cometary dust particles. Generally, primitive solar system solids can serve as a guide to interstellar dust mineralogy (Dorschner, 1968, Jones and Williams, 1987). Pyroxenes consist of linearly connected SOT (NBO=2). In the vitreous state reached by quenching melted minerals the SOT remain nearly undistorted (Si-O bond length unchanged); the Si-O-Si angles at the bridging oxygens of pyroxenes, however, scatter statistically. Therefore, the original cation oxygen symmetry of the crystal (octahedral and hexahedral coordination by O) is completely lost. The blended bands at 10 and 18 μm lose their diagnostic differences and become broad and structureless. This illustrates best the basic problem of interstellar silicate mineral diagnostics.

Optical data of glasses of enstatite (E, $Mg_2Si_2O_6$), bronzite (B, $(Mg,Fe)_2Si_2O_6$), hypersthene (H, same formula as B, but higher Fe content), diopside (D, $CaMgSi_2O_6$), salite (S, $Ca(Mg,Fe)Si_2O_6$), and hedenbergite (HB, $CaFeSi_2O_6$) have been derived. Results of E, B (Dorschner et al., 1986, 1988), and H show very good agreement with the observed

silicate features in the IR spectra of evolutionarily young objects that show "P-type" silicate signature according to the classification by Gürtler and Henning (1986). Table 1 shows compositional parameters and main characteristics of experimental SSG spectra in IR for the glasses E, B, and H. Our results fit excellently the relations derived by Koike and Hasegawa (1987) and suggest that the band ratio of the "astronomical silicate" by Draine and Lee (1984) is too low.

Table 1: Composition and spectral characteristics of pyroxene glass SSG

Parameter		E	B	H
SiO_2 content	%	57.7	56.0	52.3
MgO content	%	35.2	33.4	22.8
FeO content	%	2.7	6.6	19.8
$\lambda(10)/FWHM(10)$	μm	9.4/2.4	9.5/2.5	9.5/2.8
MAC(10)	cm^2g^{-1}	3000	3000	2430
$\lambda(18)/FWHM(18)$	μm	18.5/9.6	18.5/9.5	18.5/8.4
MAC(18)/MAC(10)		0.47	0.55	0.58

References

Dorschner, J.: 1968, Astron. Nachr. 290, 171.

Dorschner, J. and Henning, Th.: 1986, Astrophys. Space Sci. 128, 47.

Dorschner, J., Friedemann, C., Gürtler, J., Henning, Th., and Wagner, H.: 1986, Mon. Not. R. Astron. Soc. 218, 37P

Dorschner, J., Friedemann,C., Gürtler, J., and Henning, Th.: 1988, Astron. Astrophys. in press.

Draine, B.T. and Lee, H.M.: 1984, Astrophys. J. 285, 89.

Jones, A.P. and Williams, D.A.: 1987, Mon. Not. R. Astron. Soc. 224, 473.

Gürtler, J. and Henning, Th.: 1986, Astrophys. Space Sci. 128, 163.

Koike, C. and Hasegawa, H.: 1987, Astrophys. Space Sci. 134, 361.

SCATTERING BY FLUFFY GRAINS

N91-14992

J.I. Hage and J.M. Greenberg
Laboratory Astrophysics, University of Leiden

There are indications (Greenberg et. al., 1988), that fluffy (i.e. porous) particles are responsible for the observed 3.4 and 10 micron emissions of comet Halley. The absorption characteristics of small particles both solid and fluffy are needed in order to explain the Halley emissions. How isolated small solid particles react to an external radiation field is well known - the Rayleigh approximation. How these same small particles emit when assembled as fluffy aggregates is another question. To what degree are the emission spectra of isolated and aggregated particles comparable ? In order to quantify the assertion that fluffy particles produce the observed Halley infrared emission features we are performing calculations to determine the effect of porosity on the absorption characteristics of aggregates of interstellar grain-type particles. Our calculations are based on an integral representation of the scattered electromagnetic field. We present results here, with application to comet Halley.

ref. :
Greenberg, J.M., Zhao, N. and Hage, J.I. : 1988, submitted to Nature

N91-14993

LABORATORY STUDIES OF REFRACTORY METAL OXIDE SMOKES

J. A. Nuth*, R. N. Nelson** and B. Donn*
* Code 691, NASA/Goddard Space Flight Center, Greenbelt, MD 20771
**Chemistry Dept., Georgia Southern College, Statesboro, GA 30460

Studies of the properties of refractory metal oxide smokes condensed from a gas containing various combinations of SiH_4, $Fe(CO)_5$, $Al(CH_3)_3$, $TiCl_4$, O_2 and N_2O in a hydrogen carrier stream at 500 K > T > 1500 K have been performed in our laboratory. Ultraviolet, visible and infrared spectra of pure, amorphous SiO_x, FeO_x, AlO_x and TiO_x smokes will be discussed, as will the spectra of various co-condensed amorphous oxides, such as Fe_xSiO_y or Fe_xAlO_y. Preliminary studies of the changes induced in the infrared spectra of iron-containing oxide smokes by vacuum thermal annealing suggest that such materials become increasingly opaque in the near infrared with increased processing: hydration may have the opposite effect (see Fig. 1). More work on the processing of these materials is required to confirm such a trend: this work is currently in progress. Preliminary studies of the ultraviolet spectra of amorphous Si_2O_3 and $MgSiO_x$ smokes revealed no interesting features in the region from 200-300 nm. Studies of the ultraviolet spectra of both amorphous, hydrated and annealed SiO_x, TiO_x, AlO_x and FeO_x smokes are currently in progress.

Finally, data on the oxygen isotopic composition of the smokes produced in our experiments will be presented which indicate that the oxygen becomes isotopically fractionated during grain condensation. Oxygen in our grains is as much as 3% per amu lighter than the oxygen in the original gas stream. We are currently conducting experiments to understand the

mechanism by which fractionation occurs. Such processes may have observable consequences in circumstellar outflows if the effects become larger as the total pressure decreases. This might be expected if the fractionation mechanism operates during the formation of the initial molecular oxides rather than during the nucleation of the refractory grains which form from such oxides.

Figure 1. Infrared spectra of amorphous Fe-Al-silicate smokes. The lower spectrum is the initial condensate. The middle spectrum is that of a sample which was immersed in liquid water for 5 days at 378 K and then freeze-dried. The top spectrum is that of a sample which has been vacuum annealed for 16 hrs. at 1200 K. Note that a scale change occurs at 2000 cm^{-1}.

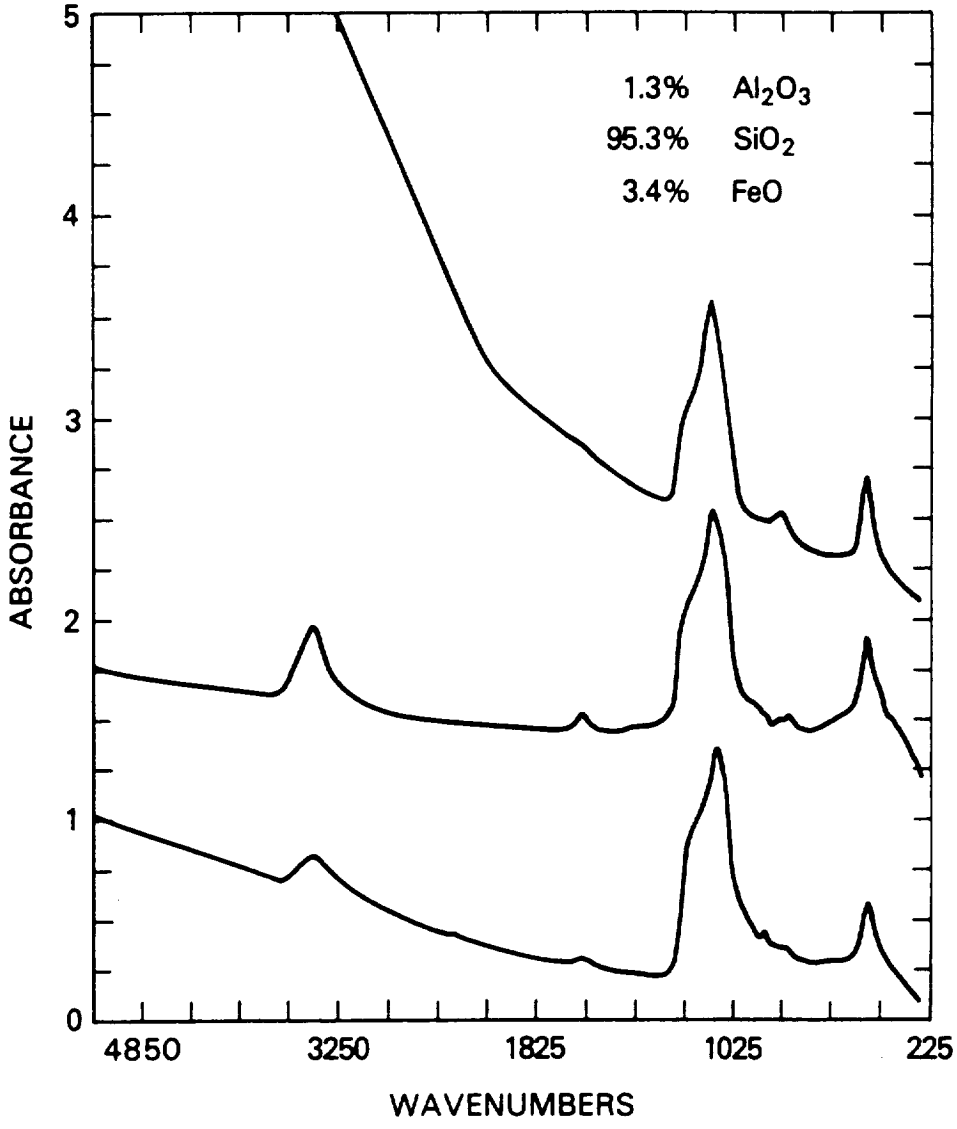

N91-14994

INFRARED SPECTRA OF CRYSTALLINE AND GLASSY SILICATES AND APPLICATION TO INTERSTELLAR DUST

J. R. Stephens, * A. Blanco, ** A. Borghesi, ** S. Fonti, ** and E. Bussoletti***
* Los Alamos National Laboratory, Los Alamos, New Mexico, USA
** University of Lecce, Lecce, Italy
***Instituto Universitario Navale, Naples, Italy

Glassy silicates have been identified as components of interstellar and circumstellar dust on the basis of agreement in the position and shape of observed bands near 10 and 20 microns with laboratory spectra of glassy silicates, particularly of olivine ($(Mg, Fe)_2SiO_4$) composition (See Dorschner and Henning, 1986 for a review of the experimental investigations). Olivine is but one of a variety of silicates that are predicted to condense from a cooling gas of "cosmic" composition in oxygen-rich stars. Other predicted condensates include the "refractory" (> 1000 C) silicates diopside ($CaMg(Si_2O_6)$) and enstatite ($(Mg, Fe)SiO_3$) as well as "low temperature" hydrous minerals including serpentine ($Mg_6(Si_4O_{10})(OH)_8$) and talc ($Mg_3(SiO_{10})(OH)_2$) (Huffman, 1977). Both refractory and hydrous minerals have been found in meteorites, and recently in interplanetary dust particles collected in the Earth's stratosphere (Zolensky, 1987)

The infrared spectra of crystalline minerals predicted in theoretical condensation sequences do not match the astronomical observations. Since the astronomical spectra are a closer match to glassy silicates, we have undertaken a study to measure the infrared spectra of glassy silicates that have compositions similar to silicate minerals predicted in theoretical condensation sequences. The data should support observations aimed at elucidating condensation chemistry in dust forming regions.

We measured the mass absorption coefficients, from 2.5 to 25 microns, of ground samples of olivine, diopside, and serpentine and also smoke samples that were prepared from these minerals. The smoke samples prepared in this way are predominantly glassy with nearly the same

composition as the parent minerals. The crystalline samples consisted of pure olivine ($(Fe_{0.1}Mg_{0.9})_2SiO_4$), serpentine, and diopside. Sample purity was confirmed by X-ray diffraction. Each mineral was ground for 10 hours and a measured mass of the powder was mixed with KBr powder for absorption measurements using the method of Borghesi et al. (1985). The smoke samples were prepared from the same samples used for grinding by vaporizing the minerals using pulsed laser radiation in air. The smoke samples formed by condensation of the resulting vapor. The smoke settled onto infrared transparent KRS-5 substrates and onto a quartz crystal microbalance used to obtain mass measurements. A description of the preparation method is given in Stephens (1980). The glassy diopside showed only diffuse electron diffraction peaks and hence was nearly amorphous, while the serpentine smoke showed a weak diffraction pattern corresponding to MgO. The smoke from olivine showed a weak diffraction pattern corresponding to Fe_2O_3 and/or Fe_3O_4.

The mass absorption coefficients, from 2.5 to 25 microns, of crystalline diopside, olivine, and serpentine and their corresponding smoke samples are shown in Figures 1, 2, and 3.

Figure 1 - Diopside Spectra

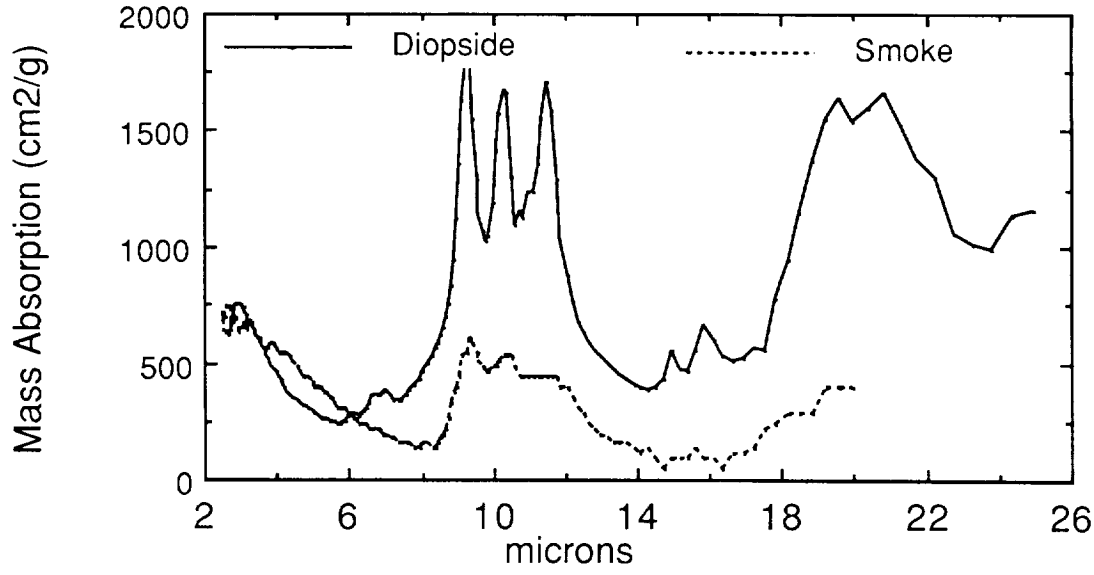

Figure 2 - Olivine Spectra

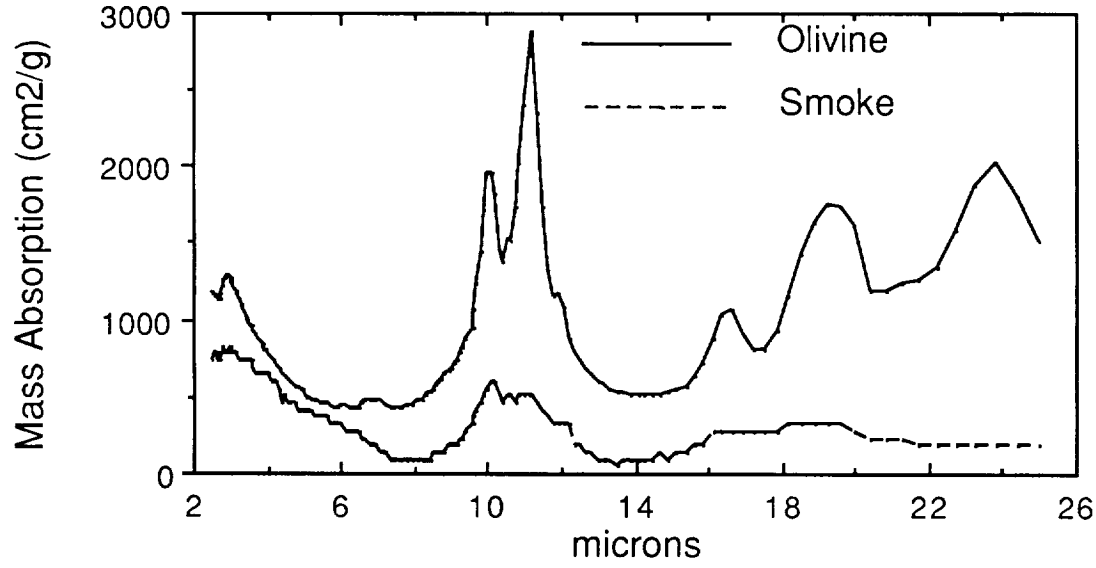

Figure 3 - Serpentine Spectra

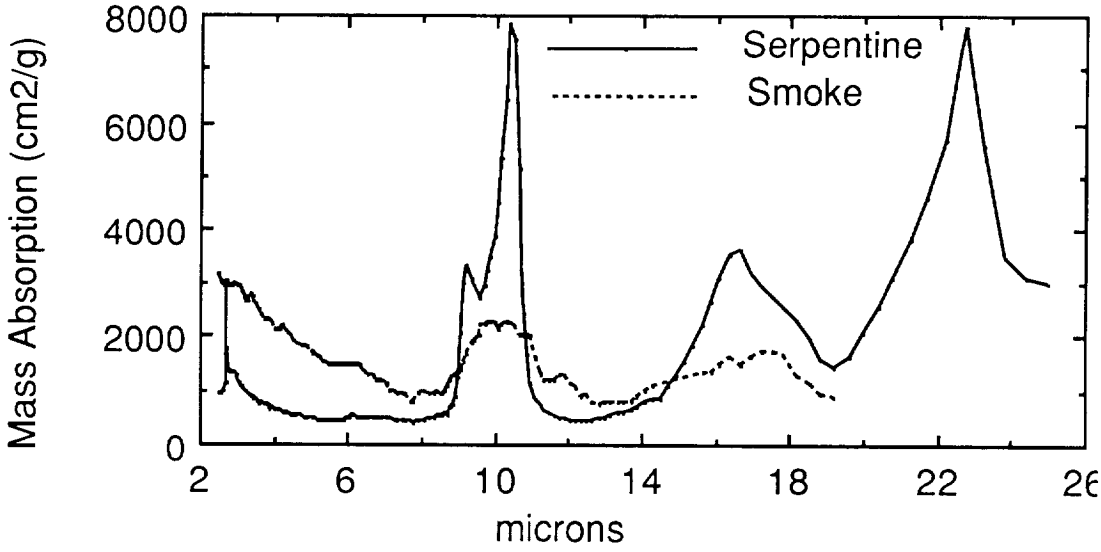

The spectra for the ground crystalline samples show sharp peaks with peak positions and mass absorption coefficients similar to spectra in the literature (diopside (Omori, 1971), olivine (Day 1975), and serpentine (Dorschner et al. 1978)) All of the crystalline samples show a broad spectral peak near 3 microns due to water absorbed during the grinding processes. The crystalline serpentine sample shows a sharp peak at 2.7 microns from OH stretching.

The smoke samples show broader and weaker peaks that are centered near the major peaks in the crystalline spectra. The serpentine smoke does not show a peak corresponding to the 2.7 micron peak in the crystalline serpentine, since the smoke does not have a layered hydrous structure. The mass absorption coefficient at the 10 micron peak of the olivine smoke is much less than the value of 1750 cm^2/g reported by Kratschmer and Huffman (1979) for amorphous olivine. Mass absorption coefficients of diopside and serpentine smokes have not been reported, but Dorschner et al. (1980) measured peak mass absorption coefficients in the range of 2000-3000 cm^2/g for a variety of Fe, Ca, and Mg protosilicates. Our serpentine smoke shows similar strength in the 10 micron feature. The range of mass absorption coefficients for the various smokes illustrates the danger of deriving dust and elemental abundances from measurements of the peak strengths in observational spectra of silicate dust. We do not presently understand the reason for the wide range of mass absorption coefficients in our smokes.

Interestingly, diopside and olivine smokes show very similar peak positions and strengths in the 10 micron band despite the range of metal cations (Fe, Mg, Ca) and metal to silicon ratios of the samples. The shape of the 10 micron peak of serpentine smoke is also similar to the other two smokes. This points out the insensitivity of the 10 micron peak to the composition and metal to silicon ratio of glassy silicates. The 20 micron features for the serpentine, olivine, and diopside smokes peak at 17.5, 19, and beyond 20 microns respectively. The weaker 20 micron silicate feature in astronomical objects we believe to be more diagnostic of the composition of glassy silicate dust than the 10 micron feature. The weakness of the 20 micron feature places strong requirements on the quality of observations needed to probe the condensation chemistry in astronomical environments.

The other striking feature of the spectra is the strong rise in extinction toward the near infrared. All of the spectra except serpentine show this trend. Stephens and Russell (1979) showed that much of the extinction seen in the near infrared spectra of ground samples of olivine is due to scattering by comparing emission (absorption) and extinction (absorption and

scattering) spectra. Emission spectra of the ground samples are needed to determine if the near infrared rise is due to absorption or scattering.

For smoke samples, which consist of smaller particles, the scattering is expected to be much smaller and the absorption should dominate. Preliminary data on the emission spectra of the serpentine and diopside smokes indicate, however, that the near infrared rise in serpentine is due to absorption, while that for diopside is due to scattering (Russell 1988). The difference in the scattering and absorption behavior of the two samples points out the difficulty in separating scattering and absorption in the near infrared and shorter wavelengths. Separation of absorption and scattering processes in this region are needed, for example, to understand the observation that circumstellar silicates show stronger absorption in the near infrared than terrestrial silicates (Jones and Merrill, 1976). More work needs to be done on synthesizing and measuring the spectral properties of a variety of silicates glasses over a wide range of wavelengths including the ultraviolet, visible, and infrared to obtain a comprehensive picture of the spectral behavior of these materials.

Borghesi, A. et al.: 1985, Astron. Astrophys., 153, 1

Day, K. L.: 1975, Ap. J., 199, 660

Dorschner, J. et al.: 1978, Astron. Nachr., 299, 269

Dorschner, J., et al.: 1980, Astrophys. and Space Sci., 68, 159

Dorschner, J. and Henning, Th.: 1986, Astrophys. and Space Sci., 128 , 47

Huffman, D. R.: 1977, Advances in Physics, 26, 12

Jones, T. W. and Merrill, K. M.: 1976, Ap. J., 209, 509

Kratschmer, W. and Huffman, D: 1979, Astrophys. and Space Sci., 61, 197

Omori, K. : 1971, Am. Minerologist, 56, 1607

Russell, R. W.: 1988, (Private Communication)

Stephens, J. R.: 1980, Astrophys. J., 237, 450

Stephens, J. R. and Russell, R. W.: 1979, Ap. J., 228, 780

Zolensky, M. E.: 1987, Science, 237, 1466

OPTICAL PROPERTIES OF IRREGULAR INTERSTELLAR GRAINS

J.M. Perrin and P.L. Lamy
Laboratoire d'Astronomie Spatiale, Marseille, France

ABSTRACT

In order to study the interaction of light with interstellar grains, we represent an irregular particle by a network of interacting dipoles whose polarizability is determined in a first approach by the Clausius-Mossoti relationship. Typically, 10000 dipoles are considered. In the case of spherical particles, the results from Mie theory are fully recovered. The main interest of this method is to study with a good accuracy the implications of surface roughness and/or inhomogeneities on optical properties in the infrared spectral range, particularly of the silicate emission features.

INTRODUCTION

Small dust particles are known to play an important role in the interstellar extinction process, but the nature of the grains and the mechanism of interaction with light are still a matter of debate. If various models of interstellar grains have been published for the last two decades (see the reviews of Mathis, 1986 and Tielens and Allamandola, 1987) none of them is able to explain the totality of the spectral features observed in the interstellar medium from the far ultraviolet to the far infrared (Mathis et al, 1977 ; Greenberg and Chlewicki, 1983 ; Greenberg and d'Hendecourt, 1985).

So a careful study of the interaction between dust and light must be conducted. When the size of the dust particle is lower than

the wavelength of the incident light, which is the case for interstellar dust particle in the infrared spectral range, approximations are used, such as the Rayleigh theory (see for example, Bohren and Huffman, 1983) to obtain extinction, absorption and scattering cross sections as well as the scattering diagram. However this approximation cannot always be used (see for example Perrin and Lamy, 1981 ; Draine and Lee, 1984) since there exists a condition on the imaginary part of the refractive index in addition to the well-known condition that the particle is small w.r.t. the wavelength. In order to study the interaction of infrared light with interstellar dust, in a general way, we first show that the classical electrodynamic equations permit to represent a dust particle by a network of interacting dipoles as first proposed by Purcell and Pennypacker (1973). We then compare the values of the extinction cross section obtained by this method and the Mie theory (Mie, 1908) for a small, homogeneous spherical dust particle of silicate in the mid-infrared spectral range [5 - 15 μm]. Finally we use this method to study the variations to extinction introduced by fluffy particles of the same mass as the spherical one.

THE ELECTROMAGNETIC FIELD SCATTERED BY INTERACTIVE DIPOLES

We consider a dust particle with no free charge, no currents and no magnetic suceptibility and which may be composed of a inhomogeneous material of complex index of refraction $n(\vec{r})$. The electromagnetic field $\vec{E}$ (with harmonic time dependance) interacting with the particle is solution of equations from classical electromagnetic theory :

$$\vec{\nabla} \times (\vec{\nabla} \times \vec{E}) - k^2 \vec{E} = k^2 [n^2(\vec{r}) - 1] \vec{E}$$

where $k = 2\Pi/\lambda$ and λ is the wavelength of the incident light.

Let us represent the dust particle by a discrete collection of dipoles ; then

$$n^2(\vec{r}) = 1 + 4\Pi \sum \alpha_i \, \delta(\vec{r} - \vec{r}_i)$$

where α_i and $\vec{r}_i$ are respectively the polarizability and the position vector of the i^{th} dipole (in the case of an anisotropic material, the method remains valid but $n(\vec{r})$ must simply be represented by a

tensor). The scattered field is the sum of the field created by each individual dipole whose electric dipole moment $\vec{d}_i$ is induced by the incident light and of the fields radiated by all other dipoles. When the dipoles are located at the nodes of a cubic "lattice", this method generalized that of Purcell and Pennypacker (1973). To obtain the value of the scattered field at a point $\vec{r}$ far away from the particle (w.r.t. the wavelength), we first calculate the dipole moment $\vec{d}_i$ at each site :

$$\vec{d}_i = \alpha_i \vec{E}(\vec{r}_i)$$

Then the total scattered field in the direction of observation defined by the unit vector $\vec{u}$ is found to be

$$\vec{E}_s(\vec{r}) \simeq k^2 \frac{e^{ikr}}{r} \sum \exp(-ik \vec{r}_i . \vec{u}) \; (\mathbb{1} - \vec{u} \otimes \vec{u}) \; \vec{d}_i$$

The dipole moments $\vec{d}_i$ may be obtained by solving a set of 6N (N = number of sites) linear equations (Shapiro, 1975).

Even with supercomputers, there is a limit to the number of dipoles which may be handled (inversion of a 6N x 6N matrix). Iteratives methodes should be considered, as first proposed by Purcell and Pennypacker (1973) ; however as their convergence process is not always satisfied, we prefer to use the Born expansion series whose physical interpetation theoretically insures the convergence (Chiappetta, 1980 ; Chiappetta et al., 1987).

The extinction cross-section is given by the optical theorem (e.g., Born and Wolf, 1964) while the absorption cross-section follows from the formulation given for instance by Jackson (1962).

COMPARAISON WITH MIE THEORY

Using the Mie theory, we calculate the extinction cross-section of a sphere of silicate of radius 0.05 μm (Fig.1a) whose complex index of refraction in the spectral range 5-15 μm is given by Draine (1985). We now consider a cubic lattice inscribed in the same sphere such that there are 25 nodes or dipoles on a diameter. Therefore, each dipole represents a local volume whose size is 0.002 μm. From

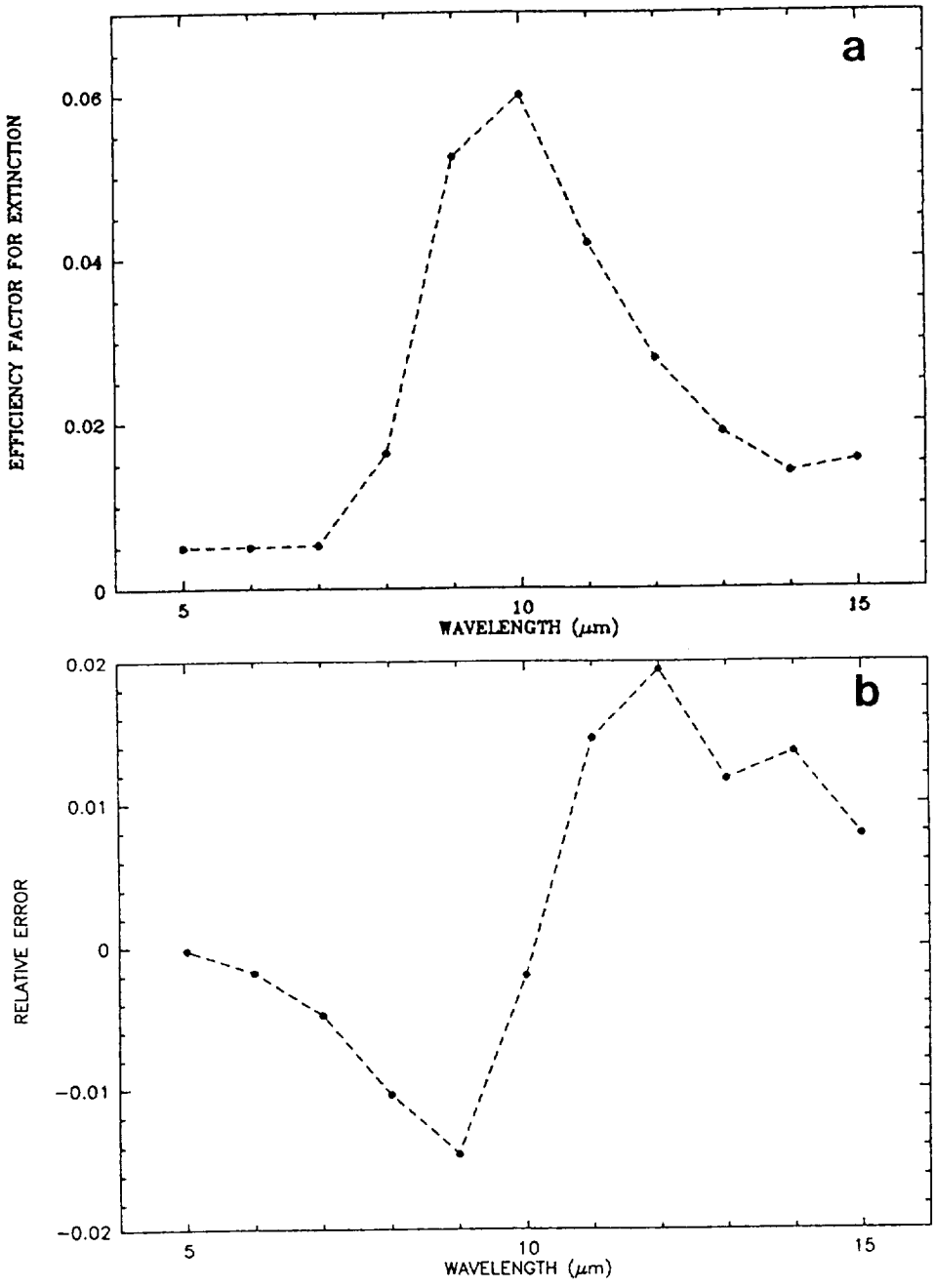

Fig. 1 : a) The efficiency factor for extinction obtained for a sphere using the Mie theory
b) Relative error between the dipole model and the Mie result for the same sphere

the point of view of the classical electrodynamic theory (i.e., from the macroscopic point of view), this local volume is the point source of the scattered field. In the present state of physico-chemical studies, at least 1000 atoms seem to be required to obtain bulk properties (e.g., Buffat and Borel, 1976). So only dust elements whose radii are > 0.001 μm can be studied as bulk, solid particles. Smaller particles must be considered as clusters of atoms or molecules and their optical properties cannot be described by a complex index of refraction (i.e. a macroscopic parameter).

In the present case, our sphere is homogeneous (for comparison with the Mie theory) the polarizability is the same for each dipole ; in a first stage, we define it from the Clausius-Mossotti relationship. Fig.1b gives the difference between the Mie and the present calculations of the extinction cross-section using the interactive dipoles model with the third order Born expansion series.

The maximum deviation resulting from this low order approximation is less than 2 % and illustrates well the validity of the proposed model.

IRREGULAR AND FLUFFY PARTICLES

We now consider an irregular, "fluffy" particle which contains the same number of dipoles as the spherical particle described in the previous section (i.e., same mass) located on a similar network (same spacing). Several sites are left vacant to create voids in the particle, the available dipoles being distributed on the external surface to make it irregular. Cross-sections of the two particles are given in Fig.2 to illustrate this process. The resulting roughness has a maximum amplitude equals to one third of the radius of the original spherical particle. We now compare in Fig.3 the efficiency factors for extinction of the two particles in the spectral range 5-15 μm. As it seems that the intrinsec error resulting from the dipole model at a given wavelength only depends on the total number of dipoles used in the calculation, the differences between the two particles are free of this type of error and therefore reflect the true effect of irregularity and fluffiness : a systematic decrease, by a factor of at least 10 % which depends upon the wavelength (henceforth, a color effect) ; in particular, the silicate "bump" is attenuated.

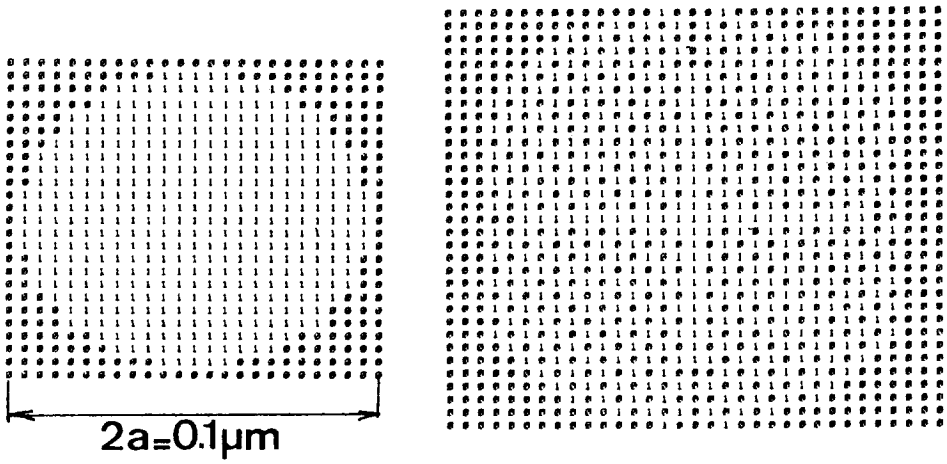

Fig. 2 : Geometrical sections of the two particles studied here : the sphere (left) and the irregular, fluffy particle (right)

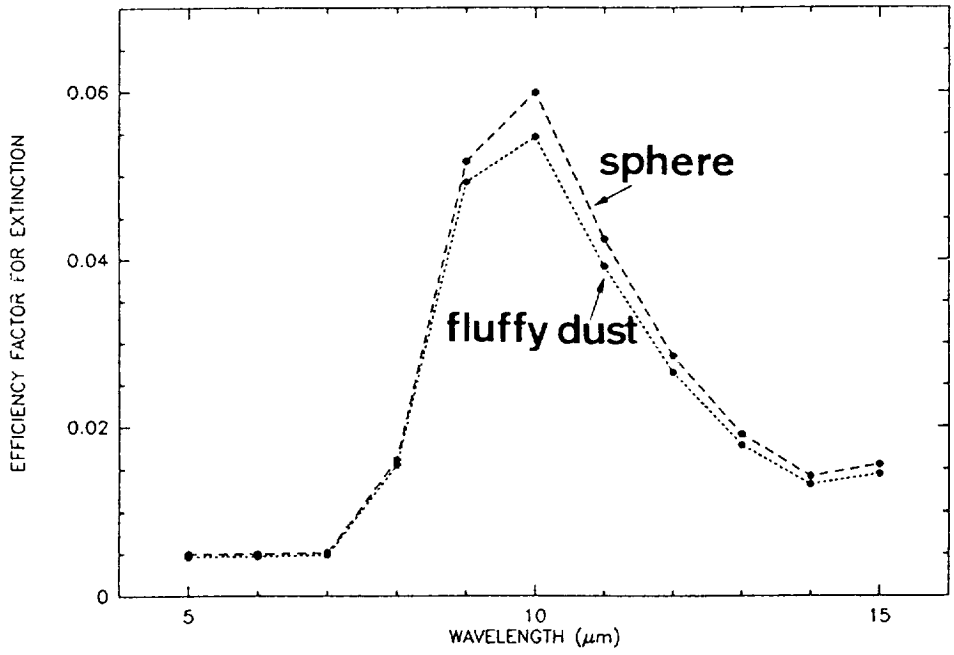

Fig. 3 : The efficiency factors for extinction for the spherical and irregular dipole models

CONCLUSION

The dipole method, originally proposed by Purcell and Pennypacker (1973) but modified by introducing the Born expansion series is shown to give very satisfactory results and therefore looks very promising for solving the problem of light interaction with irregular, fluffy particles. It is also well suited to vectorial calculation on supercomputers. Although the example discussed above corresponds to a very small size parameter ($2\Pi a/\lambda \simeq 0.03$), a clear effect is noted between the sphere and the fluffy particle of the same mass which further depends upon wavelength. The method is still in its infancy and needs further improvement such as the replacement of the Clausius-Mossoti equation by a more exact expression of the polarizability. But it is extremely general as it can handle inhomogeneous particles.

ACKNOWLEDGMENT

Computing time on the CRAY-2 has been granted by the Conseil Scientifique du Centre de Calcul Vectoriel pour la Recherche.

REFERENCES

Bohren, C.F. and Huffman, D.R. : 1983, in Absorption and Scattering of Light by Small Particles, John Wiley and Sons, New York.

Born, M., and Wolf, E. : 1964, in Principles of Optics, Pergamon Press, Oxford.

Buffat, P. and Borel, J.-P. : 1976, Phys. Rev. A13, 2287.

Chiappetta, P. : 1980, J. Phys. A13, 2201.

Chiappetta, P., Perrin, J.-M. and Torresani, B. : 1987, Nuovo Cimento 9D, 717.

Draine, B.T. : 1985, Astrophys. J. Suppl. 57, 587.

Draine, B.T. and Lee, H.M. : 1984, Astrophys. J. 285, 89.

Greenberg, J.M. and Chlewicki, G. : 1983, Astrophys. J. 272, 563.

Greenberg, J.M. and d'Hendecourt, L.B. : 1985, in Ices in the Solar System, eds J. Klinger, D. Benest, A. Dollfus and R. Smoluchowski, Reidel, Dordrecht, p.185.

Jackson, J.D. : 1962, in Classical Electrodynamic, John Wiley and Sons, New York.

Mathis, J.S. : 1986, in Interelationships among Circumstellar, Interstellar and Interplanetary Dust, eds J.A. Nuth and R.E. Stencel (NASA CP-2403), p.29.

Mathis, J.S., Rumpl, W. and Nordsieck, K.H. : 1977, Astrophys. J. 217, 425.

Mie, G. : 1908, Annals Phys. 25, 377.

Perrin, J.-M. and Lamy, P.L. : 1981, Optica Acta 28, 595.

Purcell, E.M. and Pennypacker, C.R. : 1973, Astrophys. J. 186, 705.

Shapiro, P.R. : 1975, Astrophys. J. 201, 151.

Tielens, A.G.G.M. and Allamandola, L.J. : 1987, in Interstellar Processes, eds D.J. Hollenbach and H.A. Thronson, Reidel, Dordrecht, p.397.

SECTION VI: INTERSTELLAR DUST MODELS

OBSERVATIONAL CONSTRAINTS ON INTERSTELLAR DUST MODELS

J. H. HECHT, J. A. HACKWELL, and R. W. RUSSELL
Space Sciences Laboratory, The Aerospace Corporation, Los Angeles, California 90009 USA

No single model has been able to account for all of the observed spectroscopic properties of interstellar or circumstellar dust. The reason for this is that, despite the agreement that the grains are composed of silicaceous/metal oxide and carbonaceous material, there is strong disagreement as to their exact structure and composition. This led Draine and Lee (1984) to use interstellar extinction data to define an interstellar graphitic material; new observational findings have made even that identification uncertain. But the great advantage of their approach is that they used observations at *all* of the wavelengths available to define the material. In this poster we attempt a variation of that approach. We examine recent UV and IR data and attempt to put constraints on the possible types of interstellar grain composition, and to connect these constraints with grain models. What follows is a summary of some of the important constraints imposed by the observations.

IR OBSERVATIONS

a) The astronomical "20 μm" feature, which actually occurs between 18 and 19 μm, is usually attributed to SiO bending. However, most absorptions from bulk silicates, meteoritic or interplanetary material, or laboratory cosmic dust analogues show a band longward of 20 μm. Only a few substances, such as amorphous olivine, have been shown to have an 18-19 μm feature as well as having a 9.7 μm silicate bump (see Hecht et al.,1986). In addition, the feature near 18 μm, which could also be caused by isolated MgO particles (Huffman, 1977), is apparently never found without corresponding evidence for one at 9.7 μm. This appears to rule out an independent origin for the two features.

b) The 3.1, 6.0, 6.8, and 6-7 μm absorptions seen around protostellar sources or in very dense cloud regions have been attributed to the presence on or in the silicate grains of organic ices, water ice, carbonates, or water of hydration (e. g. Hecht et al. 1986). Their absence in interstellar extinction implies that at least those silicates are free from such contamination and contradicts the recent model which attributes the 2175 Å bump in the interstellar extinction curve to hydrated silicate grains (Jones et al. 1987).

c) The UIR (or OIR) bands are almost certainly due to the presence of hydrocarbon material. They were first identified (Leger and Puget, 1984; Allamandola et al., 1985) as PAH molecules but the lack of corresponding absorption features in the UV somewhat contradicts that proposal. Other possible identifications arising from the PAH model are the presence of small amorphous CH grains also referred to as QCC or HAC (Hecht, 1986; Sakata et al. 1984; Goebel; 1986) . A very recent

suggestion which follows from an earlier proposal by Goebel(1986) is that the bands are actually due to the presence of small isolated islands of amorphous CH material in large carbon grains (Duley and Williams, 1988).

d) The 12 and 25 μm cirrus have generally been attributed to small grains, specifically the material responsible for the UIR bands. However , except for the recent proposal of large HAC grains(see above) no mechanism has been discussed for producing the 25 μm cirrus since PAHs have no distinct strong features there. However many of the IRAS spectra appear to show a distinct rise towards long wavelengths suggesting that the 12 and 25 μm emissions are indeed related. If all the cirrus emission is indeed due to carbonaceous materials does that rule out the presence of small silicate/metal oxide clusters? And, if so, why are these clusters less stable than PAH clusters? Furthermore, the absence of stable silicate clusters argues against the recent model by Jones et al.(1987) which proposes that the more volatile carbonaceous material condenses onto the more stable silicate grains.

UV OBSERVATIONS

a) The Far-UV extinction rise has been shown by Fitzpatrick et al.(1988) to have two separate uncorrelated components: a linearly increasing term and a curvature term. This is easily explained in terms of the Mathis et al. model(see Draine and Lee, 1984) whereby they are due to separate populations of silicates and carbonaceous grains. These observations apparently contradict the Jones et al. model(1987) since it attributes all the Far-UV extinction rise to carbonaceous material which coats silicate grains. A further problem with this model is that it predicts a decreasing Far-UV extinction for the bare silicate grains which is seen neither in astronomical observations nor generally in terrestrial silicates.

b) Observations by Fitzpatrick and Massa (1986) have shown that the 2175 Å bump is nearly constant in position but varies in width. These results argue aginst the graphite explanation supported in the Mathis model. Two possible explanations that involve the presence of small grains have been proposed. Hecht(1986) has argued in favor of small de-hydrogenated amorphous CH (or HAC) grain material. The variation in the width could be due to the presence of a small amount of impurities. An argument in favor of this model is that the broadening of the bump should be correlated with the strength of the Far-UV curvature since both the bump and the curvature originate in the carbon grain component, and both features are affected by impurities. This correlation has been observed by Fitzpatrick and Massa(1988). The objections to this model are the lack of its laboratory verification, and the possible indirect implication from IR observations that carbonaceous grains are present in the SMC (Roche et al. 1987). This is significant because the SMC clearly has small grains but shows no bump. The other explanation involves the presence of small OH-bearing silicate grains or small MgO grains (Jones et al. 1987). The strengths of this model are in the laboratory studies that indicate that such grains could form a bump, and the model's natural explanation of the stability of

the central wavelength of the bump peak. The deficiencies of the model involve the presence of other UV features not seen in the interstellar extinction curve, and the strength of the bump compared with other known absoption features with which the bump does not correlate i.e. IR absorption features, and the linear Far-UV rise.

Allamandola, L.J., Tielens, A.G.G.M., and Barker, J.R. :1984, Ap.J.**290**, L25
Draine, B. and Lee, H. M.: 1984, Ap.J. **285**, 89
Duley, W. W. and D. A. Williams: 1988, M.N.R.A.S. **231**, 969
Fitzpatrick, E. L. and D. Massa: 1986 Ap. J. **307**, 286
Fitzpatrick, E. L. and D. Massa: 1988 Ap. J. **328**, 734
Goebel, J. H.: 1987 in *Polycyclic Aromatic Hydrocarbons and Astrophysics* eds A. Leger et al. (D. Reidel) pp. 329-334
Hecht, J. H.: 1986 Ap. J. **305**, 817
Hecht, J. H. , R. W. Russell, J. R. Stephens, and P. R. Grieve:1986 Ap. J. **309**, 90
Huffman, D. R. :1977 Adv. Phys. **50**, 129
Jones, A. P., W. W. Duley, and D. A. Williams:1987 M.N.R.A.S. **229**, 203
Leger, A. and J. L. Puget: 1984 Astr.Ap. **137**, L5
Roche, P. F., D. K. Aitken and C. H. Smith: 1987, M.N.R.A.S. **228**, 269
Sakata, A., S. Wada, T. Tanabe, and T. Onaka: 1984, Ap. J. (Letters) **287**, L51

SIZE DISTRIBUTION OF DUST GRAINS - A PROBLEM OF SELF-SIMILARITY?

Th. Henning, J. Dorschner, and J. Gürtler
Universitäts-Sternwarte, Jena, DDR-6900, G.D.R.

Distribution functions describing the results of natural processes frequently show the shape of power laws, e.g. mass functions of stars and molecular clouds, velocity spectrum of turbulence, size distributions of asteroids, micrometeorites and also interstellar dust grains. It is an open question whether this behaviour is a result simply coming about by the chosen mathematical representation of the observational data or reflects a deep-seated principle of nature. We suppose the latter being the case.

Using a dust model consisting of silicate and graphite grains Mathis et al. (1977) showed that the interstellar extinction curve can be represented by taking a grain radii distribution of power law type

$$n(a) \propto a^{-p} \quad \text{with } 3.3 \leq p \leq 3.6 \qquad (1)$$

as a basis. Biermann and Harwit (1980) explained this finding by postulating grain-grain collisions in the extended atmospheres of those late-type stars where the mentioned grains originated. Size distribution functions of the above shape (1) with p within the mentioned range have been obtained as special solutions of a non-linear integro-differential equation describing fragmentation processes in a closed system of colliding particles (cf. Dorschner, 1981).

A totally different approach to understanding power laws like that in (1) becomes possible by the theory of self-similar processes (scale invariance). The β model of turbulence (Frisch et al., 1978) leads in an elementary way to the concept of the self-similarity dimension D, a special case of Mandelbrot's (1977) "fractal dimension". In the frame of this β model it is supposed that on each stage of a cascade the system decays to N clumps and that only the portion β N remains "active" further on. An important feature of this model is that the "active" eddies become less and less space-filling.

In the following we assume that grain-grain collisions are such a scale-invariant process and that the remaining grains are the inactive ("frozen") clumps of the cascade. In this way, a size distribution

$$n(a)\,da \propto a^{-(D+1)}\,da \qquad (2)$$

results. An analogous relation was obtained by Ferrini et al. (1982), who discussed the problem of molecular cloud fragmentation in this way. Mandelbrot (1977) gave several strong arguments in favour of a value of D ranging between 2 and 3 for such processes.

Assuming D=2.5 the power law with p=3.5 found by Mathis et al. (1977) is obtained. Although the exact value of D is a matter of further discussions it seems to be highly probable that the power law character of the size distribution of interstellar dust grains is the result of a self-similarity process. We can, however, not exclude that the process leading to the interstellar grain size distribution is not fragmentation at all. It could be, e.g., diffusion-limited growth discussed by Sander (1986), who applied the theory of fractal geometry to the classification of non-equilibrium growth processes. He received D=2.4 for diffusion-limited aggregation in 3d-space.

References

Dorschner, J.: 1982, Astrophys. Space Sci. 81, 323.

Biermann, P. and Harwit, M.: 1980 Astrophys. J. 241, L105.

Ferrini, F., Marchesoni, F., and Vulpiani, A.: 1982, Physics Lett. 92A, 47.

Frisch, U., Sulem, P.-L., and Nelkin, M.: 1978, J. Fluid Mech. 87, 719.

Mandelbrot, B.B.: 1977, Fractals: Form, Chance, and Dimension. W.H. Freeman and Co., San Francisco.

Mathis, J.S., Rumpl, W., and Nordsieck, K.H.: 1977, Astrophys. J. 217, 425.

Sander, L.M.: 1986, Nature 322, 789.

N91-14998

STOCHASTIC HISTORIES OF DUST GRAINS IN THE INTERSTELLAR MEDIUM

K. Liffman* and D.D. Clayton**
*NASA Ames Research Center, MS 245-3, Moffett Field, California, 94035 USA
**Dept. of Space Physics and Astronomy, Rice University, P.O. Box 1892 Houston, Texas, 77251 USA

The purpose of this paper is to study an evolving system of refractory dustgrains within the Interstellar Medium (ISM). This is done via a combination of Monte Carlo processes and a system of partial differential equations, where refractory dust grains formed within supernova remnants and ejecta from high mass loss stars are subjected to the processes of sputtering and collisional fragmentation in the diffuse media and accretion within the cold molecular clouds. In order to record chemical detail, we take each new particle to consist of a superrefractory core plus a more massive refractory mantle. The particles are allowed to transfer to and fro between the different phases of the ISM - on a time scale of 10^8 years - until either the particles are destroyed or the program finishes at a Galaxy time of 6×10^9 years. The resulting chemical and size spectrum(s) are then applied to various astrophysical problems with the following results:

(1) for an ISM which has no collisional fragmentation of the dust grains, roughly 10% by mass of the most refractory material survives the rigors of the ISM intact, which leaves open the possibility that 'fossilized' isotopically anomalous material may have been present within the primordial solar nebula.

(2) structured or layered refractory dust grains within our model cannot explain the observed interstellar depletions of refractory material (see fig. 1.).

&(3) fragmentation due to grain-grain collisions in the diffuse phase plus the accretion of material in the molecular cloud phase can under certain circumstances cause a bimodal distribution in grain size (see fig. 2.)

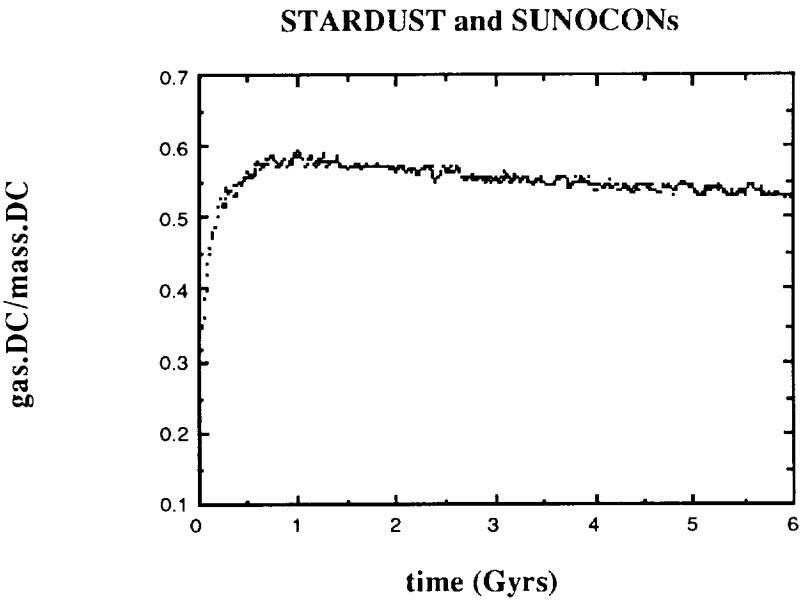

Fig. 1. The ratio of the mass of condensible gas in the diffuse medium to the total mass of the diffuse medium. As can be seen, refractory material is not sgnificantly depleted in the diffuse phase.

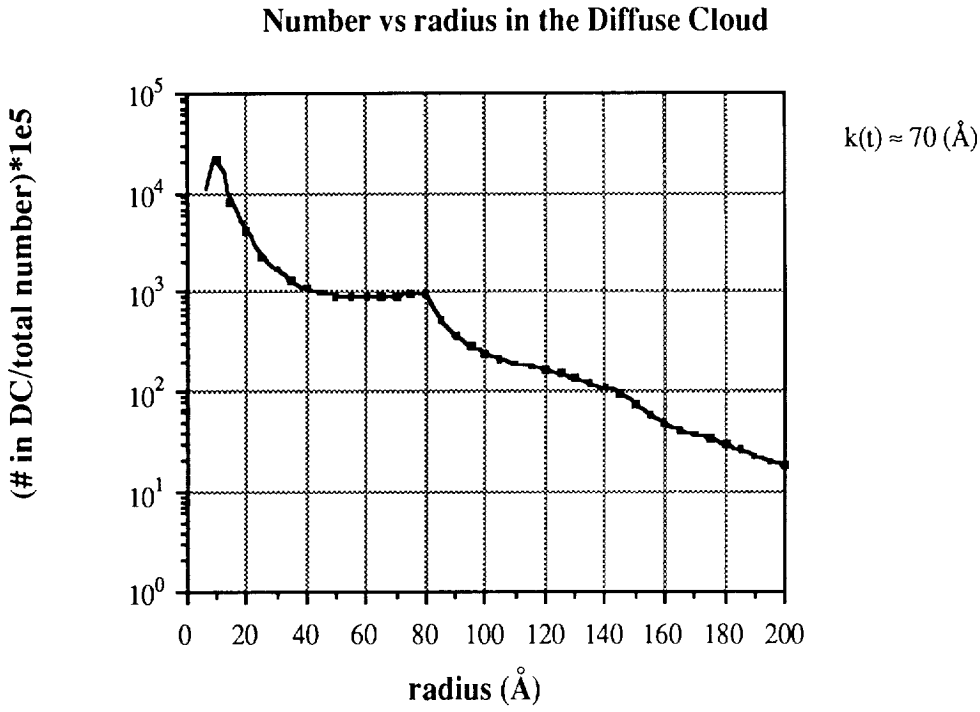

Fig. 2: Number of particles in the Diffuse Cloud over the total number of particles in the ISM versus the radii to the particles. The symbol k(t) refers to the thickness of the accreted mantle, which is a function of time.

N91-14999

Superaromatics, The Key to a Unified Cosmic Dust Theory

Lawrence R. Manuel
Berkeley CA, USA

This theory was constructed by analyzing several thousand astronomical features covering every major aspect of astrophysics and astrochemistry relating to dust. To insure consistency between disciplines the logical structure of the conclusions in each field was checked rather than accepting the current consensus. This was to eliminate the problem shown in figure 1. No substantial contradictory features are known to the author.

The analysis falls into seven major parts:

1) Kinetics of grain formation and destruction.
2) Optical spectra of the ISM.
3) Meteorite/IDP chemistry.
4) Structure of the solar system and its minor components, i. e., comets, boulders, and interplanetary dust cloud.
5) Structure and chemistry of the interstellar medium (ISM) arising from surface catalysis.
6) Dynamics of circumstellar and interstellar dust clouds, including galactic morphology.
7) The chemistry and physics of previously unidentified compounds.

Due to lack of space and time only tentative conclusions are presented here. A full explanation with references will be presented under different cover after funding is obtained.

The principle conclusion is that quantum mechanics as it is normally formulated is incomplete. The probable cause is that it is formulated with complex numbers rather than the more fundamental quaternion system. The manifestation in astrochemistry is that the most stable compounds are "superaromatic" and exotic enough to confound most classical analysis. These include the following problems:

1) They exhibit "supertransparent" phases with negligible oscillator strength so that IR absorption and visible Raman spectroscopy can fail to show most vibration modes.
2) They have large negative oxidation numbers so that generally only small fragments appear in mass spectra.
3) They generate such large matrix corrections that electron-beam analysis gives erroneous results.

The principle compounds are shown in figures 2, 3, and 4.

General

Three types of dust particles dominate:
1) Core-mantle grains aggregated into long needles, which can exceed 1 mm.
2) Small grains of 55 atoms, "ferrotile".
3) Small grains mantled with silicate, hebonite, or other minerals, which can aggregate into larger particles.

Spectral Features

The 220 nm feature is a blending of oxide absorption in small mantles with carbyne absorption in the carbonaceous mantles. The sharper diffuse-interstellar-bands arise from the central iron atom of ferrotile. Broader ones arise from decomposition products. The very broad structure arises from small mantles.

The near IR emission arises from the ferrotile. The 3.3 μm and 11.3 μm features arise from the four C-H bonds in the molecule. Features at 3.46 μm and 12.7 μm arise from a two photon dehydrogenation process.

The carbonaceous mantles have a supertransparent pass band in the near IR which allow the silicate-core features to appear. The band edges are variable, typically appearing at 1 and 20μm. A broad resonance appears at 100μm. Wide variability in emissivity at 1mm arises from ice mantling.

Meteorite/IDP Chemistry

Fresh carbonaceous matrix is a fluid, polar solvent. This leads to the filamentary carbon seen in IDPs and the cementation of grains seen in carbonaceous meteorites. Hard carbonaceous-meteorite matrix contains superaromatic spheroidal molecules in a hydrogenated diamond matrix. The dissolution of the spheroids in oxidizing acid adds to the tetrahedral carbon giving a microcrystaline diamond grain with H, O, and N as the main impurities and with some acid-insoluble spheroids containing Ne. Soluble hydrocarbons show derivation mainly from icasohedral-C rather than planar-C.

Amorphous silicate minerals nucleate on the small grains. The superparamagnetism seen in Mossbauer spectroscopy is consistent with a clustering of small grains before their incorporation into the meteorite. During metamorphosis Fe is complexed to a limited number of sites. This leads to the olivine-iron free glass-olivine sequence of mineralization. At higher levels of metamorphosis the superaromatic carbonaceous matrix can dissolve into the silicate phase. At the highest levels of decomposition iron ends up as magnetite decorations or as metallic iron.

The replacement of iron by chromium in ferrotile creates a large electron affinity in the adjacent ring. This explains the anomalously high noble gas affinity seen in chromite-carbon. Trace element affinities arising from superaromatic chemistry are apparent in most of the mineral phases of meteorites.

Solar System Structure

During the aggregation of planetesimals into planets, the carbonaceous matrix is ductile, allowing the smaller planetesimals

to survive fragmentation and become comets. At the currently colder temperatures the matrix is brittle, allowing the comets to fragment into boulders and dust. Ice reacts with silicate at 200 K allowing the microencapsulation of ice with a high volatile content. These microcapsules explode in cometary jets and during entry into the earth's atmosphere, fragmenting the material. Material close to the sun can bake into carbonaeous chrondrites.

Iridium is mostly bound into a compound that is insoluble in oxidizing acids and decomposes at 1600 C. This can survive reentry in small bodies, be incorporated in the earth's crust (but escape detection), and can then be released during shock heating by meteorite impact. This leads to an underdetermination of terrestial iridium, a gross overdetermination of cometary iridium, and a gross underdetermination of the amount of cometary material hitting the earth.

The zodiacal light shows four features characteristic of cometary material:

1) A hypervelocity component from ferrotile decomposing to iron near the sun.
2) A lobe corresponding to a sharp increase in albedo between 90 and 120 degrees arising from a spherically anisotropic complex index of refraction and seen in the Halley fly-by.
3) A sharp backscattering lobe at 177+ degrees from chondrules.
4) An emission spectrum compatible with interstellar compounds.

Interstellar Medium

The electronegative external oxygen site of ferrotile allows the protenation of the electronegative ends of molecules by proton tunneling. Thus one finds a high abundance of CNH in the ISM compared to HCN. Deuterium preferentially reacts with CNH to form the more stable isomer, so DCN is abnormally abundant compared to HCN. This site catalyzes the recombination of H II to H I and then to molecular hydrogen. The large surface area of the small grains results in a radical restructuring of ISM.

Cloud dynamics

The high catalytic activity toward recombination results in a rapid (~1 million yrs.) cycling of the gas among the cold and warm phases when adequate UV flux is present. The long length of the needles results in a high ratio of far-IR radiation pressure to gravitational pressure. This pushes the needles out of the clouds into H II regions, where they are broken down into small grains and gas. The shadowing of the UV results in a modulation of the "rocket" effect, "rockets with parasols", and leads to the chaotic structure of giant molecular clouds. A near IR source of illumination, e. g., the Becklin-Neugebauer object, can attract needles, resulting in a low gas/dust ratio. Spiral arms can push the dust into cirrus and dust lanes.

Dust dynamics varies widely among galaxies. At a metallicity less than -1, UV extinction per unit of dust may be an order of magnitude lower due to the lack of metals to generate dynamic cloud chemistry.

Astronomers at Work

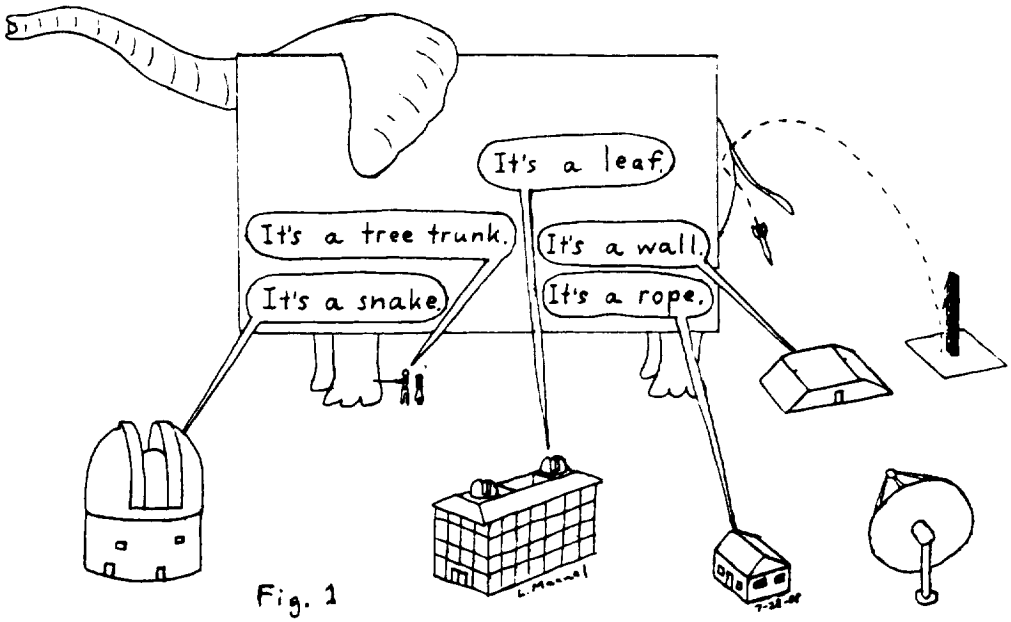

Fig. 1

Fig. 2a "Ferrotile" $FeXC_{32}H_4N_8O_7S_2$

(small grains) X = Al, Ca, S, etc.

This is the Mercator projection of an oblate ellipsoid.
See below for structure of internal ring.

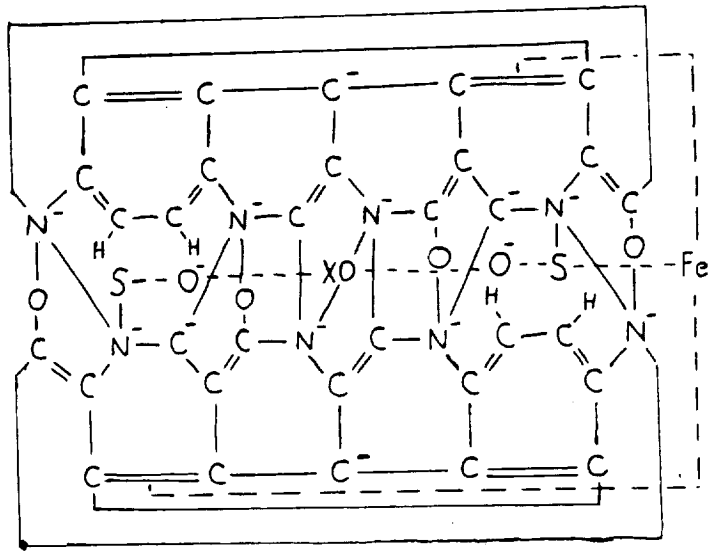

Different representations of internal ring of "ferrotile". This is sandwiched between two dehydrogenated and dehydrated "pentile" monomers.

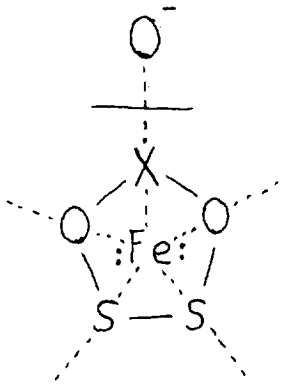

Superatomic

Fig. 2b

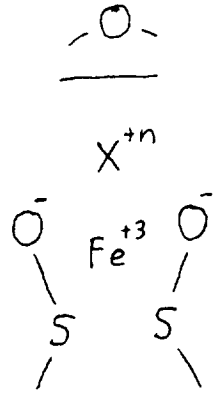

Kékulé
(matches diagram above)

Fig. 3 Magnesium "Polycoronamide"

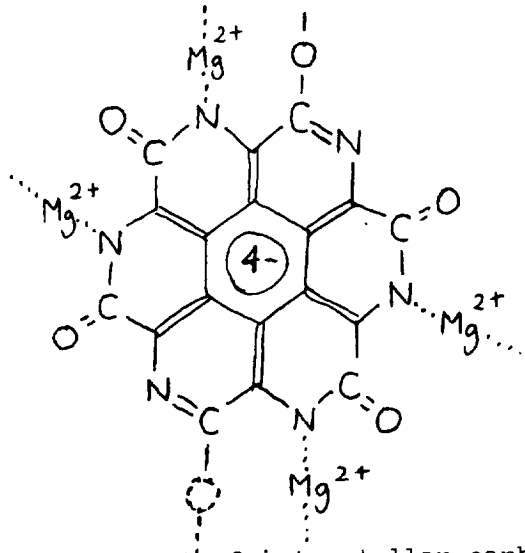

This is the main component of interstellar carbonaeous matrix, which shows a variable supertransparent pass band from about one to twenty microns (also seen in IDP's). Polycoronamide with organic cations gives a sharp mass peak at 284 daltons in laboratory UV-processed ice experiments.

Carbon polymorphs

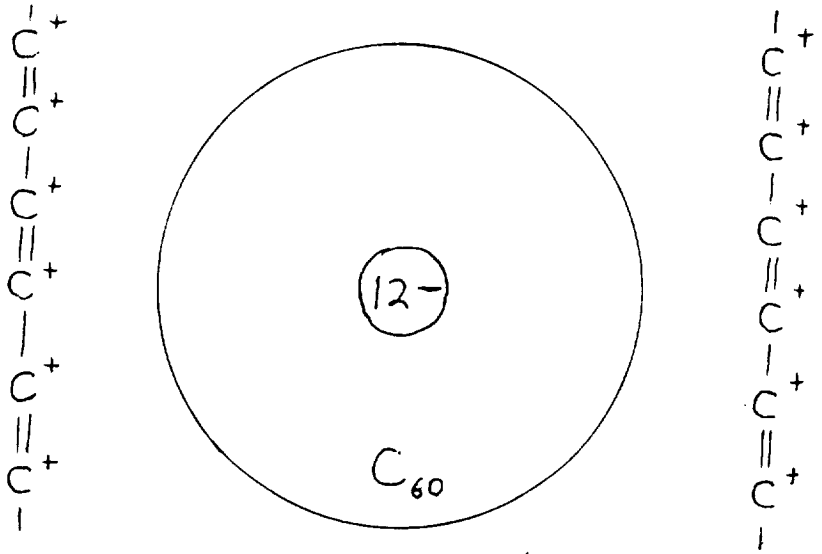

Alpha - carbyne (C_{72})

The ellipsoids are supertransparent. Only the carbyne chains appear in IR spectra and visible Raman spectra.

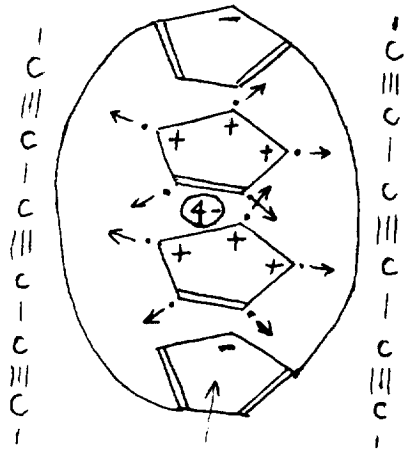

Carbon - XIV

C_{70}

(C_{82})

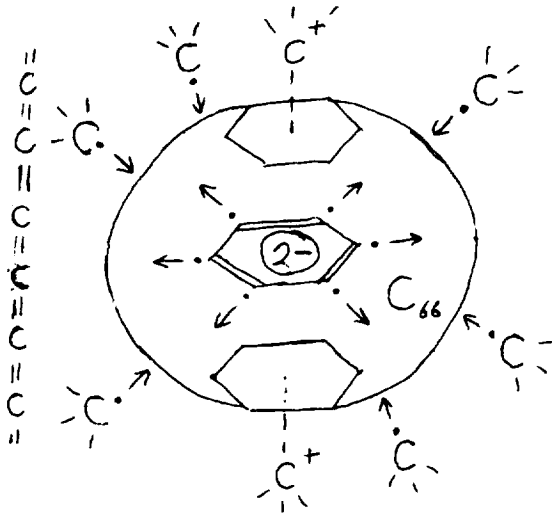

Chaoite

C_{68} (C_{74})

Fig. 4

THE ORIGIN OF MICROGRAINS

N91-15000

Theodore P. Snow[1], C. Gregory Seab[2], Richard H. Buss, Jr.[1], Karl Josafatsson[1], and Kris Sellgren[3]

[1] Center for Astrophysics and Space Astronomy
Campus Box 391
University of Colorado
Boulder, CO 80309

[2] Department of Physics
University of New Orleans
New Orleans, LA 70148

[3] Institute for Astronomy
University of Hawaii
2680 Woodlawn Dr.
Honolulu, HI 96822

Using ultraviolet and infrared techniques, we have investigated the origins of the tiny (~ 10A) grains whose presence in the interstellar medium is inferred from near-infrared photometry (Sellgren, Werner, and Dinerstein 1983; Sellgren 1984). We consider two possibilities: (1) that the grains are formed by condensation in stellar atmospheres; or (2) that they are formed by fragmentation of larger grains in interstellar shocks.

We have searched for evidence of very small grains in circumstellar environments by analyzing ultraviolet extinction curves in binaries containing hot companions, and by searching for the 3.3-micron emission feature in similar systems. The ultraviolet extinction curve analysis could be applied only to oxygen-rich systems, where small carbonaceous grains would not be expected, so these results provide only indirect information. We find a deficiency of grains smaller than 800A in oxygen-rich systems, consistent with theoretical models of grain condensation which suggest that grains grow to large sizes before injection into the interstellar medium. More direct information on carbonaceous micrograins was obtained from the search for the 3.3-micron feature in carbon-rich binaries with hot companions, whose ultraviolet flux should excite the tiny grains to emit in the infrared. No 3.3-micron feature was found, suggesting that the micrograins are absent in these systems.

In addition to the negative search for micrograins in circumstellar environments, we have also studied the possible association of these grains with shocks in the diffuse interstellar medium. Using IRAS colors as indicators of the presence or absence of the small grains (e.g Ryter, Puget, and Pérault 1987 and references cited therein), we have systematically searched for them in regions (reflection nebulae) expected to have sufficient ultraviolet flux to make them glow in the infrared. We find that the distribution is not uniform.

We propose that production of micrograins by fragmentation of larger grains in shocks could explain this uneven distribution. We note that the presence of micrograins in carbon-rich planetary nebulae may also be attributed to shock fragmentation of larger grains, since the rapid winds from planetary nebulae central stars could fragment larger grains formed during earlier mass-losing phases.

If the overall size distribution of grains in the diffuse interstellar medium is controlled by shock processing, as recent theoretical work has suggested (Seab and Shull 1985; McKee et al. 1987), then we must ask why the micrograins are not ubiquitous. It is possible that the general carbon abundance is variable with location in the galaxy, so that carbonaceous micrograins are produced only in specific regions. Another possibility is that the formation of micrograins requires shocks that are unusual in some respect such as velocity, so that only some shock-processed regions have the grains. Yet another possibility is that the micrograins are selectively destroyed by ultraviolet radiation in regions of high flux intensity (Ryter, Puget, and Pérault 1987).

Calculations in progress (Tielens et al. 1988) show that micrograins are rather easily produced in shocks; in fact it is difficult to explain how the larger grains responsible for visible extinction and polarization can survive. One suggestion is that grain coagulation is responsible, so that in effect all grains larger than micrograins are the result of the sticking of small grains to each other (Seab 1987). If so, the variable distribution of micrograins could be a density effect, since coagulation would be most efficient in relatively dense regions. Possible further observational tests of this picture will be discussed.

McKee, C. F., Hollenbach, D. J., Seab, C. G., and Tielens, A. G. G. M. 1987, Ap.J., 318, 674

Ryter, C., Puget, J. L., and Pérault, M. 1987, Astr. Ap., 186, 312

Seab, C. G. 1987, in Interstellar Processes, eds. D. J. Hollenbach and H. A. Thronson, Jr. (Dordrecht:Reidel), p. 491

Seab, C. G. and Shull, J. M. 1985, in Interrelationships Among Circumstellar, Interstellar, and Interplanetary Dust, NASA Conf. Pub. 2403, eds. J. A. Nuth III and R. E. Stencel (Washington:NASA), p. 37

Sellgren, K. 1984, Ap.J., 277, 623

Sellgren, K., Werner, M., and Dinerstein, H. 1983, Ap.J. (Lett.), 271, L13

Tielens, A. G. G. M., McKee, C., Seab, C. G., and Hollenbach, D. 1988, in preparation

Properties of Grains Derived from IRAS Observations of Dust

N91-15001

P.R. Wesselius
G. Chlewicki
R.J. Laureijs

Space Research Laboratory and Kapteyn Astronomical Institute
Groningen, The Netherlands

We have used the results of IRAS observations of diffuse medium dust to develop a theoretical model of the infrared properties of grains. Recent models based entirely on traditional observations of extinction and polarization include only particles whose equilibrium temperatures do not exceed 20 K in the diffuse interstellar medium. These "classical" grains, for which we have adopted the multipopulation model developed by Hong and Greenberg (1980), can explain only the emission in the IRAS 100 μm band. The measurements at shorter wavelengths (12, 25 and 60 μm) require two new particle populations. Vibrational fluorescence from aromatic molecules provides the most likely explanation for the emission observed at 12 μm, with PAH's containing about 10% of cosmic carbon. A simplified model of the emission process shows that PAH molecules can also explain most of the emission measured by IRAS at 25 μm.

We have identified the "warm" particles responsible for the excess 60 μm emission with small ($a \approx 0.01$ μm) iron grains. A compilation of the available data on the optical properties of iron indicates that the diffuse medium temperature of small iron particles should be close to 50 K and implies that a large, possibly dominant, fraction of cosmic iron must be locked up in metallic particles in order to match the observed 60 μm intensities. The model matches the infrared fluxes typically observed by IRAS in the diffuse medium and can also reproduce the infrared surface brightness distribution in individual clouds. In particular, the combination of iron and "classical" cool grains can explain the surprising observations of the 60/100 μm flux ratio in clouds, which is either constant or increases slightly towards higher opacities.

The presence of metallic grains has significant implications for the physics of the interstellar medium, including: 1) catalytic H_2 formation, for which iron grains could be the main site; 2) differences in depletion patterns between iron and other refractory elements (Mg, Si); 3) superparamagnetic behaviour of large grains with embedded iron clusters giving rise to the observed high degree of alignment by the galactic magnetic field.

SECTION VII: INTERSTELLAR DUST AND THE SOLAR SYSTEM

VII-A) SILICATE DUST IN COMETS

A SPECTRAL DIFFERENCE BETWEEN SILICATES IN COMET HALLEY AND INTERSTELLAR SILICATES

Humberto Campins and Eileen V. Ryan
Planetary Science Institute, SAIC, 2030 E. Speedway,
Suite 201, Tucson, Arizona, 85719 USA

We have obtained an intermediate resolution (1%) spectrum of the 8 to 13 μm region in Comet Halley which shows a prominent silicate emission feature with structure not observed before in other comets or in interstellar silicates (Figure 1). We confirm the presence of a strong 11.3 μm peak reported by Bregman et al. (1987) and find evidence for additional structure in the band. The 11.3 μm peak represents the main difference between the Halley Spectrum and that of Comet Kohoutek (Merrill 1974, Figure 2). The Kohoutek Spectrum is similar to that of the circumstellar shell around μ Ceph.

Based on a comparison with the spectra of Interplanetary Dust Particles (Sandford & Walker 1985, Figure 3), most of which are believed to be of cometary origin, we attribute the 11.3 μm peak to small crystalline olivine particles, although other minerals cannot be ruled out. Our interpretation is supported by the airborne observation of four emission peaks near 24, 28, 35 and 45 μm which can also be matched with iron-magnesium silicates including crystalline olivine. Other types of silicates (such as hydrated or amorphous) are necessary to explain the width and the 9.7 μm peak of the emission observed in Comet Halley. A complete discussion of this work has been submitted to the Astrophysical Journal.

REFERENCES

Bregman, J.D. et al.: 1987, Astron. Astrophys. 187, 616.

Merrill, K.M.: 1974, Icarus 23, 566.

Sandford, S.A. and Walker, R.M.: 1985, Astrophys. J. 291, 838.

FIGURE 1. The 8 to 12.9 μm spectrum of Comet Halley taken on 1986 January 16.08 UT using NASA's IRTF in Hawaii. The error bars are shown only when larger than the symbols. A 385K blackbody continuum has been fit to the first and last points and is represented by the solid line.

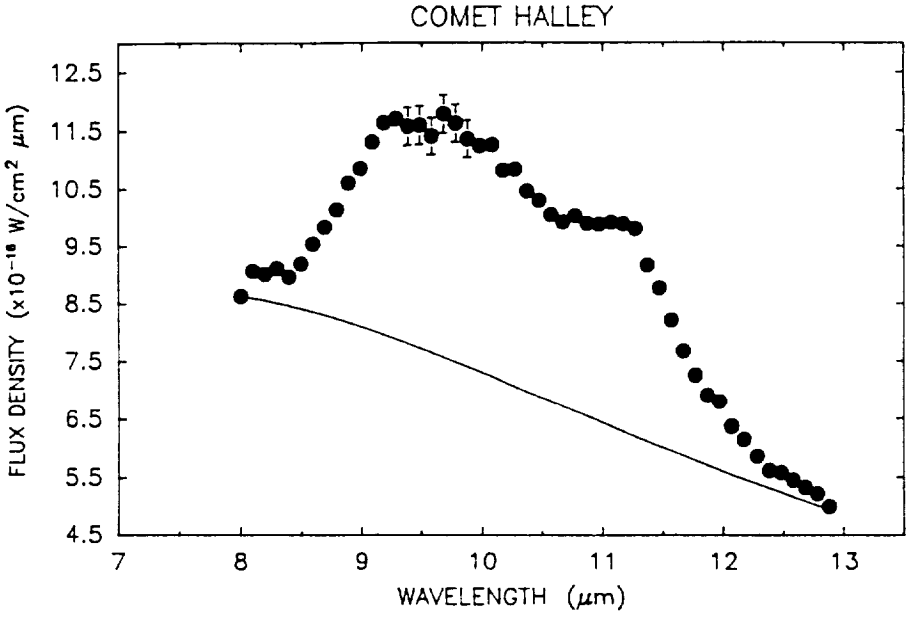

FIGURE 2. The "true" shape of the Comet Halley emission feature is shown (open circles) after dividing by the continuum in Figure 1. The Spectrum of Comet Kohoutek after dividing by a 600K continuum (Merrill 1974) is also shown (filled triangles) to illustrate the difference.

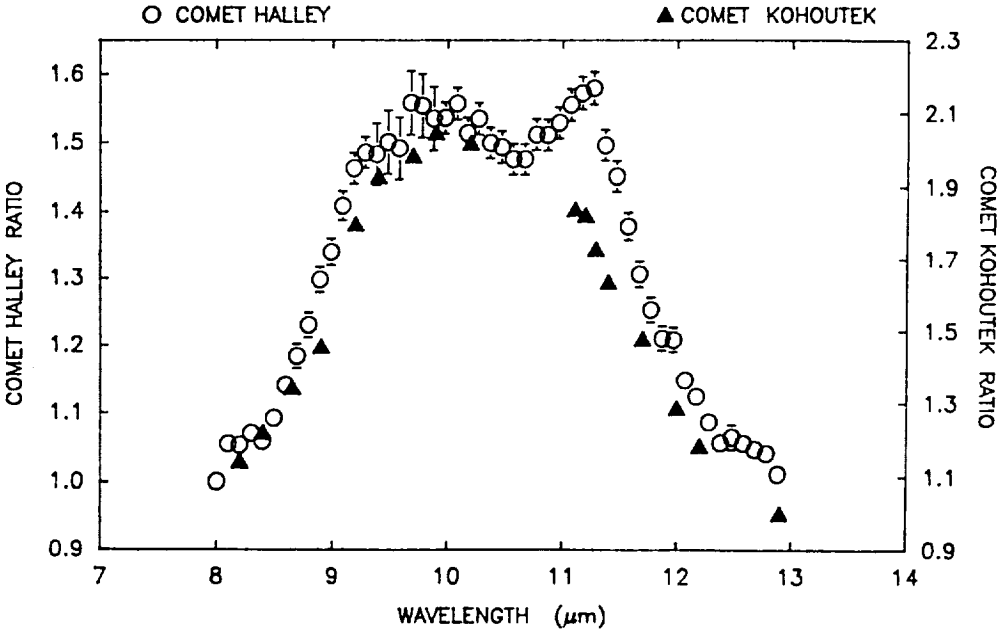

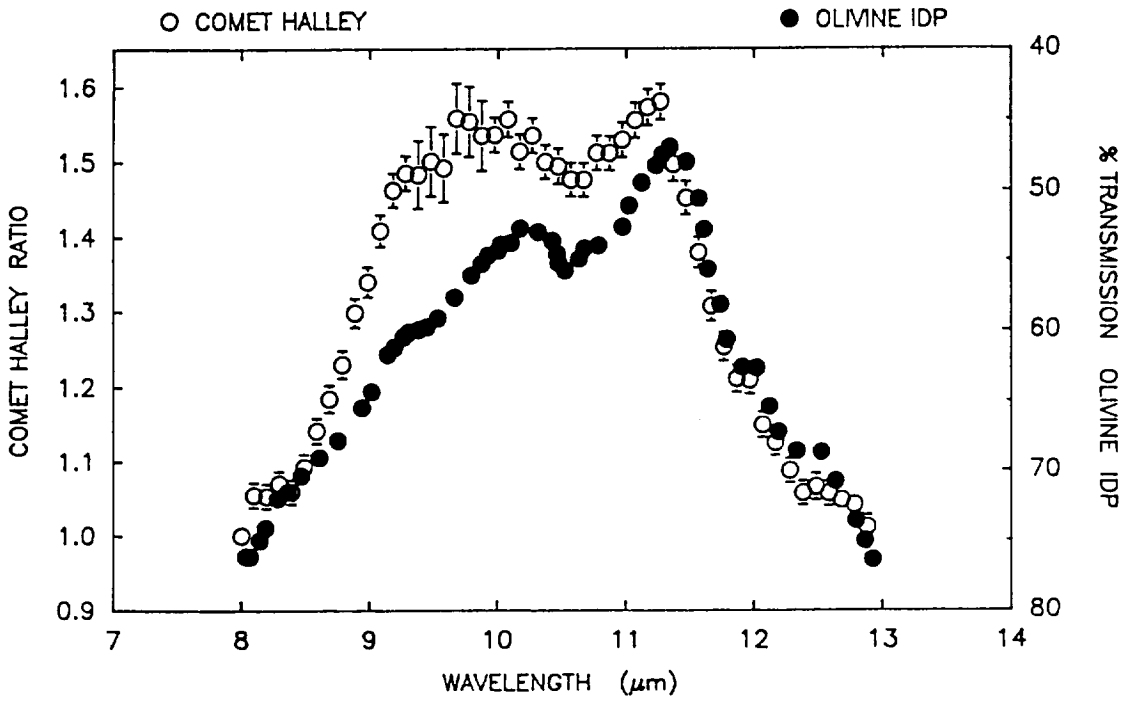

FIGURE 3. A comparison of our Comet Halley spectrum from Figure 2 (open circles) with the transmission spectrum (inverted) of the "Jedai" IDP (filled circles) from Sandford and Walker (1985). The spectrum of this particle is typical of those in the "olivine" spectral class. Note the correspondence between the two spectra longward of 10 μm.

THE NATURE OF COMETARY DUST AS DETERMINED FROM INFRARED OBSERVATIONS

K. S. Krishna Swamy, S. A. Sandford, L. J. Allamandola,
F. C. Witteborn and J. D. Bregman
NASA/Ames Research Center, Moffett Field, CA 94035

The infrared measurements of comets, the compositional information available from interplanetary dust particles (IDPs), and the recent results of flybys to Comet Halley can help in restricting the nature and composition of cometary dust models (c.f., Proceedings of the 20th ESLAB Symposium on Exploration of Halley's Comet, 1986). We have tried to incorporate some of these results into a coherent model to account for the observed cometary infrared emission.

The presence of 10 and 3.4 μm features in Comet Halley (c.f. Bregman et al. 1987; Wickramasinghe and Allen 1986) indicated the presence of at least two components in the grain material, namely silicates and some form of amorphous carbon. These two components could reside in separate grains or may be parts of composite particles. Both these cases have been considered (see Krishna Swamy et al. 1988a, 1988b). In the absence of refractive index data for cometary analogs, we have used the optical constants of olivine-rich lunar material 12009.48 (Perry et al. 1972) for the infrared region and that of α:C-H film for amorphous carbon (Angus et al. 1986). For the visible region, a value of m = 1.38-0.039i was used for the silicates, and values published by Arakawa et al. (1985) were used for the amorphous carbon. These materials should give a representative behavior of the expected results. Simple power law size distributions [$n(a) \propto a^{\alpha}$], as well as the one inferred for Comet Halley (Mazets et al. 1986a,b), were used. The absorption cross sections for single composition grains were calculated using Mie theory assuming spherical particles. Calculations for composite grains were made using Güttler theory.

The model results were compared to observational data. The strength of the 3.4 μm and 10 μm features relative to the adjacent continuum, as well as the slope of the continuum between 2500 and 1250 cm^{-1} (4-8 μm), were used as criteria for comparison. Model calculations with $\alpha = -3.5$, and also the size distribution function inferred for Comet Halley, with a mass fraction (X) of silicate to amorphous carbon grains of about 40 to 1 can fit the data. Several amorphous carbon features in the region 650 to 1400 cm^{-1} (6.1 to 7.1 μm) are expected to be present although they are weak. In fact, some of them may be present in the spectra of Comet Halley (Bregman et al. 1987). The study of IDPs indicate that some of the mineral grains are covered with a thin (< 100A) layer of carbonaceous material (see Sandford 1987). Results for a mixture of carbon-coated silicates and amorphous carbon grains require $X \approx 8$. However, silicate grains with thick carbonaceous coatings require $X > 1$ to fit the 3.4 μm feature, which is probably not reasonable in view of the lower C/Si ratio observed in IDPs.

In view of the success of the model, we have also applied it to the extensive broadband infrared observations of Comets Halley and West carried out for a wide range of heliocentric distances. The agreement for Comet Halley is quite good over the entire range of heliocentric

distances (0.59 to 2.80 AU) and wavelengths (3.8 to 20 μm). In addition, the model can also qualitatively explain the observed variation of the 3.4 μm feature with heliocentric distance in Comet Halley. As a typical case, we show in Figure 1 the results of comparison for Comet West.

Conclusions: (1) A good match is obtained for the infrared spectra of Comets Halley and West from a 40 to 1 mixture of silicate and amorphous carbon grains with a $a^{-3.5}$ size distribution function. (2) The results are consistent with compositional constraints provided by IDPs and Halley flyby data. (3) The variation of grain temperature with heliocentric distance appears to account for the major changes observed in cometary spectra.

References:

Angus, J. C., Koidl, P. and Domitz, S.: 1986, In Plasma Deposited Thin Films, ed. J. Mort and F. Jansen (Boca Raton: CRC Press), p. 89.

Arakawa, T., Dolfini, S. M., Ashley, J. C. and Williams M. W.: 1985, Phys. Rev. 31B, 8097.

Bregman, J. D., Campins, H., Witteborn, F. C., Wooden, D. H., Rank, D. M., Allamandola, L. J., Cohen, M. and Tielens, A. G. G. M.: 1987, Astr. Ap. 187, 616.

Krishna Swamy, K. S., Sandford, S. A., Allamandola, L. J., Witteborn, F. C. and Bregman, J. D.: 1988a, Icarus (in press).

Krishna Swamy, K. S., Sandford, S. A., Allamandola, L. J., Witteborn, F. C. and Bregman, J. D.: 1988b, Ap. J. (submitted).

Mazets, E. P., et al.: 1986a, Nature 321, 276.

Mazets, E. P., et al.: 1986b, In the Proceedings of the 20th ESLAB Symposium, ESA SP-250, Vol. 2, p. 3.

Ney, E. P. and Merrill, K. M.: 1976, Science 194, 1051.

Perry, C. H., Agarwal, D. K., Anastassakis, E., Lowndes, R. P., Rastogi, R. P. and Tornberg, N. E.: 1972, Moon 4, 315.

Sandford, S. A.: 1987, Fund. Cosmic Phys. 12, 1.

Wickramasinghe, N. C. and Allen, D. A.: 1986, Nature 323, 44.

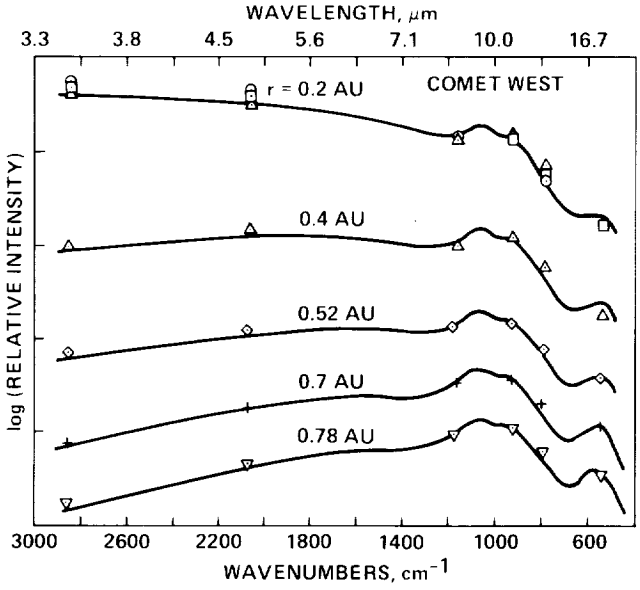

Figure 1 - Comparison of the calculated and observed 3.4 - 25 μm emission from Comet West (Ney and Merrill 1976) at solar distances of 0.2, 0.4, 0.52, 0.7, and 0.78 AU. (Model curves for $\alpha_1 = -3.5$, $\alpha_2 = -3.2$, and X = 40).

10 μm SPECTRAL STRUCTURE IN COMETS

David K. Lynch*, Ray W. Russell*, and Humberto Campins**

*The Aerospace Corporation, Space Sciences Laboratory
**Planetary Science Institute

Abstract

The 10 μm spectra of comets Halley (1982i), Wilson (1986l), Kohoutek (1973f) and Bradfield (1987s) are presented and compared. The silicate emission profiles of Halley and Bradfield are seen to be remarkably similar in that both contain a sharp break in the spectrum at 11.3 μm. Comet Bradfield does not show the same double peak structure seen in olivine and reported in Comet Halley by Campins and Ryan (1988) and Bregman, et al. (1987). We interpret the 11.3 μm signature as being due to olivine-type dust grains with at least some degree of crystallinity. Olivine alone is not enough to reproduce the shape of the 10 μm structure. However, in view of our past success in fitting interstellar dust features with the emissivity profile obtained from amorphous grains produced by laser-vaporizing olivine, this is a very appealing identification. We note that there are significant variations in olivine spectra due to compositional differences, grain size distribution and related grain temperature variations to make the olivine identification tentative. We further tentatively identify the 9.8 μm feature in Halley as being due to either amorphorous olivine or a phyllosilicate ("layer lattice"). Neither the spectra of Halley, Kohoutek, nor Bradfield exhibited the 12.2 μm feature seen in Comet Wilson, which may prove diagnostic of the composition or thermal history differences between these comets. IR spectra of various mineral samples are discussed in terms of their match to cometary spectra.

[This work was supported in the Space Sciences Laboratory by the Aerospace Sponsored Research Program and NASA contract NAS2-12370, and at the Planetary Science Institute by NASA and the NSF.]

I. Introduction

The composition of interstellar dust is so poorly known that, until recently, any statement about its make-up needed to be heavily qualified. Indeed, identifications in the 10 μm thermal window have to date amounted to little more than vague associations of the "silicate" emission feature to grossly similar features in terrestrial (and some lunar) silicates. It was shown theoretically by Gilman (1969) that it is plausible that silicates could condense from a hot cloud as it cools. This work has recently been extended by, for example, Grossman and Larimer (1974). Several workers (e.g. Day and Donn, 1978) obtained laboratory spectra which exhibited absorptivity (i.e., emissivity) peaks which were similar to the astrophysical feature at 9.8 μm, but which either had a central wavelength that did not match that seen in astronomical spectra, or did not have enough of a long wavelength tail. Stephens and Russell (1976), using laser vaporized sample of olivine were able to match the 10 μm feature in the Trapezium, and later the twenty μm feature as well (Cohen, et al., 1980). The first in situ experimental evidence that condensed silicates might indeed be present in comets was obtained by the mass spectrometer on the Halley flyby which samples comet dust (Kissel, et al., 1986).

Such compelling results add scientific weight to but not proof of the larger assertion that interstellar material has a large proportion of siliceous material (or any of the other proposed celestial grain materials, such as polycyclic aromatic hydrocarbons, hydrogenated amorphous carbons, etc.). An additional concern is that silicate-to-silicate variations in the type of fine spectral structure (features whose widths $\Delta\lambda$ are of the order of $\lambda/100$) necessary to uniquely identify the composition is complex and subtle. In view of the now well established laboratory demonstration that fine spectral features are often lost when the crystals are heated and become amorphous, the need to proceed carefully cannot be over emphasized.

Comets provide a rare astrophysical opportunity to identify the chemical composition of solar system dust because their thermal emission originates in simple, nearly isothermal, optically thin dust clouds. In this paper we analyze a simple subset of thermal emission from comets near 10 μm. The goal is to identify those features which are: 1) real, 2) present in more than one spectra, in an effort to help identify the mineralogical species responsible for thermal dust emission in comets. As an intermediate step in this analysis one derives temperatures for the cometary grains from the (assumed) grey continuum and compares the results with the blackbody radiative equilibrium temperature for the appropriate heliocentric distance to derive limits on particles sizes.

II. Five Spectra of Four Comets

Figure 1 shows five spectra taken of four comets: two of Halley, and one each of Bradfield (1987s), Wilson (1986l) and Kohoutek (1973f). Although the true shape of the spectra are accurately represented, they have been multiplied by appropriate intensity factors for convenient placement on the graph. Also note the overlay of a 300 K grey body for shape comparison. Table 1 gives the source of data and the continuum color temperature.

Table 1

		T(K)
A.	Bradfield 1987s (Lynch and Russell, 1988)	475
B.	Kohoutek 1973f (Merrill, 1974)	600
C.	Halley 1982i (Campins and Ryan, 1988)	385
D.	Halley 19821 (Bregman, et al., 1987)	320
E.	Wilson 1986s (Lynch, et al., 1988)	300

While it is obvious that the slope of any portion of a spectrum are seriously influenced by the temperature of the blackbody spectral shape it follows, the locations where the slope changes abruptly will be independent of the underlying blackbody temperature. With this in mind, we note two aspects common to most of the spectra of figure 1, and possible additional structure in the spectra of Comet Halley (see also Fig. 3).

1. A break in spectra A,C,D and possibly B at about 11.3 μm.
2. A break in spectra A,B,C and possibly D at about 9 μm.
3. Double-peak structure (9.8 and 11.3 μm) in C and D.

The meaning of these features depends on where the continuum is drawn. They could be either: a) two broad emission features at 9 or 9.8 and 11.3 μm, or b) a single broad dip at 10 μm. Campins and Ryan (1988) have proposed that olivine interplanetary dust particles (IDPs) can explain the shape of the Halley spectra longward of 10 μm.

III. Spectra of Olivine

Olivine is common rock-forming mafic (rich in Mg and Fe) mineral occurring widely on Earth. Its composition varies within two well-defined limits, being an isomorphous solid solution between forsterite (Mg_2SiO_4) and fayalite (Fe_2SiO_4).
From the low pressure gas phase olivine condenses at around 1300 K (Grossman and Larimer, 1974) although lower temperature condensates with closely related chemical composition occur down to around 800 K. Figure 2 shows several IR spectra of olivine digitized from publications of A. Hunt and Salisbury (1974), B. Zaikowski (1975), C. Day (1975), and D. Koike, et al. (1981). Several properties of the spectra are evident:

1. Two prominent peaks occur in the 10 μm region, at around 10.1 and 11.4 μm.
2. The peaks occur at somewhat different wavelengths in different samples.
3. The shapes of the peaks are different in different samples.

These spectra, though showing some differences, suggest that the spectra of olivine could be used to identify mineralogical content of cometary dust, providing that olivine's spectral variations cannot be duplicated by spectra of other minerals.

IV. Is Comet Halley's Dust Made of Olivine?

Figure 3 shows Campins and Ryan's fit of the IRTF Halley spectrum to Sandford and Walker's (1985) olivine interplanetary dust particle. It is evident that:

a. Halley's spectrum's peaks ..... ≈ 9.8 and ≈ 11.3 μm
b. Olivine IDP spectrum's peaks ..... ≈ 10.3 and ≈ 11.3 μm
c. Olivine (Fig. 2) spectrum's peaks ..... ≈ 10.1 and ≈ 11.3 μm

From this analysis we see that the structure of Halley's spectrum and olivine's spectrum, though similar, are significantly different, shortward of 10 μm. Although the 10.1 to 10.3 μm olivine features are observed to change wavelength in various samples, no crystalline olivine sample was found that had the short wavelength peak shifted to ≈ 9.8 μm. The discrepancy is enough to suggest that olivine is either not the sole content of the dust, or if it is, it's lattice structure (and thus spectral structure) has been altered in a significant manner. An equally plausible scenario involves a mineral component as yet unidentified. The main appeal of olivine as a major constituent in cometary dust is that a large fraction of IDPs contain olivine-like material and comets are believed to be the main source of IDPs (Sandford and Walker 1985). Furthermore, an amorphous olivine emission spectrum has been shown to match the 10 and 20 μm emission profile (Stephens and Russell, 1979).

V. What Causes the 9.8 μm Feature?

Our approach to identifying the 9.8 μm feature in Comet Halley's spectrum is two-fold: 1) locating minerals with known 9.8 μm emission features and compositions similar to olivine, and 2) locating minerals with the 9.8 μm feature that occur in IDPs.

Taking our cue from the tentative olivine identification of the 11.3 μm feature, we have searched for minerals whose spectra show the similar structure and which would be expected to condense from a low density plasma around 1300 K as olivine does. The following minerals are possible candidates for the mineral responsible for the 9.8 μm feature.

1. Andalusite ..... $AlSiO_5$
2. Pectolite ..... $NaCa_2Si_3O_8OH$
3. Cordierite ..... $(Mg,Fe^{3+})_2Al_4Si_5O_{18}$
4. Garnierite ..... $(Ni,Mg)_3Si_2O_5(OH)_7$
5. Hisingerite ..... $Fe_2Si_2O_5(OH)_4 \cdot 2H_2O$

The spectra of these minerals are shown in figure 4.

Andalusite is considered a metamorphic mineral and, being trimorphic with neosilicates kyanite and sillimanite, would not normally be expected to form directly from a low density plasma. However, it is not known what changes would take place in corundum (Al_2O_3) to alter it to andalusite on solar system time scales. Kyanite shows a feature too broad to reproduce the 9.8 μm cometary feature and sillimanite has a completely different 10 μm spectrum. Pectolite is an inosilicate which has both 9.8 and 11.3 μm features. Cordierite is a cyclosilicate and is commonly found with polymorphs of Al_2O_5 (see #1 andalusite above). Except for being metamorphic, cordierite might be considered a suitable candidate. Garnierite, though possessing the proper spectral shape, is probably too rare to be seriously considered because of the low nickel abundance in the solar system. Little is known about hisingerite.

The cometary feature at around 9.8 ± 0.2 μm (figure 3) may well be due to the Si–O stretching mode in phyllosilicates (Farmer, 1974). Such a feature has been seen in IDPs (Sandford and Walker, 1985), some classes of which also show the 11.3 μm feature attributed to olivine (Campins and Ryan, 1988).

Sandford and Walker found that the best IDP fit to Merrill's Kohoutek spectrum was a roughly equal mixture of layer–lattice silicates and pyroxenes (phyllosilicates and inosilicates). We find the best fit to Campins and Ryan's spectrum of Comet Halley would be roughly equal mixtures of phyllosilicates and neosilicates (olivines).

Finally, we note that amorphous olivine (Stephens and Russell, 1979) has a single feature at ≈ 9.8 μm (see Fig. 5). In view of the identification of the 11.3 μm feature with crystalline olivine, it is reasonable to suggest that both peak in Comet Halley's spectrum can be explained by a mixture of amorphous and crystalline olivine.

VI. Conclusions

Five spectra of four comets are shown to contain enough common spectral features to begin making tentative mineralogical identifications of the dust. Crystalline olivine is a likely candidate for reproducing the 11.3 μm feature in some comets. Other minerals acting together (possibly amorphous olivine and phyllosilicates similar to those identified in IDP must be present to explain the 9.8 μm feature in Comet Halley's spectrum.

References

Bregman, J.D., et al., 1987, Astron. and Astrophys., 187, 616.
Campins, H. and Ryan, E.V., 1988, (preprint).
Cohen, N.L., McCarthy, J.F., Russell, R.W. and Stephens, J.R., 1980, B.A.A.S., 11, 610.
Day, K.L., 1975, Astrophys. J., 199, 660.
Day, K.L., and Donn, B., 1978, Astrophys. J. (Letters), 222, L45.
Farmer, V.C., 1974, The Infrared Spectra of Minerals, Mineralogical Society of London.
Ferraro, J.R., 1982, The Sadtler Infrared Spectra Handbook of Minerals and Clays, Sadtler Research Laboratories, Philadelphia.
Gilman, R.C., 1969, Astrophys. J. (Letters), 155, L185.
Grossman, L. and Larimer, J.W., 1974, Rev. Geophys. and Space Phys., 12, 71–101.
Hunt, G.R. and Salisbury, J.W., 1974, AFCRL-TR-74-0625.
Kissel, J., et al., 1986, Nature, 321, 280–282.
Koike, C., Hasegawa, H., Asada, N. and Hattori, T., 1981, Astrophys. Space Sci., 79, 77.
Lynch, D.K., et al., 1988, (preprint).
Merrill, K.M., 1974, Icarus, 23, 566–567.
Russell, R.W., Lynch, D.K., and Chatelain, M., 1988, Bull. A.A.S., 20, 724.
Sandford, S.A. and Walker, R.M., 1985, Astrophys. J., 291, 838.
Zaikowski, A., Knacke, R., and Porco, C.C., 1975, Astrophys. Space Sci., 35, 97.

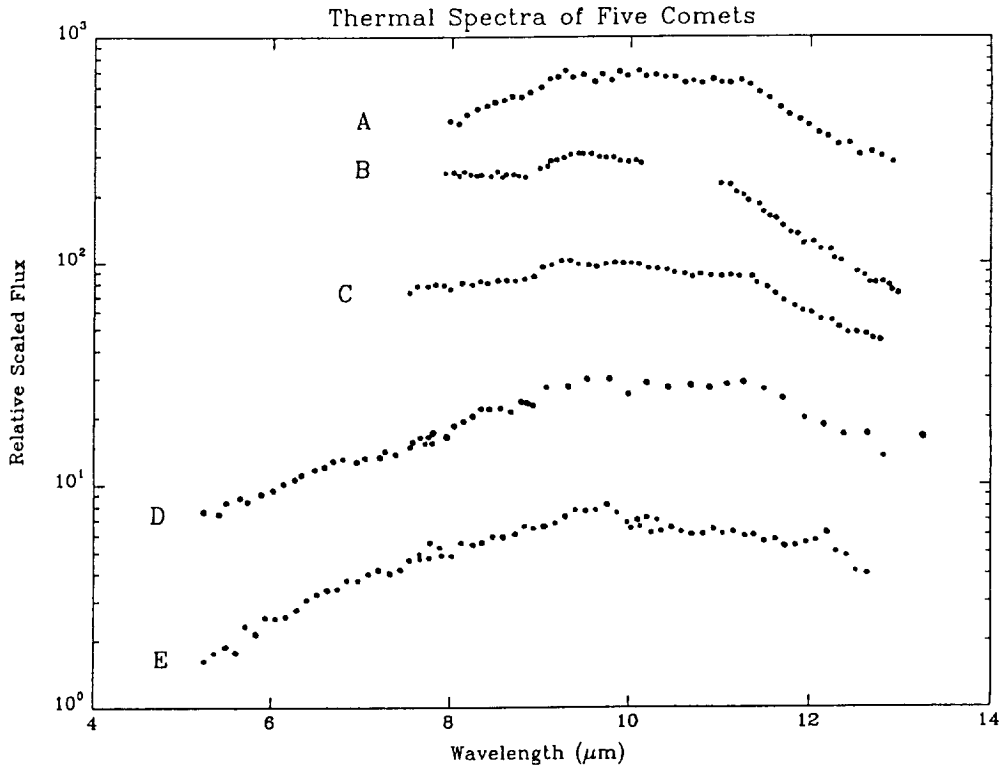

Figure 1

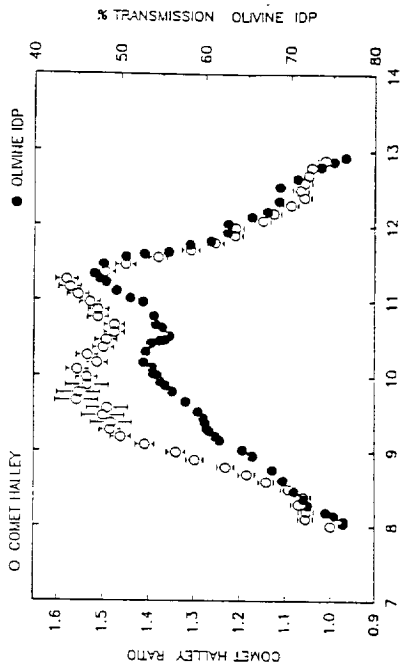

Figure 3

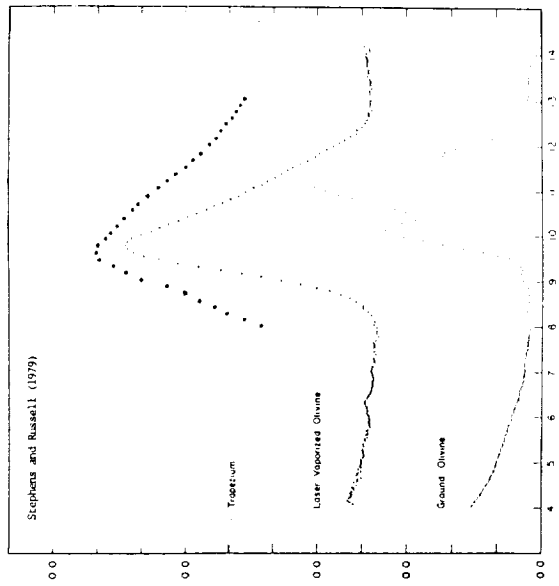

Figure 5

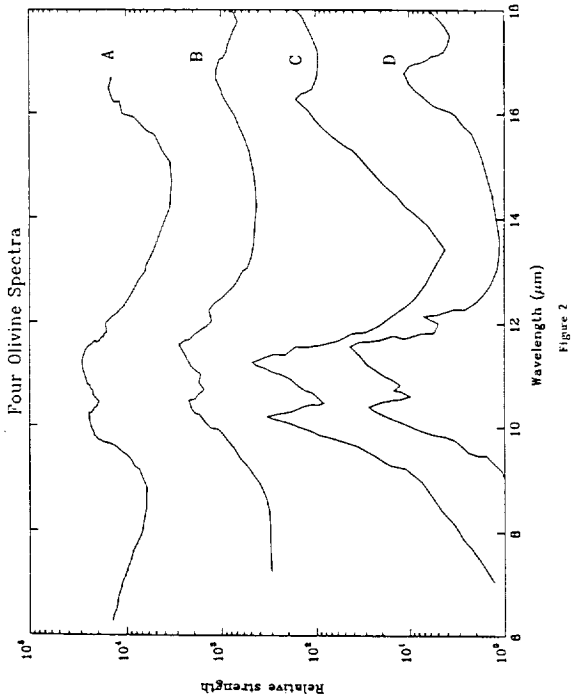

Figure 2

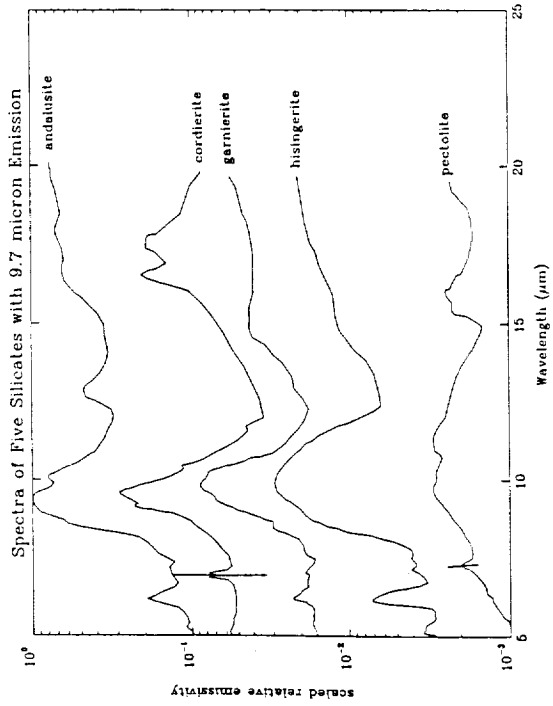

A Comparative study of the Continuum and Emission Characteristics of Comet Dust
I. Are the Silicates in Comet Halley and Kohoutek Amorphous or Crystalline ?

Zhao Nansheng, J. Mayo Greenberg and J. Hage
Laboratory Astrophysics, University of Leiden

Abstract

A continuum emission was subtracted from the 10 μm emission observed towards comets Halley and Kohoutek. The 10 μm excess emissions have been compared with BN absorption and laboratory amorphous silicates. The results show that cometary silicates are predominantly amorphous which is consistent with the interstellar dust model of comets.

1. Continuum baseline

A baseline has been calculated and a continuum emission was subsequently subtracted from the 10 μm emission features observed towards Comet Halley (Bregman et al. 1987) and Kohoutek (Merrill 1974). The IR continuum emission of a comet includes two parts: non-neutrally scattered sunlight and thermal emission.

2. 10 μm excess emission from Comets Halley and Kohoutek

The 10 μm feature of Comet Halley and Comet Kohoutek has been observed at a resolution probably sufficient to distinguish crystalline and amorphous silicates.

A comparison between the material responsible for the 10 μm feature in comets and interstellar dust may reveal something about cometary origin and evolution. Using the baseline in fig. 1 we obtain the excess emission above the 10 μm continuum observed towards Comet Halley and Kohoutek.

3. Evidence for the dominance of amorphous silicates in Comets

Figures 2, 3 and 4 show that the cometary 10 μm feature is similar to the BN object (Willner et al. 1982) which, in turn, resembles a combination of laboratory amorphous silicates (Day 1979).

The 10 μm feature of Comet Halley is distinguished by an extra 11.2 μm band which probably is produced by crystalline olivine (Sandford and Walker 1985). The question is how much crystalline olivine is present?

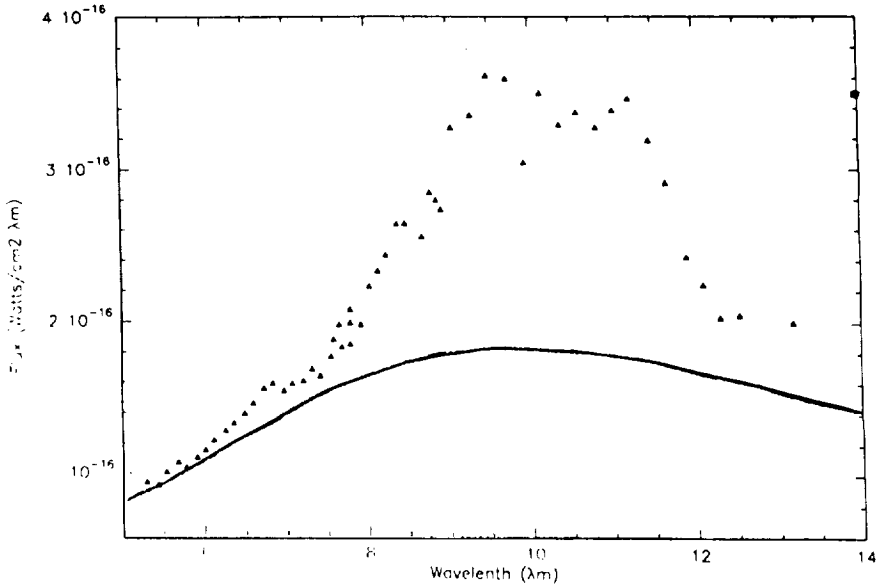

Fig. 1. Observed 10 μm emission (▲) and base line for Comet Halley (Heliocentric distance of Comet = 1.24–1.3 A.U. T = 290 K. Note that the base line or continuum here is different from Bregman et al. (1987).

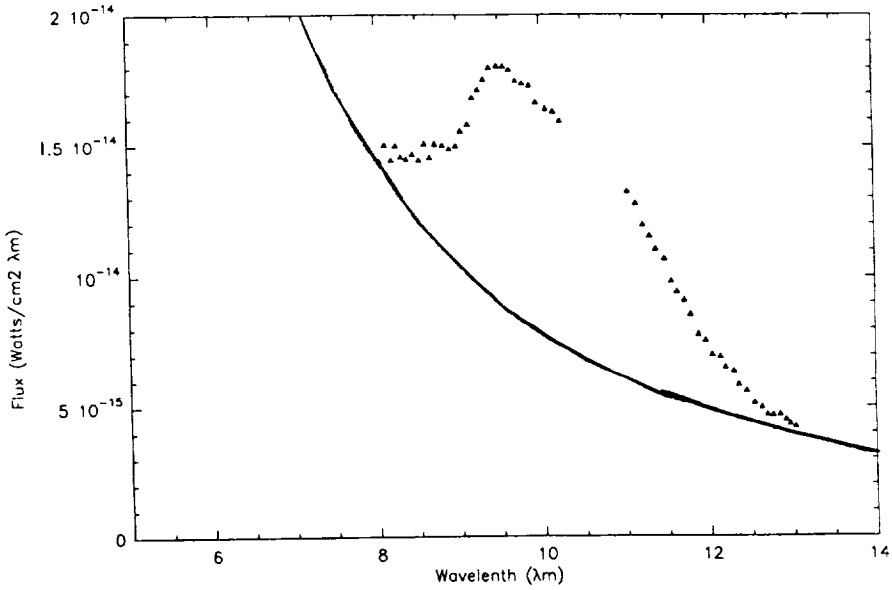

Fig. 2. Observed 10 μm emission (▲) and base line for Comet Kohoutek (Heliocentric distance of Comet = 0.4–0.23 A.U. T = 600 K.

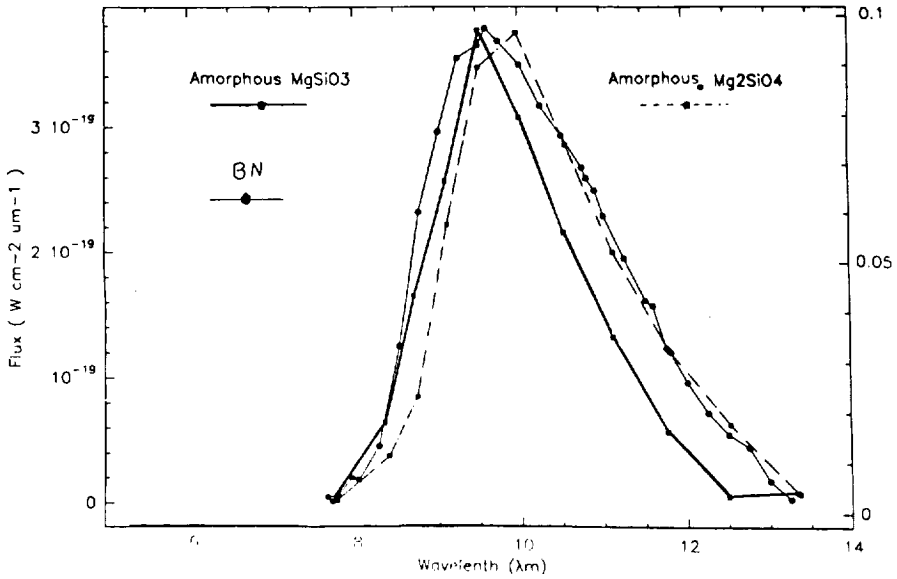

Fig. 3. Comparison of the 10 μm feature of BN and laboratory amorphous silicates.

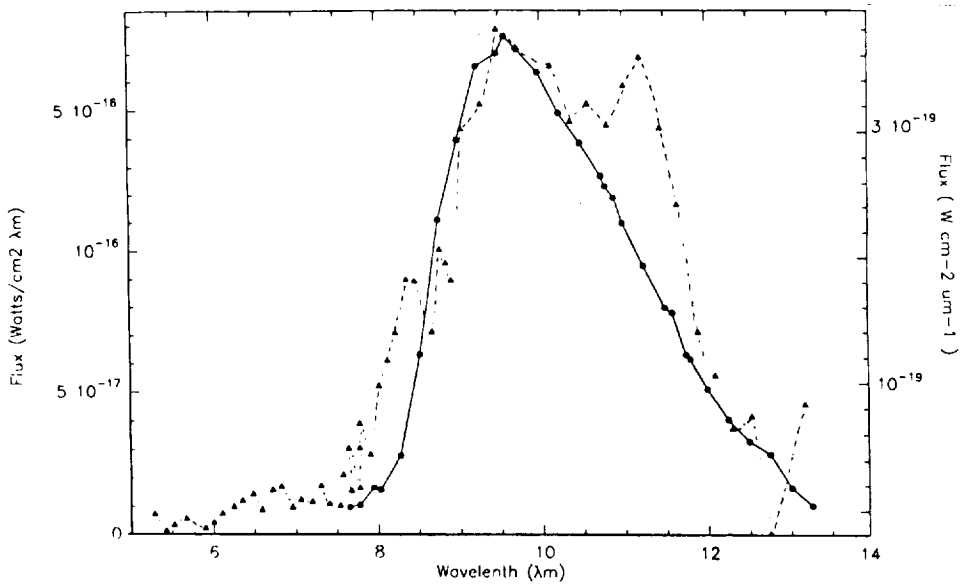

Fig. 4. Comet Halley emission (---▲---) compared with BN absorption (—●—).

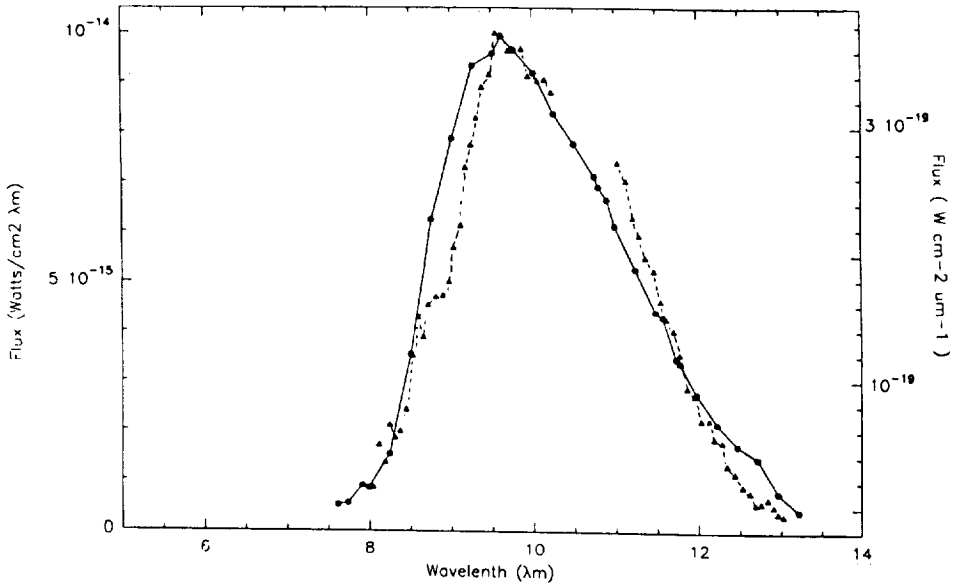

Fig. 5. Comet Kohoutek emission (---▲---) compared with BN absorption (—●—).

Since the extinction efficiency of crystalline relative to amorphous silicates is Q_{cry} / Q_{amo} = 10 (Day et al. 1974), the extra feature represents a small addition by mass. Subtracting the amorphous component (BN) from the total of Comet Halley, yields a peak ratio I_{cry} / I_{amo} = 6.5 : 14 which implies a mass ratio of crystalline to amorphous silicate = 0.05, which is indeed quite small !

4. Discussion and Conclusion

1) Cometary silicates are predominantly similar to interstellar silicates. For a periodic comet like Comet Halley, it is to be expected that some of the silicate may have been heated enough to convert to crystalline form. But apparently, this is only a small fraction of the total.

2) A comparison of Comet Halley silicates with a combination of the crystalline forms observed in IDP's seemed reasonable at first sight (Walker 1988, Brownlee 1988). But, if true, it would imply that the total silicate mass in Comet Halley dust is lower than that given by mass spectrometry data of Kissel and Krueger (1987). They estimated m_{org} / m_{sil} = 0.5 while using crystalline silicate to produce the 10 μm emission would give m_{org} / m_{sil} = 5 (Greenberg et al. 1988). This is a factor of 10 too high.

References

Bregman, J.D. et al.: 1987, *Astr. Ap.* **187**, 616.

Brownlee, D.E., *Infrared Observation of Comets Halley and Wilson*, NASA Conf. Publ. (ed. Hanner, M.).
Day, K.L., Steeyer, T.R., and Huffman, D.R.: 1974, *Ap. J.* **191**, 415.
Day, K.L.: 1979, *Ap. J.*, **234**, 158.
Greenberg, J.M., Zhao, Nansheng, and Hage, J.: 1988, *to be submitted to Nature.*
Kissel, J., and Krueger, F.R.: 1987, *Nature* **326**, 755.
Merrill, K.M.: 1974, *Icarus* **23**, 566.
Sandford, S.A., Walker, R.M.: 1985, *Ap. J.* **291**, 838.
Walker, R.M.: 1988, *Infrared observations of Comets Halley and Wilson*, NASA Conf. Publ. (ed. Hanner, M.).
Willner, S.P., et al.: 1982, *Ap. J.* **253**, 174.

VII-B) CARBONACEOUS DUST IN COMETS

THE 3.4 MICRON EMISSION IN COMETS

T.Y. Brooke,* R.F. Knacke,* T.C. Owen,* and A.T. Tokunaga**
*Dept. of Earth and Space Sciences, SUNY at Stony Brook, Stony Brook, NY 11794-2100 USA
**Institute for Astronomy, Univ. of Hawaii, 2680 Woodlawn Dr., Honolulu, HI 96822 USA

Emission features near 3.4 μm were detected in comet Bradfield (1987s) on 17 Nov 1987 UT, and, marginally, on two earlier dates, with the Cooled Grating Array Spectrometer at the NASA IRTF (Brooke et al., 1988b). The central wavelength (3.36 μm) and width (~0.15 μm) of the strongest feature coincide with those observed in comet Halley. A weaker emission feature at 3.52 μm and a strong feature extending shortward of 2.9 μm were also detected. This brings the number of comets in which these three features have been seen to three, two new (Bradfield, Wilson) and one old (Halley).

It seems almost certain that the 3.4 μm features are emissions by C-H groups in complex molecules. Based on the similarity of the 3.4 μm features in comets Halley and Wilson, we suggested that a particular set of organic compounds may be common to all comets (Brooke et al. 1988a). The absence of the feature in some comets could then be due to photodestruction or evaporation of the organics when the comet approaches the sun, in combination with a predominance of thermal emission from non C-H emitting grains. Detection of the 3.4 μm emission feature in comet Bradfield at r = 0.9 AU provides support for this argument.

Complex organics in comets could have been formed by particle irradiation of parent ices in the nucleus or been incorporated as grains at the time the comets formed. Since the most heavily irradiated layers of Halley would have been lost in its hundreds of perihelion passages, we believe the more likely explanation is that the 3.4 μm emitting material was incorporated in comet nuclei at the time of formation.

The 3.4 μm comet feature resembles, but is not identical to, the interstellar 3.29 μm (and longer wavelength) emission features and the broad 3.4 μm feature seen in absorption toward the Galactic center. Detailed comparisons of cometary and interstellar organics will require comet spectra with signal-to-noise and spectral resolution comparable to that available in spectra of the interstellar medium. Such observations are currently being planned.

Brooke, T.Y., Knacke, R.F., Owen, T.C., and Tokunaga, A.T.:1988a, Ap. J., in press.

Brooke, T.Y., Knacke, R.F., Owen, T.C., Tokunaga, A.T., Mumma, M., Reuter, D., and Storrs, A.: 1988b, in preparation.

THE PRE- AND POST-ACCRETION IRRADIATION HISTORY OF COMETARY ICES

Christopher Chyba and Carl Sagan
Laboratory for Planetary Studies, Cornell University, Ithaca, NY 14853-6801 USA

Comets Halley and Wilson exhibited similar 3.4μm emission features at $\sim$1 AU from the Sun. A simple model of thermal emission from organic grains fits the feature, provides optical depths in good agreement with spacecraft measurements, and explains the absence of longer-wavelength organic features as due to spectral heliocentric evolution (Chyba and Sagan, 1987). The model utilizes transmission spectra of organics synthesized in the laboratory by irradiation of candidate cometary ices; we have long noted that related gas-phase syntheses yield polycyclic aromatic hydrocarbons, among other organic residues (Sagan *et al.*, 1967).

We have previously concluded (Chyba and Sagan, 1987) that Halley's loss of several meters' depth with each perihelion passage, combined with the good fit of the Halley 3.4μm feature to that of comet Wilson (Allen and Wickramasinghe, 1987), argues for the primordial—but not necessarily interstellar—origin of cometary organics. Here we examine the relative importance to the formation of organics of the variety of radiation environments experienced by comets. We conclude that there is at present no compelling reason to choose any of three contributing mechanisms (pre-accretion uv, pre-accretion cosmic ray, and post-accretion radionuclide processing) as the most important.

The irradiation environments experienced by cometary ices (summarized in the accompanying table) may be divided into four categories: (1) Pre-accretion irradiation of interstellar dust by uv and low-energy cosmic rays, (2) Post-accretion irradiation of cometary interiors by incorporated radionuclides, (3) Cosmic ray irradiation over 4.6 Gyr of a comet's outer $\sim$ 10–100 m, and (4) Solar wind and ultraviolet irradiation to a depth $\lesssim$ 0.1μm during a comet's typically $\sim$1 Gyr residence in the inner Oort cloud, $\sim$3.5 Gyr residence in the outer Oort cloud, and eventual passage(s) through the inner solar system.

Even for a dynamically new comet such as Wilson, environment (4) will be unimportant for the formation of observable organics, as the outer 0.1μm of surface will be quickly shed during a comet's first passage through the inner solar system.

Ryan and Draganić (1986) have calculated the irradiation of a comet's outer layers by cosmic ray protons with energies >1 MeV. Cometary ice at a depth of 1 m experiences a dose $\sim 10^4$–10^5 Mrad; at 10 m, a dose $\sim 10^3$ Mrad; and negligible dose at much greater depths. Environment (3) may thus be contributing organics to the spectrum of the dynamically new comet Wilson, but not to that of Halley.

Below a depth $\sim$10 m, radionuclides incorporated into the comet at the time of its accretion [environment (2)] provide a dose $\sim 10^3$ Mrad throughout the entire cometary interior (Draganić *et al.*, 1984). About 80% of this dose would have been due to the extinct radionuclide ^{26}Al, thus dating from the first $\sim 10^6$ yr of a comet's lifetime. Such a calculation takes $^{26}Al/^{27}Al \sim 5 \times 10^{-5}$, as implied by isotopic analysis of meteorites, and assumes essentially cosmic abundances for most other elements. There is reason to believe this ^{26}Al abundance to be typical of

bulk interstellar dust composition, as three independent γ–ray measurements (by HEAO 3, the SMM satellite, and a balloon flight) find $^{26}Al/^{27}Al \sim 1 \times 10^{-5}$ in the ISM (Wasserburg, 1987). A ratio $^{26}Al/^{27}Al \sim 10^{-5}$ would melt no more than the innermost core of a comet ~5 km in radius (Wallis, 1980).

Both uv and and low–energy cosmic ray irradiation should significantly process volatile ices on grains in the ISM [environment (1)]. Over a $\sim 10^8$ yr molecular cloud residence, interstellar grains experience $\sim 10^7$ Mrad due to uv photons (Greenberg and Grim, 1986), and 5×10^4 Mrad due to low–energy cosmic rays (Strazzulla *et al.*, 1983). Both doses may increase substantially for those grains cycled between diffuse and dense clouds, although optically–thick clouds will shield dust from uv.

Strazzulla *et al.* (1983) have experimentally measured polymerization cross–sections for 0.1–2 MeV protons on C–rich ices; they conclude that, at the cosmic ray doses cited above, C–containing molecules in interstellar grains will be totally polymerized in times less than typical cloud lifetimes. Thus the fact that a grain's uv dose may be $\sim 10^2$–10^3 times that due to low–energy cosmic rays is not decisive for the two mechanisms' importance to the formation of interstellar organics. Even in the total absence of uv processing (as in an optically thick cloud), complete polymerization of C–containing ices would occur.

Comets must contain both solar nebula and interstellar condensates; the former may well be non–negligible (Geiss, 1987). C–containing solar nebula condensates will be irradiated by incorporated cometary radionuclides; the resulting dose $\sim 10^3$ Mrad should polymerize more than half of the C atoms present (Strazzulla *et al.*, 1983). Thus it appears that both pre– and post–accretion environments may be of importance for the formation of cometary organics. We are undertaking a well–characterized study of the infrared spectral evolution of candidate ice residues, with irradiation extending from radionuclide to interstellar doses. These experiments may exclude one or more irradiation environments: Only certain doses may yield spectra providing good fits to the 3.4μm feature in comets Halley and Wilson.

Allen, D.A. and Wickramasinghe, D.T.: 1987, *Nature* **329**, 615.

Chyba, C. and Sagan, C.: 1987, *Nature* **330**, 350.

Draganić *et al.*: 1984, *Icarus* **60**, 464.

Geiss, J.: 1987, *Astron. Astrophys.* **187**, 859.

Greenberg, J.M. and Grim, R.: 1986, *ESA SP–250* **2**, 255.

Ryan, M.P. and Draganić, I.G.: 1986, *Astrophys. Space Sci.* **125**, 49.

Sagan, C. *et al.*: 1967, *Nature* **213**, 273.

Strazzulla, G. *et al.*: 1983, *Mon. Not. R. Astr. Soc.* **204**, 59p.

Wallis, M.K.: 1980, *Nature 284*, 431.

Wasserburg, G.J.: 1987, *Earth Planet. Sci. Lett.* **86**, 129.

COMET HALLEY IRRADIATION HISTORY

ENVIRONMENT	DOSE (Mrad)	PROCESSING DEPTH	REMARKS
Inner Solar System			
Solar Wind, 1 Orbit	10^3	~0.1 μm	Comet Shielded Within ~5 AU
Solar Wind, 10^2 - 10^3 Orbits	10^5 – 10^6	~0.1 μm	
Residence in Oort Cloud			
Solar Wind, 4.6 Gyr	10^4	~0.1μm	
Cosmic Rays, 4.6 Gyr[a]	10^4 – 10^5 10^3	~ 1 m ~ 10 m	Flux May Increase Beyond Heliosphere
Radionuclides, 4.6 Gyr[a]	10^3	Entire Nucleus	Assumes no Differentiation ^{26}Al ~80%
Inner Oort Cloud			
Solar Wind, ~ Gyr	10^9	~0.1 μm	
Pre-Accretion			
Low Energy Cosmic Rays[b] 10^7 - 10^8 yr	10^4 – 10^5	~100μm	All C-containing Ices Polymerized
Interstellar UV, 10^8 yr[c]	10^7 – 10^8	~ 0.1μm	

[a] Draganić et al., 1984.

[b] Strazzulla et al., 1983.

[c] Greenberg & Grim, 1986.

N91-15008

EXPERIMENTAL EVIDENCE FOR AMORPHOUS CARBON GRAINS IN COMETS

L. Colangeli*, G. Schwehm*, E. Bussoletti**, A. Blanco***, A. Borghesi***, S. Fonti***, V. Orofino***
* Space Science Department of ESA/ESTEC, Noordwijk, The Netherlands
** Istituto Universitario Navale and Osservatorio Astronomico di Capodimonte, Napoli, Italy
*** Physics Department, University of Lecce, Lecce, Italy

1. IR SPECTRA OF COMET HALLEY

Ground based observations (Baas et al., 1986; Wickramasinghe and Allen, 1986; Knacke et al., 1987; Danks et al., 1987; Tokunaga et al., 1987) and "in situ" measurements by the IKS telescope on board the VEGA 1 spacecraft (Moroz et al., 1987) have shown the presence of a well pronounced emission feature in the spectrum of comet Halley between 3.3 and 3.7 μm, resolved in different bands (Table 1). This evidence confirms for P/Halley the presence of carbonaceous materials including CH-X bonds, in agreement with measurements by the mass spectrometers PUMA 1/2 and PIA, on board VEGA 1/2 and Giotto, respectively (Kissel et al., 1986; Jessberger et al., 1988).

The band intensity shows temporal variations relative to the continuum: a) on a daily time scale, irregular changes have been observed (Knacke et al., 1987; Wickramasinghe and Allen, 1986; Tokunaga et al., 1987); b) on a monthly time scale, an anticorrelation seems to exist between the band intensity and the continuum level (Baas et al., 1986; Knacke et al., 1987).

A main uncertainty concerns the origin of the bands at about 3.4 μm from either **molecules in gaseous phase** or **solid grains**. However, their broad profile tends to support a solid state origin. Similar absorption features have been observed in the spectrum of various galactic IR sources, as - for example - IRS 7 in Sagittarius A (Butchart et al., 1986) (Table 1). In this last case, carbonaceous grains in dense molecular clouds, close to the Galactic Centre, are considered possible carriers of the bands. Also on the base of the relations between interstellar dust and cometary materials (Greenberg, 1986) a similar attribution for the bands in P/Halley seems possible.

2. HYDROGENATED AMORPHOUS CARBON GRAINS

Hydrogenated amorphous carbon (HAC) grains with mean radius = 40 Å have been produced in laboratory by arc discharge in a controlled Ar atmosphere (p = 1 Torr) between two amorphous carbon electrodes (Bussoletti et al., 1987).

Single atoms or functional groups (H, CH_n, n=1,2,3) may link to chemically unsaturated sites of the crystalline sub-units randomly oriented to form the disordered network (Marchand, 1986). Therefore, weak bands detected in HAC absorption spectra between 3.3 and 3.5 μm are attributed to various C-H bonds (Borghesi et al., 1987). Their wavelength of occurrence and relative intensity

suggests a prevalent diamond-like (sp^3) hybridization of the crystallites in HAC grains (Table 1). Dischler et al. (1983) have analyzed the evolution of IR features in α - C:H thin films after thermal annealing, finding a progressive change of the crystalline structure from a dominant diamond-like (sp^3) character, at room temperature, to a prevalent graphite-like (sp^2) type, at 600 °C (Table 1).

HAC grains with variable sp^3/sp^2 content may be produced in space. Since in laboratory experiments this ratio seems to increase with increasing temperature, the $\sim$ 3.3 μm bands from sp^2CH_n are expected to dominate over the $\sim$ 3.4 μm features from sp^3CH_n in HII Regions and Planetary Nebulae, where T $\leq$ 1000 K (Sellgren, 1984). The opposite situation occurs in dark clouds and in comets, where the temperature is much lower. The intensity of IR bands measured in laboratory on HAC grains appears much weaker than in space conditions. The large amount of H available in space suggests that various types of **highly hydrogenated amorphous carbon grains (HHAC)** could be among the carriers of both the interstellar and the cometary bands between 3.2 and 3.6 μm.

3. SIMULATION OF COMETARY SPECTRA BY "HHAC"

The best-fit of P/Halley continuum flux recorded on March 30th (Wickramasinghe and Allen) by means of HAC extinction data (Bussoletti et al., 1987, Borghesi et al., 1987) has been obtained for a temperature T_g(HAC) $\sim$ 340 K, which can be considered as an average temperature of grains emitting in the IR range. The required HAC grain abundance is < 1 % of the total mass rate and $\sim$ 30 % of the rate for grains < 10^{-5} g, well within the limits deduced for carbonaceous grains by PUMA and PIA (Kissel et al., 1986; Jessberger et al., 1988).

To match the 3.4 μm band intensity, HHAC particles have been assumed to have the same optical properties as HAC grains but an H content sufficient to produce a 3.4 μm band stronger than in the HAC case. The Halley spectrum appears well matched if the band intensity is increased by a factor F = 7 (Figure 1). To simulate HHAC grains with various sp^3/sp^2 ratios we have scaled the results from Dischler et al. (1983) on the HAC continuum and increased the band intensity by F = 10 (Figure 2). HHAC grains with a dominant sp^2 coordination do not reproduce the observations because the 3.28 μm band dominates the 3.4 μm feature, while grains with a sp^3 content $\geq$ 65 % may account also for the 3.28 μm cometary signature. Therefore, a proper mixture of HHAC grains, with different crystalline structures but a prevalent diamond-like character, is able to give a quite good fit of the IR emission bands detected in P/Halley.

In our picture the IR continuum is attributed to amorphous carbon grains while the 3.4 μm band is due to hydrogenation effects. This scenario may allow to interpret the observed temporal behaviour of the two spectral components: a) the amount of H stuck on grains may suddenly vary in time in the thermodynamically unstationary comet environment, producing daily variations in the 3.4 μm band intensity; b) as the comet removes from the Sun the dust progressively cools down and the relative amount of H trapped onto the grains may rise as well as the 3.4 μm band intensity (monthly variations).

4. SIMULATION OF IRS 7 SPECTRUM BY "HHAC"

The approach used to simulate the cometary bands has been applied to reproduce the absorption bands detected in IRS 7 (Butchart et al., 1986). Also in this case the best-fit has been obtained by HHAC grains, for a band enhancement factor F = 7. Again, HHAC grains likely match the 3.4 μm feature, but are not able to reproduce the weaker 3.3 μm band. This goal is achieved when HHAC grains

with 33 % of sp^2 content are considered (Figure 3).

5. CONCLUSIONS

Amorphous carbon grains similar to those produced in the laboratory, but with a higher hydrogen content, appear to be good candidates to simulate both the IR continuum emission and the 3.4 μm band measured for P/Halley. The comparison of the cometary features with those detected in laboratory for carbon grains characterized by various sp^2/sp^3 ratios seems to indicate that a prevalent diamond-like (sp^3) structure should be present in cometary particles. This kind of solid particles seem also suitable to explain the daily and monthly variations of the 3.4 μm band intensity, relative to the continuum, and - at the same time - to fulfill the abundance constraints. The same grains appear to be able to reproduce the absorption bands detected in the IR galactic source IRS 7. This result may be considered as a first experimental evidence of a relation existing between interstellar dust and cometary materials.

Baas, F., Geballe, T.R. and Walther D.M.: 1986, Ap. J. (Letters) 311, L97.

Borghesi, A., Bussoletti, E. and Colangeli, L.: 1987, Ap. J. 314, 422.

Bussoletti, E., Colangeli, L., Borghesi, A. and Orofino, V.: 1987, Astr. Ap. Suppl. Ser. 70, 257.

Butchart, I., McFadzean, A.D., Whittet, D.C.B., Geballe, T.R. and Greenberg, J.M.: 1986, Astr. Ap. 154, L5.

Danks, A., Encrenaz, T., Bouchet, P., Le Bertre, T. and Chalabaev, A.: 1987, Astr. Ap. 184, 329.

Dischler, B., Bubenzer, A. and Koidl, P.: 1983, Solid State Comm. 48, 105.

Greenberg, J.M.: 1986, ESA SP-249, 47.

Jessberger, E.K., Christoforidis, A. and Kissel, J.: 1988, Nature 332, 691.

Kissel, J. et al.: 1986, Nature 321, 280.

Knacke, R.F., Brooke, T.Y. and Joyce, R.R.: 1987, Astr. Ap. 187, 625.

Marchand, A.: 1986 in "Polycyclic Aromatic Hydrocarbons and Astrophysics (ed. A. Leger, L. d'Hendecourt, N. Boccara), Reidel Dordrecht, p. 31.

Moroz, V.I. et al.: 1987, Astr. Ap. 187, 513.

Sellgren, K.: 1984, Astrophys. J. 277, 632.

Tokunaga, A.T., Nagata, T. and Smith, R.G.: 1987, Astr. Ap. 187, 519.

Wickramasinghe, D.T. and Allen, D.A.: 1986, Nature 323, 44.

Table 1. Identification of IR bands in space and in laboratory.

Configuration		Laboratory			Observations	
Type	Wavelength (μm)	Band position (μm)				
		HAC	α-C:H		P/Halley	IRS 7
		$T_{ambient}$	50	600 °C		
sp^1CH	3.02		3.03			
sp^2CH (arom.)	3.28			3.28	3.28	3.29
sp^2CH_2 (olef.)a	3.31				3.31	
sp^2CH (olef.)	3.33		3.33			
sp^3CH_3 (asym.)a	3.38	3.39			3.40	3.40
sp^2CH_2 (olef.)s	3.39					
sp^3CH_2 (asym.)a	3.42	3.42	3.42	3.42		
sp^3CH	3.43				3.44	
sp^3CH_3 (sym.)s	3.48	3.48				3.48
sp^3CH_2 (sym.)s	3.51	3.51	3.51		3.51	

Notes: "a" and "s" in column 1 indicate "antisymmeteric" and "symmetric" vibrations; P/Halley and IRS 7 bands: see references in the text.

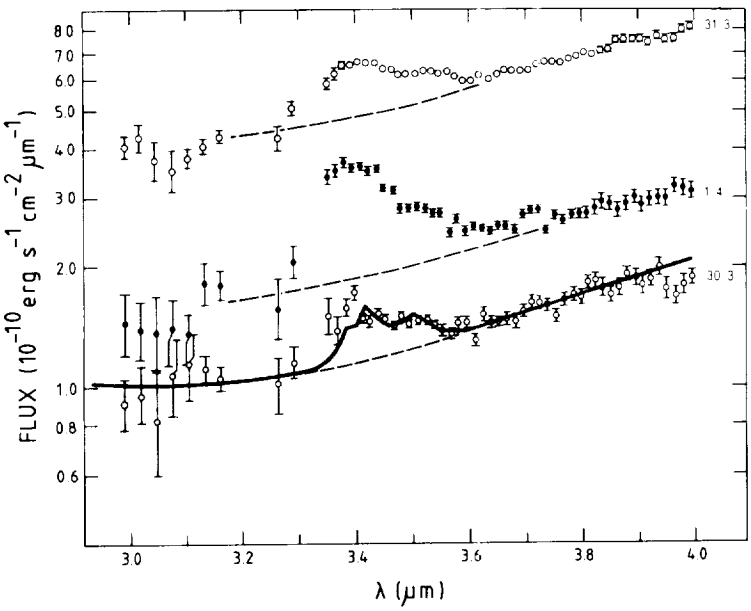

Figure 1. Best fit (solid line) of the 3.4 μm cometary band (Wickramasinghe and Allen, 1986) by means of HHAC extinction data.

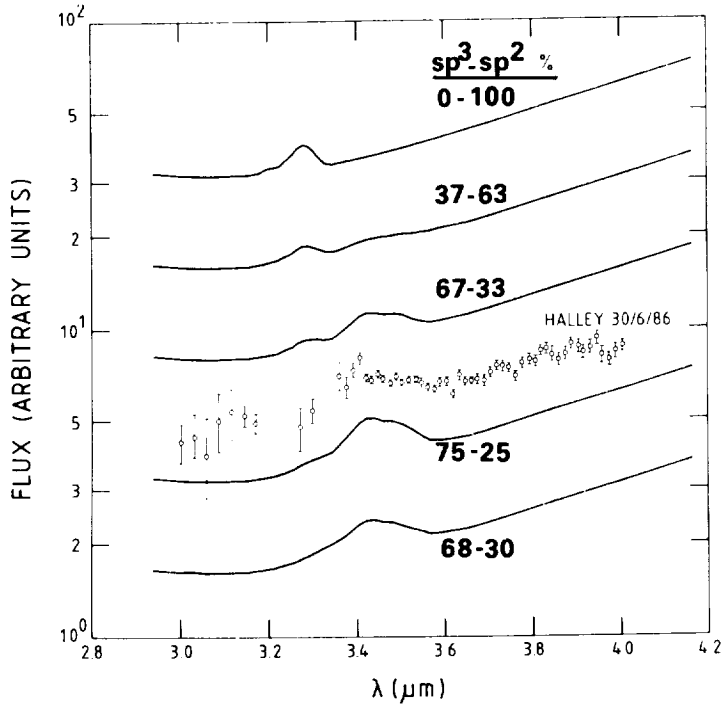

Figure 2. Emission spectra from HHAC grains with various sp^3/sp^2 ratios (Dischler et al., 1983). The Halley spectrum is reported for comparison (Wickramasinghe and Allen, 1986).

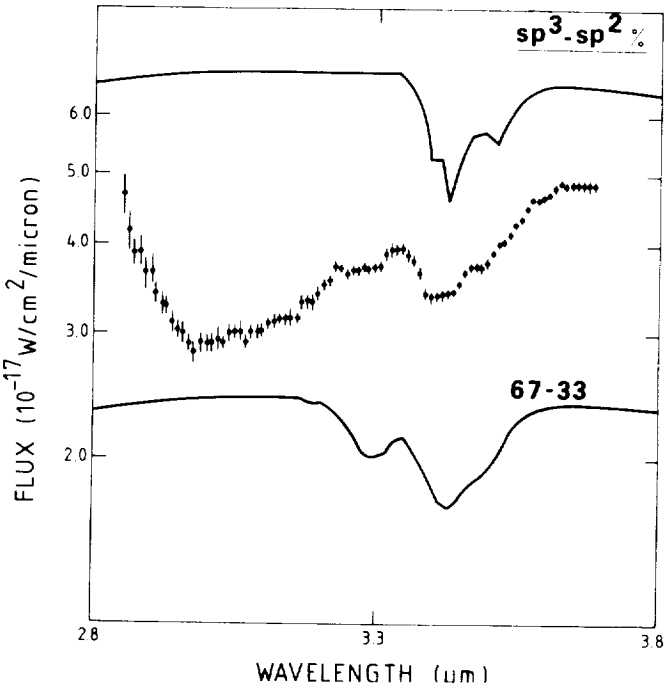

Figure 3. Ordinate displaced best fits (solid lines) of the IRS 7 spectrum (Butchart et al., 1986) by means of the extinction data for HHAC grains with various sp^3/sp^2 ratios.

VII-C) COMET HALLEY FLYBY

VEGA-GIOTTO FLYBY MISSIONS AND COMETARY COSMOGONY

B.Lang
Warsaw University, Department of Chemistry,
02-089 Warsaw, Poland

1. INTRODUCTION. The opportunity to absorb the results of the in-situ measurements as made on the board of the spacecrafts is for cometary cosmogony the most important implication of the Vega/Giotto flyby missions to Halley. Unfortunately the exploration of matter identified as ejecta from the nucleus proved its inability to define unambiguously the very chemical-mineralogical nature of the nucleus - to provide information comparable with expected from a sample return mission. However, incapable to offer an adequate empirical firm basis for a scenario describing formation of a cometary body the obtained results are significant enough to affect and to re-direct the cosmogonical thinking.

Accordingly, the understanding is to be modified of the dichotomy of cometary matter as deduced from the distinction of water-dominated volatiles and silicate-based non-volatiles. Organic carbon compounds emerged as a major constituent of cometary matter. Their discovery enabled not only to correct the views on the supposed chemical nature of the nucleus but it stimulated a search for a signature of a chemical activity accompanying ejection of matter from cometary nuclei [see, e.g., Combi and Delsemme,1986; Combi, 1987]. At the moment with all the respect to the work of Whipple [1950, 1963, 1976, 1984] it is likely that the revision of his classic concept of the icy conglomerate cannot be avoided.

Affected by the Vega/Giotto flyby missions to Halley cometary cosmogony seems to enter its new conceptual period. Of basic importance appeared the results of the in-situ measurements - mass-spectrometric, UV- and IR-spectroscopic. Chemistry has been called to explain the occurrence inside the nuclei of the variety of species as inferred from the mass-spectrometric data and to predict the results of the processes possibly involved. Cosmochemical factor has been postulated to operate behind the observed cometary phenomena. The chemistry of the interstellar medium, covering the circumstellar and interstellar dust became a natural ally of the advances in cometary cosmogony.

2. COMETARY MATTER: GENERAL. Cometary nucleus is so far inaccessible. Inaccessible in-situ is the cometary matter filling the nucleus. Far from perihelium, at temperatures as low as 20 - 30 K, or less, the nucleus is an assemblage of solids. They appear to make (on large scale) continuum that can be defined as monolithic [cf. Brandt, 1987]. However, the low bulk density of cometary nuclei- although estimated from astronomical data with rather poor precision (e.g. for Halley Rickman [1986] found 100 - 300 kg/cu.m, while Sagdeev et al. [1988] 600 (+900,-600) kg/cu.m - can be explained only with abundant microscopic pores and void spaces corresponding with chemical-mineralogical features of the microstructure.

Of particular importance for understanding the nucleus is the exploration of the ejecta. In the past the attention to the ejecta was focused on the gaseous products of sublimation of cometary ices as exposed to solar radiation while believed to be responsible for the observed cometary phenomena.

Accordingly chemistry used for explanation of cometary ejecta has been reduced to dealing with simple phase transition. In terms of such an approach generation of ejecta was viewed as a transfer of material from the interior of the nucleus to the surrounding halo or coma without any significant chemical change. The process of transfer was tacitly assumed chemically indifferent. The transferred material of the nucleus has been supposed to be aggregated in analogy with aggregation of planetary matter [cf. Donn, 1988].

The outcomes of the in-situ measurements invalidated the assumption of chemical passivity as attributed to cometary nuclei. In contrast with such a passivity is the abundance of the organic carbon compounds varying appreciably in chemical reactivity and stability while contributing in organic mantles of grains. There is no reason to refer the gaseous ejecta to cometary ices only. A need arises for a model of the cometary nucleus with cosmochemical signature consistent with a multidisciplinary approach.

3. THE EJECTA. The results of the exploration of the ejecta were recently summarized by Jessberger et al.[1988b] using an extensive reference list. The major element composition of the Halley dust was considered as a part of this summary [Jessberger et al.,1988a]. The discussed below pre-requisites of a re-orientation of cometary

cosmogony were inspired by the work of Kissel and Krueger [see Kissel et al., 1986a, b; Kissel and Krueger, 1987a, b; Krueger, 1988] involving the dust particles.

To understand the results for the dust let us look at the gaseous ejecta [Encrenaz, 1987]. Overdominant was found the contribution of water as high as 80%. Relative to water other abundances are: CO: 5 - 7%, CO2: 1.5 - 3.5%, CH4: 2 - 7%, saturated hydrocarbons: 1%, HCN: 0.1%, NH3: <10%, N: 2%. Such a composition of the ejecta hardly can be recognized as involving species previously incorporated into the nucleus. It has been believed to be converted into a mixture frozen but chemically unchanged.

The results of the chemical identification covered 20 elements distributed among 5 major (H,C,N,O,S), 7 minor (O, Mg, Al, Si, (S), Ca, Fe), and 8 trace elements (Li, B, Ti, Cr, Mn, Co, Ni, Ca). The occurrence of further 9 elements was found highly uncertain.

Among identified molecular species organic carbon compounds play a special most important role. They have been subdivided into two categories according to the level of reliability of their identifcation. Chemically they form four groups specified as CH, CNH, COH and CHON compounds. Each group consists approximately of two types of compounds: highly unsaturated ones with one triple or two double C-C bonds in 4 - 5-membered chains coexisting with cyclic unsaturated, aromatic or heterocyclic partners. The probability of the occurrence of COH is claimed to be not high. There is no doubt that the carbon compounds need a special insight and careful consideration. One can suspect that the grouped compounds resemble homologous series and probably could be derived from few initial molecules or radicals like CO, HCN, C2 - typical astrophysical species. Interacting on the surfaces of grains encrusted with various metals active as catalysts with hydrogen and other molecules such species could initiate reaction sequences leading to synthesis of polymeric carbon chains of various length, their branching and cross-linking.

It is not excluded that a computer search for an adequate chemical network would be reasonable and fruitful. The context of the interstellar chemistry seems to be both attractive and promising.

4. COMETARY ICES - WATER. If water has been brought into cometary nucleus together with grains as their component claimed to contribute in the supposed mantle then it should be regarded as endogenous i.e. to enter the basic material. However, facing the abundance of icy-rocky objects in the solar system we cannot exclude the occurrence of exogenous water in cometary nuclei - water that joined the nucleus during an episode preceding the ultimate formation of a cometary body. One can hypothesize that such an episode would include a kind of a "snowfall": condensation of water-dominated mixture of gases of composition close to the supposed cometary one. Expelled from the central warmer regions towards the colder periphery of the planetary system it would traverse the circumsolar region of swarming grains - precursors to cometary bodies. This exogenous water could penetrate a swarm of grains to condense into a dendritic structure leading to a low average density as featuring cometary bodies.

Another peculiar source of water was considered too [Krueger, 1988]: water from chemical reaction of the synthesis gas CO + H2 : its occurrence is highly probable, while the presence of a metal catalyst (Fe, Ni, Co) not excluded. So we arrived at the Fischer-Tropsch catalytic reduction-polymerization leading to formation of water:

$$(\ CO\ +\ 2\ H2\ )^{*}\ n = (\ CnH2n\ +\ n\ H2O)$$

However, the deep difference between the known laboratory conditions and those governing in the solar/galactic medium (extremely low temperatures and concentrations of reactants, variability of occurrence of catalysts) suggests a reasonable reservation.

5. COMETARY NUCLEUS AS ASSEMBLAGE OF SOLIDS. Far from the Sun cometary nuclei are composed of solids. The features echoing with their very nature are preserved only in the dust particles. The latter have been shown to be aggregates of coalesced submicron grains. Their mass distribution is ranging 6 orders of magnitude - down to $10^{**}(-19)$kg. In terms of this finding aggregation of grains preceded their swarming. It is hypothesized that nucleation and initial rise of aggregates were made possible due to supply of chemical-mineralogical material of circumstellar and interstellar origin. The high

efficiency of aggregation as demonstrated by the span of the size distribution is attributed to local conditions inside eddies produced by turbulence supposed to operate at the periphery of the solar nebula under the impact of a convective instability [cf.,e.g.,Cabot et al.,1987]. The flux of gases streaming outwards the solar system was considered by many authors [see e.g.Cameron,1984; Vityazev and Pechernikova, 1986; Rawlings et al., 1988].

The growth of the dust particles was probably close to diffusion-limited aggregation (DLA) of Witten and Sander [1983] or cluster-cluster aggregation of Meakin [1983] leading to fractal structures [Donn, 1987; Hughes, 1987].

6. CONCLUSION. The offered very fragmentary scenario is based on assumed distinct origin of cometary solids. It predicts incorporation of grains of galactic origin as aggregates evolved from smaller interstellar particles into a mass of condensate. The latter is supposed to be obtained during an episodic snowfall producing the matrix material filling the cometary nucleus.

REFERENCES

Bailey,M.: 1987, Icarus 69, 70.

Bailey,M.: 1988, in "Dust in the Universe"(M.Bailey & D.Williams Eds.)

Brandt,J.: 1987, Phil.Trans.R.Soc.Lond. A323, 437.

Cabot,W.,Canuto,V.,Hubickyj,O.,Pollack,J.: 1987, Icarus 69, 387, 423.

Cameron,A.G.W.: 1984, LPSC XV, 118.

Combi,M.: 1987, Icarus 71, 178.

Combi,M., Delsemme,A.: 1986, Astrophys.J. 308, 472.

Delsemme,A.: 1987, ESA SP-278.

Donn,B.: 1987, LPSC XVIII, 243.

Donn,B.: 1988, Astron.Astrophys. (in press).

Encrenaz,T.: 1987, Phil.Trans.R.Soc.Lond. A323, 397.

Hughes,D.: 1987, Nature 325, 231.

Jessberger,E., Christoforidi,A., Kissel,J.: 1988a, Nature 332, 691.

Jessberger,E., Kissel,J., Rahe,J.: 1988b, Preprint MPI H-1988-V20.

Kissel,J. + 22 co-authors: 1986a, Nature 321, 280.

Kissel,J. + 18 co-authors: 1986b, Nature 321, 336.

Kissel,J., Krueger,F.: 1987a, Nature 326, 755.

Kissel,J., Krueger,F.: 1987b, Sterne u.Weltraum 191.

Krueger,F.: 1988, Sterne u.Weltraum 286.

Krueger,F., Kissel,J.: 1987, Naturwissenschaften 74, 312.

Meakin,P.: 1983, Phys.Rev. A27, 604.

Rawlings,J., Williams,D., Canto,J.: 1988, Mon.Not.R.astr.Soc. 230, 695.

Rickman,H.: 1986, Uppsala Preprints in Astronomy, preprint no.8.

Sekanina,Z.: 1986, ESA-SP 250, 131.

Vityazev,A., Pechernikova,G.: LPSC XVIII, 908.

Whipple,F.: 1950, Astron.Astrophys. 111, 375.

Whipple,F.: 1963, in Moon, Meteorites, Comets (B.Middlehurst & G.Kuiper Eds.), pp.639 - 664.

Whipple,F.: 1984, in Ices in the Solar System (J.Klinger, D.Benest, A.Dollfus, R.Smoluchowski Eds.), pp.343 - 346.

Witten,T., Sander,L.: Phys.Rev. B27, 5686.n

THE COMPOSITION OF HEAVY MOLECULAR IONS INSIDE THE IONOPAUSE OF COMET HALLEY

D.L. Mitchell, R.P. Lin, K.A. Anderson, C.W. Carlson, D.W. Curtis
Space Sciences Laboratory, University of California, Berkeley, CA U.S.A.

A. Korth
Max-Planck-Institut für Aeronomie, Lindau, F.R.G.

H. Rême, J.A. Sauvaud, C. d'Uston
Centre d'Etude Spatiale des Rayonnements, CNRS, Toulouse, France

D.A. Mendis
Department of Electrical Engineering and Computer Sciences
University of California, San Diego, CA U.S.A.

The RPA2-PICCA instrument aboard the Giotto spacecraft obtained 10–210 amu mass spectra of cold thermal molecular ions in the coma of Comet Halley. Outside the ionopause (r>4700 km), the thermal energy spread of the ions limits the effective mass resolution of PICCA to about 3 amu. However, several important features of the mass spectrum are observed at this resolution (Mitchell *et al.*, 1987). Above 50 amu, there is an ordered series of mass peaks composed of three or more closely spaced masses and centered at 61, 75, 90, and 105 amu. The separations of the peak centers are characteristic of molecules rich in carbon, hydrogen, oxygen, and nitrogen. The peak abundances decrease smoothly with increasing mass. The average loss rate of 55–69 amu ions is roughly 10^{-4} per second, or four times the H_2O loss rate, which results from the photodissociation of a single H-O bond. The loss rate increases with mass to about 5.5×10^{-4} per second for 98-114 amu ions. This suggests that the heavy molecules are predominantly singly bonded, and that the number of single bonds per molecule increases with mass.

Inside the ionopause the ion temperature drops to $kT = 0.03$ eV, allowing optimal mass resolution ($\lesssim$1 amu). High resolution data were obtained from 35 to 70 amu, revealing the dominant masses at 43, 45, 47, 48, 57, 59, 61, and 63 amu. The mass composition derived from the high resolution spectra is consistent with lower resolution spectra taken just outside the ionopause, which shows that there is no abrupt change in composition across the ionopause.

The dissociation products of the long chain formaldehyde polymer polyoxymethylene (POM) have recently been proposed as the dominant complex molecules in the coma of Comet Halley (Heubner, 1987); however, POM alone cannot account for all of the features of the high resolution spectrum. The dominant masses between 55 and 70 amu are separated by 2 amu; therefore the peak width must result from variations in the C:O ratio and not from the dissociation and attachment of hydrogen atoms. The observed 63 amu molecule, for example, can be produced by replacing an H on the

methylene unit of $HOCH_2O$ with an OH, which gives the oxygen-rich molecule HOCHOHO. However, a relatively abundant 57 amu molecule cannot be produced in a similar manner without eliminating the oxygen altogether and is thus likely to result from a species unrelated to POM.

An important component of the dust at Comet Halley is particles highly enriched in carbon, hydrogen, oxygen, and nitrogen relative to the composition of carbonaceous chondrites (Clark *et al.*, 1987). Since this dust could be a source for the heavy molecules observed by PICCA, we began the search for other chemical species by determining all the molecules with mass between 20 and 120 amu which can be made from the relatively abundant C, H, O, and N, without regard to chemical structure. The only criterion for a valid molecule was that it have enough chemical bonds to hold itself together. The total number of possible CHON molecules as a function of mass shows peaks which agree quite well with the locations of the observed mass peaks in the PICCA data.

The composition of interstellar grains could be relevant to comets if the latter consist of essentially unmodified interstellar material. Laboratory experiments designed to simulate the chemical processes that take place on interstellar dust grains during the formation and evolution of icy mantles have recently been performed (Shutte, 1988). First, a gas mixture of H_2O, CO, NH_3, and CH_4 was deposited onto a 12°K aluminum "grain surface" under simultaneous ultraviolet irradiation. The UV radiation created radicals which could either react or be stored within the cold icy substrate. Subsequent warm-up of the icy mantle allowed first the radicals and then the non-radicals to diffuse and react, producing progressively more complex molecules. After warm-up to room temperature, there remained on the grain surface a refractory organic residue, which was composed of molecules which cluster near the mass peak locations observed by PICCA. Most of these molecules appear to be made up of molecular units (CH_2, NH_2, OH, and CO) connected by single bonds.

Molecules which are constructed from CH_2, NH, O, and H units connected by single bonds can produce a spectrum that closely resembles the observed high resolution spectra if the nitrogen abundance is less than about 12% (which is consistent with the CHON dust composition, Langevin *et al.*, 1987) and the C/O ratio is 1.2 to 1.4. The 2 amu alternation results since the molecules are constructed mainly from even-mass units. In order for the alternation to fall on odd masses, most molecules must have suffered a single dissociation, leaving only one open bond. This is consistent with the 55-69 amu molecules having traveled only a short distance inside the ionopause (~4000 km) relative to their observed dissociation scale length of 9300 km.

References

Clark, B.C., L.W. Mason, and J. Kissel, *Astron. Astrophys,* **187**, 779 (1987).

Heubner, W.F., *Science,* **237**, 628 (1987).

Langevin, Y., J. Kissel, J-L. Bertaux, and E. Chassefière, *Astron. Astrophys.,* **187**, 761 (1987).

Mitchell, D.L., R.P. Lin, K.A. Anderson, C.W. Carlson, D.W. Curtis, A. Korth, H. Rème, J.A. Sauvaud, C. d'Uston, and D.A. Mendis, *Science,* **237**, 626 (1987).

Shutte, W.A., Ph.D. Thesis, University of Leiden, The Netherlands (1988).

VII-D) METEORS, METEORITES, AND INTERPLANETARY DUST

ATOMIC ENVIRONMENTS IN IRON METEORITES USING EXAFS

G. Cressey (1), A. J. Dent (2), B. Dobson (2), A. Evans (3), G. N. Greaves (2), C. M. B. Henderson (4), R. Hutchison (1), R. N. Jenkins (3), S. P. Thompson (3), R. Zhu (2,5)

1 Department of Mineralogy, British Museum (Natural History), London, SW7 5BD
2 SERC Daresbury Laboratory, Warrington, WA4 4AD
3 Department of Physics, The University, Keele, ST5 5BG
4 Department of Geology, The University, Manchester, M13 9PL
5 Institute of High Energy Physics, Academia Sinica, PO Box 918, Beijing, Peoples' Republic of China.

1. Introduction

Extended X-ray Absorption Fine Structure (EXAFS) is observed as a modulation on the high energy side of an X-ray absorption edge. It occurs when the photo-ejected electron wave is scattered by neighbouring atoms in a solid, and interference occurs between the outgoing and scattered waves. The result is that the absorption spectrum carries a signature that is characteristic of the identity and disposition of scattering atoms around the absorbing atom (see e.g. Stern 1978). It may be shown that the Fourier transform of the normalized EXAFS gives directly the distance, co-ordination number and identity of scattering atoms around the absorbing atom. An analysis of EXAFS can therefore provide detailed information about the immediate environment of specific atoms in a solid and is ideally suited to the study of cosmic dusts.

We have initiated a study of cosmic dusts, using EXAFS and other techniques, at the SERC Synchrotron Radiation Source (SRS) at Daresbury, U.K. We have started this work by investigating what seems to be the simplest type of cosmic material, namely the iron meteorites, the morphology of which has been well-studied using conventional techniques.

2. Iron Meteorites

Iron meteorites have nickel content typically in the range ~ 4 - 40%. The metal normally occurs as two co-existing phases, namely kamacite (which has b.c.c. structure) and taenite (f.c.c.). A portion of the Fe-Ni phase diagram is shown in Fig. 1. Meteorites having high Ni content consist mainly of taenite, whereas those having low Ni content are mainly kamacite.

The iron meteorites investigated in the present study are Uwet (5.6% Ni), Steinbach (9.1%), Mount Edith (9.4%), Butler (15.2%) and Santa Catharina (33.6%) (see Graham et al. 1985). In some cases meteorites having intermediate nickel content were first treated to separate the kamacite and taenite phases.

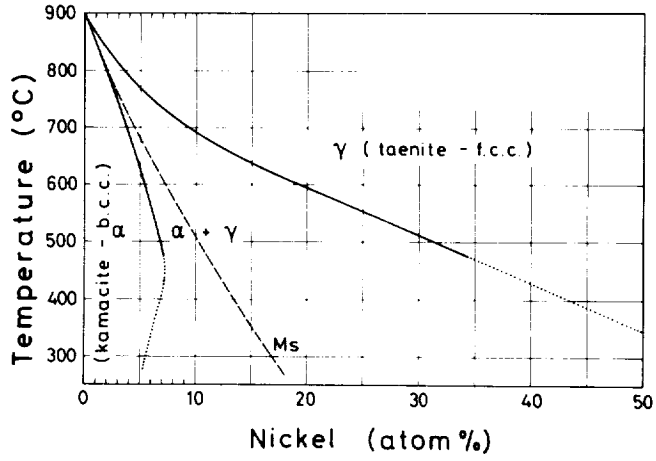

Fig. 1: Fe-Ni phase diagram (after Wasson 1974).

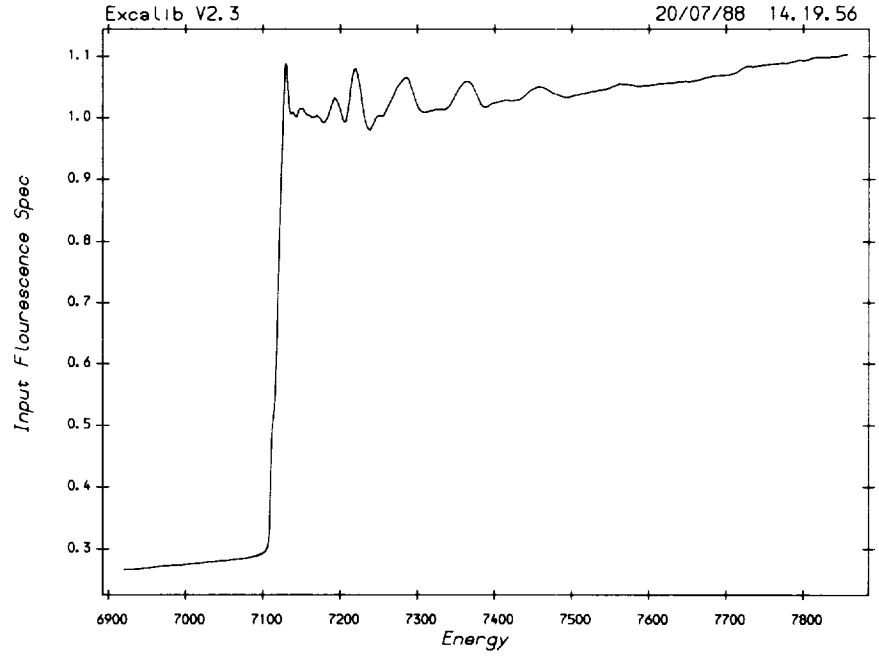

Fig. 2: Relative absorption at the Fe K-edge vs. photon energy (eV) for Butler meteorite.

3. EXAFS

We have measured the Ni and Fe K-edge EXAFS using (i) transmission mode, (ii) fluorescence mode and (iii) a photo-yield ion chamber filled with helium. Iron (b.c.c.) and nickel (f.c.c) foils were used as 'spectroscopic standards'. A typical meteoritic (Butler) EXAFS spectrum - at the Fe K-edge - is shown in Fig. 2.

Fig. 3a shows the spectrum of Ni foil, background subtracted and normalized to the post-edge region where the EXAFS is no longer visible. The Fourier transform is shown in Fig. 3b, the broken curve being a theoretical fit - including multiple scattering effects - for an f.c.c. lattice with 12 nearest neighbour Ni atoms at distance (r) 2.49 Å, 6 Ni atoms at 3.52 Å etc. Figs. 4a,b show the corresponding plots for Fe foil.

The Fourier transform of the EXAFS spectrum of the Uwet meteorite at the Fe K-edge is shown in Fig. 5a (full line); the broken curve is the Fourier transform of the Fe foil spectrum and clearly the Fe b.c.c. structure gives an extremely good fit to the meteoritic data. This result is consistent with the low Ni content of the Uwet meteorite.

The Santa Catharina meteorite consists of a mixture of kamacite and taenite phases. The Fe K-edge EXAFS for this meteorite is shown in Fig. 5b. In this case neither the Fe nor the Ni alone can adequately fit the data. Instead we find that a combination consisting of 10-20% b.c.c. and 80-90% f.c.c. fit the data well; Fig. 5b shows the fit for a 15:85 combination (broken curve). [Note that, while the general features of the Fourier transform are well described the amplitudes differ because the meteorite and foil EXAFS were obtained using photo-yield and transmission techniques respectively.]

The Butler meteorite also consists of a kamacite-taenite mixture. In this case the data at the Fe K-edge are consistent with a 60-80% b.c.c. and 20-40% f.c.c. mix (see Fig. 6a, which shows the fit for a 70:30 combination). To demonstrate that neither pure b.c.c. nor pure f.c.c. can fit the data, Fig. 6b compares the Butler Fourier transform with the Fe standard only, while Fig. 6c compares Butler with Ni only.

Again the Steinbach meteorite is a kamacite-taenite mix and the data are best fitted by a 80-100% b.c.c. + 0-20% f.c.c. combination. Fig. 7 again compares the Fourier transform for the meteorite data (Fe K-edge) with that for a 90:10 combination.

4. XANES

In addition to the EXAFS, which extends over $\geq$ 100 eV past the absorption edge, information can also be derived from the X-ray Absorption Near Edge Structure (XANES); this is the structure in the absorption close ($\lesssim$ 40 eV) to, and in, the edge step itself. Fig. 8a shows the XANES around the Fe K-edge for the Mount Edith meteorite (thin line). The thick line is the corresponding XANES for Fe foil, indicating that the bulk of the Mount Edith meteorite is b.c.c., consistent with its known composition. Fig. 8b shows the corresponding

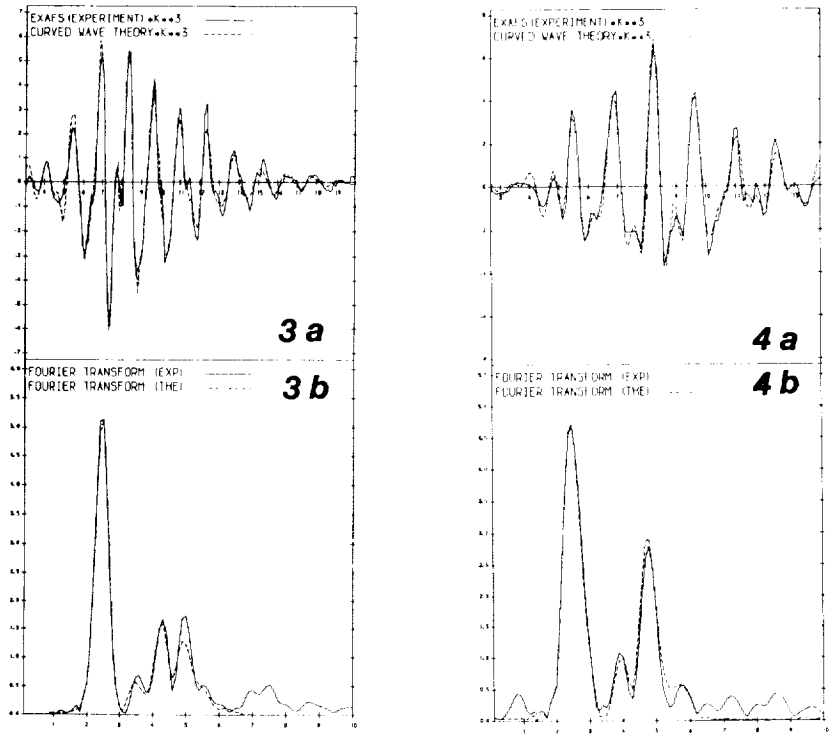

Fig. 3: (a) Normalized EXAFS of Ni foil at K-edge;
(b) Fourier transform of (a).
Fig. 4: (a),(b) As 3(a),(b) but for Fe foil.

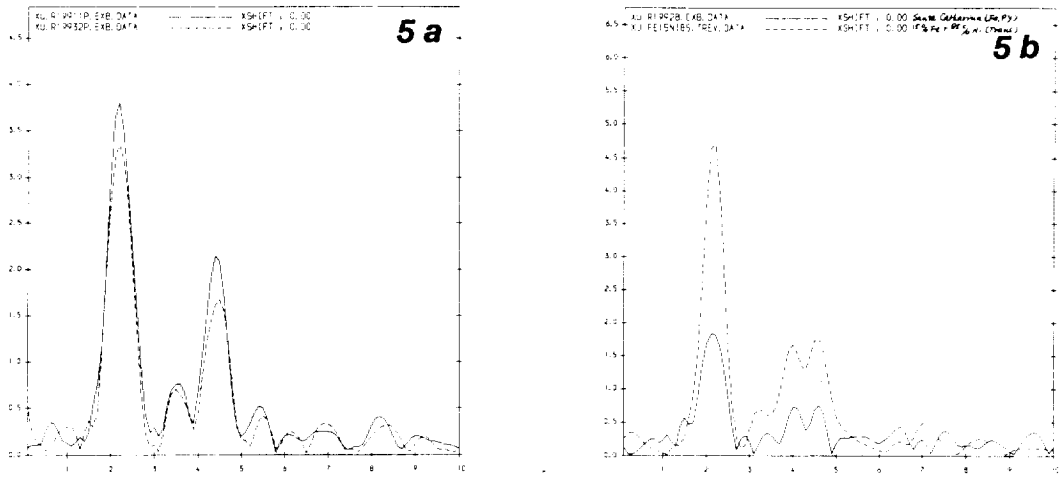

Fig. 5: (a) Fourier transform of normalized Fe K-edge EXAFS
for Uwet; see text for details.
Fig. 5: (b) As 5(a) but for Santa Catharina.

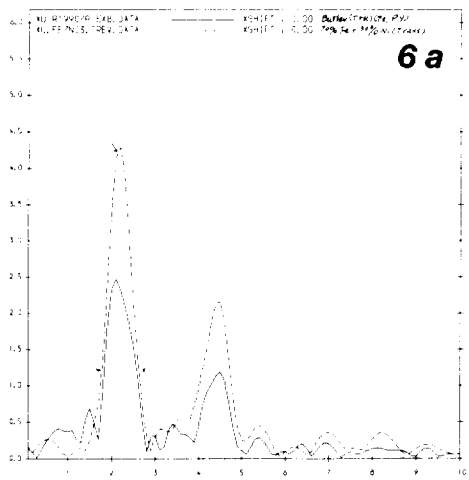

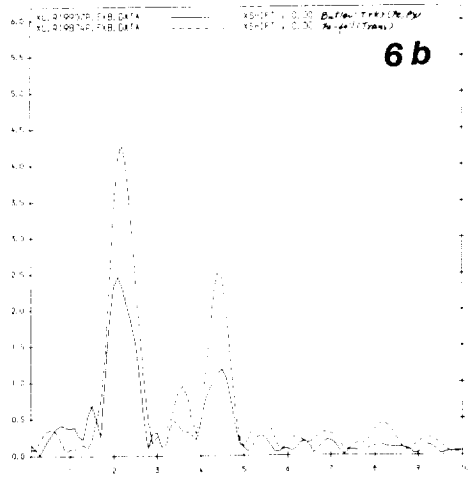

Fig. 6: (a) As 5(a) but for Butler.
Fig. 6: (b) Fourier transform of Butler Fe K-edge EXAFS + Fe foil.

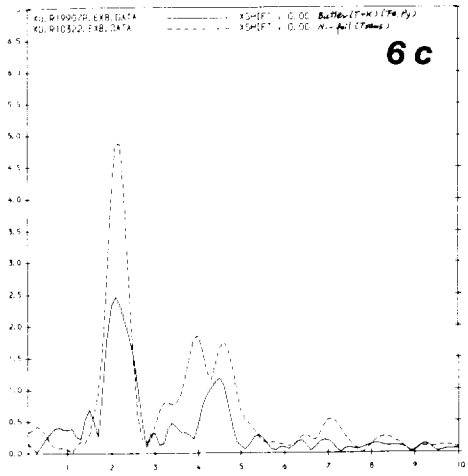

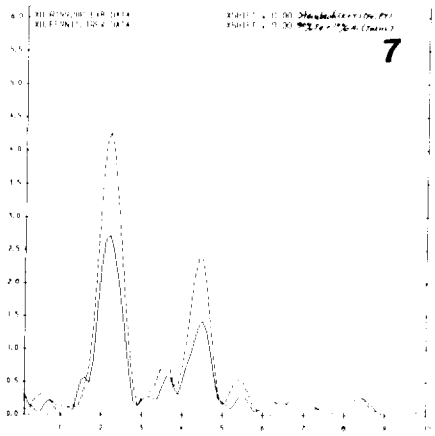

Fig. 6: (c) Fourier transform of Butler Fe K-edge EXAFS + Ni foil.
Fig. 7: As 5(a) but for Steinbach.

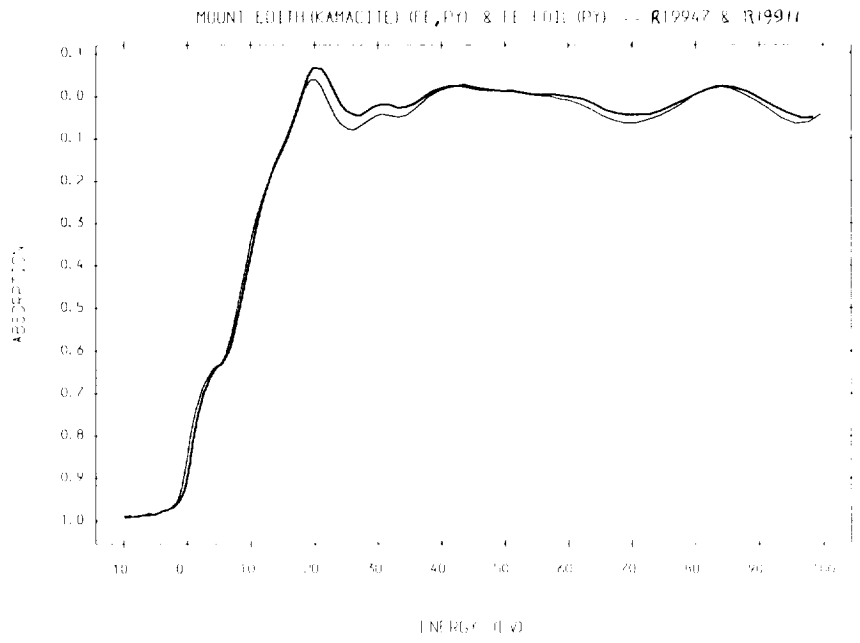

Fig. 8: (a) XANES in Fe K-edge spectrum of Mount Edith.

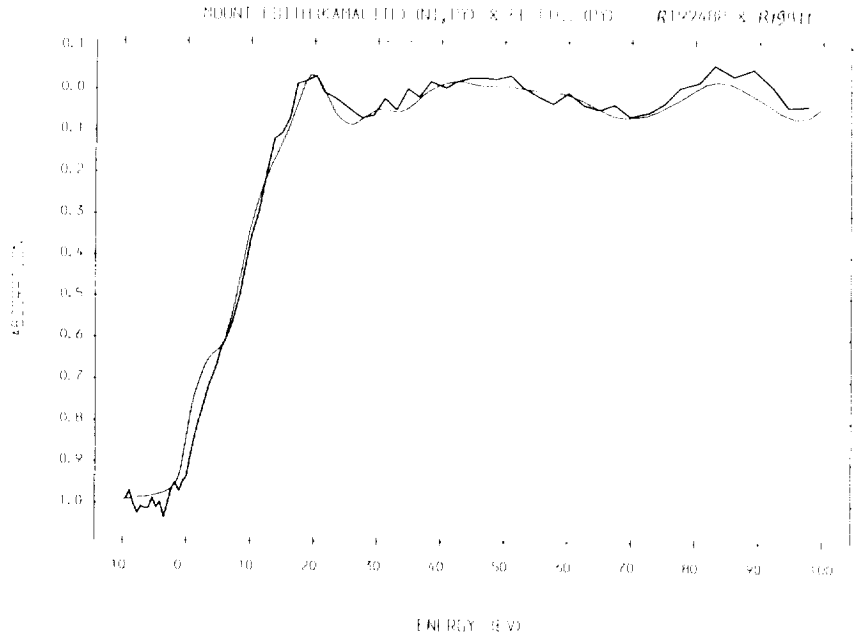

Fig. 8: (b) XANES in Ni K-edge spectrum of Mount Edith.

XANES at the Ni K-edge.

5. Conclusions and further work

Our results to date demonstrate that the relative proportions of kamacite and taenite in bulk samples can be determined with accuracy using EXAFS. Previous determinations have had to rely on optical micrograph and SEM techniques, which provide kamacite-taenite ratios in terms of the relative surface area occupation of the section under consideration; as such previous determinations have tended to be somewhat less representative of the actual bulk value. Since the kamacite-taenite ratio has direct bearing on the thermal history of iron meteorites EXAFS is capable of providing information on the cooling history of these materials (Saikumar & Goldstein 1988).

Our investigation of meteorites at the Daresbury SRS is continuing and future work will include EXAFS and powder diffraction studies of various chondritic meteorites, Brownlee (and other) particles and 'synthetic' dusts. Since EXAFS probes the local environment of specific species in the solid state this work will ultimately throw light on the likely nucleation and crystallization characteristics of cosmic (including interstellar) dusts.

References

Graham A. L., Bevan, A. W. R. & Hutchison, R., 1985,

Catalogue of Meteorites, British Museum.

Saikumar, V. & Goldstein, J. I., 1988, Geochim. Cosmochim.

Acta, **52**, 715.

Stern, E. A., 1978, Contemporary Phys., **19**, 289.

Wasson, J. T., Meteorites, Springer Verlag.

DUST OF ORIONID METEOR SHOWER IN THE EARTH ATMOSPHERE BEFORE AND AFTER HALLEY'S COMET

G. Mateshvili and Yu. Mateshvili

Abastumani Astrophysical Observatory
Academy of Sciences of the Georgian SSR

INTRODUCTION

Among the interesting questions concerning meteor streams associated with Comet Halley is the question of whether or not the activity of a meteor stream was connected with the approach of the comet to the terrestrial orbit in 1985-1986.

Meteoric aerosol getting to the upper atmosphere can be detected by twilight sounding, as has been done in former times by Link et al. in Czechoslovakia and in France [1,2] and in the USSR (in Odessa) by Kasan and Abastumani [3,4].

It has turned out that not only parameters describing some properties of aerosol can be obtained by twilight sounding, but also some characteristics concerning the structure of the stream can be derived.

Among the yearly active streams, the Orionides have always attracted the attention of scientists. The period of activity of the Orionides is October 18-26, and the maximum stream activity is October 21. Figure 1 shows the orbit of Comet Halley and that of the Earth and the dates when the orbits most closely approached one another (0.154 AU for the Orionides and 0.065 AU for the Eta Aquarides).

In detecting aerosol layers in the terrestrial atmosphere, a notion of the logarithmic intensity gradient of scattered twilight light is used, d log I/dH, where I is intensity and H is the real twilight beam height, which is a function of the wavelength observed.

We used a photoelectric photometer with an interference filter at the wavelength of 610 nm.

The observations were carried out in two points of the solar vertical; the zenith angle of the observations points was ±60°. The recording was carried on continuously in each direction during a minute, then the system was switched to the other direction. A calibration standard was recorded before each observation.

The observation dates in the Orionid periods of 1984, 1986, and 1987 are given in table 1.

RESULTS

In figures 2, 3, and 4 the logarithmic intensity gradient as a function of altitude is shown, with clearly pronounced aerosol layers, so that one can follow the layers lowering during several days.

The relations of intensities for two days, October 24 and 25, to that for October 15, i.e., for a day free from the effect of the meteor shower are also calculated for 1986. These relations for 1986 are given in figure 5 and table 2.

It can be seen from figure 5 and table 2 that after the maximum had passed, the intensity of scattered light increased throughout the middle atmosphere, which implies that some matter was distributed in it, consisting of different fractions that precipitated with different rates. Having calculated the ratio of the intensities obtained in 1986 to those of 1984, i.e., before and after the passage of Comet Halley, we found that the intensity of scattered light increased, for various altitudes, from 4 to 14 times (fig. 6).

For 1987, the ratios of intensities before and after the maximum stream (fig. 7) reveal no significant increase in intensity after the maximum of the stream, comparable with that for 1986.

Mean sizes of particles composing the layers are calculated from sedimentation velocities of the layers. Particle sedimentation velocity was determined using the Stokes-Cunningham law with the Cunningham correction,

$$V_t = \frac{2r^2}{g\eta} g(\rho_p - \rho_a)\,(1 + B\bar{l}/r)$$

where η is the air viscosity, ρ_p is the air density for the appropriate altitude, $\bar{l}$ is the mean free path of a molecule, B is a factor for which $\bar{l}r \geq 10$ (where r is the particle radius) equals 1.65. The air density for October was ascertained from CIRA-72.

For the Orionid-1984, the mean particle sedimentation velocity, from October 22–27, at altitudes of 70 to 80 km, was equal to 5.747 cm/sec. The estimated particle radii were ~0.08 μm, and the number density of particles 2.5 g/cm^3. For 1986, the mean particle radius at altitudes of 86 to 70 km, for the mean particle sedimentation velocity of 4.09 sm/sec was equal to 0.065 μm. If we assume the number density of the particles to be 2 g/cm^3, then their mass would be about 10^{-5} to 10^{-6} g.

The information about the structure of the Orionid meteor shower is taken mostly from radar measurement data as well as from visual observations. According to the data of the Spring Hill Meteor Observatory (Canada) [5] for 1958 to 1962, there are several peaks of various magnitudes in meteor hourly rates. In a number of papers (i.e., in those based on the observations carried in Kharkov, as well as in Ondřejov and Bologna [6]) either a shift of the peak of activity, or several peaks of various magnitude have been observed (figs. 8 and 9).

The results of those observations imply that the meteor shower has nonuniform, filamentary structure. This phenomenon can also be verified using twilight observation data, through amplifications of the intensities of scattered light on different heights, and in so doing, some fractions of finest particles can be detected that cannot be registered by the radar method.

In fact, three activity peaks were detected through intensity amplifications at altitudes of 80 and 90 km: on October 22, 25, and 27, 1984 (fig. 10). In 1986 and 1987, there was no possibility to embrace the whole period of activity of the Orionid meteor shower, but still one may note an amplification of scattered light intensity in the evening twilight on October 24, 1986, and another one which took place on October 21, 1987 (fig. 11).

REFERENCES

1. Link, F: Planet and Space Sci., vol. 23, no. 6, 1975.

2. Fechrenbach, U.; Frimout, D.; Link, F.; and Lippens, C.: Ann. Geophys., vol. 28, no. 2, 1972.

3. Divari, N.; and Mateshvili, Yu.: Astr. Lirk., no. 744, 1973.

4. Mateshvili, G.: Astr. Lirk., no. 1456, 1986.

5. Millman, P. M.; and McIntosh, B. A.: Canad. Jour. of Phys., vol. 42, 1964.

6. Hajdukova, M.; Hajduk, A.; Cevolan, G.; and Formiggini, C.: Astronomy and Astrophysics, vol. 187, no. 1/2, 1987.

TABLE 1.– OBSERVATION DATES

October	15	16	17	18	19	20	21	22	23	24	25	26	27
1984	---	---	---	---	---	---	---	E	E	E	E	E	M
1986	M	---	---	---	---	---	---	---	---	E	E	---	E
1987	---	E	---	---	---	E	E	M	---	---	---	---	---

Note: E is evening twilight, M is morning twilight.

TABLE 2.– RELATION OF INTENSITIES

H, km	$I_{24.X}/I_{15.X}$	$I_{25.X}/I_{15.X}$	$I_{27.X}/I_{15.X}$
40	5.5	10.7	3.8
50	3.9	6.8	3.6
60	4.0	4.8	3.5
70	3.8	4.1	3.0
80	3.2	2.9	---
90	3.0	1.7	---
100	4.0	1.9	---

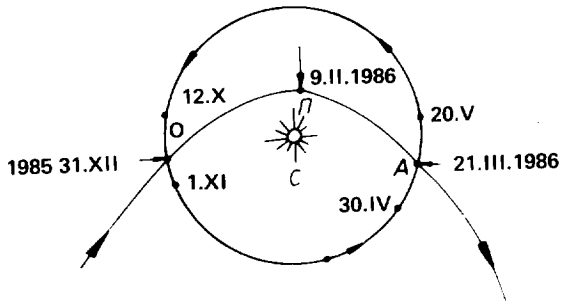

Figure 1

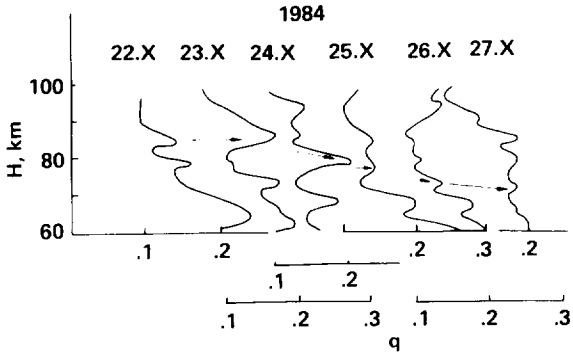

Figure 2

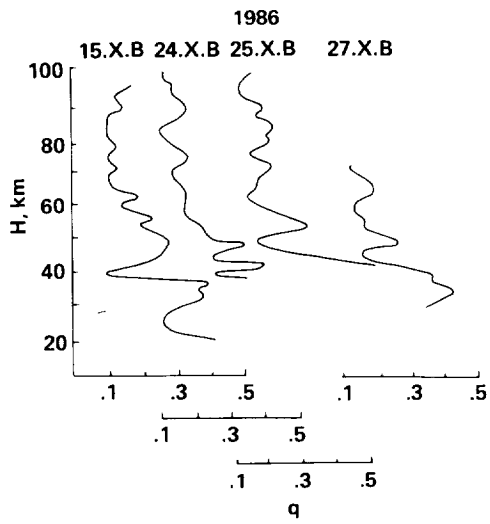

Figure 3

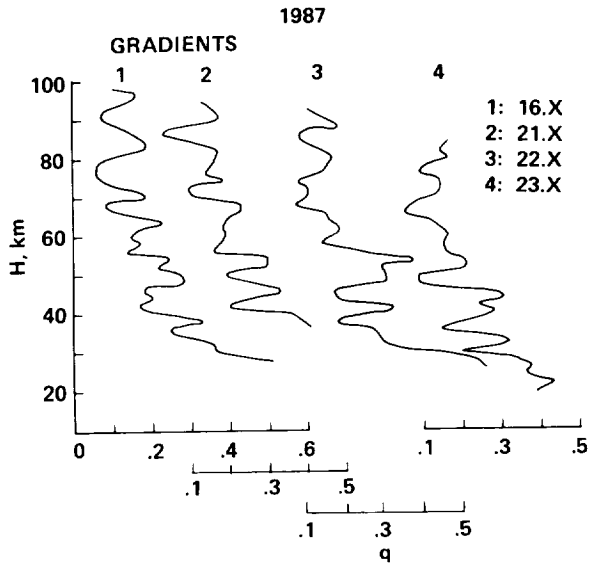

Figure 4

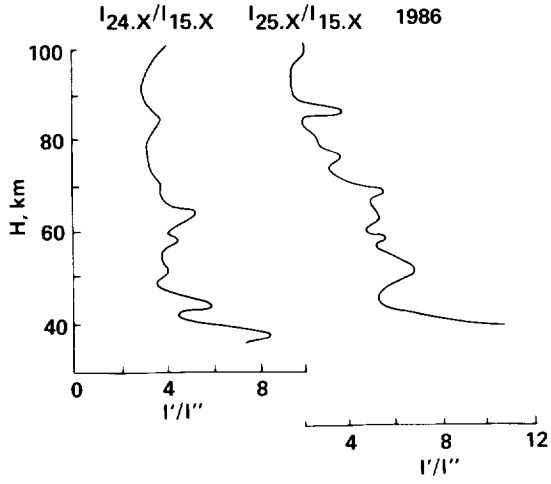

Figure 5

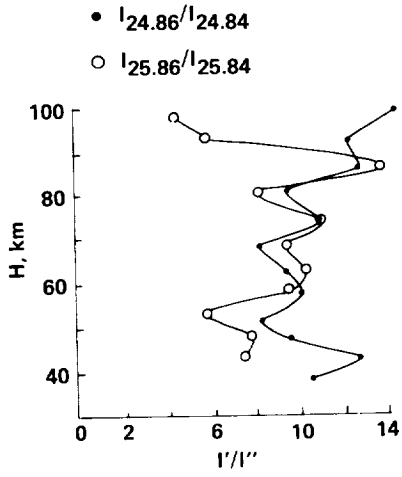

Figure 6

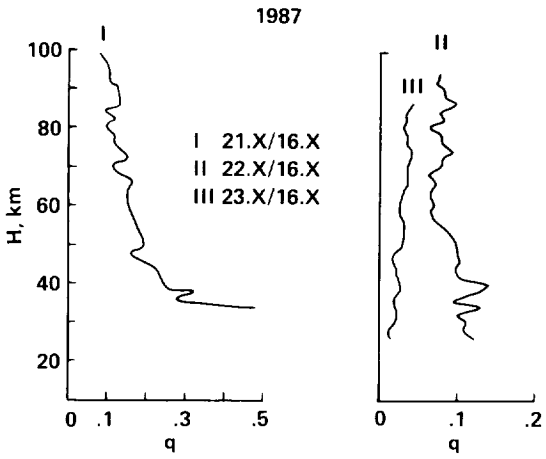

Figure 7

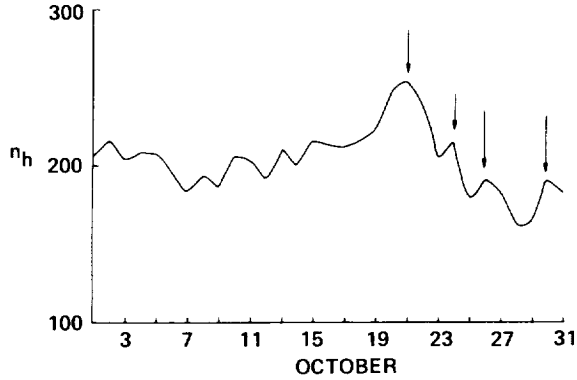

Figure 8

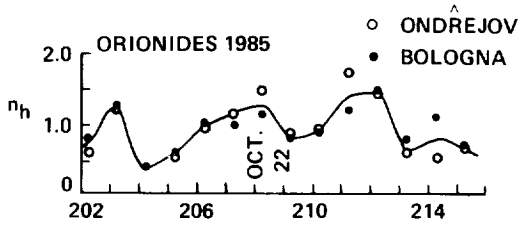

Figure 9

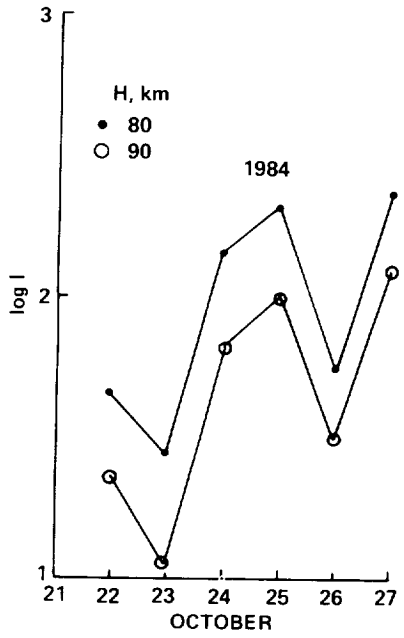

Figure 10

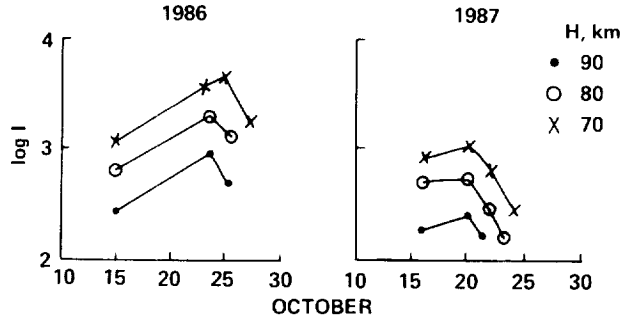

Figure 11

INFRARED EMISSION FROM INTERPLANETARY DUST

William T. Reach
Astronomy Department, University of California, Berkeley

I. INTRODUCTION

The infrared sky is dominated on large scales by emission from interplanetary dust, which produces the Zodiacal Emission (ZE), and interstellar dust (Hauser *et al.* 1984). These two components of the infrared background differ in angular and spectral distribution, allowing the two to be separated easily in some places. In this contribution, we describe our method of determining the emission from interplanetary dust near the Earth's orbit, and we compare our results to predictions for realistic materials with the interplanetary size distribution measured *in situ*.

II. OBSERVATION OF THE LOCAL VOLUME EMISSIVITY

The brightness of the ZE observed toward the north and south ecliptic poles varies sinusoidally with a period of one year, due to the inclination ($\simeq 1.8°$) of the Earth's orbit with respect to the surface of maximum interplanetary dust density. The polar brightness difference is equal to the integral of the local volume emissivity over the short path between the Earth and the symmetry plane, so we may determine the local emissivity from the amplitude of the annual brightness variation. We performed least-squares fits to the polar brightness data in the IRAS Zodiacal Observation History File, which contains the 0.5°-averaged sky brightnesses and pointing information as a function of time throughout the IRAS mission. The brightness differences are calculated from individual half-orbit scans, so that the calibration is identical. The derived local volume emissivities in the four IRAS bands are shown in Table 1. The uncertainties listed in this table are due only to the statistical uncertainty in the amplitude of the polar brightness variation.

The second method of determining the local emissivity uses the variation of the ZE brightness with the solar elongation angle, ϵ, defined as the angle between the line of sight and the sun. The gradient at $\epsilon = 90°$, *i.e.* tangent to the Earth's orbit, is equal to the local volume emissivity. We used least squares fits of the IRAS data, which cover $60° < \epsilon < 120°$, to determine the emissivities which are shown in the second row of Table 1. The least-squares fits were performed using a variety of terms in addition to those dependent on ϵ. A term proportional to the Galactic H I column density was crucial at 60 and 100μm, and significant in all four IRAS bands.

TABLE 1

Volume Emissivity of Interplanetary Dust[a]

	12μm	25μm	60μm	100μm
polar brightness variation	2.89 ± 0.03	4.85 ± 0.06	1.34 ± 0.04	0.65 ± 0.13
ecliptic plane gradient	3.19 ± 0.01	4.67 ± 0.03	1.74 ± 0.02	0.76 ± 0.04

[a] Units 10^{-29} erg cm^{-3} sec^{-1} Hz^{-1} Str^{-1}

The statistical uncertainties listed in Table 1 are underestimates of the true uncertainties, which include calibration and systematic errors. Note that since we use differential measurements, an isotropic background (instrumental or astronomical) would not affect our results directly.

III. Calculation of the Local Volume Emissivity

Assuming spherical grains, we calculated the interpalnetary emissivity using the measured optical properties of real materials and the size distribution of interplanetary dust. The interplanetary size distribution, from Grün *et al.* (1985), is constrained by satellite measurements of the particle flux in Earth orbit and by the lunar microcrater distribution (for pits larger than 7μm). Spectrum were calculated and averaged over the IRAS bandpasses, for comparison with the observations.

None of the materials is consistent with the overall level of the observed infrared emission. Those which best match the predicted spectra (silicates) predict an infrared emissivity roughly a factor of 2 fainter than observed. We cannot resolve this discrepancy, but we note that our calculations are consistent with the calibration of observations of Murdock and Price (1985).

Notwithstanding the problem with the overall brightness of the ZE, we can use the observed color ratios to constrain the constituent of interplanetary dust. Metallic grains of graphite and magnetite are inconsistent with the 12/25μm color ratio (too hot). The size distribution obtained by using lunar microcrater counts all the way down to submicron particles is also inconsistent with the observed ZE due to substantial emission by submicron grains, which are hotter than the $\sim 100\mu$m grains which produce the bulk of the emission.

IV. References

Grün, E., Zook, H.A., Fechtig, H., Giese, R.H. 1985, *Icarus*, **62**, 244.

Hauser, M.G., *et al.* 1984, *Ap. J. (Letters)*, **278**, L15.

Murdock, T.L. and S.D. Price 1985, *Astron. J.*, **90**, 375.

Reach, W.T. and C. Heiles 1988 in *Comets to Cosmology*, ed. A. Lawrence.

SECTION VIII: DUST FORMATION AND DESTRUCTION

VIII-A) DUST FORMATION

GAS-PHASE FORMATION OF SILICON CARBIDES, OXIDES AND SULPHIDES FROM ATOMIC SILICON IONS

Diethard K. Bohme, Stanislaw Wlodek and Arnold Fox
Department of Chemistry and Centre for Research in Experimental Space Science, York University, North York, Ontario, Canada M3J 1P3.

We have recently embarked on a systematic experimental study of the kinetics and mechanisms of the chemical reactions in the gas phase between ground-state $Si^+(^2P)$ and a variety of astrophysical molecules. The aim of this study is to identify the reactions which trigger the formation of chemical bonds between silicon and carbon, oxygen and sulphur and the chemical pathways which lead to further molecular growth. Such knowledge is valuable in the identification of new extraterrestrial silicon-bearing molecules and for an assessment of the gas-phase transition from atomic silicon to silicon carbide and silicate grain particles in carbon-rich and oxygen-rich astrophysical environments .

Ground-state $Si^+(^2P)$ ions are generated in our laboratory experiments in a Selected-Ion Flow Tube (SIFT) apparatus and reacted in helium buffer gas (at ca 0.35 Torr and 296 K) with added neutral molecules. Reactant and product ions are monitored as a function of the concentration of the added gas. These data provide rate constants and product distributions for the primary reactions. Secondary and higher-order reactions which lead to further ionic growth are also monitored, including the sequential growth of ions in which the silicon becomes increasingly co-ordinated. In natural environments which are partially ionized, such as diffuse or dense interstellar clouds or the atmospheres of certain stars, molecular ions formed in this manner may ultimately be neutralized by recombination with electrons without significantly disrupting their molecular composition and structure, and so provide sources for complex silicon-bearing molecules in these environments.

Ground-state silicon ions havebeen found to be unreactive toward H_2 and so should be available for reactions with other constituents in astrophysical environments in which hydrogen gas predominates (Wlodek et al, 1987).

FORMATION OF SILICON CARBIDES

Si-C bond formation has been found to be efficient with acetylene and cyanoacetylene which react rapidly with $Si^+(^2P)$ to form SiC_2H^+ by H-atom and CN elimination, respectively:

$$Si^+ + C_2H_2 \xrightarrow{0.7} SiC_2H^+ + H \quad (1a)$$

$$Si^+ + C_2H_2 \xrightarrow{0.3} SiC_2H_2^+ \quad (1b)$$

$$Si^+ + HC_3N \xrightarrow{0.7} SiC_2H^+ + CN \quad (2a)$$

$$Si^+ + HC_3N \xrightarrow{0.3} SiC_3HN^+ \quad (2b)$$

A secondary reaction of SiC_2H^+ with acetylene was observed to build up the carbon content further to produce SiC_4H^+ by H_2 elimination:

$$SiC_2H^+ + C_2H_2 \xrightarrow{0.9} SiC_4H_3^+ \quad (3a)$$

$$SiC_2H^+ + C_2H_2 \xrightarrow{0.1} SiC_4H^+ + H_2 \quad (3b)$$

SiC_2H^+ and SiC_4H^+ may neutralize by recombination with electrons or proton transfer to produce the carbide molecules SiC_2 and SiC_4. Ground-state silicon ions will also extract carbon from amines to form directly the neutral molecules SiCH and $SiCH_3$ as well as the ion $SiCH_2^+$, from acetonitrile to form $SiCH_2^+$, from acetone to form $SiCH_3$, from ethylene to form $SiC_2H_3^+$, and from methylacetylene to form $SiCH_2^+$, SiC_2H^+, and $SiC_3H_3^+$ (Wlodek and Bohme, 1988; Bohme et al, 1988).

Scheme 1 provides a summary of the observed ion chemistry which can be directed to the formation of silicon-carbide molecules.

It is interesting to note that Si^+ reacts only slowly with methane under our experimental conditions, $k = 5 \times 10^{-13}$ cm^3 molecule^{-1} s^{-1}, to form adduct ions, probably in a termolecular fashion:

$$Si^+ + CH_4 \longrightarrow SiCH_4^+ \quad (4)$$

Also diacetylene does not entrain silicon, reacting instead to form SiH:

$$Si^+ + C_4H_2 \longrightarrow SiH + C_4H^+ \quad (5)$$

FORMATION OF SILICON OXIDES

A rich chemistry was observed to be initiated and propagated with hydroxyl-containing molecules (Wlodek et al, 1987). Ground-state silicon ions were found to react with the molecules H_2O, CH_3OH, C_2H_5OH, HCOOH, and CH_3COOH to produce the silene cation $SiOH^+$ which may neutralize to form silicon monoxide:

$$Si^+ + XOH \longrightarrow SiOH^+ + X \quad (6)$$

$$SiOH^+ + e\,(B) \longrightarrow SiO + H\,(BH^+) \quad (7)$$

$SiH_3O_2^+$, which may neutralize to produce silanoic acid, is the predominat product in the reactions of $SiOH^+$ with H_2O, C_2H_5OH and HCOOH, while direct formation of silanoic acid is likely in the reaction with CH_3COOH. Further chemistry can be propagated by $SiH_3O_2^+$. It associates with H_2O and C_2H_5OH and produces $SiCH_3O_3^+$ and $SiH_5O_3^+$ with formic acid. Reaction sequences identified with CH_3OH, C_2H_5OH and HCOOH are postulated to lead to the complete saturation of Si^+ forming ions of the type $HSi(OCH_3)_3^+$, $HSi(OC_2H_5)_3H^+$, and $HSi(OH)_3H^+$ which may neutralize to generate trimethoxysilane, triethoxysilane and trihydroxysilane, respectively. Analogous reactions can be proposed which lead to the formation of tetrahydroxysilane which is a known building block for condensational synthesis of hydrated silica networks.

Scheme 1. Limited reaction scheme for the synthesis of silicon-carbide molecules initiate bu atomic silicon ions. The double arrows represent neutralization reactions such as proton transfer and electron/ion recombination.

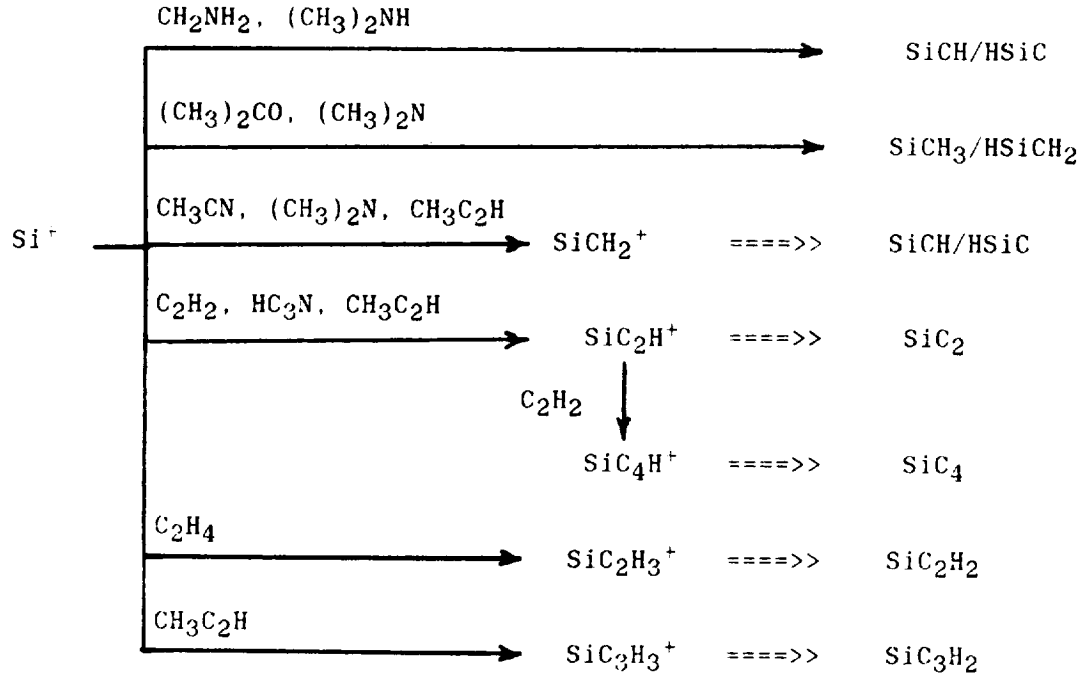

Schemes 2 and 3 provide a summary of the observed ion chemistry which can be directed to the formation of silicon-oxide molecules.

Scheme 2. Limited scheme for the synthesis of silicon-oxide molecules with ion chemistry initiates by Si^+ in ethanol and formic acid. The double arrows represent neutralization reactions such as proton transfer and electron/ion recombination.

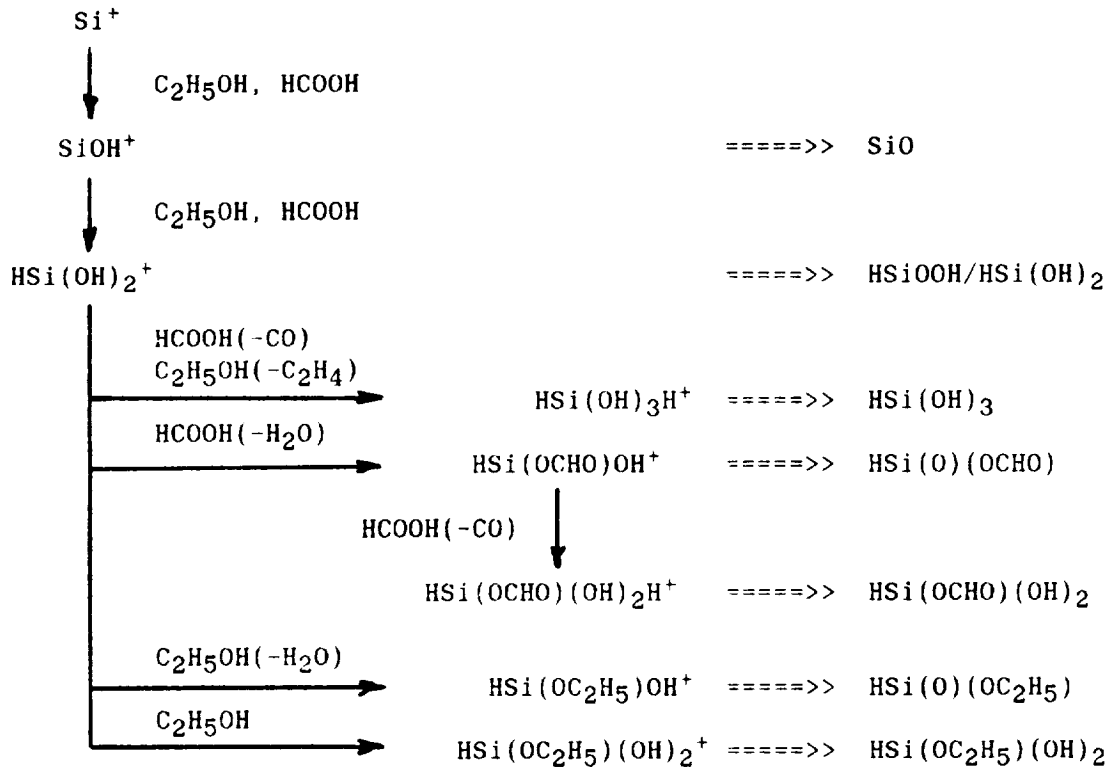

The oxidation of ground-state atomic silicon ions with diatomic and triatomic molecules not containing hydrogen was explored with O_2, NO, CO, CO_2, NO_2, SO_2, and N_2O. Bimolecular oxidation reactions which may proceed with these molecules include oxygen-atom transfer as indicated in reaction (8) and oxide-anion transfer as indicated in reaction (9). Both

$$Si^+ + XO \text{ -----> } SiO^+ + X \qquad (8)$$

$$Si^+ + XO \text{ -----> } SiO + X^+ \qquad (9)$$

reactions (8) and (9) were observed to occur rapidly when exothermic. Oxygen-atom transfer was observed with N_2O and NO_2, while oxide-anion transfer was observed to occur with NO_2 and SO_2. Slow adduct formation (with O_2, NO and CO_2), or no reaction (with CO) was observed when formation of SiO^+ or SiO was endothermic.

With N_2O oxidation was observed to proceed sequentially to produce polyoxide ions of the type SiO_n^+ as indicated in reaction (10):

$$Si^+ \xrightarrow{N_2O} SiO^+ \xrightarrow{N_2O} SiO_2^+ \xrightarrow{N_2O} SiO_3^+ \xrightarrow{N_2O} SiO_4^+ \qquad (10)$$

The production of these polyatomic ions was observed to compete with adduct formation and elimination of O_2^+ and SiO_2 which becomes important in the last two steps in the reaction sequence. The polyoxide ions pose interesting questions regarding their structure and the molecules which they may spawn upon neutralization.

Scheme 3. Limited reaction scheme for the synthesis of silicon-oxide molecules initiated by $SiOH^+$ in methanol and ethanol. The double arrows represent neutralization reactions such as proton transfer and electron/ion recombination.

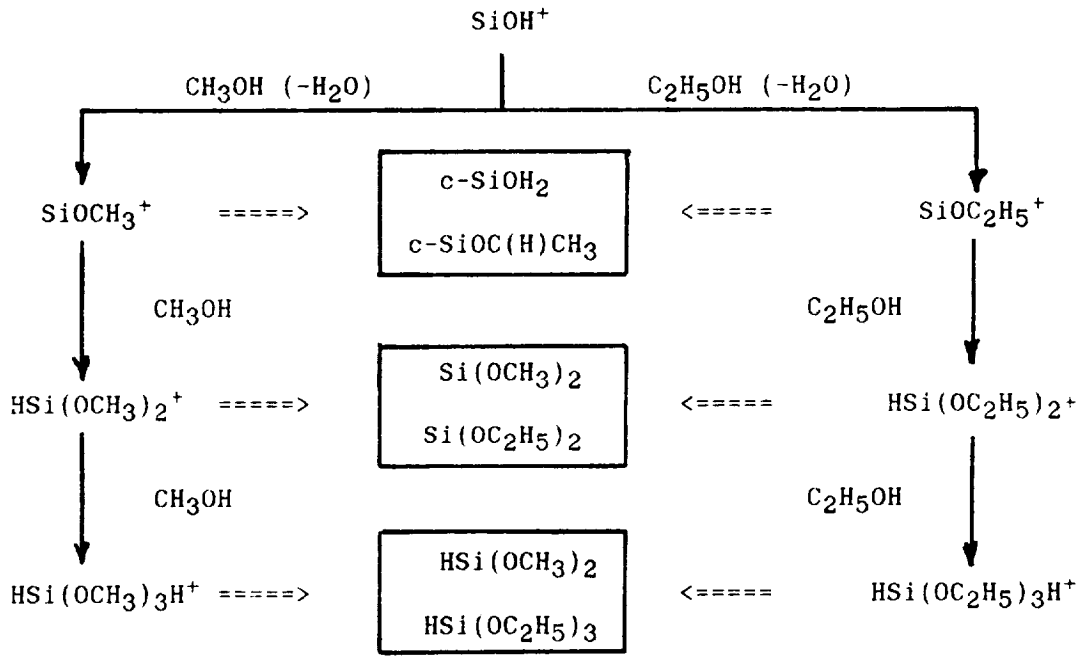

FORMATION OF SILICON SULPHIDES

Si-S bond formation was observed to proceed with H_2S and with COS in a reaction analogous to reaction (8):

$$Si^+ + H_2S \longrightarrow SiSH^+ + H \qquad (11)$$

$$Si^+ + COS \longrightarrow SiS^+ + CO \qquad (12)$$

The polysulphide ions SiS_2^+ and SiS_3^+ were observed to be formed sequentially with COS as reactant.

$$Si^+ \xrightarrow{COS} SiS^+ \xrightarrow{COS} SiS_2^+ \xrightarrow{COS} SiS_3^+ \qquad (13)$$

Charge-transfer reactions with molecules which have ionization energies lower than the recombination energies of these ions can lead to formation of the polysulphide molecules.

SUMMARY

The experimental studies reported here are providing clues to the formation of a large number of silicon-containing molecules in partially ionized astrophysical environments. For example, the gas-phase ion/molecule reactions which have been identified in our studies so far represent possible contributors to the formation of the following silicon-carbide, silicon-oxide and silicon sulphide molecules:

SiCH, SiC_2, $SiCH_3$, SiC_4, SiO, SiO_2, SiS, SiS_2, HSiOOH, $SiOCH_2$, $HSiC(H)CH_3$, $HSi(OH)_3$, HSi(O)(OCHO), $HSi(O)(OC_2H_5)$, $HSi(OCHO)(OH)_2$, $Si(OCH_3)_2$, $HSi(OCH_3)_3$, $Si(OC_2H_5)_2$, $HSi(OC_2H_5)_3$.

Current investigations are being directed toward ion/molecule reactions of $Si^+(^2P)$ which can lead to bonding with still other heavy atoms, and toward a further elucidation of the kinetics and mechanisms of the higher-order chemistry which can lead to still further growth and perhaps ultimately to the formation of small silicon-carbide and silicon-oxide particles.

Acknowledgment

We thank the Natural Sciences and Engineering Research Council of Canada for financial support of this research.

References

Bohme, D.K., Wlodek, S. and Fox, A.: 1988, in "Rate Coefficients in Astrochemistry", T.J. Millar and D.A. Williams (Eds.), Kluwer Academic Press, 193 (1988).

Wlodek, S., Bohme, D.K.: 1988, J. Am. Chem. Soc. 110, 2396.

Wlodek, S., Fox, A. and Bohme, D.K.: 1987, J. Am. Chem. Soc. 109, 6663.

N91-15015

PAH FORMATION IN CARBON-RICH CIRCUMSTELLAR ENVELOPES

Eric D. Feigelson* and Michael Frenklach**
*Dept. of Astronomy, Penn State University, University Park, Pennsylvania 16802 USA
**Dept. of Material Science and Engineering, Penn State University, University Park, Pennsylvania 16802 USA

Motivation and Summary

While there is growing observational evidence that some fraction of intestellar carbon is in polcyclic aromatic hydrocarbons, the mechanisms by which these molecules might be formed have not been extensively studied. We briefly present here, and more completely elsewhere (Frenklach and Feigelson 1988), a detailed investigation of PAH production in the outflowing molecular envelopes of carbon-rich red giant stars. The gas-phase kinetics of a chemical reaction mechanism developed by Frenklach and co-workers to study soot production in hydrocarbon flames is modified to apply in circumstellar environments. We find that astrophysically significant quantities of PAHs can be formed in carbon star envelopes provided the gas is sufficiently dense and resides for a long time in the temperature range 900 to 1100 K. The precise yield of PAHs is very sensitive to astronomical parameters of the envelope (e.g. mass loss rate, outflow velocity, acetylene abundance) and certain poorly determined chemical reaction rates.

Chemical and Astronomical Model

A chemical reaction mechanism involving >40 hydrocarbon species and >100 reactions was constructed from the models of PAH formation and growth in terrestrial pyrolytic and combustion environments (e.g. Frenklach et al. 1985, 1986). The terrestrial mechanism was shortened, revised for high temperatures and low pressures, and updated with recent rate coefficients. Four different first-ring cyclization paths are considered, including chemical activated processes. PAH growth beyond two rings is modeled with a linear lumping algorithm (Frenklach and Gardiner 1984).

Time-dependent non-equilibrium concentrations of each species was calculated for a range of density and temperature profiles characteristic of outflowing circumstellar envelopes. Most models were based on simple constant-velocity winds with density $n \sim \dot{M}/r^2v$,

temperature $T \sim r^{-\alpha}$, and time variable $t \sim r/v$. The concentration of acetylene C_2H_2 at the base of the wind must also be assumed. Published models of red giant molecular envelopes, particularly IRC +10216, were also examined.

Results

Figure 1 presents the calculated PAH production in a constant-velocity model with wind parameters $\dot{M} = 10^{-4}$ $M_\odot$/yr, v = 0.01 km/s, $[C_2H_2]/[H_2] = 10^{-4}$, $\alpha = 0.5$ and stellar parameters $R_* = 10^{14}$ cm and $T_* = 1500$ K. The top panel shows the assumed temperature and density profiles. The middle panel (right axis) shows that the calculated PAH yield increases only when $1100 > T > 900$ K. Yield is defined to be the fraction of carbon initially in C_2H_2 incorporated into molecules with >2 aromatic rings. The mean PAH size μ is generally ~40 carbon atoms per molecule. The lower panel gives the standard deviation and skewness of the PAH Asize distribution. Our models all show a wide range of PAH sizes. This contrasts with the results of Keller (1987), who concludes that PAH growth in circumstellar envelopes proceeds rapidly until extremely large molecules are formed.

A grid of wind models similar to Figure 1 indicates PAH production is very sensitive to certain wind parameters. We find the yield depends approximately as:

$$Y \approx 1\% \left(\frac{v}{10^{-2}\ \mathrm{km\ s^{-1}}}\right)^{-4.0} \left(\frac{\dot{M}}{10^{-4}\ M_\odot\ \mathrm{yr^{-1}}}\right)^{2.5}$$

and scales with the cube of the acetylene abundance. Stated from a different perspective, the yield appears to depend mainly on the density and time spent in the PAH-producing temperature range $900 < T < 1100$ K, approximately as:

$$Y \approx 1\% \left(\frac{n_{T=1000K}}{3\times10^{12}\ \mathrm{cm^{-3}}}\right)^{2.5} \left(\frac{\Delta t_{1100>T>900K}}{1\times10^{11}\ \mathrm{s}}\right)^{1.5}$$

for $R_* = 10^{14}$ cm and $0.3 < \alpha < 0.8$. Yields can exceed 90% in extreme cases. The yield for a fixed wind model can change by 1-2 orders of magnitude as certain chemical reactions rates (e.g. involving $H_2C{=}C{:}$) are varied over ranges consistent with measurements. Given these strong dependencies and uncertainties, it is difficult to predict accurately the PAH production in a given star or ensemble of stars.

Discussion

The dominant pathway we found for PAH formation in the outflowing envelopes is shown in Figure 2. The principal feature -- H abstractions followed by C_2H_2 additions -- is the same as that

identified in terrestrial acetylene pyrolysis (Frenklach et al. 1985). However, important differences are seen: in circumstellar environments the high ambient H_2 concentration suppresses H abstraction, and thus PAH production, at the high temperatures (1400-2000 K) seen under terrestrial conditions. At temperatures around 1000 K, the irreversibility of the acetylene addition step drives PAH formation and growth. Analysis also suggests that the addition of other chemical species (e.g. CO, O_2, electronically excited species) will not qualitatively affect our PAH-producing mechanism. Condensation of PAHs onto silicon carbide grains, however, should be considered.

Astronomically, our study implies that PAHs will form in carbon-rich circumstellar envelopes if their densities, $[C_2H_2]/[H_2]$ ratios, and residence times in the 900-1100 K temperature window are sufficiently high. Outflow velocities at these temperatures must be 10^{-3} times typical terminal wind velocities. Such quasi-static warm regions have in fact been observed in red giant and supergiants (Tsuji 1987), and appear in the Lafont et al. (1982) model of IRC +10216. If such conditions are sufficiently common, then the concentration of PAH molecules introduced into the interstellar medium could be substantial.

References

Frenklach, M., Clary, D. W., Gardiner W. C., and Stein, S. E.: 1985, in 20th Symp. Intl. Combustion, Pittsburgh:Combustion Inst., 887.

Frenklach, M., Clary, D. W., Yuan, T., Gardiner, W. C., and Stein, S. E.: 1986, Combust. Sci. Technol. 50, 79.

Frenklach, M. and Feigelson, E. D.: 1988, submitted to Astrophys. J.

Frenklach, M. and Gardiner, W. C.: 1984, J. Phys. Chem. 88, 6263.

Keller, R.: 1987, in PAHs and Astrophysics (A. Leger, L. d'Hendecourt and N. Boccara, eds.), Dordrecht:Reidel, 387.

Lafont, S., Lucas, R. and Omont, A.: 1982, Astron. Astrophys. 106, 201.

Tsuji, T: 1987, in Astrochemistry (M. S. Vardya and S. P. Tarafdar, eds.), Dordrecht:Reidel, 409.

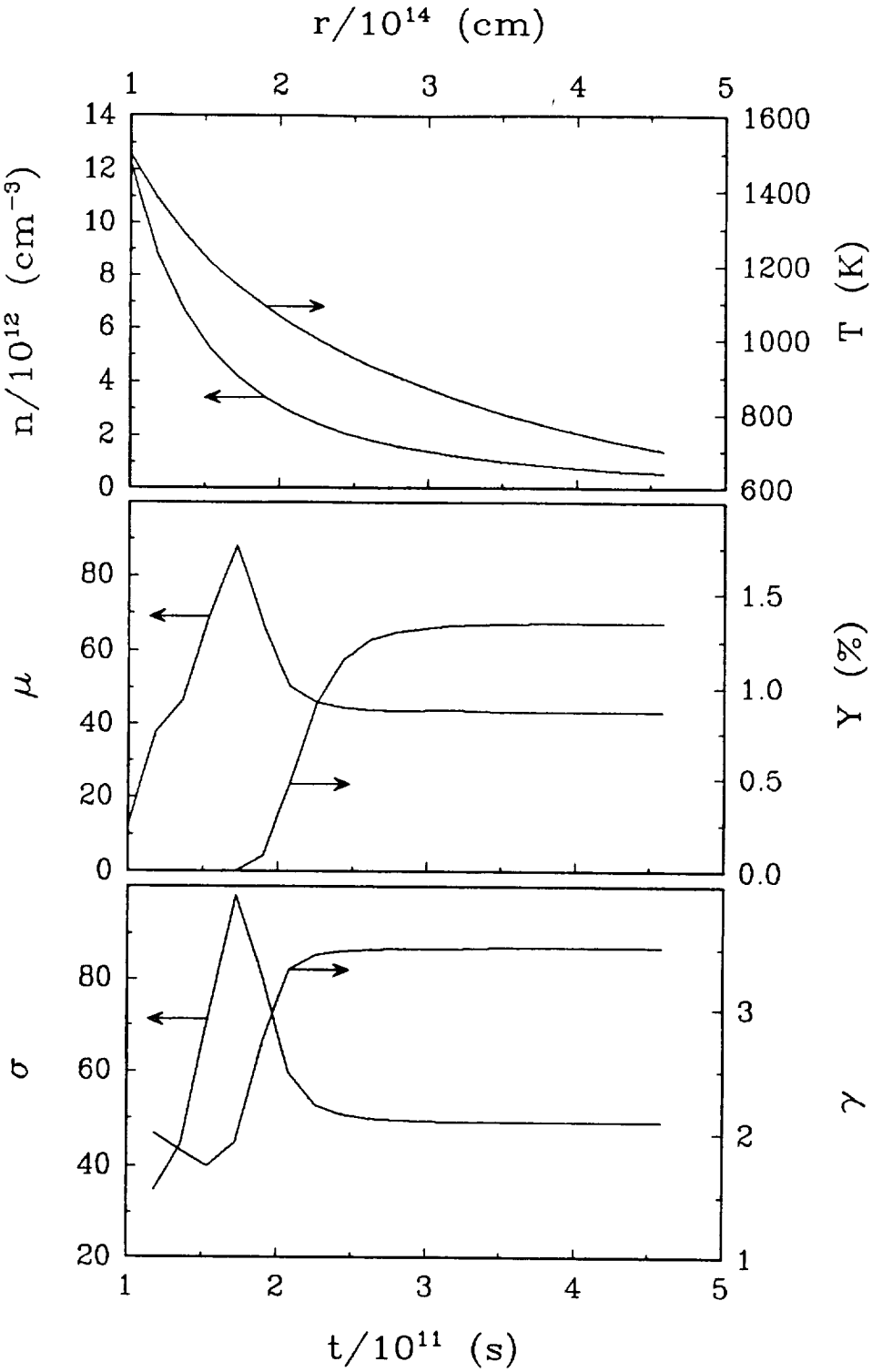
r/10^14 (cm)
1
2
3
4
5
14
12
10
8
6
4
2
0
n/10^12 (cm^-3)
1600
1400
1200
1000
800
600
T (K)
80
60
40
20
0
μ
1.5
1.0
0.5
0.0
Y (%)
80
60
40
20
σ
3
2
1
γ
t/10^11 (s)

FIGURE 1

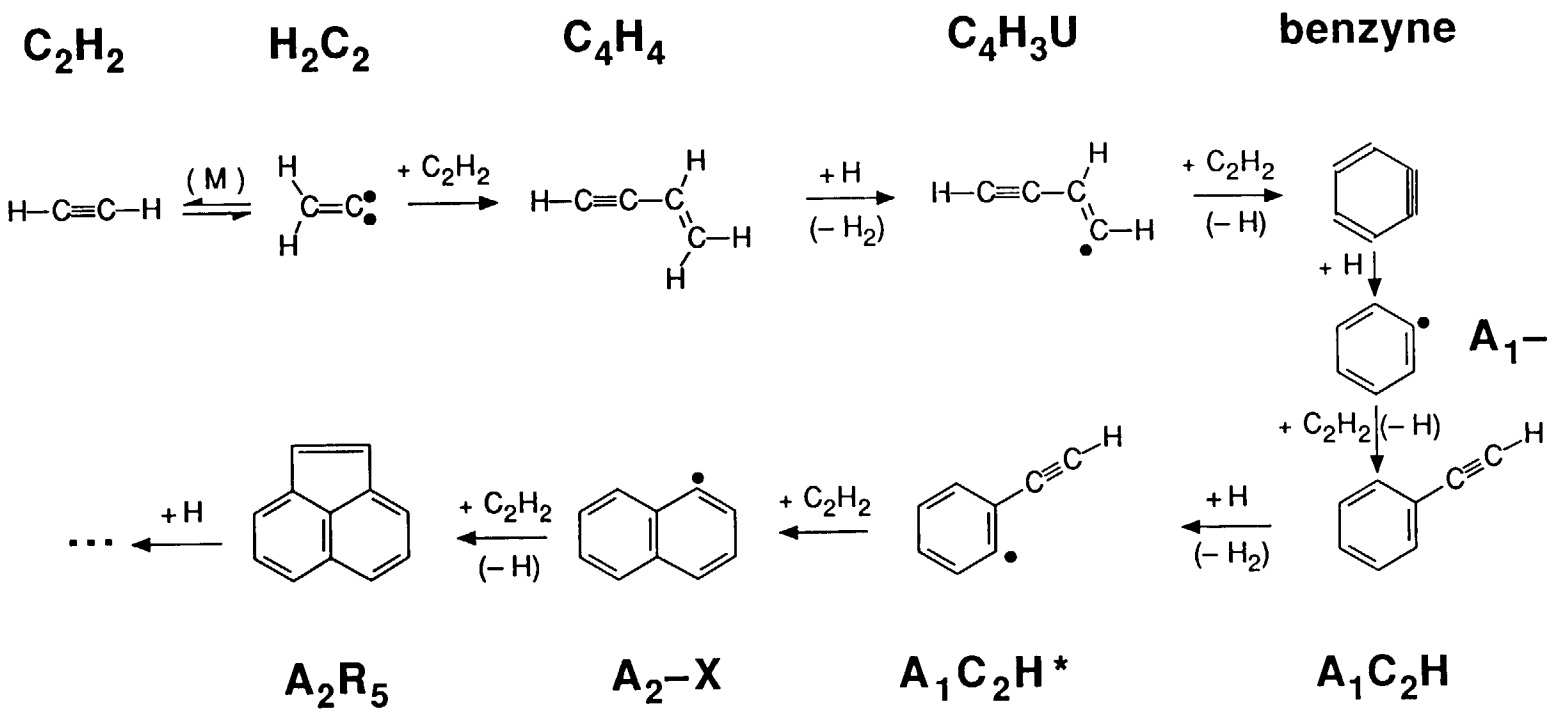
C2H2
H2C2
C4H4
C4H3U
benzyne
H–C≡C–H
(M)
+ C2H2
+H
(– H2)
+ C2H2
(– H)
+ H
A1–
+ C2H2 (– H)
+H
(– H2)
+ C2H2
+ C2H2
(– H)
+H
A2R5
A2–X
A1C2H*
A1C2H

FIGURE 2

SUBLIMATING ICY PLANETESIMALS AS THE SOURCE OF NUCLEATION SEEDS FOR GRAIN CONDENSATION IN CLASSICAL NOVAE

J.J. Matese*, D.P. Whitmire*, R.T. Reynolds**
*Physics Department, Univ. of Southwestern Louisiana, Lafayette, Louisiana 70504-4210
**NASA Ames Research Center, Moffett Field, CA 94035 USA

ABSTRACT. The problem of grain nucleation during novae outbursts is a major obstacle to our understanding of dust formation in these systems. How nucleation seeds can form in the hostile post-outburst environment remains an unresolved matter. We suggest here that the material for seeding the condensation of ejecta outflow is stored in a primordial disk of icy planetesimals surrounding the system. Evidence is presented that the requisite number of nucleation seeds can be released by sublimation of the planetesimals during an outburst.

I. INTRODUCTION

The sources of the small dust grains observed by IRAS around Vega, β-Pic and numerous other old main sequence stars are believed to be extended shells or disks of cometary material (Harper et al., 1984; Weissman, 1984). The mass of material directly seen in these systems in the form of particle sizes ≤ 1 mm is ≥ 0.01 $M_\oplus$ (Gillett, 1986). Since the optical depth in these systems implies that collision time scales are less than their ages, there must be unseen parent bodies which repopulate the smaller sizes and significantly add to the total mass contained in these disks (Whitmire et al., 1988). Indeed the conventional viewpoint is that primordial disks of icy planetesimals will survive in transplanetary regions (Kuiper, 1951; Cameron, 1962). It has been argued that the Solar System contains such a disk from which short period comets originate (Fernandez, 1980; Matese and Whitmire, 1986; Duncan et al., 1988). The mass content out to 100 AU is estimated to be $\sim$1 $M_\oplus$. It is to be emphasized that the cometary disk discussed here is distinct from the conventional isotropic inner (Hills, 1981) and outer Oort cloud.

Here we estimate the amount of dust that will be released from such a disk during a classical nova outburst. The significance of this source of dust to the grain condensation problem will then be described.

II. ANALYSIS

It has been shown (Ney, 1982) that the observed mass loss rate (volatiles and solids) for comets can be fit to the form

$$dM/dt = -kM^{2/3} \exp(-1552/T) \qquad (1)$$

where T is the local blackbody temperature in kelvins. The Boltzmann factor is appropriate for the activation energy of water release from clathrates whereas the coefficient k depends on specific surface absorptivity and activity, being smaller for older comets like Encke (Ferrin and Gil, 1988). We assume that equation (1) is applicable to smaller icy planetesimals as well. When such objects are exposed for a time t to the emerging flux of a nova outburst of luminosity $L \approx L_{Edd} = 4 * 10^4 L_\odot$ then all planetesimals of initial mass $M_0 < M_c(t)$ will be completely sublimated. One finds

$$M_c(t) = [(kt/3) \exp(-1552/T)]^3$$
$$= 3 * 10^8 g\ (t/60d)^3 \exp[-1.2(L_{Edd}/L)^{\frac{1}{4}} R^{\frac{1}{2}}(AU)]. \qquad (2)$$

In evaluating equation (2) we have conservatively adopted the value of k appropriate to Encke, $k(Encke) = 3.7 * 10^{-4}\ g^{1/3}\ s^{-1}$.

Those planetesimals of initial mass $M_c(t) < M_0 < M_{max}$ will be partially sublimated. If the initial number density of these objects is represented by the power law M_0^{-b} then the fraction of the net mass content of these objects which is released is given by

$$\epsilon(t) = C_b\ (M_c(t)/M_{max})^{2-b} \qquad (3)$$

where C_b is order(1) for $5/3 < b < 2$.

Therefore, 60 days subsequent to an outburst of $L = L_{Edd}$, planetesimals at a distance of 50 AU will have all of their volatiles sublimated and their dust released if their mass is $\leq 6 * 10^4$ g. At this distance the blackbody temperature is $\approx$ 55OK but the dust would be hotter if it radiated inefficiently. A cometary distribution with $b = 11/6$ (corresponding to a size power law of 7/2) and $M_{max} = 10^{21}$ g would release a mass fraction $\epsilon(60d) = 0.004$. The planetesimals that do survive should be stirred due to outgassing (Katz, 1988), thus providing a mechanism for collisionally repopulating the size distribution for masses $< M_c$ in the intervening time between outbursts. In turn the disk should thicken somewhat.

III. DISCUSSION

Although correlations between outburst characteristics (speed class, energy output, system velocities) and dust characteristics (production onset, optical depth) do exist (Gallagher and Starrfield, 1978), there

are enough exceptions (eg. Gehrz et al., 1988) to preclude a clear understanding of how conventional ideas can predict the location where dust begins to form and how much dust will form.

Dust growth requires a nucleation seed (a cluster exceeding a critical size where condensation is more likely than evaporation) as well as outflow properties that are conducive to an increase in size. There is considerable controversy over whether classical nucleation theory (eg. Draine and Salpeter, 1977) is applicable (Draine, 1985; Donn and Nuth, 1985) but in any case the formation of seeds is as yet an unresolved problem. We suggest that the problem can be mitigated if icy planetesimals do indeed survive in the regions around 50-100 AU as argued in the Introduction.

If 10^{-3} $M_{\oplus}$ of material is released from planetesimals during an outburst and ten percent (Ney, 1982) is in the form of solids then 3 * 10^{-10} $M_{\odot}$ of dust grains will be deposited in the disk and subjected to the ablative and accelerative effects of the outflow. This amount of material is comparable to that estimated to exist surrounding the dust-poor slow nova PW Vulpeculae (Gehrz et al., 1988). If such a dust disk is formed in an outflow where condensation is kinetically favorable and the mean grain radius enlarged by a factor of ten, then an enhancement in the mass of dust to levels estimated to exist in dust-rich novae will occur. Some distinguishing features of this model from other models that invoke preexisting dust grains or nucleation seeds (see eg. Bode and Evans, 1980) are that prior to the eruption the preponderance of pre-ablated seeds were stored, since primordial times, inside icy planetesimals having a disklike distribution. Thus first time novae are equally likely to show IR excesses.

Finally, we emphasize that the nucleation seed distribution would be disklike in our model. Therefore, independent of the distribution of ejecta from the C-O white dwarf, the distribution of condensates should also be disklike rather than isotropic.

ACKNOWLEDGEMENTS

J.J. Matese and D.P. Whitmire wish to recognize the support provided by the NASA-ASEE Summer Faculty Fellowship Program.

REFERENCES

Cameron, A.G.W.: 1962, Icarus 1, 13.

Donn, B., and Nuth, J.: 1985, Ap. J. 288, 187.

Draine, B.T. and Salpeter, E.E.: 1977, J. Chem. Phys. 67, 2230.

Draine, B.T.: 1985, NASA Conf. Pub. 2403, 19.

Duncan, M., Quinn, T. and Tremaine, S.: 1988, Ap. J. Lett. 328, L69.

Fernandez, J.: 1980, Mon. Not. R. Astron. Soc. 192, 481.

Ferrin, I. and Gill, C.: 1988, Astron. Astrophys. 194, 288.

Gallagher, J.S. and Starrfield, S.: 1978, Ann. Rev. Astron. Ap., 16, 171.

Gehrz, R.D., Harrison, T.E., Ney, E.P., Matthews, K., Neugebauer, G., Elias, J, Grasdalen, G.L., and Hackwell, J.A.: 1988, Ap. J. 329, 894.

Gillett, F.C.: 1986, Light on Dark Matter, ed. Israel, F.P. (Reidel, Dordrecht), 61.

Harper, D.A., Lowenstein, R.F., and Davidson, J.A.: 1984, Ap. J. 285, 808.

Hills, J.G.: 1981, Astron. J. 86, 1730.

Katz, J.I.: 1986, Ap. J. 309, 253.

Kuiper, G.P.: 1951, Astrophysics, ed. Hynek, J.A. (McGraw-Hill, NY), 357.

Matese, J.J., and Whitmire, D.P.: 1986, Icarus 65, 37.

Ney, E.P.: 1982, Comets, ed. Wilkening, L.L. (Univ. of Arizona Press, Tucson), 333.

Weissman, P.: 1984, Science 224, 987.

Whitmire, D.P., Matese, J.J. and Tomley, L.J.: 1988, Astron. Astrophys. Lett., in press.

DUST FORMATION AROUND M-TYPE STARS

Takashi Onaka
Department of Astronomy, Faculty of Science, University of Tokyo
Bunkyo-ku, Tokyo 113, Japan

IRAS LRS spectra (IRAS team, 1986) of M Mira variables have shown a large variation in the appearance of the 9.7 μm silicate feature, which is correlated with the shape of light curve (*cf.*, Vardya *et al.*, 1986). Onaka and de Jong (1987) and Onaka *et al.* (1988) have studied the LRS spectra of about 100 Mira variables by using simple dust shell models containing mixtures of silicate and aluminum oxide dust grains. They have shown that the aluminum oxide grains account for the observed broad feature around 12 μm and that the variation of the spectra can be interpreted in terms of the variation of the temperature at the inner boundary of silicate dust shell. They have proposed silicate mantle growth on aluminum oxide grains as a possible explanation for the results. In this report, we calculate model spectra taking account of silicate mantle growth and investigate the physical parameters which may determine the appearance of the 9.7 μm feature in M Mira variables.

In the model calculation it is assumed that aluminum oxide grains are already formed at the bottom of the circumstellar envelope because of their high condensation temperature (~ 1500 K). The growth of silicate mantle and the motion of gas and grains from $r=r_0$, where the mantle growth starts, are investigated. Sticking and sputtering processes due to the relative motion of grain to the ambient gas are taken into account. The thermal velocity is assumed to be negligible to the drift velocity. Acceleration by radiation pressure is considered in the gas motion equation. The formal solution is integrated to obtain the emergent spectra. Physical conditions inside r_0 are regarded as boundary conditions. Observed spectra are compared to model spectra to investigate the conditions at the bottom of circumstellar envelope. In modelling the envelope, a parameter C_l is introduced to take account of the density fluctuation of the envelope phenomenologically.

Silicate mantle growth on an aluminum oxide grain can be written as

$$\frac{dA}{d\bar{R}} = -\frac{F_R}{V(1+\bar{V}_d)}\left[1-\frac{A^3-1}{A_f^3-1}-\sum_i \frac{f_i}{f}S_i\right] \tag{1}$$

with $A=a/a_0$, $\bar{R}=r_0/r$, $V=v/v_0$, $\bar{V}_d=v/v_d$, and $A_f=a_f/a_0$. Here, a is the grain radius including core and mantle, a_0 the core radius, r the distance from the star, v the gas velocity, $v_0=v$ at $r=r_0$, and v_d the drift velocity of the grains relative to the ambient gas. The parameter a_f is determined by the abundance ratio of silicate to aluminum oxide, being about 3. The last term in the parentheses represents the erosion due to sputtering: f_i is the relative cosmic abundance of element i and S_i the sputtering yield taken from Kwok (1975). Sputtering is negligible unless v_d exceeds 20 km/sec. The parameter F_R describes the rate of mantle growth and is given by

$$F_R = \frac{\dot{M} f \Omega}{16\pi a_0 r_0 v \mu m_H} \approx 1.35\left[\frac{\dot{M}}{10^{-6}\,M_\odot/\mathrm{yr}}\right]\left[\frac{10\ \mathrm{nm}}{a_0}\right]\left[\frac{6\cdot10^{14}\ \mathrm{cm}}{r_0}\right]\left[\frac{10\ \mathrm{km/sec}}{v_0}\right] C_l, \tag{2}$$

where $\dot{M}$ is the mass loss rate, f the fraction of the condensible material (~ $3\cdot10^{-5}$), Ω the volume of the monomer (~ $5\cdot10^{-23}$ cm^3), μ the molecular weight (~ 1.4), and m_H the hydrogen mass.

The change of the velocity due to the radiation pressure may be given by

$$\frac{dV}{d\bar{R}} = -\frac{F_V}{V}\left[\frac{g\,A^2\,Q_p\,\bar{V}_d}{1+\bar{V}_d} - 1\right], \tag{3}$$

where Q_p is the radiation pressure coefficient of the grains and the parameters g and F_V are defined as

$$g = \frac{3\,L\,f_g}{16\pi\,c\,G\,M\,d\,a_0} \approx 9.0\left[\frac{10\text{ nm}}{a_0}\right] \tag{4}$$

and

$$F_V = \frac{G\,M}{r_0\,v_0^2} \approx 0.22\left[\frac{6\cdot10^{14}\text{ cm}}{r_0}\right]\left[\frac{10\text{ km/sec}}{v_0}\right]^2. \tag{5}$$

Here L is the stellar luminosity ($\sim 2.5\cdot10^{37}$ erg/sec), M the stellar mass ($\sim 2\cdot10^{33}$ g), f_g the mass fraction of aluminum oxide ($\sim 9.6\cdot10^{-5}$), d the density of aluminum oxide (~ 4 g/cm^3), c the light velocity, and G the gravity constant.

The drift velocity variable $\bar{V}_d$ is given, if the thermal velocity is much smaller than v_d, by

$$\bar{V}_d = \left[\frac{\dot{M}\,c\,v}{Q_p L}\right]^{1/2} \approx 0.276\left[\frac{\dot{M}}{10^{-6}\,M_\odot/\text{yr}}\right]^{1/2}\left[\frac{V}{Q_p}\right]^{1/2} C_l^{1/2}. \tag{6}$$

The emergent flux is obtained by the integration of the formal solution (Chandrasekhar, 1960):

$$F_\lambda = \pi\left[\frac{R_*}{D}\right]^2 \times\left[B_\lambda(T_*)\,e^{-\tau_\lambda} + 2\int_0^{p_\infty} p^2\,dp\int_{\phi_1}^{\phi_2} B_\lambda(T_d(r))\,k(r)\,\text{cosec}^2\phi\,\exp\left(-p\int_{\phi_1}^{\phi} k(r)\,\text{cosec}^2\phi\,d\phi\right)d\phi\right]. \tag{7}$$

Here T_* is the stellar temperature (~ 2500 K), R_* the stellar radius ($\sim 3\cdot10^{13}$ cm), D the distance to the star, and τ_λ the extinction optical depth. The input parameter p is normalized by R_*. The dust temperature $T_d(r)$ is calculated from the energy balance:

$$\int \frac{F_*(\lambda)}{r^2}\,Q_{abs}(\lambda)\,e^{-\tau_\lambda}\,d\lambda = 4\int Q_{abs}(\lambda)\,B_\lambda(T_d(r))\,d\lambda \tag{8}$$

and the volume emission coefficient $k(r)$ is given by

$$k(r) = k_0\,A^2\,Q_{abs}\,\frac{(v+v_d)_0}{v+v_d}, \tag{9}$$

with

$$k_0 = \frac{3\,f_g\,R_*\,\dot{M}}{16\pi\,d\,r_1^2\,v_0\,a_0}\left[\frac{\bar{V}_d}{1+\bar{V}_d}\right]_0 \approx 1.91\left[\frac{10\text{ km/sec}}{v_0}\right]\left[\frac{10\text{ nm}}{a_0}\right]\left[\frac{\dot{M}}{10^{-6}\,M_\odot/\text{yr}}\right]\left[\frac{\bar{V}_d}{1+\bar{V}_d}\right]_0,$$

where r_1 is the inner boundary of the aluminum oxide dust shell ($\sim 3.8\cdot10^{13}$ cm) and the suffix o represents the value at $r=r_0$. The optical constants for aluminum oxide are taken from Eriksson *et al.* (1981) and those for silicate referred to Day (1979).

In Figure 1, the radial variation of A, V, v_d, and T_d are shown for models with different a_0 and $\dot{M}$. As seen in Figure 1, the changes of V and v_d are small. The gas velocity decreases slightly at the beginning in order to adjust the boundary conditions ($v=v_0$) and the decrease is probably not realistic. However, it is small and does not make significant effects to calculated spectra. The temperature profile weakly depends

on the model parameters. Thus, calculated spectra depends mostly on the parameter F_R and k_0. If the grain size is much smaller than the wavelength in question, Q_p and Q_{abs} are approximately proportinal to the size. Therefore, F_R is proportional to $\dot{M}/a_0$ and $k(r)$ to $\dot{M}$: a_0 and $\dot{M}$ are the major parameters in this model.

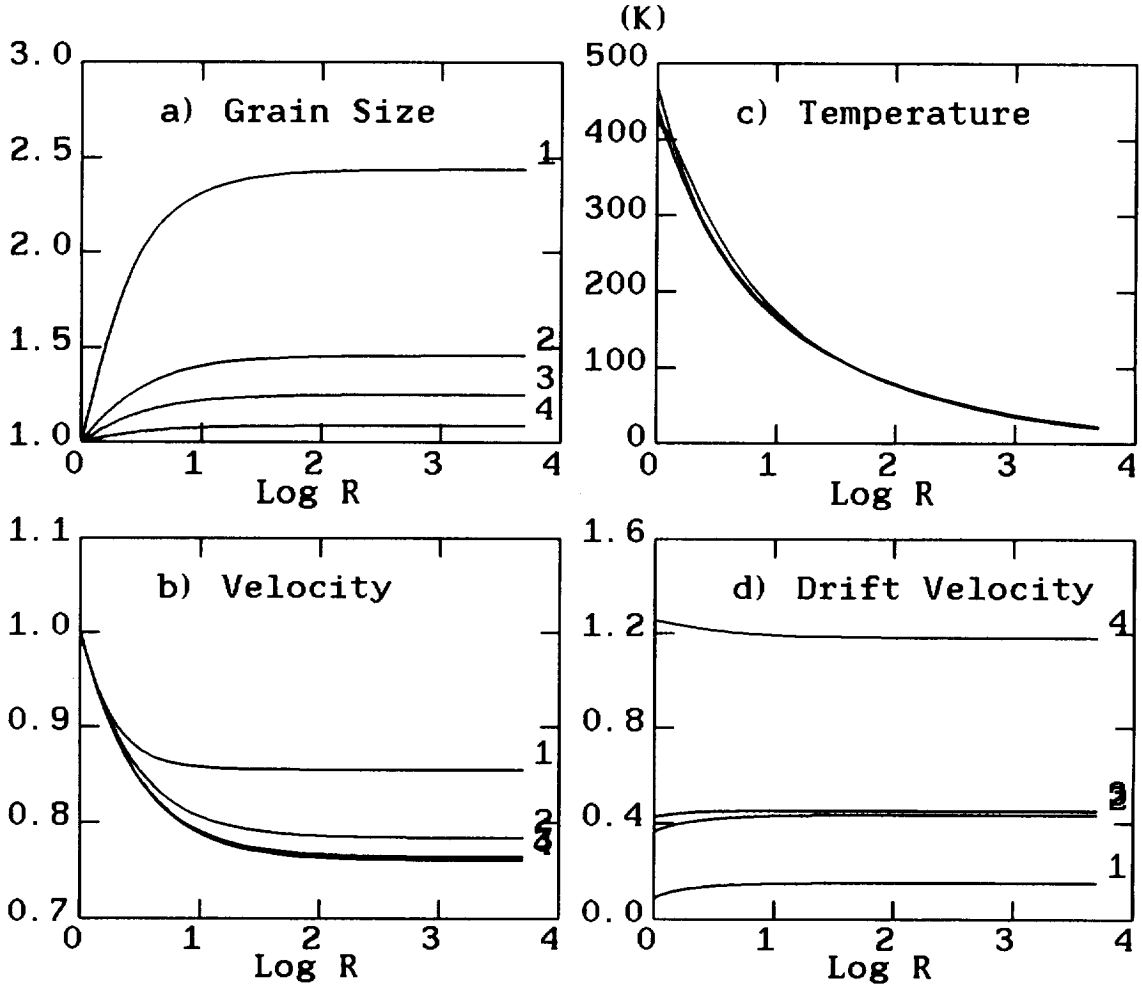

Figure 1. a) Radial distribution of grain radius normalized by core radius. b) Normalized velocity. c) Dust temperature (in K). d) Drift velocity normalized by initial gas velocity. All models are calculated with v_0=10 km/sec, C_l=1, and r_0=6·10^{14} cm. Model numbers are indicated on each curve; 1: a_0=10 nm, $\dot{M}$=10^{-5} M$_\odot$/yr, 2: a_0=100 nm, $\dot{M}$=10^{-5} M$_\odot$/yr, 3: a_0=20 nm, $\dot{M}$=10^{-6} M$_\odot$/yr, and 4: a_0=100 nm, $\dot{M}$=10^{-6} M$_\odot$/yr. The abscissa is the normalized distance (r/r_0).

A model grid was constructed for various sets of a_0 and $\dot{M}$. The *best fit* model parameters were obtained for each observed spectrum. The samples of LRS spectra are the same as in Onaka *et al.* (1988). The parameter r_0 was set to be 6·10^{14} cm since it was found to give the best fit of models to most observed spectra. Effects of v_0 and C_l were also examined. Examples of fitted spectra with LRS spectra are shown in Figure 2. Most LRS spectra of M Mira variables in the present sample are reproduced satisfactorily by the models with parameter range $10^{-6} < \dot{M} < 10^{-5}$ M$_\odot$/yr and $5 < a_0 < 400$ nm). However, in some cases, *e.g.*, RR Aql, a much larger F_R is reqiured to reproduce a *strong* silicate feature. Unless we assume a very fine core radius (~ 0.5 nm) it is difficult to have a good fit.

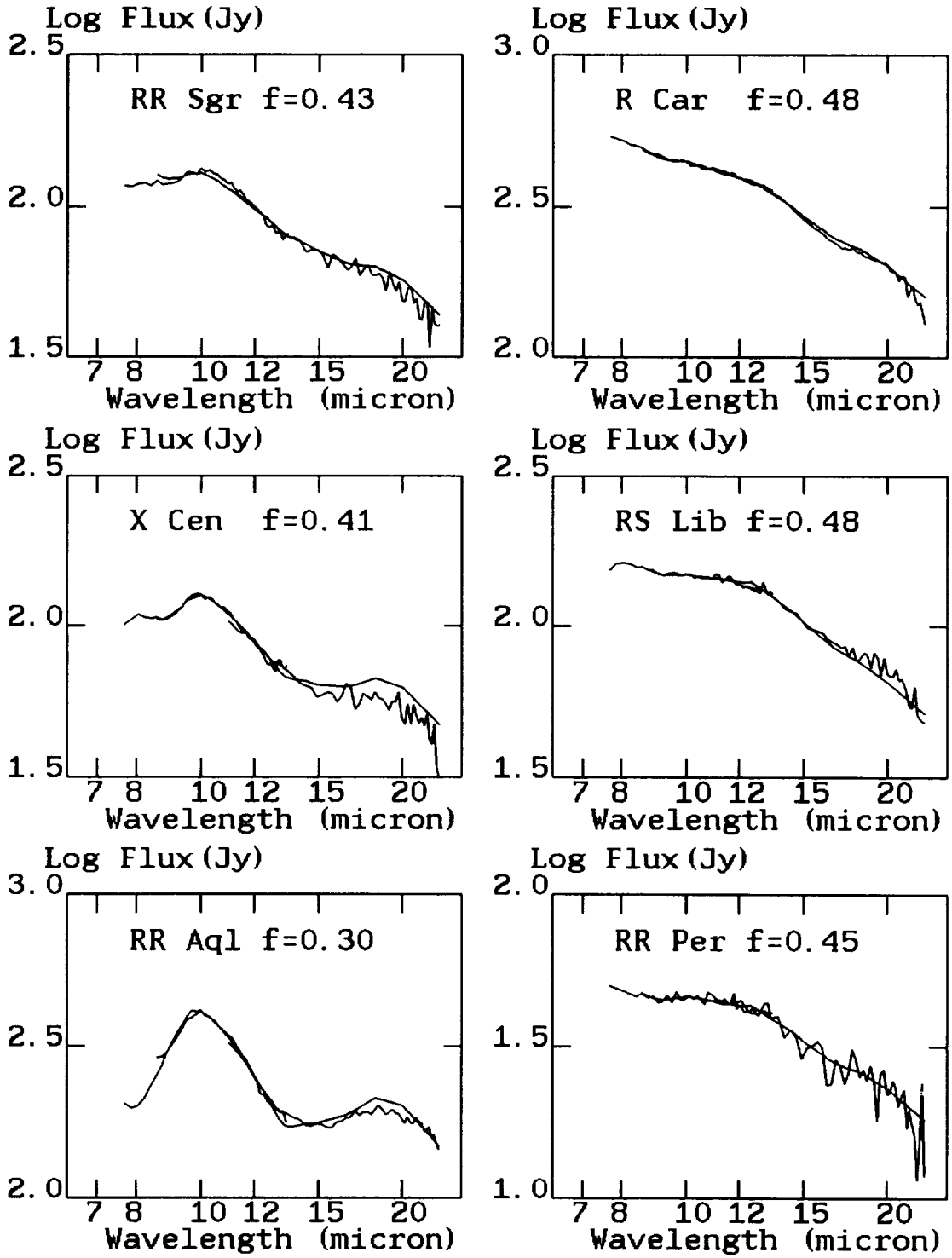

Figure 2. Examples of model spectra together with LRS spectra of M-type Mira variables. They are shown in the order of light curve asymmetry index f (*cf.* Vardya *et al.*, 1986). Model parameters are: (a_0 (nm), $\dot{M}$ (10^{-6} $M_\odot$/yr), v_0 (km/sec), and C_l) = (5, 2, 10, 10) for RR Aql, (5, 2, 7, 1) for X Cen, (10, 2, 7, 1) for RR Sgr, (200, 10, 7, 1) for RR Per, (100, 10, 10, 1) for RS Lib, and (400, 10, 7, 5) for R Car.

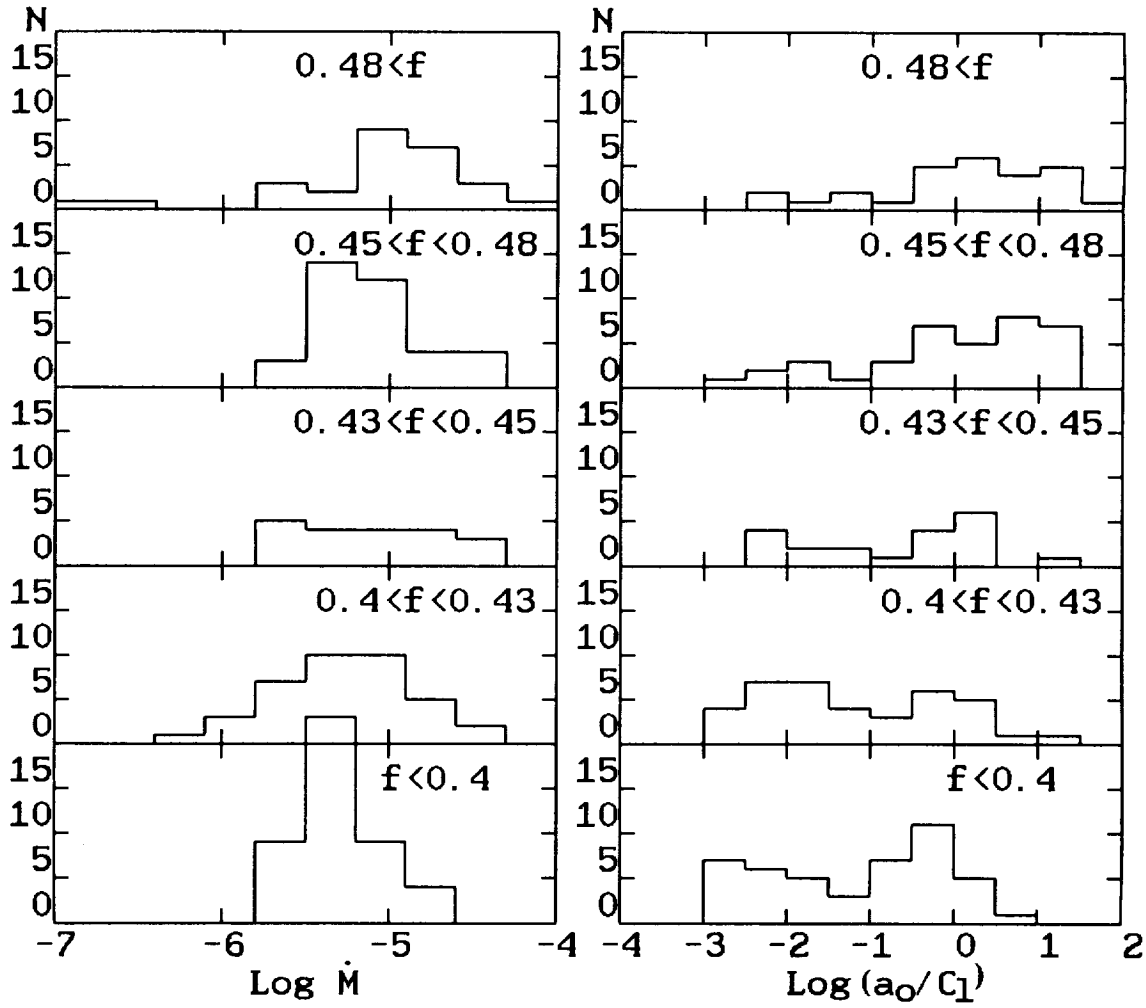

Figure 3. Distributions of model parameters Log($\dot{M}$) ($\dot{M}$ in $M_\odot$/yr) and Log(a_0 / C_l) (a_0 in nm) for stars with different light curve asymmetry index f.

Thus, we introduce a *clumpiness* parameter C_l as described in equations (2) and (6). We assume that in these stars a density fluctuation occurs and accelerates the mantle growth. It also affects the drag force (equation (6)). However, owing to the optically-thin nature of the present models, effects to the transfer equation (7) can be neglected. If we introduce C_l, the model fit becomes much improved (*e.g.*, RR Aql in Figure 2). As inferred from equations (2) and (6) it is difficult to separate the effects of C_l from those of a_0 a priori. The change of v_0 also improves the model fit. However, its effects are small since observed terminal velocities are in a small range.

The distribution of model parameters a_0 divided by C_l and $\dot{M}$ are shown in Figure 3 for five groups of stars with different light curve asymmetry index f. It is clear that for stars with small f index (asymmetric light curve) a small core radius or a large clump is required. For models of stars with large f index (symmetric light curve), somewhat larger $\dot{M}$ is obtained compared to stars with small f index. This is consistent with the observed trend of the 9.7 μm feature with f: Only stars with f <0.43 show the 9.7 μm feature and those with f >0.43 do not. If a_0 is small or C_l is large, F_R becomes large and silicate mantle grows quickly; emergent spectra show the silicate feature clearly. If a_0 is large, on the other hand, mantle growth is suppressed and the aluminum oxide feature at 12 μm is observed.

According to the present model, the observed variation in appearance of the 9.7μm feature is ascribed to the variation of grain size of core aluminum oxide grains or to the degree of density fluctuation in the circumstellar envelope. Some degree of density fluctuation is necessary unless very fine grains are assumed, although in the present analysis it is difficult to separate the effects of C_l from those of a_0. The size of aluminum oxide grains is considered to be determined by the nucleation process at the bottom of the circumstellar envelope. According to Yamamoto and Hasegawa (1977) and Draine and Salpeter (1977) the particle size in the homogeneous nucleation process is determined by the ratio of the cooling time scale of the system to the collision time scale of the condensible gas particles. In stars with small f index the shock propagates strongly and the cooling occurs rapidly, thus, small aluminum oxide grains may be formed. It may be also possible that further mutual collisions occur frequently in circumstellar envelopes of these stars and that grains are broken into small pieces (Biermann and Harwit 1980). Strong shocks may also produce a large density fluctuation. The observed variation of LRS spectra, thus, can be ascribed to the difference of the physical conditions at the bottom of the circumstellar envelope and should provide important information on the acceleration mechanism of mass loss process.

The increment at 18μm for some stars (*e.g.*, R Car in figure 2) may not be well reproduced by the present model. The dependence of silicate band strength on the temperature, which has been indicated experimentally by Day (1976) and suggested from the dust shell model analysis by Bedijn (1987), may have to be taken into account.

The author would like to thank Saneyoshi Scholarship Foundation for partial support of travel expenses to the symposium. This work was partly supported by grant-in-aid No.62420001 from the Ministry of Education, Science, and Culture, Japan.

Bedijn, P. J.: 1987, *Astr. Ap.*, **186**, 136.

Biermann, P. and Harwit, M.: 1980, *Ap. J. (Letters)*, **241**, L105.

Chandrasekhar, S.: 1960, *Radiative Transfer*, Dover Publ., New York, p23.

Day, K. L.: 1976, *Ap. J.*, **210**, 614.

Day, K. L.: 1979, *Ap. J.*, **234**, 158.

Drain, B. T. and Salpeter, E. E.:1977, *J. Chem. Phys.*, **67**, 2230.

Eriksson, T. S., Hjortsberg, A., Niklasson, G. A., and Granqvist, C. G.: 1981, *Applied Optics*, **20**, 2742.

IRAS Science Team: 1986, *Astr. Ap. Suppl.*, **65**, 607.

Kwok, S.: 1975, *Ap. J.*, **198**, 583.

Onaka, T. and de Jong, T.: 1987, in *Proc. of Late Stage of Stellar Evolution*, ed. S. Kwok and S. R. Pottash, Reidel, Dordrecht, p97.

Onaka, T., de Jong, T., and Willems, F. J.: 1988, submitted to *Astr. Ap.*

Vardya, M. S., de Jong, T., and Willems, F. J.: 1986, *Ap. J. (Letters)*, **304**, L29.

Yamamoto, T. and Hasegawa, H,: 1977, *Prog. Theor. Phys.*, **58**, 816.

N91-15018

SUBLIMATING COMETS AS THE SOURCE OF NUCLEATION SEEDS FOR GRAIN CONDENSATION IN THE GAS OUTFLOW FROM AGB STARS

D.P. Whitmire*, J.J. Matese*, R.T. Reynolds**
*Physics Department, Univ. of Southwestern Louisiana, Lafayette, LA 70504-4210
**NASA Ames Research Center, Moffett Field, CA 94035

ABSTRACT. A growing amount of observational and theoretical evidence suggests that most main sequence stars are surrounded by disks of cometary material. In this paper we investigate the dust production by comets in such disks when the central stars evolve up the red giant and asymptotic giant branch (AGB). Once released, the dust will be ablated and accelerated by the gas outflow and the fragments will become the seeds necessary for condensation of the gas. The origin of the requisite seeds has presented a well known problem for classical nucleation theory. This model is consistent with the dust production observed in M giants and supergiants (which have increasing luminosities) and the fact that earlier supergiants and most WR stars (whose luminosities are unchanging) do not have significant dust clouds even though they have significant stellar winds. Another consequence of the model is that the spatial distribution of the dust will not in general coincide with that of the gas outflow, in contrast to the conventional condensation model. A further prediction is that the condensation radius is greater than that predicted by conventional theory, in agreement with IR interferometry measurements of α-Ori.

I. INTRODUCTION

The sources of the small dust grains observed by IRAS around Vega, β-Pic and numerous other old main sequence stars (Aumann, 1985; Backman and Gillett, 1987; Walker and Wolstencroft, 1988) are believed to be disks of cometary material (Harper et al., 1984; Weissman, 1984; Matese et al., 1987). Modeling of the IR emission yields dust disk radii extending to several hundred AU (Gillett, 1986). The disk in β-Pic has been resolved optically and it extends to $\approx$1000 AU (Smith and Terrile, 1987). The mass of the small ($\sim$10μm) grains directly observed is $> 0.01 M_{\oplus}$ (e.g. Gillett, 1986). However, the lifetime of these small grains is less than the probable ages of the stars (Whitmire et al., 1988) and therefore more massive unobserved sources must also be present. Estimates of the total disk masses are highly uncertain since it must be assumed that a standard mass distribution index holds over a range from the observed small grains up to an assumed maximum mass. If

the maximum mass is taken to be comet size, total mass estimates range from $\sim$10-300$M_\oplus$(Harper et al., 1984; Weisman, 1984; Gillett, 1986). Taking into account observational bias, it is likely that most main sequence stars (including the sun) possess disks of cool orbiting grains (Aumann, 1985; Backman and Gillett, 1987), implying that the phenomenon is not indicative of young systems as originally conjectured. Further, several F-type stars with 60μm excesses have age estimates of $\approx 2 \times 10^9$ yr (Backman and Gillett, 1987).

These observations are consistent with the theoretical expectation (Kuiper, 1951; Cameron, 1962) that a primordial disk of residual unaccreted planetesimals should exist just beyond the planetary region of the Solar System. This disk has previously been invoked as the source of the observed steady state short period comets (Fernandez, 1980; Matese and Whitmire, 1986a,b) whose flux (Fernandez, 1980) and inclinations (Duncan et al., 1988) are inconsistent with their origin as captured long period comets. In addition to this residual flattened planetesimal disk there is also theoretical evidence suggesting the existence of an isotropic massive ($\sim$100 $M_\oplus$) inner Oort cloud extending inward to just outside the planetary region (Hills, 1981; Weissman, 1985; Bailey, 1983). However, since the dust clouds around β-Pic and α-Psa are known to be flattened we assume that it is the residual planetesimal disk that dominates within several hundred AU of the star.

In this paper we investigate the dust production by disk comets around intermediate mass stars ($\approx$1-10$M_\odot$) as they evolve into red giants and especially red supergiants (AGB phase). During the AGB phase the stellar luminosity can increase to 10^4-$10^5 L_\odot$, depending on mass. We will argue that if a modest population of comets ($\sim 1 M_\oplus$) exists within 100 AU of these stars they can readily supply the seeds ($\geq$ 10 A) necessary for dust condensation in the gas outflow, thereby mitigating the classical nucleation problem of statistically producing sufficient critical clusters in this environment (Donn and Nuth, 1985; Draine, 1985).

II. ANALYSIS

Iben and Renzini (1983) have modeled the evolution of intermediate mass stars in the AGB phase. The time dependence of the stellar luminosity can be written as

$$L(t) = L(0) \exp(t/\tau_L) \qquad (1)$$

where

$$L(0) = 26.5(M_i/M_\odot)^{2.68} L_\odot \qquad (2)$$

and

$$\tau_L = 6.5 \times 10^7 (M_i/M_\odot)^{-3.64} \text{yr}. \qquad (3)$$

In these formulae t = 0 at the beginning of the AGB phase, and M_i is the initial zero-age main sequence stellar mass. These formulae are applicable for masses in the range $1M_\odot \leq M_i \leq 10M_\odot$, however for masses $< 2M_\odot$, M_i should be set = $2M_\odot$. The stellar luminosity, radial distance R and black body temperature T are related by

$$L(t) = (R/AU)^2 (T(t)/280K)^4 L_\odot \qquad (4)$$

while the time-dependent black body temperature can be written $T(t) = T(0) \exp(t/\tau_T)$ where the temperature time scale $\tau_T = 4\tau_L$.

Since, in a standard cometary mass distribution, most of the mass resides in the largest bodies, we consider comets of a single mass $M_{max} \equiv 10^{21}$ g. The total mass loss rate for observed comets can be fit to the form (Ney, 1982)

$$dM/dt = -kM^{2/3} \exp(-1552K/T) \qquad (5)$$

where the Boltzmann factor is appropriate for the activation energy of water released from clathrates and the coefficient k depends on specific surface absorptivity and activity, being smaller for older comets like Encke. This semiempirical formula is applicable for black body temperatures T up to ≈700K, which encompasses the temperatures of relevance in the present analysis.

Equation (5) can be integrated to give

$$E_1\left(\frac{1552K}{T}\right) - E_1\left(\frac{1552K}{T(0)}\right) = \frac{640 \text{ yr}}{\tau_L}\left(1 - f^{1/3}\right) \qquad (6)$$

where E_1 is the Error function, $f \equiv M/M_{max}$ = fraction of original mass surviving. The numerical factor was evaluated by taking $k = 3.7 \times 10^{-4}$ g$^{1/3}$/s (comet Encke). We shall assume that the second term is negligible compared to the first, an adequate approximation after several luminosity timescales have elapsed. Eq. (6) gives the value of T when M has been reduced to fM_{max}.

We now locate that position in the disk where sublimation is maximal. Setting $\dot{M} = 0$ we find

$$\frac{\exp(-1552K/T_p)}{1552K/T_p} = \frac{640 \text{ yr}}{\tau_L} \frac{f_p^{1/3}}{2} \qquad (7)$$

where T_p is the black body temperature where the comet is undergoing peak sublimation and f_p is the surviving mass fraction at peak sublimation. T_p is also a rough lower limit to the black body temperature at the inner edge where f = 0. An adequate approximate solution to this equation is found to be

$$T_p \approx 1860K/\ln(\tau_L/400\ yr). \qquad (8)$$

Having obtained the temperature at which comets are undergoing peak sublimation rates we next determine the disk location R_p where this occurs and take this as an adequate (upper bound) approximation to the inner edge. R_p is found from

$$R_p(t) \approx (L(t)/L_\odot)^{1/2}/(T_p/280K)^2 AU \qquad (9)$$

or

$$R_p(t)/R_*(t) = \tfrac{1}{2}(T_*/T_p)^2 \qquad (10)$$

where * refers to stellar parameters. In Table 1 T_p, f_p and R_p/R_* are tabulated for several stellar masses. R_p/R_* is given for two stellar temperatures corresponding to α -Ori (oxygen supergiant) and IRC 10216 (carbon supergiant).

Table 1

			R_p/R_*	
$M_i/M_\odot$	$T_p(K)$	f_p	T_*=3300K	T_*=2300K
2	194	0.33	145	70
4	270	0.34	75	36
6	341	0.35	47	23
8	423	0.36	30	15
10	509	0.37	21	10

Finally, if one approximates that sublimation occurs only at the location of the peak sublimation

$$dM_{net}/dt \approx (dM/dR)\,(dR/dt)\big|_{R_p(t)} = (2\tau_L)^{-1}(RdM/dR)\big|_{R_p(t)} \qquad (11).$$

For any standard radial power law $RdM/dR \approx \Delta M(\tfrac{1}{2}R \to 2R)$ in order of magnitude. Therefore, if there is $\sim 1M_\oplus$ of comets available we should be releasing it at a rate

$$dM_{net}/dt \sim \Delta M/\tau_L \sim \begin{cases} 10^{-7} M_\oplus\ /yr \text{ for } M_i = 2M_\odot \\ 10^{-4} M_\oplus\ /yr \text{ for } M_i = 10M_\odot \end{cases} \qquad (12)$$

To order of magnitude this result is of general applicability and can also be used, for example, to estimate the dust production rate around red giants as well as red supergiants.

III. DISCUSSION

Although these dust production rates are incapable by themselves of explaining the observed dust clouds around most M giants and supergiants they can readily supply the seeds (> 10Å) necessary for dust condensation in the gas outflows. Seeds of radii $\sim$10Å which subsequently grow to $\sim$0.1μm represent a dust mass enhancement factor of $\sim 10^6$. The required seeds should be readily produced by ablation in the dense gas outflow, sputtering, grain-grain collisions, or they could simply correspond to the lower end of a standard mass distribution of the sublimating particles. The seeds will simultaneously be accelerated until there is little relative velocity between the seeds and the gas outflow, at which point condensation may occur rapidly. We note that the temperature T_p in Table 1 is the black body temperature at the location of those comets which are undergoing peak sublimation, but the temperature of the small condensing grains ($\lesssim$ 0.1μm) that are actually observed can be significantly higher (e.g. 1000K).

The inner radius of the best studied oxygen supergiant α-Ori has been resolved with IR interferometry and found to be ≈ 35 - 60 R_* (Bloemhof, 1984; Howell et al., 1981), consistent with the proposed model but much larger than expected by conventional condensation theory (Draine, 1985). In other cases it is often assumed that T = 1000K which implies an inner edge ≈5R_* for black body radiators (Tielens, 1988).

The proposed model is consistent with the fact that M giants and supergiants have significant dust clouds while earlier supergiants and most WR stars do not, even though they have significant mass loss via stellar winds. It is only the cool giants and supergiants that have rapidly increasing luminosities, and therefore short time scales τ_L, as they evolve. Most of the comets within a few hundred AU should be concentrated in a disk. Thus, we expect the sublimated seeds and condensed dust to be preferentially concentrated near the disk. Dust disks are compatible with the observed asymmetries in the IR emission in IRC 10216 and other cool giants (e.g. Zuckerman, 1980; Beckwith, 1985). A prediction of the model is that the spatial distribution of the dust will not in general coincide with that of the gas outflow, in contrast to conventional condensation theory. Although R_p is uncertain by a factor of ≈ 2, the model predicts that the inner disk edges will tend to be further out than suggested by conventional condensation theory, especially for the lower mass stars.

ACKNOWLEDGEMENTS

This work was supported in part by the NASA Ames/Stanford ASEE Summer Faculty Fellowship Program and by a NASA Ames University Consortium Grant.

REFERENCES

Aumann, H.H.: 1985, Publ. Astr. Soc. Pacific 97, 885.

Backman, D.E. and Gillett, F.C.: 1987, 5th Cool Star Workshop, Boulder, CO, preprint.

Bailey, M.E.: 1983, Mon. Not. R. Astr. Soc. 204, 603.

Beckwith, S.: 1985, Mass Loss From Red Giant, eds. Morris, M. and Zuckerman, B. (Reidel Pub. Co., Dordrecht), p.95.

Bloemhoff, E.E., Townes, C.H. and Vanderwyck, A.H.B.: 1984, Ap. J. (Letters) 276, L21.

Cameron, A.G.W.: 1962, Icarus 1, 13.

Donn, B. and Nuth, J.: 1985, Ap. J. 288, 187.

Draine, B.T.: 1985, NASA Conf. Pub. 2403, 19.

Duncan, M., Quinn, T. and Tremaine, S.: 1988, Ap. J. (Letters) 328, L89.

Fernandez, J.: 1980, Mon. Not. R. Astron. Soc. 192, 481.

Gillett, F.C.: 1986, Light on Dark Matter, ed. Israel, F.P. (Reidel Pub. Co., Dordrecht), p.61.

Harper, D.A., Lowenstein, R.F. and Davidson, J.A.: 1984, AP. J. 285, 808.

Hills, J.G.: 1981, Astron. J. 86, 1730.

Howell, R.R., McCarthy, D.W. and Low, F.J.: 1981, Ap. J. (Letters), 251, L21.

Iben, I. and Renzini, A.: 1983, Ann. Rev. Astron. Astrophys. 21, 271.

Kuiper, G.P.: 1951, Astrophysics, ed. Hynek, J.A. (McGraw-Hill, NY), p.357.

Matese, J.J., Whitmire, D.P., Lafleur, L.D., Reynolds, R.T. and Cassen, P.M.: 1987, BAAS 19, 830.

Matese, J.J. and Whitmire, D.P.: 1986a, Icarus 65, 37.

Matese, J.J. and Whitmire, D.P.: 1986b, The Galaxy and the Solar System, ed. Smoluchowski, R., Bahcall, J.N., Matthews, M.S., (Univ of Arizona Press).

Ney, E.P.: 1982, Comets, ed. Wilkening, L.L., (Univ. of Arizona Press, Tucson), p.333.

Smith, B.A. and Terrile, R.J.: 1987, BAAS 19, 829.

Tielens, A.G.G.M.: 1988, Carbon in the Galaxy: Studies from Earth and Space, ed. Tarter, J., NASA CP, in press.

Walker, H.J. and Wolstencroft, R.D.: 1988, preprint.

Wiessman, P.: 1984, Science 224, 987.

Wiessman, P.: 1985, Protostars and Planets II, eds. Black, D.C. and Matthews, M.S. (Univ. of Arizona Press), p.895.

Whitmire, D.P., Matese, J.J. and Tomley, L.: 1988, Astron. and Astrophys. (Letters), in press.

Zuckerman, B.: 1980, Ann. Rev. Astron. Astrophys. 18, 263.

VIII-B) DUST IN CIRCUMSTELLAR SHELLS

IR EMISSION FROM CIRCUMSTELLAR ENVELOPES OF C-RICH STARS

A. Blanco*, A. Borghesi*, E. Bussoletti**, L. Colangeli***, S. Fonti*, V. orofino*.

*Physics Department, University of Lecce, Lecce, Italy
**Istituto Universitario Navale and Osservatorio Astronomico di Capodimonte, Napoli, Italy
***ESA Space Science Department, ESTEC, Noordwijk, The Netherlands

Various authors have developed theoretical models to solve the radiative transfer equation in dust clouds surrounding a central star (Leung, 1975; Rowan-Robinson, 1980). Recently, Orofino et al. (1987) have proposed a simplified model that allows to compute the flux from circumstellar envelopes around carbon stars. The computation has been performed under the hypothesis of spherical geometry and neglecting both dust scattering contributions and the heating of inner dust by IR radiation from outer grains ("back-heating").

The use of optical properties measured in laboratory on different kinds of amorphous carbon grains (Bussoletti et al., 1987), together with those quoted in literature for graphite (Draine and Lee, 1984), has shown that observations are better fitted by amorphous carbon particles rather than by graphite grains.

In the present work we check the reliability of our model comparing its results with those obtained using the more general elaboration of Leung (1975). In particular we find that both the classical scattering by dust and the "back-heating" effects are negligible in the radiative transfer when envelopes similar to IRC+10216 are taken into consideration.

In addition we present new fits of IRC+10216 spectra, obtained when the source is in different luminosity phases, assuming amorphous carbon grains in the circumstellar envelope.

The best-fit values of the free parameters in our model are in agreement with previous determinations and with the variability phase of the source.

In these fits we have taken into account the work of Sutton et al. (1979) who found that the formation of solid grains around several Mira objects, including IRC+10216, seems to occur rather far from the central star, even if its temperature could allow the condensation of solid particles very close to the photosphere.

The same model is currently used to simulate the emission from carbon-rich sources showing the silicon carbide (SiC) feature at 11.3μm (Cohen, 1984; Baron et al., 1987). In this case extinction data for various kind of amorphous carbon and SiC grains mixtures have been used. These data have been

experimentally obtained in laboratory with the usual pellet technique (Borghesi et al., 1983).

Due to the importance of matrix effects, first of all we have investigated what would be the behaviour of the optical properties of such mixtures in vacuum.

Here we show that matrix effects are not important on the band intensity (at least within experimental errors) for mixtures with an amount of SiC up to 25% by weight.

On the other side, a matrix effect is evident for the band position, since a clear shift towards shorter wavelengths appears extrapolating from KBr to vacuum. The displacement for the mixture ($\Delta\lambda_{peak} \simeq 0.3\mu m$) is the same that has been found for SiC alone (Pégourié, 1987).

Baron, Y., de Muizon, M., Papoular, R., Pégourié, B.: 1987, Astron. Astrophys. 186, 279.

Borghesi, A., Bussoletti, E., Colangeli, L., De Blasi, C.: 1983, Infrared Phys. 23, 321.

Bussoletti, E., Borghesi A., Colangeli, L. and Orofino, V.: 1987, Astron. Astrophys. Suppl. Series 70, 257.

Cohen, M.: 1984 Monthly Notices Roy. Astron. Soc, 206, 137.

Draine, B.T. and Lee, H.M.: 1984, Astrophys. J. 285, 89.

Leung, C.M.: 1975, Astrophys. J. 199, 304.

Orofino, V., Colangeli, L., Bussoletti, E., Strafella, F.: 1987, Astrophys. Space Sci. 138, 127.

Pégourié, B.: 1987, submitted to Astron. Astrophys.

Rowan-Robinson, M. and Harris S.: 1983, Monthly Notices Roy. Astron. Soc. 202, 797.

Sutton, E.C., Betz, A.L., Storey, J.W.V. and Spears, D.L.: 1979, Astrophys. J. 230, L105.

THE INFLUENCE OF GRAIN GROWTH IN CIRCUMSTELLAR DUST ENVELOPES ON OBSERVED COLORS AND POLARIZATION OF SOME ERUPTIVE STARS

Yu. S. Efimov
Crimean Astrophysical Observatory, USSR

The existence of gas and dust envelopes for many types of stars is well known. R CrB stars are classical examples of stars where dust envelope formation takes place. Dust envelope formation was detected around the Kuwano-Honda object (PU Vul) in 1980-1981 when the star's brightness fell to 8^m. Such envelopes are also formed at nova outbursts. The process of dust envelope formation leads to appreciable variations in optical characteristics, which are seen in specific color and polarization variations in the course of light fading and the appearance of IR radiation.

The main features observed are 1) a light decrease of several magnitudes; 2) the asymmetric shapes of minima with a steep decrease and slow increase in light; 3) different amplitudes and durations of the minima; 4) the delay in minima at long wavelength with respect to the minima at short wavelength, as was observed at the time of deep minimum of PU Vul in 1980 by Kolotilov (1983); 5) the reddening of a star at the beginning and end of minima and the bluing at the centers of minima (typical of R CrB minima that were detected at the minimum of PU Vul in 1980); 6) rapid color variations at the "bottoms" of the minima; 7) exponential increase in the degree of polarization with decreasing light (as it was observed in R CrB in 1977); 8) coincidence of a polarization peak with a peak of bluing at the center of light minimum; 9) the rise of polarization up to 5-14% at the center of the minimum (observed on R CrB); 10) variation of the shape of wavelength dependence of polarization from a flat to a convex shape with the polarization maximum shifted toward long wavelengths at the time of decreasing light; 11) different values for the polarization maximum for the same amplitudes of photometric variations (observed on R CrB).

The explanation of all these features is difficult. One source of confusion may be due to the ignoring of change of optical parameters of dust particles as they grow during dust envelope formation from a thousandth part of a micrometer at the beginning to submicrometer size at the end of the process. In fact, all optical properties of dust grains are strongly dependent on the composition, shape, and size of the grains. Hence, for particles of any material and constant geometry, size variations lead to variations in the optical characteristics of particles. This implies that optical parameters of dust in the circumstellar envelope will change too.

For simplicity consider the case of a star with a thin dust circumstellar envelope of uniform density consisting of identical particles. At any wavelength λ the light decrease will be

$$\Delta m = 1.086\pi\, a^2 Q_\lambda^e n l ,$$

where a is the size of particles, Q_λ^e is the extinction factor, n is the number density, and l is the geometrical depth in the line of sight. The extinction factor Q_λ^e is the only parameter which is wavelength-dependent. For a given type of particle, the extinction factor depends on the ratio of the particle radius to the wavelength (figure 1). It is clear that for the same value of the extinction factor, in particular, its extrema will correspond to different sizes of particles. If we assume that the size of particles grows linearly with time, it follows that extinction factor extrema will come later than those in the short wavelength region. Just such a phenomenon was detected by Kolotilov (1983) in the deep minima of PU Vul in 1980.

It is known from the optics of small particles that the shape of the Q^e_λ curve may be very complex, with several local maxima with decreasing amplitudes and increasing separations. At various wavelengths the shapes of Q^e_λ curves are similar, but differ from each other in amplitude at the same radius. Thus, at each moment in time, a given particle's size corresponds to different values of extinction factors Q^e_λ at different wavelengths. This implies that variations in color index, for example, B-V, are determined by the variations of difference $Q^e_B - Q^e_V$. The color-index amplitude

$$\Delta(B-V) = 1.086\pi\, a^2(Q^e_B - Q^e_V)nl$$

may be variable as well, and its sign may be reversed several times depending on the composition of particles. For silicate-like particles with weak absorption, the sign reversals occur more often than for particles of material with high absorption like graphite or iron. This feature may be used as a rough diagnosis of dust composition (see figure 2).

Formulae for the color index and for the light amplitude also contain parameters n and l which are characteristic of stellar envelope. To eliminate or reduce these poorly known factors which depend on the envelope's composition one may consider the ratio $\Delta(B-V)/\Delta V = Q^e_V/(Q^e_B - Q^e_V)$. This ratio is a function only of dust properties. It is of interest to construct the Q^e_V, $Q^e_B - Q^e_V$ diagram as shown in figure 3. The main features of such diagrams are 1) an approximately linear growth of $Q^e_B - Q^e_V$ from zero to a maximum value which is followed by a sign reversal. The succeeding growth of particles leads to more negative values of the difference of $Q^e_B - Q^e_V$ with minimal variations of Q^e_V near its maximum value. It is equivalent to the "bluing" observed in the minima of eruptive stars with dust envelopes. When the size of particles reaches 0.2 to 0.5 mcm for silicates or little more than 0.1 mcm for graphite-like particles, rapid sign reversals may be seen, as was observed at the time of deep minimum of PU Vul in 1980 (see figure 4). The continued growth of the particles leads to neutral absorption by dust envelope and the star's color returns to its initial value.

The increasing of dust particles' size also increases the radial pressure, however. This leads to the acceleration of particles to velocities at which large particles are destroyed by collision. Small particles are then again dominant in the expelled envelope. This may explain the reddening observed at the rising branch of the minima of R CrB stars (see figure 5). The similarity between the Q^e_V, $Q^e_B - Q^e_V$ diagram and the color-magnitude diagram for PU Vul and R CrB is seen in figures 4-6. Comparison of corresponding parts of the diagrams can give a rough estimate of the mean size of the dust particles. Similar effects may also occur in optically thick envelopes as shown by Daniel (1978). Light scattering in the envelope limits the amplitude of minimum to a value which depends on the contribution of scattered radiation to total radiation and may lead to some compensation of reddening by the contribution of blue radiation from the scattered light.

Evidence of particle growth can be obtained from the shift of polarization maximum toward long wavelengths at the time of decreasing light. If particles are nonsymmetric, then any suitable alignment mechanism can lead to significant polarization. It is clear that in a system containing a star and a flattened envelope, the polarization may reach very high values (~33% in a disk-like electron envelope) if unpolarized light from a star is obscured by the dust screen. In such a case maximum polarization will occur at the time of light minimum and a nonlinear correlation between polarization and stellar brightness is expected. Such correlation was first observed at the time of the R CrB minimum in 1977 when polarization rose to 14% in the visual and the stellar magnitude fell to 8^m (see figure 6).

Since the degree of polarization depends on the contribution of polarized light from the envelope and on the fraction of aligned particles in the line of sight, any reduction of the polarization factors leads to a rapid decrease of polarization without any effect on the total absorption. Consequently, there may be events when different polarization is observed at the same light amplitudes (as found in various minima of R CrB). The behaviour of the polarization angle will vary depending on the polarization mechanism.

Hence, the model of a circumstellar dust envelope with aligned particles of changing size can be successfully applied to explain most phenomena observed at the time of light minima for a number of eruptive stars. The polarization may arise in a nonspherical dust envelope or be produced by alignment of nonspherical particles. Such a model may be useful to study similar phenomena in other types of stars. These results will be published elsewhere (Efimov, 1988) in more detail.

REFERENCES

Daniel, J.-Y., 1978. Astron. Astrophys., **64**, 345.

Dorschner, J., 1970. Astron. Nachr., **292**, 71.

Efimov, Yu. S., 1986. Ph.D. thesis, Tartu.

Efimov, Yu. S., 1988. Astron. Zh., in press.

Goncharova, R. I., 1985. Pis'ma v Astron. Zh., **11**, 855.

Kolotilov, E. A., 1983. Astron. Zh., **60**, 746.

Rosenbuch, A. E., 1986. Kinematika i fisika nebesnych tel, **2**, 29.

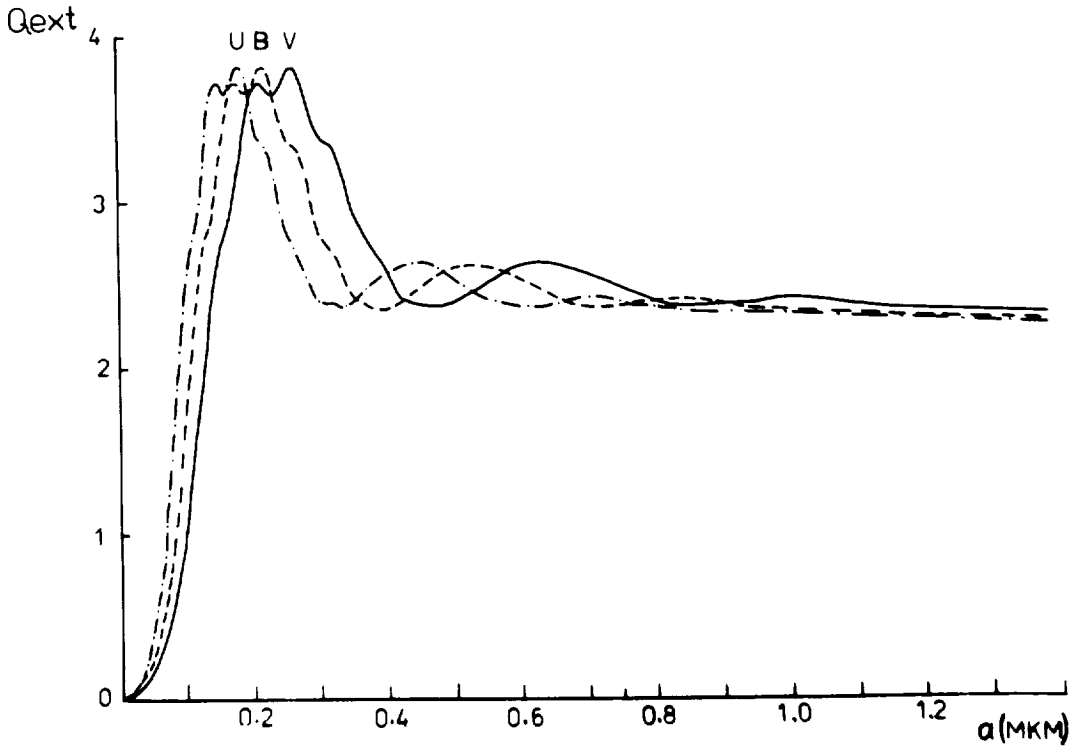

Figure 1.– The dependence of Q_λ^e on radius of particles a (mcm) in the UBV system for silicate (Dorschner, 1970).

C 7

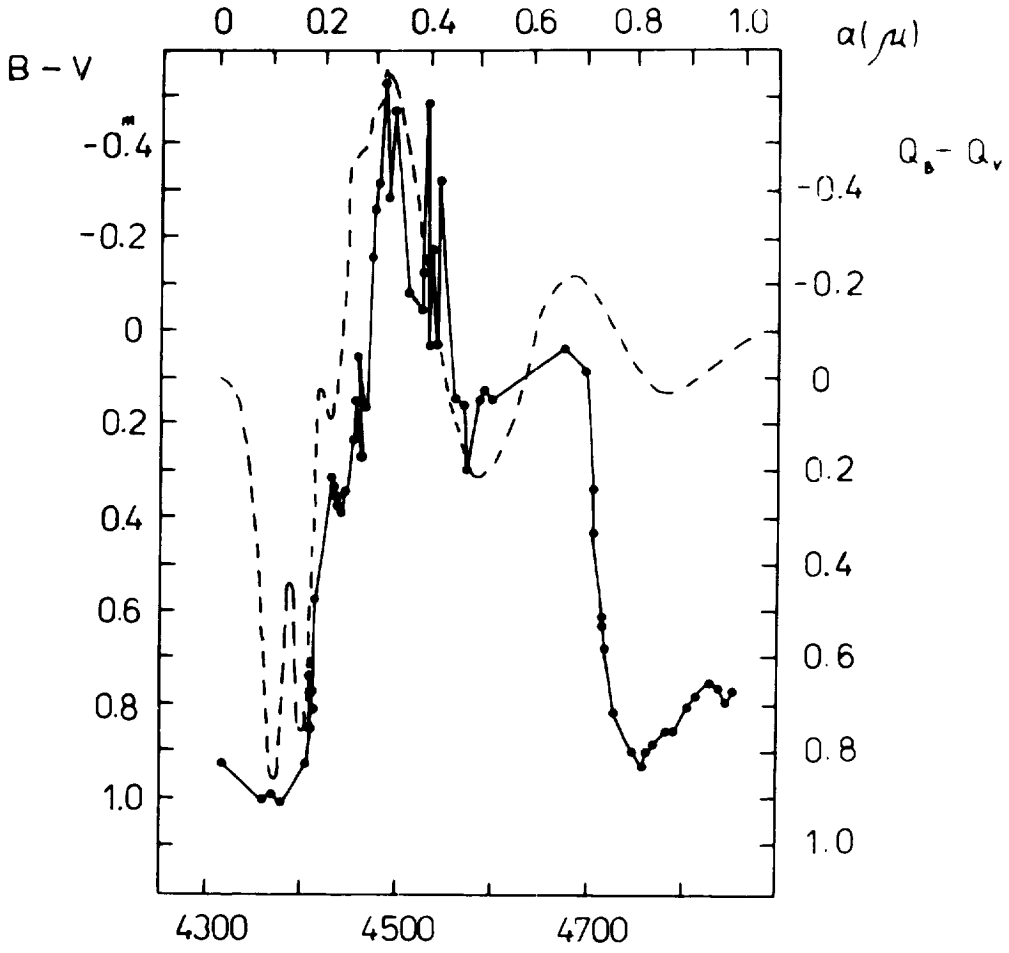

Figure 2.– The dependence of the difference $Q_B^e - Q_V^e$ for silicate (dashed line) and color B–V for PU Vul in 1980 (continuous line).

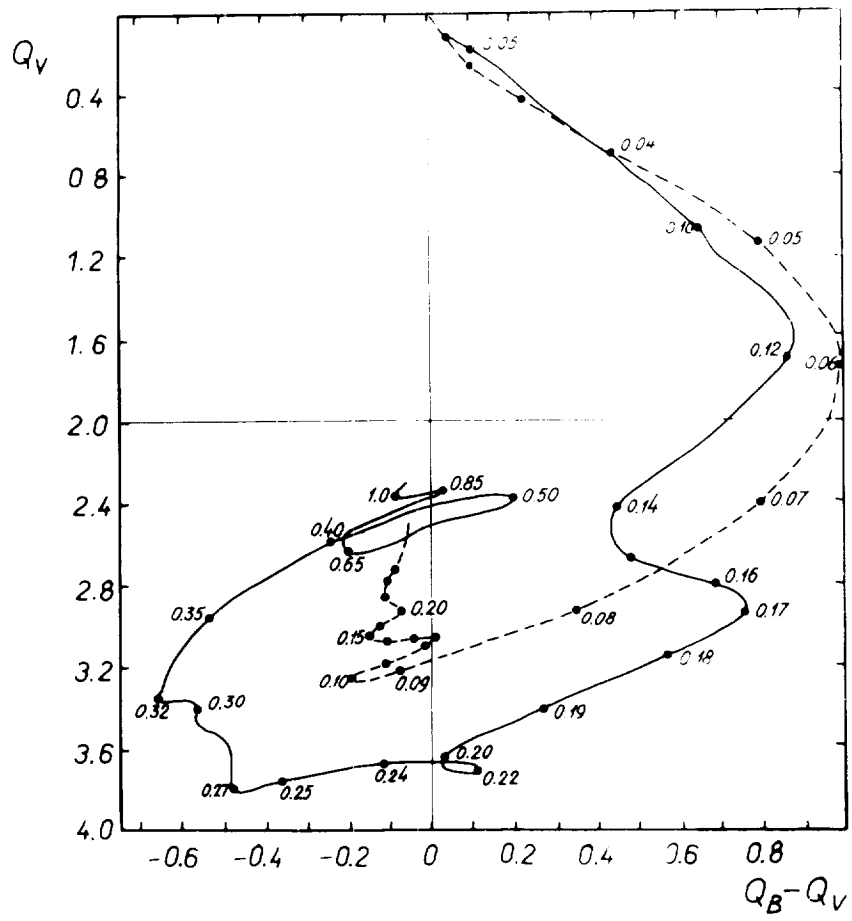

Figure 3.– The Q_V^e, $Q_B^e - Q_V^e$ diagram for silicate (continuous line) and for graphite (dashed line). The figures near the curves indicate radii of grains in mcm.

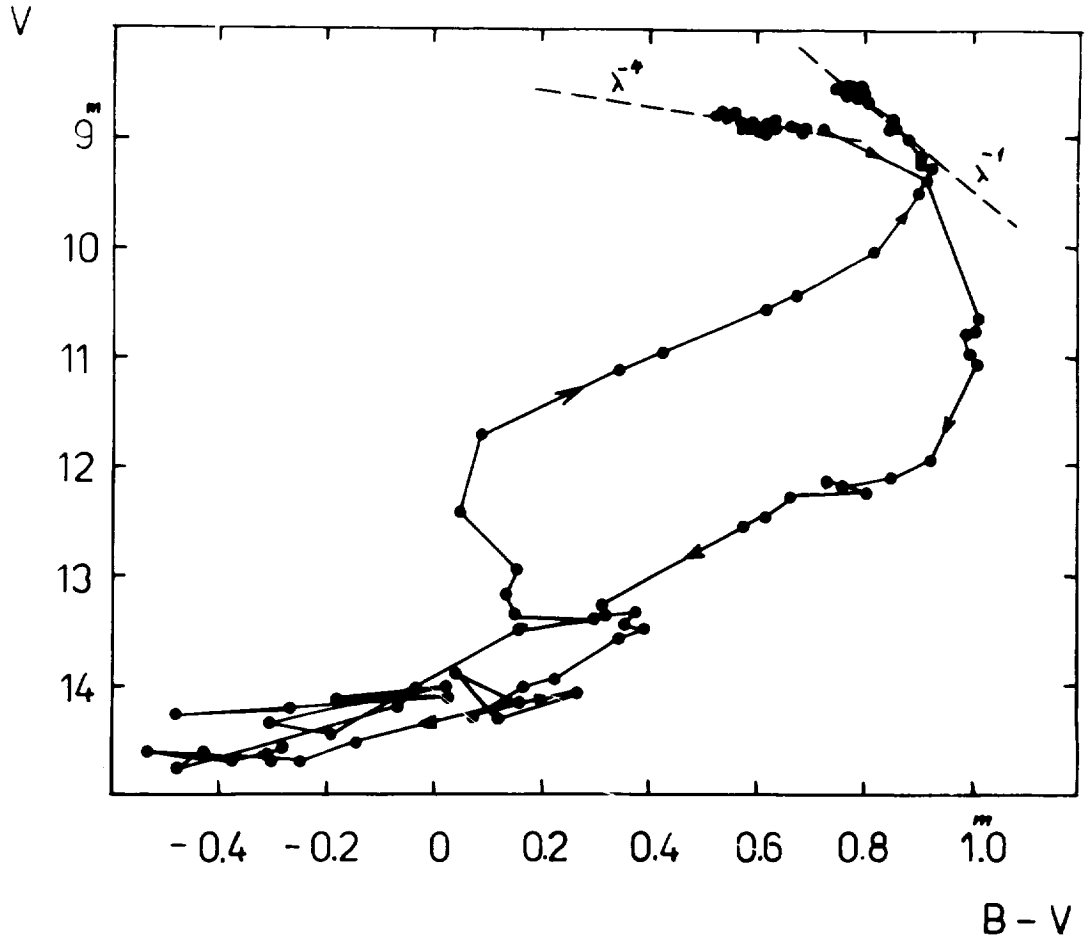

Figure 4.– The diagram V, B–V for the hot component of PU Vul in the deep minimum of 1980 (Efimov, 1988).

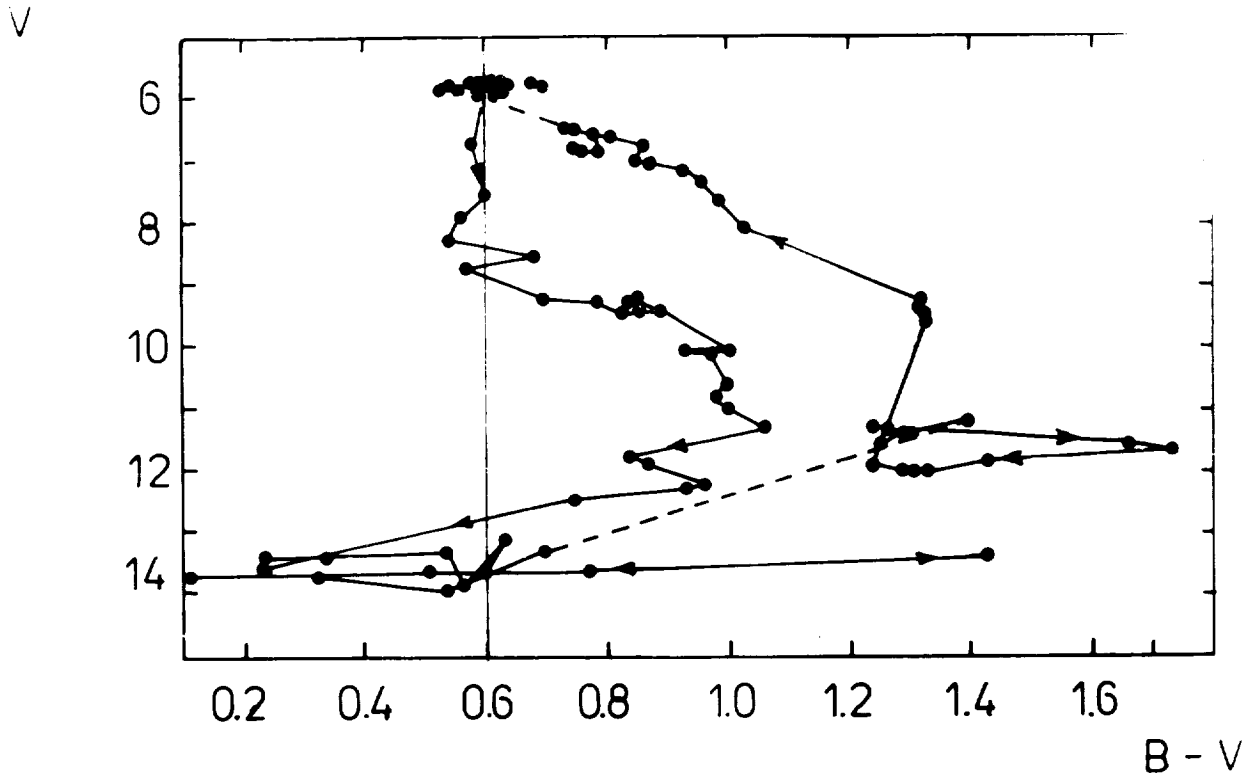

Figure 5.– The diagram V, B–V for R CrB in minimum in 1983 (Goncharova, 1985; Rosenbuch, 1986). The motion of the star in the diagram is shown by arrows.

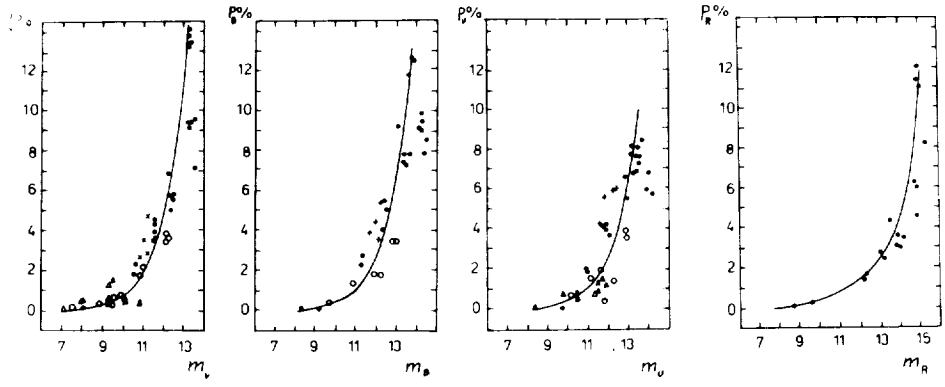

Figure 6.– The correlation between polarization and magnitude for different minima of R CrB in UBVR. Different symbols are used for different minima (Efimov, 1986).

N91-15021

USING INFRARED SPECTRAL FEATURES TO PROBE CIRCUMSTELLAR DUST SHELLS AROUND COOL STARS

Michael P. Egan and Chun Ming Leung
Rensselaer Polytechnic Institute, Troy, New York 12180–3590, USA

IRAS observations of cool stars provide low resolution spectra in the mid–infrared (7.8–22 μm) and also give fluxes at four wavelength bands (12, 25, 60, and 100 μm) from which color–color diagrams are constructed. The latter have been used to study the evolution of these stars, e.g., as an O–rich star evolves to become a C–rich star and its detached dust shell moves further away, its evolution can be tracked on a color–color diagram (Willems, 1987; Chan and Kwok, 1988).

A major factor in determining the position of either C–rich and O–rich stars on the 12–25–60 μm color–color diagram is the presence of spectral features in the mid–IR. O–rich stars show a 9.8 μm silicate feature, while C–rich stars have a SiC feature at 11.2 μm. IRAS observations (Little–Marenin, 1986) indicate that the SiC feature is quite narrow and uniform in shape showing little variation from star to star. The full width at half maximum (FWHM) is 1.6 ± 0.15 μm. On the other hand, the shape of the silicate feature varies widely among the O–rich stars, with a FWHM ranging from 2 to 3 μm.

The characteristics of circumstellar dust shells should manifest themselves both in the flux spectrum and in the details of the spectral features. To provide a coherent interpretation for these IRAS observations, we have constructed models (using the radiative transfer code of Egan *et al.*, 1988) of dust shells around O–rich and C–rich stars. We used realistic grain opacities which include spectral features of varying intrinsic widths (e.g., gaussian features at 10 μm with half width at half maximum of 0.5 and 1.0 μm). Applying various observational constraints to the models, the following conclusions emerge:

(1) The difference in variations of the shape of SiC and silicate features is due to the smaller intrinsic width of the SiC feature in the presence of varying dust temperature distributions. Spectral features with greater intrinsic width are more sensitive to changing physical conditions in the dust shell (see figure).

(2) The observed differences in the width of the silicate feature in O–rich stars are most likely due to variations in the dust shell distance from the star. Variations in shell optical depth, dust density distribution, or grain composition cannot easily account for the range of shifts observed in the silicate feature.

(3) Variations in the luminosity of the central star and in the dust shell parameters produce distinct effects on the position of a star on color–color diagrams. In particular, as the distance of the dust shell from an O–rich star increases, the intensity on the red side of the silicate feature is enhanced, resulting in a systematic shift in position of the star on the 12–25–60 μm color–color diagram. Hence a correlation between the shifts of the silicate features observed in O–rich stars and their corresponding positions on the color–color diagram would provide strong

support for the hypothesis that O–rich stars evolve to form carbon stars as their O–rich dust shells are detached (Willems, 1987)

This research was partially supported by NASA under the IRAS Data Analysis Program (funded through JPL) and under Grant NAGW–1103.

REFERENCES

Chan. S. J. and Kwok, S.: 1988, *Ap. J.*, in press.

Egan, M. P., Leung, C. M. and Spagna, G. F., Jr.: 1988, *Computer Phys. Commun.*, **48**, 271.

Little–Marenin, I.: 1986, *Ap. J. (Letters)*, **307**, L15.

Willems, F. J.: 1987, Ph. D. Thesis, Universiteit van Amsterdam, Netherlands.

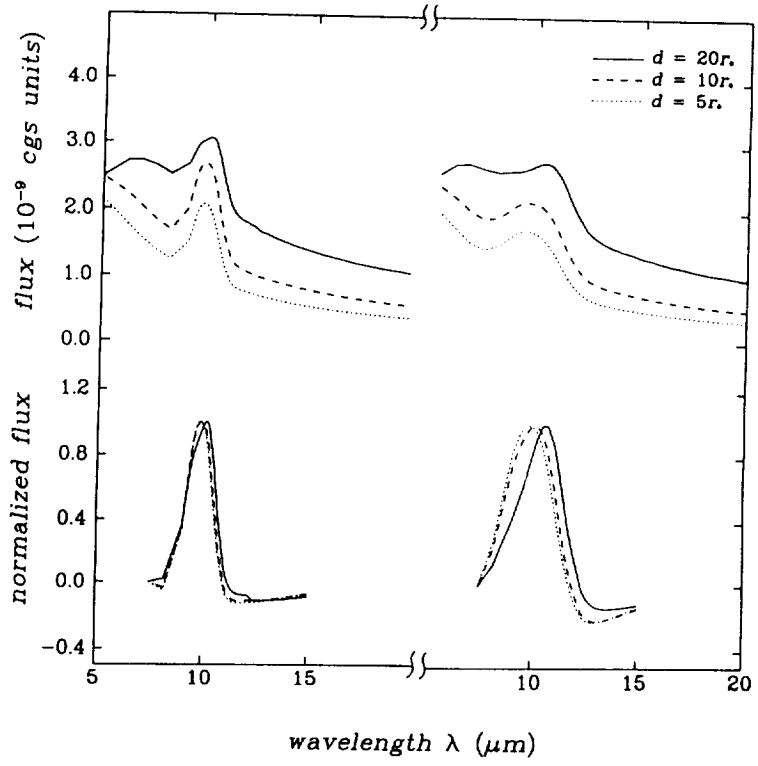

Effect of circumstellar shell distance (d) on the flux spectra of gaussian features of different intrinsic half–widths (σ): $\sigma = 0.5$ μm on the left panel and $\sigma = 1.0$ μm on the right. The normalized flux for the spectral feature is obtained by subtracting the local blackbody continuum from the spectra. Note that the wider feature on the right is more sensitive to variation in shell distances. Furthermore, the blue side of the narrower feature is affected much less than the red side by changes in the shell parameters. These two characteristics are observed in the silicate and SiC features of O–rich and C–rich cool stars respectively.

N91-15022

Carbon Stars With alpha-C:H Emission

Florence Gerbault and John H. Goebel

NASA Ames Research Center

244-10, Moffett Field CA 94035

Abstract

Many carbon stars in the IRAS LRS catalog have been found which display emission spectra that compare favorably with the absorption spectrum of alpha-C:H. These stars have largely been classified as 4X in the LRS which has led to their interpretation by others (e. g., Willems and Papoular) in terms of displaying a mixture of the UIRF's 8.6 micron band and SiC at 11.5 microns. We also find that many of these stars have a spectral upturn at 20+ microns which resembles the MgS band seen in carbon stars and planetary nebulae. We conclude that this group of carbon stars will evolve into planetary nebulae like NGC 7027 and IC 418. In the presence of hard ultraviolet radiation the UIRFs will light up and be displayed as narrow emission bands on top of the broad alpha-C:H emission bands.

N91-15023

New Circumstellar Dust Component in Oxyggen Rich Environments

John H. Goebel and Florence Gerbault

NASA Ames Research Center

244-10, Moffett Field CA 94035

Abstract

Spectra of oxygen rich stars in the IRAS LRS catalog nave been found to display two distinct classes of circumstellar excess emission. The first group has the normal silicate with emission peaking at 10 and 18 microns. The second group has an emission spectrum peaking at 13 and 20 microns. There are also spectra with a mixture of the above types. Generally the continuum temperature associated with the second group is much warmer than that associated with the normal silicate group. Laboratory spectra are compared with the new excess which associates the emission with a class of materials represented by hydrated aluminates and silicates. Possible interpretations include equilibrium condensation sequences and peculiar metal abundance ratios.

TYPE OF SILICATE FEATURE IN OXYGEN RICH STELLAR ENVELOPES

K.V.K. Iyengar and T.N. Rengarajan
Tata Institute of Fundamental Research
Homi Bhabha Road, Bombay 400005, India

The 10 μm silicate feature is seen in several types of astronomical sources. Laboratory measurements of emissivities of silicate grains of different types show variation in the absolute value and in wavelength dependence. In many astronomical studies, one has used the emissivity function derived from the Trapezium emission feature (Gillett et al., 1975). Here, we describe a statistical study of a large sample of objects about the applicability of this commonly used function (hereafter TR).For comparison, we also use another emissivity function derived for lunar silicate (LS) sample 14321 (Knacke and Thomson, 1973) which has a maximum at 10.2 μm instead of at 9.7 μm as for TR. For the present study we use the IRAS Low Resolution Spectra sources classified as 7n, having a silicate absorption feature without any atomic line emission. Most of these sources are likely to be oxygen rich stellar envelopes or hotspots in molecular clouds. Of the 66 sources listed, we selected 61 having a higher flux density in the 25 μm band than in the 12 μm band. We further restricted our study to 59 sources with S/N > 5 at about 8 μm.

For the present study, we assumed the central source to emit a Planckian spectrum characterised by a temperature T and an absorbing envelope with an emissivity dependence of type TR or LS. Values of T and τ, the absorption optical depth were obtained by minimising χ^2 between the observed and fitted spectra in the 7-13 μm range. Values of reduced χ^2 were obtained by taking the noise listed in the LRS Catalog as standard deviation. The τ values obtained correspond to 9.7μm for TR and 10.2 μm for LS.

A summary of the results is given in Table 1. Defining $R = \chi^2(TR)/\chi^2(LS)$, we give the distribution of log R for different ranges of $\chi^2(TR)$ and $\tau(TR)$. Taking all the sources, it is seen that 36% are better fitted by TR shape (log R < -0.2), 24% are better fitted by LS (log R > 0.2) and the rest 40% equally well by both. If we consider only those with $\chi^2 < 10$, the corresponding percentages are 49(TR), 13(LS) and 38 (both). The fraction of sources for which TR is not a good representation is ~ 0.2. In Fig. 1, we show two sources illustrating the difference in fits when TR(LS) is much better than LS(TR).

REFERENCES

Gillett, F.C., Forrest, W.J., Merrill, K.M., Capps, R.W., and Soifer, B.T.: 1975, Ap. J., 200, 609.

Knacke, R.F. and Thomson, R.K.: 1973, PASP, 85, 341

Table 1: Statistics of fits

	$\chi^2(TR) \leq 10$		$\chi^2(TR) \geq 10$	
	$\tau \leq 2$	$\tau \geq 2$	$\tau \leq 2$	$\tau \geq 2$
log R < -0.2	15	3	3	0
0.2 > log R > -0.2	10	4	8	2
log R > 0.2	4	1	6	3

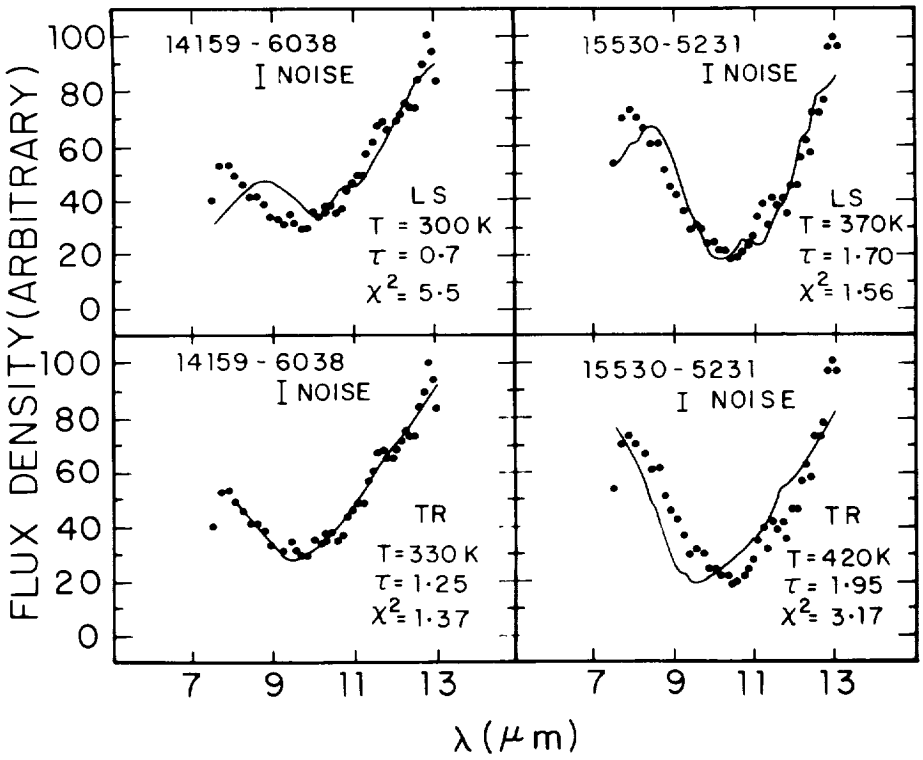

Figure 1. The observed 7-13 μm spectra (filled circles) and the best fits (continuous lines). Emissivity functions used are: TR, Trapezium; LS, lunar silicate.

INTERSTELLAR EXTINCTION AT 10-20 μm

J. P. Simpson* and R. H. Rubin**
*Lick Observatory and NASA/Ames Research Center, Moffett Field, California 94035 USA
**Astronomy Dept., U. C. L. A., and NASA/Ames Research Center, Moffett Field, California 94035 USA

The interstellar extinction function is not well determined in the infrared. Typically, for studies of H II regions and molecular clouds, one assumes that the extinction curve has the same shape as the dust emission in the Trapezium of the Orion Nebula from 8 to 13 μm. Models assuming either pure absorption or emission plus absorption are then fit to the observations of the spectra of the H II regions or molecular clouds by least squares (e.g. Gillett et al. 1975). Herter et al. (1981) extended the extinction curve to 20 μm by assuming that the 18 μm feature that is seen in emission in the dust shells surrounding oxygen rich stars (Forrest et al. 1979) has the same shape as the interstellar extinction curve. The Trapezium 10 μm feature gives good agreement with the 10 μm absorption in molecular clouds, although the general interstellar absorption to the Galactic center seems to require a narrower 10 μm feature, such as is found in the star μ Cep (Roche and Aitken 1985).

We have analysed the IRAS LRS spectra of 117 stars of excellent signal/noise with optically thin silicate dust shells. We subtracted the stellar continua (assumed to be a cool black body), and we fit the resulting dust shell spectra with simple models F_λ assuming uniform mass loss and dust temperature T as a function of distance from the star r, calculated using the optical constants for silicates of Draine (1985). That is,

$$F_\lambda = \int_{R_0}^{R_{max}} \kappa_\lambda B_\lambda(T) \rho_0 (r/r_0)^{-2} 4\pi r^2 dr$$

or in the optically thin approximation,

$$\kappa_\lambda = \frac{F_\lambda}{\int B_\lambda(T) \rho_0 (r/r_0)^{-2} 4\pi r^2 dr}.$$

From the comparison of the spectra and the models, functions for the emissivity κ_λ were derived. The temperature T_0 at the inner edge of the dust shell R_0 was chosen such that the ratio of $\kappa(18\ \mu\text{m})/\kappa(10\ \mu\text{m})$ equals 0.35 (Draine 1985). The different emissivity functions can be divided into 5 groups, which possibly represent

shells of dust of different composition, particle size, or optical depth (Simpson, in preparation). In the different groups, the 10 μm feature peaks at either 9.7 μm or 10 μm, and the width varies. The 18 μm feature has the same appearance in all classes. The average spectra for each group are plotted in Figure 1.

The emissivity function from the class with the shortest wavelength 10 μm peak and the narrowest 10 μm feature is a good match to the Trapezium emissivity function from 9.7 to 13 μm. A composite of the Trapezium feature from 8 to 11 μm and the dust shell feature from 11 to 23 μm is plotted in Figure 2. Using this function, we computed the extinction to 53 H II regions with IRAS LRS spectra by fitting absorption and emission models to the spectra by least squares. Abundances of neon and sulfur were computed for the H II regions from the neon lines at 12.8 and 15.5 μm and the sulfur lines at 10.5 and 18.7 μm. There are decreasing gradients of abundance with galactocentric radius; the abundances of neon and sulfur are also inversely proportional to the luminosities and the excitations of the H II regions. There is an apparant correlation with distance which seems to be due to selection effects on the luminosity such that the low luminosity, high abundance sources are all nearby. Any additional featureless component of the interstellar extinction would have to be less than 0.07 magnitudes/kpc at 12.8 μm and 0.07 magnitudes/kpc at 18.7 μm. These H II regions with similar galactocentric radii as the Sun are plotted in Figure 3.

REFERENCES

Draine, B. T., 1985, *Ap. J. Suppl.*, 57, 587.

Forrest, W. J., McCarthy, J. F., and Houck, J. R., 1979, *Ap. J.*, 233, 611.

Gillett, F. C., Forrest, W. J., Merrill, K. M., Capps, R. W., and Soifer, B. T., 1975, *Ap. J.*, 200, 609.

Herter, T., Helfer, H. L., Pipher, J. L., Briotta, D. A. Jr., Forrest, W. J., Houck, J. R., Rudy, R. J., and Willner, S. P., 1981, *Ap. J.*, 250, 186.

Roche, P. F., and Aitken, D. K., 1985, *M. N. R. A. S.*, 215, 425.

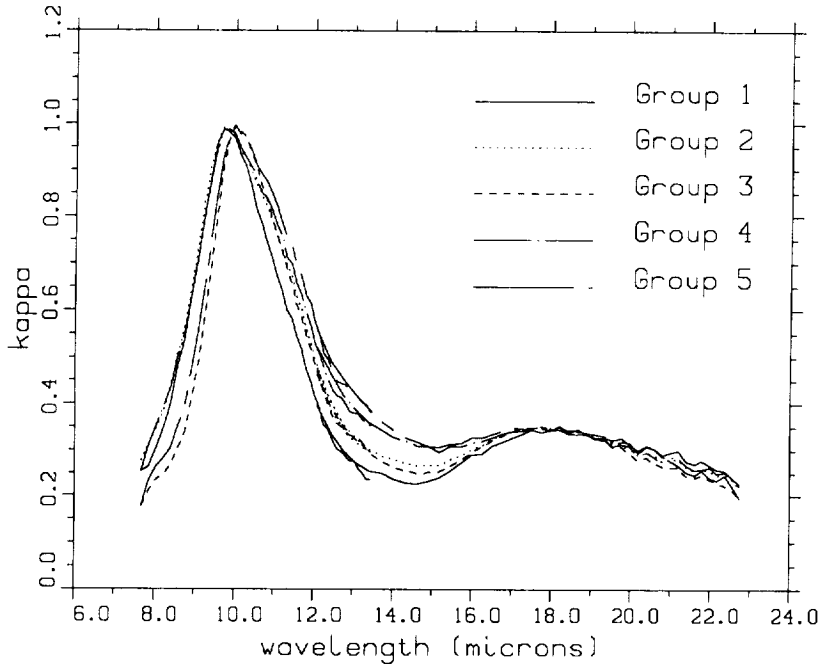

Figure 1. Average dust shell emissivities.

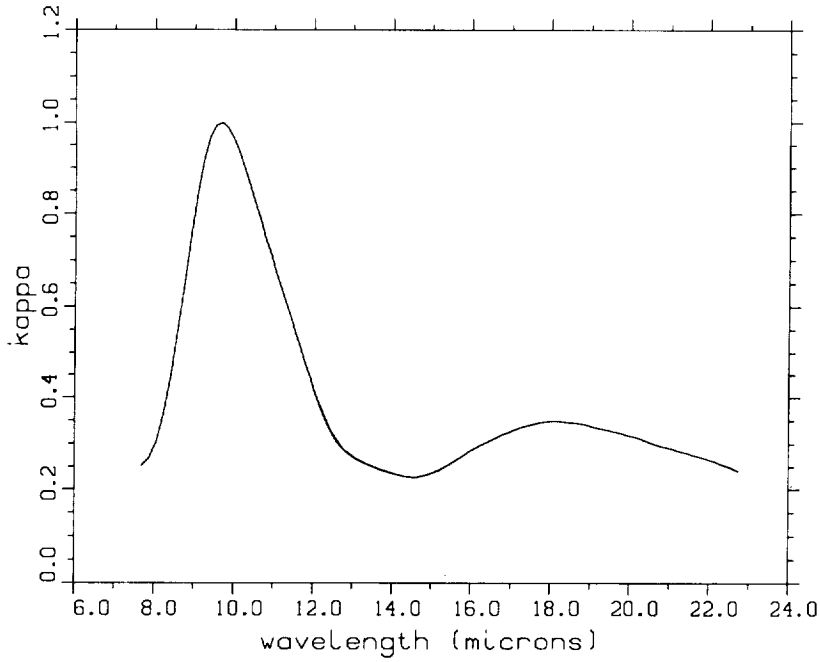

Figure 2. Composite emissivity function.

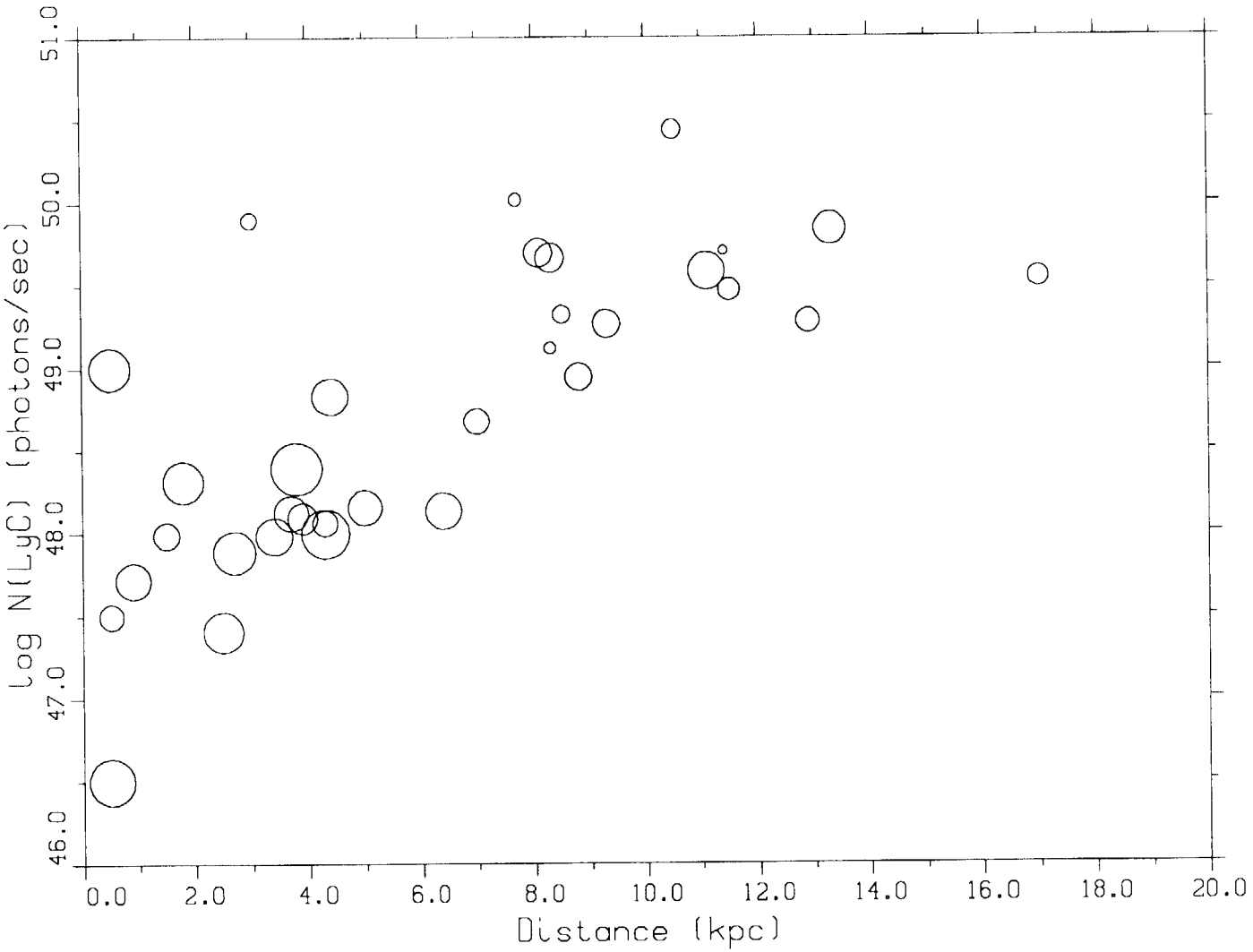

Figure 3. H II regions with similar galactocentric radii as the Sun are plotted against the number of ionizing photons and the distance from the Sun. The diameters of the plotted circles are proportional to the log of the neon abundances, which range from log Ne/H = −5.4 to −3.5.

DUST AROUND MIRA VARIABLES. AN ANALYSIS OF IRAS LRS SPECTRA.

S. Slijkhuis
Astronomical Institute, University of Amsterdam,
Roetersstraat 15, 1018 WB Amsterdam, The Netherlands.

The spatial extend and spectral appearance of the thin dust shell around Mira variables is determined largely by the dust absorptivity $Q_{abs}(\lambda)$ and the dust condensation temperature T_{cond}. Various authors have analysed mid-IR spectra to derive $Q_{abs}(\lambda)$ assuming a value of T_{cond}. Onaka et al.(1987, 1988) have derived T_{cond} assuming $Q_{abs}(\lambda)$. They fitted IRAS LRS spectra with a two component dust model: they took the measured $Q_{abs}(\lambda)$ of synthesised amorphous Mg_2SiO_4 (Day 1979) to account for the 10 and 20 μm features, and of Al_2O_3 to account for the 12 μm feature (which dominates the spectra of stars with a symmetrical optical lightcurve, Vardya et al. 1986). In general, their fits are reasonably good, but a large fraction of the spectra is not fitted very well in detail by the laboratory dust emissivities.

In the present work, we try to extract both $Q_{abs}(\lambda)$ and T_{cond} from IRAS LRS spectra. To do this, we make the assumption that the ratio of total power in the 10 μm feature to that in the 20 μm feature should be equal to that measured in other amorphous silicates (e.g. synthesised amorphous Mg_2SiO_4, Day 1979). We find that T_{cond} decreases with decreasing strength of the 10 μm feature, from T_{cond}= 1000 K to T_{cond}= 500 K (estimated error 20%). A similar result was found by Onaka et al. (1987, 1988), but they found lower values of T_{cond}. We cannot determine a value for the Near-IR dust absorptivity. Although this parameter strongly affects the condensation radius, it hardly affects the shape of the LRS spectrum (as long as the optically thin approximation is valid), because it scales the spatial distribution of the dust.

Information on the magnitude of the NIR dust absorptivity may be deduced from the unique carbon star BM Gem. This star has a LRS spectrum with silicate features indicating an inner dust shell temperature of at least 1000 K. However, on the basis of observations in the 1920s-1930s one may infer an inner dust shell radius of at least 6×10^{12} m. To have this high temperature at such a large distance, the NIR absorptivity of the dust must be high, compatible with the results found by Jones and Merrill (1976), but less compatible with "astronomical silicate" (Draine and Lee 1984).

REFERENCES

Day, K.L.: 1979, Ap.J. 234, 158

Draine, B.T., and Lee, H.M.: 1984, Ap.J. 285, 89

Jones, T.W., and Merrill, K.M.: 1976, Ap.J. 209, 509

Onaka, T., and de Jong, T.: 1987, in "Late stages of stellar
ed. S. Kwok and S.R. Pottasch (Dordrecht: Reidel), p97

Onaka, T., de Jong, T., and Willems, F.J.: 1988, submitted to
Astron.Astroph.

Tielens, A.G.G.M., and Allamandola, L.J.: 1987, in "Interstellar
processes", ed. D.J. Hollenbach and H.A. Thronson (Dordrecht:
Reidel), p397.

Vardya, M.S., de Jong, T., and Willems, F.J.: 1986, Ap.J.L. 304, L29

VIII-C) DUST IN PROTOPLANETARY NEBULAE

POLARIZATION DUE TO DUST SCATTERING IN THE PLANETARY NEBULA CN1-1

Harish C.Bhatt
Indian Institute of Astrophysics, Bangalore 560034, India

The peculiar emission-line object Cn1-1 (=HDE330036=PK330+4°1), classified both as a symbiotic star (Glass and Webster, 1973) and as a planetary nebula (Lutz, 1977, 1984), was detected by the Infrared Astronomical Satellite (IRAS) as a strong source of far-infrared radiation (Pottasch et al., 1984) indicating the presence of cool dust in the system. Bhatt and Mallik (1986) discussed the nature of the dust in Cn1-1 and argued that the object is a Type I proto-planetary nebula in a binary system.

Polarization measurements of Cn1-1 have been made recently by Schulte-Ladbeck and Magalhaes (1987). A high degree of linear polarization ($\sim$ 3%) was observed. However, they regarded Cn1-1 as a symbiotic star and considered the observed polarization to be of purely interstellar origin. We argue here that the polarization is intrinsic to Cn1-1 and is due to scattering by large (compared to the interstellar) dust grains in the protoplanetary nebula asymmetrically (bipolar?) distributed around the central star.

The wavelength (λ) dependence of the observed percent polarization $P(\lambda)$ ($P(0.35\ \mu m)=1.96$, $P(0.44\ \mu m)=2.58$, $P(0.55\mu m)=2.79$, $P(H_\alpha)=2.84$, $P(0.79\ \mu m)=2.97$; position angle $\theta = 29\pm3°$ for all λ) shows that $P(\lambda)$ increases with λ and the wavelength of maximum polarization $\lambda_{max} >> 0.55\ \mu m$, the mean interstellar value. A fit to the emprirical law: $\ln(P_{max}/P(\lambda))=K\ \ln^2(\lambda_{max}/\lambda)$ (Serkowski et al., 1975) gives $K=0.75$, $P_{max}=2.98\%$ and $\lambda_{max}=0.74\ \mu m$. The values of K and λ_{max} are rather different from the mean interstellar values $K=1.15$ and $\lambda_{max} = 0.55\ \mu m$. The value of θ ($=29\pm3°$) also differs much from $\theta = 49\pm3°$ for other normal stars (HD 141318 and HD 142919, Mathewson and Ford, 1970) in the neighbourhood of Cn1-1.

The large degree of polarization ($\sim$3% for the Cn1-1 distance of $\sim$ 450 pc) with a large λ_{max} is naturally explained if it is caused by scattering by large dust grains in the Cn1-1 nebula. The presence of large dust grains in Cn1-1 has been suggested by Bhatt and Mallik (1986). Since the H_α line is also polarized at the same level and position angle as the continuum, the dust must be asymmetrically distributed around the central star. The morphology of the protoplanetary nebula in Cn1-1 may be bipolar. Bipolarity is quite common among the Type I planetary nebulae (Peimbert and Torres -Peimbert, 1983).

The polarization observations thus support the suggestion that Cn 1-1 is a bipolar Type I planetary nebula.

Bhatt,H.C. and Mallik,D.C.V.: 1986, Astron. Astrophys. 168,248.
Glass,I.S. and Webster,B.L. : 1973, Mon. Not. R. Astron. Soc. 165, 77.
Lutz,J.H. : 1977, Astron. Astrophys. 60, 93.
Lutz,J.H. : 1984, Astrophys. J. 279, 714.
Mathewson,D.S. and Ford,V.L. : 1970, Mem. R. Astron. Soc. 74, 139.
Peimbert,M. and Torres-Peimbert,S. : 1983, in Planetary Nebulae, IAU Symp. No.103, ed. D.R.Flower, D.Reidel, Dordrecht.
Pottasch,S.R. etal. : 1984, Astron. Astrophys. 138, 10.
Schulte-Ladbeck,R.E. and Magalhaes,A.M. : 1987, Astron. Astrophys. 181, 213.
Serkowski,K., Mathewson,D.S. and Ford,V.L. : 1975, Astrophys. J. 196, 261.

CIRCUMSTELLAR GRAIN EXTINCTION PROPERTIES OF RECENTLY DISCOVERED POST AGB STARS

Richard H. Buss Jr.*, Henny J. G. L. M. Lamers**, and Theodore P. Snow Jr.*
*Center for Astrophysics and Space Astronomy, University of Colorado
**SRON Laboratory for Space Research, Utrecht

We have examined the circumstellar grains of two hot evolved post asymptotic giant branch (post AGB) stars, HD 89353 and HD 213985. Other studies have detected 3.3, 3.53, 7-9, and 11.3 μm infrared emission features toward HD 89353 but have found no 3 μm infrared emission lines toward HD 213985. From ultraviolet spectra, energy balance of the flux, and Kurucz models, we derived the extinction around 2175 Å. With visual spectra, we attempted to detect 6614 Å diffuse band absorption arising from the circumstellar grains so that we could examine the relationship of these features to the infrared features. For both stars, we did not detect any diffuse band absorption at 6614 Å, implying that the carrier of this diffuse band is not the carrier of the unidentified infrared features nor of the 2175 Å bump.

We found that the linear ultraviolet extinction of the carbon-rich star HD 89353 continued across the 2175 Å region with no sign of the bump; for HD 213985 we found the reverse: a strong, wide bump in the mid-ultraviolet. We ascertained that the 213985 bump was positioned at 2340 Å, longward of its usual position in the interstellar medium. Since we determined that HD 213985 had excess carbon, the bump probably arises from a carbonaceous grain. Thus, in view of the ultraviolet and infrared properties of the two post AGB stars, ubiquitous interstellar infrared emission features do not seem to be associated with the 2175 Å bump. Instead, the infrared features seem related to the linear ultraviolet extinction component: Hydrocarbon grains of radius $<$ 300 Å are present with the linear HD 89353 extinction; amorphous anhydrous carbonaceous grains of radius $<$ 50 Å might cause the shifted ultraviolet extinction bump of HD 213985.

REFERENCES

Lamers, H. J. G. L. M., Waters, L. B. F. M., Garmany, C. D., Perez, M. R., Waelkens, C. 1986, *Astr. Ap.*, **154**, L20.

Waelkens, C., Waters, L. B. F. M., Cassatella, A., Le Bertre, T., and Lamers, H. J. G. L. M. 1987, *Astr. Ap.*, **181**, L5.

Waelkens, C. *et al.* 1989, in preparation.

Waters, L. B. F. M., Lamers, H. J. G. L. M., Snow, T. P., Mathlener, E., Trams, N. R., Van Hoof, P. A. M., Waelkens, C., Seab, G. C., and Stanga, R. 1988, *Astr. Ap.*, in press.

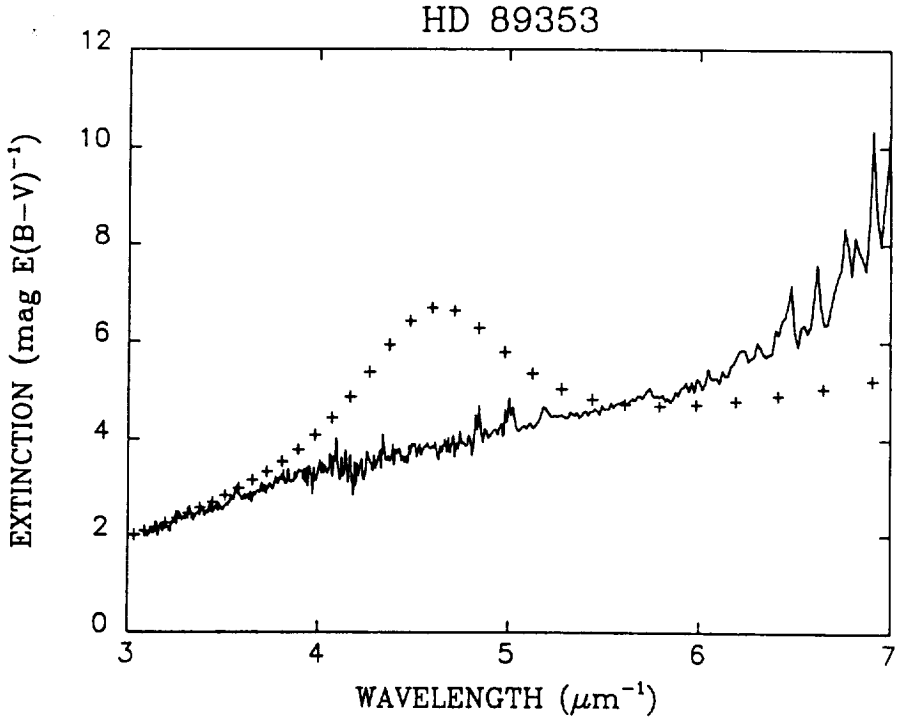

• Figure 1 –Carbonaceous protoplanetary nebula ultraviolet circumstellar extinction. HD 89353 is linear throughout; data unreliable beyond 6.7 μm. Spectral extinction has been normalized to the mean interstellar curve (crosses) at about 3.3 μm^{-1}.

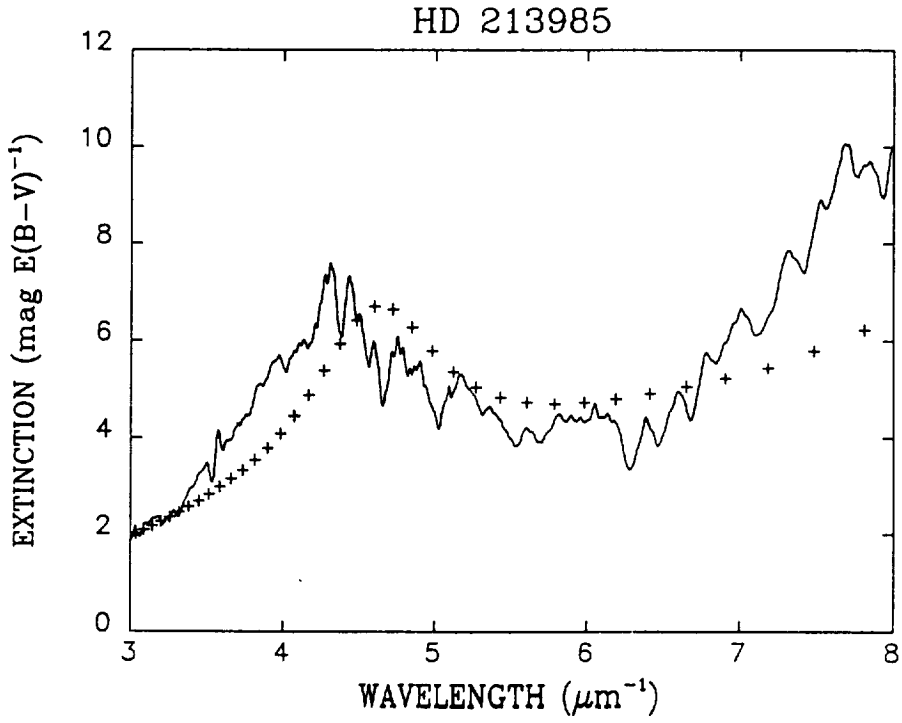

• Figure 2 –Ultraviolet circumstellar extinction normalized to the mean interstellar extinction at 3.3 μm^{-1}. HD 213985 has a shifted mid ultraviolet bump and a greater far ultraviolet rise than the interstellar medium (crosses).

COMPACT REFLECTION NEBULAE, A TRANSIT PHASE OF EVOLUTION FROM POST-AGB TO PLANETARY NEBULAE?

J.Y. Hu,[1,2] and S. Slijkhuis[2]
[1]Beijing Observatory, Academia Sinica, China
[2]Astronomical Institute, University of Amsterdam,
Roetersstraat 15, 1018 WB Amsterdam, The Netherlands

In a search of the optical counter-part of candidates of proto planetary nebulae on the plates of UK Schmidt, ESO Schmidt and POSS, 5 compact reflection nebulae associated with post-AGB stars were found. They are listed in table 1.

Table 1. IRAS sources in this study

IRAS NAME	V	d	Note
17514-1555	14.7	15"	
17195-2710	17	6	
16559-2857	14	12	prism sp: K type
16552-3050	14	12	prism sp: K type
17150-3224	15	14	brightened in period 1958-1983

A simplified model (dust shell is spherical symmetric, expansion velocity of dust shell is constant, $Q_{sca}(\lambda)$ is isotropic, and the dust grain properties are uniform) is used to estimate the visible condition of the dust shell due to the scattering of the core star's light. Under certain conditions (mass loss rate $\dot{M}$ at latest stage of AGB, the delay time dt after mass loss stopped and distance to objects) the compact reflection nebulae can be seen on the POSS or ESO/ SRC survey plates.

N91-15030

CONTINOUS INFRARED EMISSION OF PROTO- AND YOUNG-PLANETARY NEBULAE

R.Szczerba
Polish Academy of Sciences,
N. Copernicus Astronomical Center,
Laboratory of Astrophysics, Toruń, Poland

Interstellar dust is the component of interstellar medium (ISM) which determines its physical properties. An important source of new grains seem to be the outflows from the cool stars outer athmospheres. A very high rate of mass loss up to some 10^{-4} $M_\odot$/yr is common for red giants on the asymptotic giant branch which, as it is now generally accepted, are precursors of planetary nebulae (PNe). Infrared (IR) observations of PNe have established the presence of dust in these objects. As the candidates for grain materials, silicate minerals are proposed from the features at 10 μm and/or 20 μm for O- rich stars and carbon and SiC grains from the 11.5 μm feature for C- stars. While the dust in PNe may be different from that present in the ISM, it is in a better defined environment than that in a diffuse cloud, for example and so its properties and significance may be better established.

Evolutionary sequences of PNe were calculated beginning from the moment of shell ejection to its dissipation and IR spectra of the outgoing radiation were obtained for different stages of the evolution. To solve the coupled hydrodynamical and radiation transfer problem we have used computer code described and used by Yorke (1979) and Okorokov et al. (1985) in which gas and dust are treated as two separate hydrodynamical components. The models, which are calculated for two grain materials - graphite and silicate, have a size distribution of particles based on that found for the ISM by Mathis et al. (1977). In our computations we have employed the recent optical properties of graphite and "astronomical silicate" grains tabulated by Draine (1987). The details of the dust formation and growth process were neglected. We have simply assumed that silicate or graphite grains exist below some critical temperature equal to 1300 or to 1700 °K, respectively.

Infrared model spectra are compared with the IR radiation emitted by some proto- and some young-planetary nebulae. The observed IR continua can be quite well matched with our models with grains having a reasonable size range.

REFERENCES:

Draine, B.T.: 1987, Princeton Observatory Preprint,No. 213

Mathis, J.S., Rumpl, W., Nordsieck, K.H.: 1977,
Astrophys. J., 217, 425

Okorokov, V.A., Shustov, B.M., Tutukov, A.V., Yorke, H.W.: 1985,
Astron. Astrophys., 142, 441

Yorke, H.W.: 1979, Astron. Astrophys. 80, 308

THE DISCOVERY OF A HIGHLY POLARIZED BIPOLAR NEBULA

R.D.Wolstencroft*, S.M.Scarrott** and J.Menzies***
*Royal Observatory, Edinburgh, U.K.
**Department of Physics, University of Durham, U.K.
***South African Astronomical Observatory, R.S.A.

During a search for the optical counterparts of IRAS sources whose flux peaks at 25 microns we have discovered a small faint bipolar nebula in Monoceros at the position of IRAS 07131-0147.

In the CCD images displayed in fig.1 the object shows considerable structure. The central star seems relatively free of closeby nebulosity, the two lobes have a bow-tie structure with those parts nearest to the star consisting of series of small knots. The outer parts of the lobes seem to be made up of filaments streaming away from the knots.

The linear polarization map in fig.2 shows a circular pattern of vectors indicating that the system is a reflection nebula illuminated by the central star. Throughout the lobes and including the regions occupied by the knots the levels of polarization are remarkably high (~ 60-70%).

Bipolar nebulae are associated with both young and old stars. On the basis of its optical spectrum we classify the central star as a M5-6 giant. In the IRAS colour classification scheme of Van der Veen & Habing (1988) the central star is VIb which indicates that there are distinct hot and cold components of circumstellar dust and that the mass loss process may have temporarily abated. We therefore propose that our object is in the post main sequence stage of evolution and is a protoplanetary nebula.

Young protoplanetary nebulae (e.g. CRL2688) have totally obscured central stars illuminating relflective lobes whereas older ones such as M2-9 have lobes seen in emission from gas ionized by the central hot star which is clearly visible. Since the central object of IRAS07131-0147 is a relatively unobscured late type star and the lobes are seen only by reflection we suggest that this nebula is a protoplanetary nebula in an evolutionary stage intermediate between that of CRL2688 and M2-9.

Van der Veen, W. & Habing, H.J. : 1988, Astr.Astrophys. 194, 125.

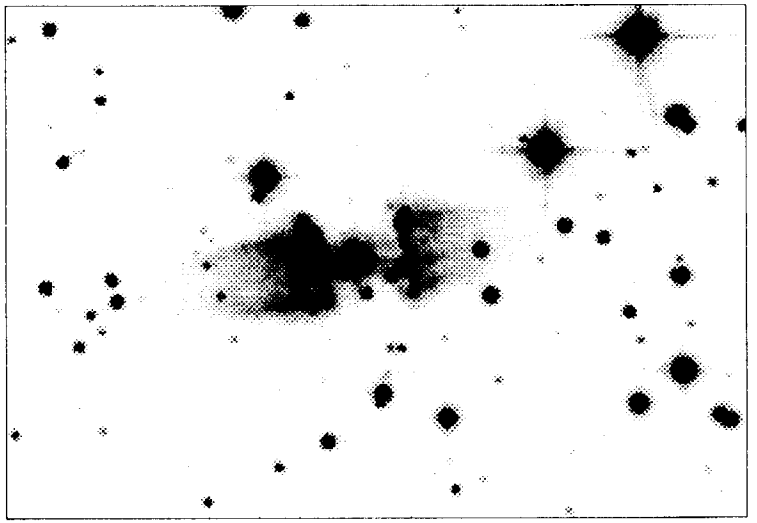

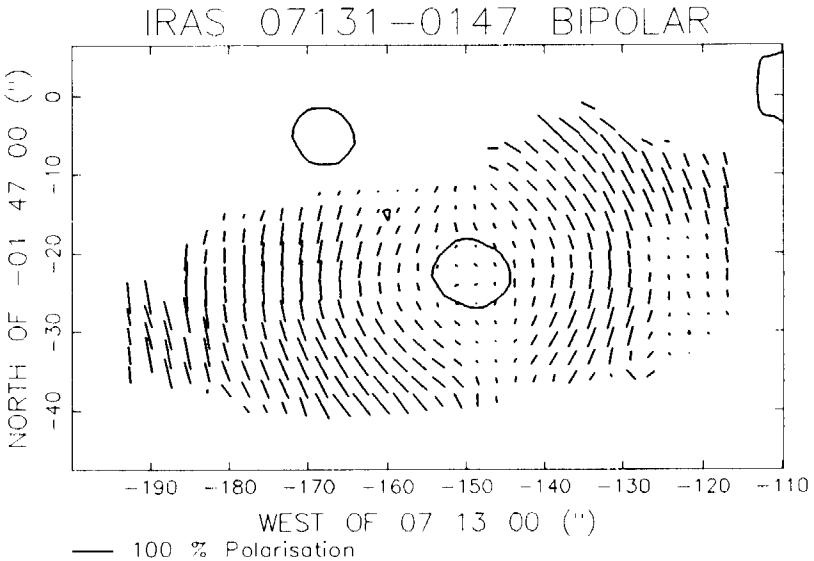

Fig.1 (top left and right).
R waveband CCD images of the IRAS 07131-0147 bipolar nebula. Note the string of knots of the inner parts of the lobes. The extent of the images is 140 by 100". Seeing was ~1".

Fig.2 (below left).
A linear polarization map of the bipolar nebula. The circular pattern is typical of a reflection nebula illuminated by a central star.

VIII-D) DUST IN SUPERNOVA REMNANTS

INFRARED EMISSION FROM THE SUPERNOVA REMNANT PUPPIS A: DUST AND GAS PARAMETERS

R. Arendt,* E. Dwek, ** and R. Petre**
*Department of Astronomy, University of Illinois, Urbana IL 61801
**NASA Goddard Space Flight Center, Greenbelt MD 20771

Abstract. We have modelled the infrared (IR) spectra of collisionally heated dust at several regions across the supernova remnant (SNR) Puppis A. Through the comparision of the actual and model spectra, we are able to narrow the possible range of gas density and temperature within these areas. From the models, we also find information on the minimum and maximum dust grain sizes, and the amount of sputtering which has occurred. Finally, for these regions, we derive the mass of gas and dust, the IR luminosity, the effective thickness, and the length of time since the dust was swept up by the SNR.

I. INTRODUCTION

Puppis A is one of the most prominent supernova remnants in the infrared. The correlation of its IR and X-ray emission is excellent, while the correlations between the IR and radio or optical emission are significantly worse. This leads us to believe that the IR emission is predominantly due to swept-up interstellar dust collisionally heated by the shocked gas within the expanding SNR. We have modelled the IR emission at several regions starting from the gas temperature and density, which are not always known uniquely, and the infrared flux densities. Next, with the selection of a grain size distribution, we determine the infrared spectrum of the dust, collisionally heated by a gas at the applicable density and temperature. We adjust the amount of sputtering and the size limits of the dust distribution to find the model spectrum which best fits the data. From the best models, we derive various physical parameters of the gas and dust at the local regions which are examined.

II. X–RAY AND IR DATA

The gas density and temperature were derived at several 6 ' diameter regions across Puppis A, through modelling the X-ray spectra obtained with the Einstein satellite's Solid State Spectrometer (SSS) (Szymkowiak 1985). These region are indicated in Figure 1.

The IR flux densities were measured from the Infrared Astronomical Satellite (IRAS) coadded data over the same regions as observed with the SSS. A planar background was subtracted from the entire region of the SNR. For region C an additional background component, with a spectrum matching that of the cloud immediately to the east, was subtracted from the observed flux densities before modelling.

III. MODELLING THE IR EMISSION

To model the observed IR emission, we used a mixture of graphite and silicate grains with a number density in the a to a+da size interval given by:

$$n_{dust}(a)\,da = n_0\,f(a)\,da,$$

where $f(a) \sim a^{-k}$, for $a_{min} < a < a_{max}$,

normalized so that $\int f(a)\,da = 1$,

and $n_0(\text{graphite}) = Z_g\,C_g\,n_{gas}$

$n_0(\text{silicate}) = Z_s\,C_s\,n_{gas}$,

where n_{gas} is the number density of the gas, C_g and C_s are constants which depend on the index (k), and the limits (a_{min} and a_{max}) of the power law distribution, and Z_g and Z_s are the dust to gas mass ratios of graphite and silicate, taken to be $Z_g = 0.0040$ and $Z_s = 0.0035$ throughout this work.

Two of the models used were an MRN distribution (Mathis, Rumpl, and Nordsieck 1977) extended to smaller grain sizes (EMRN), and an extended MRN distribution with larger grain sizes also included (EMRNL). The power law indicies of both of these distributions are were k = -3.5. The lower limits for both distributions were a_{min} (graphite) = 0.0003μm, a_{min} (silicate) = 0.0026μm, and the upper limits for the EMRN distribution were a_{max}(graphite), a_{max}(silicate) = 0.25μm, while for the EMRNL distribution the upper limits were a_{max}(graphite), a_{max}(silicate) = 1.0μm.

The fluxes from the dust models were calculated according to:

$$F(\lambda) = \sum_{\text{comp.}} \int_{a_{min}}^{a_{max}} n_{dust}(a) \left[\int_{3K}^{T_{evap.}} P(a,T_d) B_\lambda(T_d) Q_\lambda(a)\,dT_d \right] da.$$

The sum is over grain compositions. The function $P(a,T_d)$ is the temperature probabilty distribution of dust grains of size a. This function depends upon the density and temperature of the gas which is heating the dust. Under the conditions found within Puppis A, for grain sizes larger than ~0.02μm the effects of stochastic heating become less important and these grains are found within a narrow range of their equilibrium temperatures ($T_{eq}(a)$). Thus, for these larger grains we made the approximation: $P(a,T_d) = \delta(T_d - T_{eq}(a))$.

A decrease in grain size due to sputtering, Δa(sput.), was simulated by using a size distribution based on the initial distribution described above: $n_{sput}(a) \sim f(a+\Delta a(\text{sput.}))$. This sputtered grain size distribution was then used in the integral defining the flux.

For each region we created several model spectra. In most cases the EMRN dust model provided a reasonably good spectrum. Models using different amounts of sputtering and size limits were created to find better fits to the observed data, and to determine what range of variation of the dust model parameters was allowable.

IV. RESULTS

The amount of sputtering that has taken place in a region can be related to the length time (τ) for which the gas has been subjected to sputtering by: $\Delta a(\text{sput.}) = 0.005\,n_{gas}\,\tau$, where Δa(sput.) is in Å, n_{gas} is in cm^{-3}, and τ is in years (Draine and Salpeter 1979). The normalization factors needed to match the model spectra to the observed spectra are directly related to the current mass of dust in the given regions. The depletion of the dust

due to sputtering is defined as the ratio of the current dust mass to the initial dust mass before sputtering had acted to erode the grains. The mass of gas in the region is found from the initial dust mass and the dust to gas mass ratio. The mass of gas and the gas density are then used to derive the effective thickness of each region. (The width of each region examined is 1.75d pc, where d is the distance to Puppis A in kpc.) The IR luminosity is found from the integral of the spectrum over wavelength.

For each of the regions, Table 1 lists the input parameters used in calculating the model spectra, the dust model that provides the best fitting model spectrum, and various physical parameters which can be derived from the models.

TABLE 1

	Region	C	I1	I2	I3	N	R
Input Parameters	IR flux densities(Jy)						
	12μm	1.22	<1.56	<1.56	<1.56	<1.56	<1.56
	25μm	14.8	13.1	10.2	7.2	7.7	2.0
	60μm	63.2	50.7	44.7	33.7	37.9	8.9
	100μm	36.3	44.6	31.7	16.9	19.2	19.7
	Gas density (cm^{-3})	4.0	1.3	1.3	1.3	1.3	1.3
	Gas temperature (10^6 K)	3.2	5.6	5.6	5.6	10.	3.2
Best Fitting Dust Model	Size distribution	EMRN	EMRN	EMRN	EMRN	EMRN	EMRNL
	Model flux densities(Jy)						
	12μm	1.6	1.2	1.0	0.8	0.6	0.3
	25μm	14.7	10.8	9.09	6.68	7.02	1.94
	60μm	63.3	55.4	46.8	34.4	38.9	9.7
	100μm	34.9	34.8	29.4	21.6	21.5	8.38
	Δa(sput.) (Å)	6	0.0	0.0	0.0	0.0	0.0
Derived Parameters	Sputtering age (yrs)	~300	<460	<460	<460	<460	<460
	Depletion	0.906	1.0	1.0	1.0	1.0	1.0
	Dust mass ($10^{-3} M_\odot/kpc^2$)	1.59	2.13	1.80	1.32	0.96	1.27
	Gas mass ($M_\odot/kpc^2$)	0.234	0.284	0.240	0.176	0.128	0.169
	Effective thickness(pc)	0.77	1.9	2.4	1.8	1.3	1.7
	IR Luminosity ($L_\odot/kpc^2$)	174	148	125	91.5	98.2	28.0

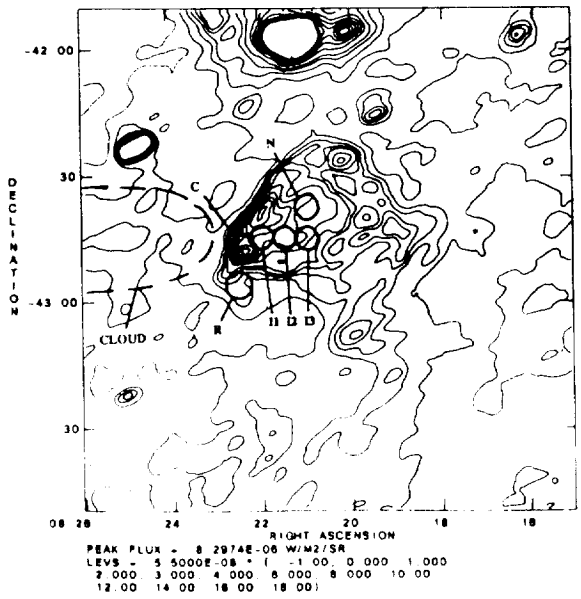

Figure 1: Puppis A at 60μ

The diamond shaped object, roughly 50' across, at the center of Figure 1 is the SNR Puppis A as seen by the IRAS at 60μm. The circles indicate the the regions observed with the Einstein SSS and analyzed by Szymkowiak (1985). To the east of Puppis A lies a cloud, visible in the IR as well as through HI and CO observations (Dubner and Arnal 1988), which is interacting with the SNR.

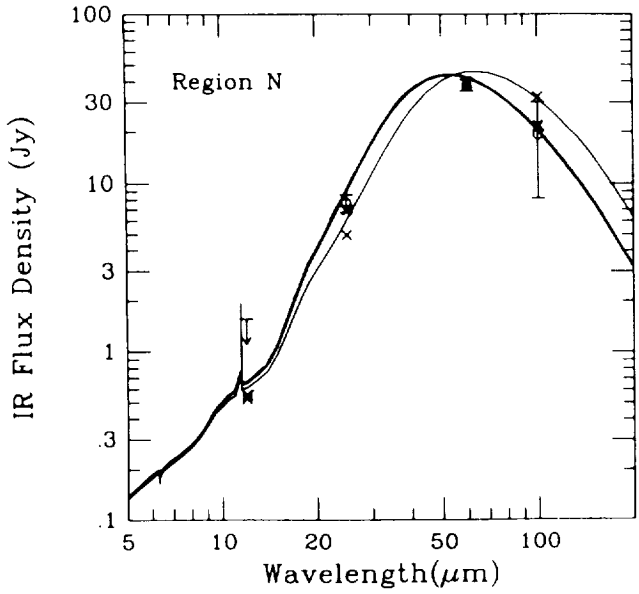

Figure 2: IR as a Diagnostic of Plasma Parameters

For region N, two different sets of gas density and temperature can be used to produce equally good models of the X-ray spectrum. However, only one of these sets leads to a good model of the IR spectrum. (heavy line : n = 1.3 cm^{-3}, T = 10^7 K; light line: n = 0.4 cm^{-3}, T = 10^7 K)

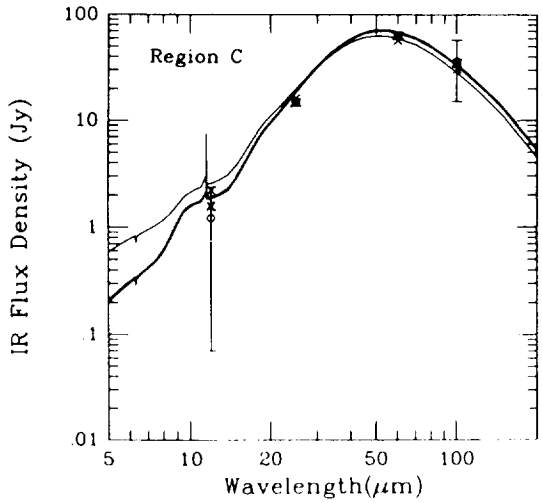

Figure 3: The Effects of Sputtering

For region C, the IR spectrum modelled from the extended MRN grain size distribution is too high at 25μm and too low at 60μm (light line). An improved spectrum results when grains with the same initial size distribution are sputtered so that all grains are decreased in size by 6A (heavy line).

Other regions show little or no evidence of sputtering, but are modelled by a less dense gas and therefore a correspondingly lower sputtering rate.

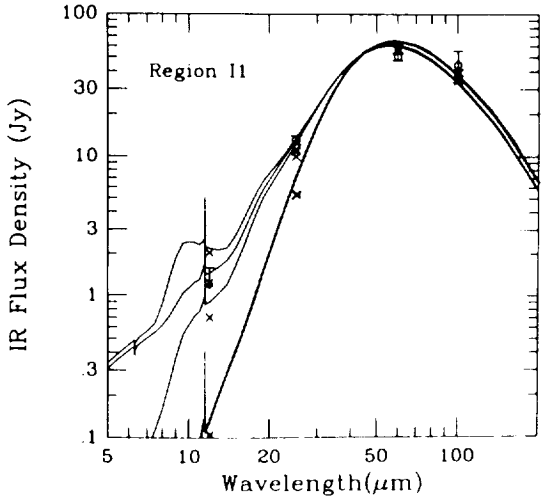

Figure 4: The Effects of Small Grains

Models of the IR spectrum based on a standard MRN size distribution underestimate the 25μm flux densities of all regions (heavy line). Extending the MRN spectrum to smaller grain sizes leads to better model IR spectra (light lines, from higher to lower: a_{min}(graphite), a_{min}(silicate) = 3A; a_{min}(graphite) = 3A, a_{min}(silicate) = 26A; a_{min}(graphite), a_{min}(silicate) = 26A). The 12μm flux density is most strongly affected by the lower limit of the grain size distribution. Unfortunately, only in region C is there any detectable IR emission.

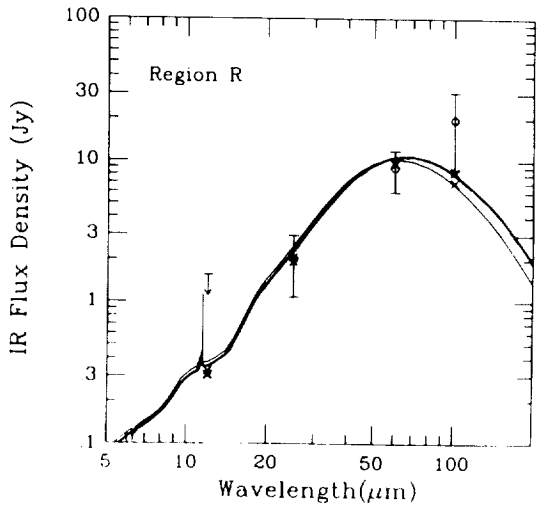

Figure 5: The Effects of Large Grains

Region R shows an observed 100μm flux density which is underestimated by the emission modelled from an extended MRN distribution of grain sizes (light line). Increasing the upper limit of the grain size distribution from 0.25μm to 1.0μm yields a spectrum with an improved fit (heavy line).

However, improved results can also be obtained by subtracting an additional background component with the same spectrum as the cloud immediatly to the east of this region.

V. CONCLUSION

Through this examination of selected regions of the SNR Puppis A, we have been able to show that: 1) the gas densities and temperatures derived from analysis of the X-ray spectra lead to good models of the IR spectra of collisionally heated dust, which provide estimates of the masses, luminosities, ages, and effective thicknesses of these regions (see Table 1), 2) the model IR spectra can be used to determine the best choice of gas density and temperature in cases where more than one combination can be used to model the X-ray spectra, 3) the standard MRN grain size distribution must be extended to smaller sizes, which are stochastically heated, to achieve the best fitting model IR spectra, 4) the limits set on the amount of sputtering which has occurred, indicate that most of the dust has resided in the hot plasma of the SNR for <450 years, and 5) the results for regions R and C indicate either the superposition of the SNR and a nearby cloud, or the presence of additional large dust grains.

REFERENCES

Draine, B. T., and Salpeter, E. E.: 1979, Ap. J., **231**, 77.

Dubner, G. M., and Arnal, E. M.: 1988, in Supernova Remnants and the Interstellar Medium, eds. R. S. Roger and L. Landecker, (Cambridge: Cambridge University Press), p.249.

Mathis, J. S., Rumpl, W., and Nordsieck, K. H.: 1977, Ap. J., **217**, 425.

Szymkowiak, A. E.: 1985, "X-ray Spectra of Supernova Remnants", NASA Technical Memo. 86169.

ON THE DETECTABILITY OF INFRARED ECHO ARCS AROUND SUPERNOVA 1987A

James E. Felten and Eli Dwek
Laboratory for Astronomy and Solar Physics, Code 685,
NASA Goddard Space Flight Center, Greenbelt, MD 20771 USA

ABSTRACT

The ring-like interstellar visual echoes of radii 33 and 54 arcsec detected around SN 1987A should coincide with infrared echoes (thermal reradiation) from dust at T ~ 15-30 K. We consider whether these infrared echoes are detectable at present. They will be brightest at ~100μm, the range of the Texas infrared photometer. Detectability depends on the ratio $\zeta \equiv \tau_a/\tau_s P(\theta)$, where τ_a and τ_s are the visual absorption and scattering optical thicknesses of the echo layer, and P is the phase function for small-angle scattering ($\theta \approx 2°$ to 4°). We need $\zeta \gtrsim 1$ for a detectable signal (~0.3 Jy), but ζ cannot be >>1; otherwise the visual echoes could not be as bright as they are. Typical dust mixtures of Mathis-Rumpl-Nordsieck type have $\zeta << 1$. ζ remains small even if a population of very small grains with power-law index as steep as ~5.5 is added. A population with even more small grains and/or fewer large grains could have $\zeta \sim 1$ and be detectable at present, but this seems unlikely. The echoes will move, but should remain accessible for many years and should be detected eventually.

The detection of arcs or rings of visual echo light around Supernova (SN) 1987A (Crotts, 1988), similar to those seen around Nova Persei in 1901 (Felten, 1988), has introduced a new element into discussions of possible infrared echoes. These visual echoes (Suntzeff *et al.*, 1988; Gouiffes *et al.*, 1988; Chevalier and Emmering, 1988) consist of light emitted by the SN around its epoch of maximum visual light (observed via the direct path around May 1987), and scattered by dust clouds in the far foreground so as to reach us with a kinematical time delay of about a year. Two clouds or layers within the Large Magellanic Cloud (LMC) are identified, at distances z ≈ 123 and 330 pc in front of the SN. These dust clouds should absorb some of the SN light at the same time and reradiate the energy thermally. In principle this produces an infrared echo coincident with the visual echo.

We have heard rumors of attempts to detect this infrared echo. Therefore we have tried to predict its expected strength and infer whether it can be detected at present. A longer account of our work appears elsewhere (Dwek and Felten, 1988). Here we merely summarize the simple physical ideas involved and the results we obtain. Detection at present is unlikely, though not impossible.

Our approach is to make some simple estimates without worrying too much about the radiative-transfer complications which would ensue if any of the visual optical thicknesses τ_e which appear in the problem were large ($\tau_e \gtrsim 1$). It is generally believed that τ_e is not large, say not >1, along lines of sight to and near the SN, though this is not certain. A value of τ_e as large as ~2 could perhaps be permitted along the direct line to the SN without doing too much violence to theories of the outburst. Below we assume that $\tau_e \approx 0.5$, i.e., $A_V \approx 0.5$, in the numbers that we use. If τ_e were as large as 2, our numbers would have to be changed a bit, but the general features of the results would not change.

How bright could such an IR echo possibly be? In mid-May 1987, the dereddened bolometric luminosity of the SN was $L_{bol} \approx 6.4\times10^{41}$ erg s^{-1} (Hamuy *et al.*, 1988; Catchpole *et al.*, 1987). The outer echo arcs arise in a dust layer about z = 330 pc in front of the SN. If this layer is thick enough ($\tau_a \gtrsim 1$) to absorb and convert essentially all the incident radiation, we get the strongest possible IR signal. The equilibrium temperature of the dust will be roughly 15-30 K, and at this temperature roughly 1/3 of the reradiated energy will go into a bandwidth ~10^{12} Hz around wavelength 100μm. This is where the echo will be strongest, and this band is accessible to the Texas infrared photometer (Harvey, Lester and Joy, 1987). It is easy to show that under these circumstances the flux density received in this band would be

$$F_\nu \approx 1.3\times10^{-15} f_s \Omega_{IR} \text{ erg cm}^{-2}\text{s}^{-1}\text{Hz}^{-1}, \qquad (1)$$

where Ω_{IR} is the beam size (sr) of the photometer and f_s is the filling factor of the bright echo knots in this beam. The Texas photometer has a beam 8×15 arcsec^2. Inspection of photos and theoretical profiles of the echo shows that it can fill this beam pretty well: $f_s \approx 0.7$. Then we find $F_\nu \approx 0.3$ Jy. This is the maximum signal achievable for $\tau_a \gtrsim 1$; for $\tau_a < 1$, $F_\nu \propto \tau_a$. This is a marginal signal for the Texas photometer, which reaches 1 Jy in ~1 hour of integration time. Thus we need a thick layer ($\tau_a \sim 1$) to have hopes of seeing it.

How thick is the actual dust layer? From the observed surface brightness of the visual echo relative to the SN, it is easy to show (Dwek and Felten, 1988; Chevalier, 1987) that $\tau_s P(\theta) \equiv \tau_e \omega P(\theta) \approx 1.1$. Here τ_s and τ_e are the visual scattering and extinction optical thicknesses of the layer, ω is the dust albedo, and $P(\theta)$ is the visual scattering phase function at scattering angle θ, where $\theta \approx 2°$ for the

outer echo ring. (This expression is rigorous for small optical depths but will remain approximately correct for $\tau_e \sim 1$. It holds even if there is heavy additional absorption, equal along the direct path to the SN and along the path through the echo layer. The only assumption is that τ_s for the echo layer itself is small, so that multiple scattering can be neglected.) This implies that, if we are to detect the infrared echo, we have to assume that

$$\zeta(\theta) \equiv \tau_a/\tau_s P(\theta) \gtrsim 1 \ . \qquad (2)$$

We could also write ζ as $\bar{Q}_a/\bar{Q}_s P$, where $\bar{Q}_a$ and $\bar{Q}_s$ are the effective mean efficiencies for absorption and scattering for the dust grains which are present.

The problem is that for typical interstellar dust mixtures ζ is small ($\ll 1$), because τ_a/τ_s is <1 and $P(2°)$ is large. Very small grains have large ζ, but large grains have small ζ, particularly at small forward angles $\theta \approx 2°$, because they scatter strongly forward. For a typical MRN mixture (Mathis, Rumpl and Nordsieck, 1977) of graphite and silicate spheres, with a power law $dn/da \propto a^{-3.5}$ in grain sizes and an upper size cutoff at $a_{max} = 0.25\mu m$, $P(2°)$ is about 8 and $\zeta(2°) \lesssim 0.1$. We have calculated ensemble properties for 14 different dust mixtures (Dwek and Felten, 1988). We took Q_a, Q_s and the asymmetry parameter g for individual spherical grains from Mie-theory calculations by Draine and Lee (1984) and Draine (1987), and assumed a Henyey-Greenstein form for the individual-grain phase function: $P(\theta)=(1-g^2)(1+g^2-2g\cos\theta)^{-3/2}$. We can increase ζ somewhat by taking an MRN mixture and adding an extra population of very small grains, but the power-law index for these small grains must be made very steep, >5.5, before ζ reaches unity. Such a dust distribution would contain more small grains than any previously suggested (e.g., Weiland *et al.*, 1986). Another way to obtain $\zeta \sim 1$ is to truncate the large-grain size distribution at a lower value a_{max}, say $0.1\mu m$ instead of 0.25. Draine and Anderson (1985) suggested such a distribution for one abnormal high-latitude Galactic cloud. The phase function then drops from $P \approx 8$ to $P \approx 2$, being strongly determined by the largest grains present. This, however, is an abnormal distribution, and the scattering by normal interstellar matter is expected to be more strongly peaked forward.

In summary, we must expect that these infrared echoes in the LMC, unless they issue from abnormal dust populations, will be one to two orders of magnitude below the present detection threshold, because the absorption optical thickness in the visual is expected to be small. The reradiated infrared echo produced at these layers by the initial ultraviolet burst from the SN should be even weaker (Dwek and Felten, 1988). It is of some interest that the visual echoes already rule out values of $\zeta \gg 1$ for these layers, because such dust would have $\tau_a \gg 1$ and would attenuate either the SN itself, or the observed visual echoes, by an additional factor $\sim \exp \tau_a$, which is not acceptable.

Finally we note that, while the infrared echoes may not be detectable at present, they are expected to remain accessible for many years at roughly the same flux level (though they move on the planes of dust). Detection should eventually be possible and should give additional information about the dust properties. We are preparing a longer paper (Felten and Dwek, 1988) on more general aspects of these echoes.

Catchpole, R.M. *et al.*: 1987, M.N.R.A.S. *229*, 15p.

Chevalier, R.A.: 1987, in *Proc. ESO Workshop on SN1987A*, ed. I.J. Danziger (Garching: ESO), p. 481.

Chevalier, R.A. and Emmering, R.T.: 1988, Ap.J. (Letters), in press.

Crotts, A.: 1988, IAU Circ., 4561.

Draine, B.T.: 1987, Princeton Obs. Preprints, No. 213.

Draine, B.T. and Anderson, N.: 1985, Ap.J. *292*, 494.

Draine, B.T. and Lee, H.M.: 1984, Ap.J. *285*, 89.

Dwek, E. and Felten, J.E.: 1988, Ap.J. (Letters), submitted.

Felten, J.E.: 1988, in *Supernova 1987A in The Large Magellanic Cloud* (Proc. 4th George Mason Astrophysics Workshop, Fairfax, Virginia, 12-14 October, 1987), ed. M. Kafatos and A.G. Michalitsianos (Cambridge: Cambridge University Press), p. 232.

Felten, J.E. and Dwek, E.: 1988, in preparation.

Gouiffes, C. *et al.*: 1988, ESO Scientific Preprint No. 591.

Hamuy, M., Suntzeff, N.B., Gonzalez, R. and Martin, G.: 1988, A.J. *95*, 63.

Harvey, P.M., Lester, D. and Joy, M.: 1987, IAU Circ., 4518.

Mathis, J.S., Rumpl, W. and Nordsieck, K.H.: 1977, Ap.J. *217*, 425.

Suntzeff, N.B., Heathcote, S., Weller, W.G., Caldwell, N., Huchra, J.P., Olowin, R.P. and Chambers, K.C.: 1988, Nature, in press.

Weiland, J.L., Blitz, L., Dwek, E., Hauser, M.G., Magnani, L. and Rickard, L.J: 1986, Ap.J. (Letters) *306*, L101.

SECTION IX: LIST OF PARTICIPANTS

LIST OF PARTICIPANTS

Achtermann, Jeff
University of Texas
Astronomy Department
R. L. Moore Hall 15.308
Austin, TX 78712

Aiello, Santi
University of Florence
Physics Department C/P CNR-IROE
via L. Pancaldo 3/45
50125 Florence, Italy

Aitken, David
Department of Physics
University of New South Wales
Campbell, Act
Australia 2600

Allamandola, Louis J.
NASA Ames Research Center
MS 245-6
Moffett Field, CA 94035

Anders, Edward
University of Chicago
5640 S. Ellis Avenue
Chicago, IL 60637

Arendt, Richard G.
349 Astronomy Bldg.
1011 W. Springfield Ave.
Urbana, IL 61801

Barker, John
University of Michigan
2106 Space Research Bldg.
Ann Arbor, MI 48109-2143

Barsella, Bruno
Istituto di Astronomia
Piazza Torricelli, 2
56100 Pisa
Italy

Bazell, David
Applied Research Corp.
NASA-Goddard
Code 685
Greenbelt, MD 20771

Benit, Jean
Department of Nuclear Engineering and
Engineering Physics
University of Virginia
Charlottesville, VA 22901

Bernard, Jean-Phillipe
Laboratoire de Physique
Route des Gatines, BP 10
91374 Verriers le Buisson
France

Bhatt, Harish
Indian Institute of Astrophysics
Room 404
Sarjapur Road
Bangalore 560 034, India

Blanco, A.
Physics Department
University of Lecce
731–Lecce, Italy

Bohme, Diethard
Department of Chemistry
York University
North York, Ontario M3J 1P3
Canada

Boulanger, F.
IPAC/Caltech
100-22
Pasadena, CA 91125

Bregman, Jesse
NASA Ames Research Center
MS 245-6
Moffett Field, CA 94035

Brooke, Tim
Department of Earth and Space Sciences
State University of New York
Stony Brook, NY 11794

Buch, Victoria
University of Illinois at Chicago
Box 4348, Chemistry Department UIC
Chicago, IL 60680

Burton, Michael
NASA Ames Research Center
MS 245-6
Moffett Field, CA 94035

Buss, Richard, Jr.
University of Colorado
Casa C. B. 391
Boulder, CO 80309

Butner, Harold M.
Department of Astronomy
University of Texas
Austin, TX 78712

Campins, Humberto
2030 E. Speedway #201
Tucson, AZ 85719

Caplan, James
Observatoire de Marseille
2 Place le Verrier
13248 Marseille Cedex 4
France

Cardelli, Jason
Department of Astronomy
University of Wisconsin-Madison
475 North Charter St.
Madison, WI 53706

Carico, David
Downs Laboratory 320-47
Caltech
Pasadena, CA 91125

Carnochan, David
Physics and Astronomy Department
University College of London
Gower Street
London, England WC1E 6BT

Casey, Sean
Yerkes Observatory
P. O. Box 258
Williams Bay, WI 53191

Caux, Emanuel
C.E.S.R. 9 Av. Du
Colonel Roche
BP 4346, 31029 Toulouse Cedex
France

Cherchneff, Isabelle
University of Michigan
Department of Atmospheric Science
Ann Arbor, MI 48109-2143

Chlewicki, Grzegorz
Laboratory for Space Research
P. O. Box 800
9700 Av Groninen
The Netherlands

Chokshi, Arati
NASA Ames Research Center
MS 245-6
Moffett Field, CA 94035

Churchwell, Ed
University of Wisconsin
Astronomy Department
475 N. Charter St.
Madison, WI 53706

Chyba, Christopher
Cornell University
Space Science Bldg.
Ithaca, NY 14853

Colangeli, Luigi
ESA Space Science Dpt. Estec
Postbus 299 Ag Nordiwjk
The Netherlands

Cudaback, David
Astronomy Department
University of California
Berkeley, CA 94720

Cugnon, Pierre
Royal Observatory of Belgium
Av. Circulaire, 3 B-1180
Brussels, Belgium

D'Hendecourt, Louis B.
Groupe de Physique des Solides
University of Paris
6 Place Jessieu 75251
Paris Cedex 05
France

DeFrees, Doug
Molecular Research Institute
701 Welch Rd., Suite 213
Palo Alto, CA 94304

DeHarveng, Lise
Observatoire de Marseille
2 Place le Verrier
13248 Marseille Cedex 4
France

Desert, Francois-Xavier
NASA Goddard
Code 685
Greenbelt, MD 20771

Deutsch, Lynn K.
Harvard-Sao
Mail Stop 10
60 Garden Street
Cambridge, MA 02138

Dones, Luke
NASA Ames Research Center
MS 245-3
Moffett Field, CA 94035

Donn, Bertram
NASA Goddard Code 69J1
Greenbelt, MD 20771

Draine, Bruce
Princeton University Observatory
Peyton Hall
Princeton, NJ 08544

Duley, W. W.
Physics Department
York University
Keele St., Toronto
Ontario, Canada M3J 1P3

Dwek, Eli
NASA Goddard
Code 685
Greenbelt, MD 20771

Efimov, Yu S.
Crimea, USSR

Egan, Michael P.
Rensselaer Polytechnic Institute
Department of Physics, RPI
Troy, NY 12180

Eiroa, Carlos
Observatorio Astronomico Nac.
c/Alfonso x11, 3
28014 Madrid, Spain

Engargiola, Gregory
Yerkes Observatory
Box 0258
Williams Bay, WI 53191

Feigelson, Eric
Pennsylvania State University
Department of Astronomy
University Park, PA 16802

Felton, James
NASA Goddard
Code 685
Greenbelt, MD 20771

Ferrara, Andrea
Istituto di Astronomia
University of Pisa
via Vettori G
Pisa, Italy

Fitzpatrick, Edward
Princeton University Observatory
Peyton Hall
Princeton, NJ 08544

Fonti, Sergio
via per Arnesano
73100 Lecce
Italy

Gehrz, R. D.
University of Minnesota
Astronomy Department
116 Church St., S. E.
Minneapolis, MN 55455

Gerbault, Florence
NASA Ames Research Center
MS 244-10
Moffett Field, CA 94035

Ghosh, Swarna Kanti
Infrared Astronomy Group
Tata Institute of Fundamental Research
Colaba, Bomba 400005, India

Giard, Martin
C. E. S. R., 9 Avenue des Colonel Roche
BP4346, 31029 Toulouse, Cedex
France

Goebel, John
NASA Ames Research Center
MS 244-10
Moffett Field, CA 94035

Greenberg, J. M.
Laboratory Astrophysics
P. O. Box 9504
2300 Ra Leiden
The Netherlands

Grim, Rudd
Laboratory Astrophysics
P. O. Box 9504
2300 Ra Leiden
The Netherlands

Haas, Michael
NASA Ames Research Center
MS 245-6
Moffett Field, CA 94035

Hackwell, James
P. O. Box 92937
The Aerospace Corporation
Los Angeles, CA 90009

Hage, J. I.
Huygens Laboratorium
Niels Bohrweg 2
2300 Ra Leiden
The Netherlands

Harris, Alan
Rutherford Appleton Laboratory
Space Astrophysics Group
Chilton, Didcot OX11 00X
England

Hecht, James H.
P. O. Box 92957
The Aerospace Corporation
Los Angeles, CA 90009

Heiles, Carl
Astronomy Department
University of California
Berkeley, CA 94720

Helou, George
IPAC, 100-22
Caltech
Pasadena, CA 91125

Hildebrand, Roger
University of Chicago
Enrico Fermi Institute
5640 Ellis Ave.
Chicago, IL 60637

Hodapp, Klaus-Werner
Institute for Astronomy
University of Hawaii
2680 Woodlawn Dr,.
Honolulu, HI 96822

Hollenbach, David
NASA Ames Research Center
MS 245-6
Moffett Field, CA 94035

Howarth, Neil
Cavendish Laboratory
Madingly Road
Cambridge, CB3 OHE
England

Huffman, Donald R.
University of Arizona
Physics Department
Tucson, AZ 85721

Hurwitz, Mark
University of California
Space Sciences Laboratory
Berkeley, CA 94720

Hyland, A. R. Harry
Mt. Stromlo/Siding Spring Observatory
Private Bag, Woden P. O.
Act 2606
Australia

Ibadov, Subhon
Institute of Astrophysics
Dushanbe 73470
USSR

Jain, S. K.
Indian Institute of Astrophysics
Bangalore 560034
India

Jenkins, Edward
Princeton University Observatory
Peyton Hall
Princeton, NJ 08544

Jones, A. P.
UMIST
Mathematics Department
P. O. Box 88
Manchester, England M60 1QD

Joseph, Charles
Department of Astrophys. Science
Princeton University
Princeton, NJ 08544

Kegel, W. L.
Institut fur Theoretische Phys
University of Frankfurt
Robert-Mayer-Strasse 10
6000 Frankfurt/Main W. Germany

Kerridge, John F.
Institute of Geophysics
University of California
Los Angeles, CA 90024-1567

Kissel, J.
MPI fur Kernsphysik
Postfach 103980
D-6900 Heidelberg
West Germany

Knacke, Roger
Earth and Space Sciences Department
State University of New York
Stony Brook, NY 11794-2100

Knude, Jens
Copenhagen University Observatory
Oster Voldgrade 3
DK-1350 Copenhagen K
Denmark

Koo, Bon-Chul
Astronomy Department
University of California
Berkeley, CA 94720

Kratschmer, W.
Max Planck Institute, Kernphysik
6900 Heidelberg
P. O. Box 103980
West Germany

Krelowski, Jacek
Institute of Astronomy
N. Copernicus University
Chopina 12/18 PL-87-100
Torun, Poland

Krueger, Frans
Engineers Bureau
Messeler St. 24
D-6100 Darmstadt 12
West Germany

Kurtz, Joe
University of Arizona
Physics Department
Tucson, AZ 85721

Lang, Bruno
Warsaw University
Department of Chemistry
Zwirki I Wigury 101
02-089 Warsaw, Poland

Lange, Andrew
Department of Physics
Berkeley, CA 94720

Laureijs, R. J.
Laboratory for Space Research
P. O. Box 800
9700 Av Groningen
The Netherlands

Leach, Sydney
Observatoire de Paris-Meudon
92190-Meudon
France

Leger, Alain
GPS – Tour 23
University of Paris 7
75251 Paris Cedex 05
France

Lequeux, James
Observatoire
13248 Marseille Cedex 4
France

Leung, Chung Ming
Rensselaer Polytechnic Institute
Department of Physics
Troy, NY 12180

Liffman, Kurt
NASA Ames Research Center
MS 245-3
Moffett Field, CA 94035

Liljestrom, Tarja
Helsinki Observatory
and Physics Laboratory
SF-00130 Helsinki, Finland

Lis, Dariusz
619 LGRC
University of Massachusetts
Amherst, MA 01003

Luan, Ling
University of California
Astronomy Department
Berkeley, CA 94720

Lynch, David K.
The Aerospace Corporation
P. O. Box 92957 MZ-266
Los Angeles, CA 90009

Magalhaes, Anontio M.
Universidade de Sao Paulo
Av. Miguel Stefano, 4200
Sao Paulo, Brazil

Manuel, Lawrence
1191 Delaware St.
Berkeley, CA 94702

Martin, Peter
C.I.T.A., University of Toronto
Ontario, Canada M5S 1A1

Massa, Derck
Applied Research Corporation
8201 Corporate Dr.
Landover, MD 20785

Matese, John
University Southwestern Louisiana
Department of Physics
Lafayette, LA 70504-4210

Mateshville, G.
Abastumani
USSR

Mathis, John S.
University of Wisconsin
Department of Astronomy
Madison, WI 53706

Matsumura, Masafumi
Astronomical Institute
Tohoku University
Sendai 980, Japan

Mattila, Kalevi
Helsink University Obs.
Tahtitorninmalu, SI-00130
Helsink, Finland

McKee, Christopher
Physics Department
University of California
Berkeley, CA 94720

Meixner, Margaret
University of California
Department of Astronomy
Berkeley, CA 94720

Menard, Francois
Department of Physics
University of Montreal
C. P. 6128, Succ. A. Montreal
Quebec, Canada H3C 3J7

Mencaraglia, Francesco
c/o CNR-IROE
via L. Pancaldo 3/45
50127 Firenze
Italy

Mendoza Gomes, Celia X.
Rijksuniversiteit Leiden
Postbus 9504; 2300 Ra Leiden
The Netherlands

Meyerdierks, Horst
Radioastronomie, University Bonn
Auf Dem Huegel 71, 5300 Bonn 1
West Germany

Mitchell, David
University of California
Astronomy Department
Berkeley, CA 94720

Moorhouse, Alan
University of Edinburgh
Department of Astronomy
Royal Observatory
Blackford Hill
Edinburgh EH 9 3HJ Scotland

Murthy, Jayant
NASA Goddard
Code 681
Greenbelt, MD 20771

Nuth, Joseph
NASA Goddard
Code 691
Greenbelt, MD 20771

Onaki, Takahashi
2-11-16 Yoyoi, Bukyo-Ko
Toyko 113
Japan

Orofino, Vincenso
via per Arnesano
73100 Lecce
Italy

Osterbrock, Donald E.
Lick Observatory
University of Santa Cruz
Santa Cruz, CA 95064

Patriarchi, Patrizio
Observatorio Astrofisico di
Arcetri
Largo E. Fermi 5
i-50125 Firenze, Italy

Pendleton, Yvonne
NASA Ames Research Center
MS 245-6
Moffett Field, CA 94035

Persi, P.
Istituto Astrofisica Spaziale
CP 67, 00044
Frascati, Italy

Pironello, Valero
University of Calabria
Italy

Prusti, Timo
Laboratory for Space Research
P. O. Box 800
9700 Av Groningen
The Netherlands

Puget, Jean-Loup
Ecole Normale Superieure
26 Rue Lhomond
F-75015 Paris
France

Reach, William T.
Astronomy Department
University of California
Berkeley, CA 94720

Rengarajan, T. N.
IR Astronomy
Tata Institute Fundamental Res.
Homi Bhabha Road
Bombay 400 005 India

Richards, Paul L.
Department of Physics
University of California
Berkeley, CA 94720

Roche, Patrick
Royal Observatory
Blackford Hill
Edinburgh, Scotland EH9 EHJ

Roellig, Thomas L.
NASA Ames Research Center
MS 245-6
Moffett Field, CA 94035

Rouan, Daniel
Department Spatial, Obs. de Paris
Bat. Iso, Obs. de Meudon
92195 Meudon Principal Cedex
France

Rubin, Robert
NASA Ames Research Center
MS 245-6
Moffett Field, CA 94035

Rudolph, Alexander
University of California
Department of Astronomy
Berkeley, CA 94720

Russell, Ray
Aerospace Corporation
El Segundo, CA 90245

Ryter, Charles
DPHG/SAP
91191 GIF Sur Yvette Cedex
France

Sakata, Akira
University of Electro-Comm.
Department Applied Physics and Chemistry
1-5-1 Chofugaoka, Chofu-Shi
Tokyo, Japan

Salama, Farid
NASA Ames Research Center
MS 245-6
Moffett Field, CA 94035

Sandford, Scott
NASA Ames Research Center
MS 245-6
Moffett Field, CA 94035

Savage, Blair
University of Wisconsin
Department of Astronomy
475 N. Charter St.
Madison, WI 53706

Scarrott, S. M.
University of Durham
Physics Department
Durham DH1 3LE
United Kingdom

Schmitt, Bernard
Huygens Laboratorium, Astrophy
Postbus 9504 2300 Ra Leiden
The Netherlands

Schutte, Willem
NASA Ames Research Center
MS 245-6
Moffett Field, CA 94035

Seab, C. Gregory
Physics Department
University of New Orleans
Lakefront
New Orleans, LA 70148

Sedlmayr, E.
Technische Universitat Berlin
Institute fur Astron. and Astrophys.
PN 8-1, Hardenbergstrase 36
D-1000 Berlin, West Germany

Seki, Munezo
College of General Education
Tohoku University
Department of Earth Sciences
Sendai 980, Japan

Sellgren, Kris
University of Hawaii
Institute for Astronomy
2680 Woodlawn Dr.
Honolulu, HI 96822

Simpson, Janet P.
NASA Ames Research Center
MS 245-6
Moffett Field, CA 94035

Slykhuis, S.
University of Amsterdam, Astr. Inst
Roetersstraat 15,
1018 WB Amsterdam
The Netherlands

Smith, Howard A.
Naval Research Laboratory
Code 41385M, Space Science Division
Washington, DC 20375

Smith, Robert
Max Planck Institute fur
ext. physics
D-8046 Garching Bei Munchen
Federal Republic of Germany

Snow, T. P.
Casa – Box 391
University of Colorado
Boulder, CO 80309

Sodroski, Thomas J.
NASA Goddard Space Flight Center
Code 685
Greenbelt, MD 20770

Sommerville, W. B.
Physics and Astronomy Department
University College London
Gower Street
London, England WC1E 6BT

Stecher, Theodore
NASA Goddard
Code 680
Greenbelt, MD 20771

Stemwede, Sally
Naval Research Laboratory
Code 4138 St.
Washington, DC 20375-5000

Stephens, John R.
Los Alamos National Laboratory
Mail Stop C-348, P. O. Box 1663
Los Alamos, NM 87545

Sudzius, J.
Astronomical Observatory
Vilnius University
Ciurlionio 29, Vilnius 232009
Lithuania, USSR

Svestka, Jiri
Prague Observatory
M846 Petrin 205
Prague, Czechoslovakia

Szcserba, Ryszard
Copernicus Astronomical Center
Laboratory for Astrophysics
UL. Chopina 12/18
87-100 Torun, Poland

Tapia, Mauricio
ESO
K. Schwarzschild Str. 2
D-8046 Garshing
West Germany

Tereby, Susan
Radio Astronomy 105-24
Caltech
Pasadena, CA 91125

Thompson, Stephen
Department of Physics
University of Keele
Keele, Staffordshire
ST5 5BG England

Tielens, A. G. G. M.
University of California
Astronomy Department
Berkeley, CA 94720

Tokunaga, Alan
Institute for Astronomy
University of Hawaii
2680 Woodlawn Dr.
Honolulu, HI 96822

Toller, Gary
Applied Research Corporation
9364 Dewitt Way
Columbia, MD 21045

Trajmar, Sandor
JPL/Caltech
4800 Oak Grove Drive
Pasadena, CA 91109

Van Buren, Dave
Space Telescope Science Center
3700 San Martin Drive
Baltimore, MD 21218

Verma, R. P.
Tata Institute Fundamental Res.
Homi Bhabha Road
Bombay, 400 005
India

Verstraete, Laurent
University of Paris
GPS-ENS, Tour 23-13
4 Place Jussieu 75251
Paris Cedex 05, France

Wainscoat, Richard J.
NASA Ames Research Center
MS 245-6
Moffett Field, CA 94035

Walker, Helen J.
NASA Ames Research Center
MS 245-6
Moffett Field, CA 94035

Walmsley, Malcolm
Max-Planck Institute Radioastron.
Auf dem Hugel 69
D-5900 Bonn 1
West Germany

Wang, Boji
Harvard-Smithsonia Center for
Astrophysics
MS 10, 60 Garden St.
Cambridge, MA 02148

Watson, William D.
University of Illinois
Loomis Laboratory
Urbana, IL 61801

Wdowiak, Thomas J.
Physics Department
University of Alabama
Birmingham, AL 35294

Weitenbeck, Anthony
St. Cloud State University
Department of Physics and Astronomy
St. Cloud, MN 56301

Werner, Michael
NASA Ames Research Center
MS 245-6
Moffett Field, CA 94035

White, Richard
University of Wyoming
Department of Physics and Astronomy
Laramie, WY 82070

Whitemore, Daniel P.
University Southwestern Louisiana
Department of Physics
Lafayette, LA 70504-4210

Whittet, Douglas
School of Phys. and Astronomy
Lancashire Polytechnic
Preston PR1 2TQ
England

Williams, David
UNIST
Mathematics Department
P. O. Box 88
Manchester, England M60 1QD

Wink, Joern -E.
IRAM
Voie 10 Domaine Universitaire
F 38406 St. Martin-D'Heres
France

Wiramihardja, Suhardja
Bosscha Observatory
Lembang 40391
Java, Indonesia

Witt, Adolf
Ritter Observatory
University of Toledo
Toledo, OH 43606

Witteborn, Fred C.
NASA Ames Research Center
MS 245-6
Moffett Field, CA 94035

Wolfire, Mark
University Of Chicago
Astronomy and Astrophysics Center
5640 S. Ellis Avenue
Chicago, IL 60637

Wolstencroft, Ramon
Royal Observatory
Blackford Hill
Edinburgh, EH 9 3HJ
Scotland

Wooden, Diane
NASA Ames Research Center
MS 245-6
Moffett Field, CA 94035

Woodward, Chick
Department of Physics and Astronomy
University of Wyoming
P. O. Box 3905
Laramie, WY 82071

Wright, Edward
Department of Astronomy
University of California
Los Angeles, CA 90024

Zhao, Nansheng
Huygens Lab. Astrophysics
Postbus 9504
2300 Leiden
The Netherlands

NASA
National Aeronautics and Space Administration

Report Documentation Page

1. Report No.	2. Government Accession No.	3. Recipient's Catalog No.
NASA CP-3036		

4. Title and Subtitle	5. Report Date
Interstellar Dust: Contributed Papers	December 1989
	6. Performing Organization Code
7. Author(s)	8. Performing Organization Report No.
A. G. G. M. Tielens and L. J. Allamandola, Editors	A 89050
	10. Work Unit No. 188-44-57
9. Performing Organization Name and Address	11. Contract or Grant No.
Ames Research Center Moffett Field, CA 94035	
	13. Type of Report and Period Covered
12. Sponsoring Agency Name and Address	Conference Publication
National Aeronautics and Space Administration Washington, DC 20546-0001	14. Sponsoring Agency Code

15. Supplementary Notes

Point of Contact: A.G.G.M. Tielens, M/S 245-6, Ames Research Center
Moffett Field, CA 94035 (415)694-6890 or FTS 464-6890

16. Abstract

The IAU Symposium 135 on Interstellar Dust was hosted and co-sponsored by NASA Ames Research Center July 26-30, 1988. The symposium was held at Santa Clara University in Santa Clara, CA. This symposium brought together 199 scientists from 19 different countries. The wide range of interest and expertise of the participants - all in some way related to interstellar dust - is reflected in the great variety of topics that were discussed during the symposium, ranging from UV, visible, and IR observations of interstellar extinction to quantum-statistical calculations of the IR emission from highly vibrationally excited polycyclic aromatic hydrocarbon molecules. During the course of the meeting, 41 invited review papers and 140 contributed papers were presented. This is a collection of the contributed papers. The invited reviews will be published in a companion volume by Kluwer Academic Publishers as part of the IAU Symposium Series.

17. Key Words (Suggested by Author(s))	18. Distribution Statement
Interstellar dust	Unclassified - Unlimited Subject Category 88

19. Security Classif. (of this report)	20. Security Classif. (of this page)	21. No. of pages	22. Price
Unclassified	Unclassified	588	A25